

Structural and Shape Reconstruction using Inverse Problems and Machine Learning Techniques with Application to Hydrocarbon Reservoirs

A thesis submitted to The University of Manchester for the degree of
Doctor of Philosophy

In the Faculty of Science and Engineering

2018

Clement Etienam
School of Chemical Engineering and Analytical Science

Contents

Contents	2
List of Figures	8
List of Tables	19
List of Abbreviations	21
Abstract	24
Declaration	25
Intellectual Property Statement	26
Acknowledgements.....	27
Preface	28
Problems and Objectives:	31
Overview of Numerical Experiments explained in Chapter Seven	32
Chapter 1 – Introduction & Literature review	38
1.1 Research Objectives	55
Chapter 2- Introduction to Petroleum Geostatistics	57
2.1 Interpolation Techniques	57
2.2 Sequential Gaussian Simulation (SGS)	59
2.3. Multiple-Point Statistics (MPS) with <i>FILTERSIM</i> Software	60
2.3.1 <i>Filters and scores</i>	61
2.3.2 <i>Filter definition</i>	63
2.3.3 <i>Pattern classification</i>	63
2.3.4 <i>Pattern partition</i>	63
2.3.5 <i>Partition method</i>	64
2.3.6. <i>Sequential simulation</i>	64
2.4 Semi-variogram	65
2.4.1 <i>Quantile function</i>	66
2.4.2 <i>Random Variables</i>	69
2.4.3 <i>Trend</i>	70

2.4.4 Semi-variogram Characteristics	70
2.4.5 Semi-variogram Modelling.....	71
The conclusion of Chapter 2.....	72
Chapter 3 – Multi-Phase Flow in Porous Media	74
3.1 Reservoir Simulation Equations	74
3.2 Two-Phase flow in porous media	77
3.3 Three-phase flow in porous media.....	77
3.4 Selection of sensitive paramters to be history matched	78
Conclusion on chapter 3.....	79
Chapter 4 –Inverse problems/Data Assimilation.....	80
4.1 Inverse Problems: Bayesian Theory	80
4.1.1 <i>Introduction to Gradients</i>	81
4.1.2 <i>Singular Value Decomposition (SVD)</i>	83
4.1.3 <i>The Bayesian posterior ensemble smoother for linear Gaussian case</i>	84
4.2 History Matching Methods.....	88
4.3 The Kalman Filter.....	89
4.4 Ensemble Kalman filter.....	92
4.4.1 <i>Measurement perturbations</i>	97
4.5 Applicability of EnKF to the Reservoir History Matching process	98
4.5.1 <i>Parametrization</i>	98
4.5.2 <i>Measurement error model</i>	100
4.5.3 <i>Induced Errors</i>	100
4.6. Ensemble square root filters	103
4.7. Ensemble smoother.....	103
4.8. Ensemble Smoother Multiple Data Assimilation (ES-MDA)	106
Conclusion on chapter 4.....	108
Chapter 5-4D Seismic and 3D Time-lapse Electromagnetic Data.....	109
5.1 Petro-Elastic Modelling	109
5.1.1 <i>Gassmann's equation</i>	109
5.2 Introduction to Electromagnetic imaging of the earth	110
5.2.1 <i>Sensitivities and the adjoint model</i>	112
5.2.2 <i>Maxwell's equation for anisotropic media</i>	112
Conclusion on chapter 5.....	114

Chapter 6 – Parametrisation Techniques 115

6.1 Introduction to the Level-set Method.....	115
6.2 Sparse Coding/Machine Learning	117
6.2.1 <i>Orthogonal Matching Pursuit</i>	118
6.2.2 <i>K-SVD Algorithm</i>	119
6.3 Discrete Cosine Transform (DCT)	122
Conclusion of chapter six	124

Chapter 7 – Methodology & Numerical Experiments..... 125

7.1 Synthetic Reservoir Models and computer specification	125
7.1.1 <i>Channelized Synthetic model-SPE 10</i>	125
7.1.2- <i>Gaussian synthetic model</i>	127
7.1.3 <i>Naturally fractured Model (NFR)</i>	129
7.1.4 <i>PUNQ-S3 synthetic model</i>	133
7.1.5 <i>Computer specification</i>	135
7.2 –Ensemble Kalman Filter- Level Set technique for an Integrated History Matching (Numerical Experiment 1)	135
<i>Novelty</i>	135
7.2.1. <i>Introduction</i>	136
7.2.2. <i>NFR modelling</i>	138
7.2.3 <i>EnKF-Level set coupling methodology</i>	141
7.2.4. <i>Results and discussions</i>	147
7.2.5 <i>Comparison between the EnKF and EnKF-Level Set History matched realisations for the SPE 10 channelised model</i>	149
7.2.6 <i>Comparison between EnKF and EnKF-Level-Set for the Gaussian model</i>	158
7.2.7 <i>Comparison between the EnKF and EnKF-Level Set History matched realisations for the NFR model</i>	165
7.2.8. <i>Conclusion and future work</i>	171
7.3 – Comparison of Ensemble-based methods integrated with imaging and regularisation techniques (Numerical Experiment 2)	172
<i>Novelty</i>	172
7.3.1 <i>Introduction</i>	172
7.3.2 <i>Algorithm specific to our synthetic reservoir</i>	173
7.3.3 <i>Results</i>	174
7.3.4 <i>Comparison between EnKF/ES-MDA</i>	174
7.3.5 <i>Covariance Localization</i>	176

7.3.6. ES-MDA-Level set coupling methodology	177
7.3.7 Conclusion	186
7.4- Improved History Matching using 4D Seismic results (Numerical Experiment 3)	186
Novelty	186
7.4.1. Introduction	187
7.4.2 Levenberg-Marquardt method	188
7.4.3 Initial ensemble construction	189
7.4.4. Fault property estimation and 4D seismic results	190
7.4.5 Absolute Transmissibility Multiplier	191
7.4.6 Multi-phase Fault Rock Properties	192
7.4.7. 4D-Seismic results and Reservoir Simulation	195
7.4.8 Quantitative inversion	196
7.4.9 Methodology	197
7.4.10 Results and Discussion	200
7.4.11. Conclusion	207
7.5 –Water Front Characterisation in History Matching Using Low-frequency Electromagnetic Data(Numerical Experiment 4)	209
Novelty	209
7.5.1. Introduction	209
7.5.2 Initial ensemble construction	210
7.5.3 A nonlinear Kaczmarz-type approach (Algebraic reconstruction technique) for EM data inversion to conductivity	210
7.5.4 The Comprehensive History matching algorithm	211
7.5.5 Reservoir synthetic model	213
7.5.6. Simulation results	216
7.5.7 EnKF-Level set with EM water saturation data assimilation	219
7.5.8 EnKF-Level set void of EM water saturation data assimilation	221
7.5.9 Comparison between EnKF-EM and EnKF models	221
7.5.10. Conclusion and future work	229
7.6 – Combining Machine learning techniques with a History Matching - Level set approach (Numerical Experiment 5)	230
Novelty	230
7.6.1 Introduction	230
7.6.2. Construction of the state space ensemble	232
7.6.3. The algorithm/Method	234

7.6.4. Results and Discussions	238
7.6.5 PUNQ-S3 synthetic model.....	238
7.6.6 Comparison studies for the PUNQ-S3 model	240
7.6.7 SPE 10 synthetic model.....	254
7.6.8 Comparison studies for SPE 10 numerical experiment	254
7.6.9. Conclusion.....	267
Chapter 8-Overall Conclusion of Numerical experiments and results in the thesis with considerations for future work	269
Appendix	274
A1 - Reservoir Fluid Properties.....	274
A.1.1 Reservoir rock-fluid interaction	274
A.1.2 Darcy's Law	282
A.1.3 Two-Phase relative permeability.....	284
A.1.4 Three-phase relative permeability	285
A.1.5 Under saturated reservoirs.....	285
A.1.6 Saturated Reservoir	285
A.1.7 Gas Expansion Factor	285
A.1.8 Volumetric Estimation of Fluid Reserves	286
A.2: The flow potential	287
A.2.1 Real gas flow potential.....	288
A.2.2 Steady and unsteady flow	289
A.3 Fluid Types.....	290
A.4 Reservoir Simulation Equations numerically solved by ECLIPSE	290
A.4.1 Multiphase flow equations	294
A.4.2 Finite Difference Model	297
A.4.3 Discretization.....	297
A.4.4 Spatial discretisation	297
MATLAB codes	303
Codes for Numerical Experiment 2- Comparison of Ensemble-based methods integrated with imaging and regularisation techniques	303
Codes for Numerical Experiment 5- Combining Machine learning techniques with a History Matching - Level set approach.....	341
Bibliography.....	353

WORD COUNT: 52,419

List of Figures

Figure 2.1: Filter and score (a) general template (b) cube-shaped template (c) From filter to score (Wu et al., 2006).....	62
Figure 2.2: Two classification method (Wu et al., 2006).....	64
Figure 2.3: Diagram showing the semi-variogram, covariance, and variance (Bohling, 2005)	69
Figure 2.4: A schematic of a semi-variogram (Bohling, 2005).....	70
Figure 2.5: A plot of semi-variance against lag showing the various semi-variogram models(Bohling, 2005)	72
Figure 3.1: Flow-chart of the reservoir modelling and uncertainty quantification workflow.	76
Figure 4.1: Comparison between KF and EnKF.....	92
Figure 4.2(a): Time-series visual representation of the EnKF	93
Figure 4.2(b): Comparison between EnKF and traditional History matching (Fahimuddin, March,2010)	93
Figure 4.3: Traditional history matching model that uses the input data simultaneously and generates a single best-matched model.....	102
Figure 4.4: Workflow chart of the EnKF.....	102
Figure 4.5: Bayesian concept description of the EnKF.	103
Figure 4.6: Bayesian concept description of the ES.....	104
Figure 4.7: Schematic showing the description of the ES-MDA.	108
Figure 5.1: A 3D-EMIT experimental setup with a dipole transmitter, q adapted from (Dorn, et al., 2007)	111
Figure 6.1: Implicit representation of the level-set function	117
Figure 6.2: Schematic showing the K-SVD algorithm	122
Figure 6.3: Illustration of the DCT algorithm implemented in a picture. (A) True image of the reference picture, and (B) Corresponding DCT cosine basis of the picture.....	123
Figure 6.4: Reconstruction of the original image is retaining a certain level of the DCT cosine basis. (A) DCT image reconstruction at 0.2%,(B) DCT image reconstruction at 1%,(C) DCT image reconstruction at 2.5% and (D) DCT image reconstruction at 4.2%.....	123
Figure 7.1(a): permeability map of the SPE 10 true model showing the 2D and 3D- 8 well configurations.....	126

Figure 7.1(b): Scatter plot of log permeability against porosity for the fine-scale model.....	127
Figure 7.2: True reservoir synthetic model.....	128
Figure 7.3: (a) 3D permeability field of the true Gaussian synthetic model showing the two well locations and (b) 2D permeability field of the true Gaussian synthetic model.....	129
Figure 7.4: Dual Porosity concept, (Lemmonier & Bourbiaux, 2010)	130
Figure 7.5: Idealization of the fractured reservoir, (Edited from Warren, J.E. & Root, P, J., 1963)	131
Figure 7.6: (a) Outcrop of the fractured reservoir (Odling E, 1997), (b) Pixel converted Training image (with a MATLAB code) used for the initial creation of permeability ensemble.....	131
Figure 7.7: (a) True dual-permeability synthetic model (fracture model) used in this work:(b) 3D true dual-permeability synthetic model used in this work.....	132
Figure 7.8(a): permeability field of the true PUNQ-S3 synthetic model showing the 2D planar permeability field and 3D model showing the six well locations.	134
Figure 7.8(b): Histogram of the true permeability and porosity field justifying the truncation value to be used in the EnKF-Level set algorithm.....	138
Figure 7.9: Log-Log type curve of NFR, (Bourdarot, G, 1998).....	139
Figure 7.10: Realisations of the different initial channelised permeability obtained by FILTERSIM algorithm obtained in S-GeMS	149
Figure 7.11: Schematic showing the representation of a pixel permeability map to its corresponding facies map, signed distance map and narrowband map.....	149
Figure 7.12: Production profile for the initial ensemble. (A) Oil production rate for the four producer wells, (B) water cut profile for four producer wells, (C) bottom hole pressure for the four injector wells, (D), Gas-oil-ratio for the four producer wells, (E) Field oil recovery ratio and (F) Initial RMSE values for the realisations. The red curve represent the true data and the blue overlay lines represents the realisations.The black dashed line (vertical) represents the historical and prediction stages.....	151
Figure 7.13: Production profile for the EnKF-Level Set history matched ensemble. (A) Oil production rate for the 4 producer wells, (B) water cut profile for 4 producer wells ,(C) bottom hole pressure for the 4 injector wells, (D), Gas-oil-ratio for the 4 producer wells, (E) Field oil recovery ratio and (F) RMSE values for the EnKF-level set history-	

matched realizations. The red curve represent the true data and the blue overlay lines represents the realisations.The black dashed line (vertical) represents the historical and prediction stages.....152

Figure 7.14: Production profile for the EnKF scheme. (A) Oil production rate for the 4 producer wells, (B) water cut profile for 4 producer wells ,(C) bottom hole pressure for the 4 injector wells, (D), Gas-oil-ratio for the 4 producer wells, (E) Field oil recovery ratio and (F) RMSE values for the EnKF history matched realizations. The red curve represent the true data and the blue overlay lines represents the realisations.The black dashed line (vertical) represents the historical and prediction stages154

Figure 7.15: Log-permeability field evolution for selected realisations. (A) #75,(B) # 80 and (C)# 70. The first column all through the panel is the initial guesses, the second columns are the EnKF updated realisation, and the third columns are the EnKF-level set updated realisations and the fourth columns is the true permeability field156

Figure 7.16: 3D Log-permeability field evolution for selected realisations. (A) #75,(B) # 85,(C)# 70 and (D) #29.157
some statistical relationship to quantify the log permeability realisations of both the updated EnKF and EnKF-level set to the true log permeability field is shown below..157

Figure 7.17: Statistical quantification of the history matched realisations showing the correlation coefficient of the permeability and porosity fields of both the EnKF(red line) and EnKF-level set(blue line) scheme to the true model. The initial ensemble is light blue (down) and the difference in production data mismatch (top)157

Figure 7.18: The Histogram of the reference permeability field justifying the use of the Level Set technique.....159

Figure 7.19: an initial model of realisations #24, #19 and #51 generated with the *SGSIM* algorithm (Deutsch & Journel, 1998) unique for the Gaussian experiment.159

Figure 7.20: (a) Facies map distribution of a model, and (b) Narrowband map of the true model.....160

Figure 7.21: The initial ensemble oil production rate profile (a), water production rate profile (b) and injector bottom hole pressure profile(c). The red curve represent the true data and the grey overlay lines represents the realisations.The black dashed line (vertical) represents the historical and prediction stages161

Figure 7.22: The EnKF-Level Set history matched ensemble oil production rate profile (top-left), water production rate profile(top-right), injector bottom hole pressure

profile(bottom-left) and oil recovery ration (bottom right). The red curve represent the true data and the grey overlay lines represents the realisations.The black dashed line (vertical) represents the historical and prediction stages	162
Figure 7.23: The EnKF history matched ensemble oil production rate profile (top-left), water production rate profile(top-right), injector bottom hole pressure profile(bottom-left) and oil recovery ration (bottom right). The red curve represent the true data and the grey overlay lines represents the realisations.The black dashed line (vertical) represents the historical and prediction stages	163
Figure 7.24: Comparison between EnKF and EnKF-Level Set RMS function (#51).....	164
Figure 7.25: Comparison between EnKF and EnKF-Level Set ensemble mean: (a) EnKF mean oil production rate profile, (b) EnKF mean water production rate profile, (c) EnKF mean injection pressure profile, (d) EnKF-Level Set mean oil production rate profile, (e) EnKF-Level Set mean water production rate profile, and (f) EnKF-Level Set mean injection pressure profile.....	164
Figure 7.26: (a) Permeability map distribution of true model, (b) EnKF-Level Set history matched realisation permeability map (#51).(c) SSIM map for the comparison, (d) Permeability map distribution of true model,(e) EnKF history matched realization permeability map (#51) and (f) SSIM map for the comparison	165
Figure 7.27: Initial dual-permeability model of some realizations: (a) dual-permeability model of # 72, (b) dual-permeability model of # 28, (c) dual-permeability model of # 92.....	166
Figure 7.28: initial ensemble pressure-production profile: (a) oil production rate profile before update, (b) water-cut production rate profile before update, (c) injection pressure profile before EnKF update, (d) Oil recovery ratio before EnKF update. The red curve represent the true data and the grey overlay lines represents the realisations.	168
Figure 7.29: Final ensemble pressure-production profile after EnKF-Level-set History-matching: (a) oil production rate profile after EnKF-Level-set update, (b) water-cut production rate profile after EnKF-Level-set update, (c) injection pressure profile after EnKF update, (d) Oil recovery ratio after EnKF-Level-set update. . The red curve represent the true data and the grey overlay lines represents the realisations.....	168
Figure 7.30: Comparison between the true model permeability field and the history matched realization: (a) True dual-permeability distribution showing Layers 1-2, and	

(b) History matched dual- permeability distribution of # 72 showing Layers 1-2, (c) History matched dual- permeability distribution of # 28 showing Layers 1-2, and (d) History matched dual- permeability distribution of # 92 showing Layers 1-2	169
Figure 7.31: Final ensemble pressure-production profile after EnKF-Level-set History matching for the best seven realisations: (a) oil production rate profile after History matching, (b) water-cut production rate profile after EnKF-Level-set update, (c) injection pressure profile after EnKF update, and (d) Oil recovery ratio after EnKF-Level-set update.....	170
Figure 7.32: Permeability reconstruction: Top-down is Layer 1-4 Column A-Initial mean, Column B-EnKF mean permeability, Column C-ES-MDA mean permeability, Column D-True permeability.....	174
Figure 7.33: Schematic showing the 5 th order Gaspari-Cohn covariance function.....	180
Figure 7.34: Production profile of initial ensemble. Top-down is for producer's 1-4.Column A: Oil production rate, Column B is water cut, and Colum C is the Gas-oil ratio. . The red curve represent the true data and the cyan overlay lines represents the realisations.The vertical dashed line represents the historical (left of this line) and predcitin stages (right of this line)	181
Figure 7.35: Well bottom hole pressure for the four injectors, field oil recovery ratio and RMS Cost function of the initial ensemble. The red curve represent the true data and the cyan overlay lines represents the realisations.The vertical dashed line represents the historical (left of this line) and predcitin stages (right of this line)	181
Figure 7.36: Production profile of ES-MDA-LS-COV. Top-down is for producers 1-4.Column A: Oil production rate, Column B s water cut and Colum C is the Gas-oil ratio. The red curve represent the true data and the cyan overlay lines represents the realisations.The vertical dashed line represents the historical (left of this line) and predcitin stages (right of this line)	183
Figure 7.37: Well bottom hole pressure for the four injectors, field oil recovery ratio and RMS Cost function of the ES-MDA-LS-COV ensemble. The red curve represent the true data and the cyan overlay lines represents the realisations.The vertical dashed line represents the historical (left of this line) and predcitin stages (right of this line)	183
Figure 7.38: Production profile of ES-MDA Standard. Top-down is for producers 1-4.Column A: Oil production rate, Column B s water cut and Colum C is the Gas-oil ratio .The red curve represent the true data and the cyan overlay lines represents the	

realisations.The vertical dashed line represents the historical (left of this line) and predcitin stages (right of this line)	184
Figure 7.39: Well bottom hole pressure for the four injectors, field oil recovery ratio and RMS Cost function of the ES-MDA ensemble. The red curve represent the true data and the cyan overlay lines represents the realisations.The vertical dashed line represents the historical (left of this line) and predcitin stages (right of this line)	184
Figure 7.40: Permeability reconstruction: Top-down is Layer 1-5 Column A-Initial mean, Column B-ES-MDA mean permeability, Column C-ES-MDA-LS-COV mean permeability, Column D-True permeability.....	186
Figure 7.41: Schematic showing the derivation of the phase-specific transmissibility multiplier.....	192
Figure 7.42: Schematic sub-methodology on updating fault parameters taking into consideration two-phase properties.....	199
Figure 7.43: Fault-zone pseudo-relative permeability modification ranges, (b) Synthetic Pc curves for fault-zone grid-blocks; the circles represent capillary threshold pressure on the drainage Pc curves. At this Swor, the oil relative permeability with imbibition Pc both go to zero.,moreover, (c)Relative transmissibility multipliers for oil and water; generated within the range of water saturation value output realized with 4D-Seismic data and simulated results.....	201
Figure 7.44: 3D Fault model of the EnKF -2 phase scheme	202
Figure 7.45: True model and 3D History matched permeability model, EnKF-FTM, and LM-2 phase FTM.....	203
(A-E) Permeability for the true model, (F-J) final permeability for the EnKF-FTM model without 4D seismic, and (K-O) final permeability for the LM-2phase with 4D seismic.	
.....	203
Figure 7.46: 3D History matched permeability model of the EnKF No-FTM and EnKF-2 phase FTM, (A-E) final permeability reconstructed by EnKF-No FTM history matching without 4D seismic, and (F-J) permeability recovered by EnKF- 2 phase FTM history matching with 4Dseismic.	204
Figure 7.47: Comparison between the History matched models of the EnKF-FTM, EnKF-2 phase FTM, EnKF No-FTM and LM-2 phase FTM: (a) oil production rate profile, (b) water production rate profile, (c) injection pressure profile and (d) RMS function comparison.....	205

Figure 7.48: Comparison between the oil recovery ratios of the history matched models of the EnKF-FTM, EnKF-2 phase FTM, EnKF No-FTM and LM-2 phase FTM: ...	205
Figure 7.49: Reconstructed impedance image of the history matched models of EnKF-FTM, EnKF-2 phase FTM, EnKF No-FTM and LM-2 phase FTM. (a) True impedance image (b) impedance image reconstructed by EnKF-2 phase FTM history matching, (c) impedance image reconstructed by EnKF-FTM history matching, and (d) impedance image reconstructed by EnKF No-FTM history matching and, (e) impedance image reconstructed by LM-2 phase FTM history matching	206
Figure 7.50: Schematic showing the coupled EnKF-level set-EM method used in this work	214
Figure 7.51: 3D True model water saturation distribution at year 6 showing the two well locations	215
Figure 7.52: True water saturation distribution of the reference/true reservoir at year 6.....	215
Figure 7.53: 3D True and reconstructed conductivity profile of synthetic model at year six from EM survey.....	217
Figure 7.54: 2D-view conductivity plume: (a) True water conductivity distribution of the reference/true reservoir, (b) Reconstructed conductivity profile	217
Figure 7.55: (a) Reconstructed conductivity profile, (b) Equivalent water saturation distribution of the reconstructed conductivity profile using Archie's law	218
Figure 7.56: (a) RMS evolution during the conductivity reconstruction and (b): RMS function evolution of the reconstructed conductivity profile	219
Figure 7.57: (a) Correlation function from 5 th order Gaspari –Cohn matrix, (b) Correlation function (sensitivity functions) from our non-linear Kazsmarz solver and (c) Correlation function arriving from the combination of both approaches	220
Figure 7.58: Comparison between EnKF-EM and EnKF production rate profile:, (a) oil production rate profile (b) water production rate profile (c) injection pressure profile and (d) History matched Realizations RMS function with and without assimilating EM data	222
Figure 7.59: Production profile of initial ensemble. (a) Oil rate match, (b) Water rate match and (c) Bottom-hole-pressure. The red curve represent the true data and the grey overlay lines represents the realisations.The vertical dashed line represents the historical (left of this line) and predcitin stages (right of this line).....	223

Figure 7.60: Production profile of EnKF-EM. (a) Oil rate match, (b) Water rate match and (c) Bottom-hole-pressure. The red curve represent the true data and the grey overlay lines represents the realisations.The vertical dashed line represents the historical (left of this line) and predcitin stages (right of this line).....	223
Figure 7.61: Production profile of EnKF ensemble. (a) Oil rate match, (b) Water rate match and (c) Bottom-hole-pressure. The red curve represent the true data and the grey overlay lines represents the realisations.The vertical dashed line represents the historical (left of this line) and predcitin stages (right of this line).....	224
Figure 7.62: Water saturation reconstruction of the various methods. (a) Initial model water saturation, (b) Water saturation recovered by EnKF (d) Water saturation distribution recovered from EnKF-EM and (d) True model water saturation distribution reconstructed from kazsmarz method	225
Figure 7.63: 3D Water saturation reconstruction of the various methods. (a) Initial model water saturation, (b) Water saturation recovered by EnKF (d) Water saturation distribution recovered from EnKF-EM and (d) True model water saturation distribution reconstructed from kazsmarz method	225
Figure 7.64: permeability reconstruction from the various methods. (a) Initial permeability model, (b) permeability recovered by EnKF (c) permeability recovered from EnKF-EM and (d) True model permeability field.....	227
Figure 7.65: 3D permeability reconstruction from the various methods. (a) Initial permeability model, (b) permeability recovered by EnKF (c) permeability recovered from EnKF-EM and (d) True model permeability field.....	228
Figure 7.66: Comparison between the EnKF-EM and EnKF SSIM metric image quality assessment: (a) injection pressure profile, (b) water production rate profile and (c) oil production rate profile.....	228
Figure 7.67: Schematic showing the <i>SELE</i> algorithm	238
Figure 7.68: an initial model of realisations #21, #11, #31 and #67 generated with the <i>SGSIM</i> algorithm (Deutsch & Journel, 1998)	240
Figure 7.69: K-SVD error convergence when creating the overcomplete learned dictionary required in the ES-MDA loop of the permeability and porosity realisations shown in (A) and (B) respectively	241
Figure 7.70: Some initial permeability K-SVD basis	242

Figure 7.71(a): shows the bottom-hole pressure, gas –oil ratio and water cut for the six producer wells of the initial ensemble. The red curve represent the true data and the cyan overlay lines represents the realisations.The vertical dashed line represents the historical (left of this line) and predcitin stages (right of this line).....	245
Figure 7.71(b): shows the bottom-hole pressure, gas –oil ratio and water cut for the six producer wells of the ensemble recovered after ES-MDA. The red curve represent the true data and the cyan overlay lines represents the realisations.The vertical dashed line represents the historical (left of this line) and predcitin stages (right of this line)	247
Figure 7.71(c): shows the bottom-hole pressure, gas –oil ratio and water cut for the six producer wells of the ensemble recovered after an ES-MDA-Level set. The red curve represent the true data and the cyan overlay lines represents the realisations.The vertical dashed line represents the historical (left of this line) and predcitin stages (right of this line).....	249
Figure 7.71(d): shows the bottom-hole pressure, gas –oil ratio and water cut for the six producer wells of the ensemble recovered after SELE. The red curve represent the true data and the cyan overlay lines represents the realisations.The vertical dashed line represents the historical (left of this line) and predcitin stages (right of this line)	251
Figure 7.72(a): Permeability field of the five models shown row-wise (left-to-right). (First row) True permeability model, (second row) mean permeability of initial ensemble, (third row) mean permeability recovered with the ES-MDA algorithm, (fourth row) means Permeability recovered with the ES-MDA-Level set algorithm and (fifth row) mean permeability recovered with the SELE scheme	252
Figure 7.72(b): 3D Permeability field of the five models. (a) True permeability model, (b) mean permeability of initial ensemble, (c) Permeability recovered with the ES-MDA algorithm, (d) permeability recovered with the ES-MDA-level set scheme and (e) Permeability recovered with the SELE method	253
Figure 7.73: Some basis function from an over-complete dictionary created with the KSVD algorithm trained for the channelised SPE 10 synthetic reservoir model used in this work.....	255
Figure 7.74: Error convergence profile during the creation of the overcomplete dictionary	256
Figure 7.75(a): initial ensemble showing the match to oil production rate (column 1), match to water cut (column 2) and match to gas oil ratio (column 3). The red curve	

represent the true data and the cyan overlay lines represents the realisations.The vertical dashed line represents the historical (left of this line) and predcitin stages (right of this line).....	258
Figure 7.75(b): initial ensemble showing the match to bottom hole pressure of the injector wells. The red curve represent the true data and the cyan overlay lines represents the realisations.The vertical dashed line represents the historical (left of this line) and predcitin stages (right of this line)	259
Figure 7.76(a): ES-MDA ensemble showing the match to oil production rate (column 1), match to water cut (column 2) and match to gas oil ratio (column 3). The red curve represent the true data and the cyan overlay lines represents the realisations.The vertical dashed line represents the historical (left of this line) and predcitin stages (right of this line).....	261
Figure 7.76(b): ES-MDA ensemble showing the match to bottom hole pressure of the injector wells. The red curve represent the true data and the cyan overlay lines represents the realisations.The vertical dashed line represents the historical (left of this line) and predcitin stages (right of this line)	261
Figure 7.77(a): ES-MDA-Level set ensemble showing the match to oil production rate (column 1), match to water cut (column 2) and match to gas oil ratio (column 3). The red curve represent the true data and the cyan overlay lines represents the realisations.The vertical dashed line represents the historical (left of this line) and predcitin stages (right of this line)	263
Figure 7.77(b): ES-MDA-Level set ensemble showing the match to bottom hole pressure of the injector wells. The red curve represent the true data and the cyan overlay lines represents the realisations.The vertical dashed line represents the historical (left of this line) and predcitin stages (right of this line).....	263
Figure 7.78(a): SEL ensemble showing the match to oil production rate (column 1), match to water cut (column 2) and match to gas oil ratio (column 3). The red curve represent the true data and the cyan overlay lines represents the realisations.The vertical dashed line represents the historical (left of this line) and predcitin stages (right of this line).....	264
Figure 7.78(b): SEL ensemble showing the match to bottom hole pressure of the injector wells. The red curve represent the true data and the cyan overlay lines	

represents the realisations.The vertical dashed line represents the historical (left of this line) and predcitin stages (right of this line)	265
Figure 7.79: Permeability field of the five models shown row-wise (left-to-right). (First row) True permeability model, (second row) mean permeability of initial ensemble, (third row) mean permeability recovered with the ES-MDA algorithm, (fourth row) means Permeability recovered with the ES-MDA-Level set algorithm and (fifth row) mean permeability recovered with the SELE scheme	266
Figure 7.80: 3D Permeability field of the five models. (a) True permeability model, (b) mean permeability of initial ensemble, (c) Permeability recovered with the ES-MDA algorithm, (d) permeability recovered with the ES-MDA-level set scheme and (e) Permeability recovered with the SELE method	267
Figure A1: Schematic of an oil reservoir	277
Figure A2: Capillary pressure schematic as it relates to the oil reservoir	280
Figure A3: Schematic showing the porosity of the rock.....	281
Figure A4: One-dimensional grid system (Crichlow, 1977).	298
Figure A5: 2-dimensional grid system (Crichlow, 1977).....	298
Figure A6: 3-dimensional grid system (Crichlow, 1977).....	298
Figure A7: Discretization in the time domain (Crichlow, 1977)	299

List of Tables

Table 4.1: Differences between Traditional based History Matching and EnKF based History matching	101
Table 7.1: Computer specification for running the numerical experiments	135
Table 7.2: RMS function of the best three realisations after EnKF and EnKF-Level Set	150
Table 7.3: RMS function of best seven realisations after EnKF and EnKF-Level Set update	161
Table 7.4: SSIM values to reference permeability and porosity field for the two history matched models of the EnKF-Level Set scheme and standard EnKF.....	164
Table 7.5: Shape factor calculation using established methods	166
Table 7.6: RMS function of best three realisations after history matching	169
Table 7.7: Shape factor function of best three realisations after history matching update	170
Table 7.8: SSIM value of average fracture distribution reconstruction to the true model	171
Table 7.9: RMS function of best seven realisations after EnKF and ES-MDA.....	175
Table 7.10: SSIM values to reference permeability and porosity field for the two history matched models of the ES-MDA and standard EnKF.....	175
Table 7.11: RMS cost function comparison EnKF-FTM, EnKF-2 phase FTM, EnKF No-FTM and LM-2 phase FTM final history matched	204
Table 7.12: Comparison of the initial and Final FTM values after EnKF/LM update for the EnKF-FTM, EnKF-2 phase FTM, EnKF No-FTM and LM-2 phase FTM final history matched models.....	205
Table 7.13: Overall cost function comparison EnKF-FTM, EnKF-2 phase FTM, EnKF No-FTM and LM-2 phase FTM final history matched	207
Table 7.14: Reference Reservoir synthetic model properties	213
Table 7.15: RMS cost function evolution of Best 7 Realisations with and without EM data.	226
Table 7.16: Overall cost function comparison between EnKF-EM and EnKF.	229
Table 7.17: RMS function of best three realisations after ES-MDA, ES-MDA-Level set and SELE update.....	243

Table 7.18: <i>SSIM</i> values to true permeability field for the four history matched models of the ES-MDA-Level-set scheme standard ES-MDA and SELE method	253
Table 7.19: RMS function of best three realisations after ES-MDA, ES-MDA-Level set and SELE	257
Table 7.20: <i>SSIM</i> values to true permeability field for the three history matched models of the ES-MDA-Level-set scheme standard ES-MDA and SELE method	267

List of Abbreviations

Chapter 1	Chapter 2
N_e -Ensemble size	β -Kriging weight
KF -Kalman Filter	μ -mean
EnKF -Ensemble Kalman Filter	S_τ -filter score
ES -Ensemble Smoother	$\text{pat}(\mathbf{u} + \mathbf{h}_i)$ -pattern nodal value
ES-MDA -Ensemble Smoother with Multiple Data Assimilation	α_i -filter node offset
cdf -cummulative density function	$f_2^i(\alpha_i)$ -gradient filter
pdf - probability density function	$f_1^i(\alpha_i)$ -average filter
FTM -Fault Transmissibility Multipliers	$f_3^i(\alpha_i)$ -curvature filter
EM -Electromagnetic	$\text{prot}(\mathbf{h}_i)$ -prototype
	σ -standard deviation
	$F^{-1}(\mathbf{p})$ -quantile function of normal distribution curve
	$\Phi^{-1}(\mathbf{p})$ -quantile function of standard normal distribution curve
	$\text{erf}(x)$ -error function
	$\Phi(x)$ -cummulative distribution
	Ψ -probability density function
	$\gamma(\mathbf{h})$ -semi-variance
Chapter 3	Chapter 4
φ -effective porosity	$\mathcal{O}(\mathbf{m})$ -objective function
S -saturation	$\nabla_m \mathcal{O}(\mathbf{m})$ -gradient of objective function
\mathbf{K} -absolute permeability	\mathbf{T} -transpose
k_r -relative permeability	\mathbf{m} -model paramters
ρ -density	\mathbf{G} -forward simulator
μ -viscosity	\mathbf{d} -observed data
$\hat{\mathbf{g}}\nabla \mathbf{z}$ -acceleration due to gravity	$\mathbf{R}(G)$ -range of the matrix
\mathbf{Q} -source and sink term	$\dim \mathbf{R}(G)$ -rank of the matrix
p -pressure	\mathbf{C}_M -model covariance matrix

ℓ, γ -phase	m_{prior} -prior mean of model parameters
\mathbf{u}_γ -darcy velocity	ε -noise
	\mathbf{C}_D -data error covariance matrix
	\mathbf{H} -information matrix in KF and EnKF
	\mathbf{F}_K -Linear model operator at time step K
	ε_k^m -Error covariance of model noise
	$\mathbf{C}_{\Psi_k}^f$ -forecast of prior covariance matrix
	\mathbf{K}_k -Kalman gain at time step K
	\mathbf{y}^j -state vector
	$\tilde{\mathbf{C}}_{MD}^f$ -Cross covariance between model and predicted data
	$\tilde{\mathbf{C}}_{DD}^f$ -autocovariance between predicted data
	γ^i -damping coefficient during ES-MDA
	N_a -iteration time during ES-MDA
	\mathbf{d}_{uc} -perturbed observed data for ensemble member

Chapter 5

K_{sat} -effective bulk modulus
K_f -single fluid bulk modulus
K_d -dry frame bulk modulus
K_m -matrix bulk modulus
G_d -shear modulus of dry frame
V_p -pulling wave velocity
$E(x)$ -Electric field
$H(x)$ -magnetic field
$J(x)$ -electric source current
$M(x)$ -magnetic source current
$\sigma(x)$ -electric conductivity
$\epsilon(x)$ -dielectric permittivity

Chapter 6

$\phi(x)$ -level set function
τ -zero level set function
T_0 -sparsity level
\mathcal{X} -sparse weights
\mathbf{y} -signal
\mathbf{D} -over complete dictionary
Δ =index set
\mathbf{r} -residual

$\mu(x)$ -magnetic permeability

Chapter 7

K_m -matrix permeability

K_f -fracture permeability

σ_o -shape factor

L -equivalent length

$\mathcal{H}(\phi(x))$ -heaviside function

$f_{Noverall}$ -Narrow band function

\circ -Hadamard product

RMSE-Root mean square error

D_{sim}^j -simulated data from ensemble

member

EnKF-LS-Ensemble Kalman Filter with

Level set

SSIM-structural similarity index metric

ρ_o =Gaspari-cohn correlation matrix

Trans-Transmissibility

T_{ABS} -Absolute transmissibility

T_p -phase specific transmissibility

multiplier

ΔI -Impedance between 2 monitoring

points

OMP-orthogonal matching pursuit

Abstract

This thesis introduces novel ideas in subsurface reservoir model calibration known as *History Matching* in the reservoir engineering community. The target of history matching is to mimic historical pressure and production data from the producing wells with the output from the *reservoir simulator* for the sole purpose of reducing uncertainty from such models and improving confidence in production forecast. Ensemble based methods such as the **E**nsemble **K**alman **F**ilter (EnKF) and **E**nsemble **S**moothening with **M**ultiple **D**ata **A**ssimilation (ES-MDA) have been proposed for history matching in literature. EnKF/ES-MDA is a Monte Carlo ensemble nature filter where the representation of the covariance is located at the mean of the ensemble of the distribution instead of the uncertain true model. In EnKF/ES-MDA calculation of the gradients is not required, and the mean of the ensemble of the realisations provides the best estimates with the ensemble on its own estimating the probability density. However, because of the inherent assumptions of linearity and Gaussianity of petrophysical properties distribution, EnKF/ES-MDA does not provide an acceptable history-match and characterisation of uncertainty when tasked with calibrating reservoir models with channel like structures. One of the novel methods introduced in this thesis combines a successive parameter and shape reconstruction using level set functions (EnKF/ES-MDA-level set) where the spatial permeability fields' indicator functions are transformed into signed distances. These signed distances functions (better suited to the Gaussian requirement of EnKF/ES-MDA) are then updated during the EnKF/ES-MDA inversion. The method outperforms standard EnKF/ES-MDA in retaining geological realism of channels during and after history matching and also yielded lower Root-Mean-Square function (RMS) as compared to the standard EnKF/ES-MDA. To improve on the petrophysical reconstruction attained with the EnKF/ES-MDA-level set technique, a novel parametrisation incorporating an unsupervised machine learning method for the recovery of the permeability and porosity field is developed. The permeability and porosity fields are posed as a sparse field recovery problem and a novel *SELE* (**S**parsity-**E**nsemble optimization-**L**evel-set **E**nsemble optimisation) approach is proposed for the history matching. In *SELE* some realisations are learned using the **K**-means clustering **S**ingular **V**alue **DK-SVD) to generate an overcomplete *codebook* or dictionary. This dictionary is combined with **O**rthogonal **M**atching **P**ursuit (*OMP*) to ease the ill-posed nature of the production data inversion, converting our permeability/porosity field into a sparse domain. *SELE* enforces prior structural information on the model during the history matching and reduces the computational complexity of the Kalman gain matrix, leading to faster attainment of the minimum of the cost function value. From the results shown in the thesis; *SELE* outperforms conventional EnKF/ES-MDA in matching the historical production data, evident in the lower RMS value and a high geological realism/similarity to the true reservoir model .**

Declaration

Author: Clement Oku Etienam

I declare that no portion of the work referred to in the dissertation has been submitted in support of an application for another degree or qualification of this or any other university or another institute of learning.

Signature:

Date:

Intellectual Property Statement

- I. The author of this dissertation, Clement Oku Etienam (including any appendices and/or schedules to this dissertation) owns certain copyright or related rights in it (the 'Copyright') and he has given The University of Manchester certain rights to use such Copyright, including for administrative purposes.
- II. Copies of this dissertation, either in full or in extracts and whether in hard or electronic copy, may be made only in accordance with the Copyright, Designs and Patents Act 1988 (as amended) and regulations issued under it or, where appropriate, in accordance with licensing agreements which the University has entered into. This page must form part of any such copies made.
- III. The ownership of certain Copyright, patents, designs, trade marks and other intellectual property (the 'Intellectual Property') and any reproductions of copyright works in the dissertation, for example graphs and tables ('Reproductions'), which may be described in this dissertation, may not be owned by the author and may be owned by third parties. Such Intellectual Property and Reproductions cannot and must not be made available for use without the prior written permission of the owner(s) of the relevant Intellectual Property and/or Reproductions.
- IV. Further information on the conditions under which disclosure, publication and commercialisation of this dissertation, the Copyright and any Intellectual Property and/or Reproductions described in it may take place is available in the University IP Policy (see <http://documents.manchester.ac.uk/display.aspx?DocID=487>), in any relevant Dissertation restriction declarations deposited in the University Library, The University Library's regulations (see <http://www.manchester.ac.uk/library/aboutus/regulations>) and in The University's Guidance for the Presentation of Dissertations. (www.researchsupport.eps.manchester.ac.uk/learning_bytes/academic_writing).

Acknowledgements

Firstly, I would like to give gratitude to Jesus, the son of God, for the gift of life.

I also want to thank the Niger Delta Development Commission (NDDC) of the Federal Republic of Nigeria, for sponsoring my PhD programme so far and the University of Manchester for giving me an enabling environment to carry out my research.

To my mentors and friends, Dr Rossmary Villegas my main supervisor and my Co-supervisor Dr Masoud Babaei, many thanks for your support, teaching and help during my PhD programme. I want to thank Dr Rossmary for her patience and excellent technical knowledge of the field of inverse problems and to Dr Masoud for improving my writing skills and also helping me with the field of Petroleum Geostatistics.

I also want to thank my friend and advisor Dr Oliver Dorn for, his collaboration and academic support so far with regards to exciting discussions and guidance in the field of time-lapse 3D electromagnetic survey and machine learning.

My appreciation also goes to Professor Konstantinos Theodoropoulos and Dr Carlos Avendano for giving me the opportunity to pursue a PhD programme at the Department of Chemical Engineering and Analytical Science. I will be forever grateful to this two for all the moral support and opportunity presented to me.

I also want to thank my recent Post-doctoral supervisor, Professor Kody Law for his guidance and comments on the quality of the thesis, with regards to the applied mathematics aspect, during the writing up period.

I will not forget friends that I made along the way; Chinonso, Mijana, Yap, Yusuf, Dauda, Joy, Yobo, Reece, also; Igor , Matz and Katie (the postgraduate administrators at School of Chemical Engineering) and Malik. You all contributed in one way or the other, towards the success of this PhD research.

Finally, I would like to thank my sweet and loving parents, Eng. and Mrs Clement Oku Ayana Etienam for the gift of education and for nurturing me all these years from infancy.

Preface

The researcher developed novel methodologies during the thesis for solving the History Matching inverse problem. The report consists of 5 numerical experiments detailed in chapter seven, which include papers that have been submitted or yet to be submitted to several high impact journals and presentations at various conferences around the world. MATLAB codes are also available to encourage other researchers to reproduce results in this thesis and for the advancement of knowledge in the field of reservoir history matching.

The numerical experiments include;

Numerical experiment 1, found in section 7.2-Ensemble Kalman filter and Level sets for Integrated History Matching:

Papers-

- “Simultaneous parameter and shape reconstruction using a coupled Ensemble Kalman Filter- Level Set technique”. Villegas R, Etienam C, Babaei M and Dorn O. Submitted to *Inverse Problems Science and Engineering*, March 2018
- “Integrated Structural Reconstruction and History Matching Using Ensemble Filter and Low-Frequency Electromagnetic Data” Etienam C, Villegas R and Babaei M. Proceeding at the 78th 2016 EAGE Conference and Exhibition, 11-15 June, Vienna, Austria.
- “History matching of Naturally Fractured Reservoirs using a coupled Level-set- Ensemble Kalman Filtering approach”. Etienam C, Villegas R and Dorn O. To be submitted to *Journal of petroleum technology*, November 2018.
- “CO2 Sequestration Using Ensemble Kalman Filter and Considering Sustainability Approach”. Villegas R., Etienam C., Rahma., F and SPE-190803-MS Proceeding at the 2018 SPE EUROPEC featured at the 2018 EAGE Conference, 11-14 June, Copenhagen, Denmark.

Conference Presentation-

- 78th EAGE Conference and Exhibition, 2016.11-15 June, Vienna, Austria.

- SPE EUROPEC featured at 2018, 80th EAGE Conference, 11-14 June, Copenhagen, Denmark.

Numerical experiment 2, found in section 7.3-Comparison of Ensemble based Methods Integrated with imaging and regularisation techniques:

Papers-

- “A Comparative study between Ensemble methods, for history matching and structural reconstruction of hydrocarbon reservoirs”. , Etienam C, Villegas R, Babaei M and Dorn o. To be submitted to *Journal of petroleum technology*, November 2018.
- “History Matching of Reservoirs Coupling Covariance Localization with a modified ES-MDA Level Set Technique”. Etienam C, Villegas R, Babaei M and Dorn O. To be submitted to *Journal of petroleum technology*, November 2018.

Numerical experiment 3, found in section 7.4-Improved History Matching using 4D Seismic results:

Papers-

- “History Matching of Reservoirs by updating fault properties using 4D seismic results and Ensemble Kalman filter”. Etienam C, Mahmood I and Villegas R. SPE-185780-MS Proceeding at the 2017 SPE EUROPEC featured at the 2017 EAGE Conference, 11-15 June, Paris, France.

Conference Presentation

- 2017 SPE EUROPEC featured at the 2017 EAGE Conference, 11-15 June, Paris, France.

Numerical experiment 4, found in section 7.5- Waterfront characterisation in History matching using low-frequency EM data:

Conference Presentation

- Society of Applied Mathematics (SIAM) Conference, issues in the Geosciences at Erlangen (September 2017), Erlangen, Germany

- “A level set ensemble Kalman filter method for history matching of production data incorporating electromagnetics”. Dorn O, Etienam C, Villegas R and Babaei M. *Society of Industrial and Applied Mathematics*, September 2018.

Numerical experiment 5, Found in section 7.6-Combining machine learning techniques with a History matching-Level set approach:

Papers-

- “Sparse orthogonal matching pursuit with a modified ES-MDA-scheme for History matching of hydrocarbon reservoirs”. Etienam C, Villegas R and Dorn O. *ECMI*, November 2018.

Conference Presentations

- Institute of Pure and Applied Mathematics (IPAM) Workshop III: Data Assimilation, Uncertainty Reduction, and Optimization for Subsurface Flow, Los-Angeles, USA. May 2017
- 20th European Conference on Mathematics for Industry (ECMI) 18-22 June 2018, Budapest, Hungary

Problems and Objectives:

Facies History matching is an active area of research. Several researchers have developed ideas in this area of study, but so far there is no consensus as to what the “best approach” to take for this optimisation problem. The researcher puts forward several novel approaches for the history matching of reservoirs.

The objectives are to;

- Postulate novel ideas to this optimisation problem. (History Matching)
- Calibrate the reservoir model using multi-physics and an extra source of data such as 4D seismic and Electromagnetic data to alleviate model ill-posedness.
- Make the optimisation solution easier and much more robust to any reservoir geometry.
- Thoroughly compare the EnKF to the ES-MDA for data assimilation efficiency for synthetic test cases.
- Solve the history matching problem of non-Gaussian reservoirs by parametrisation techniques such as the Level-set and Discrete Cosine Transform (DCT).
- Apply machine learning techniques (unsupervised learning algorithms) to history match non-Gaussian parameter distribution.

The first method in numerical experiment 2, found in section 7.3 utilises the recently developed Ensemble Smoother with Multiple Data Assimilations as the optimisation algorithm coupled with covariance localisation and the level set technique. This method is optimum in the case of channelised or turbidite reservoirs, where the aim is in retaining the underlying geology of the channels during history matching. Geological realism is maintained in this approach as well. The method in numerical experiment 5, found in section 7.6 incorporates machine learning in the minimisation scheme. This method is optimal in enforcing prior structural information by a pre-generated over-complete dictionary, a reduction in computational complexity during the Kalman gain inversion and faster arrival at the minimum of the cost function.

Overview of Numerical Experiments explained in Chapter Seven

Numerical experiment 1, found in section 7.2 introduces a methodology that couples the Level set method with the Ensemble Kalman Filter (EnKF) for the updating and representation of geological lithofacies in the reservoir with stratigraphic compartmentalisation (Jolley, et al., 2007). In the numerical experiment, a simultaneous parameter and shape reconstruction was implemented where a signed distance function re-parametrised the degraded parameter update by the classical EnKF (Villegas et al., 2018). The methodology is introduced. The initial ensemble of permeability and porosity are produced using the sequential Gaussian simulation for the second test case and *FILTERSIM* (Wu, et al., 2006) for the first test case. In the paper, a simultaneous parameter and facies reconstruction are successful.

We also apply the same methodology to Naturally Fractured Reservoirs (NFR). Naturally fractured reservoirs (NFR) having unknown fracture distributions, the characteristics of fracture distributions having a higher permeability value to the surrounding matrix are crucial for determining their production dynamics. The classical EnKF method is not adequate because the pixel-based rock property fields in the NFR are usually highly non-Gaussian which is a limitation of the EnKF with regards its Gaussian enforcement.

In this work, a misfit algorithm that combines a level set re-parameterisation scheme and the EnKF for estimating the fracture distributions of the reference three-dimensional reservoir model is proposed. Our method combines simultaneous parameter update and the level-set update using the EnKF. A narrowband function which is a matrix of ones and zero, indicating the proximity of a fracture to a matrix is included in the level set parameterisation step. The level-set value of each pixel is updated by the Kalman gain matrix and a residual vector which is the difference between the observed historical data and simulated data from the multiphase flow simulator at each data assimilation time-step.

The uncertainty in the inverse problem includes vertical permeability, effective porosity and shape factor, which is a fracture-matrix transfer function. The initial porosity and permeability field is bi-modal and is modelled using Multiple Point statistics (MPS). Also, the initial ensemble of shape factors values is modelled within

the confines of ranges set by established literature. Three-dimensional examples of water flooding in fractured reservoirs were modelled to show the proposed method. It is shown that the method is capable of capturing the main features of the fracture distributions in the reference fields as indicated by its higher structural similarity index metric (*SSIM*) of the true model porosity/permeability field. The history matches of production data also improve significantly after updating the initial model as indicated by its root-mean-square (RMS) function

MATLAB, Fortran 90 and Python based codes were developed. The results produced in the results were generated using MATLAB. The strain of computational time was alleviated as a parallel programming architecture was employed for the simulation and forwarding of each member of the ensemble. This method is suitable for reservoirs having more than one rock type with contrasting properties and fractures.

Numerical experiment 2, found in section 7.3, compares two history matching methods namely the EnKF and the Ensemble Smoother Multiple Data Assimilation (ES-MDA). The Ensemble-based methods have gained popularity as reservoir history-matching techniques. The advantages and gains typically attributed to these methods include the generation of several alternative models conditioned to data, the possibility of adjusting a large number of model parameters at a reasonable computational cost and the ease of implementation. It is clear to adapt these methods to accommodate different types of model variables and data.

Moreover, they are easily linked with commercial reservoir simulators and do not require the computation of the gradients or adjoints. Among these methods, the EnKF is by far the most investigated and attractive. Ensemble Smoothers are better suited to practical history-matching applications because they do not require updating dynamical (state) variables and consequently avoid the frequent simulation restarts required by EnKF. This numerical experiment presents the results of an investigation on the performance of a newly developed type of ES, namely, Ensemble smoother with Multiple Data Assimilation (ES-MDA), to history match production data as compared to the EnKF. The numerical experiment discusses the quality of the data matches and the permeability and porosity reconstruction.

The initial ensemble of permeability and porosity are produced using the sequential Gaussian simulation. In the paper, an $84 \times 27 \times 4$ numerical grid cell is presented. A MATLAB-based code was developed which was ran in parallel to ease the computational time in running each member of the ensemble and for the data assimilation technique. The overall results show the ES-MDA outperforming the EnKF regarding the quality of permeability and porosity reconstruction and also the computational time required for an acceptable convergence.

Also, a methodology that couples the distance based covariance localisation scheme (Houtemaker, January, 2001) with a previous Level set method in numerical experiment 1 is introduced. The assimilation scheme is the ES-MDA, and it is carried out for the updating and representation of geological lithofacies in the reservoir with stratigraphic compartmentalisation (Jolley, et al., 2007).

In that work, a simultaneous parameter and shape reconstruction was implemented, where a signed distance function re-parametrised the degraded parameter update by the classical ES-MDA. The methodology is introduced. Covariance localisation means localising the effect of an observation to the state variables that are ‘closer’ to the observations. The various localisation methods proposed in the literature have the common goal of removing the spurious terms in the cross-covariance matrix; this matrix is in turn used to update the state vectors during the ES-MDA update process. The explained procedure is done by conditioning the Kalman Gain through a localising function.

The motivation of covariance localisation is to achieve a similar level of ES-MDA performance if a larger ensemble size would have been used. However, it requires enormous computational resources to perform history matching if the ensemble size is large. The initial ensemble of permeability and porosity are produced using the MPS algorithm *FILTERSIM* (Wu, et al., 2006). In the numerical experiment, a simultaneous parameter and facies reconstruction are successfully using a developed MATLAB-based code. The strain of Computational time was alleviated as a parallel programming architecture was employed for the simulation. This method is suitable for reservoirs having more than one rock type with contrasting properties.

Numerical experiment 3, found in section 7.4 focuses on the improvement of an

integrated methodology (Villegas, et al., 2009), for the automatic history matching of compartmentalised reservoirs using 4D seismic results, stochastic initialisation and the Ensemble Kalman Filter method. The comparison of two different history matching techniques using the EnKF to update the Fault Transmissibility Multipliers (FTM) initially estimated with and without considering the 4D seismic results was demonstrated. In this numerical experiment, the parameters updated during the history matching are two-phase fault transmissibility multipliers (FTM), absolute permeability and effective porosity of a synthetic realistic 3D reservoir. The true impedance map and the changes in reservoir pressure and saturation were previously computed from 4D seismic results. The systematic estimation of two-phase fault transmissibility multipliers is based on the integration of the collected 4D seismic results and an established method validated in our previous work based on a deterministic model, using the gradient-based History Matching, Levenberg Marquardt method (LM). Geostatistical techniques were used to generate the initial geological models. The stochastic method used is the Sequential Gaussian Simulation (SGS) technique to generate 100 initial models. During history matching using the EnKF, the saturation distributions are computed from the forward modelling of a two-phase system (oil-water). The impedance maps are then estimated using the Gassmann equation and compared with the true impedance map as part of the History Matching process. To validate the results, the cost function consisting of two components is calculated, the first is the structural similarity index of the two reconstructed impedance images to the real impedance image and the second is the RMS cost function value, ℓ_2 – norm of the difference between the simulated pressure-production data and true data. The EnKF history matching using the two-phase FTM values considering 4D seismic results produced lower cost function values compared with the model using the initial FTM multiplier without considering 4D seismic results. The EnKF history matching algorithm using 4D seismic presented in this work produced results closer to the true reservoir impedance map compared to our previous 4D gradient based history matching method.

Numerical experiment 4, found in section 7.5 presents an extension of the methodology introduced in numerical experiment 1, where the novel history matching scheme is coupled with low-frequency EM results using Maxwell's equations (Dorn, et

al., 2007). The novelty is in coupling the level-set enhanced EnKF algorithm from numerical experiment 1 with the iterative nonlinear generalised Algebraic Reconstruction Technique or a non-linear Kaczmarz-type approach for the reconstruction of the water saturation distribution of the 3D oil reservoir. The main focus was to solve the conductivity profile from the Maxwell equation using inverse problem and geophysical imaging techniques to assimilate the water saturation distribution into our history matching process. The saturation distribution is inferred from low frequency cross-borehole electromagnetic induction tomography (EMIT) whereby the anisotropic or isotropic conductivity distribution of the earth is reconstructed from surface-to -borehole electromagnetic data. The inverse problem is solved by a back-propagation strategy (based on adjoint fields) and conductivity levels inferred from such inversion. This conductivity levels are converted to saturation distribution using the well-known Archie equation and then assimilated in our EnKF-History matching module and compare with one void of water saturation data assimilation. Conclusively assimilation of EM water saturation data during the EnKF inversion scheme yields a lower final RMS (Root-Mean-Square) function value to one void of EM water saturation assimilation, also EM water saturation assimilation yields a reduced number of data assimilation time steps required for an acceptable convergence.

In numerical experiment 5, found in section 7.6 introduces a novel shape reconstruction technique called '**SELE***' which denotes Sparsity-Ensemble optimization-Level-set-Ensemble optimisation implementing a coupling of a Level-set-Ensemble Smoother Multiple Data Assimilation (ES-MDA) with compressed sensing (CS) is proposed (Etienam et al., 2018). Owing to the ill-determined nature of history matching, several realisations may match quantitatively to the true model but vary qualitatively as permeability replicates. '**SELE***' solves this ill-posed inverse problem by using a sparsity promoting ES-MDA approach. An initial over-complete learned dictionary is created using an unsupervised learning algorithm called *K-SVD*. Further parametrisation to avoid a huge burden on complexity is achieved using the discrete cosine transform (*DCT*) on the initial realisations first, which is then after learned with the *K-SVD*. This *K-SVD* is combined with a greedy orthogonal, matching pursuit algorithm (*OMP*) for the parametrisation of the petrophysical properties (permeability/ or porosity fields). During the history matching step, the researcher generates the

ensemble state which consists of these sparse coefficients coupled with the level set representation of these properties. The analysed sparse coefficients are then mapped back to spatial fields using this K-SVD dictionary. The researcher shows the efficiency of our algorithm with numerical examples. The CS algorithm enhances the reconstruction of channelised geological structures by transforming the ES-MDA assimilation stage to a sparse field which represents the diverse geological scenarios in play. The researcher shows numerical examples and quantifies our '**SELE***' shape reconstruction by using a structural similarity index metric (*SSIM*). The proposed method shows rapid convergence to the true model and higher *SSIM* index to the true model permeability distribution.

.

Chapter 1 – Introduction & Literature review

This PhD thesis presents an integrated History Matching approach combining the ensemble methods such as Ensemble Kalman Filter (EnKF) and Ensemble Smoother Multiple Data Assimilation (ES-MDA) with parametrisation techniques such as the Level-set method. The initial ensembles of static properties are constructed using Geostatistics techniques. Also, machine learning techniques are infused to infer information about the pattern distribution in petrophysical static properties. Multi-physics for reservoir model calibration is achieved by assimilating extra source of data such as 4D seismic interpretation and Low-frequency electromagnetic (EM) surveys.

In the field of petroleum engineering, the primary task of history matching is improving the knowledge of parameters located in the reservoir that are not well-known such as the permeability and porosity. This is done in order to reduce the data misfit between simulated (data from the output of our reservoir simulator) and observed historical data (production, seismic and EM data)(Aanonsen et al.,2009). Additionally, the knowledge of saturation distribution and oil in place helps to reduce the uncertainty of production dynamics.

In most cases, geological reservoir models are developed using time inverted seismic which refers to data originating from seismic surveys and geological data which refer to data that pertains to the style of geological depositions. Additionally, stochastic modelling techniques are applied which are based on geostatistics and well logs data (Deutsch & Journel, 1995).

These models provide an initial estimate of the reservoirs with good accuracy at the wells but tend to decrease in accuracy in regions far away from the wells. In numerical reservoir modelling, different kind of sources of data is integrated into the reservoir model, in particular, reservoir engineering data such as PVT, well-testing, production data. Dynamic reservoir characterisation hence can be described as the process of integrating and incorporating different data into the reservoir using the fluid flow equations (Fahimuddin, 2010).

Reservoir simulation is a useful tool for the decision-making process involved in the development and management of petroleum reservoir exploitation projects. A reservoir simulation model combines fluid and rock properties with a mathematical

formulation to describe the fluid flow in the porous media. This model is subsequently used to predict the performance of the reservoir model under various operating conditions. However, to improve the predictive capability of a reservoir model, it is necessary to incorporate in this model relevant information available about the field. The process of incorporating dynamic data in reservoir models is known in the petroleum literature as history matching. (Aanonsen et al.,2009).

Reservoir history matching is the process of constraining the reservoir model to mimic actual historical dynamic production data of the reservoir to predict its future production behaviour and reduce uncertainty about the description of the reservoirs (Chang et al.,2010). History matching is an ill-posed problem because the amount of independent data available is much less than the number of variables. Hence, there exist an infinite number of combinations of the unknown reservoir properties that results in reservoir models which can match the observations. Besides that, the information accessible about the reservoir is always inaccurate and may be inconsistent. As a result, reservoir models are constructed with uncertain parameters; consequently, their predictions are also uncertain. (Aanonsen et al.,2009)

Over the last decade, increased importance has been attributed to the quantification of uncertainty in reservoir model performance predictions and reservoir model description to manage risk. Because of this obsession in the characterisation of uncertainty, it is now common to generate multiple history-matched models. However, generating multiple history-matched models may not necessarily lead to a correct assessment of uncertainty. In reality, uncertainty has no scientific meaning beyond the realm of statistics and probability. Bayesian statistics provides a straightforward theory for dealing with uncertainty.

In the application of interest in this dissertation, Bayes' theorem allows one to write down the posterior probability density function (pdf) for reservoir model parameters conditional to field measurements such as production, electromagnetic and seismic data. Then, the optimisation problem of characterising the model uncertainty in reservoir model parameters is tantamount to the problem of sampling this posterior pdf. If a set of realisations of the vector of reservoir model parameters represents a set of samples from the posterior pdf, then a correct assessment of the uncertainty in

specific outcomes of reservoir performance predictions can be generated by predicting with each model and then construct statistics for the set of outcomes. For example, one can estimate the pdf for a well's predicted oil rate at each time from a histogram of the predictions set. Markov chain Monte Carlo (MCMC) provides a theoretically attractive technique for sampling the posterior pdf for model parameters.

It is established that a properly designed MCMC method samples this pdf correctly in the limit as the number of states in the chain goes to infinity (Hastings 1970, Tierney 1994). For high-dimensional problems, MCMC typically requires a large number of iterations to provide a reasonable sampling of the desired pdf. When utilising MCMC to compute the posterior pdf of reservoir model parameters conditional to historical observed production data, computation of the probability of accepting the transition from the current state to the proposed state requires a run of the reservoir model simulator to evaluate the likelihood part associated with the posterior pdf. This requirement makes the direct application of MCMC to realistic reservoir problems computationally prohibitively.

The randomised maximum likelihood (RML) (Kitanidis 1995, Oliver et al., 1996, Reynolds et al., 1999) is a method designed for sampling a posterior pdf of a vector of model parameters conditional to a set of production history measurements. Although RML can be proved to sample correctly only if the predicted data are linearly related to the model parameters vectors (Reynolds et al., 1999) RML generates samples from different modes of the distribution so that it can approximate a non-Gaussian posterior pdf.

The application of RML to generate N_e realisations requires the minimisation of N_e objective functions, which, in general, can only be done efficiently with a gradient-based optimisation algorithm, e.g., a quasi-Newton method (Zhang & Reynolds, 2002, Gao & Reynolds, 2006). However, the efficient calculation of the gradients needed in a quasi-Newton method requires the implementation of the adjoint method (Wu et al., 1999, Li et al., 2003), and, unfortunately, the adjoint code is not commonly accessible in commercial reservoir model simulators.

Recently, the Ensemble Kalman Filter (EnKF) (Evensen 1994, Burgers et al., 1998) has emerged as an attractive option for reservoir history-matching problems because it is

easy to implement and computationally efficient. Since its introduction by Evensen (1994), the number of publications about EnKF became quite extensive. EnKF is a stochastic Monte Carlo method (Haibin & Zhang 2015, Agbalaka & Oliver 2008). EnKF has been applied in diverse research fields, including oceanography (Bertino et al., 2003, Keppenne et al., 2003), atmospheric modelling (Whitaker 2002 Houtemaker & Mitchell 2001) numerical weather prediction (Houtekamer & Mitchell , 2001) , the area of hydrology (Chen & Zhang 2006, Stordal & Oliver 2011) and petroleum reservoir inverse problems(history matching) (Aanonsen, et al., 2009). Evensen (2007) introduces a chronological set of applications of EnKF. The pioneer application for petroleum history matching problems was presented by Lorentzen et al. (2001), where EnKF was applied to two-phase flow in a drilled well to improve future predictions of the pressure behaviour from such wells.

The pioneer reservoir utilisation of EnKF was presented by Naevdal et al.(2003), where EnKF was utilised to tune permeability fields for drilled well reservoir models. Sequel to these pioneering applications, the frequency of adaptability of EnKF as a method for history-matching increased significantly. Some recent field adaptability of EnKF for history matching can be found in (Bianco et al. 2007, Evensen et al. 2007, Emerick & Reynolds 2011, Skjervheim et al. 2011). Two recent review journal papers (Aanonsen et al., 2009, Oliver & Chen 2010) summarise the main improvement and applications of the EnKF in reservoir problems from 2001 to 2010. The sequential data assimilation nature of EnKF dictates the modification of the traditional history-matching problem from a parameter-estimation optimisation problem to a parameter-state-optimisation problem (Emerick & Reynolds, 2013).

Specifically, when applying EnKF for history matching, it is compulsory to update a combined parameter-state vector, which includes the reservoir field model parameters (uncertain reservoir rock properties) and the reservoir field primary variables of the reservoir simulator (typically grid block pressure, fluid saturations in a standard black-oil reservoir simulator) (Emerick & Reynolds 2013). The reason for updating these primary variables, which represent the state of the dynamical system, is to avoid initialising the reservoir simulations from time zero (initial reservoir condition) after every sequential data assimilation stage. The assumption holds that the updated primary variables are assumed statistically consistent with those obtained by running

the reservoir simulator with the tuned set of reservoir model parameters from time zero. Unfortunately, this consistency can be proved only for problems with Gaussian statistics, linear relation between reservoir model and predicted (simulated) data and negligible model error (Thulin et al., 2011). Unfortunately, the reservoir simulator equations are highly nonlinear. At such, the theory of consistency is invalid, which may degrade the data assimilation performance (Thulin et al.. 2011)

In practice, after assimilating at time t , the reservoir model simulations may be restarted at time t_n with wrong pressure and saturation values, thereby violating the historical material balance of the field. In the extreme case, the analysis step in the EnKF may result in non-physical values for these variables, e.g., negative pressures or saturations larger than one. Wen & Chen (2006) introduced the confirming step, which consists of rerunning the simulator starting from the previous data assimilation time-step with the updated set of model parameters obtained at the current data assimilation time step to obtain physically plausible reservoir state variables. However, Zafari & Reynolds (2007) showed that this procedure is inconsistent with the linear case and should not be used.

Some iterative procedures have been proposed to overcome inconsistency because of the nonlinearity (Reynolds et al. 2006, Li & Reynolds 2009) Most of these methods can be viewed as ensemble approximations of the RML method (Aanonsen, et al., 2009). Reynolds et al. (2006) and Li & Reynolds (2009) presented two iterative forms of EnKF based on adjoint-gradients. The ensembles are used to approximate the Hessian in a Gauss-Newton type update equation. Because each ensemble member is updated based on a different gradient, these two methods are expected to be able to sample multimodal distributions, as the standard RML does (Emerick & Reynolds 2013).

The main difficulty encountered in these two iterative methods is the dependency on the adjoint implementation. Gu & Oliver (2007) introduced an iterative method called ensemble randomised maximum likelihood (EnRML), which uses the ensemble to estimate an average sensitivity matrix. With this procedure, Gu & Oliver (2007) avoided the need of adjoint-based gradients. However, because all models are updated using the same average sensitivity, EnRML is not expected to sample multiple modes of a posterior distribution (Emerick & Reynolds 2013). EnKF is also not expected

to sample multimodal distributions correctly because all models are updated based on the same Kalman gain. Moreover, because EnRML uses a rough approximation of the sensitivity matrix, the search direction is not guaranteed to be "downhill." If EnRML encounters an "uphill" search direction, the iterative procedure fails to improve the match to the historical production data.

The computational cost of these iterative procedures is typically much expensive than that of the standard EnKF. Perhaps the most straightforward procedure to overcome problems with inconsistency between updated reservoir model parameters and primary reservoir variables is to rerun the reservoir simulation using the latest ensemble of model parameters from time zero after each data assimilation. This procedure ensures consistency but requires a considerable increase in computational time. Wang et al. (2010) refer to this procedure as half-iteration EnKF (HI-EnKF).

To improve computational efficiency, Wang et al. (2010) proposed rerunning the ensemble from time zero after a data assimilation time-step only if the average relative change in the ensemble mean model is more significant than a threshold value. Using the PUNQ-S3 case (Floris et al. 2001), Wang et al. (2010) concluded that HI-EnKF and EnRML resulted in similar results. However, HI-EnKF requires much less computational time than EnRML. One crucial advantage of EnKF is the fact that it does not require adjoint implementation for computing gradients. This makes EnKF easy to adapt to several types of reservoir model parameters, several types of data and commercial reservoir simulators.

Oliver & Chen (2010) pointed out that there is a tendency to increase the types of reservoir model parameters estimated with EnKF. Gridblock porosities and permeabilities are the typical model parameters considered. However, other types of parameters including net-to-gross ratio, fluid contacts, fault transmissibilities (Etienam, et al., 2017), endpoints of relative-permeability curves facies, have been considered as model parameters using EnKF. Although EnKF has been successfully applied to history match field cases, EnKF often fails to provide a reasonable characterisation of uncertainty.

To establish that the ensemble generated by assimilation of data using EnKF represents a correct sampling of the posterior pdf for the state vector, requires one to

assume a linear-Gaussian case, which is a Gaussian prior model for the state vector, a linear relationship between predicted data and the state vector, Gaussian measurement errors, which are uncorrelated in time, and that the dynamical system (forward model) represents a first-order Markov process. (Emerick & Reynolds, 2013)

Even when the afore-mentioned assumptions hold, it is also required to let the ensemble size approach infinity to show that EnKF samples correctly because covariances are estimated from the ensemble of state vectors. Mandel et al. (2011) present a rigorous proof that, under the above conditions, EnKF converges to the standard Kalman filter (KF) when the size of the ensemble goes to infinity. Mandel et al. (2011) also point out that EnKF introduces dependence in the ensemble because the covariances are estimated based on all members of the ensemble. As a result, the final ensemble members do not represent unique and independent samples of the posterior pdf.

Houtekamer and Mitchell (2001) pointed out that because EnKF uses the same Kalman gain to update all members of the ensemble, EnKF introduces an inbreeding during the analysis. Houtekamer and Mitchell (2001) proposed a variant of EnKF using two ensembles, where the statistics computed in one ensemble is used to update the other. van Leeuwen (1999), gave a theoretical justification for the inbreeding effect. However, van Leeuwen (1999) pointed out that the primary concern in the EnKF is related to the use of small ensemble sizes. Small ensembles are necessary for computational efficiency, but they introduce sampling errors and reduce the degrees of freedom to assimilate data (Aanonsen, et al., 2009). As a result, the ensemble variance obtained once data assimilation with EnKF is completed tends to be significantly underestimated (Anderson, 2007).

The underestimation of posterior variances is an essential limitation of EnKF. Firstly, the low variance in the ensemble can make it difficult to assimilate new independent data. Secondly, but equally or more critical, underestimation of posterior variances conclusively indicates an underestimation of uncertainty in the reservoir model parameters after data assimilation. Besides the plausible underestimation of model uncertainty in the reservoir model parameters, EnKF also seems to fail to provide reasonable uncertainty quantification in the reservoir performance predictions.

Using the PUNQ-S3 case, Lorentzen et al. (2005) found that running EnKF with different initial ensembles resulted in cumulative distributions of forecasted field oil production which are not mutually consistent, i.e., the estimated distributions for each ensemble estimated a high degree of variation to represent approximations of the same cumulative density function (cdf). Thulin et al. (2011) also concluded that with only a single EnKF run, there is no control over the Monte Carlo error in the estimate of the conditional pdf. Thulin et al. (2011) proposed repeating the assimilation of data using the EnKF multiple times with different prior ensembles and using the average cdf calculated from all EnKF runs as the final probability distribution of predictions.

Comparing EnKF with RML, Tavakoli & Reynolds (2010) concluded that EnKF results in unreasonably high values of the objective function after data assimilation. A high value of the objective function is typically associated with poor data matches. However and perhaps more importantly, high values of the objective function mean that the realisations of vectors of model parameters are of extremely low probability, i.e., give a low value of the posterior pdf compared to those obtained with gradient-based optimisation algorithms

Perhaps more importantly, when applied to field cases, EnKF appears to perform reasonably well and has typically given better results than a model based on a manual history matching (Bianco et al., 2007, Evensen et al., 2007, Emerick & Reynolds 2011). Also, EnKF does not require adjoint implementation for computing gradients, which makes the method easy to adapt to several types of model parameters and commercial reservoir model simulators.

Another attractive feature of the EnKF is the sequential data assimilation, which makes the method well suited for closed-loop reservoir management problems (Jansen et al., 2005, Jansen et al., 2009, Chen et al., 2010). Even though there has been intense interest and investigation of EnKF for reservoir history-matching problems in the last decade, because of the inherent assumptions of linearity and Gaussianity and the use of limited ensemble sizes, some problems remain with the method, including the following: Excessive and incorrect reduction in the ensemble variance after data assimilation, reduced number of degrees of freedom to history-match data, nonphysical updates in model parameters and state variables, inconsistency between

updated model parameters and the primary reservoir simulator variables, relatively poor data matches when compared to gradient-based history matching methods, difficulty in preserving more complex geological features, e.g., channels and facies and finally the inability to correctly characterise uncertainty in reservoir model parameters moreover, production predictions.

The small size of the ensemble used in practice for computing the covariance's in the EnKF leads to sampling errors that produce spurious long-distance correlations with the elements of the state vector and predicted data, whereas, in reality, pixels and data at grid blocks far apart should in principle be uncorrelated. Spurious correlations can result in a non-negligible change in a component of the EnKF state vector due to the assimilation of data at a location far away from the spatial location of this component, whereas if covariances were accurately represented, no change in the component would occur. When this incorrect change occurs during the EnKF analysis step, the variance of the state component is also incorrectly reduced.

This loss of the estimated variance can make it difficult to modify the state component properly by assimilating later time data (Aanonsen, et al., 2009). Representing covariances with finite samples also limits the degrees of freedom available to update the state vector. In particular, the subvector corresponding to model parameters in any realisation of the EnKF analysed state vector at any data assimilation time-step is a linear combination of the corresponding initial N_e vectors of model parameters (Aanonsen, et al., 2009). Thus, there are at most N_e coefficients that can be adjusted to make any particular realisation consistent with all observed data. More generally, any updated vector of model parameters lies in the subspace spanned by the members of the prior ensemble. Also, Lorenc (2003) showed that if we assimilate a perfect observation, i.e., noise free with the variances of measurement errors set to zero in the update equations, we lose at least one degree of freedom.

Even though we never assimilate perfect data, it is reasonable to expect that, after several data assimilation time-steps, we will experience a reduction in the available degrees of freedom left to assimilate subsequent data. This problem is critical in situations in which it is necessary to assimilate a large number of independent data, e.g., reservoirs with several wells (Aanonsen, et al., 2009) or time-lapse seismic data

(Etienam, et al., 2017). Although increasing the size of the ensemble reduces problems caused by errors due to sampling and limited degrees of freedom, computational efficiency requires the use of a small size of the ensemble. A standard procedure for mitigating the effect of spurious correlations due to sampling errors is to replace the estimated prior (forecast) covariance at each data assimilation time step by the Schur (element-wise) product of a correlation matrix, having compact support, and the forecast covariance matrix. This technique is known as covariance localisation.

The first utilisation of localisation was presented in Houtekamer & Mitchell (2001) where a distance cut-off was utilised to the Kalman gain in a way that only model parameters within a critical distance located to the observation were updated. According to the results in Houtekamer & Mitchell (2001), the optimal radius of the cut-off increased in positive correlation with the ensemble size increase. The use of the Schur product for the covariance localisation method was introduced by Houtekamer & Mitchell (2001). In this work; the authors pointed out that localisation utilising the Schur product resulted in relatively smoother models compared to those obtained using the distance cut-off or using no localisation at all.

Anderson (2007) also presented a non-distance based localisation procedure, called a hierarchical ensemble filter. In the hierarchical ensemble filter, a small number of dissimilar ensembles are used to compute confidence factors, which are utilised to tune the regression coefficients (entries of the Kalman gain matrices). Zhang & Oliver (2010) modified the method proposed by Anderson (2007), in a way that as opposed to using multiple ensembles, we resample a single ensemble with replacement to compute bootstrapped ensembles (Emerick & Reynolds, 2013).

Another procedure that has appeared in the literature to compensate for the underestimation of posterior variances in the EnKF is known as covariance inflation (Anderson, 1999). Covariance inflation is often used in the area of oceanography, and numerical weather prediction systems (Anderson, 1999) but has rarely been applied in reservoir model calibration problems (history matching). Covariance inflation utilises an inflation factor to enlarge the covariance located in the forecast ensemble without altering the mean. The inflation factor is a tuning variable, and the “optimised” inflation factor is problem dependent. Evensen (2009) proposed an adaptive

covariance inflation procedure which computes the inflation factor based on the ensemble size and the measurements.

For facies history matching adequate knowledge of the boundaries separating the different facies is critical in making good reservoir assessment and future oil production forecasting. In general, there are two accepted methods for reservoir facies history matching and assimilating the well historical production data: stochastic methods and gradient-based methods (Chang, et al., 2010). (Jafarpour & McLaughlin, 2007)

History matching of Geological facies (non-Gaussian features) presents a challenging area in the reservoir modelling workflow also. In the area of history matching the level-set method has been applied in a gradient-based setting (Villegas, et al., 2005) (Chang, et al., 2010), where the evolving level-set functions indicate the distribution of facies and the boundaries between each facies are propagated to minimise a designated cost function. The adjoint method is then used to calculate the gradients in each optimisation step. As such, the level-set method is primarily targeting the tracing of lithofacies interfaces. Permeability estimation applying the level-set methodology has been implemented in various research studies (Villegas et al., 2005, Moreno & Aanonsen, 2008, Lorentzen et al., 2012, Lorentzen et al., 2013) The underlying inverse problem is underdetermined and ill-posed because the degree of freedom is considerably high, which yields different models that all match numerically to the true data but give widely different qualitative results (Tarrahi & Afra, 2016).

By using Gaussian statistics, the EnKF is optimal and highly efficient (Evensen, 2003). However, the Gaussian-based EnKF encounters difficulty in the estimation of facies distributions of multimodal nature (Chang, et al., 2010) (Jafarpour & McLaughlin, 2007). Another problem is in the utilisation of a large number of realisations to encapsulate the true solution of the history matching problem in the span of the ensemble members.

To overcome the problems mentioned above, the truncated Gaussian, and pluri-Gaussian procedure was proposed in parameterising the facies distribution (Liu & Oliver, 2005). In this process, multiple random fields which are Gaussian are truncated at separate regions, and each region indicates various facies type in the reservoir

(Chang, et al., 2010). Liu & Oliver (2005) utilised dual Gaussian random fields in the state vectors in their facies history matching process to attain the Gaussian requirements of EnKF. The implementation of the approach is applied for a 3D reservoir in (Agbalaka & Oliver, 2008, Lorentzen et al., 2013) where the authors decoupled the assimilation step into production data assimilation and facies data assimilation. This was implemented to avoid large changes in the updated state variable. Truncated and pluri-Gaussian models are suitable for two-point statistics which honour indicator variograms and facies proportions. Nevertheless, representation of curvilinear geometries is poorly captured with the truncated pluri-Gaussian method, for such geometries multiple-point statistics better represent such distribution (Jing & Zhang, 2013) (Strebelle, 2002).

Other similar approaches in using the EnKF to estimate facies distributions are the level-set method (which will be implemented in this work as shown in later sections) (Dorn & Villegas, 2008), discrete cosine transform (Liu & Jafarpour, 2013) and the Gaussian mixture models (Dovera & Della Rossa, 2007). Chang, et al., (2010) proposed a different method of facies history matching where a representing node system signified points for the computation of the level-set functions. The authors generated Gaussian random numbers from such level-set functions. The facies type was indicated by the sign of the level-set functions (Jing & Zhang, 2013). From these representing nodes, linear interpolation was carried out to get the level-set functions of other points in the reservoir. Dovera & Della Rossa (2007) proposed expression for the conditional variance, conditional means and Gaussian mixture model weights to enable the EnKF implementation applicable with Gaussian mixture model (Chang, et al., 2010). Moreno & Aanonsen (2007) combined the EnKF and level-set. They modelled the boundary velocity mimicking a Gaussian random field and suggested there was a “best case” initial model which was to be implicitly modelled using the level-set function. This boundary velocity was then updated with the EnKF along each assimilation stage and implemented to the original level-set functions to generate new realisations (Chang, et al., 2010). The quality of the best guess model dramatically influences the results obtained from the EnKF inversion.

The discrete cosine transforms (DCT) method implemented by (Jafarpour & McLaughlin, 2007), parameterised both state variables and the model parameters. The

leading coefficients of the retained cosine basis function were updated using the EnKF (Jing & Zhang, 2013). This method is limited to the reduction in the computational complexity. Nevertheless, the method does not provide an efficient mechanism for the incorporation of prior information on the possible structures of the subsurface fields and its inter-connectivity (Tarrahi & Afra, 2016). In this thesis a novel facies history matching method based on a coupled EnKF-level set approach is proposed and discussed in chapter 7.

The sequential data assimilation with EnKF dictates modification of the traditional history-matching problem from a parameter-estimation problem to a parameter-state-estimation problem. Specifically, when applying EnKF for history matching, we update a combined parameter-state vector, which includes the reservoir model parameters (reservoir rock properties) and the primary variables of the reservoir simulator (which includes grid block pressure and fluid saturations).

The logic for including primary variables, which represent the state of the dynamical system, is to avoid the re-run of the simulations from time zero for every data assimilation time-step. However, it requires the assumption of statistical consistency between the updated vectors of states and parameters. However, the reservoir simulator equations are highly nonlinear, and as such this assumption is often violated, resulting in low estimates of model parameters. Sequential data assimilation is a desirable feature of EnKF on the other hand when the objective is the closed-loop reservoir management (Chen and Oliver, 2010; Chen et al., 2010).

However, the simulation restarts needed by the sequential data assimilation are inconvenient when the goal is to incorporate the history matching in workflows that integrate different parts of the reservoir modelling process. These workflows require integration of different geo-modelling software, making the simulation restarts required by EnKF very inconvenient, in some cases, impossible.

The ensemble smoother (ES) was recently introduced by van Leeuwen and Evensen (1996). Unlike EnKF, ES does not assimilate historical data sequentially in time. Instead, ES calculates a global update by simultaneously assimilating all data available at once. Other than that this significant difference, ES formulation is similar to EnKF. Evensen and van Leeuwen compared ES and EnKF with Lorenz equations and concluded that

EnKF outperforms ES because the recursive assimilation updates in the EnKF keep the ensemble of states “on track” and closer to the true solution.

Recently, Skjervheim et al. (2011) compared ES and EnKF and summarised that both methods gave similar results for the reservoir history-matching problems considered in their paper. The significant gain of ES is that it avoids restarts of the reservoir simulator making ES much easier to implement and faster than EnKF. The elimination of simulation restarts also makes ES an attractive option. Applying ES for reservoir history matching converts the parameter-state-estimation problem back to a parameter-estimation problem. Thus, ES removes the parameter-state inconsistency issue observed in the sequential data assimilation with EnKF.

However, Reynolds et al. (2006) showed that EnKF is similar to applying, at each data assimilation time-step, one Gauss-Newton iteration having a full step and the sensitivity matrix replaced by an average sensitivity matrix estimated from the ensemble. With ES, all data are assimilated simultaneously, which means that a single Gauss-Newton correction is applied to condition the ensemble to all data available. Hence, ES may not be able to provide acceptable data matches when applied to reservoir history-matching problems. Emerick and Reynolds (2013) introduced a method in which the same data are assimilated multiple times with the covariance of the measurement errors multiplied by the number of data assimilations. This method is termed ES-MDA and will be used as the optimisation scheme to be compared to EnKF much later in the thesis.

It is common in history matching to have multiple model realisations that lead to a combination of property values from the inverse problem solution that is representative of the true geology (Oliver, et al., 2008). As well as matching historical data, it is critical that the reservoir model honour the subsurface geology (such as reservoirs having faults). In practicality, the entirety of a reservoir is never known with certainty on geological parameters, and so reservoir models resort to interpolating the unknowns (Etienam, et al., 2017).

Most reservoirs contain faults. A common challenge in modelling them is capturing their three-dimensional nature, along with their complex petrophysical properties that are dynamically dependent on the fluids flowing across them. Faults enhance the

vertical connectivity of reservoirs while impeding the horizontal connectivity. Naturally, this has implications for reservoir management, performance and overall economics, particularly in the case of compartmentalised reservoirs, for which a comprehensive understanding of fault dynamics has immediate practical significance (Etienam, et al., 2017).

Fault Transmissibility Multipliers (FTM) are commonly applied to the representation of faults and their values effects production dynamics in reservoir simulation. These are a function of the properties in the fault zone and associated connected grid-blocks, explicitly used in flow simulation to implicitly represent the effect of low permeability rocks to flow, without modelling grid blocks for them explicitly. (Lia et al., 1997) found fault transmissibilities to account for the most significant uncertainty on compartmentalised reserves in the North Sea and this uncertainty are subsequently carried forward to the history matching process.

Most modelling and simulation workflows do not take into consideration the multiphase dependencies of faults and transmissibility multipliers which further adds to the uncertainty. Recent studies indicate that fault transmissibility multipliers can be quantified from petrophysical parameters (Manzocchi et al., 2002, 2010) and be subsequently integrated into the history matching process. The acquisition of extensive hard data on fault properties is impractical due to the associated cost; however, they can be estimated through the integration of 4D-seismic data. Reservoir models are constrained through history matching of observed production data. The solution resulting from just measured rates and pressures is non-unique, and the role of 4D-seismic becomes crucial in significantly reducing uncertainty (Macbeth, et al., 2006). On faults, 4D-seismic data, forward modelling of rock and fluid physics relationships enables saturation inversion, and subsequently a mathematical determination of two-phase fault transmissibility multipliers as they change over time. Computing them and implementing them back into the simulation model, and evaluating the result on history matching would be discussed more in depth in the numerical experiment section in chapter 7.

Understanding the distribution and movement of injected water by incorporating various field data is vital in increasing oil recovery rates. Electromagnetic techniques have become attractive over the past few years because of their ability to overcome some of the shortcomings of seismic techniques such as mapping out images of

reservoir beneath salt layers. It is also advantageous in areas where government regulations prohibit the use of seismic equipment (Zhdanov, 2010) (Ravanelli & Hoteit, 2013). Due to increased computational ability available for reservoir engineers, Crosswell Electromagnetic tomography and controlled-source electromagnetic methods (CSEM) are the go-to methods for determining hydrocarbon reservoir when drilling for oils (Katterbauer et al., 2014). Resistivity well logging is the current standard in the oil industry for determining hydrocarbon reservoirs. CSEM survey methods(Hu et al., 2009) originated from academic studies focused on the oceanic lithosphere in the 1980s. The method has attracted limited focus due to the success of 3D seismic methods, low oil prices, and shallow water environment. Cross-well electromagnetic tomography originally originated in the 1970s from Korea where the Korean Government utilised it to detect tunnels. This method is effective in determining hard rock but is disadvantageous due to high high-frequency attenuation within the transmission lines (Katterbauer et al., 2014). Lower frequencies yield to lower attenuation but have high dispersion that could not be used with traditional techniques. Advances in electromagnetic methods gave rise to the development of low-frequency receivers capable of rejecting background noise while amplifying measured signals (Wilt et al., 1995). Building on the achievements of Wilt, et al(1995).(Wilt & Alumbaugh, 2003), (Marsala, et al., 2008) carried out experiments on the Haradh field located in Saudi Arabia where the authors mapped the fluid distribution and monitored the injected water movement. The author achieved high EM data for well separations of over 850m.

With the rapid advancement in Crosswell Electromagnetic imaging, there has been a pressing need to improve the interpretation and processing of the data. Conventional approaches are to simplify Maxwell's equation to a second order partial differential equation and then invert this equation to obtain the conductivity profile (Abubakar, et al., 2008). History matching incorporating electromagnetic data will be discussed much later in the thesis.

Against the above-mentioned limitations in the methodologies presented, a modified algorithm to the work of Villegas et al., (2005) is modified and proposed employing the EnKF to solve and analyse the inverse problem in 3D, initially assimilating the

production data including the injector pressure, water, and oil production rates, and then carrying out a parameter update using the EnKF and a level-set function.

In this thesis, the researcher presents a novel methodology for the history matching of a black oil reservoir that preserves the shape of the channels and facies using the level-set method in combination with geostatistic, low-frequency Electromagnetic data, 4D-seismic data and machine learning techniques. To current knowledge, a coupling of this kind with the introduction of a narrow band matrix fused with machine learning is novel.

There are eight chapters in this thesis;

Chapter one presents the introduction, literature review and objectives of this work.

Chapter two introduces the concept of Petroleum Geostatistics, terminologies and general knowledge necessary for our initial ensemble creation using two-point statistics and the multiple-point statistics. It also introduces the method used in constructing our initial ensemble for the history matching process. The sequential Gaussian simulation (SGS) and the multiple-point statistics algorithm *FILTERSIM* is discussed. It is worth mentioning that 80% of the EnKF based history matching success is attributed to the construction and selection of the initial ensemble.

Chapter three discusses the flow in porous media, reservoir rock-fluid interaction, the fundamental governing equation relevant to our forward modelling and the parameters to be history-matched in this research.

Chapter four introduces the concept of inverse problems and how the inverse problem peculiar to this case (History matching) is solved using the Bayesian technique. We also introduce the Kalman filter (KF) and show a natural evolution beginning from the Kalman filter to the ensemble Kalman filter. The Ensemble Smoother (ES) and the recently Ensemble Smoother with Multiple Data Assimilation (ES-MDA) is also discussed.

Chapter five introduces Multiphysics techniques for reservoir inverse modelling. Multiphysics enhances the reservoir model calibration by taking into consideration extra source of data such as Electromagnetic and 4D-seismic data.

Chapter six introduces the various parametrisation techniques employed in this thesis. They include the level set method and its direct application to our reservoir case, discrete cosine transform and machine learning techniques (unsupervised learning techniques).

Chapter seven describes the various numerical experiments, novel implementations and methodology implementing the novel ideas developed during the research. Chapter seven is the central part of the thesis and it is the researcher's independent and novel work.

Chapter eight enumerates on the conclusions in the thesis and direction of the future work.

The appendix contains relevant background knowledge on reservoir engineering and MATLAB codes for reproducing the novel experiments conducted in chapter 7.

1.1 Research Objectives

Calibrating complex subsurface geological models against dynamic well observations is not a trivial issue. This challenging inverse problem is known as history matching in oil and gas literature. Robust and geologically consistent inversion technique is necessary due to the highly non-linear nature of the interaction between reservoir parameters and the well responses. Incorporation of all available reservoir data is vital for producing an accurate reservoir model that mimics the actual real case field scenario. For such a model to be built there is a clear need for both the reservoir engineers and geoscientists to come together and make necessary input into the realisation of such reservoir models (Biondi, 1998).

Reservoir data that are available include well logs, conceptual geologic models, production data, electromagnetic data and seismic data. History matching is the process of constraining reservoir models to dynamic production data, and its primary objective is to make reasonable production forecast and at the same time reducing the uncertainties in such a production forecast. History matching also modifies a prior model of a reservoir and gives an updated model of the reservoir whereby the forecast as said before is tremendously reduced. In more recent years, significant progress in the use of automated history matching methods such as the ensemble-based methods

and the gradient-based method has been explored in the oil and gas community. One of the challenging problems in reservoir engineering is to arrive at an estimation of the petrophysical properties such as porosity and permeability by incorporating the production history using inverse modelling.

Most of the time reservoir engineers aim to have an accurate description of the reservoir necessary in predicting future performance with regards to field production and decision-making strategies. The ability to propose accurate predictions for the reservoir history matching process is related to the data assimilation method being employed as well as the means of collecting data. To collect a good amount of data necessary for the data assimilation process a right amount of wells have to be drilled in the area of interest, we see an inverse relationship between the cost of drilling a well and the quality and quantity of data necessary for the data assimilation method. History matching is a highly non-linear, underdetermined and ill-posed problem owing to the complexity and insufficiency of observation data from the reservoirs. (Dorn & Villegas, 2008). It then means that reservoir models can match the observed measurements numerically but qualitatively give a different forecast to reality.

In this PhD thesis, the objectvie and novelty of this work are;

1. Solving model ill-posedness and facies history matching by parametrising the static properties (permeablity and porosity) reconstruction using the level-set methodology (Osher & Fedkiw, 2003) coupled with the EnKF/ES-MDA to get a reliable inversion of observed measurements
2. Multi-physics inversion coupling 4D seismic for reservoir model caliberaion and history matching.
3. Multi-physics approach coupling electromagnetic data for history matching a synthetic black oil reservoir.
4. Unsupervised machine learning techniques are applied to enforce prior structural information on channelised reservoirs during the ensemble based history matching sequence.

Chapter 2- Introduction to Petroleum Geostatistics

“Geostatistics can be described as the collection of numerical techniques that deal with the characterisation of spatial attributes employing primary random models like the way in which time series analysis characterises temporal data” (Bohling, 2005). It can also be described as synthesising geological data using statistical methods (Bohling, 2005). In this chapter, the following geostatistical methods for the creation of our initial ensemble of static properties (i.e. permeability and porosity) will be described

There are three significant components of geostatistics namely; (Bohling 2005)

- 1) Kriging: A method that is used to generate the best linear unbiased estimate at each location. It is an optimal interpolation procedure.
- 2) Stochastic simulation: This technique generates multiple equi-probable images of the variable under consideration
- 3) (semi) variogram analysis: It deals with the characterisation of spatial correlation

2.1 Interpolation Techniques

To generate the initial ensemble members (static rock properties such as permeability and porosity) that will be used in the EnKF/ES-MDA analysis we, first of all, have to understand the various methods employed by geostatisticians to achieve this process. Most of this work is gotten from (Bohling 2005)

- 1) Kriging: A form of best linear unobserved estimate (BLUE) with an estimated mean rather than an assumed mean.

$$\hat{X}(x) = \sum_{k=1}^n \beta_k X_k \quad (2.1)$$

X is the spatial position of the value(unobserved) being estimated. β is estimated by considering the covariance between the prediction points and the observations.

Let the mean

$$\mu_{X(X)} = \sum_{i=1}^m a_i g_{i(X)}$$

(2.2)

$g_i(X)$ is a function which specifies the spatial position of X , a_i is the kriging weight coefficient

β the kriging weight is obtained as the solution to the matrix equation

$$K\beta = M$$

(2.3)

M and K depend on the mean and covariance.

- 2) Linear Regression: The process of fitting a curve to the data and using that curve to extrapolate/interpolate. This process uses only geometry and the data values in determining the curve (by minimising the sum of squared errors).
- 3) Best Linear Unbiased Estimation (BLUE): It is similar to Linear Regression, except that in this case the correlation is used instead of the geometry to obtain the best fit. In this method, our estimate at the location that is unobserved is expressed as X_{n+1} such as porosity or permeability

Let X_{n+1} be the unobserved location (a linear combination of the observations X_1, X_2, X_n)

$$\widehat{X_{n+1}} = \mu_{n+1} + \sum_{k=1}^n \beta_k (X_k - \mu_k)$$

(2.4)

β_k Determined from the first and second moment (mean and covariance)

Cost Function is a function of the input prices and output quantity. Its value is the cost that is incurred in making those output quantity given its input prices

Error Estimation is known as the difference between a true value and an estimated value of value to be predicted or a parameter. There is uncertainty about the accuracy of a physical measurement to be estimated.

Geostatistical Algorithms These algorithms model the spatial distribution of uncertainty. The variogram is mainly used in geostatistics for modelling the relationship between the distance and variance, i.e., the correlation of a variable that exists with itself through space. They are divided into two categories which are

- a) Simulation: this relies on the definition of a stochastic model (a random field), an algorithm used to construct realisations of the model and a spatial domain. Convergence of such algorithms is in some cases asymptotic.
- b) Kriging: as explained earlier in section 2.1.

2.2 Sequential Gaussian Simulation (SGS)

It is a variogram based simulation algorithm which draws their spatial pattern from a variogram model. The variogram model is used to simulate high entropy distributions (Deutsch & Journel, 1995). They are robust and have great ease of conditioning to both hard and soft data. They allow simulation on irregular grids and do not require rasterising. Some of the simulation algorithms include SGSIM (Sequential Gaussian Simulation), SISIM (Sequential Indicator Simulation) COSISIM (Sequential Indicator Co-simulation), DSSIM (Direct Sequential Simulation) COSGSIM (Sequential Gaussian Co-simulation)

Its covariance matrix fully characterises a set of Gaussian Random Variable (RV) and mean vector. A Gaussian Random Function (RF) model is the ultimate model when dealing with just two-point statistics. The *SGSIM* algorithm delivers an image with patterns honouring two locations because of the entropy maximisation nature. This algorithm estimates the variance by the kriging variance and the mean by the kriging estimate. The value that is drawn from that distribution is then used as the conditioning data. A normal score transform is necessary to convert the original data to a Gaussian distribution. The detailed steps in *SGSIM* are;

- I. Transformation of the data to normal space
- II. Establishing a grid network and the coordinate system(*Zreal*)

- III. Allocating data to the nearest grid nodes
- IV. Determine a random path suitable for all the grid nodes
 - a) Find nearby data and the previously simulated grid nodes
 - b) Construct the conditional distribution by kriging
 - c) Get simulated values from the conditional distribution
- V. Check results
 - a) Does it honour the hard data?
 - b) Does it honour the histogram: $N(0, 1)$ - a mean of zero and a variance of one?
 - c) Does it honour the variogram?
 - d) Does it honour the concept of the geology of the reservoir?

We then back-transform to the original data if all conditions above are satisfied. The variogram modelling is explained shortly in section 2.4.

2.3. Multiple-Point Statistics (MPS) with *FILTERSIM* Software

FILTERSIM belongs to the family of multiple-point statistics (MPS). Before this, there were two means of simulating facies models which are the pixel-based method and the object-based method (Wu et al., 2006). The pixel-based method builds the simulated algorithms by one pixel at a time and has ease of conditioning hard data to the simulation. The pixel-based method is slow and cannot replicate complex geometries in a reservoir. Object-based methods, on the other hand, build the realisations by dropping on the simulation grid one pattern or object at a time. Conditioning of data used using object-based method is very complicated. MPS combines the strength of both approaches by operating pixel-wise with the conditional probabilities for the pixels values being recognised as the conditional proportion from a training image depicting the geometry and distribution of the patterns that is dominant in the actual field (Wu et al., 2006).

The training image (TI) which is a depiction (conceptual) is built through the algorithm *TI GENERATOR* from SGeMS in this thesis. MPS tasks are to morph the TI to honour the local conditioning data. The *SNESIM* algorithm of Strebelle (Strebelle, 2000) scans the TI once and saves the conditional proportions available in the TI in a search tree data structure, from where they can be retrieved fast. *SNESIM* is optimal for modelling facies distribution and not continuous distribution and is very limited by the number of categories it can handle. The *FILTERSIM* algorithm (Wu, et al., 2006) is less memory demanding and can handle both continuous and categorical variables. *FILTERSIM* uses linear filters and classifies the training patterns found in a filter score space of reduced dimension. Then similar training patterns are then stored in a class characterised by a prototype which is an average pattern. In the simulation, the prototype that is closest to the conditioning data event is determined. A pattern inferred from that prototype class is drawn and then pasted onto the simulation grid. *FILTERSIM* saves the central location of the training pattern in its memory and hence reducing the computer RAM demand.

2.3.1 Filters and scores

A filter can be defined as the set of weights that are associated with a specific configuration or template (Wu et al., 2006).

$\tau_j = \{u_o; h_i, i = 1, \dots, j\}$ Each node $u_i = u_o + h_i$ of the template is described by a relative offset vector $h_i = (x, y, z)_i$ from u_o the template centre. For a j -nodes template found in the *TI* the k^{th} associated filter is $\{f_k(h_i), i = 1, \dots, j\}$. The configuration of a filter can be of any shape as depicted in figure 2.1.

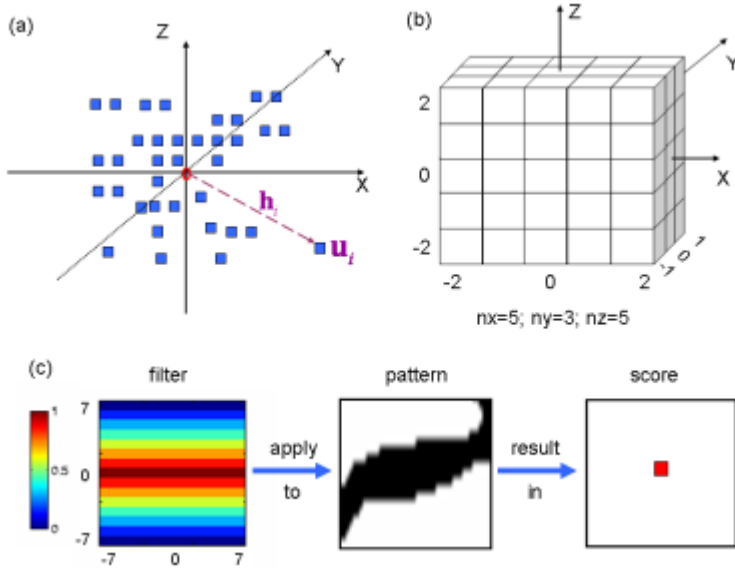


Figure 2.1: Filter and score (a) general template (b) cube-shaped template (c) From filter to score (Wu et al., 2006).

A search pattern is retrieved from the TI template. This template is rectangular in size ($n_x n_y n_z$) are positive odd integers. The filter configuration is required to be the same as the search template in a way that this filter is applied to the training pattern that is located at u the centre. The filter score is given as

$$S_t(u) = \sum_{i=1}^n f(h_i) \cdot pat(u + h_i) \quad (2.5)$$

$pat(u + h_i)$ is the pattern nodal value

A set of F filters is required to capture the numerous characteristics in a training pattern hence equation 2.5 is modified to

$$s_t^k(u) = \sum_{i=1}^n f(h_i) \cdot pat(u + h_i) \quad (2.6)$$

Where $k = 1, \dots, F$

2.3.2 Filter definition

There are three filters provided by *FITERSIM*, (Wu et al., 2006) which are the gradient filter, average filter, and curvature filter. Let n_i be the template size in the i^{th} direction and $m_i = (n_i - 1)/2$ and $\alpha_i = -m_i, \dots, +m_i$ be the filter node offset in the i^{th} direction, the default filters are; (Wu et al., 2006).

- Gradient filter: $f_2^i(\alpha_i) = \frac{\alpha_i}{m_i} \epsilon[-1,1]$
- Average filter: $f_1^i(\alpha_i) = 1 - \frac{\alpha_i}{m_i} \epsilon[0,1]$
- Curvature filter: $f_3^i(\alpha_i) = \frac{2\alpha_i}{m_i} - 1 \epsilon[-1,1]$

They are nine default filters for 3D data and six filters for 2D data.

2.3.3 Pattern classification

In general, sliding the F filters over the K -category training image results in an FK score maps, whereby each local training pattern is described by an FK -length vector in the filter score space. Similar training patterns show similar FK scores. Therefore, similar patterns can be grouped. A pattern class is defined by a pattern prototype $prot$, which is known as the point-wise average of the training patterns falling into a particular class. A prototype is a pattern group ID.

For continuous training image,

$$prot(h_i) = \frac{1}{c} \sum_{j=1}^c pat(u_j + h_i), i = 1, \dots, j \quad (2.7)$$

h_i is the offset location in the template τ_j , c is the replicates found in that prototype class, u_j is the training pattern centre.

2.3.4 Pattern partition

To maximise efficiency, a two-step approach is suggested which is

- i. Grouping all the training patterns into a rough pattern. This rough pattern is known as parent classes and is characterised by its prototype.

- ii. Further pattern classification of the parent classes of patterns that are too diverse in patterns into children classes.

2.3.5 Partition method

They are two general classification methods which are K-Mean clustering partition (Wu, et al., 2006) and the cross partition (Wu, et al., 2006). The K-Mean clustering works as follows: for an input number of clusters, the algorithm finds the centroid of every cluster and then assigns training patterns to a specific cluster by the distance between the cluster centroids and training pattern. Although the K-Mean clustering creates better pattern groups with a reasonable number of replicates, it is slow compared to the cross partition.

The cross partition involves partitioning independent filter scores into equal frequency bins. The cross-partition is fast but gives rough estimates yielding many classes that have few or no replicate as depicted in figure 2.2

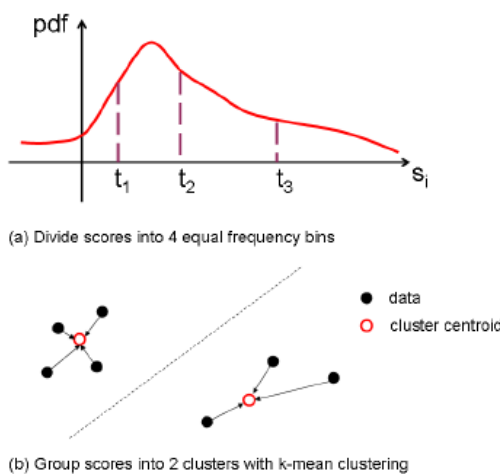


Figure 2.2: Two classification method (Wu, et al., 2006)

2.3.6. Sequential simulation

Once the prototype list is created (for all the children and parents) built from the training patterns, simulated realisations can then be generated.

For the single grid *FILTERSIM* simulation, the algorithm from Wu et al., (2006) is used.

The distance found between the *dev* and the prototype closest to it is calculated as

$$d = \sum_{i=1}^j \omega_i \cdot |dev(u + h_i) - prot(u_o + h_i)| \quad (2.8)$$

Where,

j is number of nodes in the search template τ

ω_i is weight associated to each of the template node

U is the node centre of the data event

h_i is the search template node offset τ

U_o Is the centre node location of the prototype

FILTERSIM utilises servo system intensity factor to reproduce the target better instead of just randomly drawing a pattern gotten from the closest prototype class.

2.4 Semi-variogram

Geostatistical methods and routines are implemented in the primary reservoir modelling packages such as Petrel and Eclipse used in the generation of permeability, facies, and porosity for the reservoir. Geostatistical methods are optimised when the data employed stationary (that is the variance and mean does not vary significantly in space) or normally distributed

For a normal distribution (Gaussian distribution), the following characteristics apply

- 1) The mean=mode=median
- 2) The symmetry is equal to the mean
- 3) The area under a normal distribution curve=1
- 4) The spread of a normal distribution is determined by the standard deviation σ .
The smaller this value, the more concentrated the data will be.

2.4.1 Quantile function

A quantile function is defined as the inverse of a cumulative distribution function. A probit function is the quantile function of a standard normal distribution,(a distribution where the mean is 0 and the standard deviation , σ is 1)

$$F^{-1}(p) = \mu + \sigma\sqrt{2} \operatorname{erf}^{-1}(2p - 1) = \mu + \sigma\Phi^{-1}(p)$$

(2.9)

$$\Phi^{-1}(p) = \sqrt{2}\operatorname{erf}^{-1}.p \in (0,1)$$

(2.10)

$\Phi^{-1}(p)$ is the quantile function of a standard normal distribution curve

$F^{-1}(p)$ is the quantile function of the normal distribution curve.

μ = mean, σ is the standard deviation

X= any continuous or discrete random variable, example porosity

$$\operatorname{erf}(x) = \text{error function} = \frac{1}{\sqrt{\pi}} \int_{-x}^x e^{-t^2} dt$$

(2.11)

Moreover, is the probability of a random variable that has a normal distribution with mean=0 and variance= $\frac{1}{2}$

The cumulative distribution function is given by,

$$\Phi(x) = \frac{1}{\sqrt{2\pi}} \int_{-\infty}^x e^{-\frac{t^2}{2}} dt = \frac{1}{2} \left[1 + \operatorname{erf}\left(\frac{x}{\sqrt{2}}\right) \right]$$

(2.12)

Equation 2.9 holds true for a standard normal distribution (for mean=0 and standard deviation=1)

$$F(x) = \frac{1}{2} \left[1 + \operatorname{erf}\left(\frac{x - \mu}{\sigma\sqrt{2}}\right) \right]$$

(2.13)

The probability density function (pdf) (indicated as) Ψ , of a continuous random variable, is

$$\Psi = \frac{1}{\sigma\sqrt{2\pi}} e^{-\frac{z^2}{2}}$$

(2.14)

where z is referred to as the standard or normal score value.

$$Z = \frac{x - \mu}{\sigma}$$

(2.15)

From basic statistics, we know that correlation and covariance are the measures of similarity that exists between two different variables. In geostatistics, we are more interested in the measurement of the same variable that is made some distance apart from each other. This distance between two points of the same variable is known as the “lag.”

Using the GSLIB software (Deutsch & Journel, 1995), it is possible to obtain the three statistical values, correlation, covariance, and semi-variance. Following standard geostatistical practice, the following notation (Bohling, 2005) is then used.

U : is the vector of spatial coordinates(x, y for a 2D representation of our example)

$Z(u)$: is the variable under consideration that is a function of the spatial location (porosity in our example). It is referred to as the tail variable

h : is the lag vector that represents the separation that occurs between the two spatial locations in consideration

$Z(u+h)$: is known as the lagged version of the porosity variable (or any other variable) under consideration. It is often referred to as the head variable

The scatterplot of the tail versus head variable is often referred to as an h -scattergram.

Let $N(h)$ =number of pairs that is separated by a lag h

Covariance:

$$C(h) = \frac{1}{N(h)} \sum_{\alpha=1}^{N(h)} [z(u_\alpha)] \cdot z(u_\alpha + h) - m_o \times m_{+h}$$

(2.16)

Correlation:

$$\rho(h) = \frac{C(h)}{\sqrt{\sigma_o \cdot \sigma_{+h}}}$$

(2.17)

Semi-variance:

$$\gamma(h) = \frac{1}{2N(h)} \sum_{\alpha=1}^{N(h)} [z(u_\alpha + h) - z(u_\alpha)]^2$$

(2.18)

moreover, it is the measure of the dissimilarity between the head and the tail values It is also a measure of the moment of inertia (a spread of an h-scattergram) about the 45° line shown in figure 2.3

$$m_o = \frac{1}{N(h)} \sum_{\alpha=1}^{N(h)} z(u_\alpha)$$

(2.19)

= mean of the tail

and

$$m_{+h} = \text{mean of the head} = \frac{1}{N(h)} \sum_{\alpha=1}^{N(h)} z(u_\alpha + h)$$

(2.20)

$$\sigma_o = \text{standard deviation of the tail} = \frac{1}{N(h)} \sum_{\alpha=1}^{N(h)} [z(u_\alpha) - m_o]^2 \quad (2.21)$$

$$\sigma_{+h} = \text{Standard deviation of the head} = \frac{1}{N(h)} \sum_{\alpha=1}^{N(h)} [z(u_\alpha + h) - m_{+h}]^2 \quad (2.22)$$

A plot of the correlation versus the lag is known as the correlogram, and the plot of the semivariance and lag is known as the semi-variogram. The covariance is sometimes referred to as the covariance function. The semi-variogram is a covariance function inverted as shown in Figure 2.3.

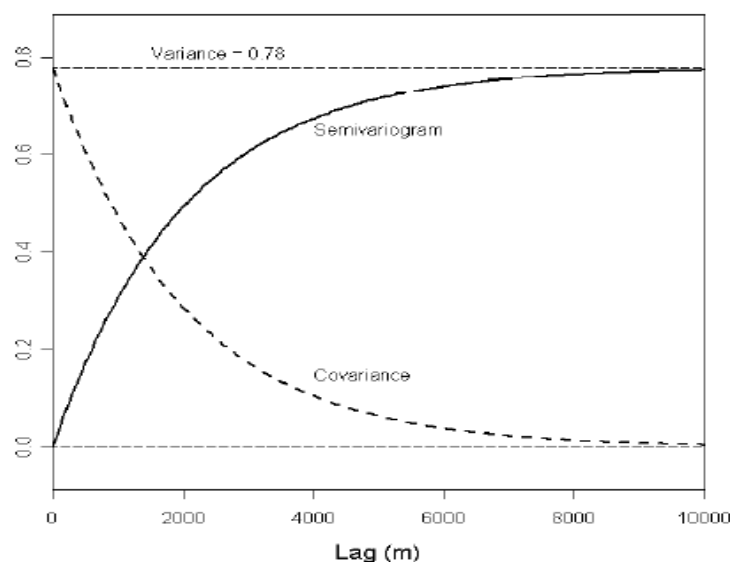


Figure 2.3: Diagram showing the semi-variogram, covariance, and variance (Bohling, 2005)

Technocrats in the field of Geostatistic are interested in the semi-variogram because it filters spatially varying mean and averages squared difference of the variable. (Bohling, 2005) The semi-variogram can also be applied whenever the first differences of the variable $Z(u) - Z(u + h)$ are second-order stationary. It is referred to as *intrinsic hypothesis* that is a weak requirement as compared to the second-order stationarity of the variable (Bohling, October 2005).

2.4.2 Random Variables

A random variable (*RV*) is one which gives a series of outcomes, each having a specific frequency or probability of occurrence. X denotes it, and the outcomes are denoted as

$\{x_i, i = 1, \dots, n\}$ for a discrete variable having n outcomes or $\{x \in [x_{min}, x_{max}]\}$ for a continuous variable bounded by a maximum and minimum value.

2.4.3 Trend

In cases where the semi-variogram continues to rise beyond the global variance is an indication of a significant spatial trend in the variable leading to a negative correlation between values of the variable separated by large lags. There are three options for dealing with lag that are:

- 1) Ignore the problem and continue using a linear and power variogram
- 2) Fit a trend surface and work with residuals from the trend
- 3) Finding a trend-free direction and using the variogram in that direction as the variogram for the variable's random component.

2.4.4 Semi-variogram Characteristics

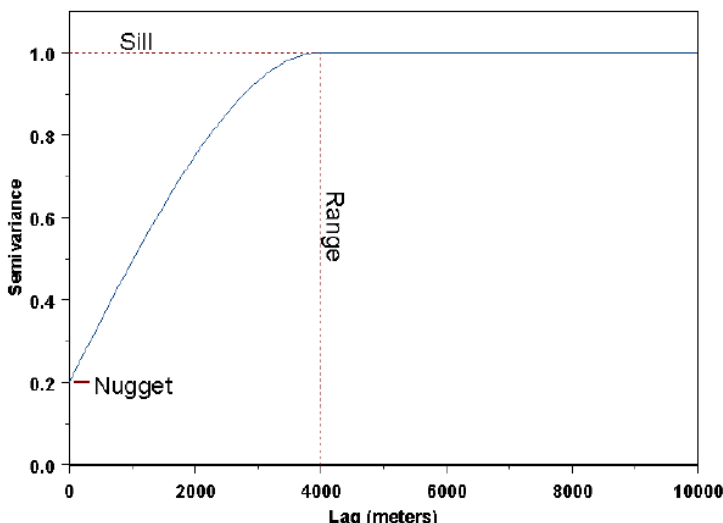


Figure 2.4: A schematic of a semi-variogram (Bohling, 2005)

Figure 2.4, shows the significant aspects of a semi-variogram which will be discussed below.

- 1) Range: This is the lag distance at which the semi-variogram will reach the sill value. Beyond the range, autocorrelation is virtually zero.
- 2) Sill: This is the semi-variance value at which the variogram levels off. It is also known as the amplitude of a component of the semi-variogram

- 3) Nugget: The nugget is used to show variability at distances that are smaller than the typical sample spacing that includes the measurement error.

2.4.5 Semi-variogram Modelling

An empirical model is usually replaced by a semi-variogram model for the sake of the stochastic simulation that will be implemented when generating different numbers of realisation. The Kriging algorithm will require access to the semi-variogram model values of the lag distances than those used for modelling the empirical semi-variogram. (Bohling, 2005) The semi-variogram model needs to be non-negative definite for the system of kriging equations to be non-singular. (Bohling, 2005)

Geostatisticians choose from a plethora of acceptable or illicit semi-variogram models. The models used can either be exponential, Gaussian, spherical, Nugget and power.

Taking a = practical range, c = sill and h = lag distances, we will have the following description below,

Gaussian:

$$g(h) = c \cdot \left[1 - \exp \left[\frac{-3h^2}{a^2} \right] \right] \quad (2.23)$$

Exponential:

$$g(h) = c \cdot \left[1 - \exp \left[\frac{-3h}{a} \right] \right] \quad (2.24)$$

Spherical:

$$g(h) = \begin{cases} c \cdot \left[1.5 \left(\frac{h}{a} \right) - 0.5 \left(\frac{h}{a} \right)^3 \right] & \text{if } h \leq a \\ c & \text{if } h > a \end{cases} \quad (2.25)$$

Nugget:

$$g(h) = \begin{cases} 0 & h = 0 \text{ or } c \text{ if otherwise} \\ c & \end{cases} \quad (2.26)$$

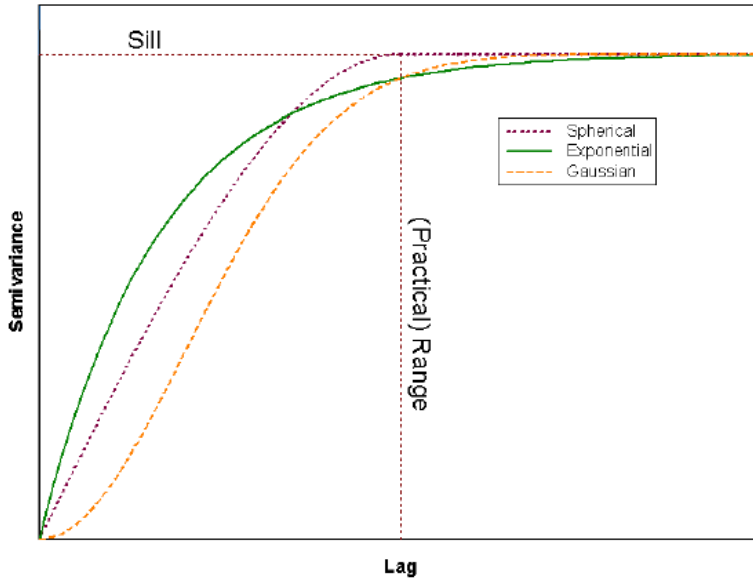


Figure 2.5: A plot of semi-variance against lag showing the various semi-variogram models(Bohling, 2005)

The nugget model represents discontinuity at the origin that arises due to small-scale variation. The exponential and spherical models show linear behaviour, adequate for representing properties with a higher level of short-range variability. Models having a finite sill like the Gaussian, spherical and exponential are referred to as transition models. (Bohling, October 2005)

The conclusion of Chapter 2

- In this chapter, the necessary information in the field of Geostatistics has been discussed.
- Concepts such as kriging and sequential Gaussian simulation (SGS) for two-point statistics generation for the initial creation of static properties (i.e. permeability and porosity) have been explained.
- For the channelised system, a variogram based model is not enough to exhibit the spatial covariance features of the underlying reservoir geometry hence the use of multiple point statistics (MPS).

- The MPS scheme discussed in detail is *FILTERSIM*, which makes the conditioning of hard data and representation of higher order statistics possible.

Chapter 3 – Multi-Phase Flow in Porous Media

The flow in porous media is complex when compared to flow in pipes or conduits. In porous media, there are no defined paths for the fluid to flow through making the estimation of pressure and flow capacity robust. Fluid flow in porous media has been analysed over the years through the means of analytical methods or experimental methods (Craft & Hawkins, 1991). The flow in porous media is explained by a dictionary of specific concepts that must first be understood before we can formulate the required equations for the reservoir fluid flow simulator. These concepts include reservoir rock, and fluid properties flow potential, relative permeability, multi-phase, single phase, fluid compressibility. A detailed description of these parameters is found in the appendix.

3.1 Reservoir Simulation Equations

A petroleum reservoir is typically an underground porous medium whereby gas or oil is trapped stratigraphically or structurally. In most situations, analytical solutions to the mathematical models that will be developed in subsequent chapters are obtainable after making assumptions that simplify the reservoir boundary conditions, geometry, and properties. In many cases, it is not very trivial to develop analytical solutions to practical issues due to the unpredictable and complex behaviours of the multiphase fluid flow, irregular shape of the reservoir, the nonlinearity of the governing equations. As a result of these reasons, these models must be solved in numerical methods using finite element or finite difference. Reservoir simulation can be said to provide numerical simulations to the hydrodynamic fluid problem in the petroleum well system using a digital machine today. It is a very powerful tool used today by reservoir engineers in solving a variety of fluid flow situations involved in the recovery of gas and oil from the porous media of the reservoir.

Applications of reservoir simulation are the prediction of the future performance of the reservoirs so that informed decisions can be made to optimise the economic recovery of the hydrocarbons from the reservoirs. Reservoir simulation can also be employed to know the dynamic behaviour of the recovery mechanism. In petroleum reservoir engineering, the numerical simulation applied through the reservoir simulator is the only way that is used to obtain reliable solutions for the reservoir system. It is because the reservoir systems are very complex. The numerical solutions

do this by providing results at the discrete points in the temporal and spatial domains. The development of the reservoir simulator for the different reservoir systems and the corresponding recovery systems requires a sound knowledge of applied sciences and mathematics which begins with the elaboration of the finite difference equations of the mathematical model of the fluid flow that occurs in a type of reservoir system. It is then followed by numerical modelling followed by computer programming followed by the generation of simulation software used in the end application.

In this work, these equations are not solved directly. Instead, the Eclipse reservoir simulator is used. The overall scheme of the process is shown in the figure 3.1 .The irregular size of the grid blocks, non-linearity of the equations and heterogeneity of the reservoir are caused by these properties (pressure-dependent). All these factors are considered in the finite difference equations.

The basic equations required to generate the necessary equations describing the flow of hydrocarbon through porous media (forward problem) are:

- 1) Conservation of energy
- 2) Conservation of momentum
- 3) Conservation of mass
- 4) Equation of state
- 5) Rate Equation (Darcy's Law)

The selection of the meaningful parameters to be history matched is discussed in section 3.3

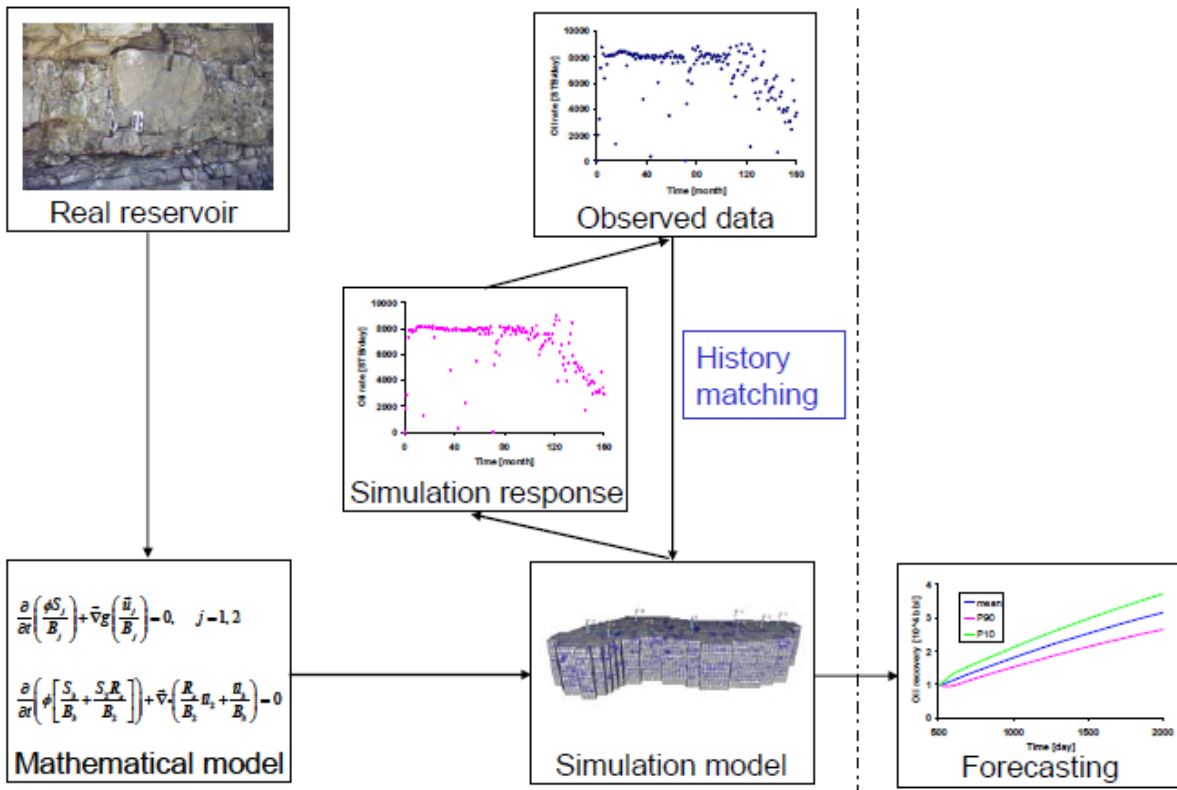


Figure 3.1: Flow-chart of the reservoir modelling and uncertainty quantification workflow.

Detailed derivation of the forward problem can be found in the Appendix

3.2 Two-Phase flow in porous media

For a two-phase flow of oil and water, the forward problem is described by the combination of Darcy's law and continuity equation as:

$$\varphi \frac{\partial S_\ell}{\partial t} = \nabla \cdot (K \frac{k_{r\ell}}{\mu_\ell} [\nabla p_\ell + \rho_\ell \hat{g} \nabla z]) + Q_\ell \quad (3.1)$$

where φ is the effective porosity, S_ℓ is the phase saturation for water and oil indicated hereafter with superscripts w and o respectively, K is the absolute permeability, $k_{r\ell}$ is the phase relative permeability, ρ_ℓ is the phase density, μ_ℓ is the phase viscosity, $\hat{g} \nabla z$ is the acceleration due to gravity. Q_ℓ are the source and sink terms representing the phase production and injection. The equation is solved comprehensively by adding auxiliary equations for capillary pressure between oil and water ($p_{cow} = p_o - p_w$) and the relationship between oil and water saturations ($S_o + S_w = 1$).

3.3 Three-phase flow in porous media

For a three-phase flow model of gas, oil and water the forward problem is fully derived using the combination of Darcy's law and continuity equation. In the following, the index notation $\gamma \in \{o, w, g\}$ is used for indicating the quantities relating to oil, water and gas respectively. We then write the continuity equation as,

$$\nabla \cdot \left(\frac{\rho_w}{B_w} u_w \right) - Q_w = - \frac{\partial}{\partial t} \left(\frac{\varphi \rho_w}{B_w} S_w \right) \quad (3.2)$$

$$\nabla \cdot \left(\frac{\rho_o}{B_o} u_o \right) - Q_o = - \frac{\partial}{\partial t} \left(\frac{\varphi \rho_o}{B_o} S_o \right) \quad (3.3)$$

$$\nabla \cdot \left(\frac{\rho_g}{B_g} u_g + \frac{R_{so}\rho_g}{B_o} u_o \right) - Q_g = - \frac{\partial}{\partial t} \left[\varphi \left(\frac{\rho_g}{B_g} S_g + \frac{R_{so}\rho_g}{B_o} S_o \right) \right] \quad (3.4)$$

Where u_γ is the Darcy velocity of each phase

$$u_\gamma = -\frac{k_{r\gamma}}{\mu_\gamma} K (\nabla p_\gamma - \rho_\gamma \hat{g} \nabla z) \quad (3.5)$$

$$S_o + S_w + S_g = 1 \quad (3.6)$$

$$p_o - p_w = p_{cow} \quad (3.7)$$

$$p_g - p_o = p_{cgo} \quad (3.8)$$

S_γ and p_γ is the phase saturation and phase pressure, $k_{r\gamma}$ are the relative permeabilities, $k_{r\gamma}$ is the phase relative permeability, ρ_γ is the phase density, μ_γ is the phase viscosity. B_γ is the phase formation volume factor. R_{so} is the solution gas-oil ratio, p_{cgo} is the gas-oil capillary pressure. z is the vertical coordinate (height) and \hat{g} denotes the magnitude of the gravitational acceleration.

3.4 Selection of sensitive parameters to be history matched

They are two criteria needed for selecting the sensitive parameters for history matching (Aanonsen S, 2009)

- a. Uncertainty ranges of value associated with the parameter
- b. The result in sensitivity to the parameter with regards the output from simulation.

They are two major classes of collected data in the reservoir, namely

- i. Static data: They are not associated with the movement of fluid in the reservoir such as geology data, core analysis, electrical logs, geostatistics, absolute permeability and effective porosity.
- ii. Dynamic data: They are associated with the movement of the fluid in the reservoir such as production history, pressure shut in the survey, well-testing data analytics, gas oil ratio, bottom hole pressure.

Absolute permeability and effective porosity have a significant influence on reservoir performance. In this work, the properties to be history matched and evaluated are the absolute permeability and the effective porosity as well as the water saturation distribution.

The absolute permeability plays a significant role in the facies classification of the reservoir. Areas of high permeability are designated sand while areas of low permeability are designated shale in this thesis.

Conclusion on chapter 3

- In this chapter, the vital reservoir rock-fluid properties necessary in reservoir simulation and modelling in porous media and also the two-phase and three-phase flow to be used in the synthetic numerical experiments in later chapters has been discussed.
- A general flowchart in the reservoir modelling workflow as also been explained.

Chapter 4 -Inverse problems/Data Assimilation

The process of building a reservoir model by incorporating all available data during the life cycle of a petroleum reservoir is known as reservoir characterisation. The ability to forecast petroleum production under different reservoir scenarios is crucial to the management of a reservoir. A consistent mathematical framework is used by reservoir engineers to reduce the uncertainty of the forecast. Data commonly available for this characterisation include well logs, acoustic, seismic surveys and production history data of the reservoir. These data are utilised to estimate the state and parameters in a mathematical skeleton of the reservoir that is concurrently fed into a numerical reservoir simulator. It is known that several models might match a given reservoir production data. Hence, these parameters and state models are treated as inverse problems (Tarantola, 2005). Traditionally for inverse problems; system parameters are higher than system outputs making the whole process non-unique.

The general steps in history matching considered in the thesis are;

- 1) The proper parametrisation of parameters that could affect the history matching of the reservoir model
- 2) A laid out objective function for the optimisation of the reservoir model is chosen
- 3) Reduction of the objective function to a minimum by selecting a proper optimisation technique(design and implementation)
- 4) The cost of the flow simulator and optimisation technique.

4.1 Inverse Problems: Bayesian Theory

The use of a set of observed measurements, d , to infer a set of model parameters, m , is known as an inverse problem. Given specific observations which are the observed data of the state variable (data that is a direct function of state variables); the aim is to infer information about the model parameters which includes some uncertainty. The main focus is on discrete inverse problems (system characterised by a few or a finite number of parameters). History matching is an example of a discrete inverse problem. In such situations, the number of data is always finite, and the data always contain some measurement errors. It is impossible to estimate the parameters of a reservoir

model correctly from inconsistent, inaccurate and insufficient data using a forward model that most likely will contain some modelling errors. In most cases, we always have some prior information about the realism and plausibility of the reservoir model. In history matching, these include a geological model that is constructed from cores, logs and seismic data and also some information on the depositional environment.

4.1.1 Introduction to Gradients

To understand the ensemble minimisation scheme, we, first of all, have to talk about the concepts of gradients. Gradients play a significant role in most inverse problems (Tarantola, 2005) and at such a detailed description of them is required. In subsequent sections, we will derive ensemble representations of these gradients since actual computing of them are prohibitive and difficult.

Let m be a column vector, $g(m)$ be a real valued function.

$g = g(m) = [g_1(m) \ g_2(m) \dots g_{N_d}]$ is a $1 \times N_d$ matrix, N_d is the total number of measurements.

$$m = \begin{bmatrix} m_1 \\ m_2 \\ \vdots \\ m_{N_m} \end{bmatrix} \quad \nabla_m = \begin{bmatrix} \frac{\partial}{\partial m_1} \\ \vdots \\ \frac{\partial}{\partial m_{N_m}} \end{bmatrix} \quad (4.1)$$

$$\nabla_m m^T = \begin{bmatrix} \frac{\partial}{\partial m_1} \\ \vdots \\ \frac{\partial}{\partial m_{N_m}} \end{bmatrix} \begin{bmatrix} m_1 & m_2 & \dots & m_{N_m} \end{bmatrix} = I_{N_m} \quad (4.2)$$

$$\begin{aligned} \nabla_m g(m)^T &= \begin{bmatrix} \frac{\partial}{\partial m_1} \\ \vdots \\ \frac{\partial}{\partial m_{N_m}} \end{bmatrix} \begin{bmatrix} g_1(m) & g_2(m) & \dots & g_{N_d} \end{bmatrix} = \begin{bmatrix} \frac{\partial g_1}{\partial m_1} & \frac{\partial g_2}{\partial m_1} & \frac{\partial g_{N_d}}{\partial m_1} \\ \vdots & \vdots & \vdots \\ \frac{\partial g_1}{\partial m_{N_m}} & \frac{\partial g_2}{\partial m_{N_m}} & \frac{\partial g_{N_d}}{\partial m_{N_m}} \end{bmatrix} \\ &= [\nabla g_1 \ \nabla g_2 \ \dots \ \nabla g_{N_d}] \end{aligned}$$

(4.3)

Let A be $N_d \times N_d$ covariance matrix with entries that are independent of the $N_m \times 1$ vector m , let G be $N_d \times M$ with entries that are independent of m , we define d as a constant N_d dimensional column vector and define the objective function in Eqn.(4.4) as;

$$O(m) = (Gm - d)^T A(Gm - d) = (m^T G^T - d^T) A(Gm - d) \quad (4.4)$$

$$\begin{aligned} \nabla_m O(m) &= [\nabla_m(m^T G^T - d^T)] A(Gm - d) + [\nabla_m((m^T G^T - d^T) A^T)(Gm - d)] \\ &= G^T A(Gm - d) + G^T A^T(Gm - d) \end{aligned} \quad (4.5)$$

If A is symmetric,

$$\nabla_m O(m) = 2G^T A(Gm - d) + G^T \quad (4.6)$$

A real symmetric $N \times N$ matrix A is referred to be positive definite if for every real N -dimensional column vector $x \neq 0$, $x^T Ax > 0$

Theorem (Tarantola, 2005):

Let A be a $N \times N$ real matrix

- i. If A is real symmetric ($A^T = A$), Then the eigenvalues $\{\lambda\}_{i=1}^N$ of A are real and A has a set of orthonormal eigenvectors, $\{x\}_{i=1}^N$
- ii. A is positive definite if and only if all the eigenvalues of A are positive
- iii. If A is positive definite, then A is nonsingular. Moreover, if $\{\lambda_i, x_i\}_{i=1}^N$ are the eigenpairs of A , then $\left\{\frac{1}{\lambda_i}, x_i\right\}_{i=1}^N$ are the eigenpairs of A^{-1} .

Consider the forward problem,

$$d = Gm \quad (4.7)$$

We pose the inverse problem as given the noisy data, d_{obs} solve, $Gm = d_{obs}$

G is the sensitivity matrix, The null space of G is the set of all vectors in $S(m) \equiv R^{N_m}$ that satisfy $Gm = 0$

The null space of G is denoted by $N(G)$. Let $\dim N(G) = \ell > 0$. If m_0 is a solution of $Gm_0 = d_{obs}$ and $\{m_k\}_{k=1}^{\ell}$ is a basis for $N(G)$, then for any scalars, $\alpha_j, j = 1, 2, \dots, n, m = m_0 + \sum_{j=1}^{\ell} \alpha_j m_j$ is a solution of Eqn. 4.7

The range of the $N_d \times N_m$ matrix G denoted as $R(G)$ is the set of all vectors d in $S(d) = R^{N_d}$ such that there exists at least one m in $S(m) = R^{N_m}$ which satisfies $Gm = d$

The dimension of the range of the $N_d \times M$ matrix G is denoted by $\dim R(G)$ and is called the rank of G . The rank of G is equal to the number of linearly independent columns of G which is also equal to the number of linearly independent rows of G .

$R(G) \leq \min\{N_d, N_m\}$. If $R(G) = \min\{N_d, N_m\}$, G is said be of full rank.

To pose the solution of the inverse problem, $Gm = d_{obs}$ we minimize the least square problem posse as

$$\|Gm - d_{obs}\|_2^2 \quad (4.8)$$

$$O(m) \equiv (Gm - d_{obs})^T (Gm - d_{obs}) \quad (4.9)$$

Equating to zero and rearranging gives,

$$G^T Gm = G^T d_{obs} \quad (4.10)$$

We apply the Singular value decomposition to find the least square solution of the minimum norm.

4.1.2 Singular Value Decomposition (SVD)

There exists an $N_d \times N_m$ orthogonal matrix U , an $N_m \times N_m$ orthogonal matrix V and an $N_d \times N_m$ matrix Λ such that

$$G = U\Lambda V^T \quad (4.11)$$

$$\Lambda = \begin{bmatrix} \Lambda_q & 0 \\ 0 & 0 \end{bmatrix} \quad (4.12)$$

Where $\Lambda_q = diag(\lambda_1, \lambda_2 \dots \lambda_q)$ with $\lambda_1 \geq \lambda_2 \geq \lambda_q \geq 0$. $q = min\{N_d, N_m\}$

SVD solution of Equation 4.10 is

$$m_{est} = V \begin{bmatrix} \Lambda_q^{-1} & 0 \\ 0 & 0 \end{bmatrix} U^T d_{obs} = V_r \Lambda_r^{-1} U_r^T d_{obs} \quad (4.13)$$

4.1.3 The Bayesian posterior ensemble smoother for linear Gaussian case

A probabilistic point of view is the best form of obtaining a clear solution of an inverse problem (Kirsch, 1996). It is assumed that model parameter prior information is utilised as a pdf. The general relationship between posterior information of a variable with the prior information is related according to the Bayesian formulation described by the equation below,

$$posterior\ pdf \propto Likelihood\ function\ pdf \times Prior\ pdf \quad (4.14)$$

The success of the solution is based on the fact that the model must have continuous consistency with the measured data and physical constraints. The solution of the Bayesian formula is picked from the posterior distribution. (Omre, 2000). The main reason for utilising the Bayesian approach is to honour prior geological data of the reservoir.

Assuming any random variable (which is multivariate Gaussian) of the reservoir, such as porosity, the probability density function of the model reservoir variable is written thus,

$$p(m) \propto a \exp\left(-\frac{1}{2}(m - m_{prior})^T C_M^{-1}(m - m_{prior})\right)$$
(4.15)

In the equation above,

m_{prior} = Best prior estimate (mean) of parameters for the reservoir field

m = Model parameters vectors

C_M = covariance matrix of the model variable normally constructed through geostatistical tools.

a = constant.

Expected porosity is described by the prior information of the reservoir configuration.

In the analysis of the reservoir, we take into consideration the data collected. The data gathered from the field is known as the true data, and it is related to the observed data by the equation below,

$$d_{obs} = d_{true} + \varepsilon$$
(4.16)

d_{obs} = Observed data (oil production rate, water cut produced or Gas-Oil-Ratio)

d_{true} = true data

ε = the measurement noise that accounts for the limited functionality of the measurement equipment.

For full Gaussian linearity, we can assume the pdf of the data noise to be,

$$p(d_{obs}|m) = b \exp\left(-\frac{1}{2}(d_{obs} - Gm_{prior})^T C_D^{-1}(d_{obs} - Gm_{prior})\right)$$
(4.17)

C_D = covariance matrix of the measurement noise. It is non-diagonal for real field seismic data and diagonal for production data. It also defines the correlation that exists between the noises of the data.

Baye's theorem states that,

$$p(m|d_{obs}) = \frac{p(m) p(d_{obs}|m)}{p(d_{obs})} \quad (4.18)$$

$$= \frac{p(m) p(d_{obs}|m)}{\int p(U)du p(d_{obs}|u)} \quad (4.19)$$

The conditional pdf can then be derived as,

$$\begin{aligned} p(m|d_{obs}) &= c \exp(-\frac{1}{2}(m - m_{prior})^T C_M^{-1}(m - m_{prior}) \times (-\frac{1}{2}(d_{obs} - \\ &Gm_{prior})^T C_D^{-1}(d_{obs} - Gm_{prior})) \end{aligned} \quad (4.20)$$

c =normalizing constant

The aim is the minimisation of the objective function $Q(m)$ in the equation below,

$$Q(m) = Qm(m) + Qd(m) \quad (4.21)$$

$$\begin{aligned} Q(m) &= \frac{1}{2}(m - m_{prior})^T C_M^{-1}(m - m_{prior}) + \frac{1}{2}(d_{obs} - \\ &Gm_{prior})^T C_D^{-1}(d_{obs} - Gm_{prior}) \end{aligned} \quad (4.22)$$

$Qm(m)$ = model mismatch term that provides normalisation for the Hessian matrix.

$Qd(m)$ =data mismatch term

If we assumed the relationship between model and predicted data is linear i.e.
 $g(m) = Gm$, then the posterior mean in Eqn.4.20 is

$$\bar{m} = m_{prior} + C_M G^T (G C_M G^T + C_D)^{-1} (d_{obs} - Gm_{prior}) \quad (4.23)$$

Characterising uncertainties in future productions from the reservoir is vital. Realising the posterior pdf is done by sampling methods such as the MCMC (Marko chain Monte Carlo), the Rejection sampling method, and the Randomized maximum likelihood. (Aster R, 2005)

Data assimilation is the process of combining data and information from actual observations into a numerical model that is geophysical. It is a probability distribution of both the analysed data and forecast data. The analysis step is executed using Baye's theory. Integration of the model forward in time is done using the Fokker-Plank equation that is outrageously expensive. Hence, other simplifying models are used instead (Evensen, 2003). The Kalman filter is used to represent normal probability distributions with their means and covariances. It is unrealistic to maintain covariance's over large data hence an ensemble of data is preferred in this assimilation.

One such method is the use of the ensemble Kalman Filter (EnKF). The EnKF updates the ensemble sequentially in time to adhere and honour to the new production data at the time they are available. The forecast in the EnKF is known as the forward integration that is followed by the analysis step (updating of state variable). The results give an updated ensemble that is conditioned on already known production data and as such gives optimal predictions of future productions (Evensen G, 2007). It should also be known that EnKF gives a known solution space that is spanned by uncertainties (prior pdf) with sufficient degrees of freedom.

The ensemble (realisations) of simulations represents the probability distributions in the EnKF, and the covariance is assumed to be the covariance of the ensemble sample (Ehrendorfer, 2007). In the process of reservoir history matching it is usually assumed that the initial state of the reservoir is known and before any assimilation, the joint probability of the critical reservoir parameters characterised (Oliver D, 2008). The data of observations are dependent on the current state of the reservoir only, and the previous state of the reservoir are neglected, leading to another exciting conclusion that suggests the probability density of the state variables and parameters are defined recursively. Conditioning of the reservoir with the most recent data available and prior information is done with the Baye's theory. This process enables us to sample the

posterior distribution utilising the likelihood term and prior information. The EnKF updates the reservoir models in a recursive sequential manner during the history matching process.

4.2 History Matching Methods

History matching is known as the process of adjusting the variables and parameters such as permeability and porosity found in a reservoir simulation model to match the observation of pressures, rates, saturation and other variables vital in assessing reservoir performance (Aanonsen et al.,2009). History matching requires the minimisation of the mismatch between all computed values and measurements and also the prior and current model parameters requiring numerous various iterations which makes the whole process computationally expensive (Aanonsen et al.,2009). The assessment of uncertainty is vital in a good history match. The general method for estimating uncertainty will be to generate multiple initial realisation models, history match each one of them and then simulate for future production on each of the models. In using the EnKF, the model can be used to forecast the production for the next few years with some uncertainties. The up-gradation of the model is achieved by collecting the updated new data having reduced uncertainty, in this procedure; the process of history matching does not end before the life of the field ends.

The goals of assisted history matching are;

- i. Honour Observations
- ii. Maintain geological realism
- iii. Have a predictive power not just regarding matching the physics of the field production but also regarding the fluid distribution
- iv. It should give at least some reasonable estimate of uncertainties for the reservoir development and also manage risk, ideally to characterise the posterior pdf
- v. Be compatible with the institution/company simulation tools
- vi. Be computationally feasible

The two broad classification of history matching is;

- I. Gradient-based (classical) method (Deterministic algorithm): Some methods include the Gauss-Newton method, Conjugate Gradient (CG) method, Steepest Descent method and Levenberg-Marquardt algorithm (Oliver, 1996). The gradient of the objective function is used as the minimisation criteria. A significant disadvantage of this approach is that it does not describe the spatial covariance model as shown by the parameters(model)
- II. Stochastic Algorithm (probabilistic): This algorithm takes a considerable amount of computational time when compared to the deterministic method. In this work, the stochastic approach was used in the form of the ensemble Kalman Filter. The stochastic approach is more suitable to the non-unique nature of history matching because of the generation of some equal probable reservoir models. It theoretically reaches the global optimum. Some examples include the Genetic Algorithm, Simulated Annealing, and the Kalman Filter.

4.3 The Kalman Filter

The method of assessing the posterior distribution recursively is done with the aid of the Kalman filter (Kalman, 1960). The idea of the best linear unbiased estimate is achieved by using the Kalman filter, assuming linear dynamics and Gaussian statistics (Luenberger, 1967). The posterior is assumed Gaussian because the likelihood and the prior distribution is Gaussian as well, and its covariance and means define it. The Kalman filter evolves the probable error covariance matrix and model state with time (most likely). The derivation of the EnKF and the Kalman filter algorithm follows the work of Skjervheim (2007).

$\Psi(x, t)$ Represents the unknown variable constituted by the model state $u(x, t)$ and model parameter, $m(x, t)$

Let,

$$d_k = H_k \Psi_k + \varepsilon_k^0 \quad (4.24)$$

and $\varepsilon_k^0 \sim N_m(0, C\varepsilon_k^0)$, H_k is referred to as the observation operator that relates the true model state, Ψ_k to the observations d_k and ε_k^0 is known as the Gaussian data noise. Its estimation will be explained subsequently. d_k is the observation of data (observed oil production rate, bottom hole pressure or water cut).

$$\Psi_k = F_K \Psi_{k-1} + \varepsilon_k^m \quad (4.25)$$

where F_K is known as the linear model operator ε_k^m is Gaussian model noise.

$C\varepsilon_k^0$ and $C\varepsilon_k^m$ are known as the error covariance of the data and model noise respectively.

The initial prior distribution expectation, $E(\Psi_0 = \Psi_0^{\text{init}})$ and the covariance, $\text{Cov}(\Psi_0)$ is equal to $C_{\varepsilon_0}^{\text{init}}$, both assumed to be Gaussian.

$$\Psi_0 \sim N_q(\Psi_0^{\text{init}}, C_{\varepsilon_0}^{\text{init}})$$

Assuming known posterior distribution at time t_{k-1} , characterised by $g(\Psi_{k-1}: d_{k-1:1})$. Hence, we arrive at

$$\Psi_{k-1}: d_{k-1:1} \sim Nq(\Psi_{k-1}^a, C_{\Psi_{k-1}}^a) \quad (4.26)$$

Combining equation 4.25 and 4.26 we can define the prior distribution

$$g(\Psi_{k-1}: d_{k-1:1}), \text{ as} \\ \Psi_k: d_{k-1:1} \sim Nq(\Psi_k^f, C_{\Psi_k}^f) \quad (4.27)$$

Ψ_k^f is the first guess mean or prior mean and $C_{\Psi_k}^f$ the prior covariance.

$$C_{\Psi_k}^f = E \left[(\Psi_k - \Psi_k^f)(\Psi_k - \Psi_k^f)^T \mid d_{k-1:1} \right] \quad (4.28)$$

From equation 4.27 we can write the prior moments as

$$\Psi_k^f = F_K \Psi_{k-1}^a$$

(4.29)

$$C_{\Psi_k}^f = F_K C_{\Psi_{k-1}}^a F_k^T + \mathcal{C} \varepsilon_k^m \quad (4.30a)$$

$(\Psi_{k-1} : d_{k-1:1})$, is known as the joint distribution and can be evaluated as

$$\binom{\Psi_k}{d_k}_{\llbracket l|d \rrbracket_{k-1:1}} \sim N_{q+mk} \begin{pmatrix} \Psi_k^f \\ d_k^f \end{pmatrix} \begin{bmatrix} C_{\Psi_k}^f & H_k^T C_{\Psi_k}^f \\ H_k C_{\Psi_k}^f & C_{\Psi_k}^f \end{bmatrix} \quad (4.30b)$$

The covariance and the analysis mean are given by

$$\Psi_k^a = \Psi_k^f + K_k(d_k - H_k \Psi_k^f) \quad (4.31)$$

$$C_{\Psi k}^a = (1 - K_k H_k) \Psi_k^f \quad (4.32)$$

K_k =Kalman gain matrix.

$$K_k = C_{\Psi k}^f H_k^T \left(H_k C_{\Psi k}^f H_k^T + C \varepsilon_k^0 \right)^{-1} \quad (4.33)$$

The Kalman filter theory assumes the state space models are linear having Gaussian statistics and a posterior distribution $g(\Psi_{k-1}; d_{k-1})$ which is subject to analytical methods and Gaussian as well. The overall objective is to create a sample from the posterior pdf $g(\Psi_k; d_{k-1})$ distribution using various sampling strategies such as Markov Chain Monte Carlo (MCMC) and rejection sampling. The comparison between KF and EnKF is depicted in figure 4.1.

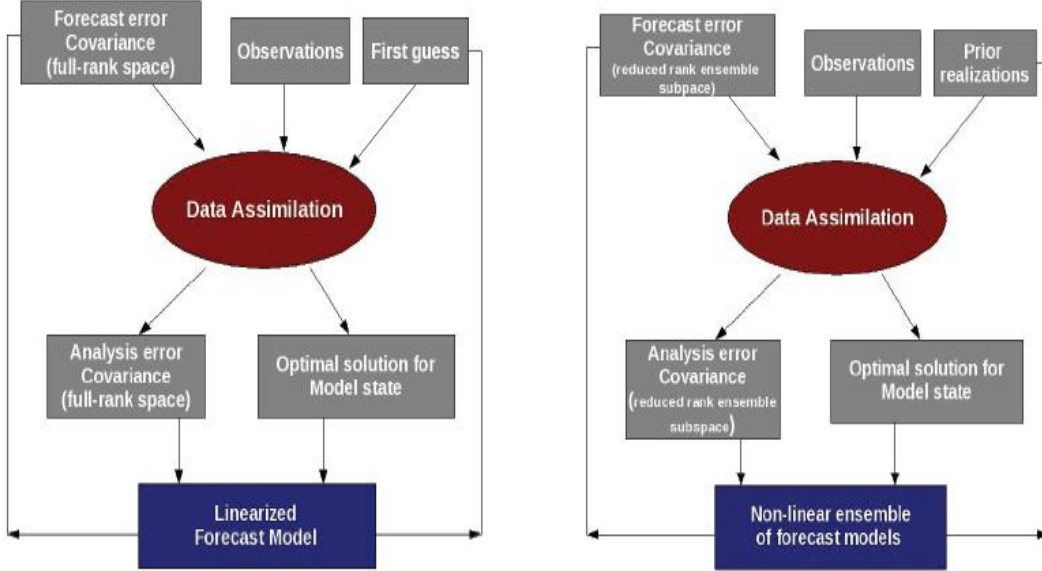


Figure 4.1: Comparison between KF and EnKF

From the analysis of the Kalman filter, it has been seen that the degree of freedom as it shows to the choice of the mean would be too significant in the analysis of the posterior probability; hence, an ensemble of data is required to limit the degree of freedom of such pdf. The EnKF is a sequential Bayesian inversion process (Monte Carlo in nature) and was first utilised by Geir Evensen when the author assimilated data for non-linear ocean models (Evensen, 1994). The Fokker-Plank equation as said earlier is solved by the use of the EnKF and the pdf of interest are represented by their ensemble of data. The combined parameter and state estimations are solved and approximated by the utilisation of the EnKF (Evensen, 2009).

4.4 Ensemble Kalman filter

The time-series visual representation of the EnKF is depicted in figure 4.2(a).

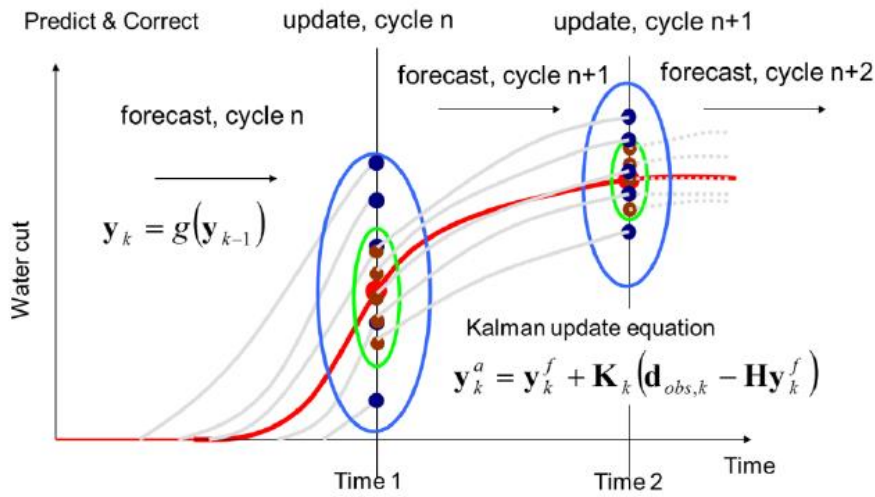


Figure 4.2(a): Time-series visual representation of the EnKF

The main difference between the Kalman filter and the EnKF is merely the sample covariance of the ensemble substitutes the covariance matrix. The explanation of the EnKF would be enumerated shortly. The comparison between EnKF and traditional history matching is depicted in figure 4.2(b).

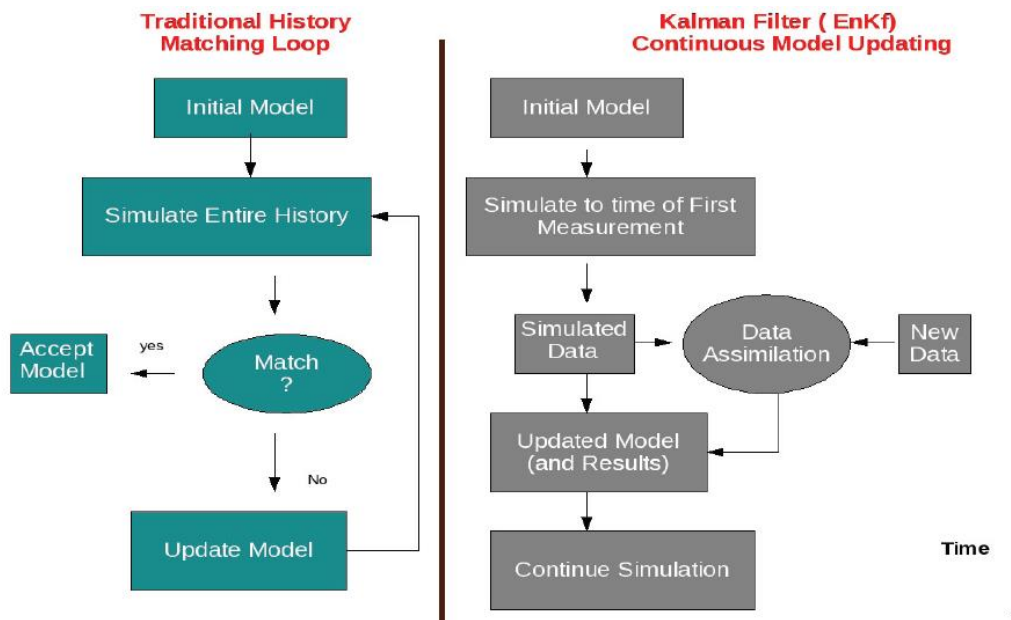


Figure 4.2(b): Comparison between EnKF and traditional History matching (Fahimuddin, March,2010)

The ensemble members are not independent of each other because the EnKF ties them together. The excellent advantage of the EnKF is that by just advancing each member of the ensemble we can advance the overall pdf in time.

The algorithm is similar to the Kalman filter but with the mean in the Kalman filter replaced by the ensemble mean in the EnKF.

For a non-linear space model,

$$d_k = h_k \Psi_k + \varepsilon_k^0 \quad (4.34)$$

$$\Psi_k = G(\Psi_{k-1}) + \varepsilon_k^m \quad (4.35)$$

$G: R_{N_y} - R^m$ represents the non-linear model operator that maps from the model space to data space

$h_k: R_{N_y} - R^{mk}$ Represents the non-linear measurement operator relating Ψ_k to d_k

And

$$\varepsilon_k^m \sim N_q(0, C\varepsilon_k^m) \quad (4.36)$$

$$\varepsilon_k^0 \sim N_{m_k}(0, C\varepsilon_k^0) \quad (4.37)$$

Another option for solving non-linearity in the state space problem is the Extended Kalman filter (EKF). (Maybeck, 1979). EKF is formulated based on a set of linear approximations making it an inefficient filter, hence, the introduction of the EnKF to analyse the equation bearing in mind the time evolution of the pdf of the model variable. In EnKF, the observations are treated as linear, and there is a reformulation of the non-linear state space (Evensen, 2003).

EnKF propagates equiprobable ensemble realisations of an initial set of realisations throughout time to assimilate new data whenever they become available.

$$\text{Let } \tilde{W}_k = [(\Psi_k, h_k(\Psi_k))] \quad (4.38)$$

Rewriting equation 4.34 as,

$$d_k = H_k \tilde{W}_k + \varepsilon_k^0 \quad (4.39)$$

where $H_k \in R^{m_k \times N_y}$ is the measurement operator(linear) that picks data from \tilde{W}_k

From now on we will use ψ_k in place of \tilde{W}_k

We define the matrix that holds the ensemble members

$$\psi_k = \psi \in R^{N_y \times N_e} \quad (4.40)$$

$$\psi = y^j \in \mathcal{R}^{N_y \times N_e}, j = 1, \dots, N_e \quad (4.41)$$

where N_e is the number of realisations; y^j are the state vectors and N_y is the number of grids were the unknown parameters are to be estimated In an ensemble of state vectors. Each state vector is represented as:

$$y_k^j = \begin{Bmatrix} m \\ u_k \\ d_k \end{Bmatrix}^j \in \mathcal{R}^{N_m + N_u + N_d} \quad (4.42)$$

Where k is the time step. The model state vectors, for now, consist of the reservoir parameters (all the static parameters we want to update) (m), state variables (u) and the simulated production data (d). The parameters are variables that do not vary in time such as permeability and porosity; whereas state variables are variables that vary with time such as the saturation and pressure for all phases (Chang, et al., 2010). The observations/simulated data consist of facies and dynamic historical production records. The state vector, for each ensemble member j , y_k^j is made up of

- Natural logarithm of the permeability value found in each grid cell(static variable): $\ln(K_i)$ where $i = 1, \dots, N_y$
- Porosity value found in each grid cell (static variable): φ_i where $i = 1, \dots, N_y$
- The pressure at all grid cells (dynamic variable): P_i where $i = 1, \dots, N_y$
- Water saturation at all grid cells (dynamic variable): $S_{w,i}$ where $i = 1, \dots, N_y$
- Bottom hole pressure at the production well: BHP_k
- Oil production rate: Q_o at the production well
- Water production rate: Q_w at the production well

The methodology for the EnKF includes two unique sequential stages: the forecasting stage and the assimilation stage. Each ensemble member undergoes the forecast step independently as,

$$y_k^{p,j} = G(y_{k-1}^{a,j}), j = 1, \dots, N_e \quad (4.43)$$

Where G is the forecast operator which represents the reservoir simulator.

Superscripts a and p represent the analysed and predicted estimates. The parameter update/assimilation step is carried out as,

$$\langle y_k^p \rangle = y_k^{p,j} \times 1_{N_e} \quad (4.44)$$

$1_{N_e} \in R^{N_e \times N_e}$ is a matrix, and each element of this matrix is equal to $1/N_e$

$$C_{y_k^p} \approx \frac{1}{N_e - 1} \sum_{j=1}^{N_e} \left\{ [y_k^{p,j} - \langle y_k^p \rangle] [y_k^{p,j} - \langle y_k^p \rangle]^T \right\} \quad (4.45)$$

4.4 1 Measurement perturbations

The vector of observations $d_k \in R^{m_k}$ with m_k being the number of measurements is reformulated as an ensemble of perturbed measurements expressed as,

$$d_k^i = d_k + \epsilon_k^{0,i} \text{ and } i = 1, 2, \dots, N_e \quad (4.46)$$

The observations (perturbed) can then be stored in the columns of the matrix as

$$D_k = (d_k^1, d_k^2, \dots, d_k^{N_e}) \in R^{m_k \times N_e} \quad (4.47)$$

The ensemble of perturbed observations can then be represented as,

$$E_k = (\epsilon_k^{0,1}, \epsilon_k^{0,2}, \dots, \epsilon_k^{0,N_e}) \quad (4.48)$$

The ensemble error covariance matrix of the observations can be expressed as,

$$C_{d_k} = \frac{E_k E_k^T}{N_e - 1} \quad (4.49)$$

EnKF is a sequential simulation with a Kriging update (refer to chapter 2), and it is based on a variance minimising scheme.

Hence, applying the Kriging update, we arrive at the equation below,

$$y_k^{a,j} = y_k^{p,j} + K_k(d_{obs,k} + \epsilon_k^{0,j} - H_k y_k^{p,j}), j = 1, \dots, N_e$$

The ensemble Kalman gain is,

$$K_k = C_{y_k^p} H_k^T \left(H_k C_{y_k^p} H_k^T + C_{d_k} \right)^{-1}$$

(4.50)

where $C_{y_k^p}$ is the predicted state covariance matrix at time step k , T stands for the transpose of a matrix and C_{d_k} is the data error covariance matrix at time step k . The partial entries of the cross covariance for Eqn.(4.50) are calculated so as to avoid the computationally prohibitive calculation of the entire matrix, explained in the algorithm. K_k is referred to as the Kalman gain matrix and is defined later. H_k (a matrix of 0's and 1's) is the operator that picks observation from the well locations in the ensemble states, at time step k , where measurements are being assimilated, and it gives the inference between the state vector and the observation vector . Also $d_{obs,k}$ is defined as the observation data at the present/ current time step. $\epsilon_k^{0,j}$ is the observation error.

4.5 Applicability of EnKF to the Reservoir History Matching process

The attractive nature of the EnKF is that it provides an ideal setting for the prediction and updating of reservoir simulation models in real time. There is an improvement in the model parameters each time new, and online data are assimilated. Future prediction of the production from the reservoir model is possible because the analysed ensemble is conditioned on the previous data of the reservoir model (Evensen, 2009).

There are three steps for the history matching of reservoir models using the EnKF, namely

- 1) Parametrisation: Uncertain parameters are identified, and a model solution certainty are identified
- 2) Prior model error selection: A prior error model is selected and specified for the parameters chosen which are based on the initial analysis(uncertain)
- 3) Solution method: The last step is the selection of a solution method

4.5.1 Parametrization

In the traditional history matching procedure, there are only a selected number of parameters that are chosen for the history matching process. These restricted sets of parameters are used for the optimisation process. These parameters are selected from

among a host of others based on their sensitivity and how much effects it causes in the objective function of choice. Selection of the relevant parameters (that is parameter estimation) has three significant steps which are

- i. Mathematical model construction: The various mathematical models as being fully described in chapter 5 and they include Darcy's law, the equation of state, mass conservation law, capillary pressure and relative permeability relationships.
- ii. Objective function: It computes the discrepancy between the data and the simulator response for a set of parameters.
- iii. Optimisation (choosing a minimisation algorithm)

The primary parameters that affect the history matching process are

- a) Porosity (φ): This has the capacity of modifying the estimated oil initially in place (OIIP) and hence affecting the initial material balance of the reservoir model. This parameter was history matched in this work
- b) Permeability(K_h): The flow of fluid through the porous media and the water breakthrough is affected by this parameter. This parameter was history matched in this work
- c) Water-oil contact(WOC); The volume of oil is determined from the boundary of the oil and water, and also the location of the optimal length of a horizontal producing well is also influenced by the WOC
- d) Gas-oil contact(GOC)
- e) Vertical transmissibility: This parameter affects the vertical communication in the reservoir.
- f) Fault transmissibility: This parameter was kept constant in this work.

The state vector is updated by the EnKF contains both static variable and dynamic variables. Static variables consist of geological data, core data, 3D seismic data, and logs. Dynamic data (historical data) consists of well test data, time-lapse (4D seismic data) production data (oil, water, BHP and flow rate.)

The ensemble EnKF state vectors can be represented as follows

$$\begin{array}{ccc}
 \text{Update} & \text{Forecast} & \text{Covariances} \\
 \left(\begin{array}{c} \varphi \\ K_h \\ P \\ S_W \\ WOC \\ multz \end{array} \right)_j = \left(\begin{array}{c} \varphi \\ K_h \\ P \\ S_W \\ WOC \\ multz \end{array} \right)_j + \sum_i a_i \left(\begin{array}{c} C(\varphi, d_i) \\ C(K_h, d_i) \\ C(P, d_i) \\ C(S_W, d_i) \\ C(WOC, d_i) \\ C(multz, d_i) \end{array} \right)
 \end{array} \quad (4.51)$$

The covariance occurs between updated variable and predicted measurements. The variable a_i denotes the impact and effect each ensemble member will have on the updated ensemble.

Prior error models give a clear understanding of the uncertainty of the initial analysis of the parameters chosen. These uncertainties are then presented as probability density function (pdf). These uncertain parameters have a standard deviation reflecting the spread in uncertainty and a mean that is equal to the best estimate.

4.5.2 Measurement error model

In the ensemble analysis, it will be noticed that the prior realisations would become closer and closer to the observations example production data and hence decrease the ensemble spread. The errors of the production measurement are drawn from a Gaussian distribution that has a zero value for the mean and standard deviations of the actual measurement value. Appropriate filters are required to remove the possible data outliers.

4.5.3 Induced Errors

They are four sources of uncertainty in reservoir performance forecasting which are:

- i. Model characterisation
- ii. Scaling
- iii. Mathematical
- iv. Data quality

Traditional history matching updates static parameters such as permeability and porosities and then updates it until the match is reached by rerunning the model in an iterative loop. Traditional history matching searches the minimum of the cost function which solves for the mode of the posterior pdf. The EnKF, on the other hand, solves for the mean of the pdf. This is because the mean is easier to estimate with a small amount of ensemble size. The difference between traditional history matching and EnKF based History matching is shown in Table 4.1

Table 4.1: Differences between Traditional based History Matching and EnKF based History matching

Traditional based History Matching (Gradient-based)	EnKF based History Matching
<ul style="list-style-type: none"> • Entire history production data are matched at the same time • Repeated flow simulations of the entire history • Time-consuming • Complicated gradient-based method coefficient sensitivity • CPU-intensive • Difficulty in assessing uncertainty • Repetition of the history matching process with different initial models • Not fully automated 	<ul style="list-style-type: none"> • Production data at the sequentially assigned time are required and matched only • Flow simulations continue from the last point of the simulation • Less time-consuming • CPU-friendly • Computations for multi-modal probability density functions for the first and second order moments becomes problematic in the course of the simulation • Low application for highly non-linear and non-Gaussian reservoir problems

Figure 4.3 depicts Traditional history matching model that uses the input data simultaneously and generates a single best-matched model.

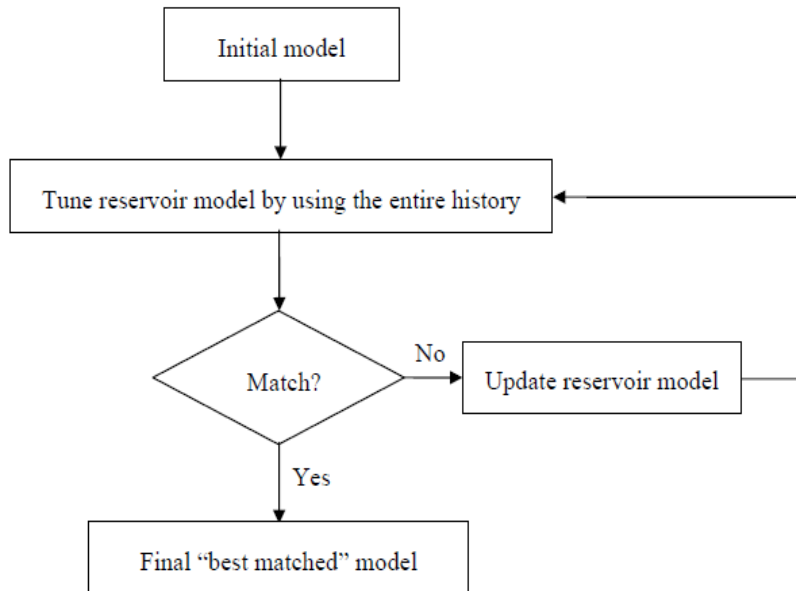


Figure 4.3: Traditional history matching model that uses the input data simultaneously and generates a single best-matched model.

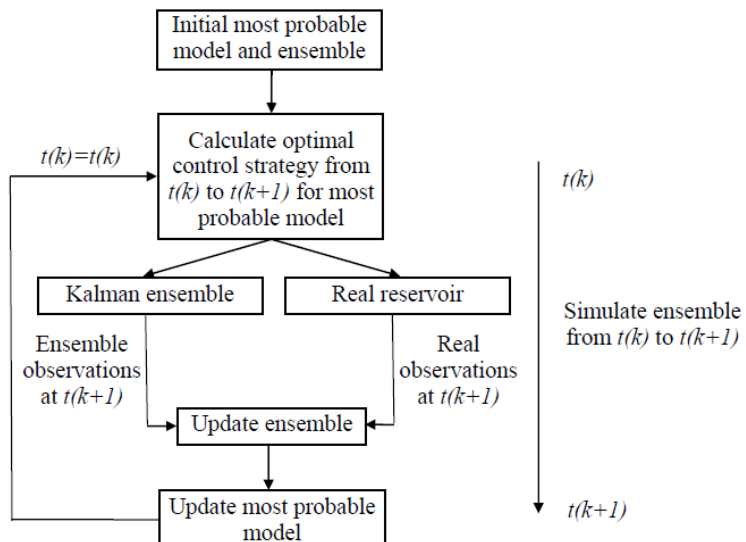


Figure 4.4: Workflow chart of the EnKF.

Bayesian concept description of the EnKF is shown in figure 4.5

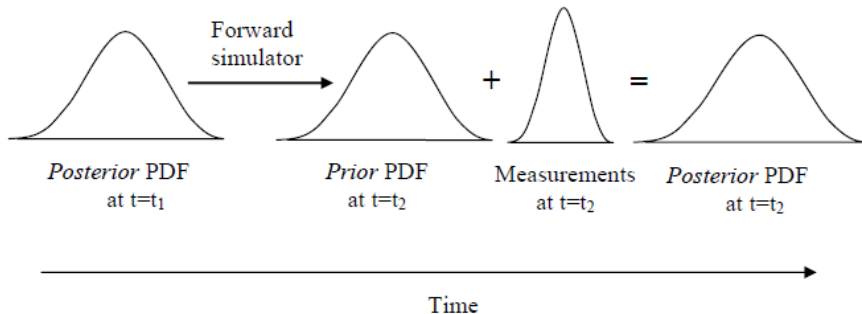


Figure 4.5: Bayesian concept description of the EnKF.

4.6. Ensemble square root filters

Ensemble square root filter (EnSRF) is a generic terminology for a set of ensemble-based implementations of the Kalman filter which do not require perturbing the observations during the data assimilation (Evensen, 1994). There is an extensive literature about square root filters in the oceanography and numerical weather prediction research areas. Similar to covariance inflation, these methods have rarely been used in reservoir history-matching applications. The primary motivation for these methods is to avoid additional sampling errors caused by the perturbed observation scheme used in the EnKF (Evensen, 2003).

4.7. Ensemble smoother

The ensemble smoother (ES) was previously introduced by van Leeuwen and Evensen (1996). In contrary to EnKF, ES does not assimilate data sequentially in time. Instead, ES calculates a global update by simultaneously assimilating all data available at once. Other than that this significant difference, ES formulation is similar to EnKF. Evensen and van Leeuwen compared ES and EnKF with Lorenz equations and concluded that EnKF outperforms ES simply because the recursive updates in the EnKF keep the ensemble of states “on track” and closer to the true solution.

Recently, Skjervheim et al. (2011) compared ES and EnKF and summarised that both methods gave similar results for the reservoir history-matching problems considered in their paper. The primary gain of ES is that it avoids restarts of the reservoir simulator making ES much easier to implement and faster than EnKF. The elimination of simulation restarts also makes ES an attractive option. Applying ES for reservoir history matching converts the parameter-state-estimation problem back to a parameter-

estimation problem. Thus, ES removes the parameter-state inconsistency issue observed in the sequential data assimilation with EnKF.

However, Reynolds et al. (2006) showed that EnKF is similar to applying, at each data assimilation time-step, a single Gauss-Newton iteration with a full step and the sensitivity matrix replaced by an average sensitivity matrix estimated from the ensemble. With ES, all data are assimilated simultaneously, which means that a single Gauss-Newton correction is applied to condition the ensemble to all data available. Hence, ES may not be able to provide acceptable data matches when applied to reservoir history-matching problems

From Equation 4.23, re-writing here again,

$$\bar{m} = m_{prior} + C_M G^T (G C_M G^T + C_D)^{-1} (d_{obs} - G(m_{prior})) \quad (4.52)$$

Where $m = \begin{Bmatrix} m_{static} \\ G(m) \end{Bmatrix}$

A Monte Carlo sampling is used to approximate the prior pdf. A set of N_e samples is created from the prior pdf, $m_j^{prior}, j = 1 \dots N_e$, we can then approximate the covariance matrix of samples. Bayesian concept description of the ES is shown in figure 4.6.

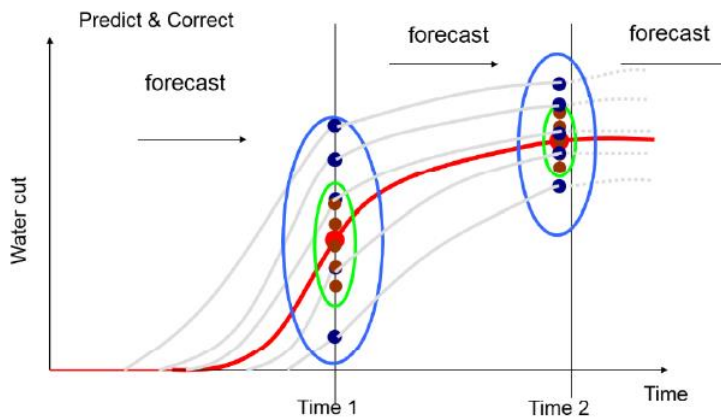


Figure 4.6: Bayesian concept description of the ES.

We derive the ensemble smoother to be an approximation to RML-Gauss-Newton equation with the full step where all the ensemble members are updated with the

same average sensitivity matrix Reynolds et al. (2006). The equivalence between ES and Gauss-Newton is shown below.

$$m_j^{\ell+1} = m_{uc,j} - C_M G_{\ell,j}^T (C_D + G_{\ell,j} C_m G_{\ell,j}^T)^{-1} \times (g(m_j^\ell) - d_{uc,j} - G_{0,j}(m_j^\ell - m_{uc,j})) \quad (4.53)$$

Doing a single iteration with $\ell = 0$ (initial guess), set $m_j^a \equiv m_j^1, m_j^f = m_{uc,j}$ and $d_j^f = g(m_{uc,j})$, then

$$m_j^a = m_j - C_M G_{0,j}^T (C_D + G_{0,j} C_m G_{0,j}^T)^{-1} \times (d_j^f - d_{uc,j}) \quad (4.54)$$

Assuming that $\overline{d^f} = d^f(\bar{m}^f) = g(\bar{m}^f)$, a first-order Taylor series expansion gives

$$d_j^f - \overline{d^f} = g(m_{uc,j}) - g(\bar{m}^f) = G(\bar{m}^f)(m_j^f - \bar{m}^f) \equiv \bar{G}(m_j^f - \bar{m}^f) \quad (4.55)$$

$$\begin{aligned} \tilde{C}_{MD}^f &= \frac{1}{N_e - 1} \sum_{j=1}^{N_e} (m_{uc,j} - \bar{m}^f) (d_j^f - \overline{d^f})^T \\ &= \frac{1}{N_e - 1} \sum_{j=1}^{N_e} (m_j^f - \bar{m}^f) (\bar{G}(m_j^f - \bar{m}^f))^T = C_M \bar{G}^T \end{aligned} \quad (4.56)$$

$$\begin{aligned} \tilde{C}_{DD}^f &= \frac{1}{N_e - 1} \sum_{j=1}^{N_e} (d_j^f - \overline{d^f}) (d_j^f - \overline{d^f})^T \\ &= \frac{1}{N_e - 1} \sum_{j=1}^{N_e} (\bar{G}(m_j^f - \bar{m}^f)) (\bar{G}(m_j^f - \bar{m}^f))^T = \bar{G} C_M \bar{G}^T \end{aligned} \quad (4.57)$$

Replacing $G_{0,j}$ by \bar{G} in equation 4.55 and using equation 4.55 and 4.56 gives the ensemble smoother equation

$$m_j^a = m_j^f + \tilde{C}_{MD}^f (\tilde{C}_{DD}^f + C_D)^{-1} \times (d_{uc,j} - d_j^f) \quad (4.58)$$

\tilde{C}_{MD}^f is the estimated covariance between the forecast models and forecast data and

\tilde{C}_{DD}^f is the autocovariance of predicted data.

Algorithm: ES

1. Generate an ensemble of realisations from the prior geological model

$$m_j^0 = m_j^f \text{ for } j = 1, 2, \dots, N_e$$

2. For $j = 1, 2, \dots, N_e$ sample $d_{uc,j}$ from $\mathcal{N}(d_{obs}, C_D)$

- a) For each member of the ensemble, perturb the observation vector using

$$d_{uc,j} = d_{obs} + C_D^{\frac{1}{2}} z_d, \text{ where } z_d \sim \mathcal{N}(0, I_{N_d})$$

- b) Update the ensemble using equation 4.58
-

In The ES, explicit computation of large covariances are avoided, it is reasonably robust and can be automated in workflows. ES is faster and easier to implement than the EnKF. It gives no inconsistency between the states and the static parameters. It is easily parallelizable. In matching the data, we can only adjust N_e coefficients (ensemble size). The initial ensemble is important. Moreover, there is a possibility of ensemble collapse particularly when the measurement error is low. Every time one perfect datum is assimilated, you lose one degree of freedom in the ensemble (Emerick & Reynolds, 2012). Covariance localization helps to ameliorate spurious correlations between the parameters and the measurements. These occur when using a small ensemble size.

4.8. Ensemble Smoother Multiple Data Assimilation (ES-MDA)

The ES-MDA was proposed by Emerick & Reynolds (2013), and it is motivated by the analogy of the ES/EnKF with a single iteration of Gauss-newton iteration (Emerick & Reynolds, 2013) and the need to provide some form of regularisation and damping at early iteration. It avoids statistical inconsistencies between updated models parameters and states that are a common occurrence with EnKF. In ES-MDA we assimilate the same data multiple times with an inflated covariance C_D .

Let m denote the petro physical properties to be estimated, G the reservoir simulator, d^0 a dimensional vector that contains all the true measurements in a certain time interval, containing measurements errors with zero mean and covariance C_D , N_e is the number of realisations in the ensemble; The parameter update/assimilation step is carried out as,

$$m_j^a = m_j^f + \tilde{C}_{MD}^f (\tilde{C}_{DD}^f + \gamma^i C_D)^{-1} \times (d_{uc,j} - d_j^f) \quad (4.59)$$

γ^i is the data error covariance inflation factor at the i^{th} data assimilation iteration and is selected a priori before the history matching loop. The simplest choice of γ is $\gamma^i = N_a$, for all iteration times where N_a is the data assimilation times. In this work, we use equal value of γ for

$$\sum_{i=1}^{N_a} \frac{1}{\gamma^i} = 1 \quad (4.60)$$

The condition in equation 4.60 ensures than single and multiple data assimilations are equivalent to the linear-Gaussian case. The ES-MDA samples correctly the linear-Gaussian case (Emerick & Reynolds, 2012).

Algorithm: ES-MDA

3. Choose the number of data assimilations, N_a and the coefficients γ^i for $i = 1, 2, \dots, N_a$
 4. For $i = 1$ to N_a
 - c) Run the ensemble from time zero
 - d) For each member of the ensemble, perturb the observation vector using $d_{uc,j} = d_{obs} + \sqrt{\gamma^i} C_D^{\frac{1}{2}} z_d$, where $z_d \sim \mathcal{N}(0, I_{N_d})$
 - e) Update the ensemble using equation 4.59
- end(for)
-

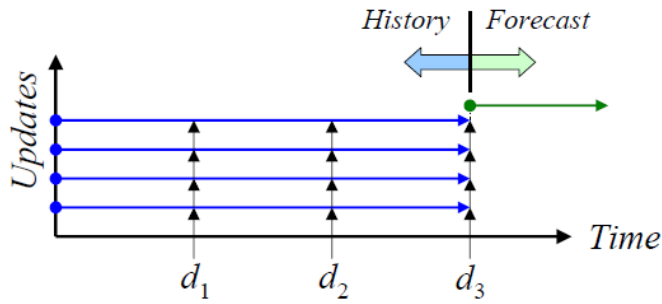


Figure 4.7: Schematic showing the description of the ES-MDA.

\tilde{C}_{MD}^f and \tilde{C}_{DD}^f are calculated from the updated ensemble at each iteration.

Conclusion on chapter 4

- We have discussed the various taxonomy in the field of inverse problem
- Solution to the inverse problems such as the classical and the stochastic methods was fully described
- The Stochastic Bayesian method for the solution to the inverse problem was fully endorsed owing to the uncertainty in subsurface reservoir evaluation.
- A logical flow beginning with the Kalman filter to the ensemble Kalman filter was discussed
- The ES-MDA has been put forward as a solution to the inconsistency between the updated static properties (permeability and porosity) and the updated dynamic reservoir properties (saturation and pressure) arising from the EnKF.

Chapter 5-4D Seismic and 3D Time-lapse Electromagnetic Data

5.1 Petro-Elastic Modelling

Petro elastic modelling (PEM), also known as a simulator to seismic modelling is a critical element of the time-lapse history matching and quantitative time-lapse seismic routines, linking seismic survey to the reservoir simulator. A PEM represented a set of elastic properties such as bulk and shear moduli assigned to each cell of a reservoir simulation model and obtained using associated fluid and rock properties. This makes PEM applicable for forwarding modelling of seismic properties using fluid conditions at a given time, effectively substituting composition of the reservoir fluids. It is well established that the quality and reliability of history matched reservoir simulation model is directly linked to the quality of the PEM. (Macbeth, et al., 2006)

5.1.1 Gassmann's equation

Being introduced in 1951, Gassmann's theory remains by far the main tool for petroelastic modelling allowing calculation of saturated bulk modulus as a function of porosity, bulk density, porous rock frame bulk modulus, rock matrix bulk modulus and fluid bulk modulus (Gassmann, 1951). Gassmann's theory assumes reservoir to be composed of an isotropic and homogeneous material with perfectly interconnected pore network. Due to the violation of the underlying assumptions, Gassmann's equation commonly fails to work in rocks with complicated rock mineralogy and in carbonate rocks. Carbonate rocks frequently possess multiple pore types with low pore connectivity causing problems for application of Gassmann's theory. Similar problems can be encountered when the equation is applied to a shale sand reservoir where pores are also poorly connected. (Smith et al., 2003):

The measure of resistance to uniform compression of a substance is referred to as the bulk modulus. The Gassmann equation allows for the calculation of, the resulting effective bulk modulus increase K_{sat} [Pa], of a rock saturated with a single fluid of modulus K_f , in terms of the dry frame bulk modulus K_d , the matrix bulk modulus K_m and porosity φ , G^* and G_d are the shear modulus of the wet and dry frame respectively

$$K_{sat} = K_d + \frac{\left(1 - \frac{K_d}{K_m}\right)^2}{\frac{\varphi}{K_f} + \frac{1-\varphi}{K_m} - \frac{K_d}{K_m^2}} ; G^* = G_d$$

(5.1)

The P and S wave velocities can be expressed as functions of bulk and shear modulus

$$V_P = \sqrt{\frac{K + \frac{4}{3}G}{\rho}} \quad V_S = \sqrt{\frac{G}{\rho}}$$

(5.2)

The effective fluid modulus for a mixture of fluids is given by:

$$\frac{1}{K_f} = \sum_i S_i / K_i , \rho_{sat} = \rho_{dry} + \varphi \sum_i S_i \rho_k ,$$

(5.3)

Where S_i and K_i refer to the fluid saturation and fluid modulus at time-step i . The density of the fluid saturated rock is: Where ρ_k is the fluid density at time-step k .

5.2 Introduction to Electromagnetic imaging of the earth

In nature, brine and sea water are good electrical conductors while the solid earth and hydrocarbons are poor electrical conductors (Dorn et al., 2007). In imaging conducting fluid, a plume found underground (for example the shape of the waterfront in a typical water flooding process) a practical way of achieving such is to make electromagnetic measurements between boreholes or between a borehole and surface arrays. The Ground Penetrating Radar (GPR) (Alumbaugh & Morrison, 1995) uses waves in the radio to microwave range of frequencies. GPR methods used in imaging conductivity employ high frequencies ($\geq 100MHz$) to have signals that propagate through the earth like a wave. At these frequencies, the depth of penetration is very shallow and no deeper than 5 meters into the Earth in dry soil, while the maximum depth of about 2 meters in wet soil as a result of high local wave attenuation. (Dorn et al., 2007)

Electromagnetic Induction Tomography (EMIT) has been investigated as a promising new tool for imaging conductivity variations in the earth (Alumbaugh & Morrison,

1995) having a depth of penetration greater than GPR. The source of this set up is a magnetic field that is generated by its currents flowing in the wire coils. This source is produced in one borehole, and the received signals are measured changes in the magnetic field found in another, distant borehole. The method is also feasible in combination with surface receivers and sources. The main tasks now are in the imaging of the electrical conductivity variations in the earth using diffusive waves (from about 1 to 20 kHz) and developing an inversion technique different from the GPR waves. A plethora of field techniques has been developed and applied to collect EM data, (Alumbaugh & Morrison, 1995) the algorithms needed for inverting the magnetic field data to produce the desired images of the electrical conductivity have not been up to date. The method used in the inversion is based on the work of Dorn et al. (2007) and the aim is to produce better images of the electrical conducting fluids (water saturation) in the reservoir by using dependable inversion techniques over great distances.

EMIT is more advantageous than other imaging techniques in that we can make use of existing wells in the play and the surface to do the imaging. There is also no need to make ground contact since the signals are received and transmitted inductively (no need for ground penetrating electrodes) making this technology non-invasive.

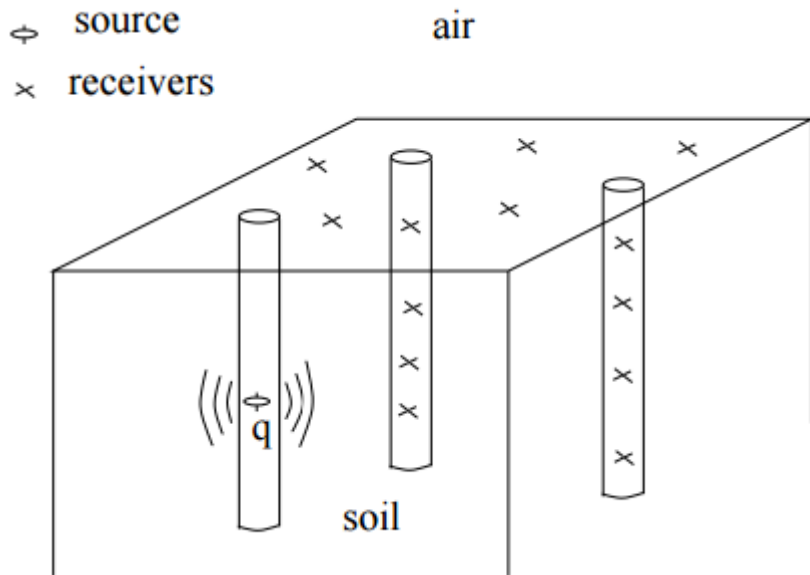


Figure 5.1: A 3D-EMIT experimental setup with a dipole transmitter, q adapted from (Dorn, et al., 2007)

The inversion method is done with an “adjoint technique”. A depiction of a single EMIT set up is shown in figure 5.1.

This technique allows the inverse problem to be solved approximately by using the same forward modelling code twice. In diffusive frequency ranges the problem of resolution comes into question. Our physical knowledge of resolution is based on the concept of *Rayleigh criterion* for resolving the power of an aperture whereby two-point source location of radiation is assumed to be resolvable if the maximum of a diffraction pattern that is found in one source coincides with the first minimum of the other(Dorn et al., 2007) . This spatial separation of the two objects depends on the ratio of the wavelength of the radiating sources to the size of the aperture. For diffusive frequencies the wavelength is not applicable, a better approach, in this case, is to define the *sensitivity functions*.

5.2.1 Sensitivities and the adjoint model

Sensitivity functions are concentrated in straight lines joining the source to the receiver, and the back projection occurs on these lines In EMIT the receivers and the sources are not located within the boundaries of the imaging domains, the propagating fields are vector fields giving us a rich variety of sensitivity function. The nonlinear *Kaczmarz-type approach* (or the ‘single-step adjoint-field inversion method’) is used for solving the inversion problem(Dorn et al., 2007) . This method is an iterative technique, and it applies successive corrections to an initial guess for the distribution of the parameter. Each correction is calculated by ‘back projecting’ a filtered part of the residuals along straight hose lines into the domain (imaging) corresponding to the incoming direction of the waves. An adjoint technique is used for calculating the sensitivities(Dorn et al., 2007) .

The sensitivity functions are related to Frechet derivatives defined on some reference parameter. They show how the receiver measurements change if we slightly perturb the reference parameter distribution at specific position found in the medium. The Frechet derivative is also a Jacobian matrix of the underlying forward operator, and the sensitivity functions are rows or columns of the Jacobian matrix

5.2.2 Maxwell’s equation for anisotropic media

$$\nabla \times H(x) - (i\omega\epsilon(x) + \sigma(x))E(x) = J(x) \quad (5.4)$$

$$\nabla \times E(x) + i\omega\mu(x)H(x) = M(x) \quad (5.5)$$

$$\nabla \cdot \epsilon E(x) = 0, \nabla \cdot \mu H(x) = 0 \quad (5.6)$$

$E(x)$ =electric field, $H(x)$ =magnetic field, $J(x)$ =electric source current,
 $M(x)$ =magnetic source current, $\omega = 2\pi f$ is the angular frequency, $i = \sqrt{-1}$

$\sigma(x)$ =electrical conductivity in Siemens per meter(S/m), $\epsilon(x)$ =dielectric permittivity in Farad per metre (F/m) and $\mu(x)$ =magnetic permeability in Henry per metre (H/m)

For anisotropic media, we will have,

$$\nabla \times H(x) - b(x)E(x) = J(x) \quad (5.7)$$

$$\nabla \times E(x) + a(x)H(x) = M(x) \quad (5.8)$$

$$a = i\omega\mu, b = i\omega\epsilon + \sigma \quad (5.9)$$

In another form,

$$q(x, t) = q(x)e^{i\omega t} = \begin{pmatrix} J(x) \\ M(x) \end{pmatrix} e^{i\omega t} \quad (5.10)$$

Eqn.5.7. and Eqn.5.8 provide a model for the propagation of the electric field and the magnetic field that is emitted by the source q , and that we can measure the magnetic field $H(d_n)$ for the N discrete detector positions $d_n, n=1, \dots, N$.

In most geophysical applications the coefficient a in Eqn. 5.8 varies less significantly in the region of interest. In this work, we assume that a is known in the whole reservoir domain. The coefficient b is assumed to be unknown in the medium and is going to be recovered from the data.

The inverse problem is as follows, assuming for many source distributions $q_j = (J_j M_j)^T$, $j=1,...p$, the corresponding magnetic fields $H_j(d_n)$ measured at the receiver locations ,we will find a parameter distribution \vec{b} such that for the solution of $(\vec{E}_j, \vec{H}_j)^T$ of ,

$$\nabla \times \vec{H}_j - b \vec{E}_j = J_j \quad (5.11)$$

$$\nabla \times \vec{E}_j + a \vec{H}_j = M_j \quad (5.12)$$

The magnetic field values found at the receiver position coincide with the data.

Conclusion on chapter 5

- In this chapter, we have described the extra source of data usually integrated into the reservoir modelling calibration
- Gassman fluid substitution method for computing acoustic impedance required in our novel seismic history matching approach has been described
- Electromagnetic data inversion to conductivity has also been described which will be used in the novel history matching scheme incorporating electromagnetics

Chapter 6 – Parametrisation Techniques

6.1 Introduction to the Level-set Method

The level set methods are techniques used for computing moving boundaries in a variety of settings (Osher & Fedkiw, 2003). The level set methods employ dynamics to the implicit surfaces where a function can be defined regarding its zero iso-contours known as τ where

$$\tau = \{x \in \mathbb{R}^n | f(x) = 0\} \quad (6.1)$$

A typical example of such is a circle of a given radius separating two domains in the two-dimensional space shown in figure 6.1. The implicit surface is defined as a function $\varphi(x)$ such that everything inside the circle negative and everything outside the circle is positive, implicitly defining two subdomains, Ω^+ and Ω^-

The level set methodology is briefly described here. More information on the procedure can be found in (Osher & Fedkiw, 2003). We assume τ to be a closed curve found in a domain Ω partitioned into two regions namely, D^c and D where D^c is the complement of D represented as $\frac{\Omega}{D}$

We define the function ϕ which satisfies the following properties as,

$$\phi(x) > 0 \text{ for } x \in D \quad (6.2)$$

$$\phi(x) < 0 \text{ for } x \in D^c \quad (6.3)$$

$$\phi(x) = 0 \text{ for } x \in \tau \quad (6.4)$$

Where τ is the zero level set of the function ϕ . The unit normal n to the surface is given by,

$$n = \frac{\nabla \phi}{|\nabla \phi|}$$

The level set method has been used in tracking simulating and modelling the motion of dynamic interfaces (Moreno & Aanonsen, 2008). The velocity field v determines this motion of the surface and is a function of position. The evolution of the surface is mathematically described as,

$$\frac{\partial \phi}{\partial t} + v \cdot \nabla \phi = 0, \phi(x, 0) = \phi_0(x) \quad (6.6)$$

$\phi_0(x)$ is the initial level set function, t is the artificial time. Rewriting equation (above) using the normal velocity v_n we arrive at a new expression,

$$\frac{\partial \phi}{\partial t} + v_n \cdot \nabla \phi = 0, \phi(x, 0) = \phi_0(x) \quad (6.7)$$

$$v_n = v \cdot \frac{\nabla \phi}{|\nabla \phi|} \quad (6.8)$$

A solution of equation 6.7 is known as the level set equation, solution of this equation over time describes the evolution of the interface. In Villegas et, al.,(2008) the level set function was used in adjoint inverse problems dealing with shape reconstruction (Villegas, et al., 2005). In that work, they described an objective function first and then used a gradient method to determine the velocity of the evolving boundary in such a way that the objective function was reduced sequentially. In this work, the level set function will be used to represent the parameter fields (permeability and porosity fields) in the EnKF/ES-MDA history match procedure.

For a given reservoir having just two facies, the parameter field can be written as,

$$p(x) = p_1 H(\phi(x)) + p_2 (1 - H(\phi(x))) \quad (6.9)$$

Where,

$$H(\phi(x)) = \begin{cases} 1, & \phi(x) > 0 \\ 0, & \phi(x) \leq 0 \end{cases} \quad (6.10)$$

$$H(\phi(x)) = \begin{cases} 1, & \phi(x) > 0 \\ 0, & \phi(x) \leq 0 \end{cases} \quad (6.11)$$

H is known as the Heaviside function and p_1 and p_2 are the facies parameter values.

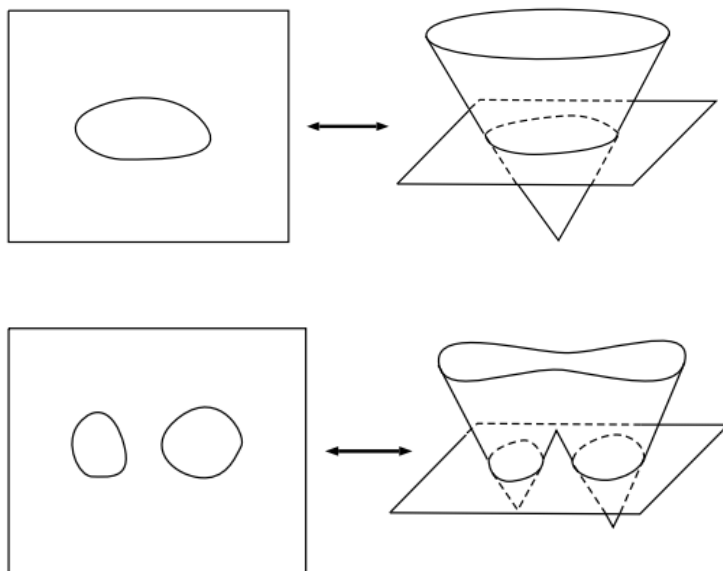


Figure 6.1: Implicit representation of the level-set function

6.2 Sparse Coding/Machine Learning

Sparse coding can be described as the process of computing the representation coefficients, X , based on the given signal Y and the dictionary D . This process, commonly referred to as atom “decomposition”, requires solving which is typically done by a “pursuit algorithm” that finds an approximate solution, as a unique determination of sparsest representations proves to be an NP-hard problem (Aharon, et al., 2006). In this section, several such algorithms and their prospects for success are described. Sparse coding is an essential tool in designing dictionaries, hence it is essential to have a good overview of methods for achieving it. The most straightforward pursuit algorithms are the Matching Pursuit (MP), Orthogonal Matching Pursuit (OMP) (Tropp & Gilbert, 2007). These are referred to as greedy algorithms that select the dictionary atoms sequentially. These methods are very

simple, involving the computation of inner products between the signal and the dictionary atoms, and possibly deploying some least squares solvers or projections

6.2.1 Orthogonal Matching Pursuit

For an estimate of sparsity T_0 for a field that is represented by a vector of weights \mathcal{X} in a d-dimensional space, the OMP algorithm attempts to recover the signal \mathcal{Y} by using a linear combination of T_0 basis atoms(basis elements) from an over complete dictionary D . The dictionary being a collection of basis represents a particular domain unique to a signal representation and can be modified to suit a particular problem (Aharon, et al., 2006). The OMP algorithm then solves the optimization problem.

$$\min_{\mathcal{X}} \|\mathcal{X}\|_0 \text{ subject to } \|\mathcal{Y} - D\mathcal{X}\|_2 < \eta \quad (6.12)$$

It solves this optimisation problem by projecting the data iteratively onto a dictionary and then finding a set of basis elements that are correlated the most with the residuals. $\|\mathcal{X}\|_0$ is the ℓ_0 -norm and it represents the signal sparsity level \mathcal{X} . η is the error tolerance.

The OMP algorithm initial inputs are the estimates of sparsity T_0 for the sparse- signal \mathcal{X} , the dictionary D of rank $N_y \times d$ with d being the same as the size of the row of the sparse coefficients in the ensemble N_e and the N_y -dimensional data vectors. The idea in OMP is in constructing an approximation to the signal \mathcal{Y} (the spatial permeability/porosity field) by undergoing an iteration process. During each iteration, the local optimum of the solution is computed. This technique is calculated by finding the column vectors in D (the over-complete K-SVD learned dictionary) which closely matches a residual vector indicated as r . The reader may refer to Tropp & Gilbert, (2007) for further information. In this work, OMP is used to enforce a sparse representation of the unknown spatial permeability and porosity field to make the inverse problem less ill-posed.

Algorithm: Orthogonal Matching Pursuit(OMP) Algorithm

- Input: Dictionary D , data vector(spatial permeability ensemble) \mathcal{Y} , error threshold η , an estimate of sparsity T_0
- Initialization : Set $x_0 = 0, r_0 = \mathcal{Y}, t = 0 \Delta_0 = 0$
- Do while $\|r_{t-1}\|_2 < \eta$
 - a) Define the index of the basis elements with the least deviation from the residual

$$\lambda_t = \arg \max_{j=1..d} |\langle r_{t-1}, D_j \rangle| \quad (D_j \text{ are the row vectors of } D)$$

b) Next, augment the index set as,

$$\Delta_t = \Delta_{t-1} \cup \lambda_t$$

c) Compute,

$$x_t = \underset{x}{\operatorname{argmin}} \| \mathcal{Y} - D\Delta_t x \|_2$$

Where x_t is our required sparse permeability field

d) Compute the new residual as,

$$r_t = \mathcal{Y} - D\Delta_t x_t$$

- Set $t = t + 1$
- End do
- Print: Index set Δ_t , Sparse final solution x_t and residual r_t

6.2.2 K-SVD Algorithm

A key criterion of sparse coding is the identification of a basis (domain) in which the field or signal under consideration can be modelled as sparse. A sparse domain describes one whereby any signal located in that domain can be adequately

represented by a linear combination requiring a few basis elements (Candes, et al., 2006) . The Wavelets (Jafarpour, 2011) and the Discrete Cosine Transform (DCT) (Jafarpour & McLaughlin, 2007) are examples of such sparse domains. In this work, we construct a sparse domain that is suited for inverse problems in reservoir engineering (history matching). Such algorithms modified for history matching are known as *dictionary learning algorithms* (Elsheikh, et al., 2013). For a set of training signals Y of size N_y (which is also the dimension of our unknown permeability field) the dictionary learning algorithm finds the basis elements necessary to construct a dictionary D whereby its sparse linear combinations represents each of the vector space found in the training set of signals Y . The corresponding weights of the signals are given as X and are calculated by solving the optimisation problem,

$$\{X, D\} = \arg \min_{X, D} \sum_{i=1}^{N_y} \|Y_i - DX_i\|_2^2 + \gamma \|X_i\|_1 \quad (6.13)$$

$$\|D_i\|_2^2 \leq 1, \quad \forall i = 1, \dots, N_y \quad (6.14)$$

X_i and Y_i are the individual training signals and coefficient vectors in X and Y respectively D_i are the atoms of the dictionary D which penalizes the ℓ_1 – norm of X_i . This is a difficult non-convex problem to solve, even in an approximate manner (Elsheikh, et al., 2013).

A computationally feasible dictionary learning algorithm that can solve equation (6.13) is the K-SVD algorithm. The KSVD is NP-hard (level of computational complexity, i.e. *non-deterministic polynomial time*), and it solves the ℓ_0 – norm equivalent of the problem enumerated in equation (6.13) by using a repetitive two-step approach (Aharon, et al., 2006) .The two steps are the sparse coding stage for updating the coefficient of the matrix X_i making use of any pursuit algorithm(a sparsity inducing method), next, we update each column of the dictionary elements D in a sequential order by changing the values of the coefficient column. These second procedure freezes X_i concurrently finding a better D . This is done to represent the signal Y_i

(several permeability/porosity realizations generated from our geostatistical software).

For further studies on the K-SVD, the reader may refer, to (Aharon et al., 2006) . A brief algorithm of the procedure is shown below

Algorithm: K-SVD Dictionary learning

Initialisation: Set the normalised dictionary matrix(randomised)

$D^{(0)} \in \mathbb{R}^{N_y \times d}, T_0 = sparsity\ level$

Set iteration count $q = 1$

Repeat computation until convergence,

Stage 1: Sparse coding stage, Compute X_i for $i = 1, \dots, N_y$

$$\min_x \|y_i - Dx\|_2^2 \text{ subject to } \|x\|_0 \leq T_0$$

Stage 2: Codebook(Dictionary)Update stage, For $k = 1, 2, \dots, d$

- We define those groups of codewords that use \mathcal{D}_k ,

$$w_k = \{i | 1 \leq i \leq N_y, x_i(k) \neq 0\}$$

- Compute

$$E_k = Y - \sum_{j \neq k}^n d_j x^q$$

- Obtain E_k^R by choosing the specific columns which corresponds to those elements that initially used d_k in their representation
- Apply the SVD decomposition computation on $E_k^R = U \Delta V^T$
- Update $d_k = u_1, x_R^k = \Delta(1,1). v_1$

Set iteration count $q = q + 1$

In this work, the K-SVD is used to generate the dictionary D used to transform the permeability and porosity field from a spatial domain to a sparse domain and back. The creation of the over complete dictionary is done off-line and once before the commencement of history matching with the EnKF/ES-MDA. A schematic showing the implementation of the K-SVD.

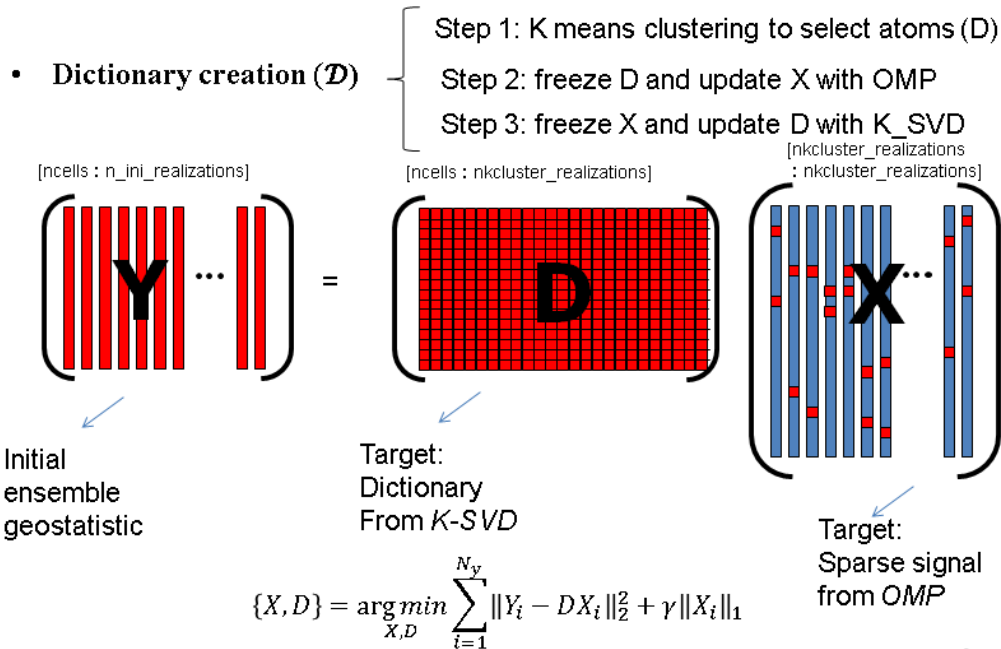


Figure 6.2: Schematic showing the K-SVD algorithm

6.3 Discrete Cosine Transform (DCT)

The two-dimensional forward DCT of an image $u(n_{xy})$ can be described as;

$$v(\Theta, \omega) = \frac{\alpha(\Theta)\alpha(\omega)}{\sqrt{N_x N_y}} \sum_{m=0}^{N_x-1} \sum_{n=0}^{N_y-1} u(n_x n_y) \cos \left[\frac{\pi(2n_x + 1)\Theta}{2N_x} \right] \cos \left[\frac{\pi(2n_y + 1)\omega}{2N_y} \right] \quad (6.15)$$

$$\alpha(j) \equiv \begin{cases} \frac{1}{\sqrt{2}} & j = 0 \\ 1 & otherwise \end{cases}$$

Where $\Theta = 0, \dots, N_x - 1$ and $\omega = 0, \dots, N_y - 1$.

Similarly, the inverse two-dimensional DCT transform is then derived as

$$\begin{aligned}
& u(n_x, n_y) \\
&= \frac{2}{\sqrt{N_x N_y}} \sum_{\theta=0}^{N_x-1} \sum_{\omega=0}^{N_y-1} \alpha(\theta) \alpha(\omega) v(\theta, \omega) \cos \left[\frac{\pi(2n_x + 1)\theta}{2N_x} \right] \cos \left[\frac{\pi(2n_y + 1)\omega}{2N_y} \right]
\end{aligned} \tag{6.16}$$

Where $n_x = 0, \dots, N_x - 1$ and $n_y = 0, \dots, N_y - 1$

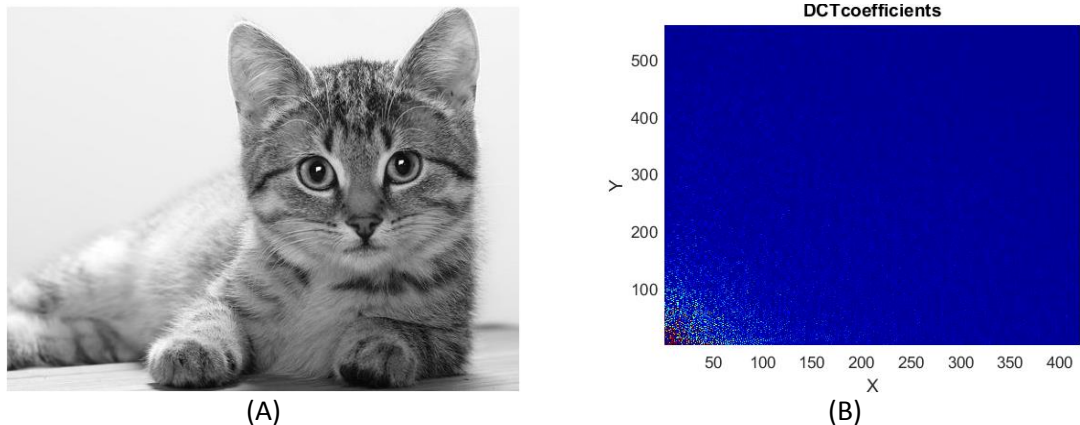


Figure 6.3: Illustration of the DCT algorithm implemented in a picture. (A) True image of the reference picture, and (B) Corresponding DCT cosine basis of the picture

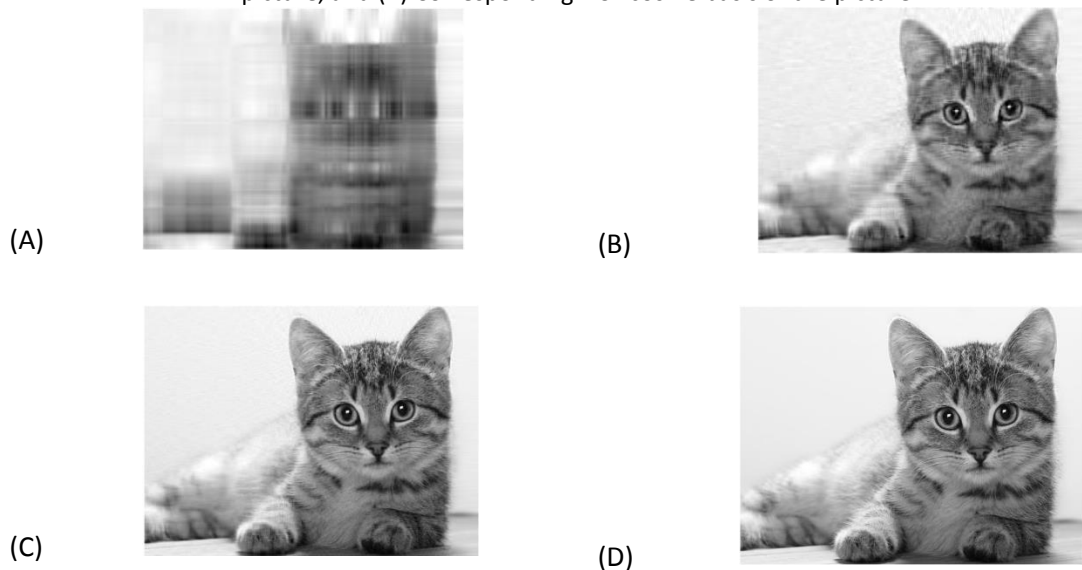


Figure 6.4: Reconstruction of the original image is retaining a certain level of the DCT cosine basis. (A) DCT image reconstruction at 0.2%, (B) DCT image reconstruction at 1%, (C) DCT image reconstruction at 2.5% and (D) DCT image reconstruction at 4.2%

Figure 6.3 shows an illustration of the DCT algorithm implemented in a picture. (A) True image of the reference picture, and (B) Corresponding DCT cosine basis of the

PhD Thesis

picture. Figure 6.4 shows reconstruction of the original image in figure 6.5 retaining a certain level of the DCT cosine basis. (A) DCT image reconstruction at 0.2%,(B) DCT image reconstruction at 1%,(C) DCT image reconstruction at 2.5% and (D) DCT image reconstruction at 4.2%

Conclusion of chapter six

- In this chapter, sparse parametrisation techniques required to alleviate model ill-posedness during the inverse problem parameter estimation stage has been discussed.
- Unsupervised machine learning techniques have been described which are vital for our novel **SELE** history matching technique

Chapter 7 – Methodology & Numerical Experiments

In this chapter, the developed ideas during this thesis would be implemented to 4 synthetic reservoir models. The fluid flow through these synthetic models (forward problem) would first be described and their corresponding novel approaches for parameter estimation (inverse problem) would be described after that.

7.1 Synthetic Reservoir Models and computer specification

In this thesis, four synthetic reservoir models are utilised to test the developed ideas.

The Synthetic models are;

- The Channelized SPE-10 model
- The Gaussian sandstone Model
- The Natural fractured dual permeability- porosity model
- The PUNQ-S3 model

7.1.1 Channelized Synthetic model-SPE 10

The channelised synthetic SPE-10 model (Christie & Blunt., 2001) is built on a mesh with grid blocks in principal axes as $Nx = 120$, $Ny = 60$, $Nz = 5$, based on the SPE10 model as shown in figure 7.1, having four injector wells and four producer wells (8 wells in total) as shown in figure 7.1 . Each gridblock is $30m \times 30m \times 60m$ in the x, y and z directions, respectively. The reservoir has a thickness of 100m and is located at a depth of 2,680m. The producer is controlled by the BHP constraint of 100 bars. The injectors are controlled individually by the injector rate of 10,000 to 5,000 Sm³/day, towards the end of the 10 years history period.

This is done to avoid early water breakthrough in the producer well, boost the reservoir pressure required for a cost-effective drawdown and also to sustain an oil production plateau for the duration of time. The simulation lasts for 3,600 days, and the injection starts on the first day. The commercial ECLIPSE 100 reservoir simulator (Schlumberger GeoQuest, 2014) is used for reservoir simulation. The observation data includes production data: oil production rate of the four producers, water cut of the four producers, and the BHP of the four injector wells. The permeability and porosity distribution are highly correlated. The SPE 10 is a three-dimensional geostatistical realisation of the Jurassic Upper Brent sequence in the North Sea, namely the Upper Ness formation (Petterson *et al.*, 1990). The permeability tensor is a diagonal tensor,

where two of the horizontal components of permeability are equal ($k_x=k_y$) and the vertical component is assumed to be one-tenth that of the horizontal ($k_z=0.1k_x$). From Fig. 7.1, it is quite clear that the Upper Ness formation is characterised by large variations in permeability, with values covering 8 orders of magnitude, from $9e-4\text{mD}$ up to 20,000 mD (Fig. 7.1.). Similarly, the porosity values span four orders of magnitude, where roughly 4.1% of all cells are comprised of porosity values of 0.001 (0.1%), and 0.14% of all cells are populated with the maximum porosity of 0.4 (40%). This variation in the permeability and porosity fields relates to the depositional environment of the reservoir, namely in rivers or delta-plain continental environments, which has lead to the creation of multiple sets of amalgamated sand bodies with good connectivity and large correlation lengths, imposed upon a background of low-permeability shales and coals (Christie & Blunt., 2001) (Fig.7.1).

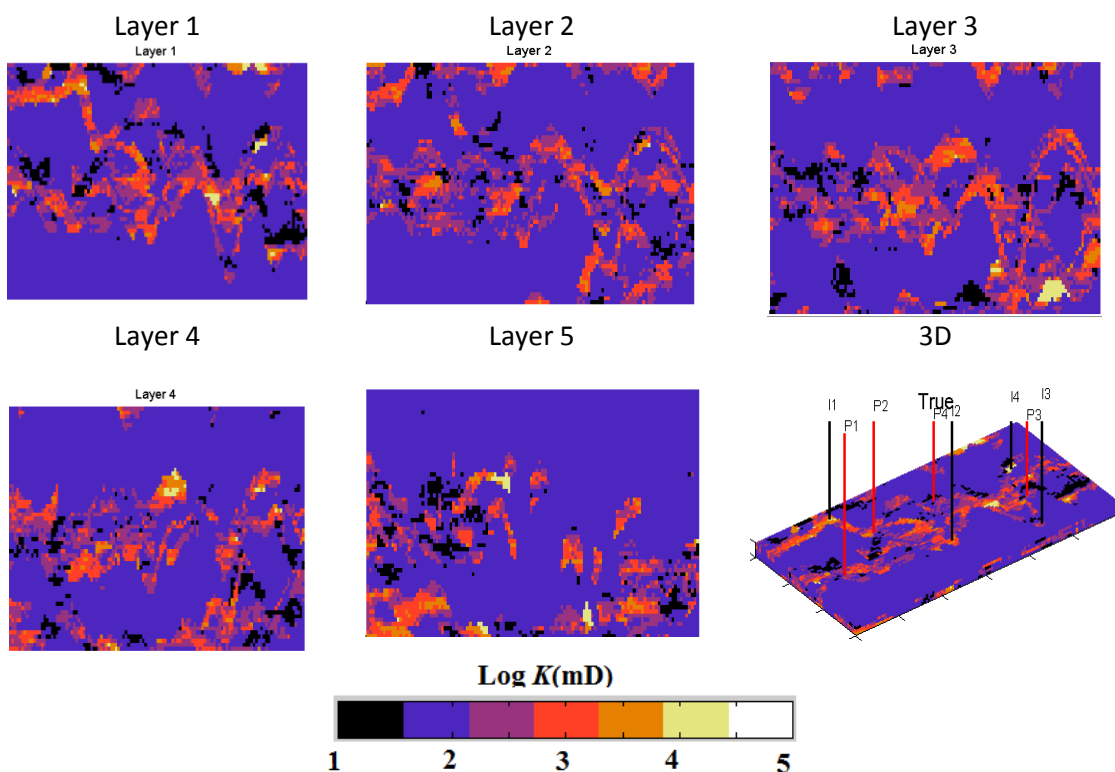


Figure 7.1(a): permeability map of the SPE 10 true model showing the 2D and 3D- 8 well configurations

The scatter plot of the horizontal permeability of each cell against its corresponding porosity (Figure 7.1(b)) suggests that there is a rudimentary relationship between the two petrophysical properties. Higher porosities will tend to correspond to higher

permeabilities, yet the statistical spread is significant, with a coefficient of determination (R^2) of 0.62 and a correlation coefficient of 0.29 (Fig. 7.1(b)). For porosities less than 20%, a single value can correspond to permeability values ranging between seven orders of magnitude, owing to the large heterogeneity of the domain.

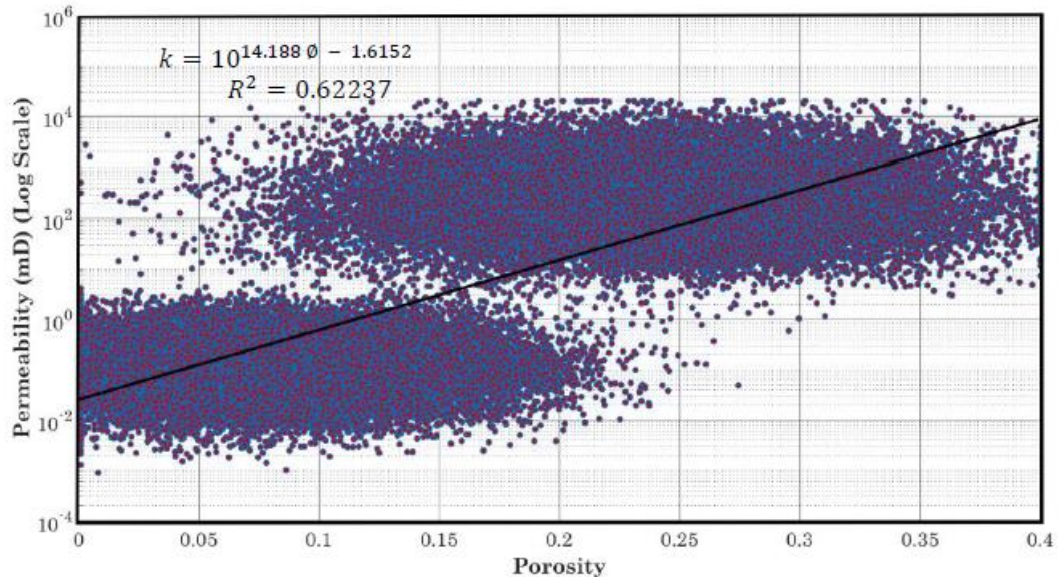


Figure 7.1(b): Scatter plot of log permeability against porosity for the fine-scale model.

7.1.2- Gaussian synthetic model

The next model we will consider is a ‘Gaussian looking’ synthetic model. This model is synthetic and is newly created for research purpose in the thesis. The model exhibits a non-Gaussian distribution of its absolute permeability field histogram but looks Gaussian by physical, visual inspection. The synthetic 3D reservoir model is a model built on a mesh with grid blocks in principal axes as $N_x = 84$, $N_y = 27$, $N_z = 4$, having one water injector well and one oil producer well and a single fault separating the reservoir into two parts (as shown in Figure 7.2). Each gridblock is 100 ft \times 100 ft \times 50 ft in the x, y and z directions, respectively. The synthetic reservoir has a thickness of 200 ft and is located at a depth of 4,000 ft (Figure 7.2). The producer well is controlled by the BHP constraint of 140 psia. Initial reservoir pressure is 4,000 psia at the top. The model is represented by a block of clastic deposits with dimensions of 84 \times 27 \times 4, intersected by a low-permeability straight fault with transmissibility multiplier of 0.745×10^{-3} . Each of the grid cells represents 50,000 ft³. For the purpose of petroelastic modelling, realistic rock mineralogy was assumed, with the fractions of quartz and feldspar being 0.6 and 0.4 respectively. The pore space of the reservoir is

saturated with a mixture of light oil of 38 API and saline brine (Demirbas, et al., 2008). The reservoir possesses uniformly distributed initial pressure of 4000 psi and saturation of 0.85. Reservoir temperature of 103°C was assumed to be constant throughout production period.

The injector well is controlled by the water injector rate of 15,000 to 10,000 STB/day towards the end of the seven years history period. This is done to discourage early water breakthrough in the producer well, boost the reservoir pressure required for a cost-effective drawdown and also to sustain an oil production plateau for the duration of time. The reservoir simulation lasts for 2,500 days, and the injection of water starts on the first day. The residual oil saturation is set to 0.2. The commercial ECLIPSE 100 reservoir simulator (Schlumberger GeoQuest, 2014) is used for reservoir simulation also. The observation data includes production data: oil production rate, water production rate of the producer well, and the BHP of the injector well. Facies type is observed at well locations.

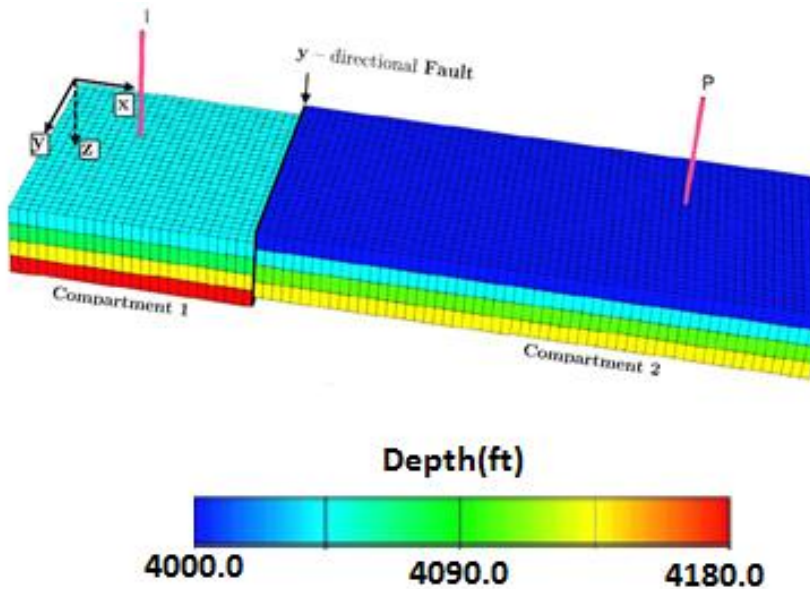


Figure 7.2: True reservoir synthetic model

The production data are assimilated at the given intervals (time steps) as specified in the reservoir forward simulation run. Pressure-production measurement errors are generated from a Gaussian distribution with mean equal to zero, and the standard deviation is given to about 1% of the actual measurement data. Facies observations are assumed to be noiseless. Figure 7.3a shows a 3D representation of our true permeability model. Figure 7.3b shows the corresponding 2D layer by layer map of the true permeability model.

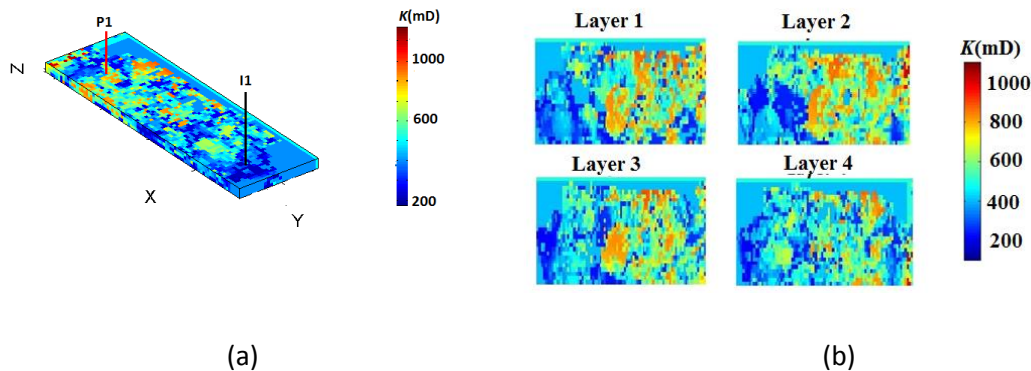


Figure 7.3: (a) 3D permeability field of the true Gaussian synthetic model showing the two well locations and (b) 2D permeability field of the true Gaussian synthetic model

7.1.3 Naturally fractured Model (NFR)

The modelling of an NFR-DP-DK (Dual porosity-Dual permeability) model is entirely different from a classical sandstone reservoir. In Naturally-fractured reservoirs (NFR) there is a considerable difference in the petrophysical properties such as porosity and permeability between the rock matrix and the fracture. The fracture poses a more significant influence in the fluid flow and production behaviour as a result of its high permeability distribution. In most cases, the fracture distribution and proportion are mostly unknown. A good estimation of the distribution of the fracture is vital in reservoir production optimisation. Most NFR formations are carbonate reservoirs and contain about 60% of the world's proven oil reserves (Carbonate Reservoirs, 2016). Naturally fractured reservoirs consist of vugs, matrix blocks and irregular fracture.

The matrix-fracture dynamic interaction mainly controls the rates of production from hydrocarbon reservoirs. The dual porosity/permeability model first introduced by (Barenblatt et al., 1960) describes a reservoir consisting of two interacting media which are the fracture and the matrix. Warren and Root (1963) presented a dual porosity model which assumed no cross flow between matrix to matrix, restricting flow to between the matrix and fracture. The concept of shape factor introduced by Barenblat et al. (1960) was introduced to simulate the matrix-fracture flow. An idealistic way of determining if a reservoir is fractured is from the well test. If the permeability value gotten from the well test is higher than that realised from cores, then we have an indication that the reservoir is fractured.

Four types of fractured reservoirs exist which are;

1. Fractures account for most of the reservoir permeability and porosity,
2. the matrix consists of low or no permeability with medium or low porosity with the fractures having permeability and providing the necessary flow capacity for the reservoir,
3. fractures assist permeability in a reservoir having moderate or high matrix permeability and porosity,
4. lastly, the fractures create a barrier to flow and do not contribute to the reservoir permeability or porosity.

In this work, model two is adopted, which implies the matrix having a moderate to high porosity with low permeability and the fracture having a low porosity with high permeability. The dual permeability/dual porosity model implies a fractured reservoir, having two overlapping media, fracture and matrix, with the exchange of fluid between them. This is depicted in figure 7.4

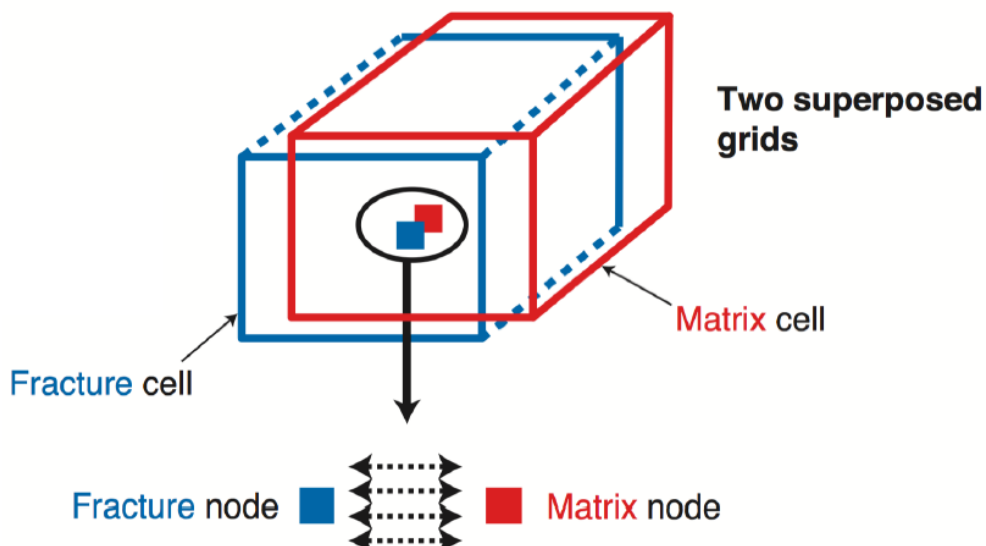


Figure 7.4: Dual Porosity concept, (Lemmonier & Bourbiaux, 2010)

To characterise the flow behaviour encountered in a fractured medium, Warren and Root (1963) discretised the solution domain to the fracture and the matrix. The authors proposed that the idealisation of the fractured medium consist of discrete volumetric parameters having primary porosity, co-joined by their secondary porosity, in a dependant directional way, as shown in figure 7.5

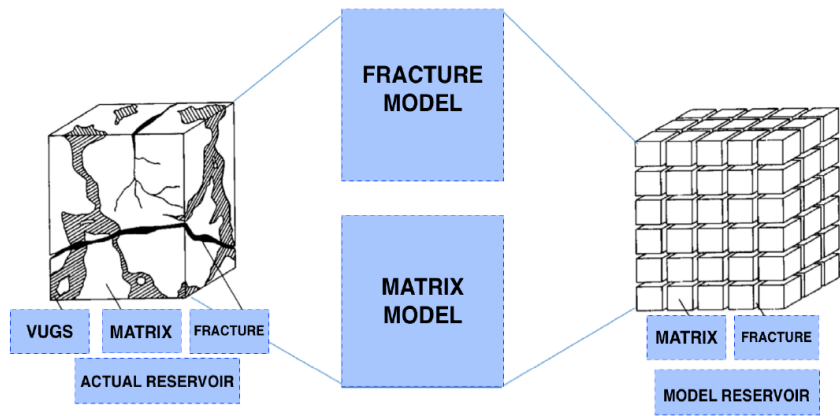


Figure 7.5: Idealization of the fractured reservoir, (Edited from Warren, J.E. & Root, P.J., 1963)

The approach is limited in its assumption of pseudo-steady-state flow and the lack of consideration of dual-permeability, implying no fluid transfer from matrix to the matrix (Elfeefi, 2014). To circumvent this problem an upscaling method approach referred to as shape factor was introduced to model the fluid transfer between the two porous regions. The theory of using the shape factor approach will be discussed in subsequent sections. The NFR model is synthetic and newly created for research purpose in the thesis.

A JPEG image of a realistic NFR outcrop shown in figure 7.6a is converted to a pixel continuous training image, figure 7.6b. This is then used as the training image model for the *FILTERSIM* algorithm

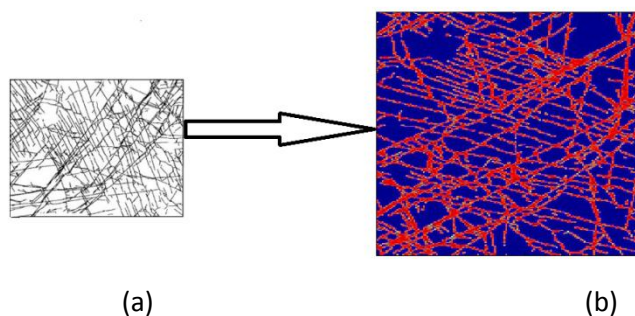


Figure 7.6: (a) Outcrop of the fractured reservoir (Odling E, 1997), (b) Pixel converted Training image (with a MATLAB code) used for the initial creation of permeability ensemble.

The 2D fracture model is shown in figure 7.7a with its corresponding 3D cartoon in figure 7.7(b).

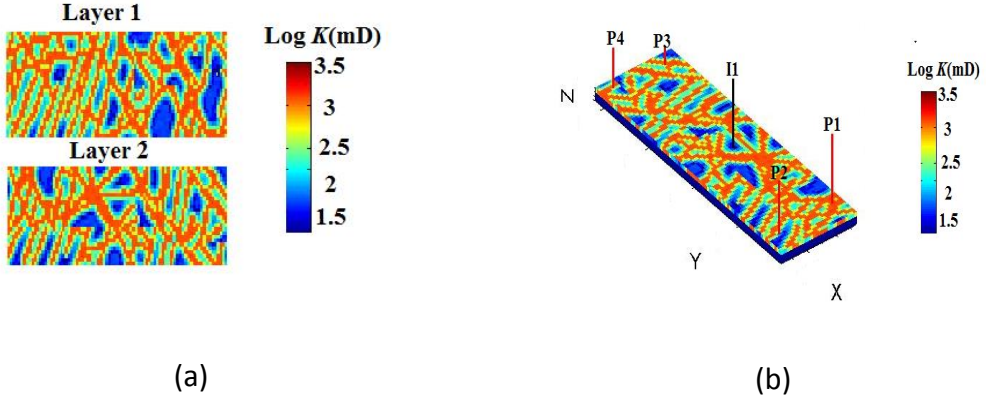


Figure 7.7: (a) True dual-permeability synthetic model (fracture model) used in this work:(b) 3D true dual-permeability synthetic model used in this work

We use the two-phase flow of oil and water in an NFR described by the combination of Darcy's law and continuity equation as (Kleppe, 2003):

$$\varphi \left(\frac{\partial S_\ell}{\partial t} \right)_f = \nabla \cdot \left(\kappa \frac{k_{r\ell}}{\mu_\ell} [\nabla p_\ell + \rho_\ell g e_z] \right)_f + Q_{mf}'_\ell, \quad \ell = w \text{ and } o \quad (7.1)$$

$$\varphi \left(\frac{\partial S_\ell}{\partial t} \right)_m = \nabla \cdot \left(\kappa \frac{k_{r\ell}}{\mu_\ell} [\nabla p_\ell + \rho_\ell g e_z] \right)_m - Q_{mf}'_\ell, \quad (7.2)$$

Equation 7.3 allows the direct transport within the matrix block system itself (Kleppe, 2003)

$$Q_{mf}' = \sigma \lambda (P_m - P_f) \quad (7.3)$$

where φ is the effective porosity, f and m represent the fracture and matrix respectively, $P_{m,f}$ represents the pressure of the matrix and fracture block respectively, σ is the shape factor, λ is the transmissibility ratio, S_ℓ is the phase saturation for water and oil indicated hereafter with superscripts w and o , respectively; κ is the absolute permeability, $k_{r\ell}$ is the phase relative permeability, ρ_ℓ is the phase density, μ_ℓ is the phase viscosity, $g e_z$ is the acceleration due to gravity.

Finally Q_ℓ combines the source and sink terms representing the phase production and injection. The equation is solved by adding auxiliary equations for capillary pressure between oil and water ($p_c = p_o - p_w$) and the relationship between oil and water saturations ($S_o + S_w = 1$). The transmissibility λ is calculated as,

$$\lambda = \sigma \times r_w^2 \times \frac{K_m}{K_f} \quad (7.4)$$

r_w is the effective matrix block length, $K_{m,f}$ is the matrix and fracture absolute permeability

Absolute permeability fields are relevant parameters for our forward model. The boundaries separating the lithological fracture distribution permeability are highly uncertain because they consist of few direct measurements of rock properties at the well locations and well test. The flow through the model is dominated mainly by the permeability and porosity hence a Dual-Permeability model is used for the simulation in Eclipse.

7.1.4 PUNQ-S3 synthetic model

The PUNQ-S3 is a small-size synthetic 3D reservoir engineering model. The reservoir model is based on a real field that was managed by Elf Exploration Production as shown in figure 7.8(a). The PUNQ-S3 model consists of $19 \times 28 \times 5$ grid blocks, where 1761 are active. The grid-blocks have equal 180-meter sides in x- and y-directions. The heights of the grid blocks are varying. figure 7.8(a) shows the top layer of the reservoir, including six production wells. The reservoir is bounded by a sealing fault in the east and south and is bounded by a strong aquifer in the west and north. This aquifer ensures high reservoir pressure and makes injection wells redundant. The red zone in the figure below indicates a gas cap. The production schedule is divided into two sections. The first section lasts eight years and is considered as a history matching phase. This section consists of one year of extended well testing, a 3-year shut-in period and four years of production. During this period, the wells are operated on target oil rates. When running the ES-MDA, we run the first eight years in a history matching mode, which indicates that the wells are steered according to the observed values generated by running the simulator using the “true” permeability and porosity fields. The rates utilised in this study are those specified in the description of the

PUNQ-S3 example. The second section consists of 8.5 years of production. A shut-in test is performed for two weeks each year for all wells (during this phase). The wells are controlled using a target oil rate of 150 scm/day. If the bottom hole pressure goes below 120 bar, this value is used as a target pressure. Further, if the gas/oil ratio is greater than 200 scm/scm, the oil rate in the wells is reduced by a value of 0.75. Measurements from all six wells were used during the assimilation period. This includes bottom hole pressures, gas-oil ratios, and water cuts. The measurement uncertainties for these measurements are collected from the PUNQ-S3 website¹⁴. The shut-in pressure has a noise value of 1 bar whereas flowing pressure has a noise level of 3 bar. The gas-oil ratios have a measurement uncertainty of 10 % before gas breakthrough and 25 % after the gas breakthrough. The water cut has 2 % uncertainty before water breakthrough and 5% after. The measurements noise is assumed uncorrelated, and we have used the same noise level generating the observations as when running the algorithm. The commercial ECLIPSE 100 reservoir simulator (Schlumberger GeoQuest, 2014) is used for reservoir simulation. Facies type is observed at well locations.

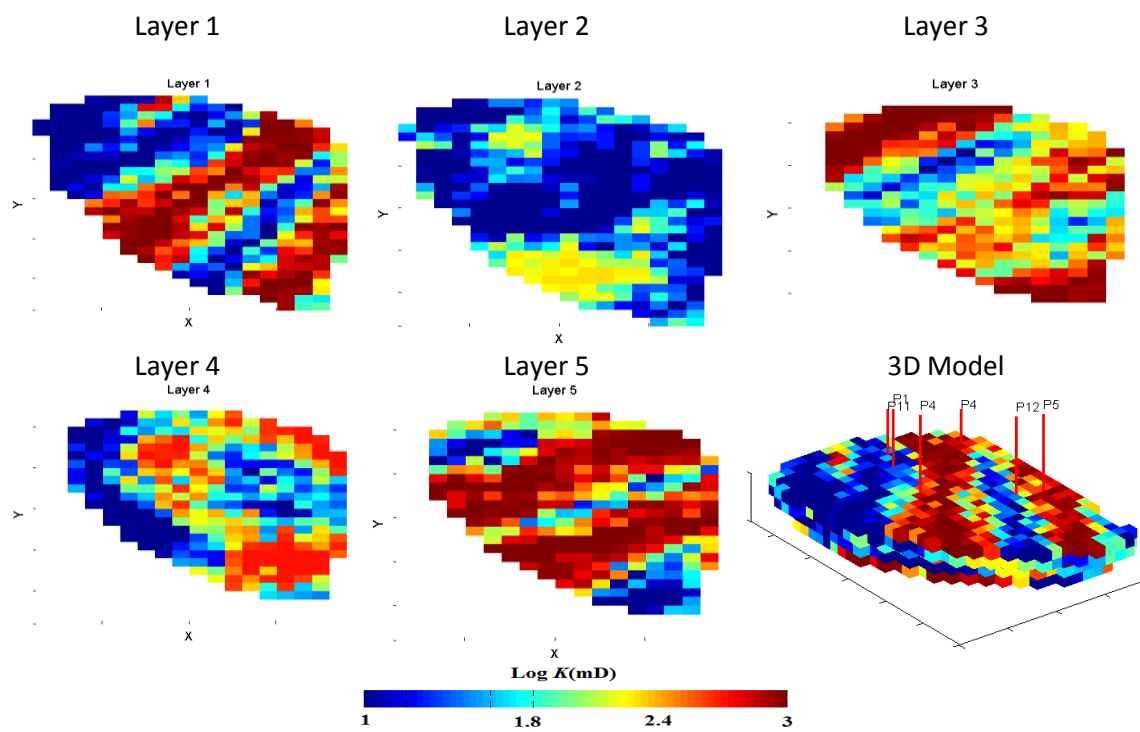


Figure 7.8(a): permeability field of the true PUNQ-S3 synthetic model showing the 2D planar permeability field and 3D model showing the six well locations.

7.1.5 Computer specification

The computer specification for the desktop computer used for conducting the numerical experiments is shown in Table 7.1.

Table 7.1: Computer specification for running the numerical experiments

Type	Desktop
Model	Dell Optiplex 790
Operating system	Windows 7 Enterprise 64-bit
Processor	Intel (R) Core(TM) i5-2400
	CPU@ 3.10 GHz, 3101 Mhz,
	4Cores(s), 4 Logical
	Processor(s)
RAM	8.00GB

Table 7.1 shows the computer specification needed to run the numerical experiments in the thesis

7.2 -Ensemble Kalman Filter- Level Set technique for an Integrated History Matching (Numerical Experiment 1)

Novelty

In this numerical experiment, a novel method for the automatic history matching of reservoirs with multiple lithofacies is introduced. The method estimates geological reservoir properties and facies boundaries by combining Ensemble Kalman Filter (EnKF) with the Level Set method. Each iteration of the automatic history matching involves the simultaneous update of the parameter field, porosity, and permeability, with the standard EnKF scheme and facies distribution. Computational time is reduced compared to Ensemble Kalman Filter (EnKF) as the Level Set evolves only around the boundary between different facies. A boundary known as the “narrow-band matrix” preserves shapes of the adjacent facies region and prevents the degradation in the classical EnKF inversion. The proposed algorithm is implemented on a synthetic 3D reservoir model with water flooding. An initial ensemble of permeability and porosity fields is created using the sequential Gaussian simulation (SGS) for the Gaussian case and a multiple-point geostatistical algorithm (*FILTERSIM*) for the channelised case. The root mean square of the pressure and production data was used as the functional

metric to measure the performance of the developed method. The proposed method outperforms the standard EnKF algorithm, regarding the accuracy of the reconstructed permeability, by preserving the boundaries. This is demonstrated based on the average structural similarity index ($SSIM$) of the reconstructed permeability image to the true or reference permeability image.

7.2.1. Introduction

The novelty of this work is the automatic history matching of the reservoir properties and lithofacies distribution by updating the level-set function using the narrow-band function and honouring the dynamic and static well data in each data assimilation time-step by applying regularisation approaches.

The current work is differentiated from Villegas, et al., (2005) and advantageous in first using the EnKF to solve the inverse problem rather than a combination of the so called-Adjoint technique(for a computationally cheap estimation of the gradient) in combination with a steepest descent method (the authors used a propagation and back propagation technique for updating the absolute permeability field). In our developed methodology in this paper, there is no explicit estimation of the gradient or its adjoints, making the procedure applicable to any reservoir flow simulator. In Villegas et al., (2005), the authors updated the absolute permeability field simultaneously with the Level Set representation of the permeability field, with a correction term. This correction term consists of the gradient(computed with the adjoint technique) and the residual term(the difference between the observed historical data and simulated data from their 2D forward simulator). The novel method is applied to a 3D synthetic reservoir as to a 2D reservoir for the latter. The current work is differentiated to Lorentzen et al., (2012) by applying a successive parameter update with the EnKF data assimilation simultaneously with the Level Set update with the update term in the EnKF equation explained in subsequent chapters. Unlike in Lorentzen et al., (2012) were the authors assigned a constant permeability value for the two different facies type after the update, the pixel values of the permeability update are preserved and update the shape of the facies only with a 3D narrow band function. The narrowband function which is a function indicating where a particular facies is in proximity with its conjugate is a matrix of zeroes and ones. This narrow

band function will be multiplied with the update term using an Hadarmad or Schur product.

Effective porosity and absolute permeability fields are relevant parameters for our forward model. The boundaries separating the lithological units of porosity and permeability are highly uncertain because they consist of a few direct measurements of rock properties at the well locations. Next, the procedure to reconstruct boundaries separating permeability of different lithofacies areas in the reservoir will be presented.

The threshold for truncation for the Gaussian model permeability/porosity field is 470mD/0.24 and for the channelised case permeability/porosity field is 100mD/0.1805 respectively

Algorithm: EnKF

- Construct the matrix y^j and y'^j ($y^j - \text{mean}(y^j)$)
- Compute the matrix $\text{Sim(simulatd data)} = H \times y$
- Compute the matrix Hy' and the singular value decomposition of $Hy' + E$ to get $U0, Z0, V0$
- Compute the matrix $\Lambda = Z0 \times Z0^T$
- Compute the matrix $X1 = \Lambda^{-1} \times U0^T$
- Compute the matrix $X2 = X1 \times (d_{obs,k} + \varepsilon_k^j - \text{Sim})$
- Compute the matrix $X3 = U0 \times X2$
- Compute the matrix $X4 = (Hy')^T \times X3$
- Update the state space ensemble by $y^{a,j} = y^j + y'^j \times X4$

In this numerical experiment, the non-Gaussian permeability/porosity distribution is represented with the more Gaussian looking signed distance function to adhere to the Gaussian requirements of EnKF.

To select the threshold values, the true permeability and porosity histogram are analysed (Figure 7.8(b)), from the Figure 7.8(b) below, the threshold value for the bimodal distribution occurs at approximately 2 (100 antilog) and 0.1805. These are the threshold values to be used in the novel EnKF-Level set approach.

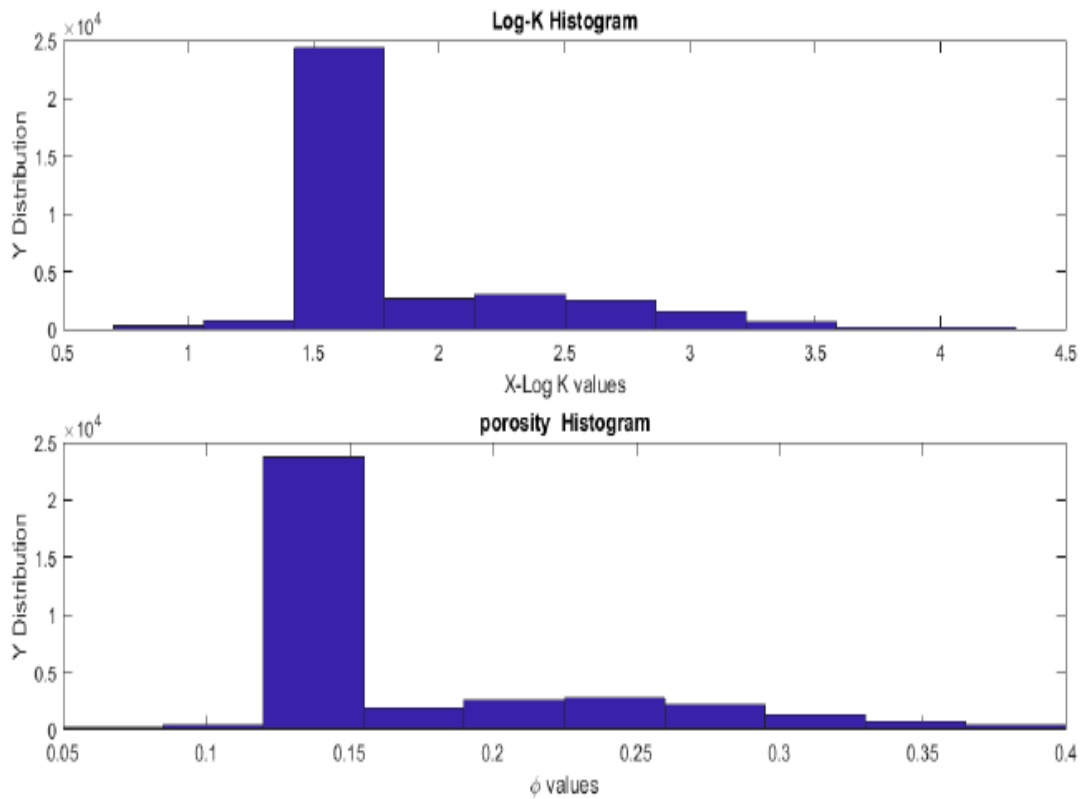


Figure 7.8(b): Histogram of the true permeability and porosity field justifying the truncation value to be used in the EnKF-Level set algorithm.

7.2.2. NFR modelling

In NFR, fluid starts to flow earlier in the fractures compared to the matrix blocks due to the higher permeability distribution in the fractures; this period is known as flow from fractures. The next zone is the transition zone which is the period the matrix block starts to flow. The transition zone can be seen in figure 7.9. The shape of the transition zone is controlled by the transmissibility. The larger the transmissibility, the higher the ease of flow through the matrix. The third period consists of a matrix and fracture flow. The shape factor of an NFR is the relative quantity of contact area that is available for the matrix-fracture flow, and the relative influence of matrix block geometry on the cross-flow rate between the matrix and fracture. (IF & Frykman, 2005).

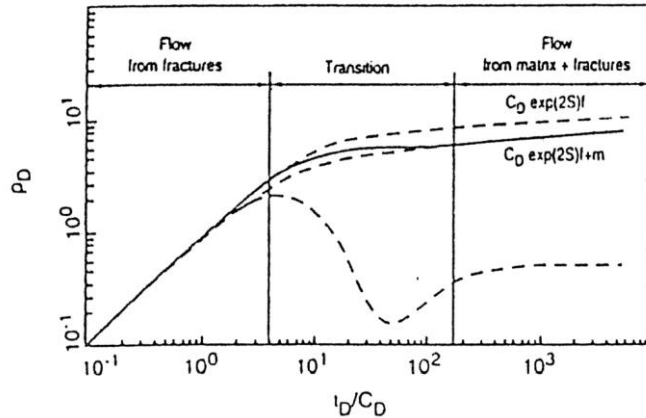


Figure 7.9: Log-Log type curve of NFR, (Bourdarot, G, 1998)

Several shape factors have been proposed to model flow in a dual permeability/porosity model and are discussed accordingly;

1. Warren and Root (1963): This model is based on an assumption on pseudo-steady state and the fractures are assumed to be space in a uniform manner

$$\sigma o = \frac{4n(n+2)}{L^2} \quad (7.5)$$

Where σo is the shape factor and L is the Equivalent length; $L_{x,y,z}$ is the Length of matrix block in x , y and z and is calculated as

$$L = \frac{3L_x L_y L_z}{L_x + L_y + L_z} \quad (7.6)$$

2. Kazemi et al. (1976)

This is an improvement on Warren and Root (1963) by applying the method to a multi-phase flow system using a finite difference method scheme

$$\sigma o = 4 \left(\frac{1}{L_x^2} + \frac{1}{L_y^2} + \frac{1}{L_z^2} \right) \quad (7.7)$$

3. Coats(1989)

$$\sigma o = 8 \left(\frac{1}{L_x^2} + \frac{1}{L_y^2} + \frac{1}{L_z^2} \right) \quad (7.8)$$

4. Lim and Aziz (1994)

The authors proposed an analytical solution method revealing in the process that the shape factor is a time-dependent parameter. They employed constant flow rate boundary conditions of pressure diffusion. (Heel et al., 2006)(K.S & W.K.S., 2013)(Mora & Wattenbarger, 2009)

$$\sigma_o = \pi^2 \left(\frac{1}{L_x^2} + \frac{1}{L_y^2} + \frac{1}{L_z^2} \right) \quad (7.9)$$

5. Chang (1993)

The authors derived an alternative of a single-phase shape factor, consisting of a constant flow rate which is the boundary conditions. The conclusions realised from the authors led them to the same conclusion as Lim and Aziz (1994) stating the shape factor is a time-dependent parameter (Mora & Wattenbarger, 2009) (Heel et al., 2006)

$$\sigma_o = 12^2 \left(\frac{1}{L_x^2} + \frac{1}{L_y^2} + \frac{1}{L_z^2} \right) \quad (7.10)$$

6. Quintard and Whitaker (1996)

The authors assumed fracture permeability to be infinitely making the application to the work in this paper impractical. (K.S & W.K.S., 2013)

$$\sigma_o = 16.54^2 \left(\frac{1}{L_x^2} + \frac{1}{L_y^2} + \frac{1}{L_z^2} \right) \quad (7.11)$$

F. I and P. Frykman (2005) proposed a method for the irregular fracture networks and matrix blocks. The authors proposed a continuous-time random walk (CTRW) in 3 dimensions for characterising the shape factor, a random walk of a particle passing through the matrix block is simulated. The random walk time is then recorded as the particle encounters a fracture. The walk time is then summed up and averaged for several particles, and the shape factor is then calculated. (IF & Frykman, 2005)

These models will be used in generating the initial ensemble of shape factors to be included in the state space parameter for history matching. Next, the coupling of the Level-set technique with the EnKF to accommodate the non-Gaussian limitation of the standard EnKF will be introduced.

7.2.3 EnKF-Level set coupling methodology

In this work, a, two-facies system where the distribution of the parameter facies is modelled using a level-set function is considered. The parameters of the model are the signed distance of each pixel towards the boundary of the other facies where the signed distance is the Euclidean distance of a cell towards the boundary of the nearest non-zero facies in the

$$\sqrt{(x_1 - x_2)^2 + (y_1 - y_2)^2 + (z_1 - z_2)^2} = \phi(x) \quad (7.12)$$

In Eqn. (7.12), (x_1, y_1, z_1) and (x_2, y_2, z_2) are the coordinates of the two locations of the zero and nearest non-zero facies respectively.

For the given reservoir having just two facies, the parameter distribution can be written as:

$$\begin{pmatrix} K(x) \\ \varphi(x) \end{pmatrix} = \begin{pmatrix} K_{high}\mathcal{H}(\phi(x)) + K_{low}(1 - \mathcal{H}(\phi(x))) \\ \varphi_{high}\mathcal{H}(\phi(x)) + \varphi_{low}(1 - \mathcal{H}(\phi(x))) \end{pmatrix} \quad (7.13)$$

Where K_{high} and φ_{high} is the permeability/porosity of the high permeability/porosity area and K_{low} and φ_{low} is the permeability/porosity of the low permeability/porosity area, and

$$\mathcal{H}(\phi(x)) = \begin{cases} 1 & \phi(x) > 0 \\ 0 & \phi(x) \leq 0 \end{cases}, \quad (7.14)$$

Where \mathcal{H} is known as the Heaviside function with 1 in the high permeability/porosity area and 0 in the low permeability/porosity area. We then construct the state space ensemble accordingly. The state space ensemble for the Gaussian experiment to be

explained later, consisting of one producer well and one injector well, with three measurements being assimilated is shown in Eqn. 7.15. It consists of the log-absolute permeability, effective porosity, signed distance function of both the permeability and porosity fields and simulated production data from the current time step

$$y_k^j = \left\{ \begin{array}{l} \ln(K_{i,k}) \\ \varphi_{i,k} \\ \phi(K)i_{i,k} \\ \phi(\varphi)i_{i,k} \\ P_i \\ S_{w,i} \\ BHP_k(\text{injector well}) \\ Qo(\text{producer well}) \\ Qw(\text{producer well}) \end{array} \right\}^j \in \mathcal{R}^{N_\phi + N_\varphi + N_u + N_d}$$

(7.15)

The state space ensemble for the SPE-10 channelised experiment to be explained later consists of four producer wells, and four injector wells, with 16 measurements being assimilated at each time step is;

$$y_k^j = \left\{ \begin{array}{l} \ln(K_{i,k}) \\ \varphi_{i,k} \\ \phi(K)i_{i,k} \\ \phi(\varphi)i_{i,k} \\ P_i \\ S_{w,i} \\ BHP_k(\text{injector well } 1 - 4) \\ Qo(\text{producer well } 1 - 4) \\ Qg(\text{producer well } 1 - 4) \\ \text{water-cut(producer well } 1 - 4)) \end{array} \right\}^j \in \mathcal{R}^{N_\phi + N_\varphi + N_u + N_d}$$

(7.16)

The ensemble state for the NFR model is described as

$$y_k^j = \left\{ \begin{array}{c} \ln(K_{i,k}) \\ \phi(K)i_{,k} \\ \sigma_o \\ P_i \\ S_{w,i} \\ BHP_k(\text{injector well}) \\ Qo(\text{producer well}) \\ \text{water cut(producer well)} \end{array} \right\}^j \in \mathcal{R}^{N_\phi + N_\varphi + N_u + N_d}$$

(7.17)

The parameter update is performed using the Eqn. 7.18

$$y_k^{a,j} = y_k^{p,j} + K_k(d_{obs,k} + \varepsilon_k^j - H_k y_k^{p,j}) \circ f_{Noverall}, j = 1, \dots, N_e$$

(7.18)

$f_{Noverall}$ is a matrix of $\in \mathcal{R}^{N_y \times N_e}$ with each element to be one. The row and columns of the $f_{Noverall}$ matrix equivalent to the signed distance of both the permeability and porosity field is replaced with f_N

$$f_{Noverall}[N_{ysigned(K+\varphi)} : N_e] = f_N \in \mathcal{R}^{N_{ysigned(K+\varphi)} \times N_e}$$

where f_N is the 3D narrow band (N.B.) function consisting of zeroes' and one's, reshaped to a column vector, to be inserted into the 2D $f_{Noverall}$ matrix. It is a matrix indicating were the low permeability/porosity facies is in proximity to the high permeability/porosity facies in the reservoir (boundary location). f_N is built from the Heaviside operation from Eqn. 18 peculiar to the absolute permeability/porosity field. The parameter $| \circ |$ signifies a Hadamard product operation. The EnKF-Level Set coupling/ update is done with Eqn. (7.18). We retain the full update on the ensemble state y and the boundaries of the signed distance function by element-wise multiplication with the $f_{Noverall}$ 2D matrix. The narrow band matrix preserves the shape of the facies and it is a matrix consisting of ones in a small pixel neighborhood of the boundaries separating two different facies type and zero elsewhere (Villegas, et al., 2005). The importance of the narrow band matrix was studied by (Villegas, et al., 2005). In principle, a conflict may occur between the update to the log-permeability field/ porosity field and to the signed distance of the permeability field/porosity field (after re-parametrization) in Eqn. (7.18), when this situation occurs, the Level Set update takes priority. The values assigned during this conflict resolution are explained shortly.

In evaluating the filter performance applying the estimated parameters in the history matching process, the estimated porosity and permeability from the last time step is used as the initial ensemble for the simulator with the dynamic variables. The root-mean-square-error (RMSE) function for each ensemble member (i) is defined as

$$\text{RMSE}(i) = \left(\frac{1}{N} \sum_{k=1}^N \sum_{j=1}^{N_{\text{data}}^k} \left(\frac{D_{\text{obs}}^j(k) - D_{\text{sim},i}^j(k)}{\sigma_{n,j}} \right)^2 \right)^{\frac{1}{2}} \quad (7.19)$$

N : Number of data assimilation time steps where measurements are assimilated (measurement times)

N_{data}^k : Number of data collected at each time step k

i : Ensemble member index

k : Time index

j : Metric or response (history matched metric or response)

$D_{\text{obs}}^j(k)$: Observed data metric for metrics j (Data equivalent in state space ensemble) at time step k .

$D_{\text{sim}}^j(k)$: Simulated data from simulator for metrics j (Data equivalent in state space ensemble) at time step k .

$\sigma_{n,j}$: Observed data standard deviation for metrics j (Data equivalent in state space ensemble).

The iterative algorithm for the automatic history matching and facies reconstruction, using our coupled EnKF-Level Set method is summarised as follows:

Algorithm: EnKF-Level Set

- Input the initial permeability and porosity ensemble generated with SGS for Gaussian case and *FILTERSIM* for Channelised/NFR case (at time k), K_k^f, φ_k^f , Production observation data $d_{\text{obs},k}$

- *Do* $k = 1, \dots$ end of production history
 - Time restart from each successive time step k
 - Forward simulate K_k^f and φ_k^f to next time – step k*

Obtain the production simulated data $d_{sim,k}$

- Truncate K_k^f and φ_k^f at given permeability/porosity threshold (470mD/0.24 for Gaussian case and 100mD/0.1805 for channelised case)
- Set $\begin{pmatrix} K_k^f \\ \varphi_k^f \end{pmatrix} = \begin{pmatrix} K_{k-1}^a \\ \varphi_{k-1}^a \end{pmatrix}$ (for $k \neq 1$)
If $\begin{pmatrix} K_{k(EnKF)}^f \\ \varphi_{k(EnKF)}^f \end{pmatrix} > threshold$, then $S(\phi_{k(EnKF)}^{f,j}) = 1$ else $S(\phi_{k(EnKF)}^{f,j}) = 0$
- Generate two facies system using signed distance function by
$$\text{Signed distance} = ((Sx_1 - Sx_2)^2 + (Sy_1 - Sy_2)^2 + (Sz_1 - Sz_2)^2)^{\frac{1}{2}} = \phi_k^{f,j}$$
- Generate the state vector
$$y_k^{f,j} = [K_{(s)k}^f, \varphi_k^f, \phi_{k(K)}^f, \phi_{k(\varphi)}^f, Pressure_k^f, Saturation_k^f, d_{sim,k}]^T$$
- Conduct EnKF data analysis with historical production data $d_{obs,k}$
- Update the EnKF state space by implementing a point by point element wise multiplication of overall narrow – band function($f_{overall}$) as

$$y_k^{a,j} = y_k^{f,j} + K_{kalman-gain(k)}(d_{obs,k} + \varepsilon_k^j - H_k y_k^{f,j}) \circ f_{overall}$$

- Output K_k^a and φ_k^a obtained from $y_k^{a,j}$

$$\text{If } \begin{pmatrix} K_{k(EnKF)}^a \\ \varphi_{k(EnKF)}^a \end{pmatrix} > Threshold, \text{ then } S(\phi_{k(EnKF)}^{a,j}) = 1 \text{ else } S(\phi_{k(EnKF)}^{a,j}) = 0$$

$$\text{If } \phi_{k(K \& \varphi)}^{a,j} < 0 \text{ then } S(\phi_{k(EnKF-Level-set)}^{a,j}) = 0 \text{ else } S(\phi_{k(EnKF-Level-set)}^{a,j}) = 1$$

- If $(S(\phi_{k(EnKF-Level-set)}^{a,j}) = S(\phi_{k(EnKF)}^{a,j}))$ = then
 $\begin{pmatrix} K_{k(EnKF-Level-set)}^a \\ \varphi_{k(EnKF-Level-set)}^a \end{pmatrix} = \begin{pmatrix} K_{k(EnKF)}^a \\ \varphi_{k(EnKF)}^a \end{pmatrix}$
elseif $(S(\phi_{k(EnKF-Level-set)}^{a,j}) \neq S(\phi_{k(EnKF)}^{a,j}))$. AND. $(S(\phi_{k(EnKF-Level-set)}^{a,j}) = 1)$ then
 $\begin{pmatrix} K_{k(EnKF-Level-set)}^a \\ \varphi_{k(EnKF-Level-set)}^a \end{pmatrix} = 1.05 \times Threshold \text{ permeability/porosity value}$
endif

if $S(\phi_{k(EnKF-Level-set)}^{a,j}) \neq S(\phi_{k(EnKF)}^{a,j}).AND.(S(\phi_{k(EnKF-Level-set)}^{a,j}) = 0))$

then

$$\begin{pmatrix} K_{k(EnKF-Level-set)}^a \\ \varphi_{k(EnKF-Level-set)}^a \end{pmatrix} = 0.95 \times \text{Threshold permeability/porosity value}$$

endif

- Output $\begin{pmatrix} K_{k(EnKF-Level-set)}^a \\ \varphi_{k(EnKF-Level-set)}^a \end{pmatrix}$
- Honour the permeability and porosity values from actual well data by enforcing a non-update on the pixel location in the simulation grid
- Set iteration count $k = k + 1$
- If $K_{kalman-gain(k+1)} = K_{kalman-gain(k)}$ then
 - end do
- end program

the History matching approach incorporating a combined level set-adjoint method, of reservoirs containing more than two facies is possible with the currently proposed method.

The iterative algorithm for the automatic history matching and facies reconstruction of the NFR model, using our coupled EnKF-Level set method is summarised as follows:

- 1) Firstly an initial permeability ensemble guesses which will honour the prior geostatistical knowledge of the synthetic fracture reservoir is generated using MPS scheme *FILTERSIM* (Wu, et al., 2006). To estimate the distribution of permeability conditioned at two well locations and also the initial value of shape factor.
- 2) For $k = 1, \dots$ end of production history
 - a. Forward simulate each realisation (ensemble state) to the next time step k
 - b. Obtain the simulated well production data accordingly
 - c. Next, the facies of permeability values are generated by truncating at the 100 mD threshold. Permeability above 100 mD are designated fractures and below 100mD designated matrix.

- d. Then build the narrowband function (N.B.) which is a matrix with 1 in a small neighbourhood of the boundaries separating two different facies type.
 - e. The facies indicator functions (0 and 1) are parameterised using the signed distance function, about the boundary separating the two facies system. This is the initial level set function $\phi_k^{p,j}$.
 - f. Construct the ensemble state as shown in Eqn. (7.17)
 - g. Update the ensemble state as done in Eqn. (7.18)
 - h. After the update from step g, assign areas with positive signed distance as facies code 1, while areas with negative signed distance as facies code 0.
 - i. Rectify the conflict between the pixel update and level set update. Give priority to the Level set update
 - j. Output $y_k^{k+1,j}$ and set $y_k^{k,j} = y_k^{k-1,j}$
 - k. Re-run the simulator with $y_k^{k,j}$ and assimilate data at this new time step k
- 3) End for
- 4) The stopping criterion, in this case, is when there no noticeable change in the Kalman gain matrix or when we assimilate all the historical production data.

7.2.4. Results and discussions

In this section three synthetic test case reservoirs are considered, namely;

1. The SPE 10 channelised reservoir model
2. A ‘Gaussian-looking’ reservoir (having non-Gaussian histogram distribution of its permeability/porosity field), The reservoir no clear channel pattern by its visual inspection but has a non-Gaussian histogram distribution of its absolute permeability and effective porosity field.
3. The NFR-DP-DK model

In this section two experiments will be conducted to test the efficiency of our history matching algorithm to the true model; EnKF, EnKF-Level Set. Although there are several other geostatistical methods to create an initial distribution of the facies and permeability distribution the multiple-point-statistics(MPS) method, *FILTERSIM* (Wu, et

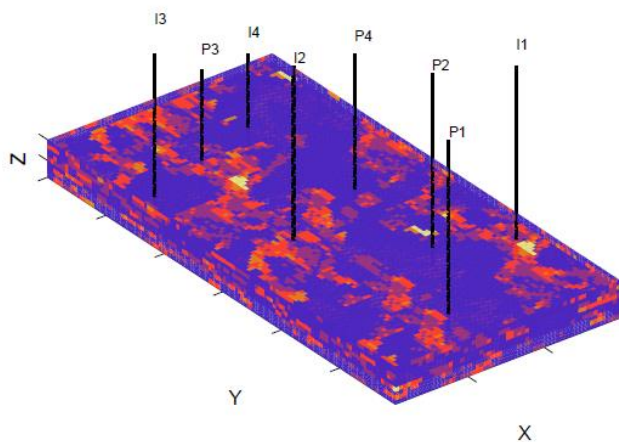
al., 2006) is chosen for its ease of conditioning to hard well data and the attractive nature in its successive facies and petrophysical generation.

(a) EnKF-Level Set

The 100 realisations of permeability models are generated with the MPS method *FILTERSIM*, (Wu, et al., 2006) as shown in figure 7.10 and the method enumerated with the level set as shown in figure 7.11.

(b) EnKF

100 realisations of permeability models are generated with the MPS method *FILTERSIM* (Wu, et al., 2006). The classical EnKF approach, as enumerated in (Evensen, 2003) is used without any Level Set parametrisation.



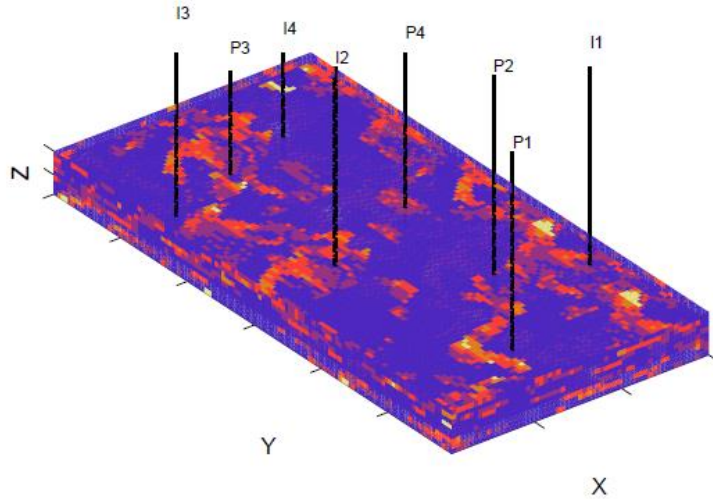


Figure 7.10: Realisations of the different initial channelised permeability obtained by *FILTERSIM* algorithm obtained in S-GeMS

7.2.5 Comparison between the EnKF and EnKF-Level Set History matched realisations for the SPE 10 channelised model

We compare the performance of the methods, EnKF and EnKF-Level Set, using the RMS function considering production data, and the structural similarity (*SSIM*) index.

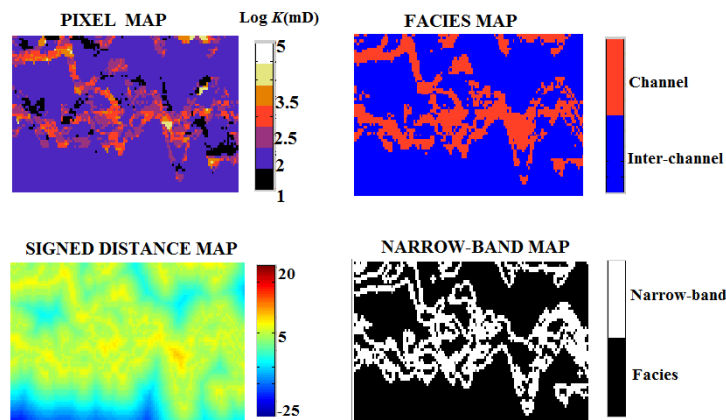


Figure 7.11: Schematic showing the representation of a pixel permeability map to its corresponding facies map, signed distance map and narrowband map.

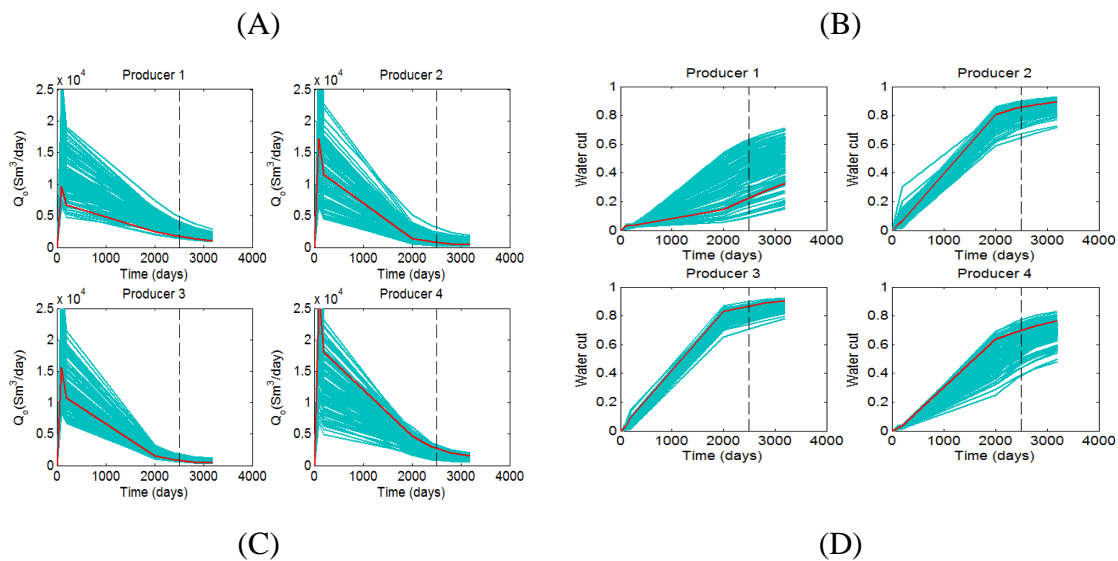
Eqn. (7.19) is used to calculate our RMSE value. Starting with a stochastic realization generated by MPS (Wu, et al., 2006), and focusing on the best realization #75, the convergence for the EnKF history matching was achieved in 36 assimilation time steps with an RMSE error of 24.21, the convergence of the EnKF-Level Set was achieved in 18 assimilation time steps with an RMSE error of 4.85. Table 7.2 below reports the effectiveness of the EnKF-Level set algorithm. The initial RMSE values for some of the

realisations are displayed in column 2. In the comparison of the final RMSE value for each method, the proposed EnKF-Level Set approach (column 4) yields lower RMSE values when compared to the EnKF method (column 3).

Table 7.2: RMS function of the best three realisations after EnKF and EnKF-Level Set

Realisation no.	Initial RMSE value	Final RMSE value using EnKF	Final RMSE value using EnKF-Level Set
75	3250.33	24.21	4.85
80	1230.83	14.78	7.78
70	445.87	9.58	6.26
29	2400	15.43	8.84

Figure 7.12 below shows the production profile for the initial ensemble. (A) Oil production rate for the 4 producer wells, (B) water cut profile for 4 producer wells ,(C) bottom hole pressure for the 4 injector wells, (D), Gas-oil-ratio for the 4 producer wells, (E) Field oil recovery ratio and (F) Initial RMSE values for the realizations. We see the initial spread of the realisations about the true data very wide. The black curve represent the differentiation of time into the historical stage and prediction stage. To the left of the black curve we have the historical stage and to the right of the curve we have the prediction stage. Figure 7.13 below shows the production profile for the EnKF-Level Set history matched ensemble. (A) Oil production rate for the 4 producer wells, (B) water cut profile for 4 producer wells ,(C) bottom hole pressure for the 4 injector wells, (D), Gas-oil-ratio for the 4 producer wells, (E) Field oil recovery ratio and (F) RMSE values for the EnKF-level set history-matched realization.



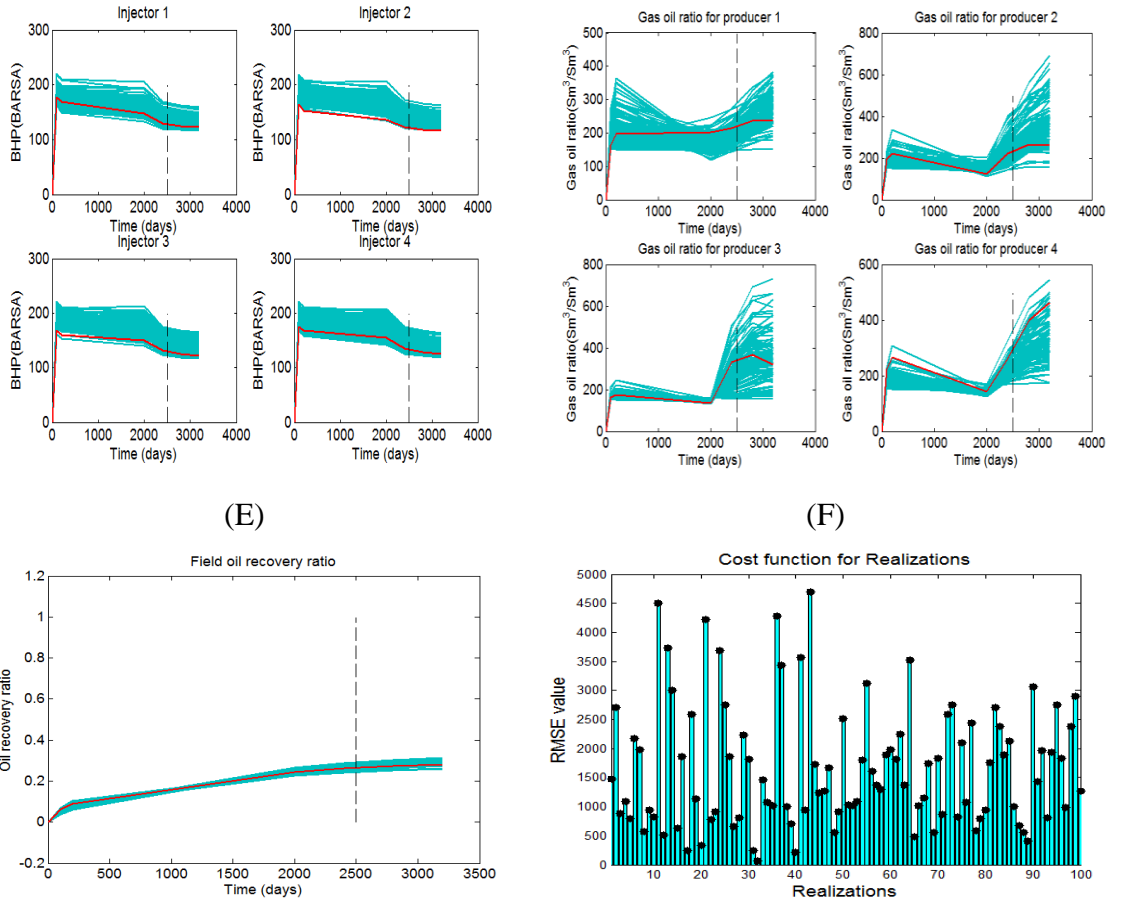


Figure 7.12: Production profile for the initial ensemble. (A) Oil production rate for the four producer wells, (B) water cut profile for four producer wells, (C) bottom hole pressure for the four injector wells, (D), Gas-oil-ratio for the four producer wells, (E) Field oil recovery ratio and (F) Initial RMSE values for the realisations. The red curve represent the true data and the blue overlay lines represents the realisations. The black dashed line (vertical) represents the historical and prediction stages

We see in figure 7.13 a decrease in the spread of the ensemble indicating the filter is minimising the uncertainty in production forecast. Likewise in figure 7.14 EnKF without any Level set parametrisation reduces the spread in the ensemble. EnKF although fails to reduce the spread in the bottom-hole pressure of injector wells 1,3 and 4. This may be due to the poorly characterised facies of the permeability field, resulting in incorrect oil-water flow in the sand facies.

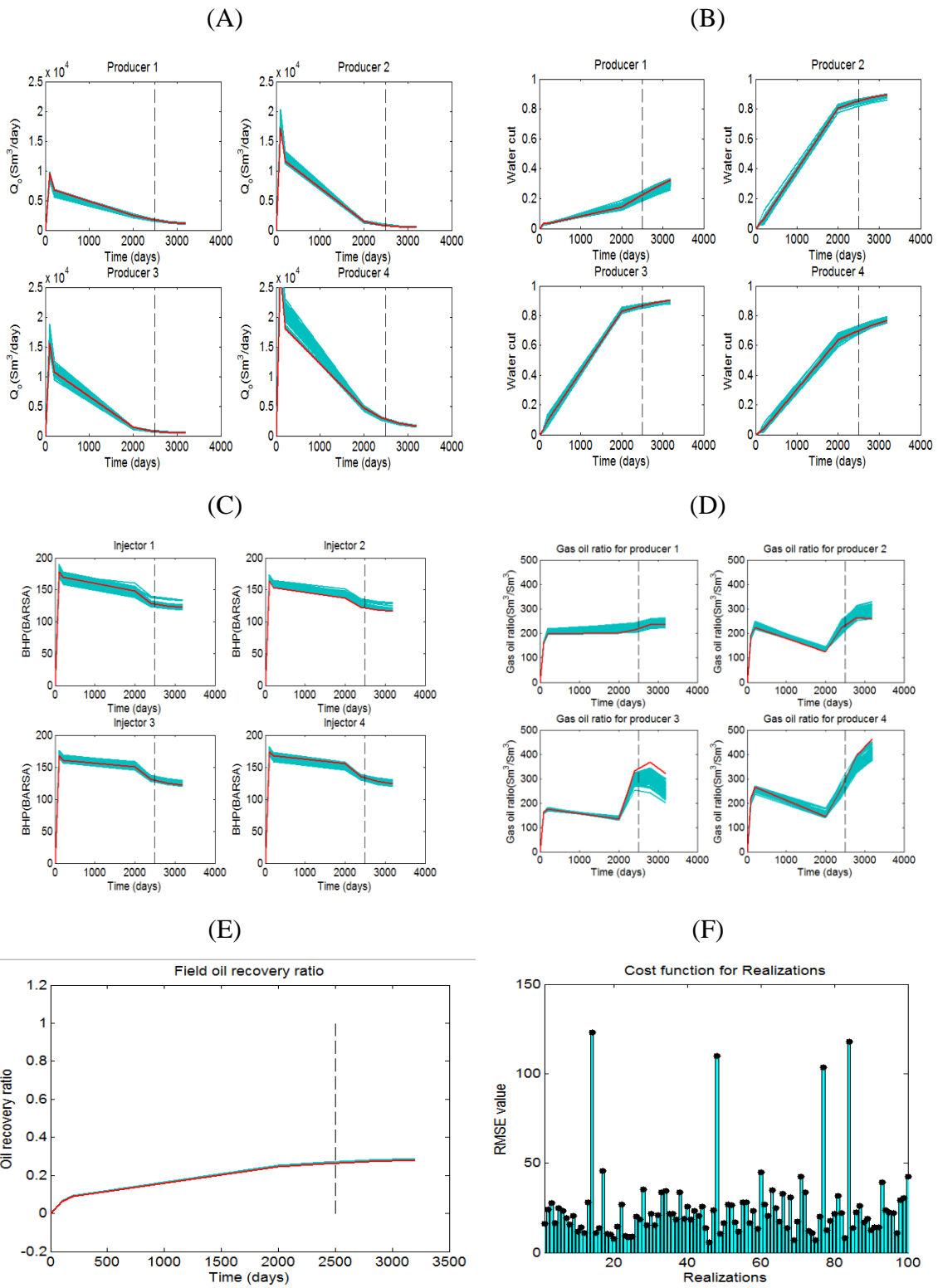
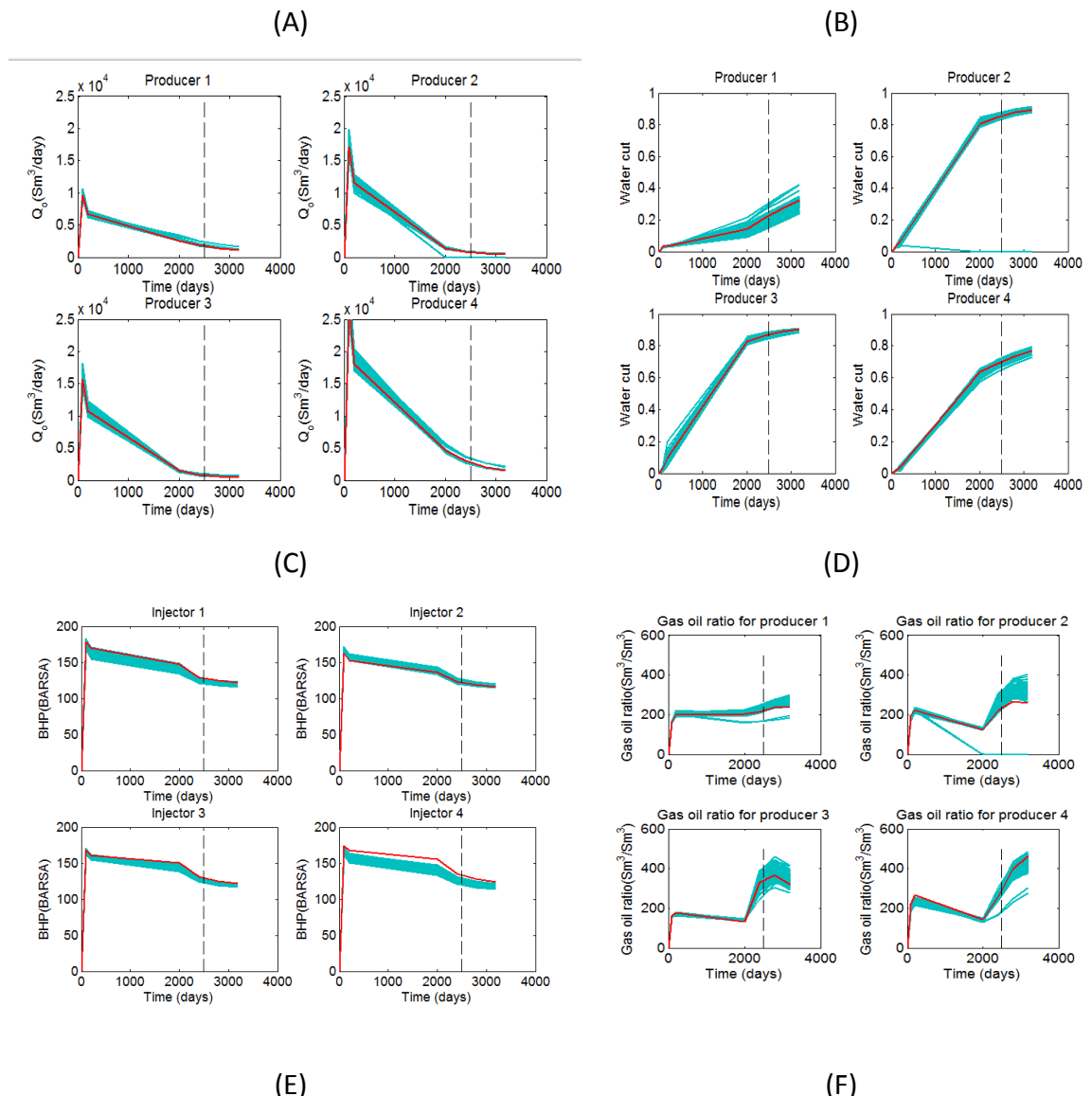


Figure 7.13: Production profile for the EnKF-Level Set history matched ensemble. (A) Oil production rate for the 4 producer wells, (B) water cut profile for 4 producer wells ,(C) bottom hole pressure for the 4 injector wells, (D), Gas-oil-ratio for the 4 producer wells, (E) Field oil recovery ratio and (F) RMSE values for the EnKF-level set history-matched realizations. The red curve represent the true data and the blue

overlay lines represents the realisations. The black dashed line (vertical) represents the historical and prediction stages

Figure 7.14 below shows the production profile for the EnKF scheme. (A) Oil production rate for the 4 producer wells, (B) water cut profile for 4 producer wells , (C) bottom hole pressure for the 4 injector wells, (D), Gas-oil-ratio for the 4 producer wells, (E) Field oil recovery ratio and (F) RMSE values for the EnKF history matched realization.



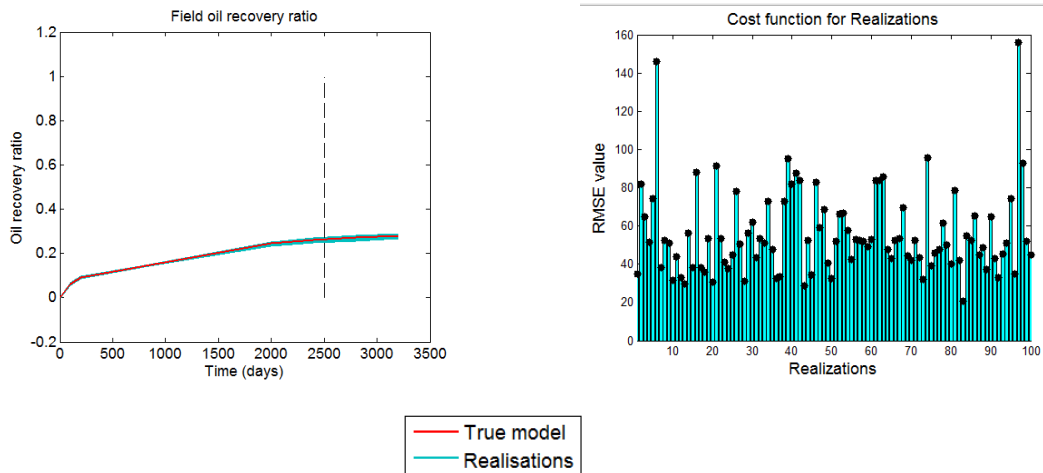


Figure 7.14: Production profile for the EnKF scheme. (A) Oil production rate for the 4 producer wells, (B) water cut profile for 4 producer wells , (C) bottom hole pressure for the 4 injector wells, (D), Gas-oil-ratio for the 4 producer wells, (E) Field oil recovery ratio and (F) RMSE values for the EnKF history matched realizations. The red curve represent the true data and the blue overlay lines represents the realisations.The black dashed line (vertical) represents the historical and prediction stages

An open source algorithm *SSIM* (Wang, et al., 2004) (Mathworks, 2016) is used to compare the EnKF-Level Set history matched reconstructed permeability realisation. *SSIM* is an image metric quantifier that analyses the visual impact of three identities of an image: structure, contrast, and luminance (s , c , and l). For further description of the algorithm, the reader may consult (Mathworks, 2016). Explaining *SSIM* further, a value of 1 means complete similarity while the value of -1 indicates complete dissimilarity.

SSIM is defined as:

$$SSIM(x, y) = [l(x, y)]^\alpha \times [c(x, y)]^\beta \times [s(x, y)]^\gamma \quad (7.20)$$

where

$$l(x, y) = \frac{2\mu_x\mu_y + C_1}{\mu_x^2 + \mu_y^2 + C_1}, \quad (7.21a)$$

$$c(x, y) = \frac{2\sigma_x\sigma_y + C_2}{\sigma_x^2 + \sigma_y^2 + C_2}, \quad (7.21b)$$

$$s(x, y) = \frac{\sigma_{xy} + C_3}{\sigma_x \sigma_y + C_3} \quad (7.21c)$$

$\mu_x, \mu_y, \sigma_x \sigma_y$, and σ_{xy} are the local means, standard deviations, and cross-covariance for images x (reference image or true model maps), and y (either of the history matched realisations using the EnKF or EnKF-Level Set module). If $\alpha = \beta = \gamma = 1$, and $C_3 = C_2/2$, $C_1 = (B_1 L)^2$, $C_2 = (B_2 L)^2$ where C_1 and C_2 are two variables that stabilises the division with a weak denominator, L is the dynamic range of the value of the pixels, $B_1 = 0.01$ and $B_2 = 0.03$, the index then becomes:

$$SSIM(x, y) = \frac{(2\mu_x\mu_y + C_1)(2\sigma_{xy} + C_2)}{(\mu_x^2 + \mu_y^2 + C_1)(\sigma_x^2 + \sigma_y^2 + C_2)} \quad (7.22)$$

To show the superiority of the EnKF-level set over the standard EnKF four realisations evolution is shown from the initial guess to the history matched model using both the standard EnKF and EnKF-level set. The log permeability field of the realisations are compared to the true log permeability field.

Figure 7.15 shows the Log-permeability field evolution for selected realisations. (A) #75, (B) # 80, and (C) # 70. The first column all through the panel is the initial guesses, the second columns are the EnKF updated realisation, the third columns are the EnKF-level set updated realisations, and the fourth columns are the true permeability field. We see how the EnKF-level set method is capable of maintaining the bi-modal distribution of the true permeability field as compared to the EnKF that completely smears out non-Gaussian features.

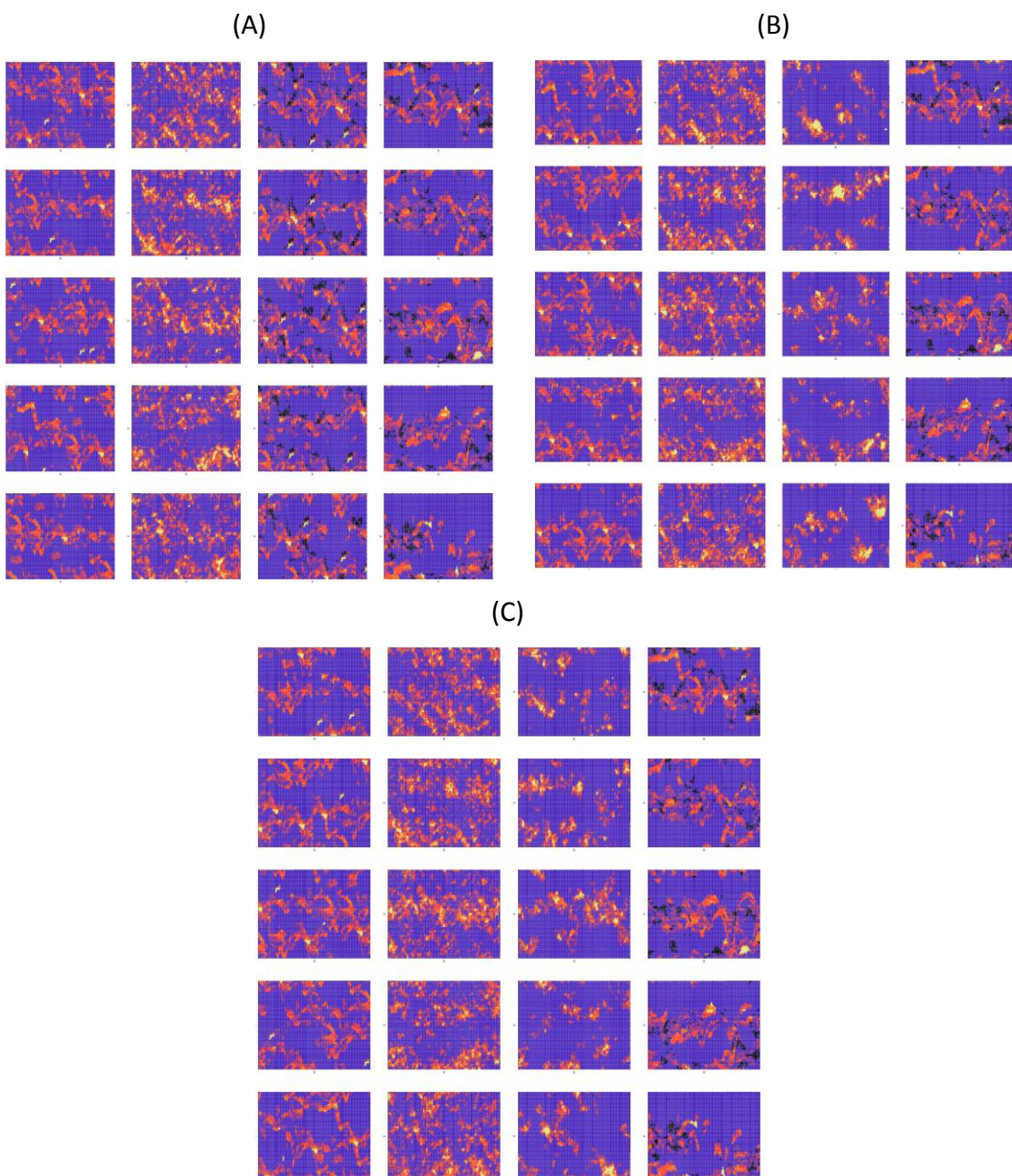


Figure 7.15: Log-permeability field evolution for selected realisations. (A) #75,(B) # 80 and (C)# 70. The first column all through the panel is the initial guesses, the second columns are the EnKF updated realisation, and the third columns are the EnKF-level set updated realisations and the fourth columns is the true permeability field

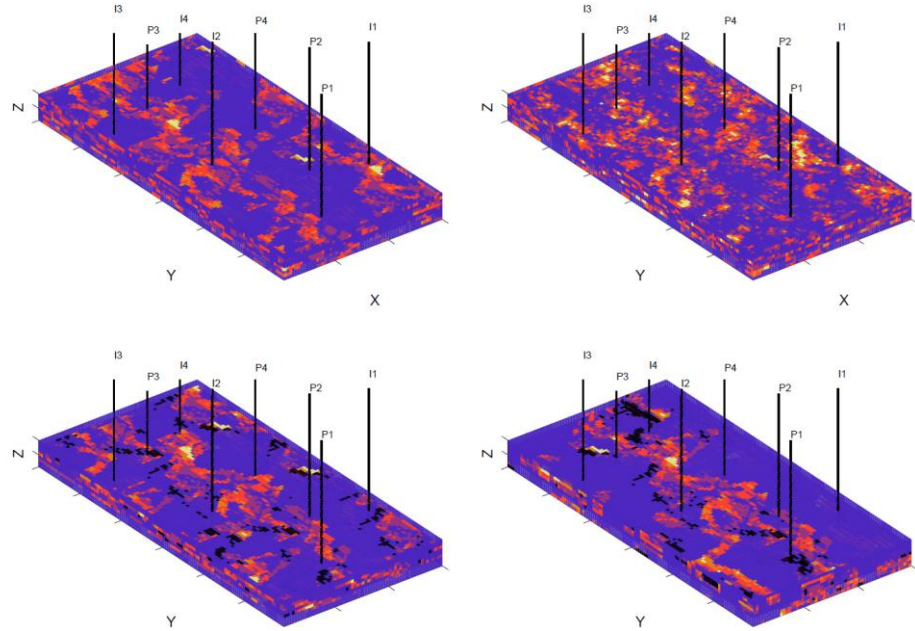


Figure 7.16: 3D Log-permeability field evolution for selected realisations. (A) #75,(B) # 85,(C) # 70 and (D) #29.

some statistical relationship to quantify the log permeability realisations of both the updated EnKF and EnKF-level set to the true log permeability field is shown below

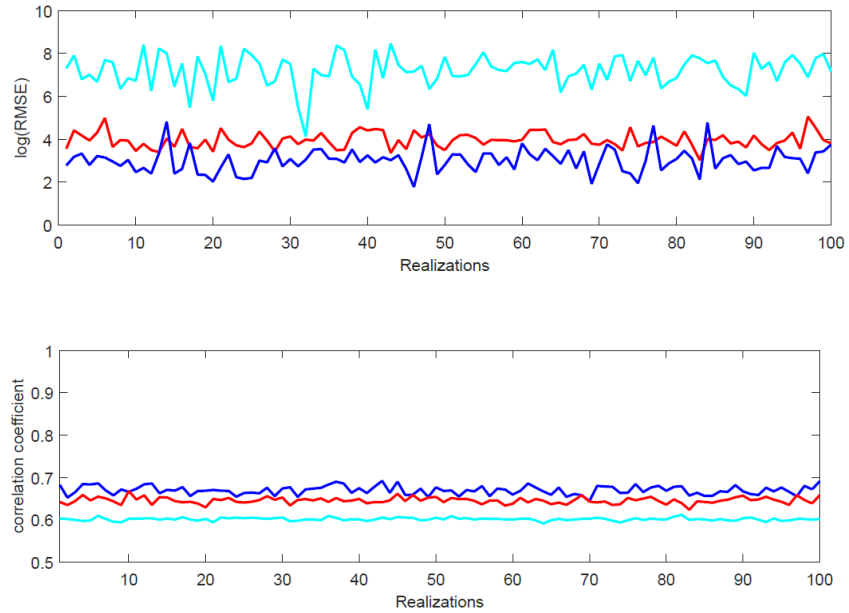


Figure 7.17: Statistical quantification of the history matched realisations showing the correlation coefficient of the permeability and porosity fields of both the EnKF(red line) and EnKF-level set(blue line) scheme to the true model. The initial ensemble is light blue (down) and the difference in production data mismatch (top)

In summarising the results of this section,

The Enkf-level set gave a lower RMSE value than the EnKF scheme. The log permeability realisations of the EnKF-level set showed a higher correlation coefficient (70%) than that of the EnKF (40%). Channel connectivity was maintained in the EnKF-level set because of the strict enforcement of the narrow band scheme, while channel connectivity and rearrangement were destroyed by the EnKF. This transformation from non-Gaussian to Gaussian by use of the signed distance function, optimal for use in the EnKF modulation and a topological update alone on the boundary of adjacent conjugate facies type, in conjunction with the narrow band function, made sure we retained the original shape of the initial ensemble generated by the MPS scheme *FILTERSIM*, and hence gave realistic channel like connectivity in the final update.

7.2.6 Comparison between EnKF and EnKF-Level-Set for the Gaussian model

For the Gaussian reservoir presented in this thesis, the stochastic technique that proved to produce more suitable initial guesses from the well data was SGS, producing lower RMSE function values. This experiment uses two points initial ensemble construction inferring the necessary covariance from a variogram. The initial ensemble, generated by GSlib (Deutsch & Journel, 1998), constitutes 100 realisations of permeability field conditioned to the well location. The corresponding porosity ensemble is generated from the initial relationship between the true porosity field and true permeability field:

$$\varphi = 0.000134313 \times K + 0.1781797 \quad (7.23)$$

Where K the permeability (mD) ensemble is generated from SGS and φ is the porosity ensemble. All other parameters are kept constant without uncertainty. Figure 7.18 shows the histogram of the reference permeability distribution, showing its non-Gaussian attribute. This justifies the use of our Level Set approach and the truncation value of 470mD. Figure 7.19 shows some initial realisations generated with SGS for the Gaussian experiment.

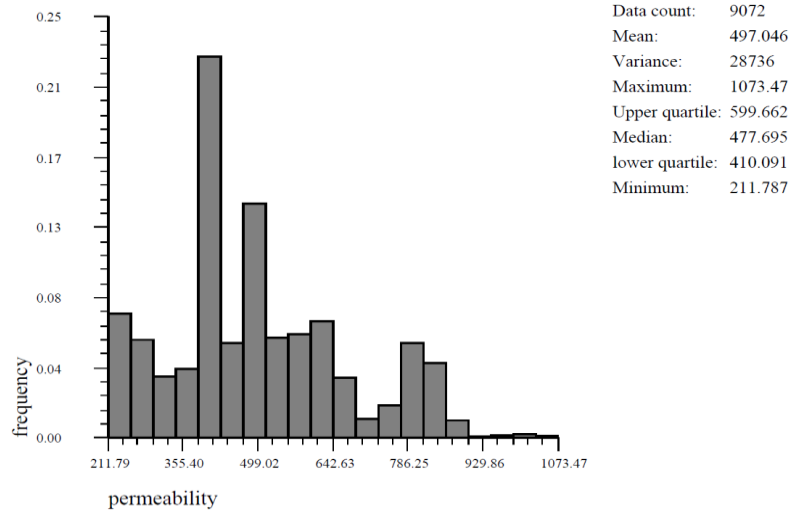


Figure 7.18: The Histogram of the reference permeability field justifying the use of the Level Set technique

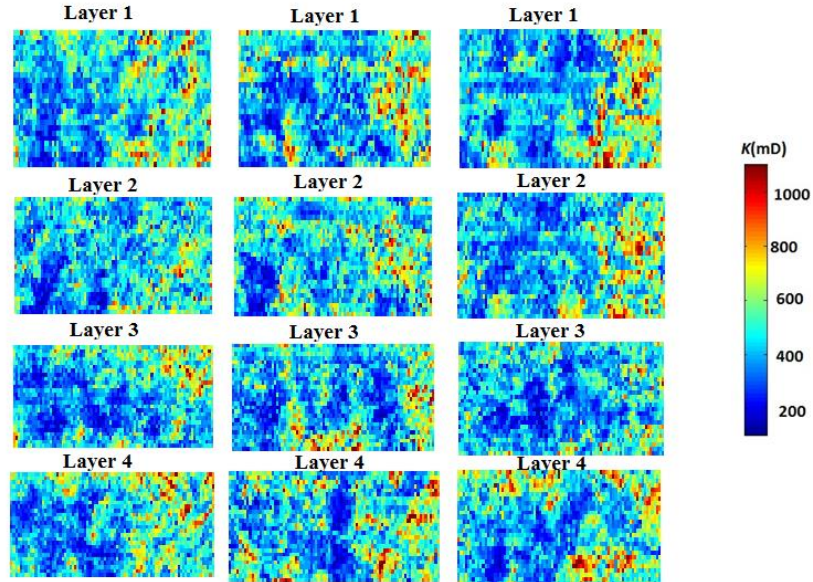


Figure 7.19: an initial model of realisations #24, #19 and #51 generated with the SGSIM algorithm (Deutsch & Journel, 1998) unique for the Gaussian experiment.

The narrowband function consists of a matrix with ones in a definite pixel neighbourhood of the boundaries separating two different facies type and zeroes elsewhere. Figure 7.20(b) shows a schematic of the narrow band application to this study, the figure 7.20(a) shows the Heaviside function/facies map as it applies to the reservoir model in a binary representation for the true model and history matched realisation #51 for both the EnKF and EnKF-Level Set.



Figure 7.20: (a) Facies map distribution of a model, and (b) Narrowband map of the true model

To analyse and compare the performance of the two methods, EnKF and EnKF-Level Set, the RMSE function considering pressure and production data, and the structural similarity (*SSIM*) index are considered. The permeability and the porosity are modified in each step, and other parameters are kept constant. The proposed EnKF-Level Set involves an additional update to estimate the new Level Set function at each time step.

Starting with a stochastic realisation generated by SGS, the EnKF history matching algorithm yielded an RMSE error of 9.2 after the assimilation of data in the history period. Using the proposed method, EnKF-Level Set history matching; the algorithm yielded an RMSE error of 1.62 after the assimilation of data in the history period. Table 7.3 below reports the effectiveness of including the level-set parameterisation. The initial RMSE values for some of the realisations are displayed in column 2. In the comparison of the final RMSE value for each method (with and without Level Set), the proposed EnKF-Level Set approach (column 4) yields lower RMSE values when compared to the standard EnKF method (column 3). In all the realisations listed, realisation #84 gave a slightly better value when using the standard EnKF to the EnKF with level-set parameterisation. This may be due to covariance error as enumerated in (Agbalaka & Oliver, 2008). Accumulation of covariance error becomes more noticeable in using an ensemble size lower than 100, in such cases, the technique known as covariance localisation highlighted by (Agbalaka & Oliver, 2008) (Houtekamer & Mitchell , 2001) should be utilised. For the case of ≥ 100 ensemble size, the effects of error covariance are not pronounced as an error in posterior estimates decreases by a factor of $\frac{1}{\sqrt{N}}$. The higher the ensemble size, the lower the error in sampling from the posterior pdf (Agbalaka & Oliver, 2008).

Table 7.3: RMS function of best seven realisations after EnKF and EnKF-Level Set update.

Realisation no.	Initial RMSE value	Final RMSE value using EnKF	Final RMSE value using EnKF-Level Set
2	56.64	21.23	14.15
13	242.23	34.34	21.25
24	175.67	42.31	31.20
19	56.22	18.82	10.31
51	45.31	15.2	1.62
84	81.49	25.26	25.93
45	38.38	33.21	4.23

Figure 7.22 and figure 7.23 shows the EnKF-Level Set and EnKF final history matched ensemble response to the true model pressure-production data. The superiority of our proposed model is clear in the quality of ensemble match with the true model.

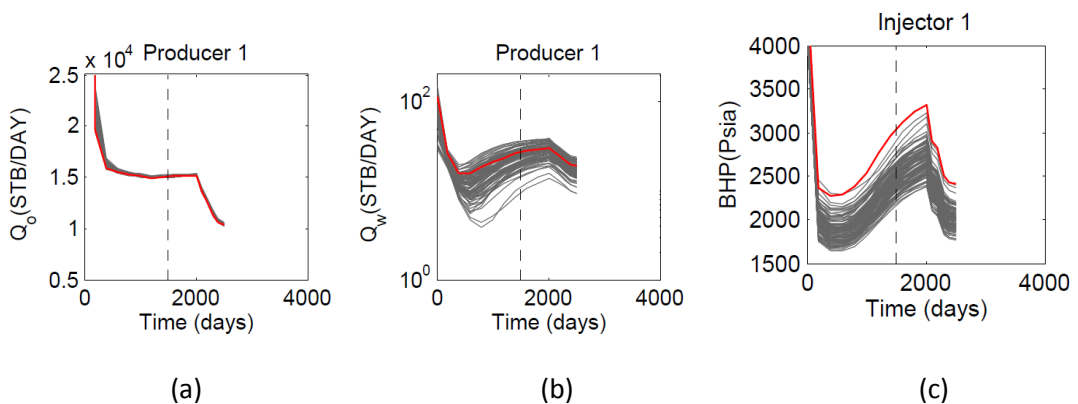


Figure 7.21: The initial ensemble oil production rate profile (a), water production rate profile (b) and injector bottom hole pressure profile(c). The red curve represent the true data and the grey overlay lines represents the realisations. The black dashed line (vertical) represents the historical and prediction stages

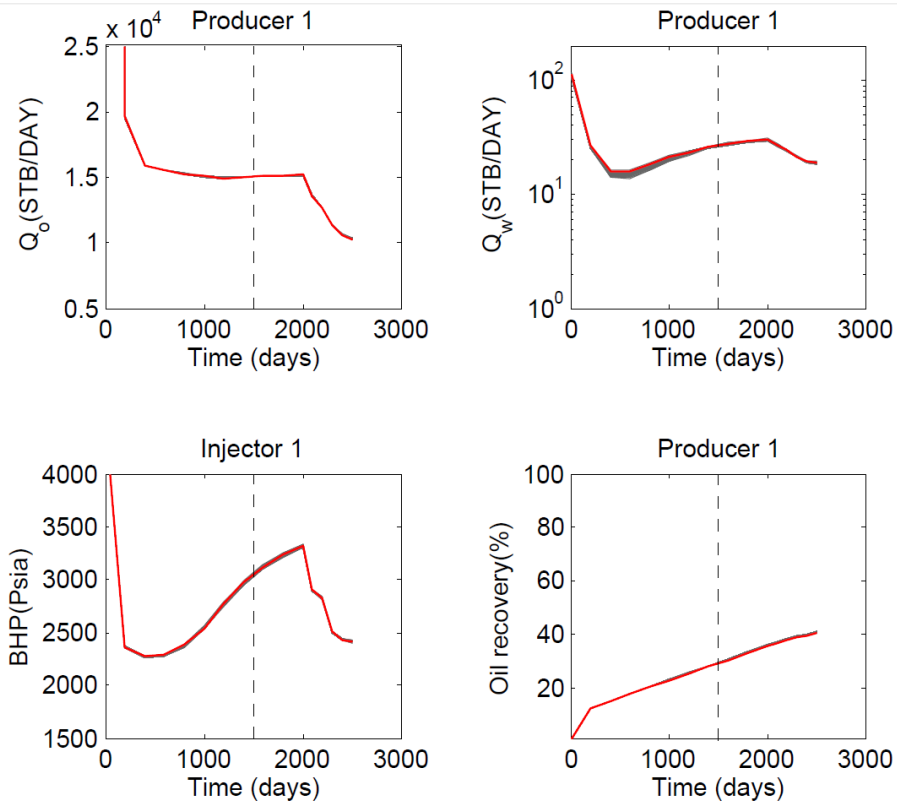


Figure 7.22: The EnKF-Level Set history matched ensemble oil production rate profile (top-left), water production rate profile (top-right), injector bottom hole pressure profile (bottom-left) and oil recovery ration (bottom right). The red curve represent the true data and the grey overlay lines represents the realisations. The black dashed line (vertical) represents the historical and prediction stages

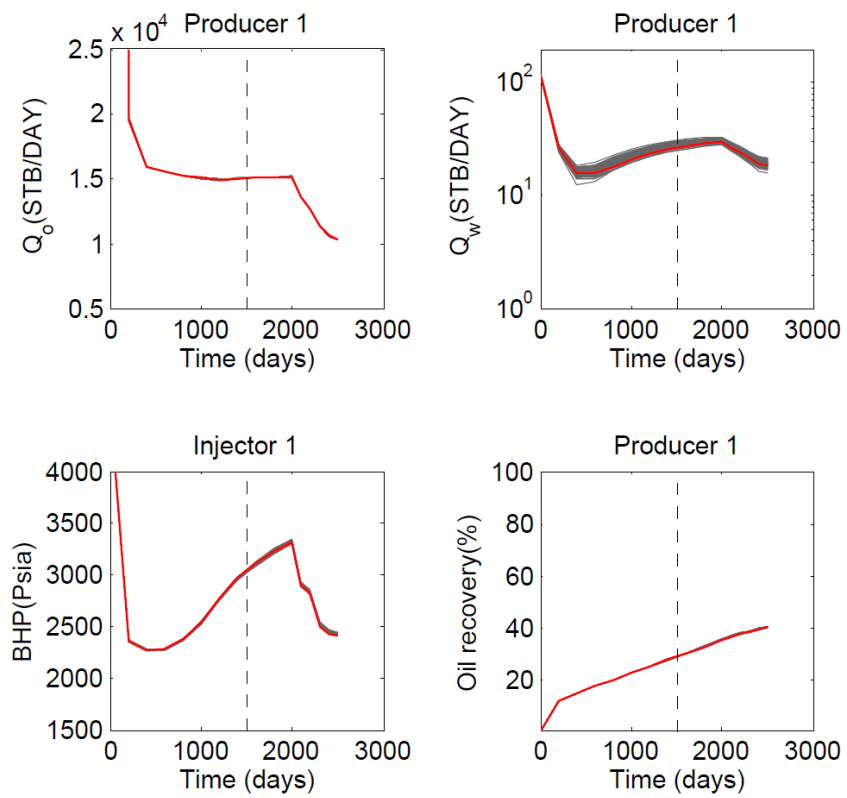


Figure 7.23: The EnKF history matched ensemble oil production rate profile (top-left), water production rate profile (top-right), injector bottom hole pressure profile (bottom-left) and oil recovery ration (bottom right). The red curve represent the true data and the grey overlay lines represents the realisations. The black dashed line (vertical) represents the historical and prediction stages

Figure 7.24 (which is vital to show the supremacy of the EnKF-level set method to conventional EnKF) shows the numerical simulation results and the RMS function of both methods with regards to observed production data. It is clear the EnKF-Level Set method outperforms the standard EnKF method by reducing the RMSE function value after the end of historical data assimilation. The nature of Q_w matching is better for the EnKF-Level set than the conventional EnKF approach. The EnKF-Level Set method gave a lower RMSE, and the possible reasons are enumerated below:

- I. The boundaries separating two different facies was updated in the Level Set update stage. This update was superior to the EnKF parameter update step. Pixel values having a positive Level Set function of 1 were replaced with 475 mD. During this conflict, if a pixel value gave a permeability value lower than the 470 mD threshold during the parameter update with the EnKF, it was replaced this new value of 475mD. In summary, the Level Set update took more priority than the parameter update.
- II. In doing this, the basic facies shapes are preserved, making it less distorted. This gave rise to the higher SSIM value.
- III. In ill-posed reconstruction such as history matching, the higher the number of wells drilled(or data assimilated) the better the parameter reconstruction, for reservoirs having few wells with few informative data there is a high tendency for ‘ghost-artefacts’ to be regenerated in areas of low sensitivity(areas far away from the well locations). The Level-set evolution takes care of such ghost generation and assigns a fixed value during the EnKF update.

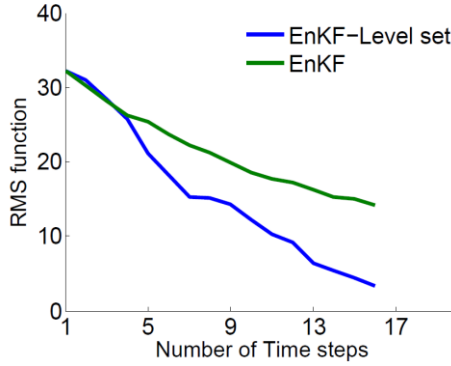


Figure 7.24: Comparison between EnKF and EnKF-Level Set RMS function (#51).

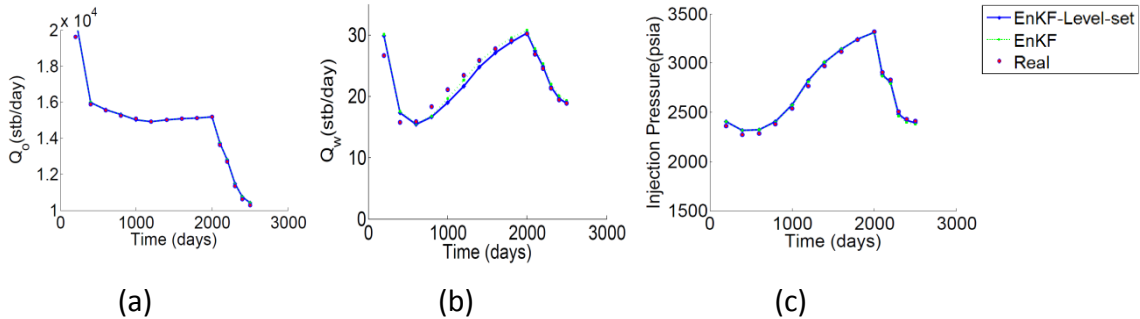


Figure 7.25: Comparison between EnKF and EnKF-Level Set ensemble mean: (a) EnKF mean oil production rate profile, (b) EnKF mean water production rate profile, (c) EnKF mean injection pressure profile, (d) EnKF-Level Set mean oil production rate profile, (e) EnKF-Level Set mean water production rate profile, and (f) EnKF-Level Set mean injection pressure profile.

Table 7.4 reports the layer-by-layer, and overall field comparison of *SSIM* of the true model permeability (figure 7.26 (b & e)) and its corresponding *SSIM* map to the history matched realisation obtained with the EnKF-level-set (columns 3 & 5) and EnKF modules (columns 2 & 4).

Table 7.4: *SSIM* values to reference permeability and porosity field for the two history matched models of the EnKF-Level Set scheme and standard EnKF.

Layer	<i>SSIM</i> value of permeability (EnKF)	<i>SSIM</i> value of permeability (EnKF-Level Set)	<i>SSIM</i> value of porosity (EnKF)	<i>SSIM</i> value of porosity (EnKF-Level Set)
Layer 1	0.7231	0.8924	0.7341	0.8796
Layer 2	0.5423	0.7841	0.5433	0.7782
Layer 3	0.6645	0.7822	0.6723	0.7693
Layer 4	0.5397	0.7021	0.5423	0.7002
Overall	0.6174	0.7902	0.6230	0.7818

In the $SSIM$ value highlighted in Table 7.4, we see that the EnKF-Level Set history matched realisation gave a higher similarity to the true model than the realisation obtained through the EnKF alone procedure. The overall $SSIM$ value of the EnKF-Level Set model was higher than the EnKF model for both the permeability and porosity reconstruction. Figure 7.26 shows the comparison between the true model (Figures 7.26 (a & d)) and the history matched permeability maps obtained using the EnKF-Level Set algorithm (Figures 7.26(b)) and the classical EnKF algorithm (Figures 7.26(e)). The corresponding $SSIM$ maps for the two procedures are shown in figure 7.26(c) and figure 7.26(f)

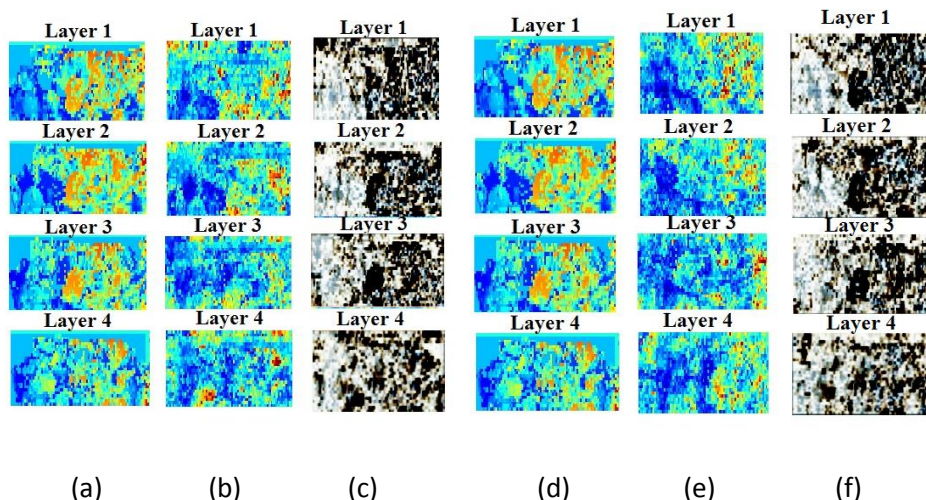


Figure 7.26: (a) Permeability map distribution of true model, (b) EnKF-Level Set history matched realisation permeability map (#51).(c) SSIM map for the comparison, (d) Permeability map distribution of true model,(e) EnKF history matched realization permeability map (#51) and (f) SSIM map for the comparison

7.2.7 Comparison between the EnKF and EnKF-Level Set History matched realisations for the NFR model

Some initial realisations are generated using *FILTERSIM* with the training image described in section 7.1

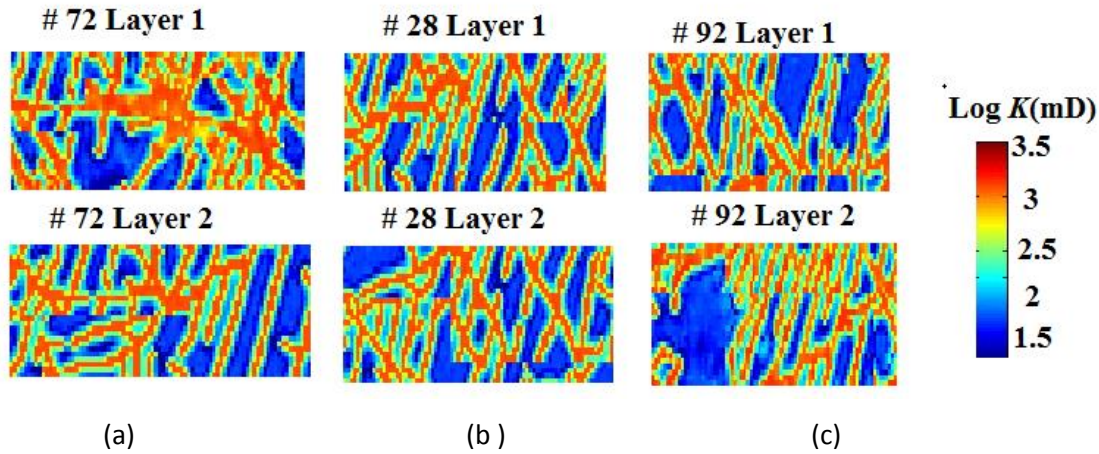


Figure 7.27: Initial dual-permeability model of some realizations: (a) dual-permeability model of # 72, (b) dual-permeability model of # 28, (c) dual-permeability model of # 92.

Initial ensemble shape factor calculation

To generate the initial ensemble of shape factor to be included in the history matching loop, several shape factor model discussed in section 2.4 is employed using $L_{x,y,z}$ to be 80,20,5 and $n = 3$, the various shape factor are shown in Table 7.5. An ensemble of shape factor is populated using the mean of the distribution and its equivalent standard deviation bounding the span of the distribution to 0.17 and 11.68. The true model utilized a shape factor of 0.6 based on the postulation of Warren and Root.

Table 7.5: Shape factor calculation using established methods

Methods	Shape Factor
Warren and Root	0.6
Kazemi	0.17
Coats	0.34
Lim and Aziz	0.42
Chang	6.15
Quintard and Whitaker	11.68

The effectiveness of the proposed methodology

Figure 7.28 shows the initial ensemble pressure-production profile: (a) oil production rate profile before update, (b) water-cut production rate profile before update, (c)

injection pressure profile before update, (d) Oil recovery ratio before update, Figure 7.29 shows the final ensemble pressure-production profile after EnKF-Level-set History-matching: (a) oil production rate profile after EnKF-Level-set update, (b) water-cut production rate profile after EnKF-Level-set update, (c) injection pressure profile after EnKF update, (d) Oil recovery ratio after EnKF-Level-set update, Figure 7.31 Comparison between the true model permeability field and the history matched realization: (a) True dual-permeability distribution showing Layers 1-2, and (b) History matched dual- permeability distribution of # 72 showing Layers 1-2, (c) History matched dual- permeability distribution of # 28 showing Layers 1-2, and (d) History matched dual- permeability distribution of # 92 showing Layers 1-2

Root-mean-square (RMS) function

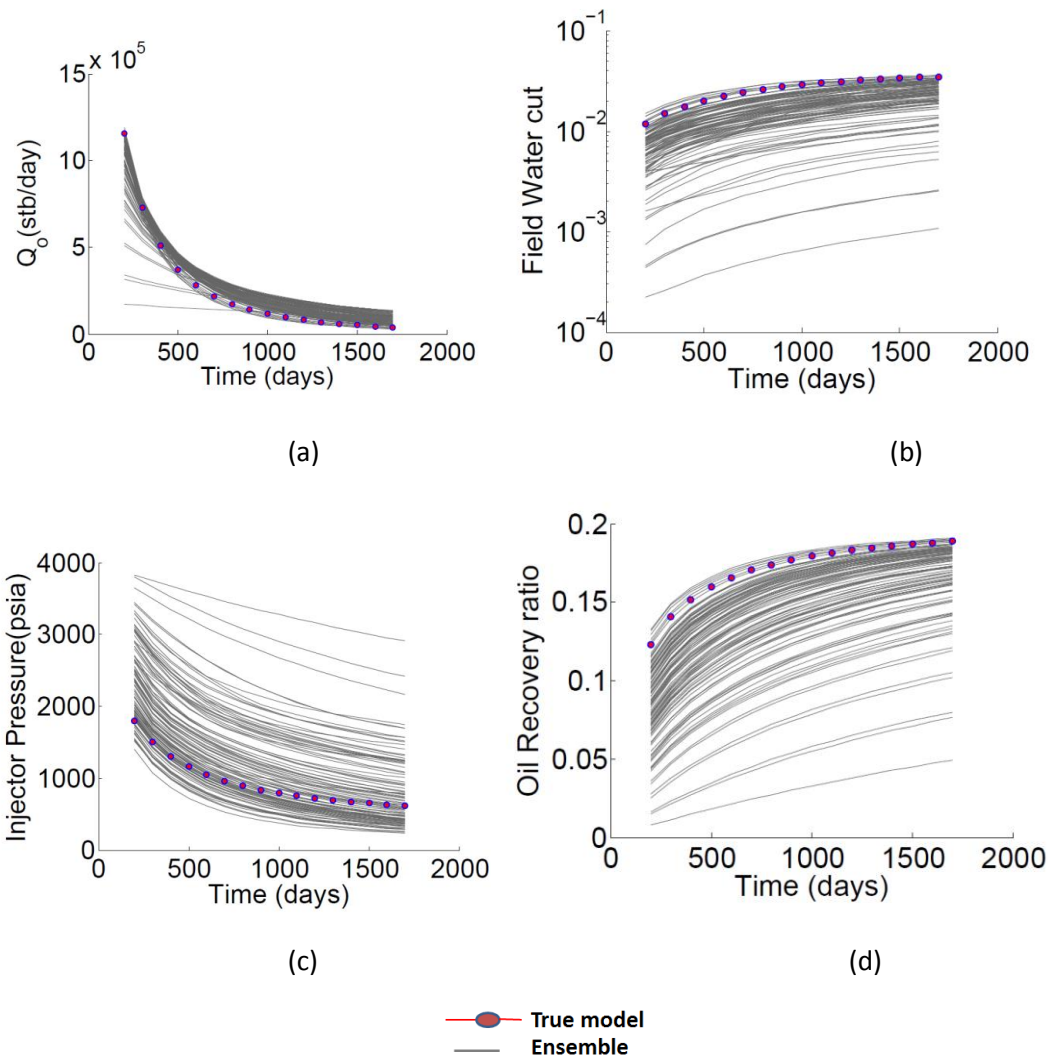


Figure 7.28: initial ensemble pressure-production profile: (a) oil production rate profile before update, (b) water-cut production rate profile before update, (c) injection pressure profile before EnKF update, (d) Oil recovery ratio before EnKF update. The red curve represent the true data and the grey overlay lines represents the realisations.

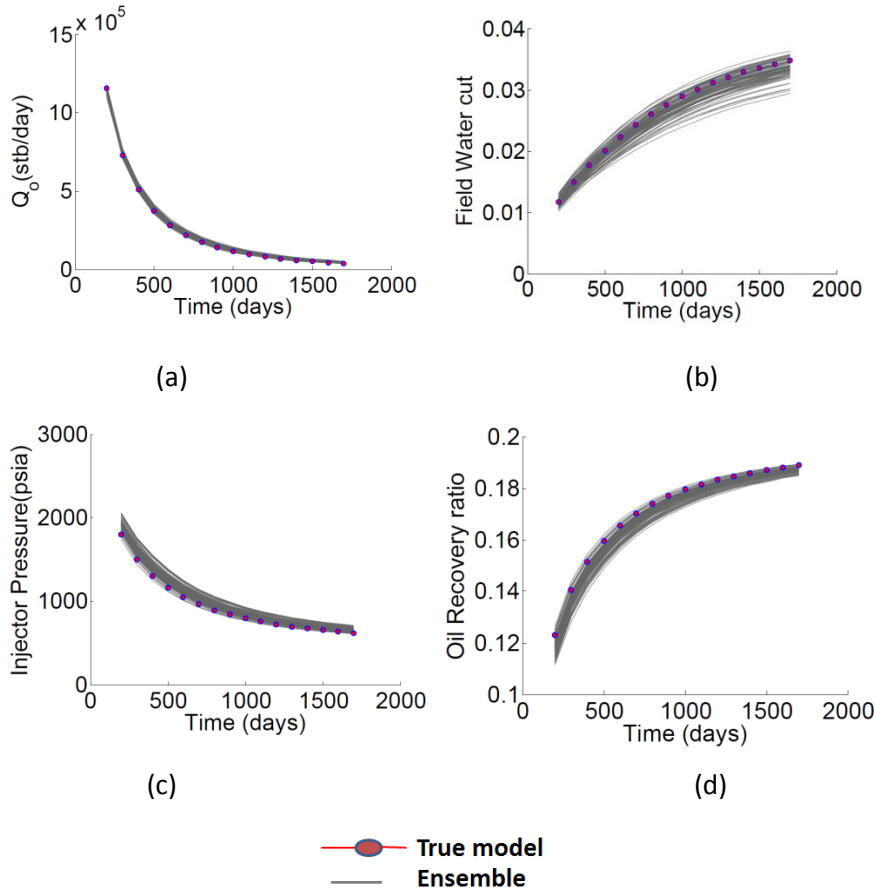


Figure 7.29: Final ensemble pressure-production profile after EnKF-Level-set History-matching: (a) oil production rate profile after EnKF-Level-set update, (b) water-cut production rate profile after EnKF-Level-set update, (c) injection pressure profile after EnKF update, (d) Oil recovery ratio after EnKF-Level-set update. . The red curve represent the true data and the grey overlay lines represents the realisations.

The initial and final RMS value of the ensemble is reported in Table 7.6

Realisation # 72 is the best history matched member with the least deviation to the true pressure-production data.

Table 7.6: RMS function of best three realisations after history matching

Realisation no.	Initial RMS value	Final RMS value using EnKF-Level set History matching scheme
28	153.60	4.22
92	29.87	6.62
72	251.44	2.41

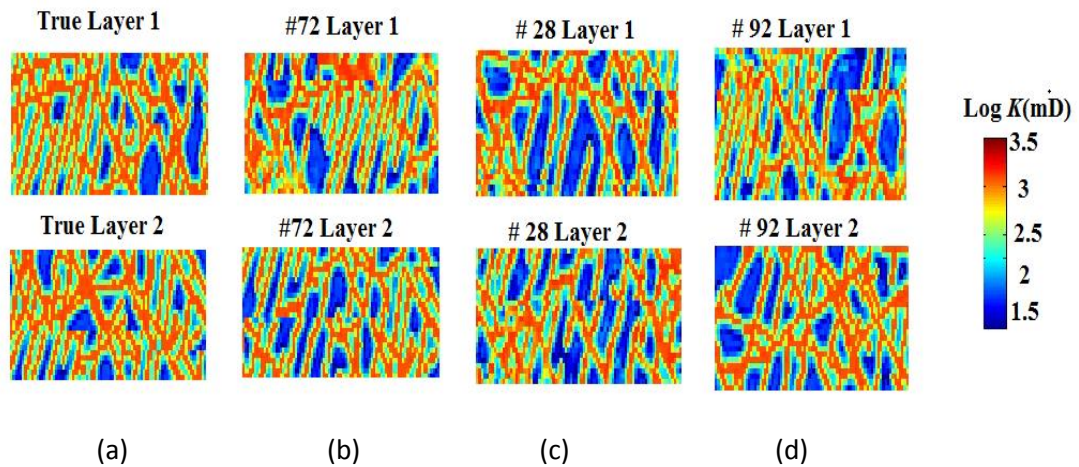


Figure 7.30: Comparison between the true model permeability field and the history matched realization: (a) True dual-permeability distribution showing Layers 1-2, and (b) History matched dual-permeability distribution of # 72 showing Layers 1-2, (c) History matched dual- permeability distribution of # 28 showing Layers 1-2, and (d) History matched dual- permeability distribution of # 92 showing Layers 1-2

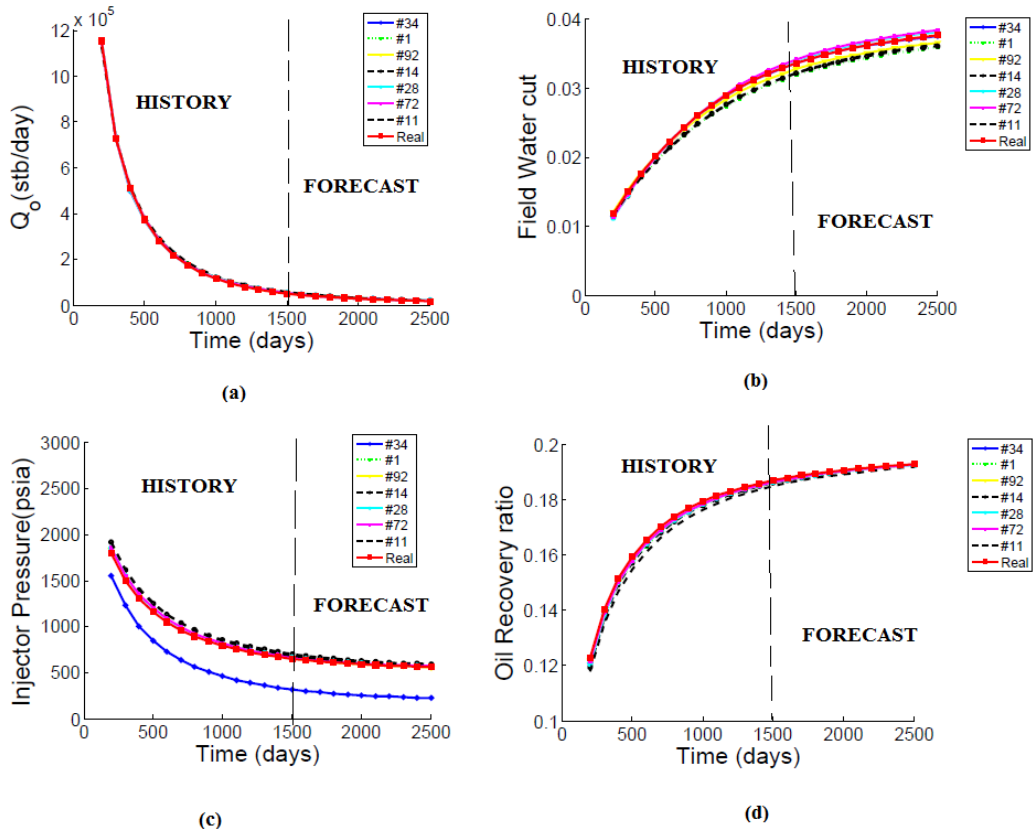


Figure 7.31: Final ensemble pressure-production profile after EnKF-Level-set History matching for the best seven realisations: (a) oil production rate profile after History matching, (b) water-cut production rate profile after EnKF-Level-set update, (c) injection pressure profile after EnKF update, and (d) Oil recovery ratio after EnKF-Level-set update.

Shape Factor comparison

To show the effectiveness of our EnKF-Level-set scheme in the handling of several parameters automatically during history matching, the initial and final matched shape factor value is reported in Table 7.7. Realisation #72 gives the closest shape factor to the original shape factor used in the true model which was 0.6

Table 7.7: Shape factor function of best three realisations after history matching update

Realisation no	Initial Shape factor value	Final shape factor after History matching
28	7.2	1.24
92	1.35	0.73
72	8.34	0.64

Structural Similarity Index Metric (SSIM)

SSIM (Wang, et al., 2004) is used to compare the EnKF-level set history matched reconstructed permeability realisation. The SSIM value for the fracture distribution reconstruction is reported in Table 7.8

Table 7.8: SSIM value of average fracture distribution reconstruction to the true model

Realisations	<i>SSIM</i> value of average fracture distribution reconstruction
28	0.621
92	0.68
72	0.77

Realisation #72 gave the best fracture network reconstruction with SSIM value of 77%.

7.2.8. Conclusion and future work

- In this section, an algorithm for coupling the EnKF and level-set parameterisation for the history matching of porosity and permeability/facies distributions of reservoirs in 3D has been developed
- With the known prior knowledge of the permeability/facies distribution, the initial realisations were created with two-point Statistics (SGS) and multiple-point statistics (*FILTERSIM*).
- It was observed that the EnKF-Level Set algorithm was superior to the standard EnKF method regarding the RMSE value realised after the assimilation of historical production data.
- The average *SSIM* value for the EnKF-Level Set gave a higher value when compared to the standard EnKF method.
- The effectiveness of the narrow-band matrix and how it helps to preserve the facies shapes during the EnKF assimilation stage is shown.
- The method is successful in characterising the non-Gaussian behaviour of fracture distributions in NFR and also channels in the SPE 10 model
- Further work will be to assimilate alternative source of data such as 4D seismic and conductivity into our inversion scheme and to employ compressed sensing

in our EnKF-Level Set algorithm to reduce the domain of the inversion and improve the permeability/facies reconstruction.

7.3 – Comparison of Ensemble-based methods integrated with imaging and regularisation techniques (Numerical Experiment 2)

Novelty

Ensemble Kalman filter (EnKF) is frequently used for history-matching applications. The repeating simulation runs during the EnKF scheme discourages the application of EnKF when the production history of the well is long, and the target is to incorporate the history matching to several aspects in the reservoir-geophysics workflow for calibrating the model. The ensemble smoother (ES) is a reasonable alternative to be used in such cases. In this numerical experiment, a variant of the ensemble smoother (ES-MDA) is utilised. The researcher compares the history matching result of the recently proposed ES-MDA to EnKF on a Gaussian synthetic reservoir. This advanced method is inspired by the equivalence between single and multiple data assimilations for the linear-Gaussian case. The proposed ES-MDA method is tested on a Gaussian sandstone reservoir. The results show that the ES-MDA provides better data matches than those obtained with EnKF, EnKF by reducing the RMS from 14.25 for the EnKF to 3.5 for the ES-MDA and having a computational cost compared with the computational cost of EnKF.

7.3.1 Introduction

In this work, for the second case which is a channelised reservoir, the distance based covariance localisation scheme (Houtemaker, January,2001) is coupled with a previously developed Level set method in section 7.1. The assimilation scheme is the ES-MDA, and it is carried out for the updating and representation of geological lithofacies in the reservoir with stratigraphic compartmentalisation (Jolley, et al., 2007). In section 7.1, a simultaneous parameter and shape reconstruction was implemented where a signed distance function re-parametrised the degraded parameter update by the classical ES-MDA. The researcher introduces the methodology. Covariance localisation means localising the effect of an observation to the state variables that are ‘closer’ to the observations. The various localisation

methods proposed in the literature have the common goal of removing the spurious terms in the cross-covariance matrix; this matrix is in turn used to update the state vectors during the ES-MDA update process. This is done by conditioning the Kalman Gain through a localising function. Each localisation scheme distinguishes itself from each other by how this localising function, also known as the Schur product or the multiplier function, is computed. The motivation of covariance localisation is to achieve a similar level of ES-MDA performance if a larger ensemble size would have been used. However, it requires enormous computational resources to perform history matching if the ensemble size is large.

In this numerical experiment, the researcher analyses the performance between the ES-MDA and a modified EnKF modulation. The modified EnKF modulation requires re-running the simulator from time zero with the updated static properties during the data assimilation stage.

7.3.2 Algorithm specific to our synthetic reservoir

The ES-MDA algorithm is enumerated below.

- 1) Generate the initial ensemble (100 realisations) of permeability using the SGSim (Deutsch & Journel, 1998) for the Gaussian test case.
- 2) Choose the number of assimilation iteration N_a and run the subsection 1 to N_a times
 - a. Forward simulate the 100 models using the multiphase flow simulator, in this case, the ECLIPSE 100 reservoir simulator. (Schlumberger GeoQuest, 2014)
 - b. Augment the ensemble state with the permeability and porosity field, with the predicted production data from the forward problem
 - c. For j=1: production history
 - i. Carry out the ES-MDA analysis using Eqn. (8).
 - d. End for
- 3) Specify the stopping criterion, in this case; the simulation stops when N_a iterations has concluded.

7.3.3 Results

7.3.4 Comparison between EnKF/ES-MDA

To compare the effectiveness of the three methods, EnKF/ES-MDA, two different criteria are considered, the RMS function considering pressure and production data, and the structural similarity ($SSIM$) index. The permeability and the porosity are modified in each step, and other parameters are kept constant.

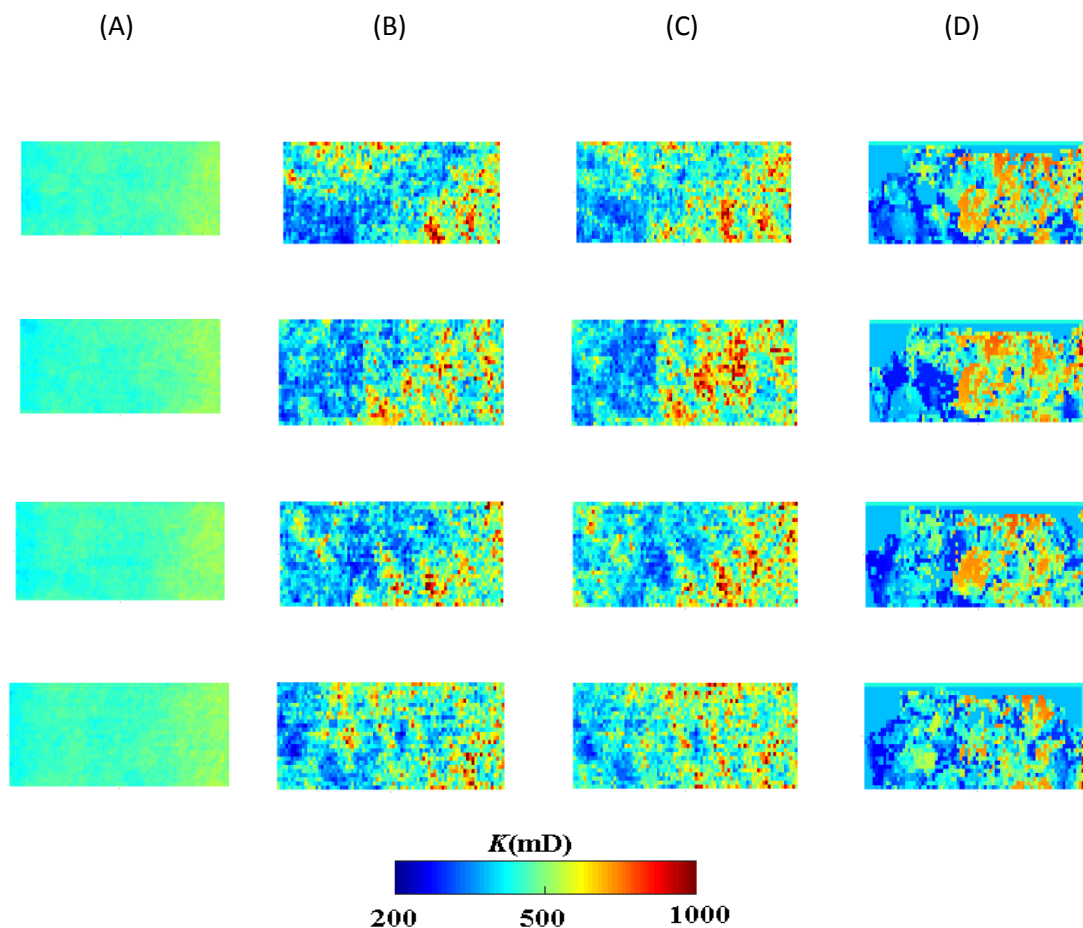


Figure 7.32: Permeability reconstruction: Top-down is Layer 1-4 Column A-Initial mean, Column B-EnKF mean permeability, Column C-ES-MDA mean permeability, Column D-True permeability

Starting with a stochastic realisation generated by SGS, the EnKF history matching algorithm yielded an RMS error of 14.2 after the assimilation of data in the history period. Using the ES-MDA method for history matching, an RMS error of 3.35 after four iterations were realised. Table 7.9 below reports the superiority of the ES-MDA over the EnKF. The initial RMS values for some of the realisations are displayed in column 2. In the comparison of the final RMS value for each method (EnKF to ES-MDA),

the proposed ES-MDA (column 4), yields lower RMS values when compared to the standard EnKF method (column 3).

Table 7.9: RMS function of best seven realisations after EnKF and ES-MDA.

Realisation no.	Initial RMS value	Final RMS value	Final RMS value
		using EnKF	using ESMDA
6	54.64	21.23	14.15
13	342.23	34.34	21.25
32	245.67	42.31	31.20
37	56.22	18.82	10.31
93	32.31	14.2	3.35
63	125.39	25.26	25.93
75	58.38	33.21	4.23

SSIM is used to compare the EnKF-level set history matched reconstructed permeability realisation.

Table 7.10 reports the layer-by-layer and overall field comparison of *SSIM* of the true model permeability and porosity maps to the history matched realisation obtained with the ES-MDA (columns 3 and 5) and EnKF modules (columns 2 and 4).

Table 7.10: SSIM values to reference permeability and porosity field for the two history matched models of the ES-MDA and standard EnKF.

Layer	SSIM value of permeability (EnKF)	SSIM value of permeability (ES-MDA)	SSIM value of porosity (EnKF)	SSIM value of porosity (ES- MDA)
Layer 1	0.7231	0.8924	0.7341	0.8796
Layer 2	0.5423	0.7841	0.5433	0.7782
Layer 3	0.6645	0.7822	0.6723	0.7693
Layer 4	0.5397	0.7021	0.5423	0.7002
Overall Field	0.6174	0.7902	0.6230	0.7818

In the *SSIM* value highlighted in Table 7.10, we see that the ES-MDA history matched realisation gave a higher similarity to the true model than the realisation obtained through the EnKF. The overall *SSIM* value of the ES-MDA model was higher than the EnKF model for both the permeability and porosity reconstruction

7.3.5 Covariance Localization

Covariance localisation means localising the effect of an observation to the state variables that are ‘closer’ to the observations. It is a technique used in history matching to eliminate filter divergence and spurious correlations which are found in both standard EnKF/ES/ES-MDA methods. It selectively assimilates data during the update step by adjusting the correlation between the data measured at a location A and the model parameters or data measured at a further location B to be zero, therefore eliminating long-distance non-zero spurious correlations and increasing the degrees of freedom available for data assimilation. It is usually applied with a Schur product.

The various localisation methods proposed in the literature have the common goal of removing the spurious terms in the cross-covariance matrix; this matrix is in turn used to update the state vectors during the ES-MDA update process. This is done by conditioning the Kalman Gain through a localising function. Each localisation scheme distinguishes itself from each other by how this localising function, also known as the Schur product or the multiplier function, is computed. The motivation of covariance localisation is to achieve a similar level of ES-MDA performance if a larger ensemble size would have been used. However, it requires enormous computational resources to perform history matching if the ensemble size is large

ρ is the localization function or multiplier function, this is a specified parameter for covariance localization. It is introduced to modify the Kalman Gain during update step for both EnkF and ES-MDA. The symbol ‘ \circ ’ is an element-by-element multiplication operator known as the Schur product (Gaspari and Cohn, 1999).

To implement the Schur product in covariance localisation, a correlation function with local support, ρ is defined. The term local support refers to the function taking on non-zero values in a small region and being zero elsewhere. The function ρ is usually defined to be the compactly supported fifth order piecewise rational function defined by Gaspari and Cohn as shown below.

$$\rho$$

$$= \begin{cases} -\frac{1}{4}\left(\frac{|z|}{c}\right)^5 + \frac{1}{2}\left(\frac{|z|}{c}\right)^4 + \frac{5}{8}\left(\frac{|z|}{c}\right)^3 - \frac{5}{3}\left(\frac{|z|}{c}\right)^2 + 1, & 0 \leq |z| \leq c, \\ \frac{1}{12}\left(\frac{|z|}{c}\right)^5 - \frac{1}{2}\left(\frac{|z|}{c}\right)^4 + \frac{5}{8}\left(\frac{|z|}{c}\right)^3 + \frac{5}{3}\left(\frac{|z|}{c}\right)^2 - 5\left(\frac{|z|}{c}\right) + 4 - \frac{2}{3}\left(\frac{|z|}{c}\right), & c \leq |z| \leq 2c, \\ 0, & 2c \leq |z|. \end{cases}$$

$$m_j^a = m_j^f + \rho o \left(\tilde{C}_{MD}^f (\tilde{C}_{DD}^f + \gamma^i C_D)^{-1} \times (d_{uc,j} - d_j^f) \right) \quad (7.25)$$

7.3.6. ES-MDA-Level set coupling methodology

Figure 7.33 shows the novel history matching technique using the covariance localisation Level set technique.

Our proposed algorithm termed **ES-MDA-LS-COV** is enumerated below.

1. Generate the initial ensemble (100 realisations) of permeability using the *FILTERSIM* (MPS) method (Wu, et al., 2006) for the channelised test
2. Choose the number of assimilation iteration N_a and run the subsection 1 to N_a times
 - a) Forward simulate the 100 models using the multiphase flow simulator, in this case, the ECLIPSE 100 reservoir simulator. (Schlumberger GeoQuest, 2014)
 - b) Truncate the spatial permeability and porosity field to arrive at the categorical facies field. Compute the signed distance function and the corresponding narrowband function
 - c) Compute the 5th order Gaspari-Cohn correlation matrix as depicted in figure 7.33
 - d) Augment the ensemble state with the spatial permeability and porosity field, level set functions of the permeability and porosity field with the predicted production data from the forward problem
 - e) For j=1: production history
 - i. Carry out the ES-MDA analysis using Eqn. (7.25).
 - f) End for
 - g) Recover the analysed spatial permeability and porosity pixel fields
 - h) Obtain the facies indicator field of the updated spatial permeability and porosity field by truncating at the relevant threshold mark
 - i) Rectify the conflict between the updated level set function and the updated facies indicator function of the spatial permeability and porosity field

- j) Give preference to the updated level set function and populate the permeability and porosity field for the next run with the values from (i)
- 3. Specify the stopping criterion, in this case; the simulation stops when N_a iterations has concluded.

The mathematical algorithm is described

Algorithm: ES-MDA-LS-COV

1. Input the initial permeability and porosity ensemble generated with SGS for Gaussian case and *FILTERSIM* for Channelized case (at time k), K_k^f, φ_k^f , Production observation data $d_{obs,k}$,
2. Choose the number of data assimilations, N_a and the coefficients γ^i for $i = 1, 2, \dots, N_a$
3. For $i = 1$ to N_a
 - a) Run the ensemble from time zero,
 - b) Obtain the production simulated data d_j^f
 - c) Truncate $K_{(spatial)k}^f$ and $\varphi_{(spatial)k}^f$ at given permeability/
 - d) Set $\begin{pmatrix} K_k^f \\ \varphi_k^f \end{pmatrix} = \begin{pmatrix} K_{k-1}^a \\ \varphi_{k-1}^a \end{pmatrix}$ (for $k \neq 1$)
 - e) If $\begin{pmatrix} K_{k(spatial)}^f \\ \varphi_{k(spatial)}^f \end{pmatrix} > threshold$, then $S(\phi_{k(spatial)}^{f,j}) = 1$ else $S(\phi_{k(spatial)}^{f,j}) = 0$
 - f) Generate two facies system using signed distance function by
Signed distance = $((Sx_1 - Sx_2)^2 + (Sy_1 - Sy_2)^2 + (Sz_1 - Sz_2)^2)^{\frac{1}{2}} = \phi_k^{f,j}$
 - g) Compute the initial narrow band function f
 - h) For each ensemble realisation, perturb the observation vector using
$$d_{uc,j} = d_{obs} + \sqrt{\gamma^i} C_D^{\frac{1}{2}} z_d, \text{ where } z_d \sim \mathcal{N}(0, I_{N_d})$$
 - i) Compute the 5th order Gaspari correlation matrix using Eqn. (10)
 - j) Generate the state vector
$$y_k^{f,j} = [K_k^f, \varphi_k^f, \phi_{k(K)}^f, \phi_{k(\varphi)}^f, d_{sim,k}]^T$$
 - k) Do $k=1$:production history

-
- Update the ES – MDA state spase
 - $y_{k+1}^{a,j} = y_k^{f,j} + \left(\tilde{C}_{MD}^f (\tilde{C}_{DD}^f + \gamma^i C_D)^{-1} \times (d_{uc,j} - d_j^f) \right)$ if overall
 - Update and compute foverall from $\phi_{k(K \& \varphi)}^{a,j}$ gotten from $y_{k+1}^{a,j}$
- I. End do
4. Output K_k^a, φ_k^a and $\phi_{k(K \& \varphi)}^{a,j}$ obtained from $y_k^{a,j}$
 If $\binom{K_{k(spatial)}^a}{\varphi_{k(spatial)}^a} > Threshold$, then $S(\phi_{k(spatial)}^{a,j}) = 1$ else $S(\phi_{k(spatial)}^{a,j}) = 0$
 If $\phi_{k(K \& \varphi)}^{a,j} < 0$ then $S(\phi_{k(Level-set)}^{a,j}) = 0$ else $S(\phi_{k(Level-set)}^{a,j}) = 1$
 5. If $(S(\phi_{k(Level-set)}^{a,j}) = S(\phi_{k(spatial)}^{a,j}))$ = then
 $\binom{K_{k(ES-MDA-LS-COV)}^a}{\varphi_{k(ES-MDA-LS-COV)}^a} = \binom{K_{k(spatial)}^a}{\varphi_{k(spatial)}^a}$
 elseif $(S(\phi_{k(Level-set)}^{a,j}) \neq S(\phi_{k(spatial)}^{a,j}))$. AND. $(S(\phi_{k(Level-set)}^{a,j}) = 1)$ then
 $\binom{K_{k(ES-MDA-LS-COV)}^a}{\varphi_{k(ES-MDA-LS-COV)}^a} = 1.05 \times Threshold$ permeability/porosity value
 endif
 if $S(\phi_{k(Level-set)}^{a,j}) \neq S(\phi_{k(spatial)}^{a,j})$. AND. $(S(\phi_{k(Level-set)}^{a,j}) = 0)$ then
 $\binom{K_{k(ES-MDA-LS-COV)}^a}{\varphi_{k(ES-MDA-LS-COV)}^a} = 0.95 \times Threshold$ permeability/porosity value
 endif
 6. Output $\binom{K_{k(ES-MDA-LS-COV)}^a}{\varphi_{k(ES-MDA-LS-COV)}^a}$
 7. Honour the permeability and porosity values from actual well data by enforcing a non-update on the pixel location in the simulation grid
 8. Set iteration count $i = i + 1$
 - a. end for
- end program
-

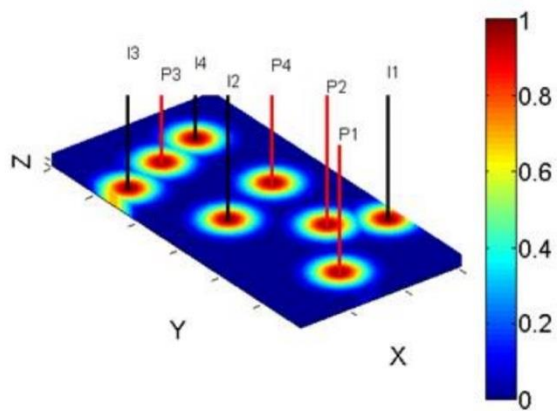


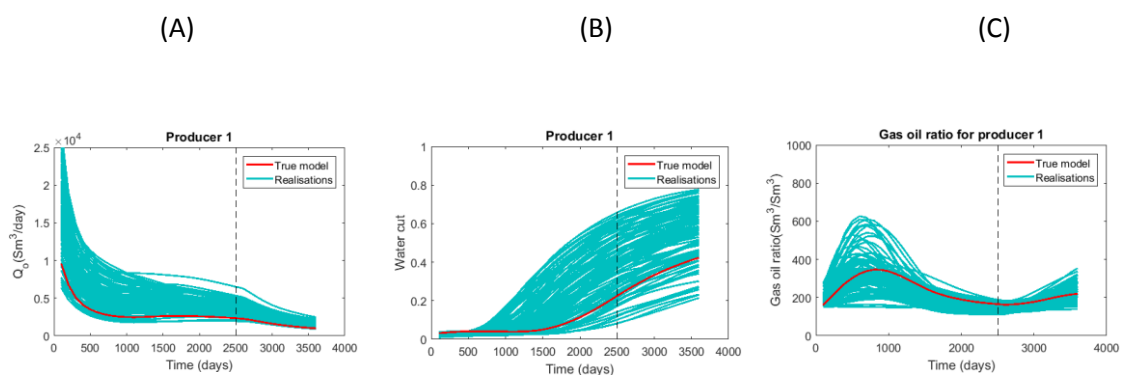
Figure 7.33: Schematic showing the 5th order Gaspari-Cohn covariance function

Results and discussions for the novel ES-MDA Level set-Covariance localisation scheme

Two experiments are conducted;

- Experiment 1 is using 100 ensemble members generated from *FILTERSIM* with covariance localisation and Level set. It is called **ES-MDA-LS-COV**
- Experiment 2 is using 100 ensemble members generated from *FILTERSIM* using the standard ES-MDA. It is called ES-MDA standard

Figure 7.34 shows the production profile of the initial ensemble. Top-down is for producers 1-4. Column A: Oil production rate, Column B is water cut, and Column C is the Gas-oil ratio, Figure 7.35 shows the Well bottom hole pressure for the four injectors, field oil recovery ratio and RMS Cost function of the initial ensemble



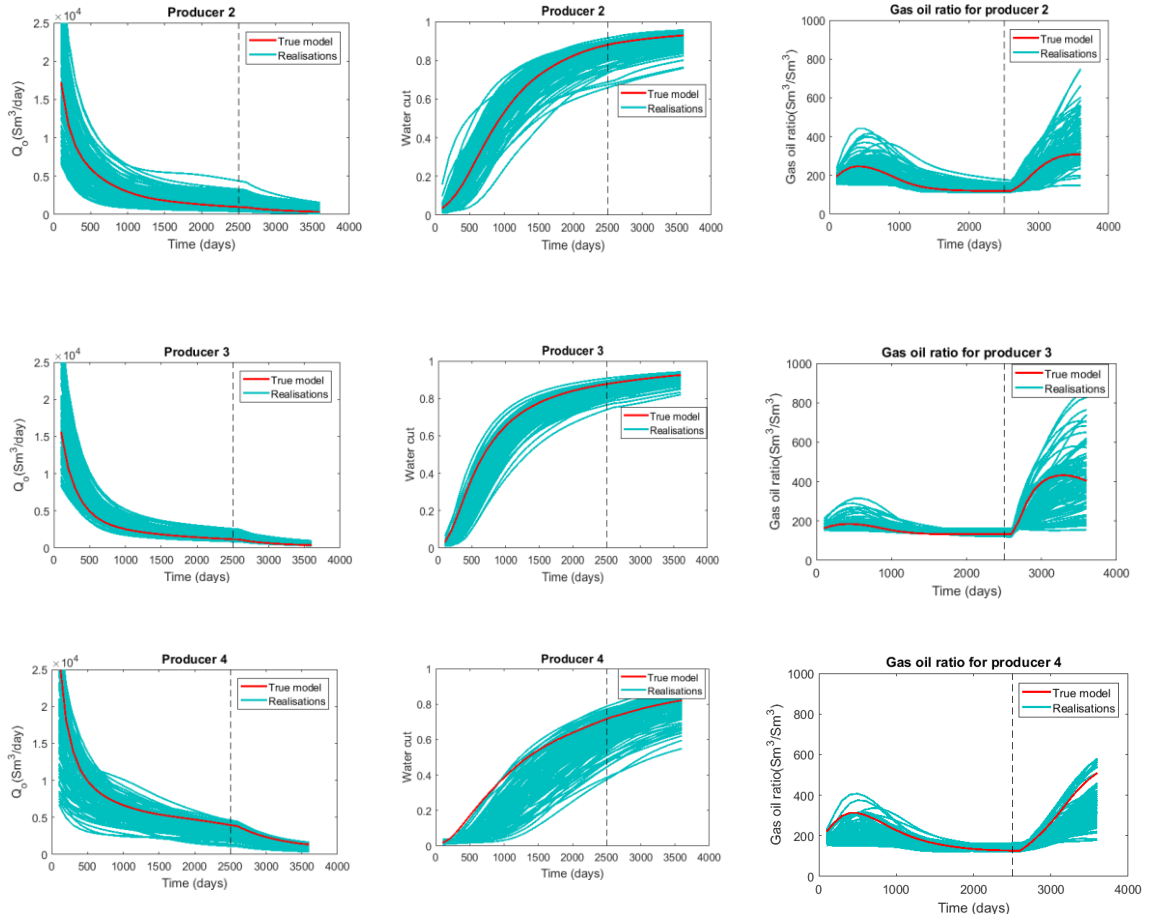


Figure 7.34: Production profile of initial ensemble. Top-down is for producer's 1-4. Column A: Oil production rate, Column B is water cut, and Column C is the Gas-oil ratio. . The red curve represent the true data and the cyan overlay lines represents the realisations.The vertical dashed line represents the historical (left of this line) and prediction stages (right of this line)

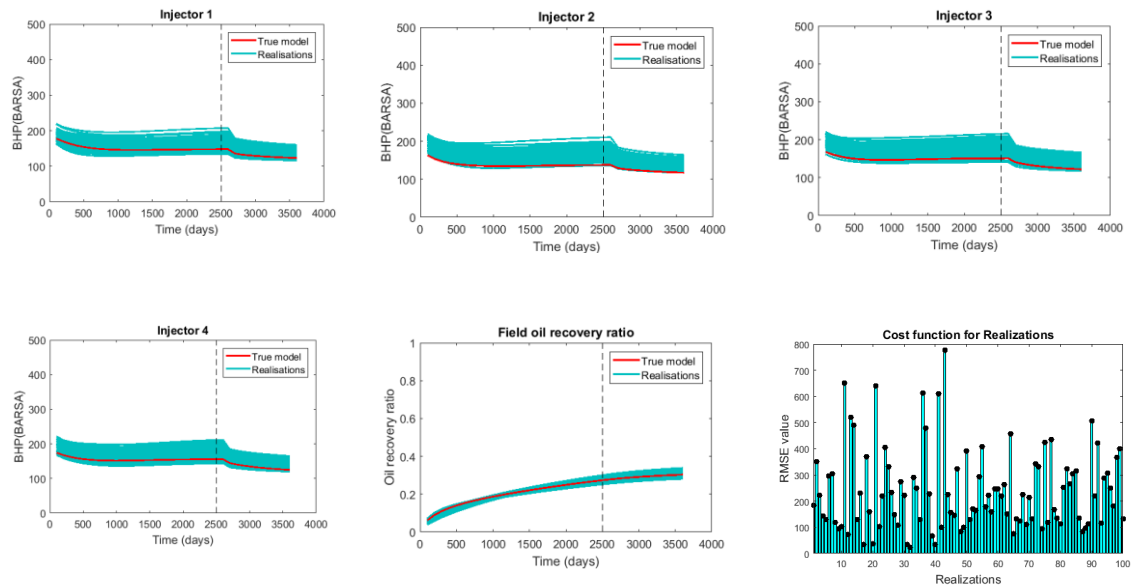


Figure 7.35: Well bottom hole pressure for the four injectors, field oil recovery ratio and RMS Cost function of the initial ensemble. The red curve represent the true data and the cyan overlay lines

represents the realisations. The vertical dashed line represents the historical (left of this line) and prediction stages (right of this line)

We see in figure 7.34 -7.36 a decrease in the spread of the ensemble. Figure 7.36 shows the production profile of ES-MDA-LS-COV ensemble. Top-down is for producers 1-4. Column A: Oil production rate, Column B is water cut, and Column C is the Gas-oil ratio, Figure 7.37 shows the Well bottom hole pressure for the four injectors, field oil recovery ratio and RMS Cost function of the ES-MDA-LS-COV ensemble

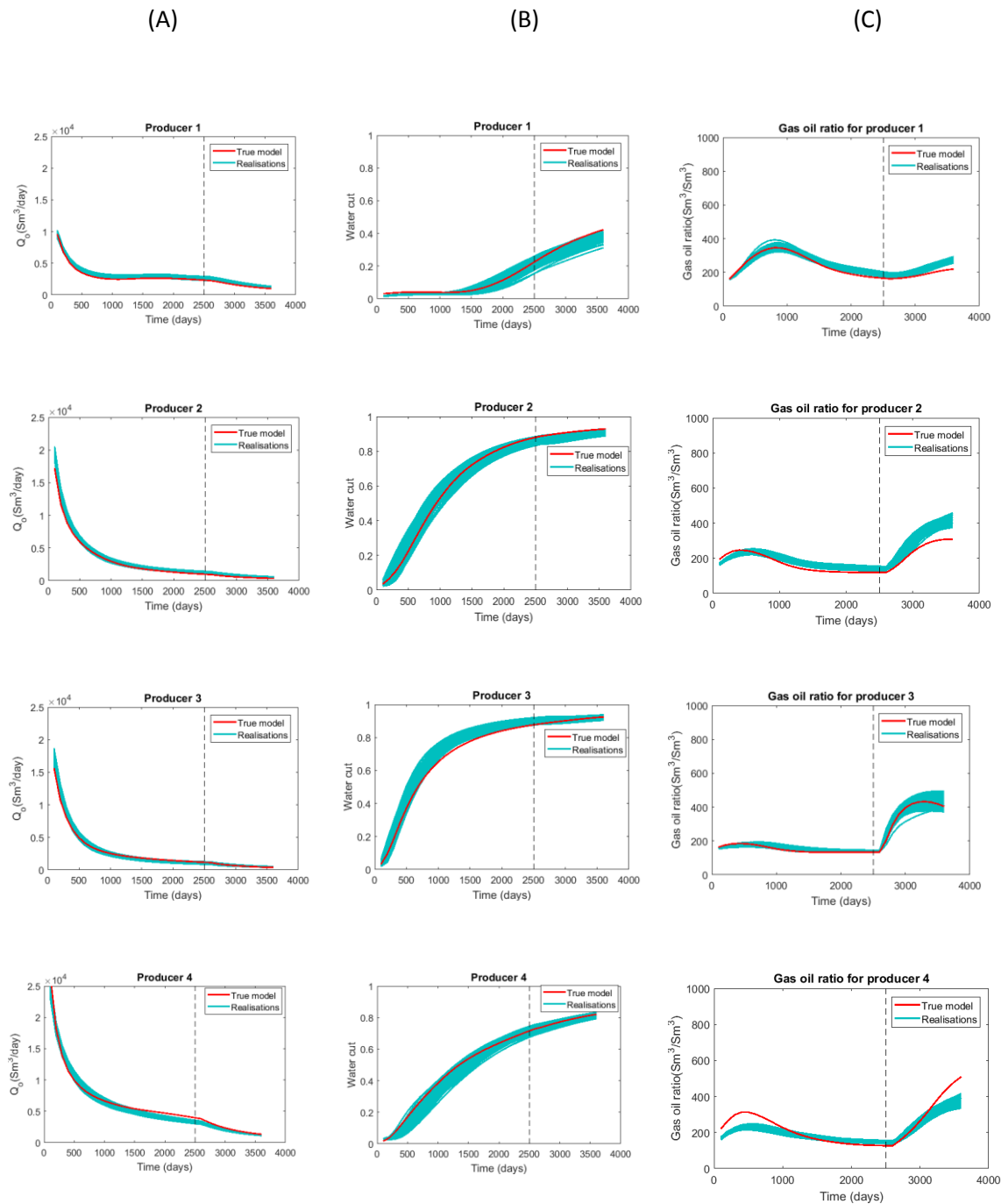


Figure 7.36: Production profile of ES-MDA-LS-COV. Top-down is for producers 1-4.Column A: Oil production rate, Column B s water cut and Colum C is the Gas-oil ratio. The red curve represent the true data and the cyan overlay lines represents the realisations.The vertical dashed line represents the historical (left of this line) and prediction stages (right of this line)

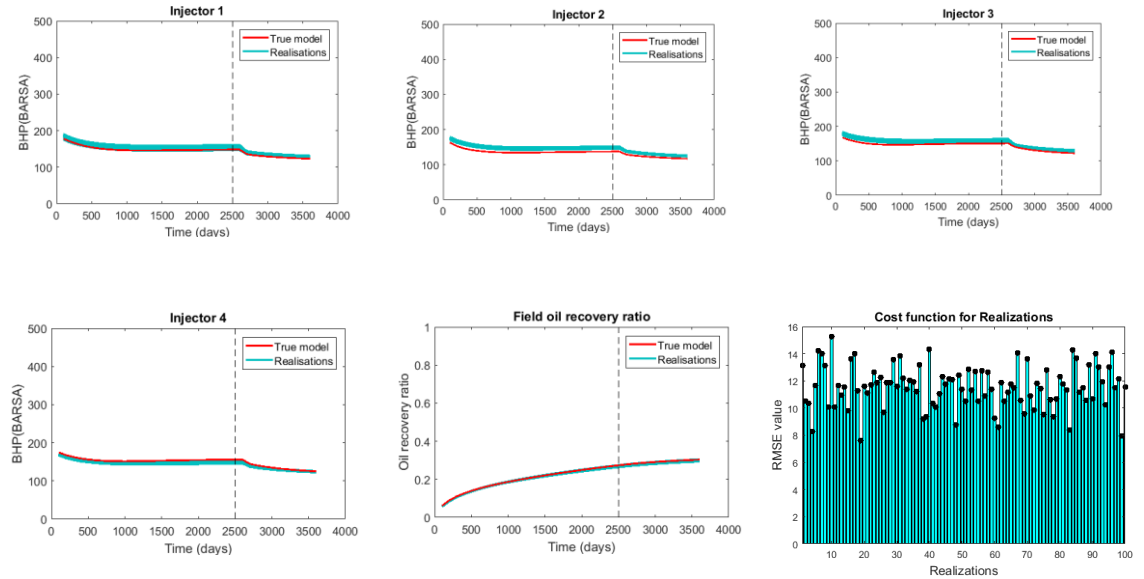
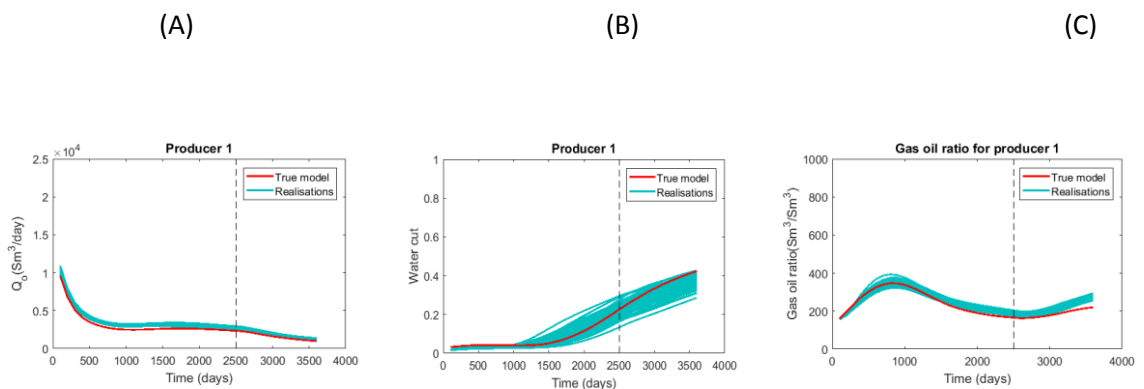


Figure 7.37: Well bottom hole pressure for the four injectors, field oil recovery ratio and RMS Cost function of the ES-MDA-LS-COV ensemble. The red curve represent the true data and the cyan overlay lines represents the realisations.The vertical dashed line represents the historical (left of this line) and prediction stages (right of this line)

Figure 7.38 shows the production profile of ES-MDA ensemble. Top-down is for producers 1-4.Column A: Oil production rate, Column B is water cut, and Colum C is the Gas-oil ratio, Figure 7.39 shows the Well bottom hole pressure for the four injectors, field oil recovery ratio and RMS Cost function of the ES-MDA ensemble.



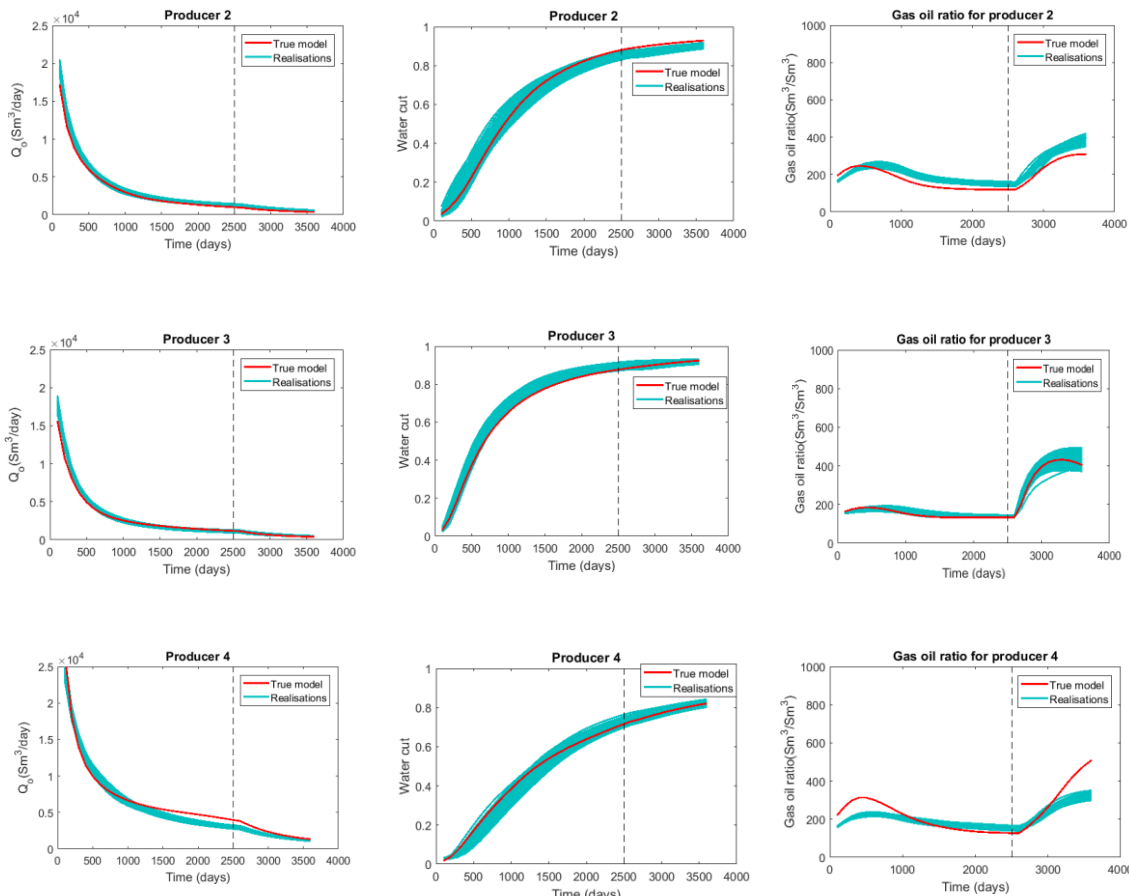


Figure 7.38: Production profile of ES-MDA Standard. Top-down is for producers 1-4.Column A: Oil production rate, Column B s water cut and Colum C is the Gas-oil ratio .The red curve represent the true data and the cyan overlay lines represents the realisations.The vertical dashed line represents the historical (left of this line) and prediction stages (right of this line)

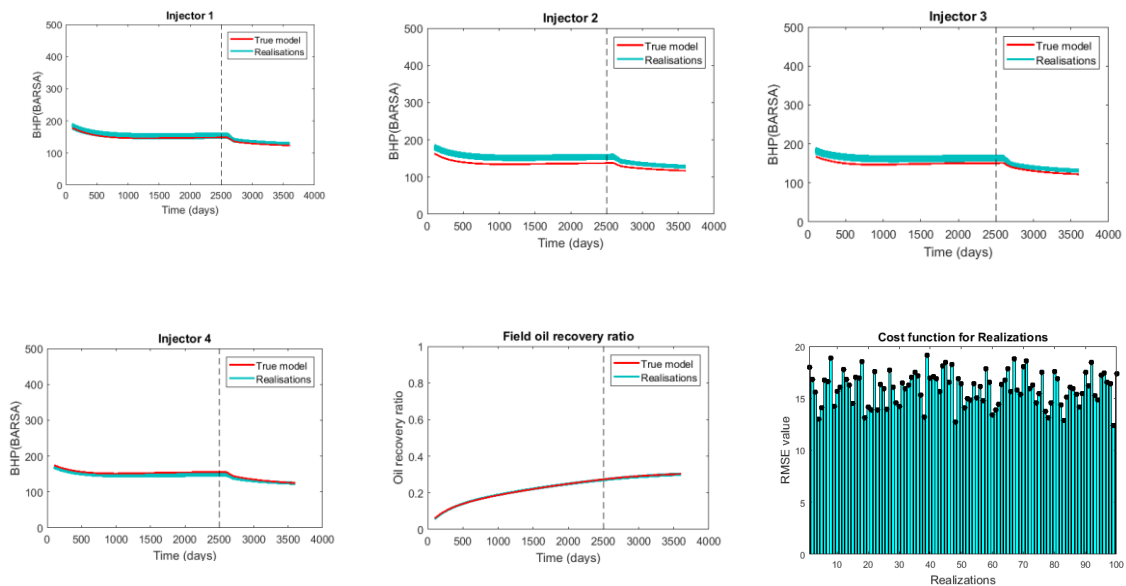
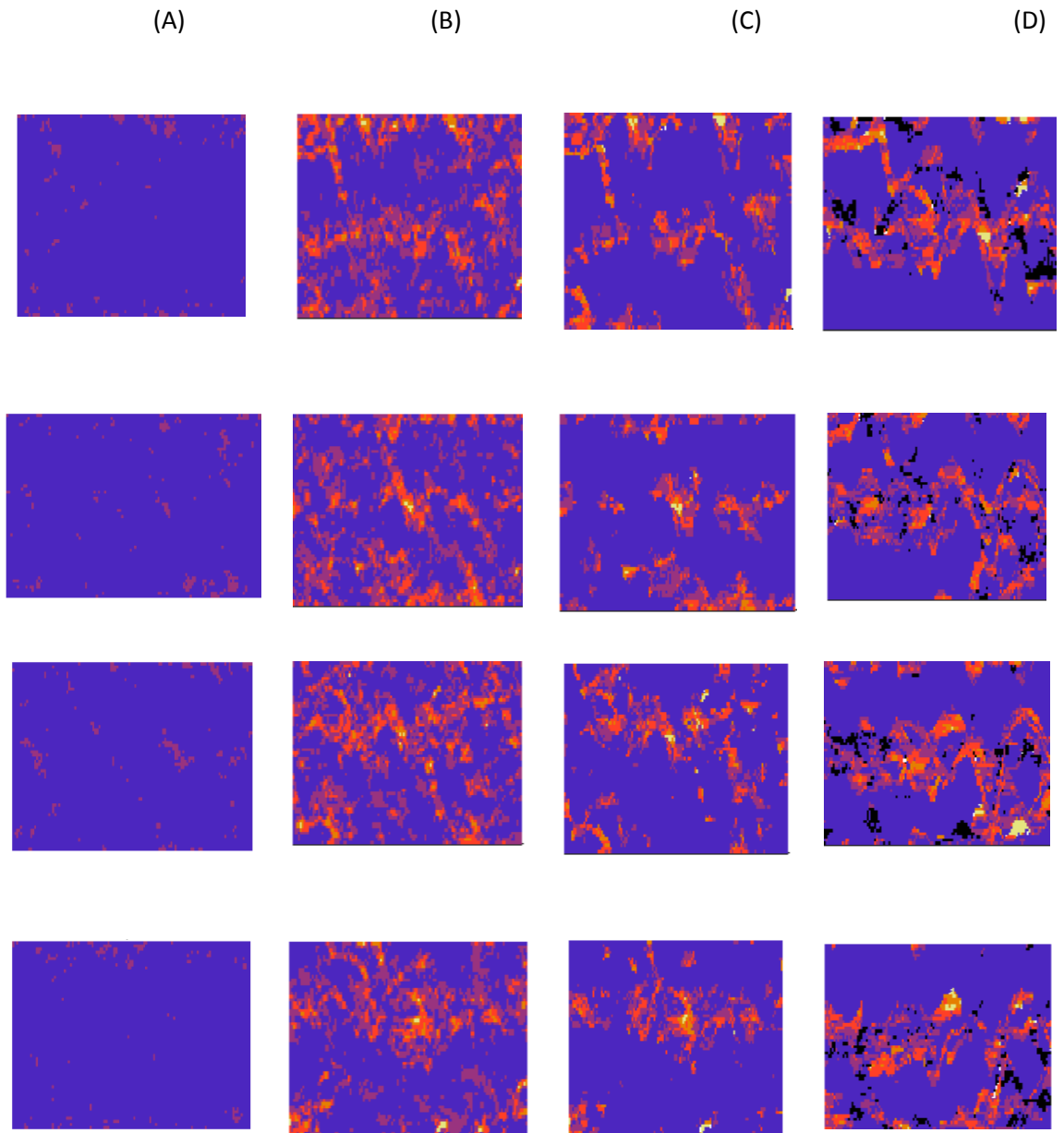


Figure 7.39: Well bottom hole pressure for the four injectors, field oil recovery ratio and RMS Cost function of the ES-MDA ensemble. The red curve represent the true data and the cyan overlay lines

represents the realisations. The vertical dashed line represents the historical (left of this line) and prediction stages (right of this line)

Figure 7.40 shows the permeability reconstruction: Top-down is Layer 1-5 Column A-Initial mean, Column B-ES-MDA mean permeability, Column C-ES-MDA-LS-COV mean permeability, Column D-True permeability. From figure 7.40 we see a perseverance of the bi-modal distribution of the permeability and high similarity to the true model as at when compared to the model recovered with the standard ES-MDA.



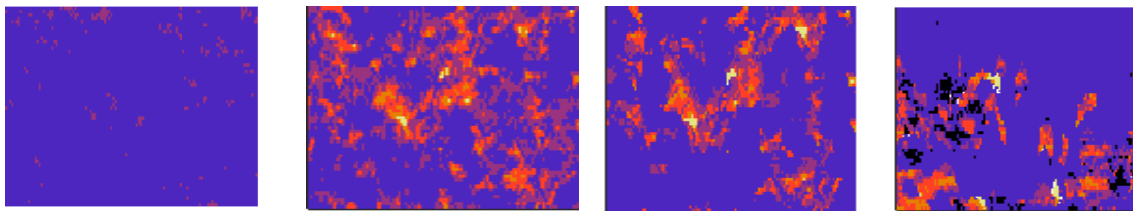


Figure 7.40: Permeability reconstruction: Top-down is Layer 1-5 Column A-Initial mean, Column B-ES-MDA mean permeability, Column C-ES-MDA-LS-COV mean permeability, Column D-True permeability

7.3.7 Conclusion.

- In this work, the performance of the EnKF/ES-MDA is compared based on the nature of permeability/porosity reconstruction.
- With the prior knowledge of the permeability distribution, the initial realisations were generated with two-point Statistics (SGS). It was observed that the ES-MDA algorithm was superior to the standard EnKF method regarding the RMS value realised after the assimilation of historical production data.
- The average $SSIM$ value for the ES-MDA set gave a higher value when compared to the standard EnKF method.
- The researcher also compared the performance of the ES-MDA standard with the ES-MDA modified with level set and covariance localisation.
- Covariance localisation localised the effect of an observation to the state variables that are ‘closer’ to the observations.
- Filter divergence and spurious long-range correlations were reduced leading to a better permeability reconstruction to the standard ES-MDA implementation.
- The method gave a lower RMS deviation to the true model as a result of the geometry of the channels being in close agreement to the true permeability model.

7.4- Improved History Matching using 4D Seismic results (Numerical Experiment 3)

Novelty

This work expantiates on the improvement of an integrated methodology for the automatic history matching of compartmentalised reservoirs using 4D seismic results, stochastic realisations and the Ensemble Kalman Filter method. The comparison of

different history matching approaches using the Ensemble Kalman Filter (EnKF) to update the Fault Transmissibility Multipliers (FTM) which is initially estimated with and without considering the 4D seismic results are compared. In this study, the main parameters updated during the history matching are two-phase fault transmissibility multipliers (FTM), effective porosity and absolute permeability of a synthetic 3D reservoir. The true impedance map and the various changes in reservoir pressure and saturation were computed a-priori from 4D seismic results. The systematic computation of two-phase fault transmissibility multipliers is based on the integration of the collected 4D seismic results and a previous method validated in our previous work based on a deterministic model, using the Levenberg Marquardt method (LM). The stochastic method used employed the Sequential Gaussian Simulation (SGS) technique to generate 100 initial models. During history matching, the saturation distributions are computed from the forward modelling of a two-phase system (oil-water). The impedance maps are estimated using the Gassmann equation and compared with the true impedance map as part of the History Matching loop. In validating the results, the cost function consisting of two components is calculated, the first is the structural similarity index of the reconstructed impedance images to the real impedance image and the second is the RMS value, ℓ_2 – norm of the difference between the true (real) and the simulated pressure-production data. The EnKF history matching using the two-phase FTM values considering 4D seismic results produced lower cost function values compared with the model using the initial FTM multiplier without considering 4D seismic results. The EnKF history matching algorithm using 4D seismic presented in this work produced results closer to the true reservoir impedance map compared to our previous 4D gradient based history matching method.

7.4.1. Introduction

On faults, 4D-seismic data, forward modelling of rock and fluid physics relationships enables saturation inversion, and subsequently a mathematical determination of two-phase fault transmissibility multipliers as they change over time. Computing them and implementing them back into the simulation model, and evaluating the result on history matching makes up the first part of this work.

The second part of this work is in using the Ensemble Kalman Filter to determine the history matched value of the FTM and determine its RMS value about deviation from

the observed data. The final FTM value obtained from the EnKF and our LM gradient method are compared together. The quality of the initial realisations is a significant factor in the success of the EnKF history matching process and hence, influences its results. In this work, the permeability field, porosity field and the FTM were treated as the uncertain parameters. The permeability and porosity fields were modelled using two-point statistics from the geostatistical software used in this work (Deutsch & Journel, 1998). The idea of this paper is aimed at reconstructing the permeability, porosity and impedance fields by assimilating the pressure data, production data and 4D seismic during the history matching scheme.

We compare and analyse the performance of the ensemble Kalman filter (EnKF) over the LM gradient method developed in our previous work. The production data to be assimilated are the injector pressure, water, and oil production rates. This numerical experiment is arranged in this order: Section 7.4.2 discusses the problem formulation and background methods. This section contains the forward model used for this work, EnKF methodology for history matching, Levenberg-Marquardt gradient method for history matching, initial ensemble construction with the SGS methods. Section 7.4.3 discusses the one-phase and multiphase fault modelling utilised in this work. Section 7.4.4 enumerates on 4D seismic which includes the forward modelling and quantitative inversion scheme. Section 7.4.5 explains the derivation of the basic methodology in our Gradient-based deterministic and EnKF stochastic history matching scheme; Section 7.4.6 gives several numerical examples and discussion of the results obtained. Section 7.4.7 presents conclusions and indications for future research.

7.4.2 Levenberg-Marquardt method

The Levenberg-Marquardt (LM) method was implemented to solve some of the limitations presented by the Gauss-Newton method such as it becoming infeasible for large-scale inverse problems due to the extensive computational expense of generating sensitivity matrices at each iteration. Furthermore, the Gauss-Newton approach has been reported to show slow convergence or unacceptable matches of pressure data, in cases of bad initial estimates (Wu, et al., 1999) and considering that computing all sensitivity coefficients is impractical if the amount of observation data and the number of model parameters are large, (Bi, et al., 2000).

$$\begin{aligned}
\delta m^{l+1} = & \frac{m^l - m_{prior}}{1 + \lambda_l} \\
& + C_M^{-1} G_l^T [(1 + \lambda_l) C_D + G_l^T C_M G_l^T]^{-1} \left[\frac{G_m(m^l - m_{prior})}{1 + \lambda_l} \right. \\
& \left. - (g(m^l) - d_{obs}) \right]
\end{aligned} \tag{7.26}$$

λ_l = Levenberg-Marquardt parameter evaluated at the l^{th} iteration step (Liang, 2007)

This is necessarily a modification of the Gauss-Newton method to the Hessian matrix, and appropriate “trust region” amendments (More & Sorensen, 1983) to improve convergence and avoid the need for estimating a step length (Oliver & Chen, 2010). The Levenberg-Marquardt procedure is a combination of two minimisation methods: the steepest descent method and the Gauss-Newton method. In the steepest descent method, the sum of squared errors is minimised by updating the parameters in the direction of steepest descent. In the Gauss-Newton procedure, the sum of the squared errors is minimised by assuming the least squares function to be locally quadratic and finding its minimum. The value λ_l controls the search direction; as it becomes large, and the parameters are far from the optimal value, the Levenberg-Marquardt iteration behaves similarly to the steepest-descent method (linear convergence). When λ_l is small, and the parameters are close to the optimal value, the iteration behaves similarly to the Gauss-Newton method (quadratic convergence). The key drawback of gradient-based methods is that they do not consider spatial covariance models exhibited by model parameters and tend to be computationally costly due to the calculation of sensitivities (Oliver et al., 2008)(Etienam et al., 2017) (Oliver, et al., 2008).

7.4.3 Initial ensemble construction

We use the Sequential Gaussian Simulation for absolute permeability and effective porosity modelling. Sequential Gaussian Simulation (SGS) is used in the estimation of the permeability property at regions where the permeability values were not made known by constraining the simulation to the permeability at the well locations (Deutsch & Journel, 1998). The procedure uses geostatistical assumptions on the parameter distribution in the reservoir indicated in the semi-variogram. SGS then creates an ensemble of realisation which honours the properties at the two well

locations. Open source geostatistical software (Deutsch & Journel, 1998) was used to generate 100 realisations of permeability and porosity values. The semi-variogram model employed in this paper is Gaussian.

7.4.4. Fault property estimation and 4D seismic results

In this section, the modelling of fault properties concerning one phase and multiphase flow will be discussed.

A common challenge on modelling faults in reservoir models is capturing their three-dimensional nature, along with their complex petrophysical properties that are dynamically dependent on the fluids flowing across them. Faults enhance the vertical connectivity of reservoirs while impeding the horizontal connectivity. Naturally, this has implications on reservoir performance and overall economics, particularly in the case of compartmentalised reservoirs, for which a comprehensive understanding of fault dynamics has immediate practical significance. Fault Transmissibility Multipliers (FTM) is commonly applied to the representation of faults and their effects on production in reservoir simulation.

These are a function of the properties in the fault zone and associated connected grid-blocks, explicitly used in flow simulation to implicitly represent the effect of low permeability rocks other barriers to flow without modelling grid blocks for them explicitly. Lia et al., (1997) established that fault transmissibilities account for the most significant uncertainty on reserves in the North Sea, and this uncertainty is subsequently carried forward to the history matching process. Recent studies indicate that fault transmissibility multipliers can be quantified from petrophysical parameters (Manzocchi et al., 2002, 2010). Fault thickness and permeability data has enabled FTM values to be computed and subsequently linked to grid block faces associated to the fault zone, thus taking into consideration the effect of faults on fluid flow (Knipe et al., 1998; Zijlstra et al., 2007; Al-Busafi, 2005).

Furthermore, it has been discovered that history matching North Sea production data showed improved results when taking into consideration fault transmissibility multipliers generated from realistic rock property data. Jolley et al., 2007, implemented locally derived fault properties, and systematically calculated fault permeability and absolute transmissibility multipliers. FTM values were derived from

the property grids of the up-scaled model using relations and correlations from (Manzocchi, et al., 1999)

7.4.5 Absolute Transmissibility Multiplier

After the generation of a reliable structural model, the next step is to account for the effect of faults on fluid flow. Reservoir simulators such as Eclipse™ calculate the flux between grid-blocks as a function of transmissibilities between them. The transmissibility between two grid-blocks (1 and 2) refers to the average harmonic permeability between their centres, divided by the distance between them. Most commercial simulators incorporate a similar approach as (Manzocchi, et al., 1999) in the analytical representation of faults. For a system of n distinct regions between grid-block centres:

$$Trans = \left[\sum_{i=1}^n \frac{L_i}{k_i} \right]^{-1} \quad (7.27)$$

Where n denotes the number of distinct permeability regions, i denote each region, L_i is the length of each region and k_i is the permeability. For a system of two adjacent grid blocks

$$Trans_{1,2} = \frac{2T_{ABS}}{\frac{L_1}{k_1} + \frac{L_2}{k_2}} \quad (7.28)$$

In the simplified case of a homogeneous reservoir, zone where $\mathbf{L}_1 = \mathbf{L}_2 = \mathbf{L}$ and $\mathbf{k}_1 = \mathbf{k}_2 = \mathbf{k}$

$$T_{ABS} = \left[1 + \frac{t_f}{L} \left(\frac{k - k_f}{k_f} \right) \right]^{-1} \quad (7.29)$$

For the fault in the question of this study, the system is represented by two grid-blocks of lengths L_1 and L_2 , permeabilities k_1 and k_2 , and a fault with a thickness t_f , and permeability k_f separating them (3 distinct permeability regions, $n=3$) as shown in figure 7.41.

$$TransF_{1,2} = \frac{2}{\frac{L_1 - t_f}{k_1} + \frac{2t_f}{k_f} + \frac{L_2 - t_f}{k_2}} \quad (7.30)$$

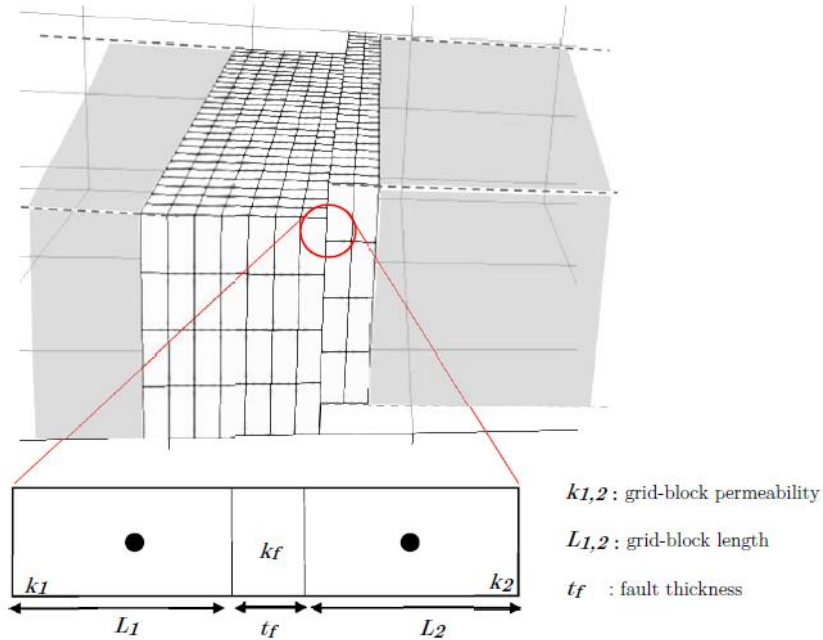


Figure 7.41: Schematic showing the derivation of the phase-specific transmissibility multiplier

The absolute single phase transmissibility multiplier, in this case, is the ratio of transmissibility between the two grid-blocks calculated by including the fault rock, against that calculated by excluding it.

$$T_{ABS} = \left[1 + t_f \frac{\left(\frac{2}{k_f} - \frac{1}{k_1} - \frac{1}{k_2} \right)}{\left(\frac{L_1}{k_1} + \frac{L_2}{k_2} \right)} \right]^{-1} \quad (7.31)$$

7.4.6 Multi-phase Fault Rock Properties

Historically multiphase flow properties of faults have not been widely considered in simulation and history matching (Fisher & Jolley, 2007), and existing studies focus primarily on improving geological and petrophysical understanding on exploration fault seal analysis. Fault rocks have smaller pore throats. This means that if they are water-wet, they can be expected to have waters saturations close to that of the free water level and negligible relative permeability to oil and gas. The surrounding adjacent reservoirs have lower water saturation, and subsequently lower relative permeability to water, resulting in substantial cross-fault water flow being rather unlikely (Fisher & Jolley, 2007).

At a certain height above the free water level, the buoyancy force from the

hydrocarbon column could be high enough to overcome the fault rock threshold pressure, allowing it to have a finite relative permeability to petroleum (Zijlstra, et al., 2007). Results from relative permeability measurements on fault rocks show that for buoyancy forces of most hydrocarbon columns, the effective permeability of the fault rock to hydrocarbons can be two or more orders of magnitude lower than their absolute permeabilities (Al-Hinai et al., 2006). This implies the fault transmissibility to hydrocarbons can be significantly higher than the estimate based on single-phase permeability only. Laboratory studies associated with multiphase fault rock properties have yielded data on capillary pressures (threshold and intrusion) across the range of saturation, Knipe et al., 1997; Pittman, 1981. The software application has been embedded into literature through three main methods of capillary pressure and relative permeability measurements.

Pseudo-relative permeability and capillary pressure functions were computed for grid-blocks proximal to the fault to obtain effective flow properties for the fault zone, by Manzocchi et al., (2002). Al-Busafi et al., (2005) proposed an approach whereby the fault was included in the simulation model as a discrete feature. Zijlstra, et al., 2007 practically extended on Manzocchi, et al., 2002 by dividing faults into three zones based on the position about the free water level, followed by subsequent calculations of absolute permeability, threshold pressure and transmissibility multipliers based on laboratory results. (Al-Hinai et al., 2006) Moreover, (Zijlstra et al. 2007) have attempted implementing multiphase flow properties of faults by taking into account capillary pressure and relative permeability of siliciclastic fault rocks of a southern North Sea Rotliegend reservoir with a 250 bar pressure differential build up between across a fault. Al-Hinai, et al., (2006), portrayed the fault as discrete grid-blocks by applying local grid refinement, followed by assigning individual capillary pressure and relative permeability curves to the grid-blocks.

The principal disadvantage of this lies in the impractical simulation times that arise with the increasing number of grid blocks, especially when considering field-scale simulation. Being a sand-rich reservoir, the presence of clay entrainment and cementation was considered to present insufficient permeability reduction ability to result in such a pressure differential. Zijlstra, et al., (2007), applied the relative permeability attributes of clay-poor fault rock into the simulation model with sufficient production history, resulting in swift history matches, in stark contrast to previous

many unsuccessful runs using trial and error based methods of determining transmissibility multipliers.

Overall, the practical significance of considering multiphase properties of fault rocks have become more evident in the studies that have taken place. When considering two-phase flow (oil, water), the effective phase permeability is a product of the absolute single phase permeability k , and the saturation dependent relative permeability k_{rp} . Implementing this concept into the single phase expression for Transmissibility leads to the phase transmissibility; I derive our relevant multiphase equations below accordingly;

$$Trans_p = \left[\sum_{i=1}^n \frac{L_i}{k_i k_{rp,i}} \right]^{-1} \quad (7.32)$$

The subscript p denotes the phase, oil or water. $k_{rp,i}$ is the relative permeability of a region i .

The saturation in grid-blocks is dynamic, changing as a function of both distance and time, along with relative permeability throughout the simulation. Equation (7.32), as a result, is dependent on saturation through k_{rp} . Following (Manzocchi, et al., 2002), a multiphase analogy is therefore implemented through the two phase transmissibility multiplier T_p ; the phase specific ratio of transmissibility between the grid-block centers, both including and excluding the fault.

In the case of the simulation model of this study, $Trans_p$ including the fault is given by:

$$\left[\frac{L_1}{k_1 k_{rp,1}} + \frac{t_f}{k_f} + \frac{L_2}{k_2 k_{rp,2}} \right]^{-1} \quad (7.33)$$

Simulation results indicate the permeability on either side of the fault zone to be the same, so $k_1=k_2=k$.

$Trans_p$ Excluding the fault properties is given by:

$$\frac{2k k_{rp}}{L_1 + L_2} \quad (7.34)$$

Where k_{rp} is the relative permeability of a given phase in the grid-blocks at a given saturation S_w .

$$T_p = \frac{\left[\frac{L_1}{k_1 k_{rp} 1} + \frac{t_f}{k_f} + \frac{L_2}{k_2 k_{rp} 2} \right]^{-1}}{\frac{2k k_{rp}}{L_1 + L_2}}$$
(7.35)

7.4.7. 4D-Seismic results and Reservoir Simulation

4D Seismic is the repeat acquisition of seismic data over time, enabling the determination of changes that occur in the reservoir due to production and injection. The principal value with regards to history matching is the ability to incorporate the additional information in constraining or updating the reservoir model, either at a field or localised scale. The most direct use of time-lapse data lies in the qualitative monitoring of changes in the reservoir, by identifying zones in which the seismic attributes (i.e. impedance) has changed over time and quantitatively linking them to changes in pressure and saturation. Quantitative integration of 4D seismic data with history matching workflows is a highly active domain(Etienam et al., 2017) , regarding constraining reservoir models along with production data to improve the distributional characterisation of porosity and permeability.

4D Seismic integration on specific fault zone parameters in history matching has been relatively sparsely explored in the literature. Villegas et al., (2009) presented a method of optimising fluid-rock properties in compartmentalised reservoirs by using 4D seismic results following the methodology of Manzocchi et al., (1999) on a realistic synthetic model. The workflow indicated that considering multiphase fault properties into the updated model, lead to lesser iterations in history matching. Benguigui et al.(2014) applied a similar methodology and incorporated 4D seismic results, on single-phase absolute transmissibility multipliers, on the North Sea, Heidrun field, resulting in an improved match. When time-lapse data is obtained from repeat surveys, it can be quantitatively linked to dynamic reservoir changes. This is performed through numerical approximations of the seismic impedance, estimated through rock and fluid physics relations, ultimately enabling the computation of pressure and saturation estimates that can compare to well data and reservoir simulation predictions. The overall process can be summarised in two steps, forward modelling of rock and fluid physics, followed by quantitative inversion (Etienam, et al., 2017)

7.4.8 Quantitative inversion

Time-lapse seismic signatures can be calibrated with observed historical data from wells through a reservoir simulator. When this is performed on a field over which two or more repeat surveys carried out at different operational calendar times, the correlation coefficients that relate the seismic signature difference to the reservoir's pressure and saturation changes can be estimated. By using seismic attributes such as impedance, that varyingly responds to changes in the reservoir, changes in pressure and saturation can be determined (Macbeth, et al., 2006). Seismic attributes such as impedance are typically computed at a chosen horizon, such as the top, base or an intra-reservoir layer. This is referred to as the initial baseline survey at a picked horizon of interest (Cole, et al., 2002). Seismic impedance is the product of seismic wave velocity, and the density of the rock it is travelling through. The principal factors it is dependent on are rock type (R), thickness (T), porosity (φ), pressure (P) and saturation (S_o, w), and can be expressed in the form of a function,

$$I = I(x, y, T, \varphi, P, S) \quad (7.36)$$

The thickness and porosity term can be ignored in the case of a non-compacting reservoir for negligible production or injection induced changes in T and φ .

A repeat survey response $I_r(x, y)$, can be expressed as a function of the baseline survey $I_b(x, y)$, and changes over time-lapse through a 1st order Taylor expansion.

$$I_r(x, y, P, S) \approx I_b(x, y, P_i, S_i) + \frac{\delta I}{\delta P} \Delta P + \frac{\delta I}{\delta S} \Delta S_o \quad (7.37)$$

ΔP and ΔS_o are changes in reservoir pressure and oil saturation. The right hand side partial derivatives are largely dependent on the initial state of the reservoir and fluid physics. The above equation leads to a linear approximation of the time-lapse seismic attribute ΔI , estimated through the difference between the baseline and repeat survey. Equation (7.37) rearranged and normalized becomes (Macbeth, et al., 2006),

$$\frac{\Delta I(x, y)}{\bar{I}_b} \approx \frac{\Delta P(x, y)}{\bar{P}_i} + \frac{\Delta S_o(x, y)}{\bar{S}_{oi}} \quad (7.38)$$

\bar{P}_i and \bar{S}_{oi} are the initial average reservoir pressure and oil saturation. \bar{I}_b is the baseline average response. Despite being a simplified linear approximation, equation (7.38) remains applicable given that ΔP and ΔS_o are not very large ($\Delta P \approx 5 - 10 \text{ MPa}$, $\Delta S_o \approx 1 - S_{wc}$), determined through rock physics modelling and laboratory

measurements by (Macbeth, 2004)

7.4.9 Methodology

7.4.9.1 Pseudo-relative Permeability Functions and capillary pressure considering 4D seismic

In this section the initial maximum and minimum value of k_{rp} , P_c , T_p to be used in the history matching scheme are estimated. This is necessary to estimate the minimum and maximum values of these dynamic variables required in the history matching loop. Being a dynamic property, if we are to consider applying two-phase properties to the fault transmissibility multiplier, it must be indexed to the saturation of the grid-block upstream to the fault (Manzocchi, et al., 2002). This is necessary to derive grid-block specific pseudo-relative permeability functions that are inclusive of the properties of the fault rock and the upstream grid-block. This subsequently enables the two-phase analogue of single phase multipliers to be back-computed from the grid-block pseudo-relative permeability functions for oil and water (Mahmood & Villegas, 2016). Pseudo-relative permeabilities refer to the incorporation of more information into the rock physics of grid-blocks. They are applied to reduce the dimensionality of reservoir simulation models and take into consideration intra-grid-block variations in rock properties (Al-Otaibi & Al-Majed, 1998). The grid-blocks in up-scaled simulation models are considerably large, and pseudo-relative functions enable taking into account the effects of detailed geology and saturation distributions through a practical approach, as opposed to modelling many grid-blocks for the fault rock. Ideally pseudo-relative functions should be computed from the fine-grid simulation model, however as this is not available for the context of this project, they were computed by the upscaled course-grid outputs. Pseudo-relative permeability curves were generated for the fault-zone grid-blocks following Kyte & Berry, (1975), using the relation:

$$k'_{rp} = \frac{\mu_p q_p}{T_{12} dP_p} \quad (7.39)$$

Where the phase viscosity μ_p , phase specific cross-fault flow rate q_p , and transmissibility between grid-blocks on either side of the fault, T_{12} are obtained from the simulation model. The pressure difference between the corresponding grid-block centers P_p , is computed from both the 4D-Seismic pressure outputs and simulation

results, and compared. In the case studied in this paper the time-step specific difference was found to be negligible between the real and simulated outputs, and so for consistency the base case dP_p values were used in subsequent calculations. The pseudo-functions are now indexed to the fault-zone grid-blocks through the simulation data file, along with the synthetic capillary pressure functions, resulting in an updated fault model, with distinct fluid physics properties.

The relative transmissibility multiplier T_{rp} are defined following Manzocchi, et al., (2002) using Eqn.7.35.

Values of fault-rock absolute permeability k_f , are obtained from the literature (Knipe, et al., 1997). Fault thickness t_f is obtained from the simulation model. $k_{rp\ 1,2}$ denotes the relative phase permeability of grid-blocks at a given saturation S_w , obtained from the saturation outputs of 4D-Seismic quantitative inversion and previously generated pseudo-relative permeability functions. Both the base case model and S_w outputs from 4D-Seismic indicated a higher S_w at the lower layers across the reservoir. To preserve this effect, a subdivision was applied to the data file fault region section. Analytically both T_{rp} and $k_{rp\ 1,2}$ are functions of water saturation, enabling the back-calculation of the relative transmissibility multiplier T_{rp} as a grid-block property

$$T_{rp(Sw)} = \frac{k'_{rp}}{k_{rp}} \quad (7.40)$$

Relative transmissibility multipliers were calculated for fault-rock absolute permeability ranging from 0.1 to 10 mD.

In the base case, fault-zone specific capillary pressure curves were not defined, and the same functions applied to all the grid blocks in the model. Synthetic capillary pressure curves were generated for the fault-zone grid-blocks following Ringrose et al., 1992.

$$P_c = 3S^{e^{-2/3}} \left(\frac{\phi}{k}\right)^{0.5} \quad (7.41)$$

Where S^e is the effective wetting phase saturation, ϕ is the porosity, and k is the absolute single-phase permeability. The wetting phase in this case is water, and the static average for the fault-zone grid-blocks is calculated from the time-lapse S_w data outputs at the initial time-steps. An average of 0.25 was taken for the top two layers, and 0.30 for the lower two layers. In order to simulate fault-zones of varying absolute permeability, P_c curves were generated at intervals between 0.01mD and 10mD

Two sets of synthetic P_c curves were created, for the top two fault-zone layers and the bottom two fault-zone layers, based on the average fault-zone S_w at the initial and final data outputs from 4D-Seismic. This was done to preserve the effect of natural buoyancy driven downwards flow of water and any potential impact on cross-fault water flow at different depths following injection. Furthermore, both the base case model and S_w outputs from 4D-Seismic indicated a higher at the lower layers across the reservoir.

7.4.9.2 Deterministic history matching with Levenberg Marquardt

In this method the phase-specific transmissibility multiplier T_p were estimated considering 4D seismic results. In this approach, the value of k_{rp} which is the relative permeability of a given phase in the grid-blocks at a given saturation S_w is estimated from 4D seismic. Eqn.7.35. is employed for this computation.

The sub-methodology on updating fault parameters taking into consideration two-phase properties is elaborated in figure 7.42 below.

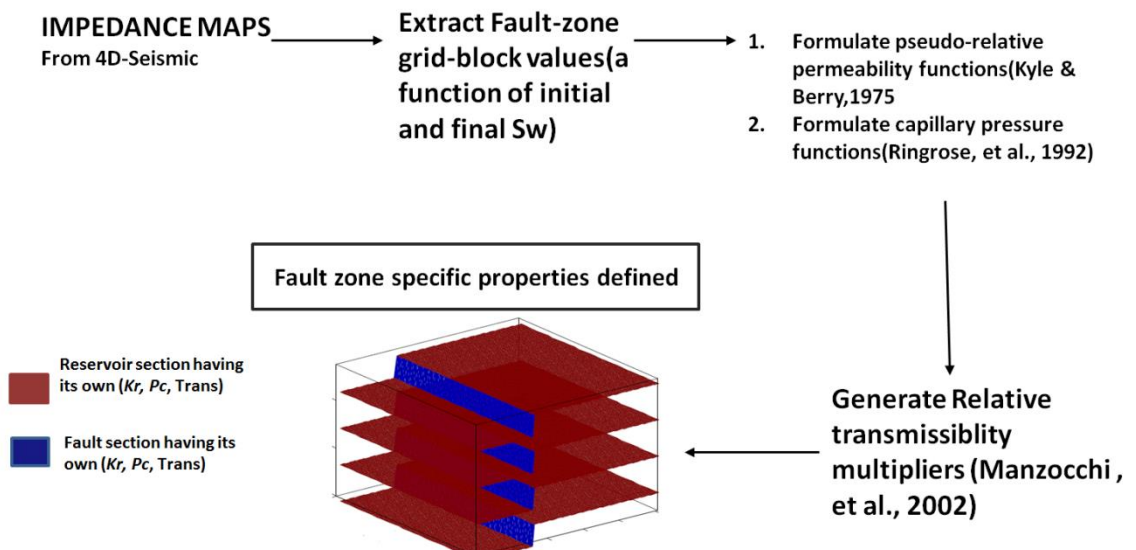


Figure 7.42: Schematic sub-methodology on updating fault parameters taking into consideration two-phase properties

7.4.9.3 EnKF history matching with and without 4D seismic

The EnKF scheme, estimating an initial value of FTM (phase-specific in this case) to generate an initial ensemble of FTM values is estimated. The maximum and minimum FTM values are determined.

7.4.9.4 EnKF including FTM as an uncertainty (without 4D seismic)

This experiment is termed **EnKF-FTM**, and it uses 2 points initial ensemble construction inferring the necessary covariance from a variogram. The initial ensemble is generated from our geostatistical software (Deutsch & Journel, 1998). 100 realisations of permeability field conditioned to the well location are generated. The corresponding porosity ensemble is generated from the initial relationship between the real permeability field and real porosity field according to the equation below

$$\varphi = 0.000134313 \times K + 0.0981797 \quad (7.42)$$

Where K the permeability ensemble is generated from our geostatistical simulator and φ is the porosity ensemble. All other parameters except the FTM parameter are kept constant without any uncertainty. The FTM ensemble is generated from a Gaussian distribution having 0.05(default FTM value estimated without considering 4D seismic) as the mean (initial guess) with a standard deviation of 0.005.

7.4.9.5 EnKF including the phase-specific FTM as an uncertainty considering 4D seismic

This experiment is termed **EnKF-2phase FTM**. The initial ensemble is generated as in Eqn. 7.42. The 2phase FTM value of 0.0039 is derived to generate an ensemble of FTM values derived from 4D seismic, having 0.0039 as the mean and a standard deviation of 0.0005. The EnKF algorithm is used for the history matching of the pressure-production data.

7.4.10 Results and Discussion

7.4.10.1 Pseudo-relative Permeability Functions and capillary pressure using 4D seismic

In this section, the results from our methodology to estimate the maximum and minimum value of K_{rp} , p_c and T_{rp} . Are shown

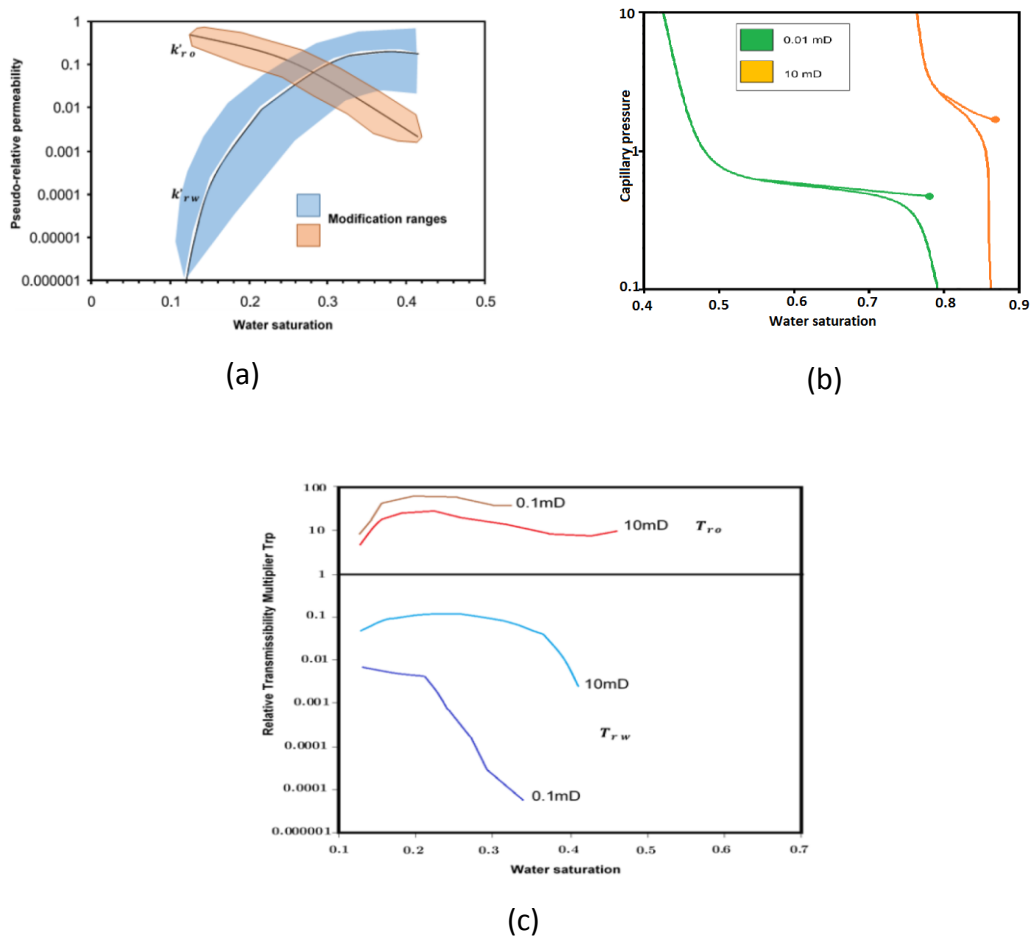


Figure 7.43: Fault-zone pseudo-relative permeability modification ranges, (b) Synthetic P_c curves for fault-zone grid-blocks; the circles represent capillary threshold pressure on the drainage P_c curves. At this S_w or, the oil relative permeability with imbibition P_c both go to zero., moreover, (c)Relative transmissibility multipliers for oil and water; generated within the range of water saturation value output realized with 4D-Seismic data and simulated results

7.4.10.2 LM scheme

This experiment is termed **LM-2 phase FTM**. The 2phase FTM value of 0.0039 is derived and used as the value of FTM in the model. The Levenberg-Marquardt procedure utilised in the SimOPT software is utilised in this case. This is a deterministic form of history matching the pressure production data. The reader may consult (Liang, 2007) for more information on the procedure.

7.4.10.3 EnKF excluding FTM as an uncertainty (Base case)

This experiment is termed **EnKF-no-FTM**. The initial ensemble is generated as in. In this experiment, the EnKF history matching algorithm void of FTM as an uncertain parameter is carried out. The fixed FTM value in the simulator DATA file is 0.002.

7.4.10.4 EnKF including FTM as an uncertainty (void of 4D seismic)

The results show that the match to the observed production data is high. The model also has a negligible match to the true impedance map; this is because impedance (4D seismic) was not assimilated during the EnKF inversion scheme.

7.4.10.5 EnKF including the phase-specific FTM as an uncertainty considering 4D seismic

This section shows results implemented from the novel methodology

Figure 7.44 shows the 3D Fault model of the experiment (indicating the well locations)

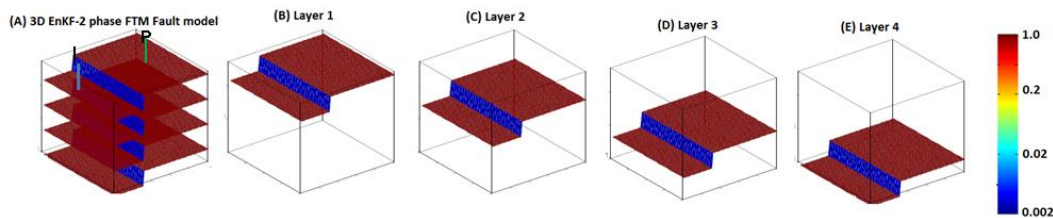


Figure 7.44: 3D Fault model of the EnKF -2 phase scheme

7.4.10.6 Comparison of the four models

To compare the overall performance of the four models, **EnKF-FTM**, **EnKF-2 phase FTM**, **EnKF No-FTM** and **LM-2 phase FTM**, two different criteria are considered,

- The RMS function considering production data and pressure,
- The structural similarity (*SSIM*) index of the reconstructed impedance image to the true impedance image.

Four experiments were conducted as indicated above, and in each experiment, the realisation with the least RMS function and highest impedance map *SSIM* values was chosen for this discussion. The realisations chosen for this result (out of the 100 generated realisations) were;

- Realization #54 for EnKF-No-FTM(base case) and LM-2phase
- Realization #62 for EnKF-2 phase FTM and EnKF-FTM

Table 7.11 below reports the RMS function for the four experiments and it indicates in which cases the 4D seismic results were considered. Figure 7.45 shows the reconstructed permeability fields of the models under consideration using the Ensemble Kalman Filter and the gradient methods Figure 7.46 shows the further reconstructed permeability fields of the models with the implementation of the 2-phase specific FTM scheme using the Ensemble Kalman Filter method.

Figure 7.47 shows the comparison between EnKF-FTM, EnKF-2 phase FTM, EnKF No-FTM and LM-2 phase FTM final history matched ensemble response to the true model pressure-production data.

We see in Table 7.12 the performance of the four models as it pertains to the match of the true FTM value of 0.002. The EnKF-2 phase FTM gives the closest match to this value because the initial FTM value estimated from 4D seismic gave good proximity as an initial guess to the true FTM value of 0.002.

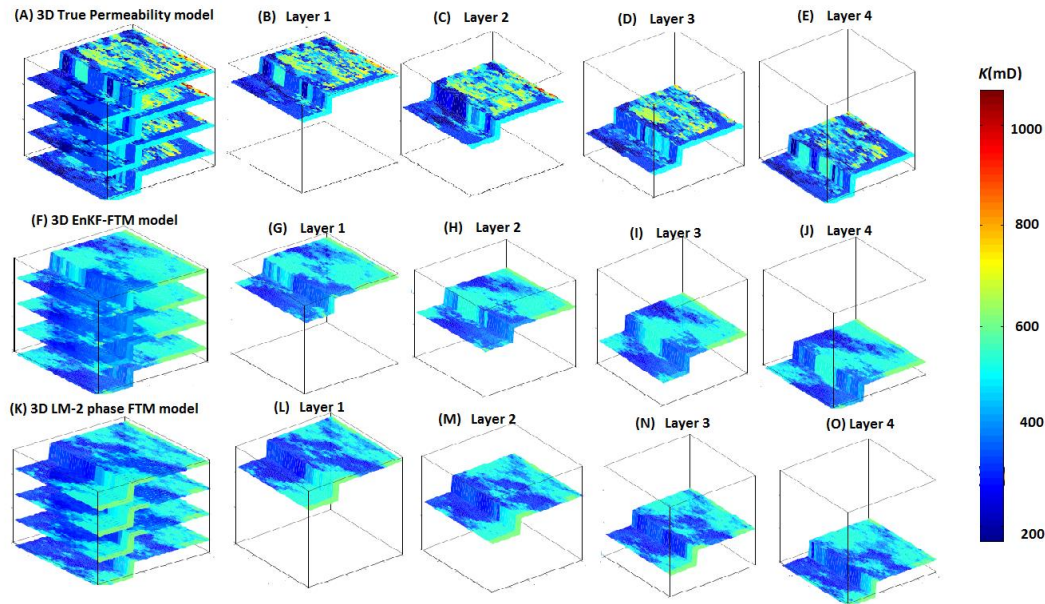


Figure 7.45: True model and 3D History matched permeability model, EnKF-FTM, and LM-2 phase FTM.

(A-E) Permeability for the true model, (F-J) final permeability for the EnKF-FTM model without 4D seismic, and (K-O) final permeability for the LM-2phase with 4D seismic.

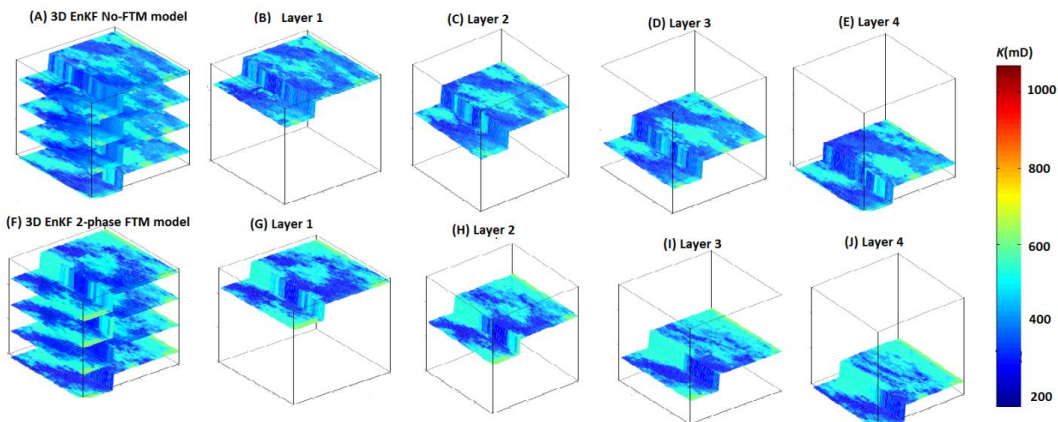
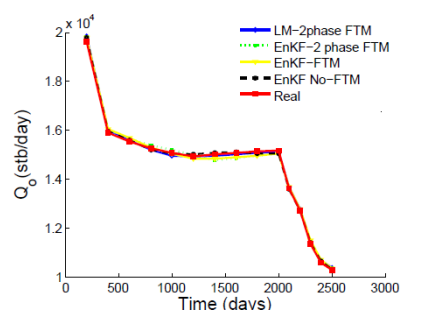


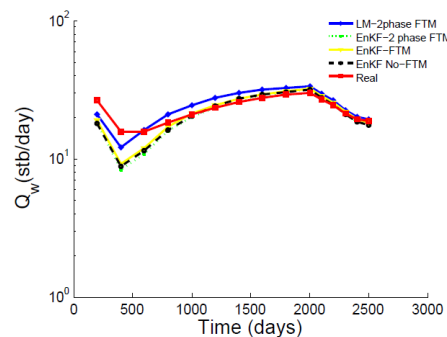
Figure 7.46: 3D History matched permeability model of the EnKF No-FTM and EnKF-2 phase FTM, (A-E) final permeability reconstructed by EnKF-No FTM history matching without 4D seismic, and (F-J) permeability recovered by EnKF- 2 phase FTM history matching with 4Dseismic.

Table 7.11: RMS cost function comparison EnKF-FTM, EnKF-2 phase FTM, EnKF No-FTM and LM-2 phase FTM final history matched

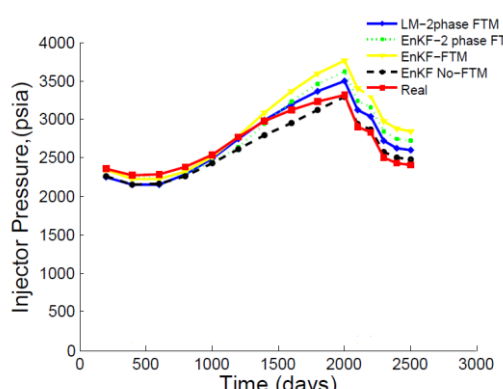
Model	4D seismic	RMS value
EnKF-FTM	No	4.97
EnKF-2 phase FTM	Yes	2.98
EnKF-No FTM	No	5.26
LM-2 phase FTM	Yes	9.64



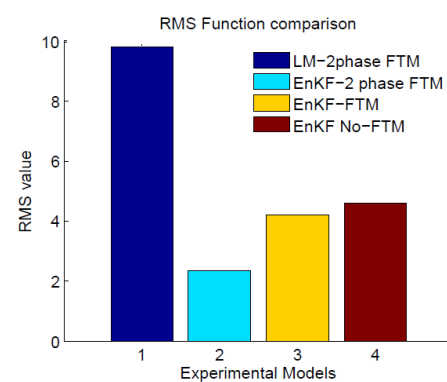
(a)



(b)



(c)



(d)

Figure 7.47: Comparison between the History matched models of the EnKF-FTM, EnKF-2 phase FTM, EnKF No-FTM and LM-2 phase FTM: (a) oil production rate profile, (b) water production rate profile, (c) injection pressure profile and (d) RMS function comparison.

To test the effectiveness and show the uncertainty of our various history matching scheme we compare the oil recovery ratio of the four models under observation with the true model oil recovery ratio. We see a very good match all round as indicated in Figure 7.48 of the four models under consideration to the true model. The LM-2 Phase FTM history matched model shows a slight deviation towards the end of the production period compared to the other ensemble-based methods. This corroborates earlier work by (Oliver, et al., 2008) in the superiority of the EnKF over the classical gradient method.

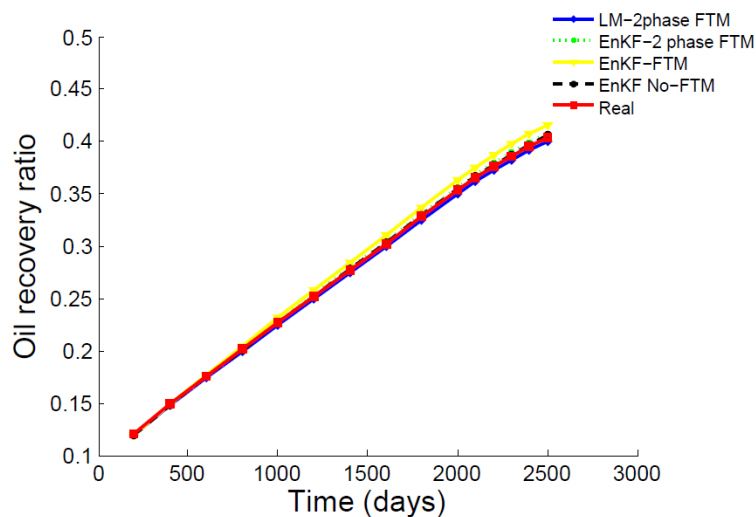


Figure 7.48: Comparison between the oil recovery ratios of the history matched models of the EnKF-FTM, EnKF-2 phase FTM, EnKF No-FTM and LM-2 phase FTM:

Table 7.12: Comparison of the initial and Final FTM values after EnKF/LM update for the EnKF-FTM, EnKF-2 phase FTM, EnKF No-FTM and LM-2 phase FTM final history matched models

Experimental model	Initial FTM vale	Final FTM value after EnKF/LM update (LM update for last model)
EnKF-FTM	0.056	0.0016
EnKF-2 phase FTM	0.0043	0.0023

EnKF No-FTM	0.002	0.002
LM- 2phase FTM	0.0039	0.0000035

We see in Table 7.12 that the EnKF No-FTM model had a constant FTM value of 0.002. This is because FTM was excluded as an uncertainty in the history matching process.

Structural Similarity Index Metric (SSIM)

SSIM (Wang, et al., 2004) is used to compare the EnKF-FTM, EnKF-2 phase FTM, EnKF No-FTM and LM-2 phase FTM final impedance maps of the history matched models. we derive our *SSIM* Normalized cost function as,

$$\text{SSIM Normalised Cost function} = \text{abs}(1 - \text{Average SSIM index value}) \quad (7.43)$$

Figure 7.49 shows the reconstructed impedance maps of the 4 history matched models under investigation to the true impedance map.

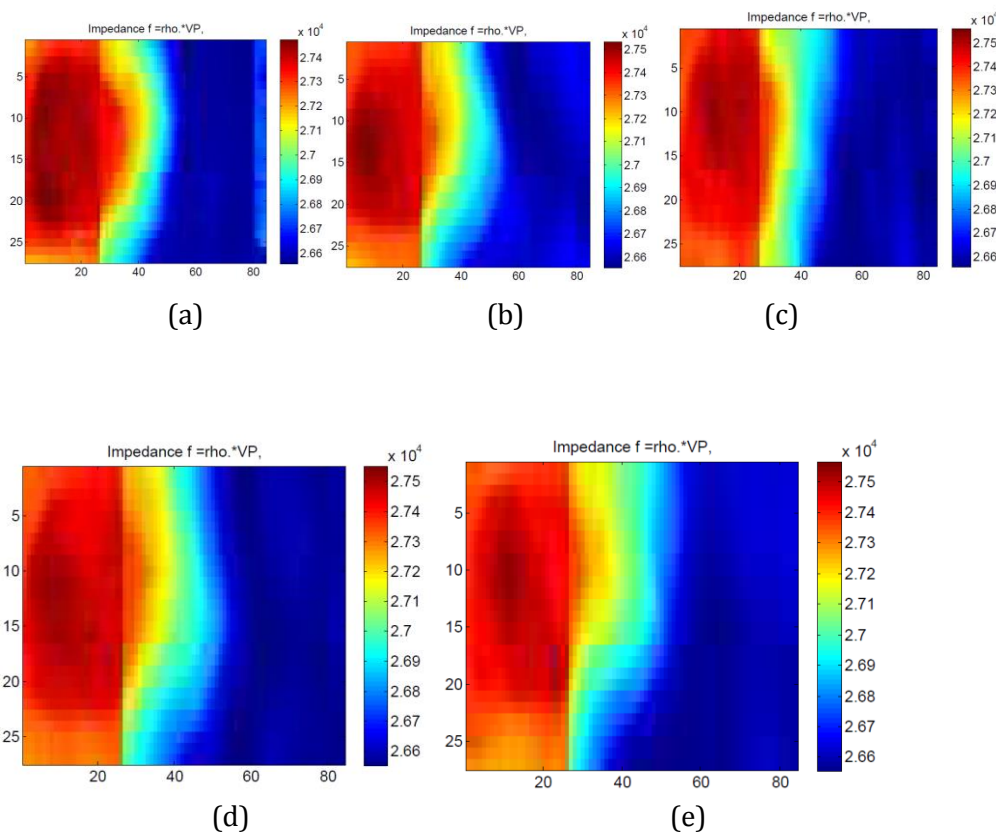


Figure 7.49: Reconstructed impedance image of the history matched models of EnKF-FTM, EnKF-2 phase FTM, EnKF No-FTM and LM-2 phase FTM. (a) True impedance image (b) impedance image reconstructed by EnKF-2 phase FTM history matching, (c) impedance image reconstructed by EnKF-FTM history

matching, and (d) impedance image reconstructed by EnKF No-FTM history matching and, (e) impedance image reconstructed by LM-2 phase FTM history matching

The overall cost function for the history matching process taking into account the RMS cost function and SSIM cost function is described in Eqn.7.44. Moreover, the values reported in Table 7.13.

$$Overall\ cost\ function = \frac{(SSIM\ Normalised\ Cost\ Function + RMS\ function)}{2} \quad (7.44)$$

Table 7.13: Overall cost function comparison EnKF-FTM, EnKF-2 phase FTM, EnKF No-FTM and LM-2 phase FTM final history matched

Experimental Model	SSIM	SSIM Normalised Cost function	RMS function	Overall cost function
EnKF-FTM	0.7645	0.2355	4.97	2.603
EnKF-2 phase FTM	0.8522	0.1478	2.98	1.564
EnKF- No FTM	0.7480	0.252	5.26	2.756
LM 2 -phase FTM	0.8715	0.1285	9.64	4.884

7.4.11. Conclusion

- In this work, the assimilation of FTM as a history match uncertainty improved the history matching performance and decreased the RMS error to the true production historical data.
- More specifically, assimilation of the 2-phase FTM value in the model using the Ensemble Kalman Filter method and 4D seismic results(**EnKF-2 phase**), matched comparatively with EnKF with an initial ensemble of FTM values generated from a Gaussian random distribution.

- Overall the EnKF-2phase considering 4D seismic results scheme gave better history match value and a closer impedance map reconstruction to the true model impedance map.
- The LM-2phase FTM module produces a good impedance map reconstruction; however, this method was inferior to the EnKF scheme. A possible explanation would be that the standard gradient method searches for the most probable model in a local minimum of search space, while the EnKF searches for the most probable model in a global minimum of search space.
- In conclusion, assimilating more data during the EnKF inversion scheme leads to a reduced RMS function value to the pressure-production historical data; also, assimilating 2 phase specific FTM value is beneficial in impedance map reconstruction and better reliable decision making and forecast in future oil production and exploration.

7.5 -Water Front Characterisation in History Matching Using Low-frequency Electromagnetic Data(Numerical Experiment 4)

Novelty

In this work, a novel history matching level-set enhanced ensemble Kalman filter (EnKF) algorithm from our previous work is coupled with time-lapse EM surveys using a non-linear Kaczmarz-type approach for the estimation of water saturation distributions in an oil reservoir from EM data. The main focus is on the coupling of the inverse Maxwell problem in geophysical imaging with the fluid flow estimation from production data. The water saturation field is inferred from low frequency cross-borehole electromagnetic induction tomography (EMIT) data using the well-known Archie equations. These internal computations of saturations are then plugged into one step of the Ensemble Kalman filter for matching well data by modifying some reservoir parameters. Numerical results show that this integrated assimilation of EM inferred internal water saturation data during the EnKF inversion technique yields in an efficient way improved results compared to history matching without integrating time-lapse EM data.

7.5.1. Introduction

Reservoir history matching is the process of constraining the reservoir model to mimic actual historical dynamic production data of the reservoir to make bold assumptions about the future production behaviour of such reservoir and reduce uncertainty with those assumptions (Chang, et al., 2010) . There are two accepted methods implemented in reservoir history matching for the estimation of facies distribution by assimilating the well historical production data: stochastic methods and Gradient-based method (Chang, et al., 2010) (Aanonsen, et al., 2009)

Focusing on the electromagnetic, a developed two-step reconstruction algorithm for the EM tomography of water saturation distribution in a 3D reservoir which uses level sets and adjoints fields (Dorn, et al., 2007) is coupled with our modified ensemble Kalman filter (EnKF)-level set algorithm. This method is differentiated from the previous work where the level set was used in parametrising the permeability field for the facies reconstruction with the EnKF. The level set technique for representing the water

saturation plume is fused with and the adjoint field methodology for solving the non-linear inverse problem. In each case, an adjoint and a forward model are solved based on the permittivity distribution corresponding to the initial level set functions (Dorn, et al., 2007). A correction to these level set function based on these two runs is compared. The water saturation distribution computed from the conductivity levels (through the level set functions) through the Archie equation is assimilated during the EnKF inversion process together with the pressure and production data of the reservoir. A modified algorithm, employing the EnKF to solve the inverse problem in 3D is presented. The production data to be assimilated are the injector pressure, water, and oil production rates. In this work, a parameter update using the EnKF and a level-set function update using the pre-calculated Kalman gain matrix multiplied by the innovation vector is computed. The innovation vector is a vector showing the difference between the observed historical data and the simulated data obtained from the reservoir simulator. This approach is capable of utilising the same forward, and adjoint runs in an effective manner for the estimation of conductivity from low-frequency EM data yielding a reduction in computational complexity.

7.5.2 Initial ensemble construction

The sequential Gaussian simulation is used for the initial ensemble construction. Sequential Gaussian Simulation (SGS) is used in the estimation of the permeability property at regions where the permeability values were not made known by constraining the simulation to the permeability at the well locations (Deutsch & Journel, 1998). The procedure uses geostatistical assumptions on the parameter distribution in the reservoir indicated in the semivariogram. SGS then creates an ensemble of realisation which honours the properties at the well locations and all Gaussian. A MATLAB code written for this work was then used to truncate the permeability values at two different thresholds to represent the two lithofacies namely high permeability areas and low permeability areas.

7.5.3 A nonlinear Kaczmarz-type approach (Algebraic reconstruction technique) for EM data inversion to conductivity.

The algorithm is briefly discussed here. We use a given data for one frequency and one source at a time during the update of the linearised residual operator after each

realisation of the incremental corresponding correction δb . The reader may consult (Dorn et al., 2007) for more information.

Algorithm: Non-linear adjoint field ART inversion

$$\bar{b}_p^{(0)} = b^{(0)}$$

Sweep_loop: DO $i = 1, I_{max}$

$$b_p^{(i)} = b^{(i-1)}$$

Source_loop: DO $j = 1, p$

$$\delta b_j^{(i)} = -R'_j(b_{j-1}^i) \times \hat{C}_j \times R_j(b_{j-1}^i)$$

$$b_j^{(i)} = b_{j-1}^{(i)} + \kappa_j \delta b_j^{(i)}$$

END DO source_loop

END DO sweep_loop

$b^{(0)}$ is an initial guess for b and I_{max} is the total number of sweeps. κ_j is the step size in step j . \hat{C}_j is a numerical linear approximation. $R_j(b_{j-1}^i)$ is the forward residual operator. $-R'_j(b_{j-1}^i)$ is the adjoint residual operator.

The reconstruction of the conductivity plume based on this algorithm is shown in Figure 7.56

7.5.4 The Comprehensive History matching algorithm

The resulting iterative algorithm for the shape/facies reconstruction using our coupled EnKF-Level set-EM method is roughly summarised as follows and shown in Figure 7.50

- 1) Firstly generate initial permeability and porosity ensemble guesses which will honour the prior geostatistical knowledge of the reservoir employing standard geostatistical software packages.

- 2) The Kalman Gain multiplied by the innovation vector (the difference between the observed and simulated value from Schlumberger's ECLIPSE 100™ (Schlumberger GeoQuest, 2014) is stored and saved from every EnKF data assimilation step.
- 3) If the time step is at year 6, include the difference between the reconstructed water saturation distribution from our ART modulation and the simulated water saturation of each of the realisations from ECLIPSE 100™ into the innovation vector

$$Innovation\ vector = (d_{obs,k} + \varepsilon_k^j - H_k y_k^{p,j}) \quad (7.45)$$

- 4) Two facies system, one for high permeability area and low permeability area, are generated. The facies distribution is modelled using a level set function. The model parameters are the signed distance of each pixel towards the boundary of the other facies, that is, the signed distance is the Euclidean distance of a cell towards the boundary of the other facies in the reservoir. r is the radius of the similar facies code separated from the conjugate with its boundary

$$Signed\ distance = ((i - a)^2 + (j - b)^2 + (k - c)^2)^{\frac{1}{2}} - r = \phi_k^{p,j}$$

- 5) Next, build the narrowband N.B matrix. This matrix consists of ones in a small neighbourhood of the boundaries separating two different facies type.
- 6) The facies indicator functions (which are 0 for shale and 1 for sand) are parametrised using the signed distance function in step 4 about the boundary separating the two facies system. This is the initial level set function $\phi_k^{p,j}$
- 7) The previously calculated Kalman gain multiplied with the innovation, and the narrowband matrix is added to this signed distance function to get a new signed distance function $\phi_k^{a,j}$. This is the analysed level set function.

- 8) Assign areas with positive signed distance value facies code 1 for high permeability, while areas with negative signed distance assigned facies code 0 for low permeability.
- 9) The algorithm stops when there is no noticeable change in the Kalman gain matrix or when all historical data has been assimilated.

Mathematically, the algorithm is described below as;

$$\phi_k^{a,j} = \phi_k^{p,j} + K_k(d_{obs,k} + \varepsilon_k^j - H_k y_k^{p,j}) \times f \quad (7.46)$$

f = Narrow band matrix, $\phi_k^{p,j}$ =Prior level set function ensemble of permeability, K_k =Kalman gain matrix (obtained from parameter update), $d_{obs,k}$ =Observed data (Qoil, Qwater, and Pressure). ε_k^j =Gaussian error, $\phi_k^{a,j}$ =Analysed level set function ensemble of permeability, H_k =information matrix

7.5.5 Reservoir synthetic model

The commercial ECLIPSE 100™ reservoir simulator (Schlumberger GeoQuest, 2014) is used for reservoir simulation with a dead oil PVT type. Measurement errors are drawn from a Gaussian distribution with mean equal to zero and the standard deviation is given to about 1% of the actual measurement data. The synthetic reservoir model is summarised in Table 7.14, and our 3D reservoir water saturation synthetic model is shown in figure 7.51.

Table 7.14: Reference Reservoir synthetic model properties

Property	Value
Grid Configuration	$84 \times 27 \times 4$
Grid size	$100 \times 100 \times 50 \text{ ft}$
Well configuration	2-spot
# of producers	1
# of injectors	1
Simulation period	7yrs

Integration step length	0.44yrs
# of integration steps	16
Reservoir depth	4,000ft
Initial Reservoir pressure	4,000psia
Integrated data	Injector Well pressure, producer oil and water rates, water saturation from EM data (at 6 th year only)
Injector's constraint	15,000 to 10,000 STB/day
Producer's constraint	140psia
Uncertain parameters to estimate	Distributed permeability, porosity and water saturation distribution

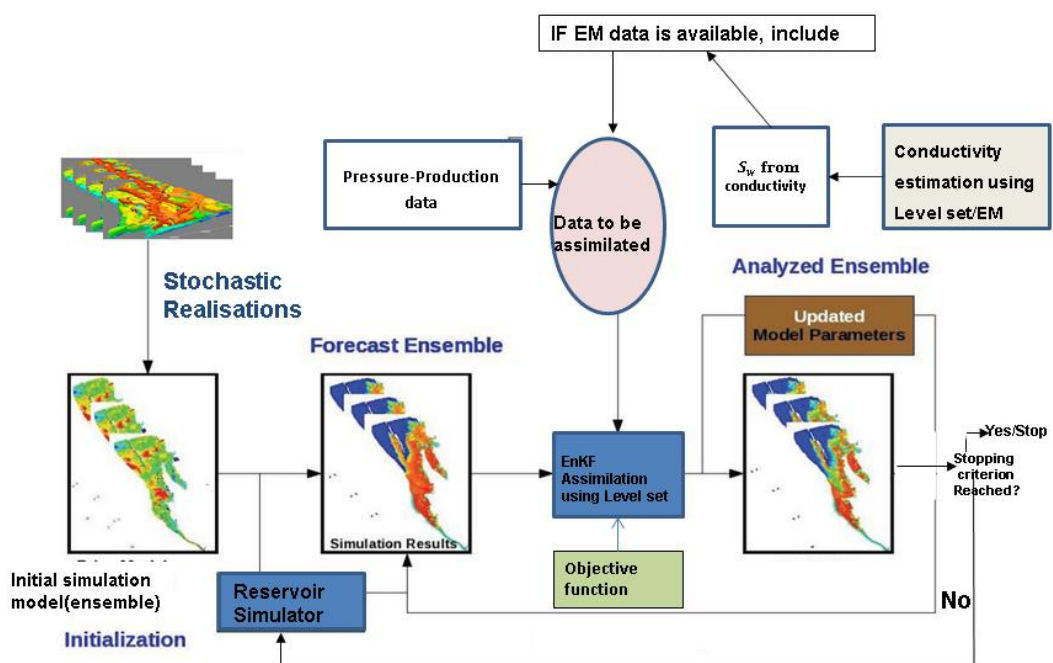


Figure 7.50: Schematic showing the coupled EnKF-level set-EM method used in this work

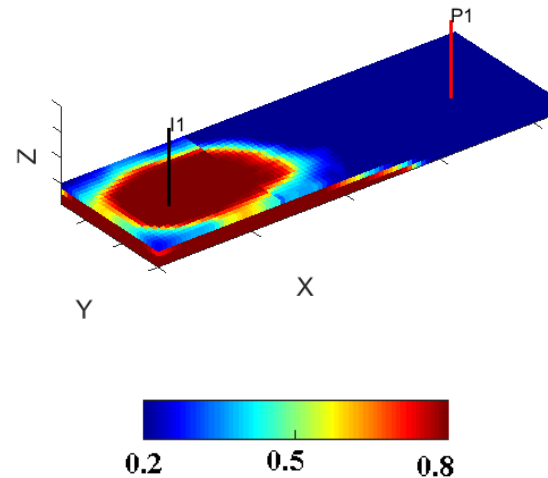


Figure 7.51: 3D True model water saturation distribution at year 6 showing the two well locations

Figure 7.52 shows the layer by layer water saturation maps of the true reservoir model.

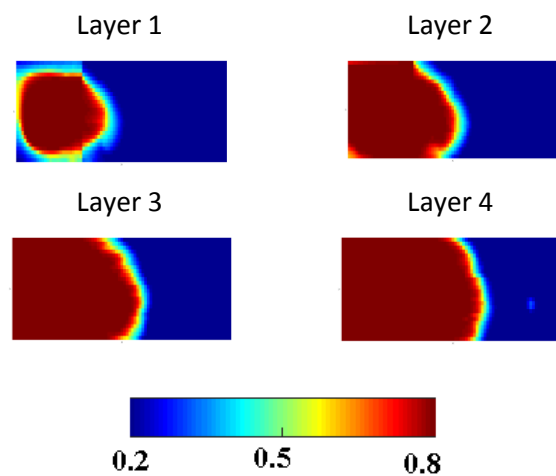


Figure 7.52: True water saturation distribution of the reference/true reservoir at year 6

The pressure maps were similarly analysed but since the novel method is targeting the motion of the propagating water front, water saturation maps are preferably shown and analysed.

7.5.6. Simulation results

EM conductivity/water Reconstruction

To convert the conductivity output from our Maxwell solver, we employ the Archie law. Archie's law states that the logarithm of conductivity is linearly related to the logarithm of porosity and saturation (Archie, 1942)

$$\log(\sigma) = \log(\sigma_w) + m\log(\kappa\varphi) + n\log(S_w) \quad (7.47)$$

With σ_w being the scaled water conductivity (Siemens/m), φ is the effective porosity, S_w is the water saturation distribution. The parameters κ, m, n are constants as specified in (Archie, 1942) (Hill & Milburn, 1956) and σ_w is given by the IJWC-equation (Report and Dresser, 1982)

$$\sigma_w = \left[\left(0.0123 + \frac{36,475}{10c_{salt}^{0.995}} \right) \frac{82}{1.8T_w + 39} \right]^{-1} \quad (7.48)$$

In this work the values used are; $T_w=20^{\circ}\text{C}$ which is the temperature of the injected water, σ =conductivity(Siemens/m) $C_{salt} = 35,000\text{ppm}$, which is the salt concentration, $m=1.83, n = 2$ (Rider, 2002)¹

The idea is including water saturation distribution inverted from conductivity levels through the Maxwell solver, as part of the observation data during the EnKF inversion scheme.

The reconstructed conductivity is shown in figure 7.54. Two-dimensional cross-sectional water saturation maps are shown in figure 7.55

¹ RL(resistivity log) is an electric log that measures formation resistivity to the flow of electric current Resistivity being the opposite of conductivity ,Applications include: Determination of hydrocarbon zone ,Estimation of water saturation, Estimation of hydrocarbon saturation¹

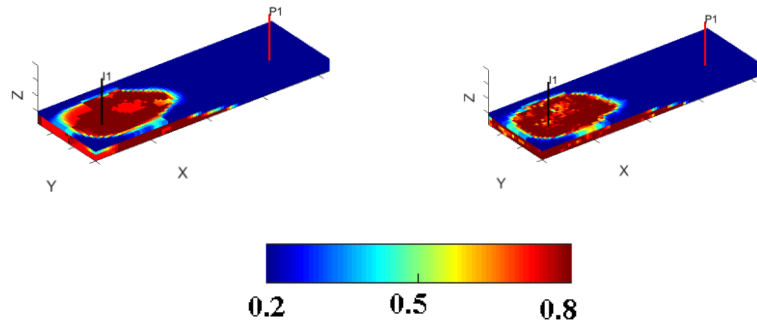


Figure 7.53: 3D True and reconstructed conductivity profile of synthetic model at year six from EM survey

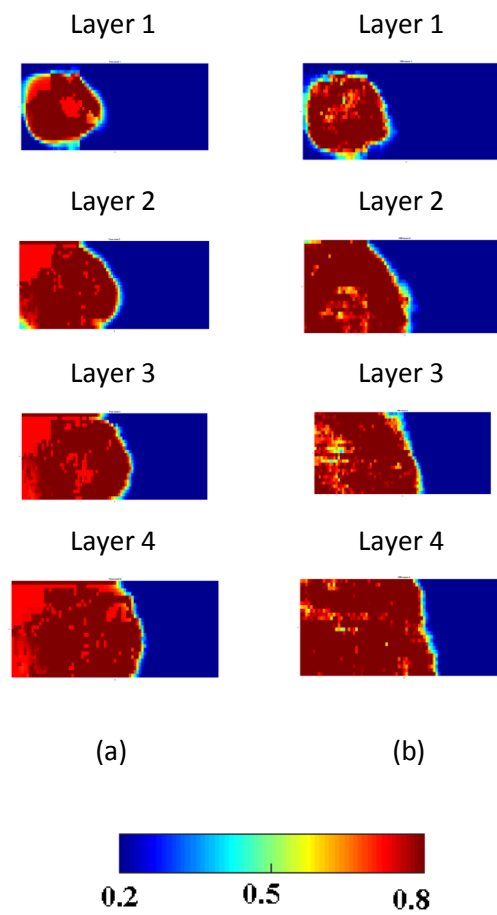


Figure 7.54: 2D-view conductivity plume: (a) True water conductivity distribution of the reference/true reservoir, (b) Reconstructed conductivity profile

Figure 7.54 shows a cross-sectional 2D water saturation map and reconstructed conductivity levels from our Maxwell solver. Figure 7.55 shows a comparison between

the true water saturation maps and the water saturation maps of the reconstructed conductivity levels shown in figure 7.55(b), inverted by using Eqn. (7.48)

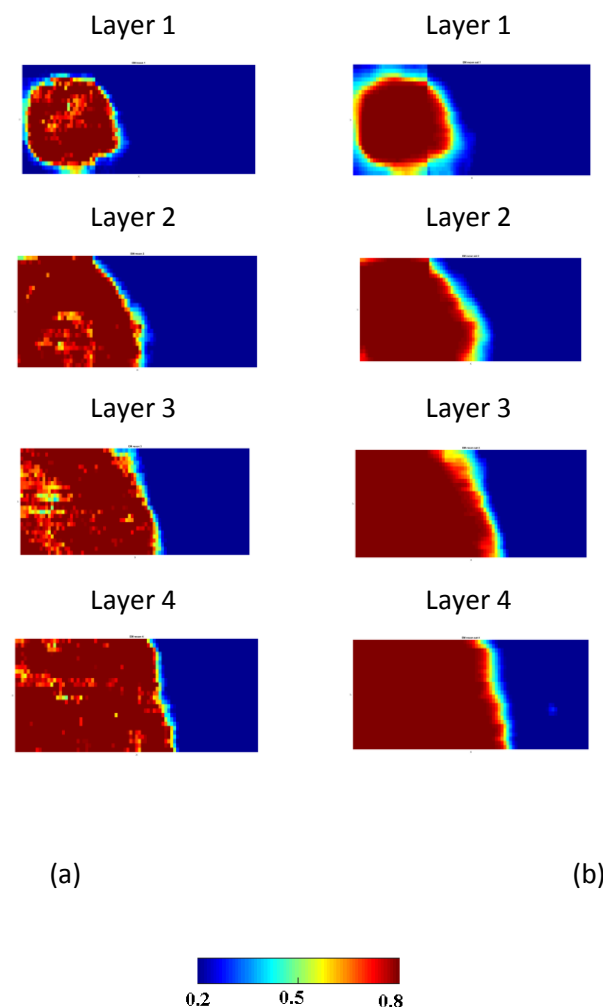


Figure 7.55: (a) Reconstructed conductivity profile, (b) Equivalent water saturation distribution of the reconstructed conductivity profile using Archie's law

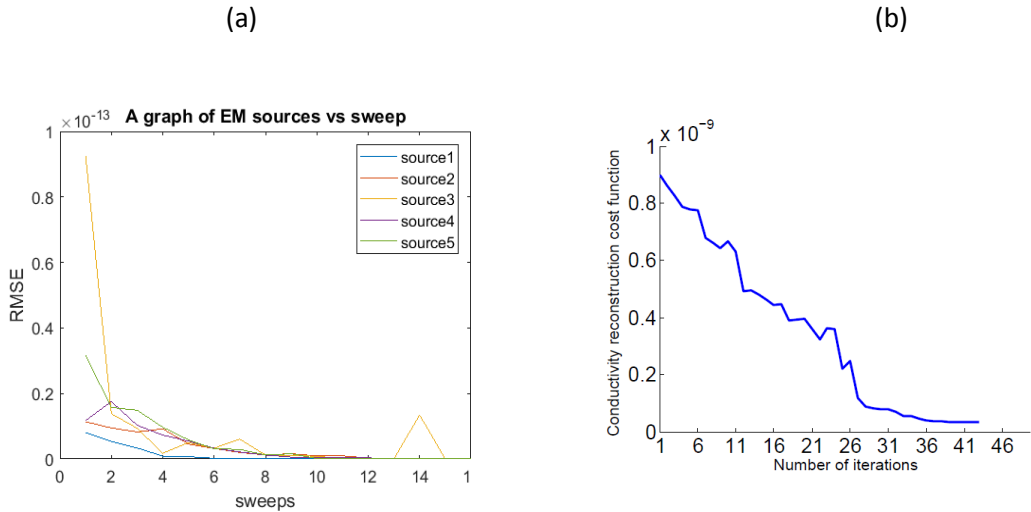


Figure 7.56: (a) RMS evolution during the conductivity reconstruction and (b): RMS function evolution of the reconstructed conductivity profile

7.5.7 EnKF-Level set with EM water saturation data assimilation

This experiment is known as ‘EnKF-EM’. We construct the initial ensemble, using SGS. 100 realisations of permeability field conditioned to the well location are then generated with our geostatistical software (Deutsch & Journel, 1998). The corresponding porosity ensemble is generated from the initial relationship between the true permeability field and true porosity field according to the equation below

$$\varphi = 0.000134313 \times K + 0.0981797 \quad (7.49)$$

Where K is the permeability ensemble and φ the porosity ensemble. All other parameters are kept constant without any uncertainty. We run the history matching module as enumerated in section 7.5.4, including water saturation innovation vector between the reconstructed water saturation distribution form EM data and the simulated water saturation distribution from ECLIPSE 100™ at the 6th year as recommended in (Saito, et al., 2006). To ameliorate the effect of spurious correlation in the covariances of the Kalman gain, localisation matrix as shown in Figure 7.57 are utilised.

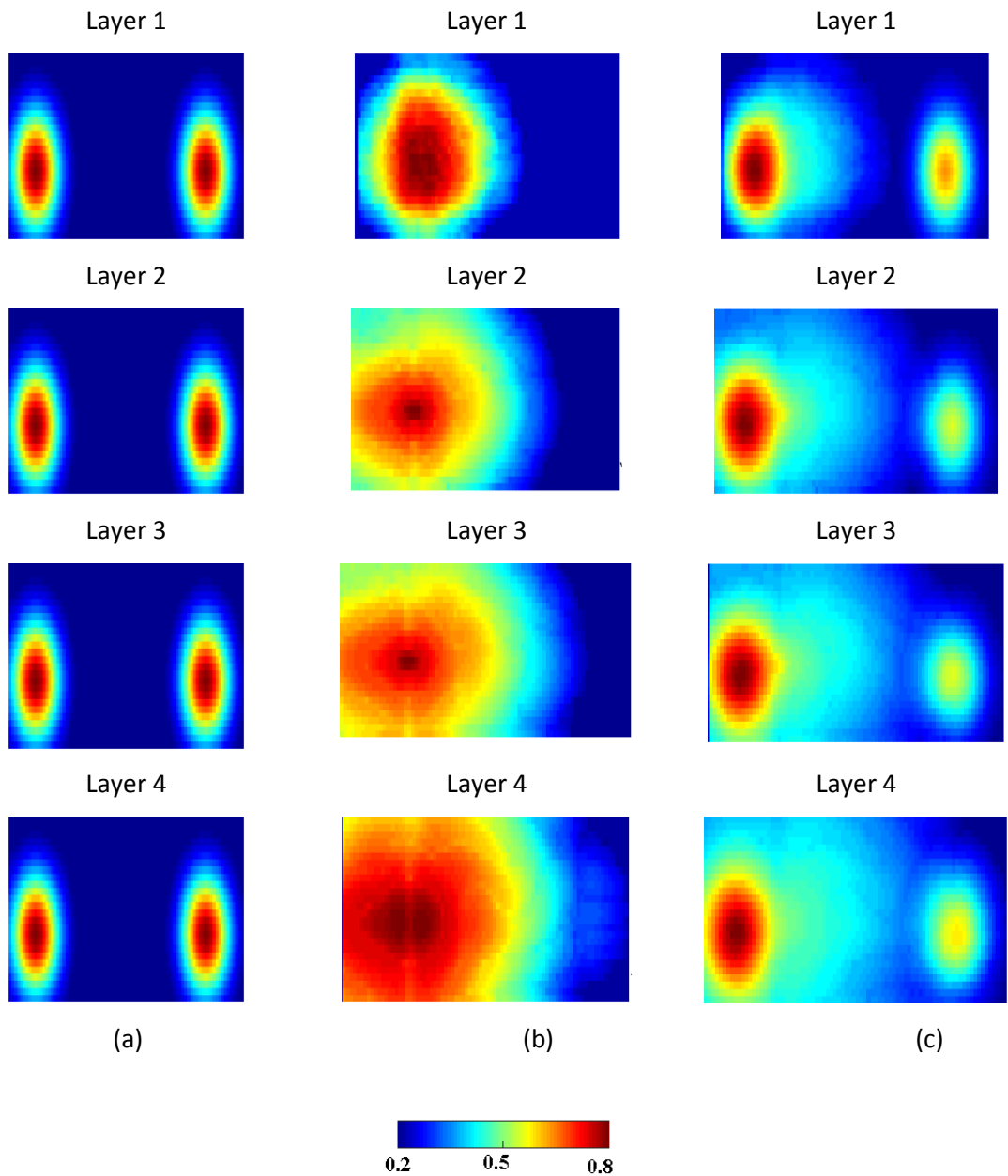


Figure 7.57: (a) Correlation function from 5th order Gaspari –Cohn matrix, (b) Correlation function (sensitivity functions) from our non-linear Kazsmarz solver and (c) Correlation function arriving from the combination of both approaches

7.5.8 EnKF-Level set void of EM water saturation data assimilation

This model is known as ‘EnKF’. This numerical experiment begins with an initial ensemble construction of permeability realisations, and the corresponding porosity ensemble. The history matching module assimilating only pressure-production data is then initiated.

7.5.9 Comparison between EnKF-EM and EnKF models

In comparing the performance of the models, EnKF-EM and EnKF, two different criteria are considered, the RMS function considering production data and pressure, and the structural similarity (*SSIM*) index.

Root-mean-square (RMS) function

Starting with a stochastic realisation generated by SGS, the convergence for the EnKF history matching was achieved in 16-time steps with an RMS error of 3.35. Assimilating EM data in the EnKF-EM history matching, the convergence was achieved in 13-time steps with an RMS error of 1.97. Table 7.15 below reports the effectiveness of including water saturation data as part of the observation metric (in the innovation vector). In the comparison of the final RMS value for each method, the proposed EnKF-EM approach yields lower RMS values when compared to the standard EnKF method. In the 100 realisations used for this work, 90% of the ensemble gave lower RMS value with the EnKF-EM approach compared to the EnKF. Figure 7.58 shows the comparison between the EnKF-EM and EnKF final history matched ensemble response to the true model pressure-production data. The superiority of our proposed model is clear in the quality of water saturation distribution match with the true model shown in figure 7.62. Figure 7.58(d) shows the numerical simulation results and the RMS function of both methods with regards to observed production data. It is clear the EnKF-EM method outperforms the EnKF algorithm by reducing the RMS function value and the number of time steps required

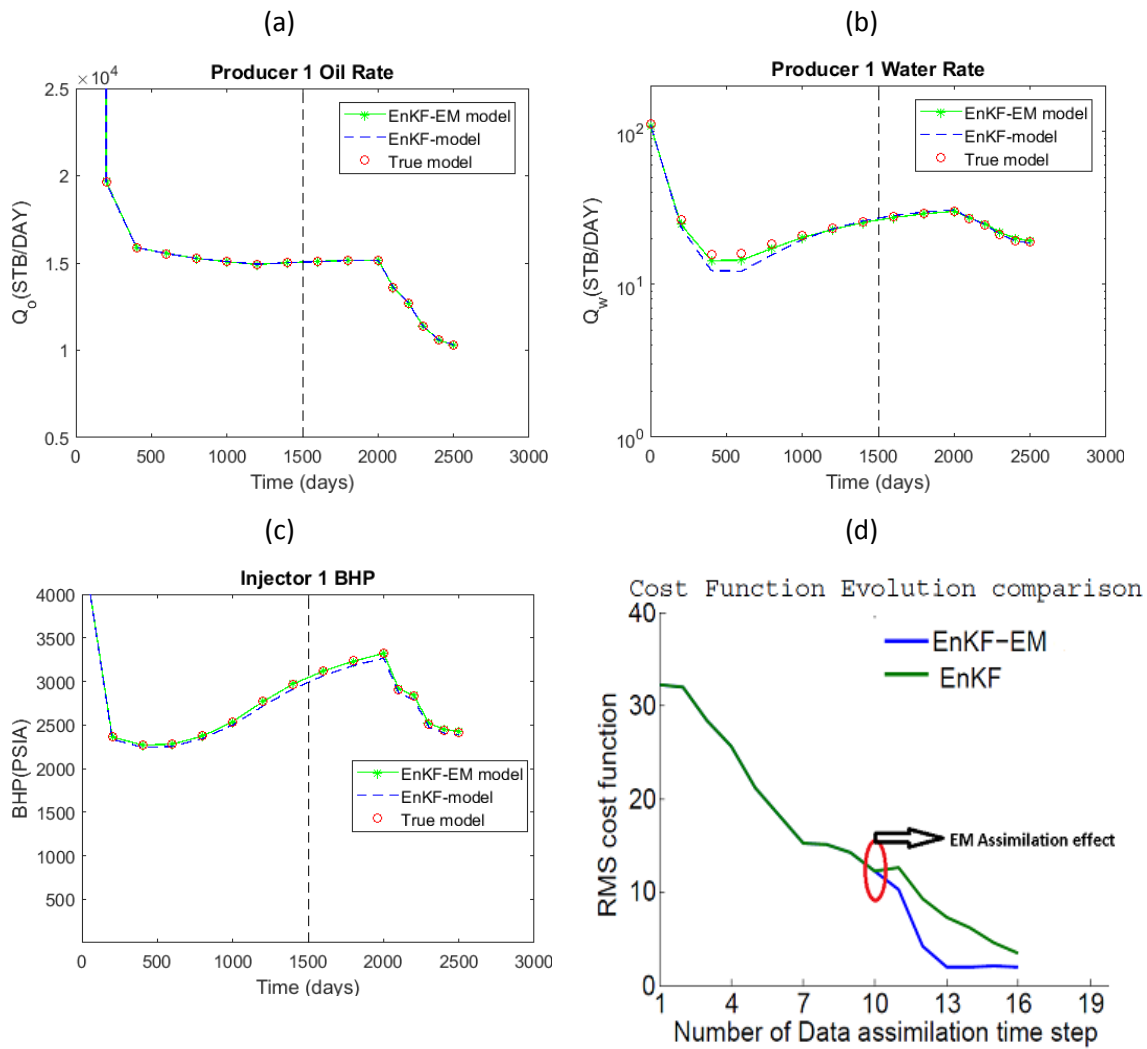
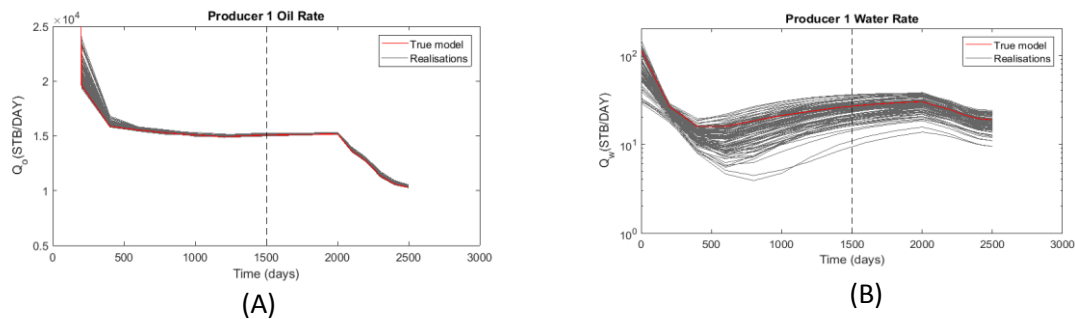
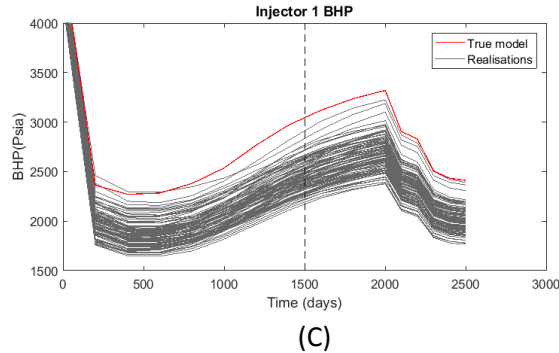


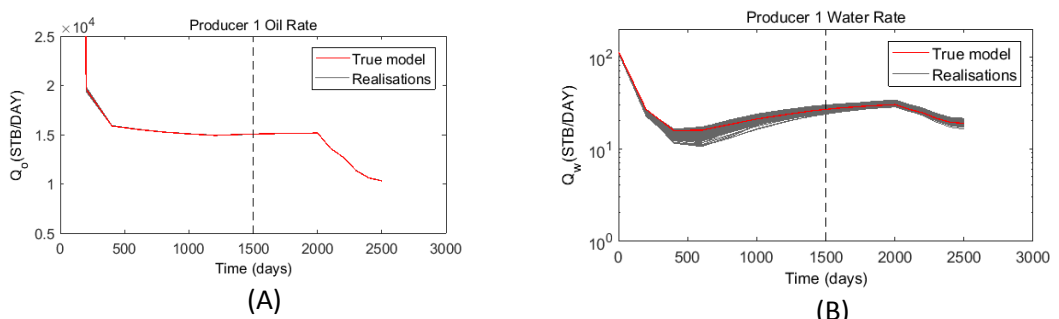
Figure 7.58: Comparison between EnKF-EM and EnKF production rate profile:, (a) oil production rate profile (b) water production rate profile (c) injection pressure profile and (d) History matched Realizations RMS function with and without assimilating EM data





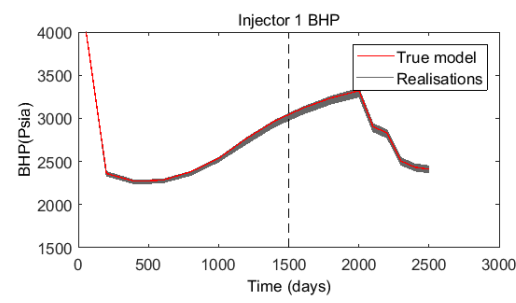
(C)

Figure 7.59: Production profile of initial ensemble. (a) Oil rate match, (b) Water rate match and (c) Bottom-hole-pressure. The red curve represent the true data and the grey overlay lines represents the realisations. The vertical dashed line represents the historical (left of this line) and prediction stages (right of this line)



(A)

(B)



(C)

Figure 7.60: Production profile of EnKF-EM. (a) Oil rate match, (b) Water rate match and (c) Bottom-hole-pressure. The red curve represent the true data and the grey overlay lines represents the realisations. The vertical dashed line represents the historical (left of this line) and prediction stages (right of this line)

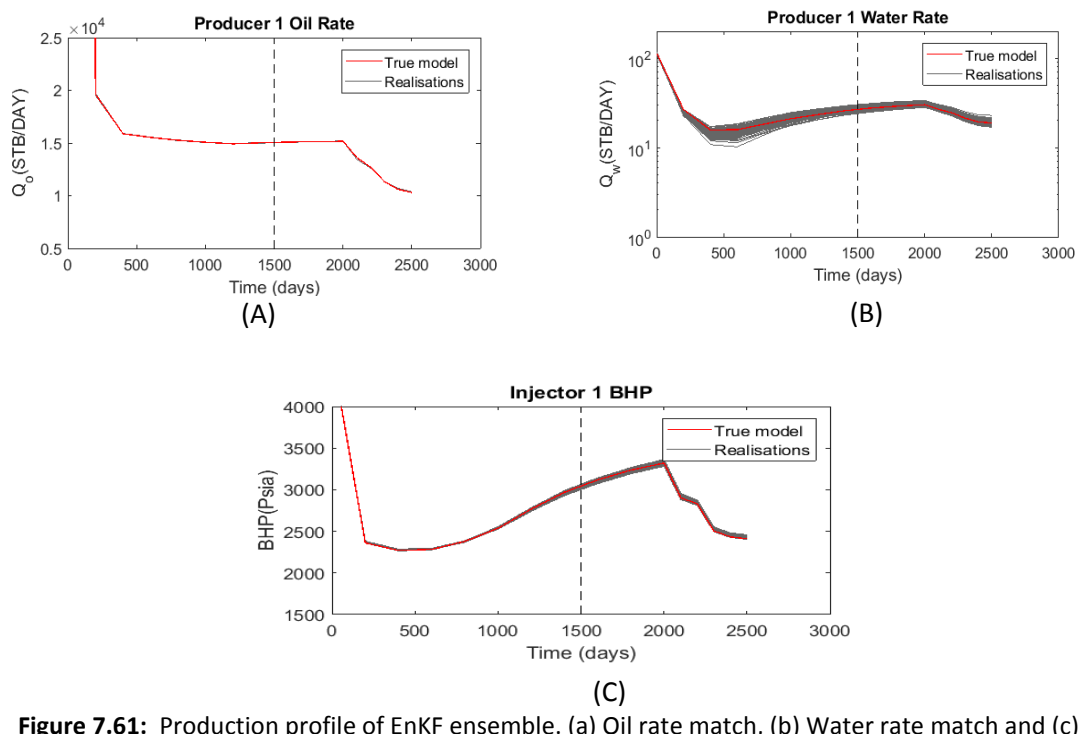
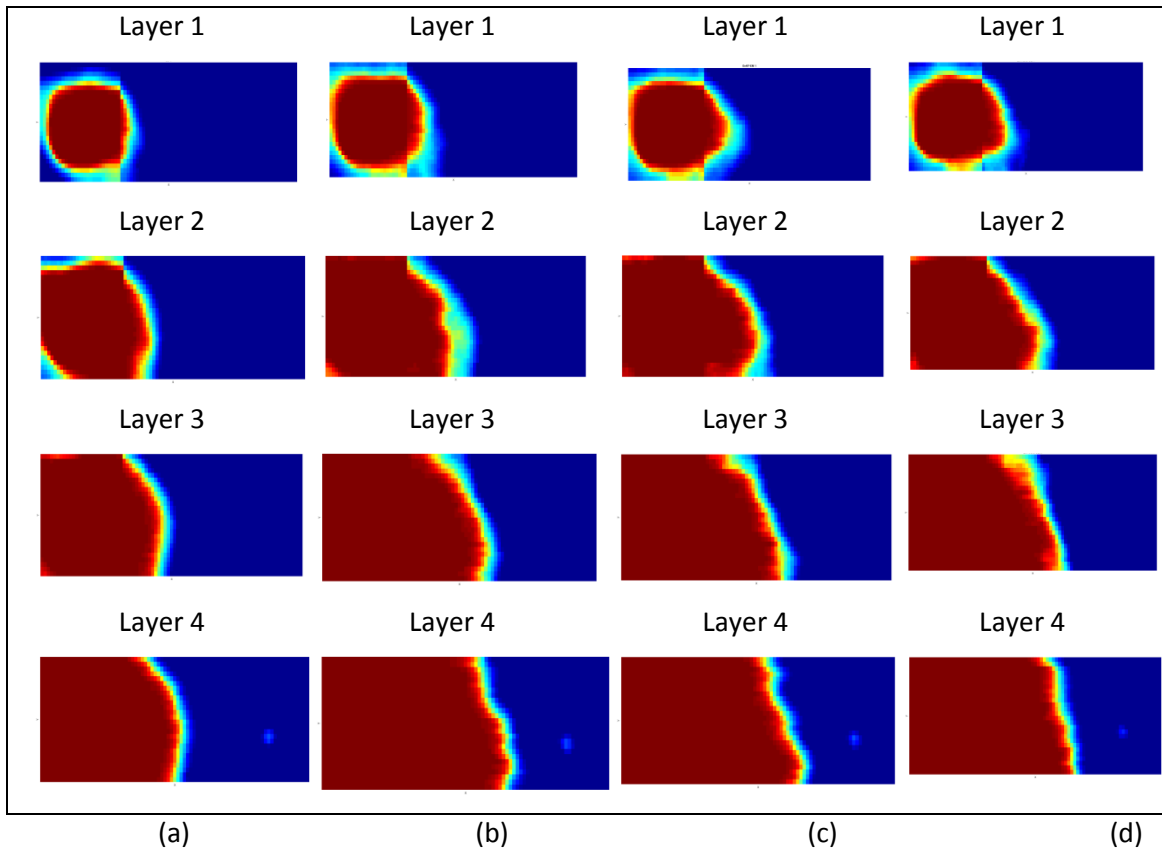


Figure 7.61: Production profile of EnKF ensemble. (a) Oil rate match, (b) Water rate match and (c) Bottom-hole-pressure. The red curve represent the true data and the grey overlay lines represents the realisations. The vertical dashed line represents the historical (left of this line) and prediction stages (right of this line)



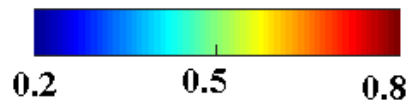


Figure 7.62: Water saturation reconstruction of the various methods. (a) Initial model water saturation, (b) Water saturation recovered by EnKF (d) Water saturation distribution recovered from EnKF-EM and (d) True model water saturation distribution reconstructed from kazsmarz method

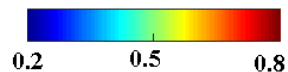
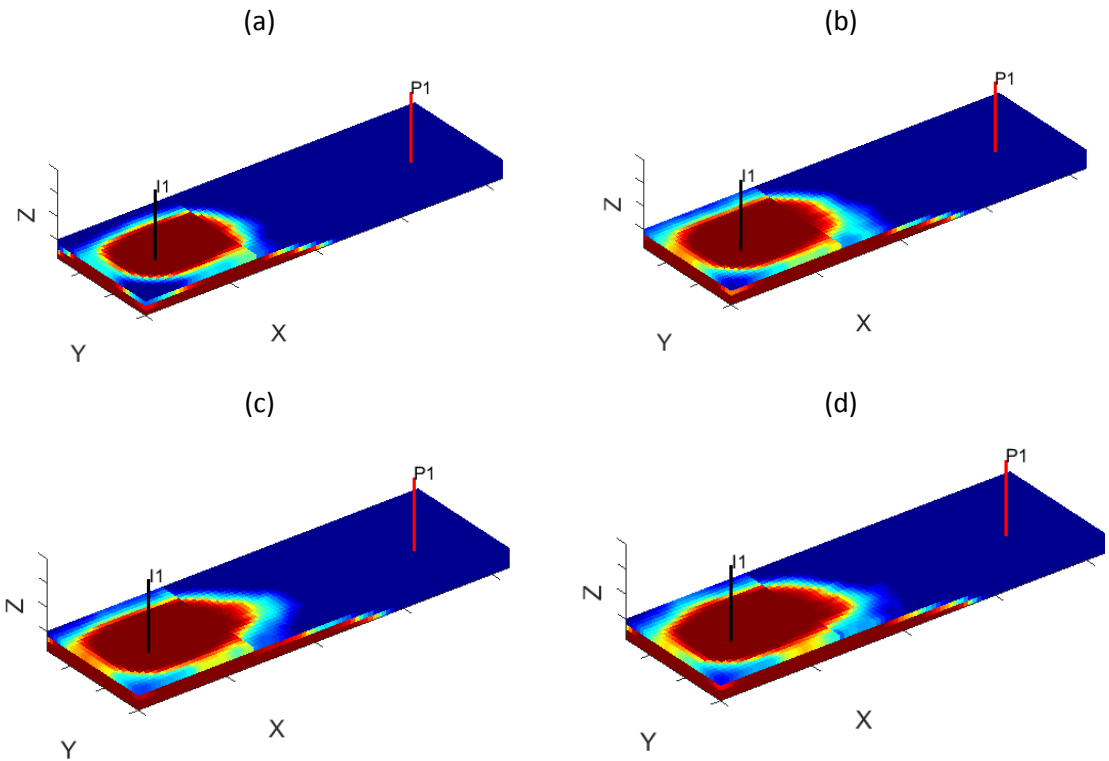


Figure 7.63: 3D Water saturation reconstruction of the various methods. (a) Initial model water saturation, (b) Water saturation recovered by EnKF (d) Water saturation distribution recovered from EnKF-EM and (d) True model water saturation distribution reconstructed from kazsmarz method

In figure 7.62 and 7.63, it is clear the EnKF-EM recovered water saturation front captures the true water propagation in the true model.

Table 7.15: RMS cost function evolution of Best 7 Realisations with and without EM data.

Realisation	RMS value with EM data assimilation	RMS data without EM data assimilation
6	14.78	29.11
17	12.23	29.65
30	32.51	45.50
33	9.23	15.71
93	1.97	3.37
54	18.39	29.01
41	38.38	47.17

SSIM (Wang et al., 2004) is used to compare the EnKF-EM, and EnKF history matched reconstructed water saturation distribution realisation to the true model.

SSIM cost function is defined as,

$$SSIM \text{ Normalised Cost function} = abs(1 - Average \ SSIM \ index \ value)$$

(7.50)

Figure 7.64 shows the average *SSIM* comparison of the EnKF-EM and EnKF permeability field to the true model permeability field.

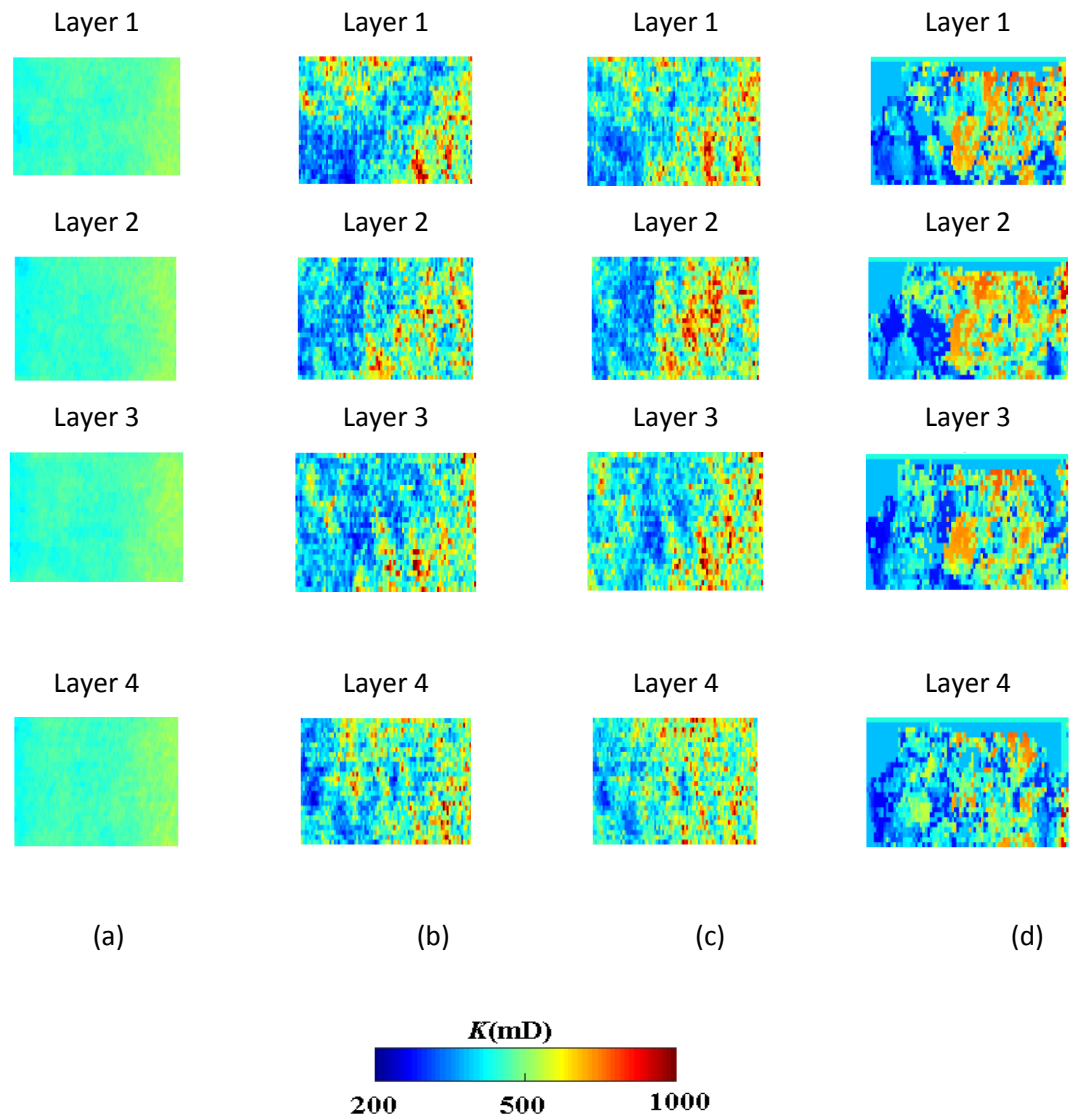


Figure 7.64: permeability reconstruction from the various methods. (a) Initial permeability model, (b) permeability recovered by EnKF (c) permeability recovered from EnKF-EM and (d) True model permeability field

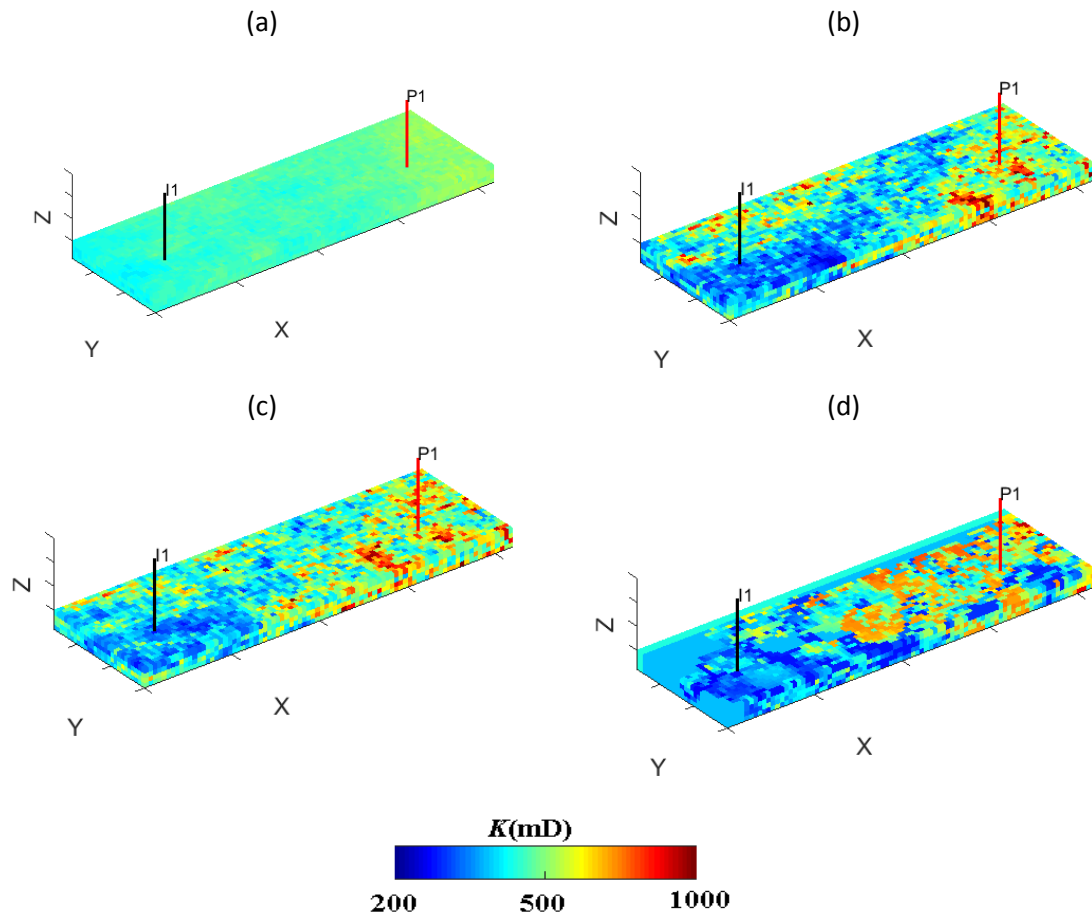


Figure 7.65: 3D permeability reconstruction from the various methods. (a) Initial permeability model, (b) permeability recovered by EnKF (c) permeability recovered from EnKF-EM and (d) True model permeability field

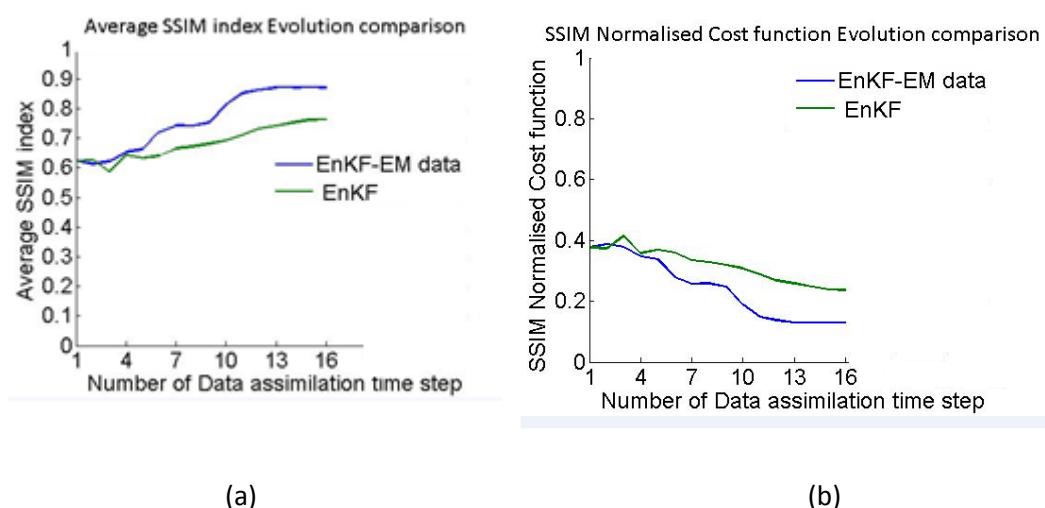


Figure 7.66: Comparison between the EnKF-EM and EnKF SSIM metric image quality assessment: (a) injection pressure profile, (b) water production rate profile and (c) oil production rate profile.

The overall cost function for the history matching process taking into account the RMS cost function and SSIM Normalised cost function is described in eqn.7.51. Moreover, the values reported in Table 7.16.

$$\text{Overall cost function} = \frac{(SSIM \text{ Normalised Cost Function} + RMS \text{ function})}{2} \quad (7.51)$$

Table 7.16: Overall cost function comparison between EnKF-EM and EnKF.

Model	SSIM Normalised Cost Function	RMS function	Overall cost function
EnKF-EM	0.129	1.97	1.05
EnKF	0.181	3.35	1.77

7.5.10. Conclusion and future work

- In this work, an approach for coupling the EnKF and level set parametrisation for the history matching of reservoirs in 3D was developed.
- With the prior knowledge of the permeability/facies distribution, the initial realisations were generated with two-point Statistics (SGS)).
- A developed process from our previous work for updating the parameters using the EnKF inversion scheme and updating the level-set function simultaneously together was fused with our ART-Level set module.
- Electromagnetic data are more sensitive to changes in water saturation and hence can reduce significantly ensemble spread and in so doing provide more accurate results.
- Assimilation of water saturation distribution from EM method increased the history matching performance and decreased the RMS error.
- History matching without the EM data assimilation had a 15% offset from true data as at when compared with history matching with EM data.

7.6 – Combining Machine learning techniques with a History Matching - Level set approach (Numerical Experiment 5)

Novelty

In this work, a novel shape reconstruction technique called '**SELE**' which denotes Sparsity-Ensemble optimization-Level-set-Ensemble optimisation implementing a coupling of a Level-set-Ensemble Smoother Multiple Data Assimilation (ES-MDA) with compressed sensing (CS) is proposed. Due to the ill-posed nature of history matching, realisations may match quantitatively to the true model but vary qualitatively as permeability replicates. '**SELE**' solves this ill-posed inverse problem by utilising a sparsity promoting ES-MDA approach. An initial over complete learned dictionary is created using an unsupervised learning algorithm called *K-SVD*. Further parametrisation to avoid a huge burden on complexity is achieved using the discrete cosine transform (*DCT*) on the initial realisations first, which is then after learned with the *K-SVD*. *K-SVD* is combined with a greedy orthogonal, matching pursuit algorithm (*OMP*) for the parametrisation of the petrophysical properties (permeability/ or porosity fields). During the history matching step, generate the ensemble state which consists of these sparse coefficients coupled with the level set representation of these properties. The analysed sparse coefficients are then mapped back to spatial fields using this *K-SVD* dictionary. The efficiency of the algorithm with numerical examples is shown. The CS algorithm enhances the reconstruction of channelised geological structures by transforming the ES-MDA assimilation step to a sparse domain representing the diverse geological scenarios in play. Numerical examples are shown and quantify our '**SELE**' shape reconstruction by using a structural similarity index metric (*SSIM*). The proposed method shows rapid convergence to the true model and higher *SSIM* index to the true model permeability distribution.

7.6.1 Introduction

The reconstruction of subsurface features from production data has long been a challenge in the reservoir engineering community as a result of the small number of observations that are available to identify their spatial arrangements in the subsurface (Jafarpour, 2011). In current trends, the Ensemble Smoother with Multiple Data

Assimilation (ES-MDA) method has been used for the estimation of subsurface petrophysical parameters such as permeability (Emerick, 2018). The standard ES-MDA approach fails to capture this spatial distribution accurately.

Image processing and signal reconstruction offer novel methods for history matching, one of these are compressed sensing (CS) (Jafarpour & McLaughlin, 2007) (Jafarpour, 2011) (Liu & Jafarpour, 2013). CS provides a means of maximising the quality of reconstruction from fields exhibiting sparsity (Candes, et al., 2006) . CS allows for improved recovery involving sparse domain signals by the use of a reduced number of observations. It does this by exploiting prior information on the sparsity of the signal. Focusing on the general reservoirs under consideration, the reservoir field is classified as a sparse field recovery problem because of the high uncertainty associated with the spatial distribution of the petrophysical properties. In classical reservoir modelling, only hard data at the well locations are known from core analysis or well-test, the rest of the field-wide data is inferred from kriging or stochastic simulation (Deutsch & Journel, 1998) (Wu, et al., 2006). Discrete Cosine Transform (DCT) in (Jafarpour & McLaughlin, 2007) and the Wavelet transforms in (Jafarpour, 2011) have been used for sparsity promoting representation under the EnKF methodology. From this work, it was noted that the gains realised from this sparse representation were limited to the reduced computational complexity, the methods were deficient in providing an efficient system in incorporating prior subsurface structural information (Khaninezhad, et al., 2012). In (Khaninezhad, et al., 2012), a detailed study was done by the authors to investigate the influence of sparse geologic dictionaries that were used as prior information in an inverse process. The authors concluded that the diverse geologic dictionaries led to a wider and more reliable estimation which was attributed to the dictionary elements.

In this work, the researcher proposes a new method based on compressed sensing to improve the reconstruction of permeability/facies using combined level-set and ES-MDA. The proposed scheme is described as follows. First, augment the ensemble state with the sparse petrophysical properties gotten after activating the OMP algorithm on the spatial permeability and porosity ensemble field, the level set functions of the

permeability and porosity fields with the forecasted simulated data. The analysed state vector consists of the updated sparse coefficients and the updated level set functions updated at just the boundary of each facies. The resulting updated spatial permeability and porosity field are gotten from a multiplication of the over-complete dictionary with the updated sparse coefficients. The resulting update of the spatial permeability field and the level set functions are compared together. The conflict in each update is rectified giving more precedence to the level set update (Etienam et al., 2018).

7.6.2. Construction of the state space ensemble

The state space ensemble for the Gaussian experiment to be explained later as shown in Eqn. 7.52. It consists of the sparse coefficient of the permeability and porosity field, signed distance function of both the permeability and porosity fields and simulated production data from the current time.

$$y_k^j = \left\{ \begin{array}{l} K_{i(\text{sparse})}, \\ \varphi_{i,(\text{sparse})} \\ \phi(K)i_{,k} \\ \phi(\varphi)i_{,k} \\ P_i \\ S_{w,i} \\ Qo(\text{producer well } 1 - 6) \\ Qw(\text{producer well } 1 - 6) \\ Qg(\text{producer well } 1 - 6) \end{array} \right\}^j \in \mathcal{R}^{N_\phi + N_\varphi + N_u + N_d} \quad (7.52)$$

The state space ensemble for the channelised experiment to be explained later is shown below,

$$y_k^j = \left\{ \begin{array}{l} K_{i(\text{sparse})}, \\ \varphi_{i(\text{sparse})} \\ \phi(K)i_{,k} \\ \phi(\varphi)i_{,k} \\ P_i \\ S_{w,i} \\ BHP_k(\text{injector well } 1 - 4) \\ Qo(\text{producer well } 1 - 4) \\ Qg(\text{producer well } 1 - 4) \\ \text{water-cut(producer well } 1 - 4) \end{array} \right\}^j \in \mathcal{R}^{N_\phi + N_\varphi + N_u + N_d}$$
(7.53)

The parameter update is performed using the Eqn. (7.54)

$$y_k^{a,j} = y_k^{f,j} + \tilde{C}_{MD}^f (\tilde{C}_{DD}^f + \gamma^i C_D)^{-1} \times (d_{uc,j} - d_j^f) \circ f_{Noverall}, j = 1, \dots, N_e$$
(7.54)

$f_{Noverall}$ is a matrix of $\in \mathcal{R}^{N_y \times N_e}$ with each element to be one. I then replace the row and columns of the $f_{Noverall}$ matrix equivalent to the signed distance of both the permeability and porosity field with f_N

$$f_{Noverall}[N_{ysigned(K+\varphi)} : N_e] = f_N \in \mathcal{R}^{N_{ysigned(K+\varphi)} \times N_e}$$

where f_N is the 3D narrow band (N.B.) function consisting of zeroes' and one's, reshaped to a column vector, to be inserted into the 2D $f_{Noverall}$ matrix. It is a matrix indicating were the low permeability/porosity facies is in proximity to the high permeability/porosity facies in the reservoir (boundary location). f_N is built from the Heaviside operation explained earlier peculiar to the absolute permeability/porosity field. The parameter $| \circ |$ signifies a Hadamard product operation. The *SELE* update is done with Eqn.7.54. Retain the full update on the ensemble state y and the boundaries of the signed distance function by element-wise multiplication with the $f_{Noverall}$ 2D matrix. The narrow band matrix preserves the shape of the facies and it is a matrix consisting of ones in a small pixel neighborhood of the boundaries separating two different facies type and zero elsewhere (Villegas, et al., 2005). In principle, a conflict may occur between the update to the log-permeability field/ porosity field and to the signed distance of the permeability field/porosity field (after re-parametrization)

in Eqn. (7.54), when this situation occurs; the Level Set update takes priority. The values assigned during this conflict resolution are explained shortly.

7.6.3. The algorithm/Method

Our new shape reconstruction algorithm is '**SELE**'. This signifies '**S**parsity-**E**nsemble optimisation-**L**evel-set **E**nsemble optimisation'. (Etienam et al, 2018). The proposed algorithm **SELE** algorithm is enumerated below.

1. Generate **Nr** realisations of different permeability/porosity geologic distributions using the MPS scheme *FILTERSIM* (Wu, et al., 2006). Where **Nr**=2000 in this work.
2. These **Nr** realisations are trained with the K-SVD algorithm in Eqn. (6.13) to create an over-complete dictionary matrix of rank grid size of reservoir \times 1500.
3. Generate the initial ensemble (100 realisations) of permeability using the *FILTERSIM* (MPS) method (Wu, et al., 2006) for the channelised test case and *SGSIM* (Deutsch & Journel, 1998) for the Gaussian test case.
4. Choose the number of assimilation iteration N_a and run the subsection 1 to N_a times
 - a. Forward simulate the 100 models using the multiphase flow simulator, in this case, the ECLIPSE 100 reservoir simulator. (Schlumberger GeoQuest, 2014)
 - b. Truncate the spatial permeability and porosity field to arrive at the categorical facies field. Compute the signed distance function and the corresponding narrowband function
 - c. Convert the spatial permeability and porosity field to sparse using the Dictionary created from (2) in conjunction with the Orthogonal Matching Pursuit algorithm (OMP) from Eqn. (6.12)
 - d. Augment the ensemble state with the sparse permeability and porosity field, level set functions of the permeability and porosity field with the predicted production data from the forward problem
 - e. For j=1: production history
 - i. Carry out the ES-MDA analysis using Eqn. (7.54).
 - f. End for

- g. Recover the spatial domain by multiplying the updated sparse ensemble from step e with the over-complete dictionary created from step 2
 - h. Obtain the facies indicator field of the updated spatial permeability and porosity field by truncating at the relevant threshold mark
 - i. Rectify the conflict between the updated level set function and the updated facies indicator function of the spatial permeability and porosity field
 - j. Give preference to the updated level set function and populate the permeability and porosity field for the next run with the values from (i)
5. Specify the stopping criterion, in this case; the simulation stops when N_a iterations has concluded.

The mathematical algorithm is described

Algorithm: SELE

1. Input the initial permeability and porosity ensemble generated with SGS for Gaussian case and *FILTERSIM* for Channelized case (at time k), K_k^f, φ_k^f , Production observation data $d_{obs,k}$, dictionary D (computed off-line and once using the K-SVD algorithm), sparsity level T_0
2. Choose the number of data assimilations, N_a and the coefficients γ^i for $i = 1, 2, \dots, N_a$
3. For $i = 1$ to N_a
 - a) Run the ensemble from time zero,
 - b) Transform the spatial permeability ensemble to sparse domain
 - i. $K_{(sparse)k}^f = OMP(K_{(spatial)k}^f, D_{(permeability)}, T_0)$
 - ii. $\varphi_{(sparse)k}^f = OMP(\varphi_{(spatial)k}^f, D_{(porosity)}, T_0)$
 - iii. Obtain the production simulated data d_j^f
 - c) Truncate $K_{(spatial)k}^f$ and $\varphi_{(spatial)k}^f$ at given permeability/porosity threshold Set
 - d) $\begin{pmatrix} K_k^f \\ \varphi_k^f \end{pmatrix} = \begin{pmatrix} K_{k-1}^a \\ \varphi_{k-1}^a \end{pmatrix}$ (for $k \neq 1$)

-
- e) If $\binom{K_{k(spatial)}^f}{\phi_{k(spatial)}^f} > threshold$, then $S(\phi_{k(spatial)}^{f,j}) = 1$, else $S(\phi_{k(spatial)}^{f,j}) = 0$
- f) Generate two facies system using signed distance function b

$$\begin{aligned} \text{Signed distance} &= ((Sx_1 - Sx_2)^2 + (Sy_1 - Sy_2)^2 + (Sz_1 - Sz_2)^2)^{\frac{1}{2}} \\ &= \phi_k^{f,j} \end{aligned}$$

- g) Compute the initial narrow band function f

- h) For each ensemble realisation, perturb the observation vector

$$\text{using } d_{uc,j} = d_{obs} + \sqrt{\gamma^i C_D^{-2}} z_d, \text{ where } z_d \sim \mathcal{N}(0, I_{N_d})$$

- i) Generate the state vector

$$y_k^{f,j} = [K_{(sparse)k}^f, \varphi_{(sparse)k}^f, \phi_{k(K)}^f, \phi_{k(\varphi)}^f, d_{sim,k}]^T$$

- j) Do k=1:production history

- i. Update the ES –

MDA state space by implementing a point by point element

- ii. multiplication of overall narrow –

band function(foverall)as

- iii. $y_{k+1}^{a,j} =$

$$y_k^{f,j} + \left(\tilde{C}_{MD}^f (\tilde{C}_{DD}^f + \gamma^i C_D)^{-1} \times (d_{uc,j} - d_j^f) \right) o foverall$$

- iv. Update and compute foverall from $\phi_{k(K \& \varphi)}^{a,j}$ gotten from $y_{k+1}^{a,j}$

- k) End do

- l) Output $K_{(sparse)k}^a, \varphi_{(sparse)k}^a$ and $\phi_{k(K \& \varphi)}^{a,j}$ obtained from $y_k^{a,j}$

- m) Transform the analysed ensemble to spatial domain

$$K_{(spatial)k}^a = D \times K_{(sparse)k}^a$$

$$\varphi_{(spatial)k}^a = D \times \varphi_{(sparse)k}^a$$

$$\text{If } \binom{K_{k(spatial)}^a}{\varphi_{k(spatial)}^a} > Threshold, \text{ then } S(\phi_{k(spatial)}^{a,j}) = 1 \text{ else } S(\phi_{k(spatial)}^{a,j}) = 0$$

If $\phi_{k(K \& \varphi)}^{a,j} < 0$ then $S(\phi_{k(Level-set)}^{a,j}) = 0$ else $S(\phi_{k(Level-set)}^{a,j}) = 1$

If ($S(\phi_{k(Level-set)}^{a,j}) = S(\phi_{k(spatial)}^{a,j})$) = then

$$\begin{pmatrix} K_{k(sele)}^a \\ \varphi_{k(sele)}^a \end{pmatrix} = \begin{pmatrix} K_{k(spatial)}^a \\ \varphi_{k(spatial)}^a \end{pmatrix}$$

elseif ($S(\phi_{k(Level-set)}^{a,j}) \neq S(\phi_{k(spatial)}^{a,j})$). AND. ($S(\phi_{k(Level-set)}^{a,j}) = 1$)

then

$$\begin{pmatrix} K_{k(sele)}^a \\ \varphi_{k(sele)}^a \end{pmatrix} = 1.05 \times \text{Threshold permeability/porosity value}$$

endif

if $S(\phi_{k(Level-set)}^{a,j}) \neq S(\phi_{k(spatial)}^{a,j})$. AND. ($S(\phi_{k(Level-set)}^{a,j}) = 0$) then

$$\begin{pmatrix} K_{k(sele)}^a \\ \varphi_{k(sele)}^a \end{pmatrix} = 0.95 \times \text{Threshold permeability/porosity value}$$

endif

n) Output $\begin{pmatrix} K_{k(sele)}^a \\ \varphi_{k(sele)}^a \end{pmatrix}$

o) Honour the permeability and porosity values from actual well data
by enforcing a non-update on the pixel location in the simulation
grid

4. Set iteration count $i = i + 1$

end for

end program

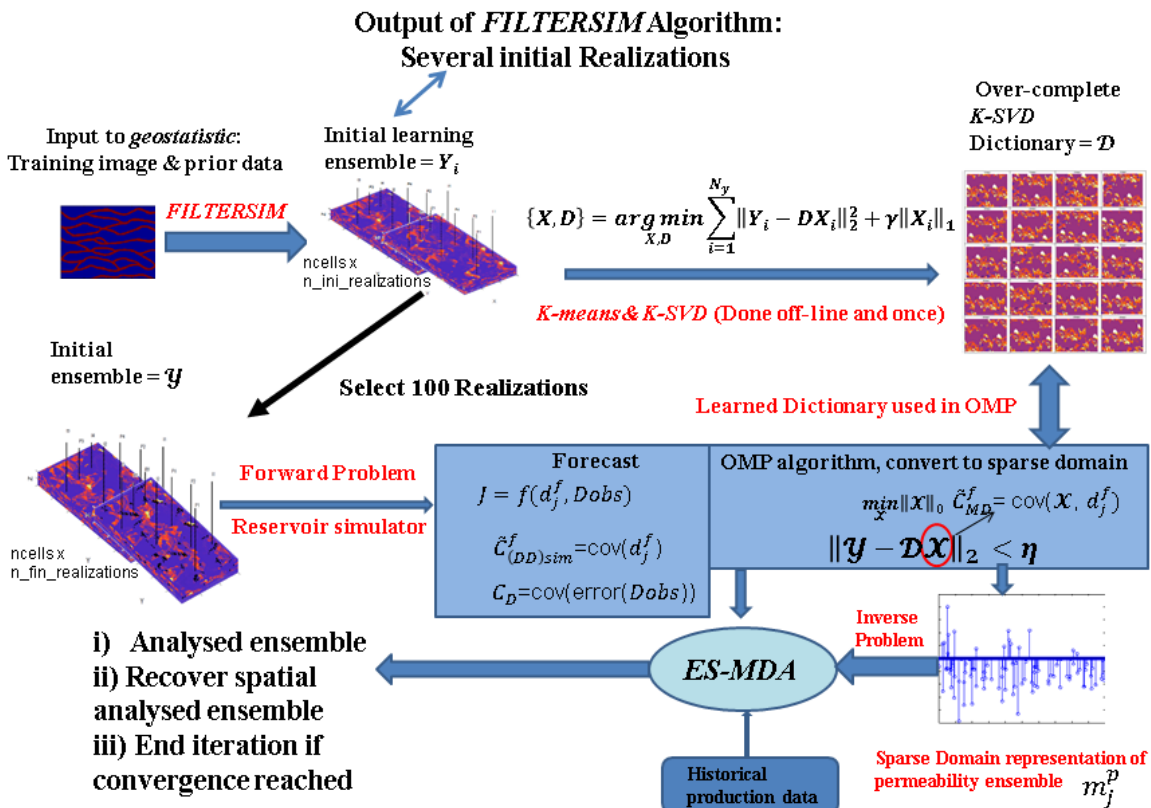


Figure 7.67: Schematic showing the **SELE** algorithm

7.6.4. Results and Discussions

In this section, we would discuss the implementation of the **SELE** algorithm to two synthetic test cases. The first test case is the PUNQ-S3 synthetic model and the second case is the SPE 10 channelised synthetic model.

7.6.5 PUNQ-S3 synthetic model

We carry out this K-SVD dictionary creation off-line before the History matching loop.

For both cases, to make the SELE method applicable to large field cases (models having more than 50,000 pixels), the DCT algorithm could be conducted on the initial ensemble generated apriori before history matching. The significant leading cosine basis (shown in the left corner of the figure) is retained. The K-SVD can then be used on this retained basis to produce a geological overcomplete dictionary of cosine basis as depicted in Figure 6.4. Figure 7.69 shows the K-SVD error convergence when creating the overcomplete learned dictionary required in the ES-MDA loop of the permeability and porosity realisations shown in (A) and (B) respectively

Experiments to be conducted

In this section, we conduct three numerical experiments to test the efficiency of our history matching algorithm to the PUNQ-S3 true model.

(a). *SELE* method

The 100 realisations of permeability models are generated with the sequential Gaussian simulation method enumerated in (Deutsch & Journel, 1998) and the method enumerated in section 7.63 with steps 1-12.

(b). ES-MDA-level set

The 100 realisations of permeability models are generated with the sequential Gaussian simulation method enumerated in (Deutsch & Journel, 1998), and the method enumerated in section 7.63, 1-12 without any sparse parametrisation on the permeability and porosity field is implemented are implemented.

(c). ES-MDA

100 realisations of permeability models are generated with the sequential Gaussian simulation method enumerated in (Deutsch & Journel, 1998). The ES-MDA approach is used without any Level-set and sparse parametrisation.

7.6.6 Comparison studies for the PUNQ-S3 model

To compare the accuracy of the three methods, ES-MDA, ES-MDA-Level Set and SELE methods two different criteria are considered, the RMS function considering production data, and the structural similarity ($SSIM$) index. The permeability and the porosity are modified in each step, and other parameters are kept constant. Figure 7.69 shows some initial realisations of model #21, #11 and #31 and #67

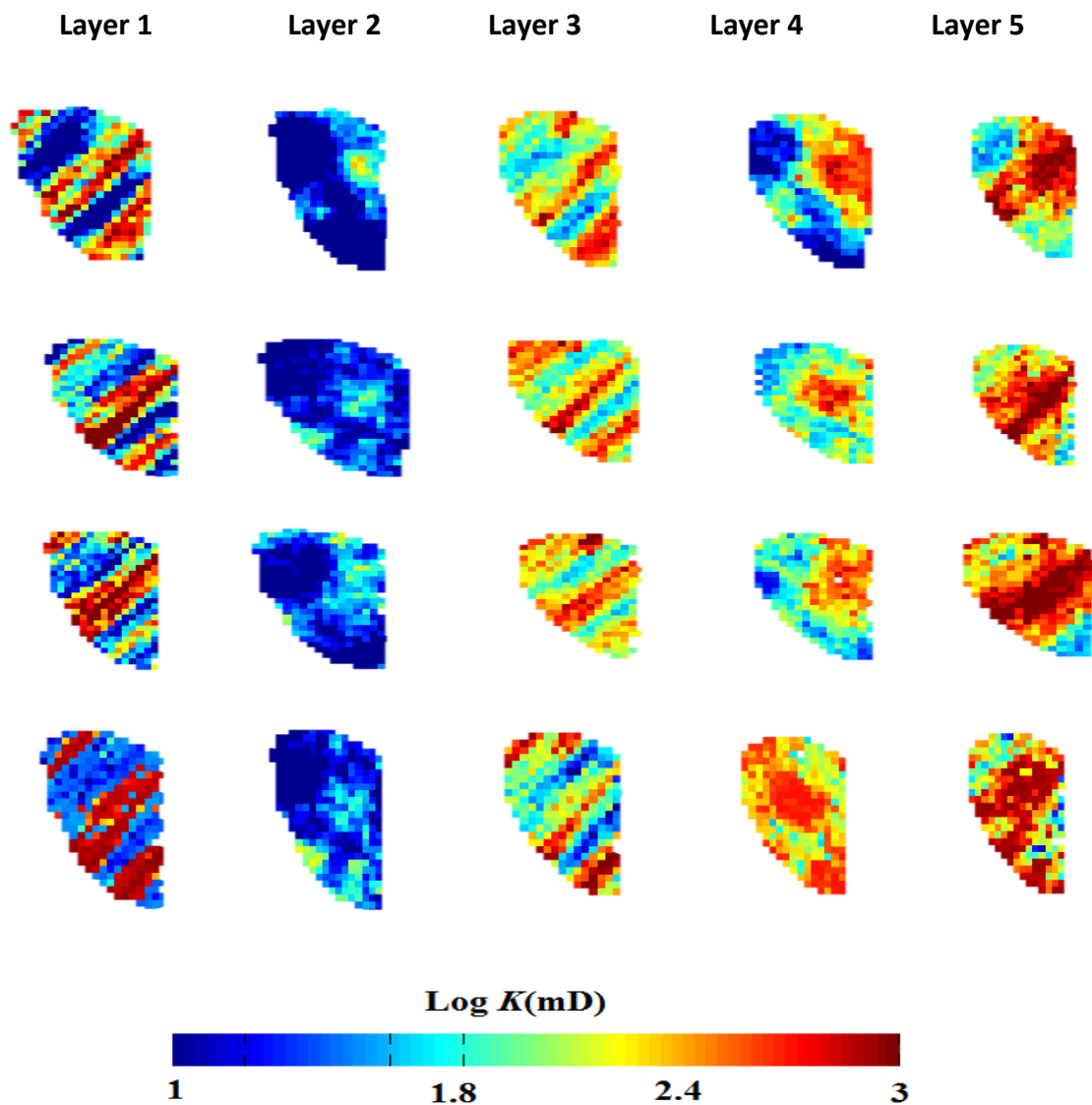


Figure 7.68: an initial model of realisations #21, #11, #31 and #67 generated with the SGSIM algorithm (Deutsch & Journel, 1998)

K-SVD Dictionary learning

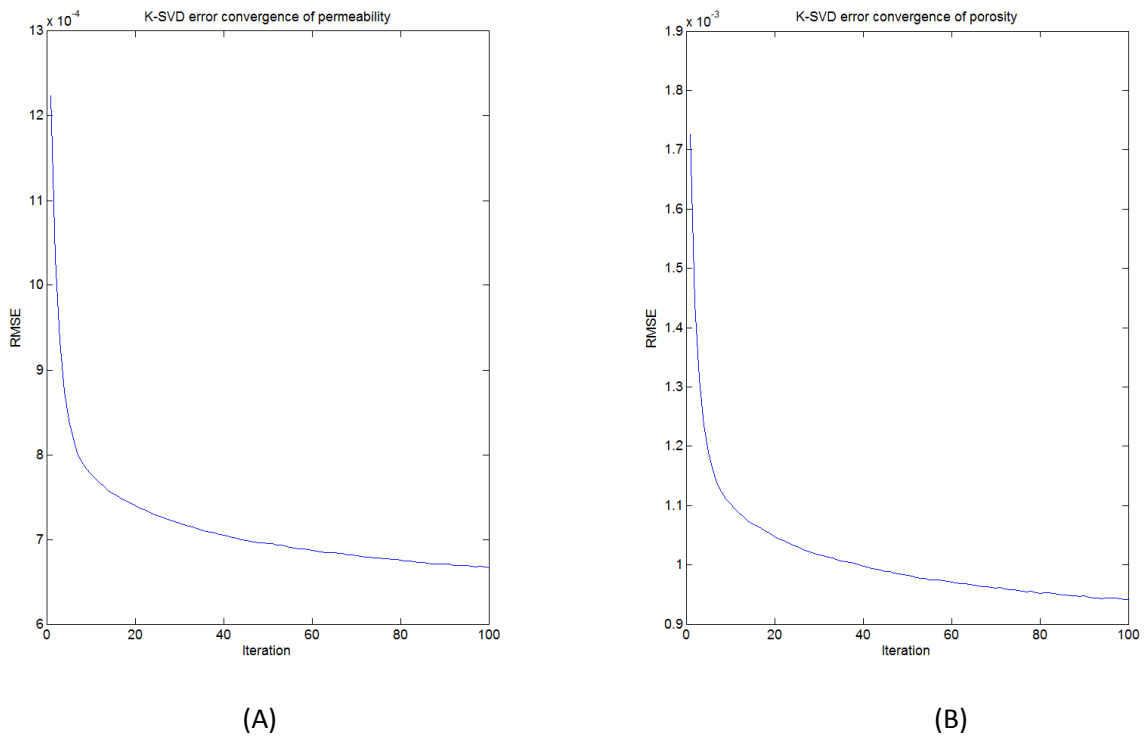
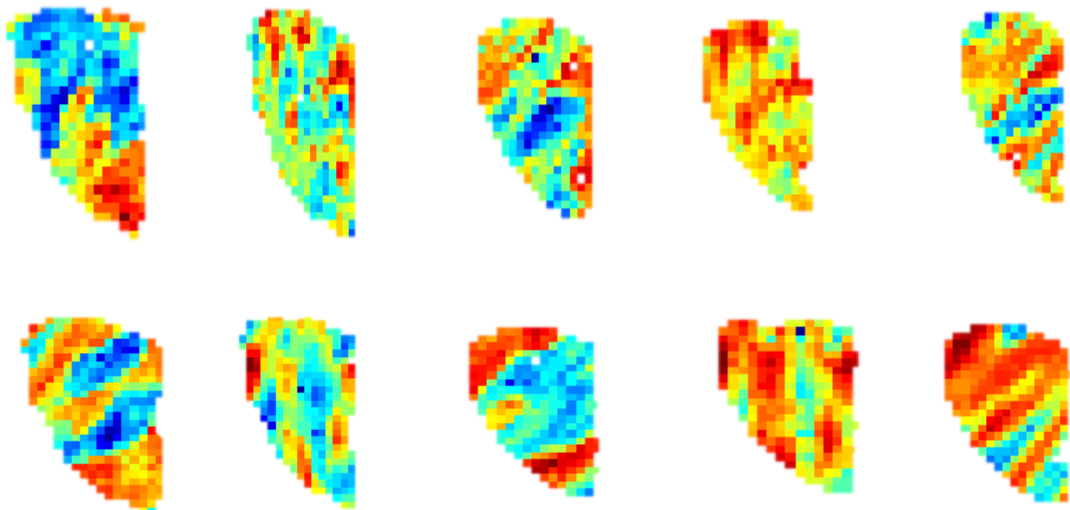


Figure 7.69: K-SVD error convergence when creating the overcomplete learned dictionary required in the ES-MDA loop of the permeability and porosity realisations shown in (A) and (B) respectively

Figure 7.70 shows some initial permeability K-SVD basis

Layer 1 Layer 2 Layer 3 Layer 4 Layer 5



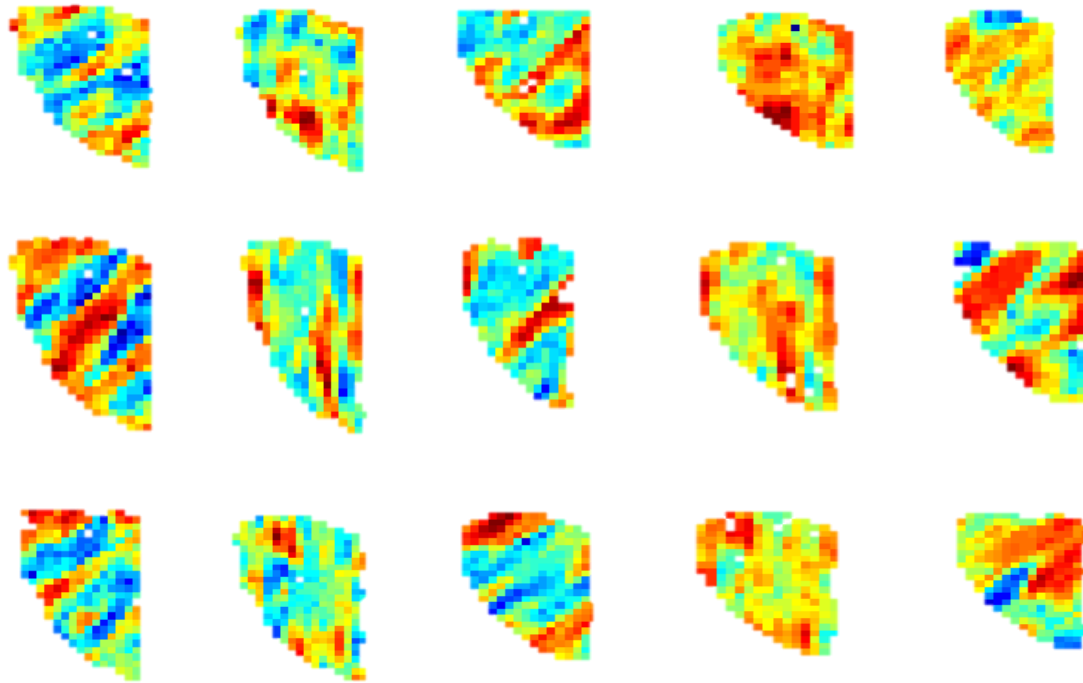


Figure 7.70: Some initial permeability K-SVD basis

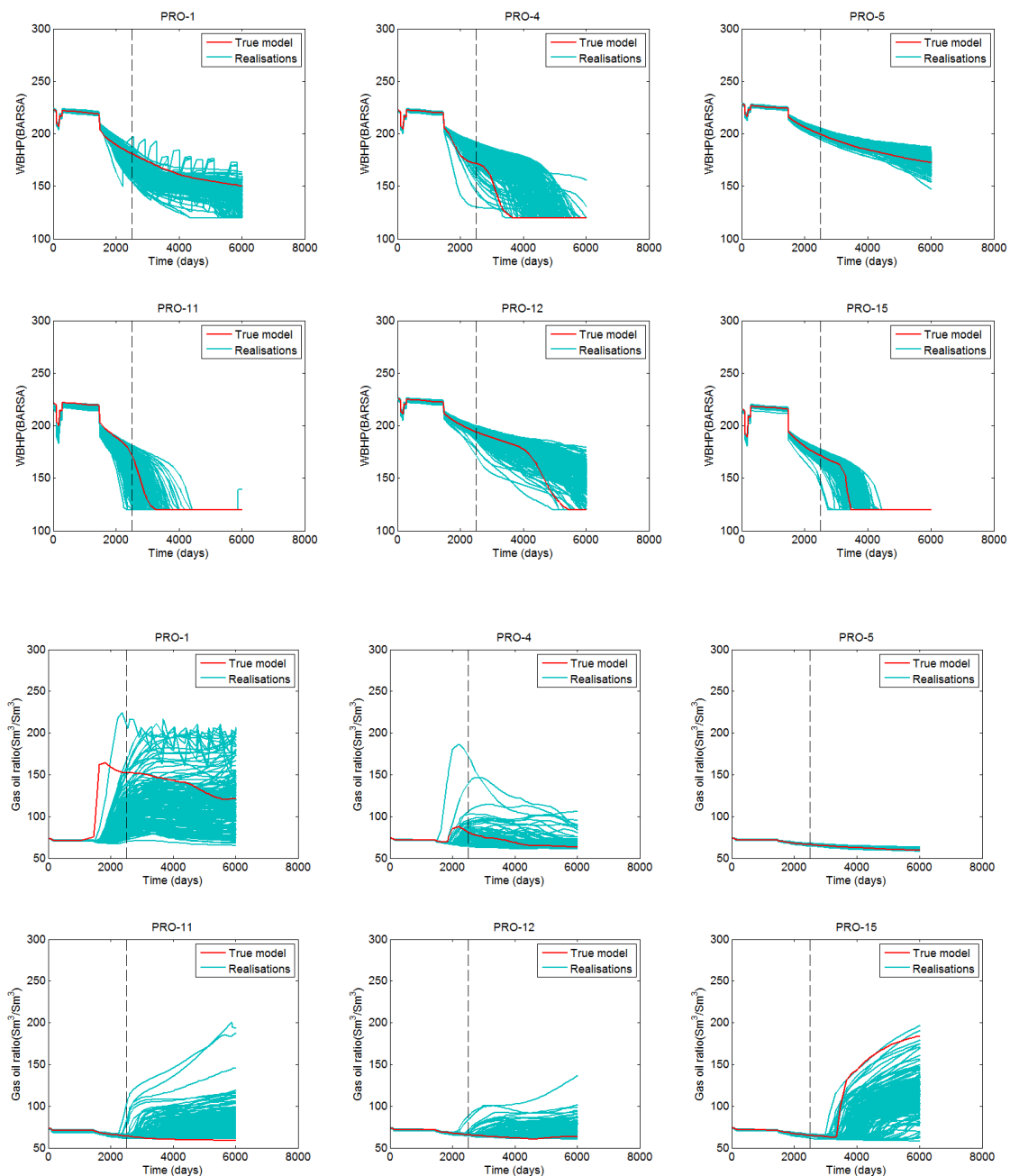
Root-mean-square (RMS) function

Eqn. (7.19) is used to calculate our RMS value. Starting with a stochastic realization generated by SGS (Deutsch & Journel, 1998), and focusing on the best realization #31, the convergence for the ES-MDA history matching was achieved in 6 iterations with an RMS error of 19.8, the convergence of the ES-MDA-Level set was achieved in 5 iterations with an RMS error of 5.5,. Using the proposed method SELE history matching, the convergence was achieved in 4 iterations with an RMS error of 0.84. Table 7.17 below reports the effectiveness of the SELE algorithm. The initial RMS values for some of the realisations are displayed in column 2. In the comparison of the final RMS value for each method, the proposed SELE approach (column 5) yields lower RMS values when compared to all other methods(column 3 and 4)

Table 7.17: RMS function of best three realisations after ES-MDA, ES-MDA-Level set and SELE update

Realisation no.	Initial RMS value	Final RMS value using ES-MDA	Final RMS value using ES-MDA-Level set	Final RMS value using SELE
21	24.33	14.21	4.2	3.32
11	71.67	52.22	22.13	10.34
31	42.83	19.8	5.5	0.84
67	234	14.34	3.21	1.45

Figure 7.71(a) shows the bottom-hole pressure, gas –oil ratio and water cut for the six producer wells of the initial ensemble. Figure 7.71(b) shows the bottom-hole pressure, gas –oil ratio and water cut for the 6 producer wells of the ensemble recovered after ES-MDA, Figure 7.71(c) shows the bottom-hole pressure, gas –oil ratio and water cut for the 6 producer wells of the ensemble recovered after ES-MDA-Level set and Figure 7.71(d) shows the bottom-hole pressure, gas –oil ratio and water cut for the 6 producer wells of the ensemble recovered after SELE



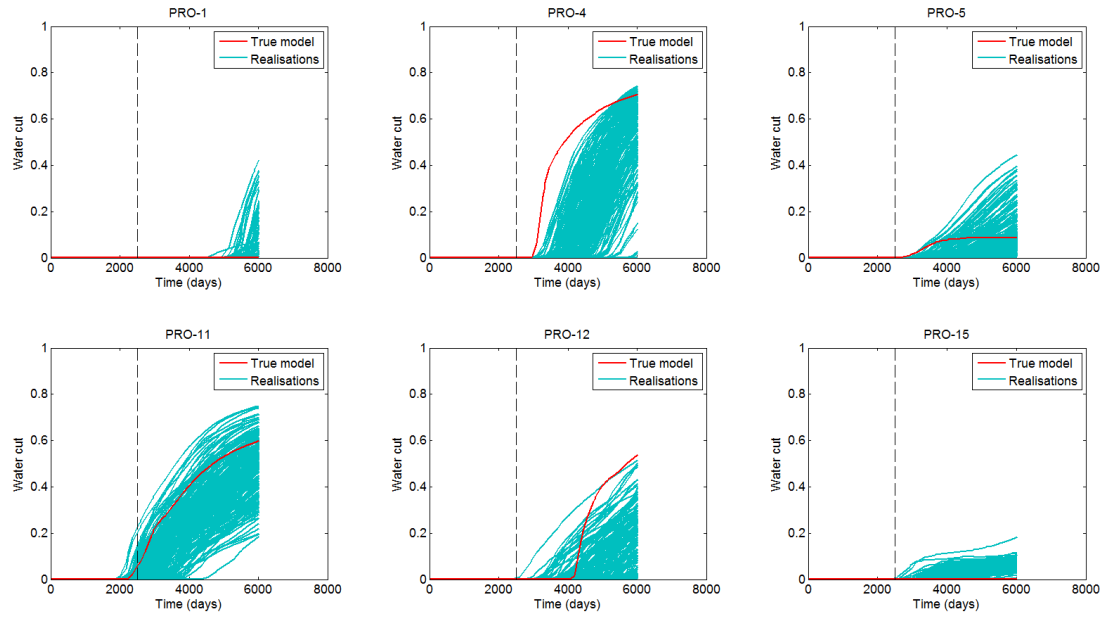
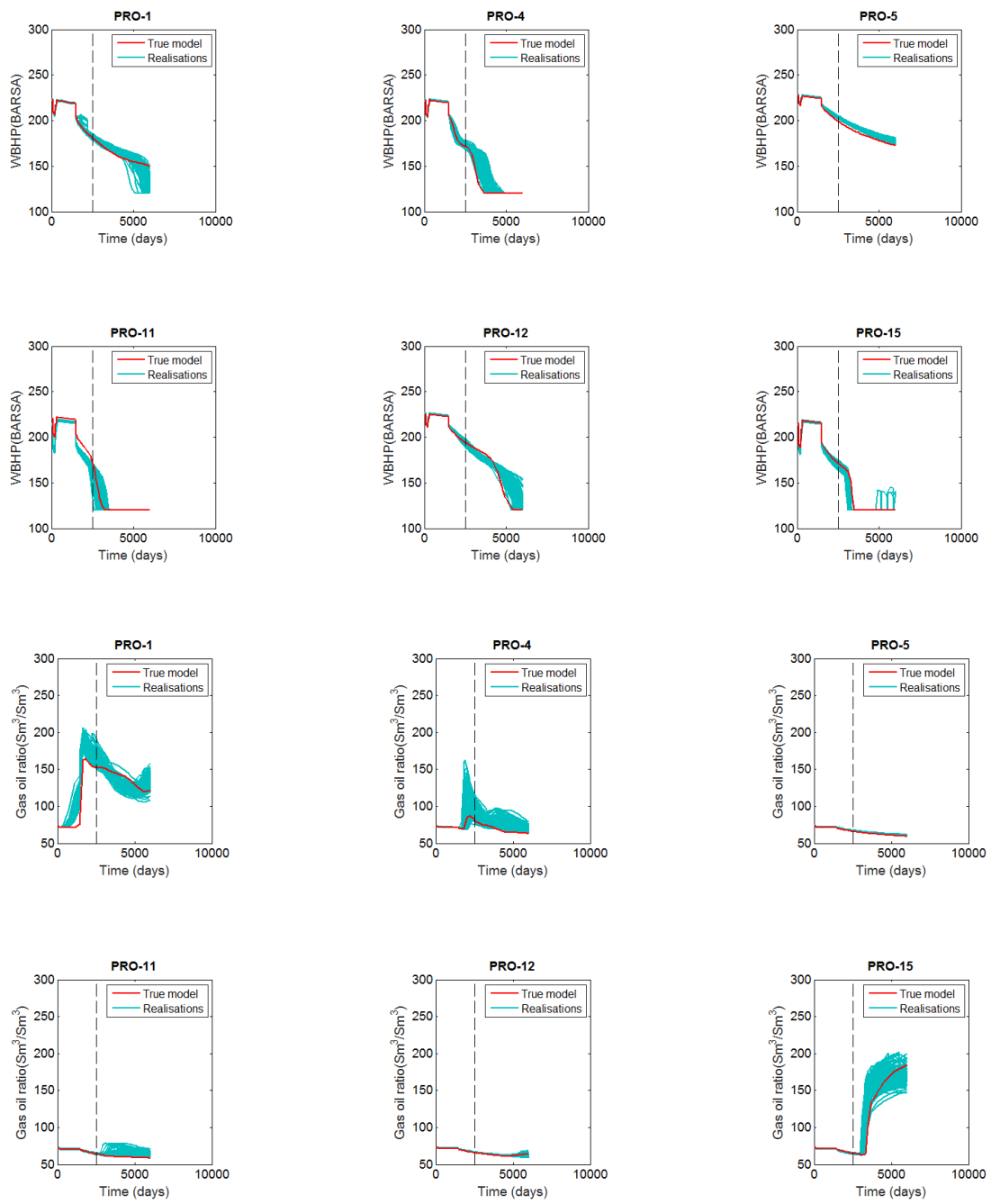


Figure 7.71(a): shows the bottom-hole pressure, gas –oil ratio and water cut for the six producer wells of the initial ensemble. The red curve represent the true data and the cyan overlay lines represents the realisations. The vertical dashed line represents the historical (left of this line) and predcition stages (right of this line)

Notice the large spread of the ensemble members about the true data. This is typical for the initial ensemble repsonses to the true production data.



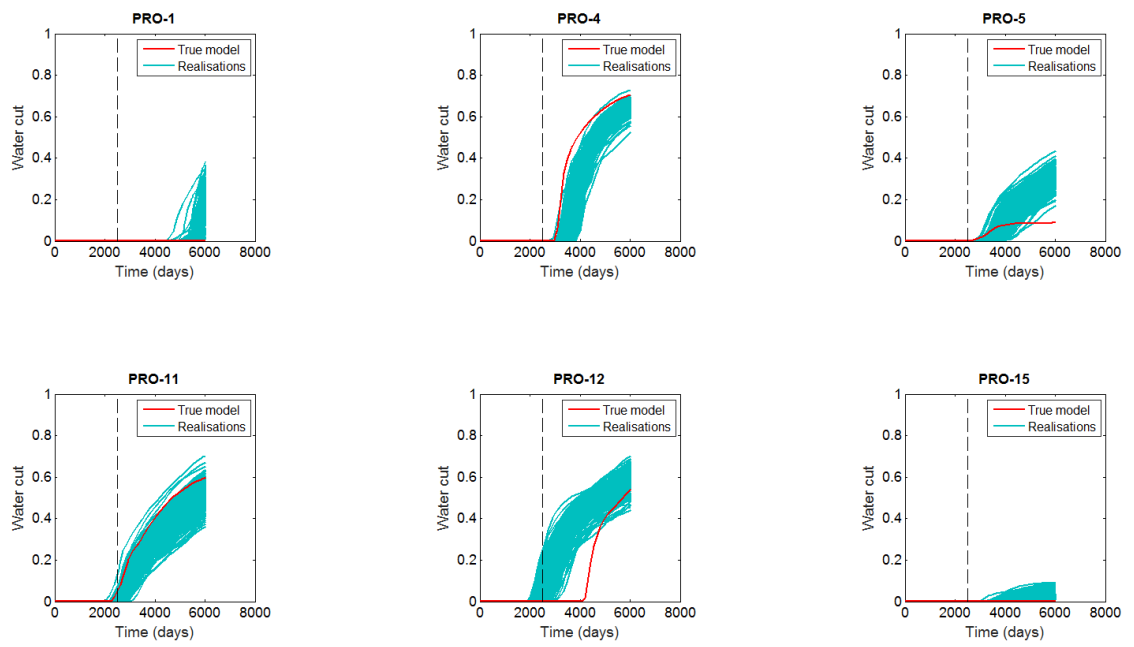
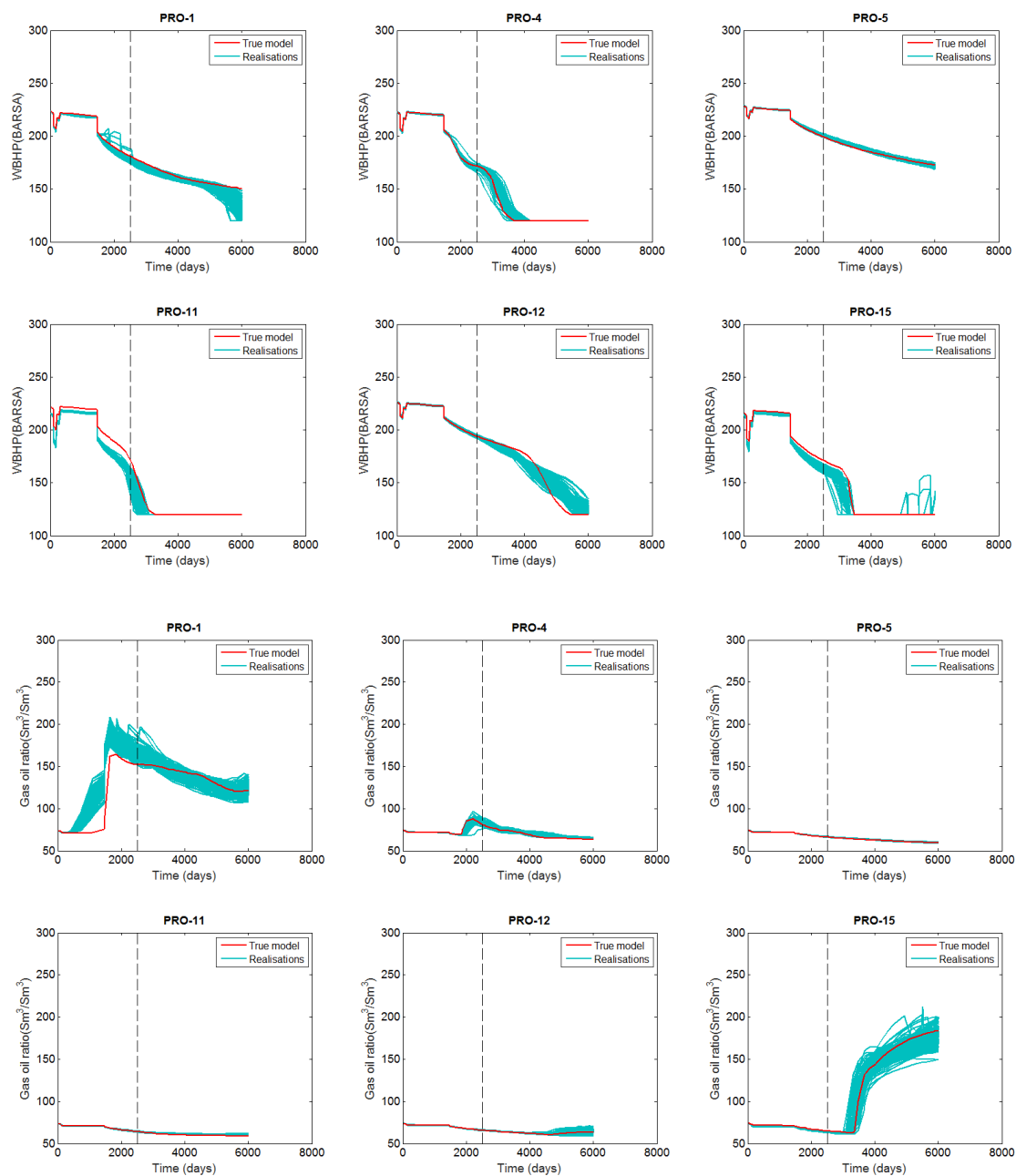


Figure 7.71(b): shows the bottom-hole pressure, gas –oil ratio and water cut for the six producer wells of the ensemble recovered after ES-MDA. The red curve represent the true data and the cyan overlay lines represents the realisations. The vertical dashed line represents the historical (left of this line) and predcitin stages (right of this line)

Notice the decrease in spread of the ensemble members about the true data. This is shows that ES-MDA is reducing the spread in the ensemble variance.



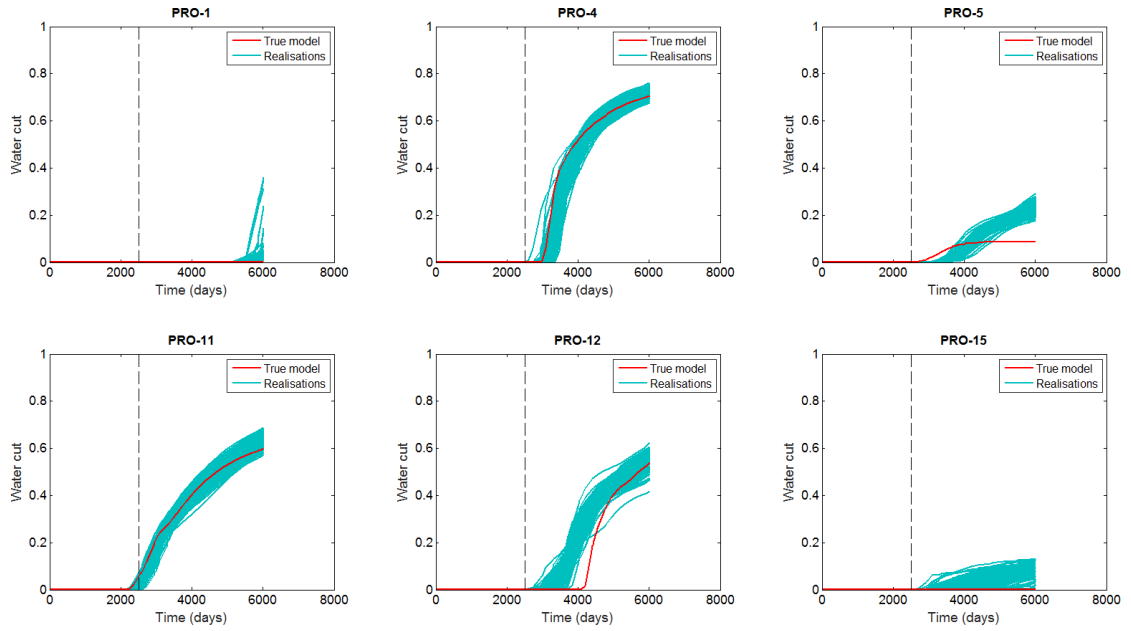
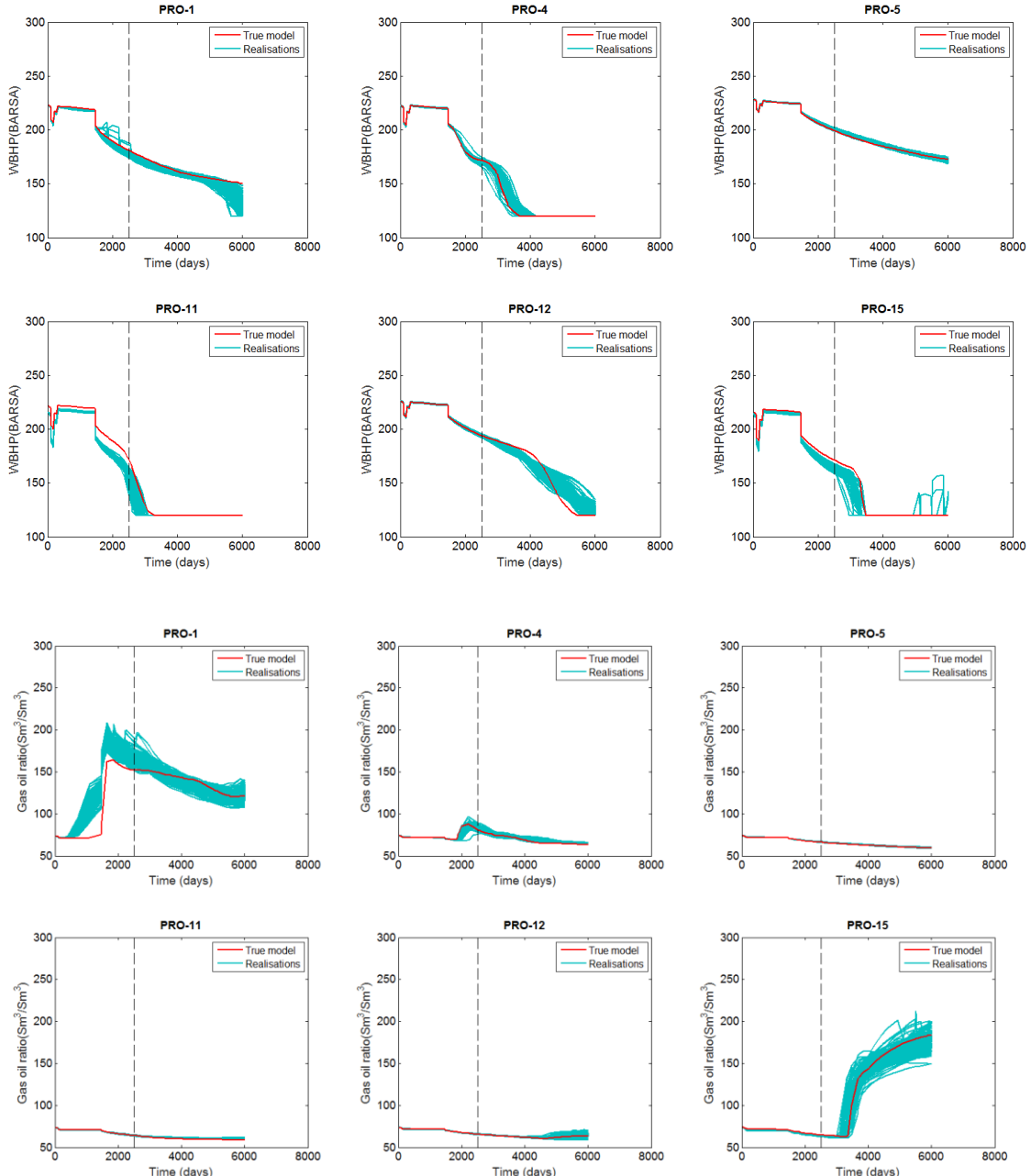


Figure 7.71(c): shows the bottom-hole pressure, gas –oil ratio and water cut for the six producer wells of the ensemble recovered after an ES-MDA-Level set. The red curve represent the true data and the cyan overlay lines represents the realisations. The vertical dashed line represents the historical (left of this line) and predctin stages (right of this line)



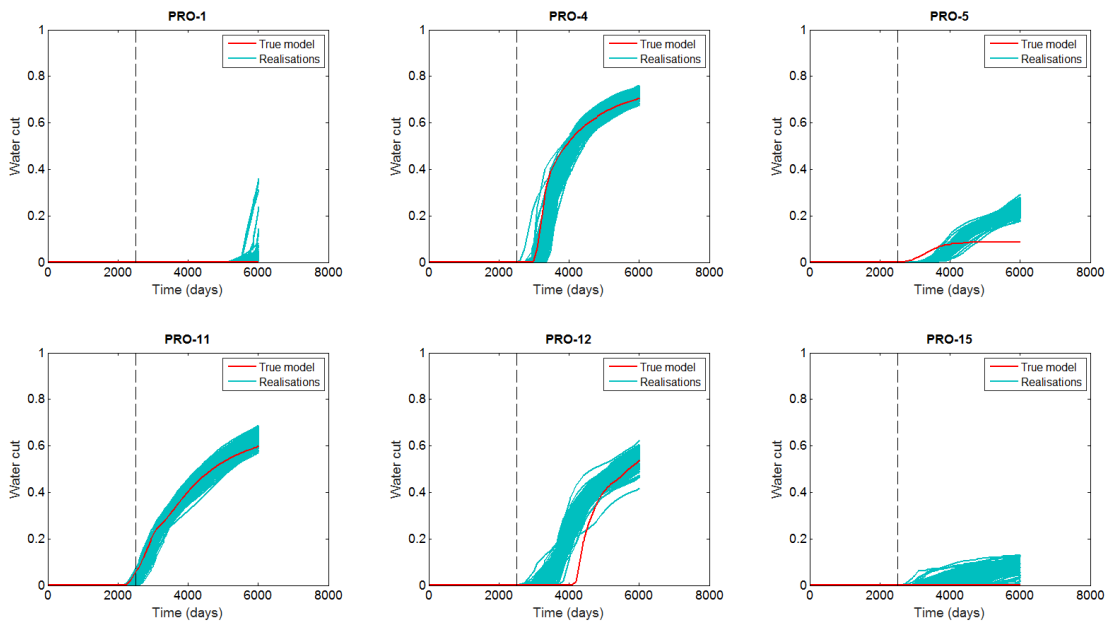


Figure 7.71(d): shows the bottom-hole pressure, gas –oil ratio and water cut for the six producer wells of the ensemble recovered after SELE. The red curve represent the true data and the cyan overlay lines represents the realisations. The vertical dashed line represents the historical (left of this line) and predictin stages (right of this line)

Structural Similarity Index metric (SSIM)

SSIM (Wang et al., 2004) is used to compare the history matched reconstructed permeability realisations to the true model permeability map. Figure 7.72(a) shows the permeability field of the five models shown row-wise (left-to-right). (First row) True permeability model, (second row) mean permeability of initial ensemble, (third row) mean permeability recovered with the ES-MDA algorithm, (fourth row) mean permeability recovered with the ES-MDA-Level set algorithm and (fifth row) mean permeability recovered with the SELE scheme. Figure 7.72(b) shows the 3D Permeability field of the five models. (a) True permeability model, (b) mean permeability of initial ensemble, (c) Permeability recovered with the ES-MDA algorithm, (d) permeability recovered with the ES-MDA-level set scheme and (e) Permeability recovered with the SELE method

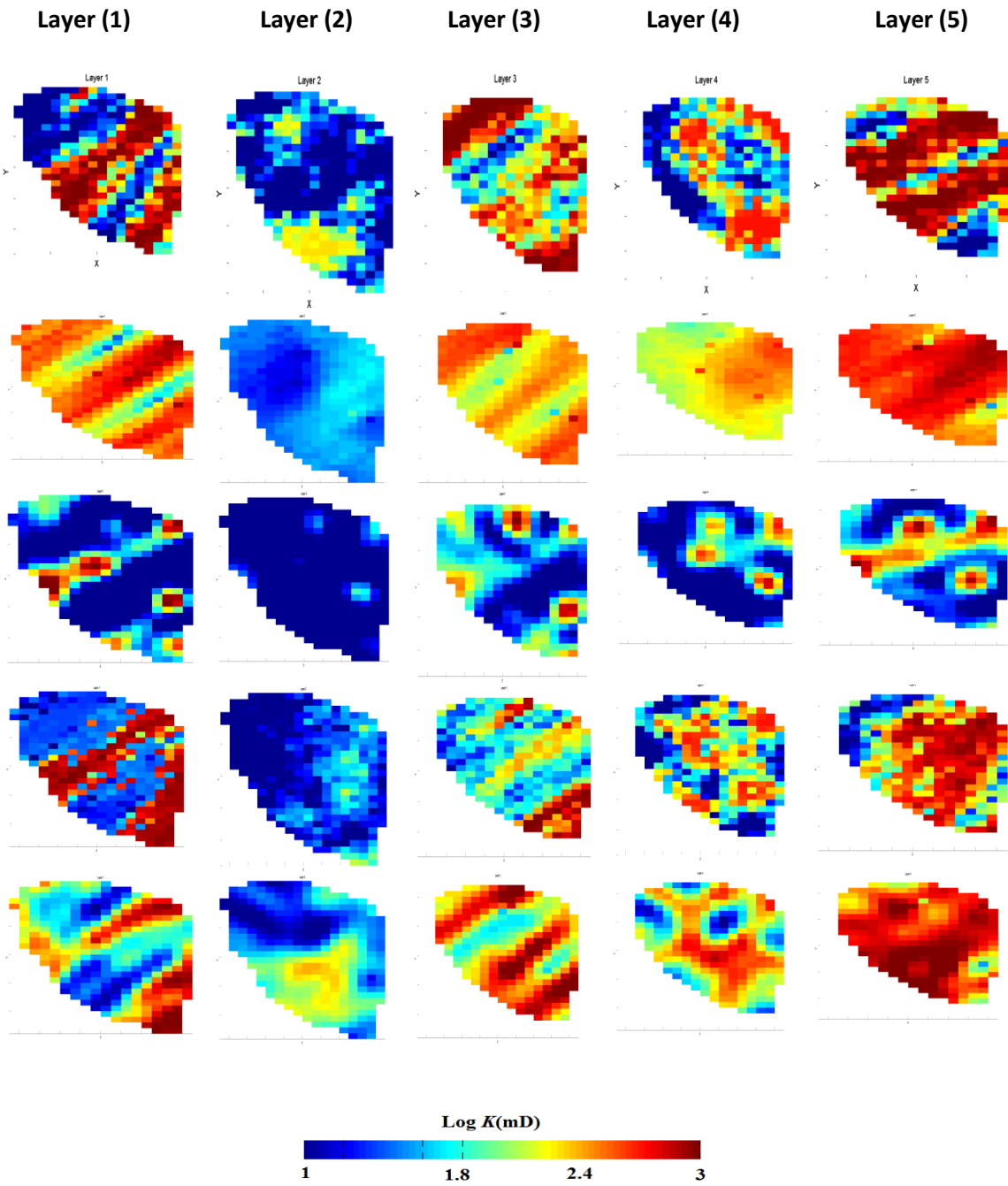


Figure 7.72(a): Permeability field of the five models shown row-wise (left-to-right). (First row) True permeability model, (second row) mean permeability of initial ensemble, (third row) mean permeability recovered with the ES-MDA algorithm, (fourth row) means Permeability recovered with the ES-MDA-
Level set algorithm and (fifth row) mean permeability recovered with the SELE scheme

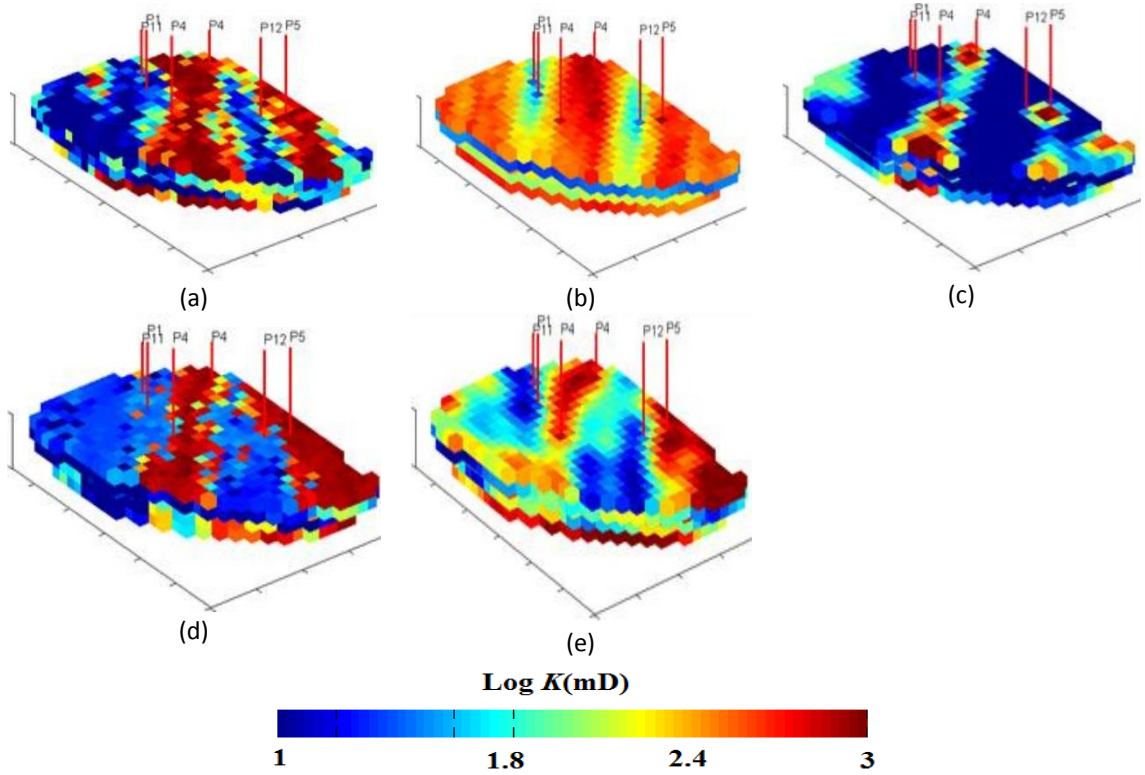


Figure 7.72(b): 3D Permeability field of the five models. (a) True permeability model, (b) mean permeability of initial ensemble, (c) Permeability recovered with the ES-MDA algorithm, (d) permeability recovered with the ES-MDA-level set scheme and (e) Permeability recovered with the SELE method

Table 7.18: SSIM values to true permeability field for the four history matched models of the ES-MDA-Level-set scheme standard ES-MDA and SELE method.

Method	SSIM value of average permeability reconstruction
SELE	0.885
ES-MDA-Level set	0.792
ES-MDA	0.522

In the SSIM value highlighted in Table 7.18, we see that the SELE and ES-MDA-Level set history matched realisation gave a higher similarity to the true model than the realisation obtained through the standard ES-MDA

7.6.7 SPE 10 synthetic model

The Channelised SPE 10 synthetic model is studied with the developed novel methodology.

Figure 7.73 reports some basis function from an over-complete learned dictionary created with the KSVD algorithm trained for the reservoir model used in this work.

Numerical Experiments

In this section, three experiments are conducted to test the efficiency of our history matching algorithm to the true model namely; ES-MDA, ES-MDA-Level set, *SELE*

(A). ES-MDA-level set

The 100 realisations of permeability models are generated with the MPS method *FILTERSIM*, and the method enumerated in section 7.63 without any sparse parametrisation are implemented.

(B). ES-MDA

100 realisations of permeability models are generated with the MPS method *FILTERSIM*. The classical ES-MDA approach is used without any Level-set parametrisation.

(C). SELE

100 realisations of permeability models conditioned to the well locations are generated with the MPS method *FILTERSIM*. The method enumerated in section 7.63, steps 1-12 are implemented for this experiment.

7.6.8 Comparison studies for SPE 10 numerical experiment

The performance of the three methods, ES-MDA, ES-MDA-Level Set and SELE are compared using the RMS function considering production data, and the structural similarity (*SSIM*) index. Figure 7.74 shows the error convergence profile during the creation of the overcomplete dictionary by K-SVD for each iteration count.(refer to section 6.2.2 on K-SVD)

K-SVD Dictionary learning

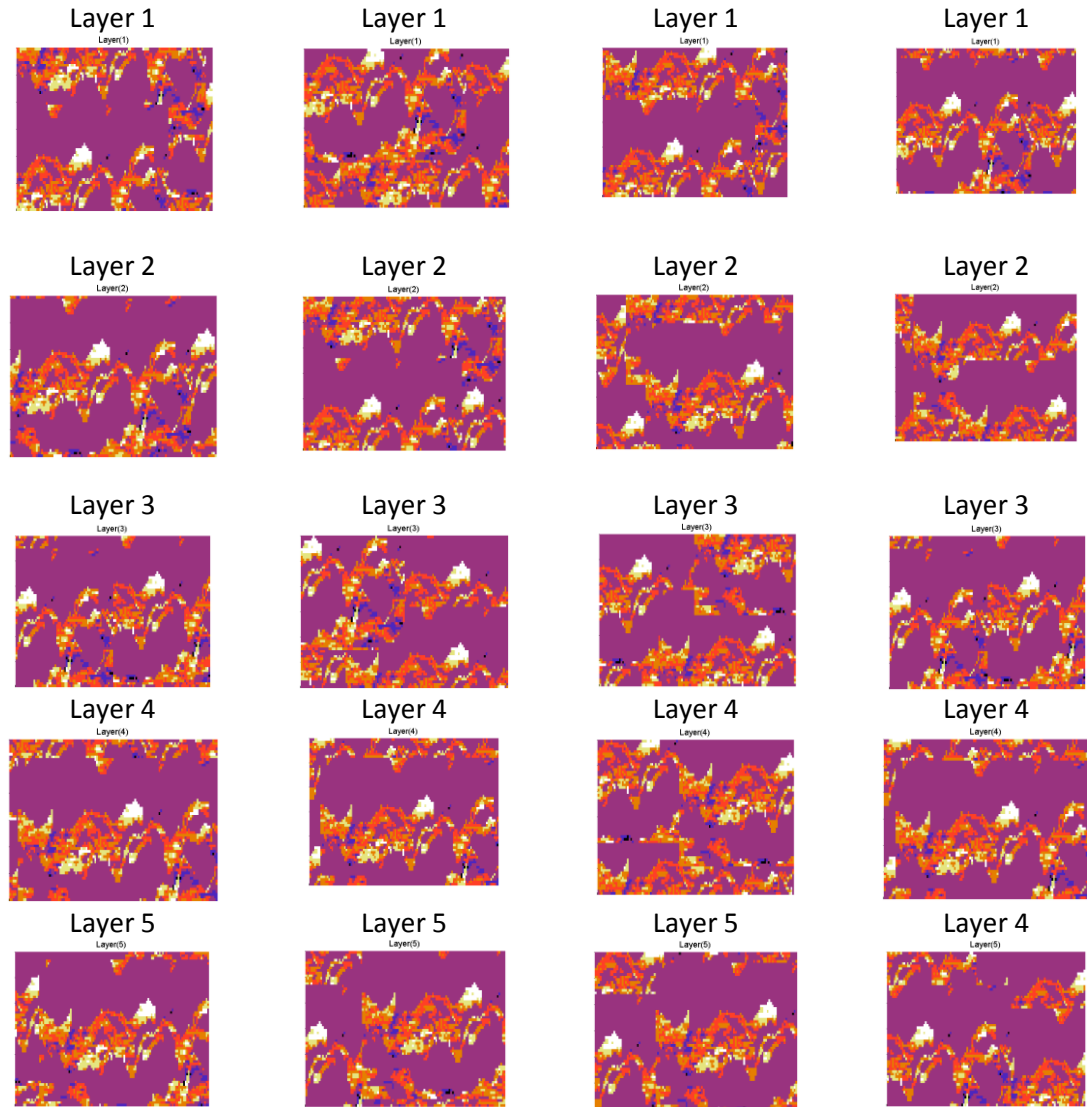


Figure 7.73: Some basis function from an over-complete dictionary created with the KSVD algorithm trained for the channelised SPE 10 synthetic reservoir model used in this work.

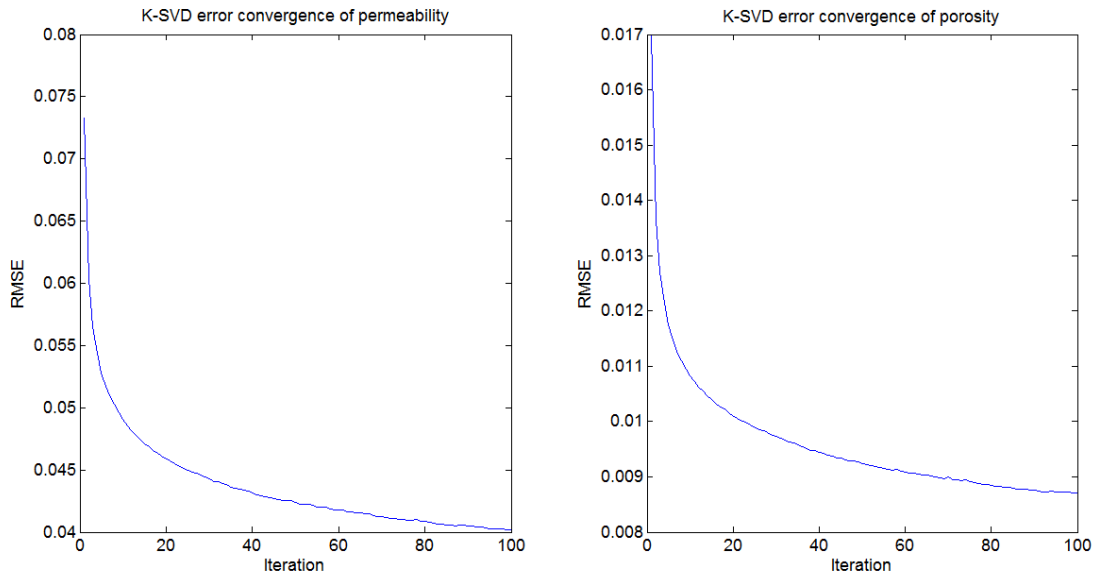


Figure 7.74: Error convergence profile during the creation of the overcomplete dictionary

Root-mean-square (RMS) function

Eqn. (7.19) is used to calculate our RMS value. Starting with a stochastic realization generated by MPS (Wu, et al., 2006), and focusing on the best realization #41, the convergence for the ES-MDA history matching was achieved in 8 iterations with an RMS error of 9.8, the convergence of the ES-MDA-Level set was achieved in 6 iterations with an RMS error of 8.1. Using the proposed method SELE history matching, the convergence was achieved in 4 iterations with an RMS error of 1.34. Table 7.19 below reports the effectiveness of the SELE algorithm. The initial RMS values for some of the realisations are displayed in column 2. In the comparison of the final RMS value for each method, the proposed SELE approach (column 5) yields lower RMS values when compared to all other methods(column 2,3 and 4)

Table 7.19: RMS function of best three realisations after ES-MDA, ES-MDA-Level set and SELE

Realisation no.	Initial RMS value	Final RMS value using ES-MDA	Final RMS value using ES-MDA- Level set	Final RMS value using SELE
13	49.33	24.21	9.2	4.32
56	43.83	12.8	7.1	1.34
92	56.87	24.58	11.26	6.44

Figure 7.75(a) shows the initial ensemble showing the match to oil production rate (column 1), match to water cut (column 2) and match to gas oil ratio (column 3). Figure 7.75(b) shows the initial ensemble matches to bottom hole pressure of the injector wells

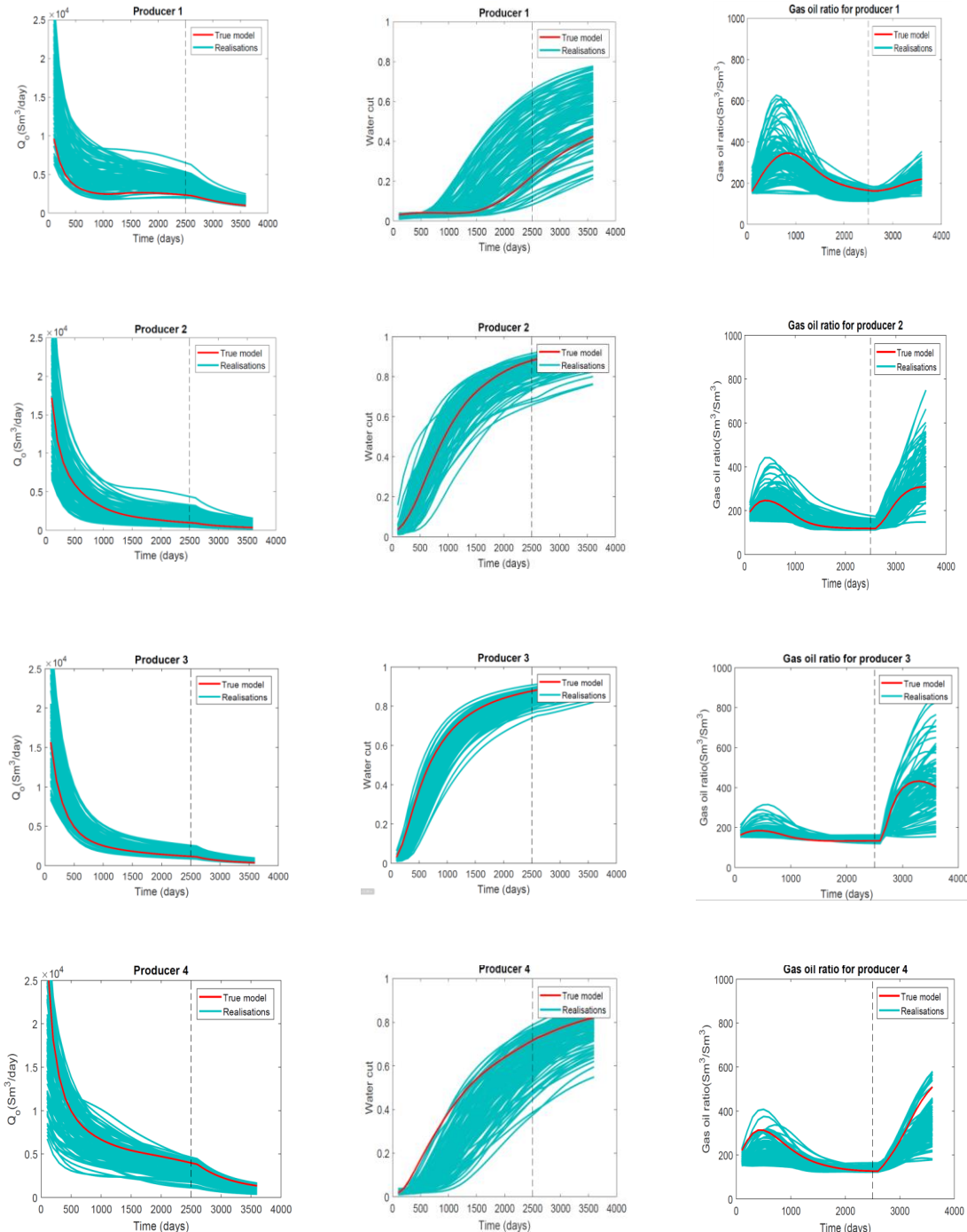


Figure 7.75(a): initial ensemble showing the match to oil production rate (column 1), match to water cut (column 2) and match to gas oil ratio (column 3). The red curve represent the true data and the cyan

overlay lines represents the realisations. The vertical dashed line represents the historical (left of this line) and predictin stages (right of this line)

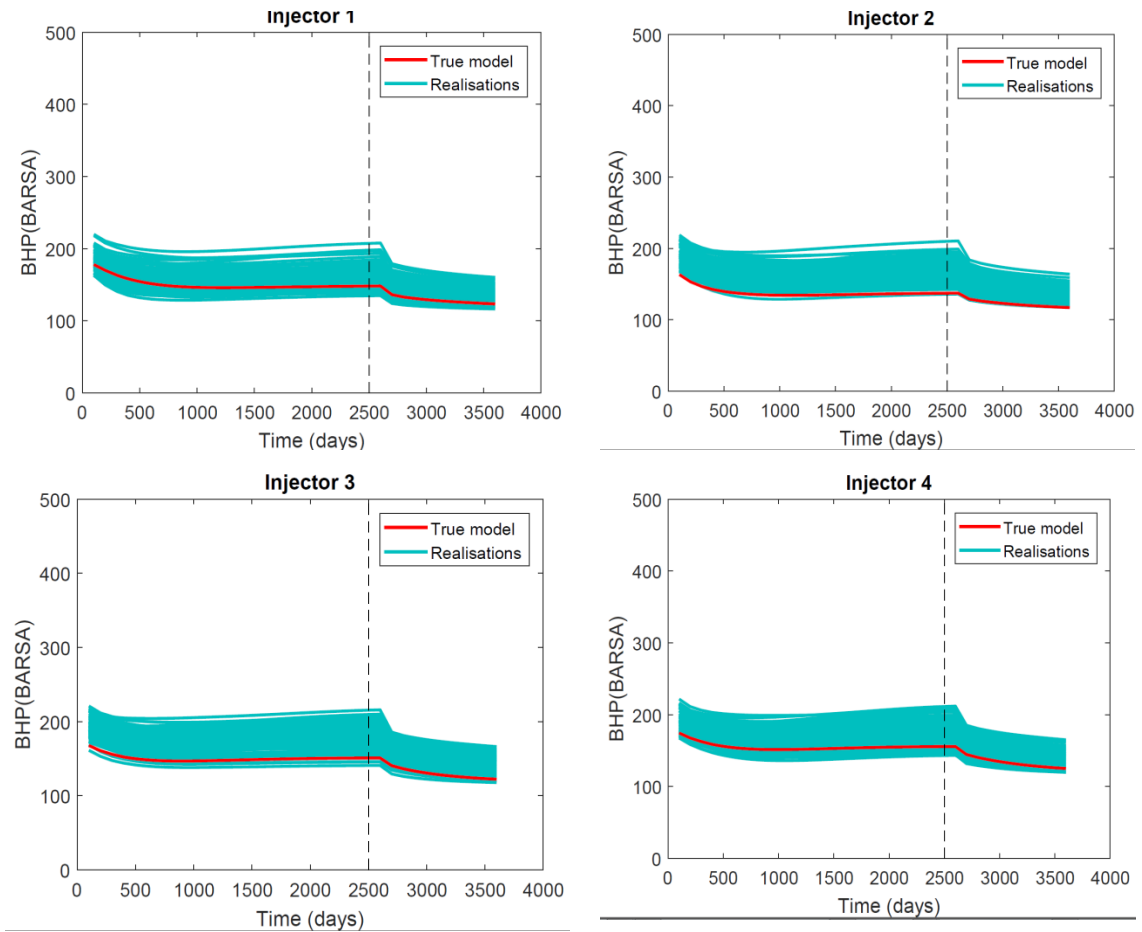
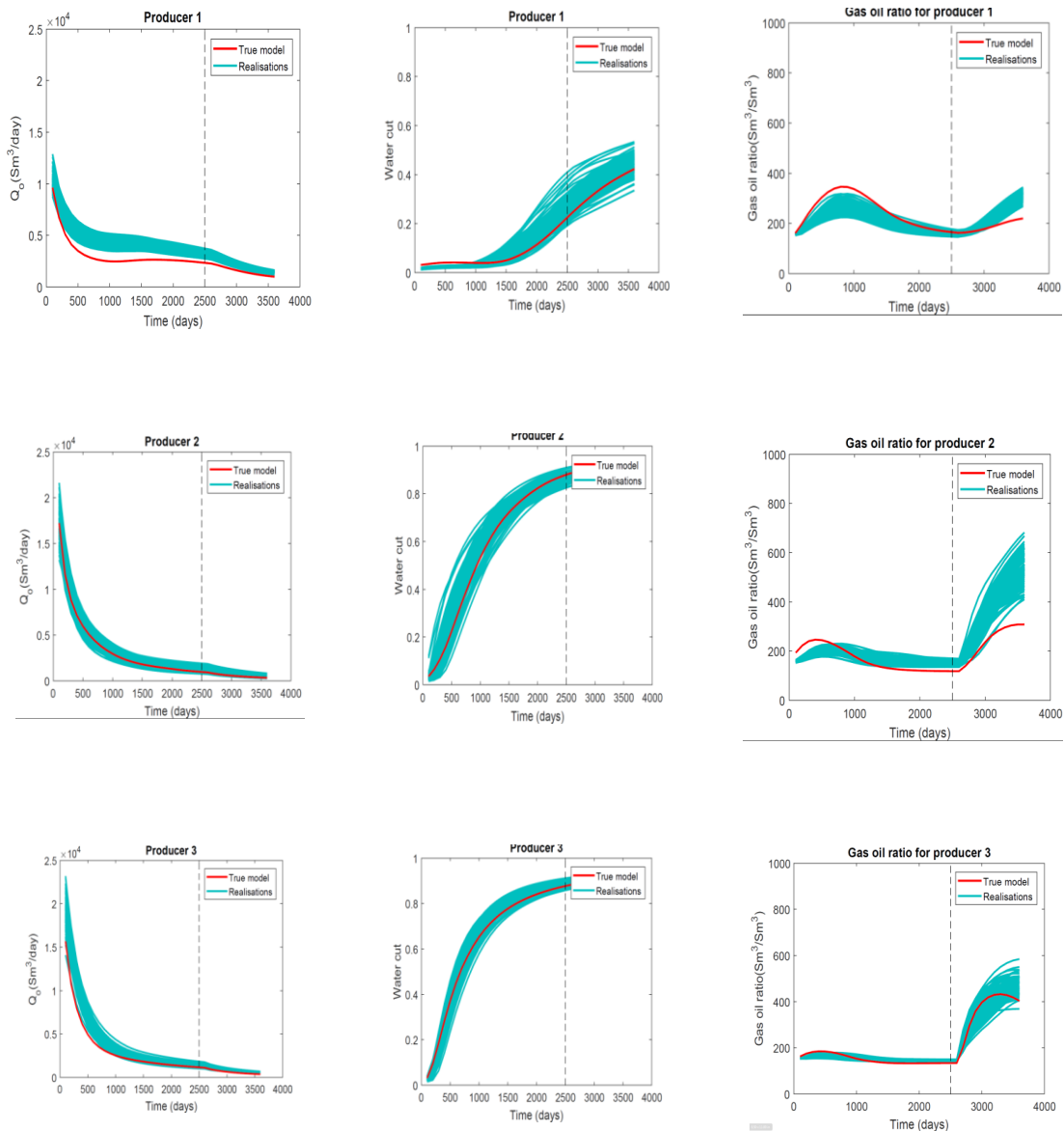


Figure 7.75(b): initial ensemble showing the match to bottom hole pressure of the injector wells. The red curve represent the true data and the cyan overlay lines represents the realisations. The vertical dashed line represents the historical (left of this line) and predcitin stages (right of this line)

Figure 7.76(a) shows the ES-MDA ensemble showing the match to oil production rate (column 1), match to water cut (column 2) and match to gas oil ratio (column 3). Figure 7.76(b) shows the ES-MDA ensemble matches to bottom hole pressure of the injector wells



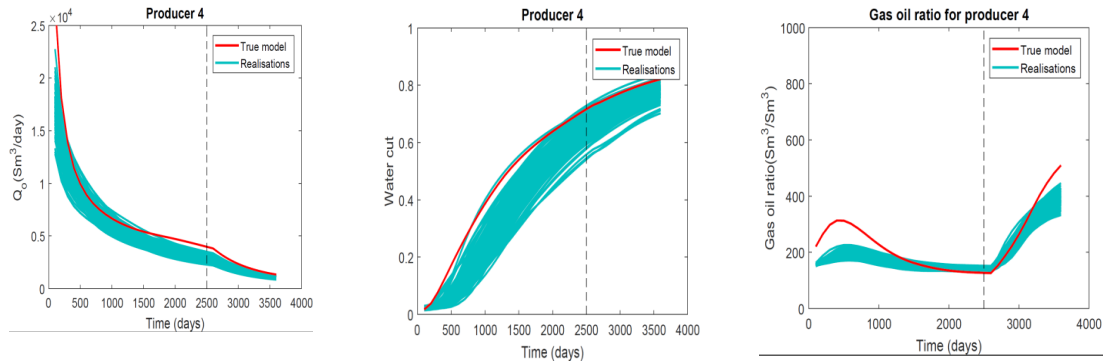


Figure 7.76(a): ES-MDA ensemble showing the match to oil production rate (column 1), match to water cut (column 2) and match to gas oil ratio (column 3). The red curve represent the true data and the cyan overlay lines represents the realisations. The vertical dashed line represents the historical (left of this line) and predcitin stages (right of this line)

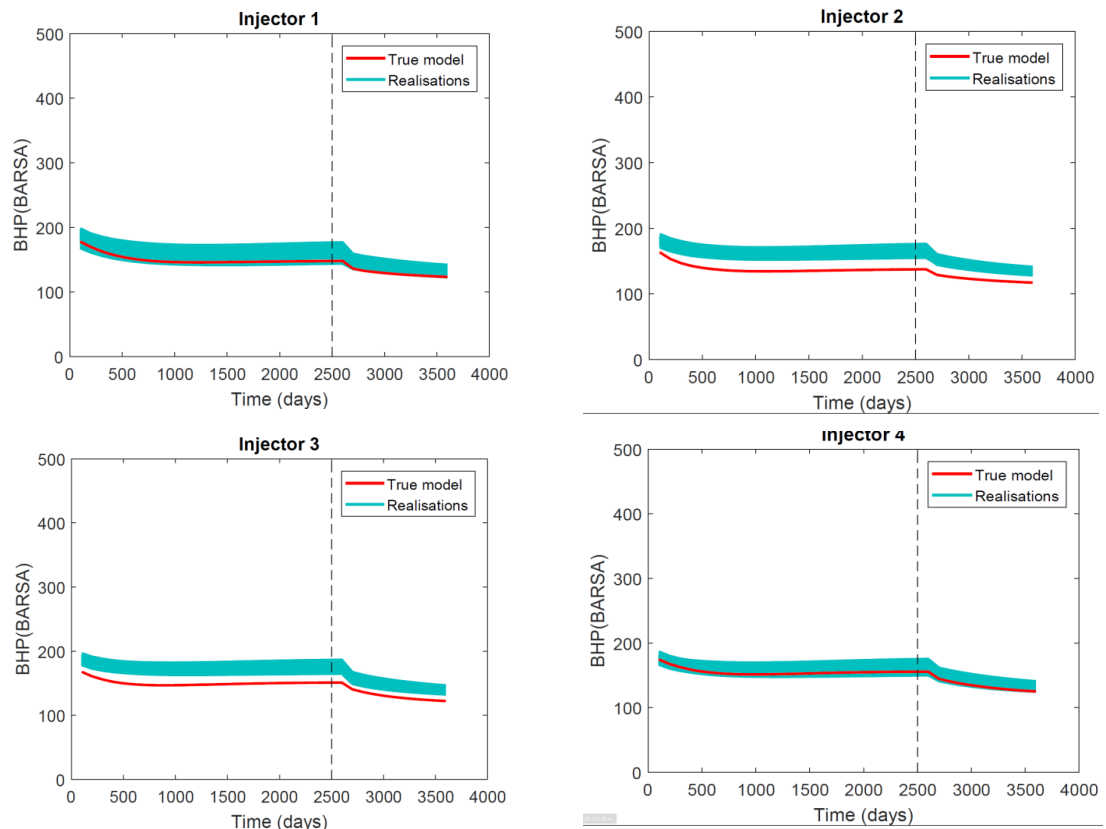


Figure 7.76(b): ES-MDA ensemble showing the match to bottom hole pressure of the injector wells. The red curve represent the true data and the cyan overlay lines represents the realisations. The vertical dashed line represents the historical (left of this line) and predcitin stages (right of this line)

Figure 7.77(a) shows the ES-MDA-Level set ensemble showing the match to oil production rate (column 1), match to water cut (column 2) and match to gas oil ratio

(column 3). Figure 7.77(b) shows the ES-MDA-Level set ensemble matches to bottom hole pressure of the injector wells

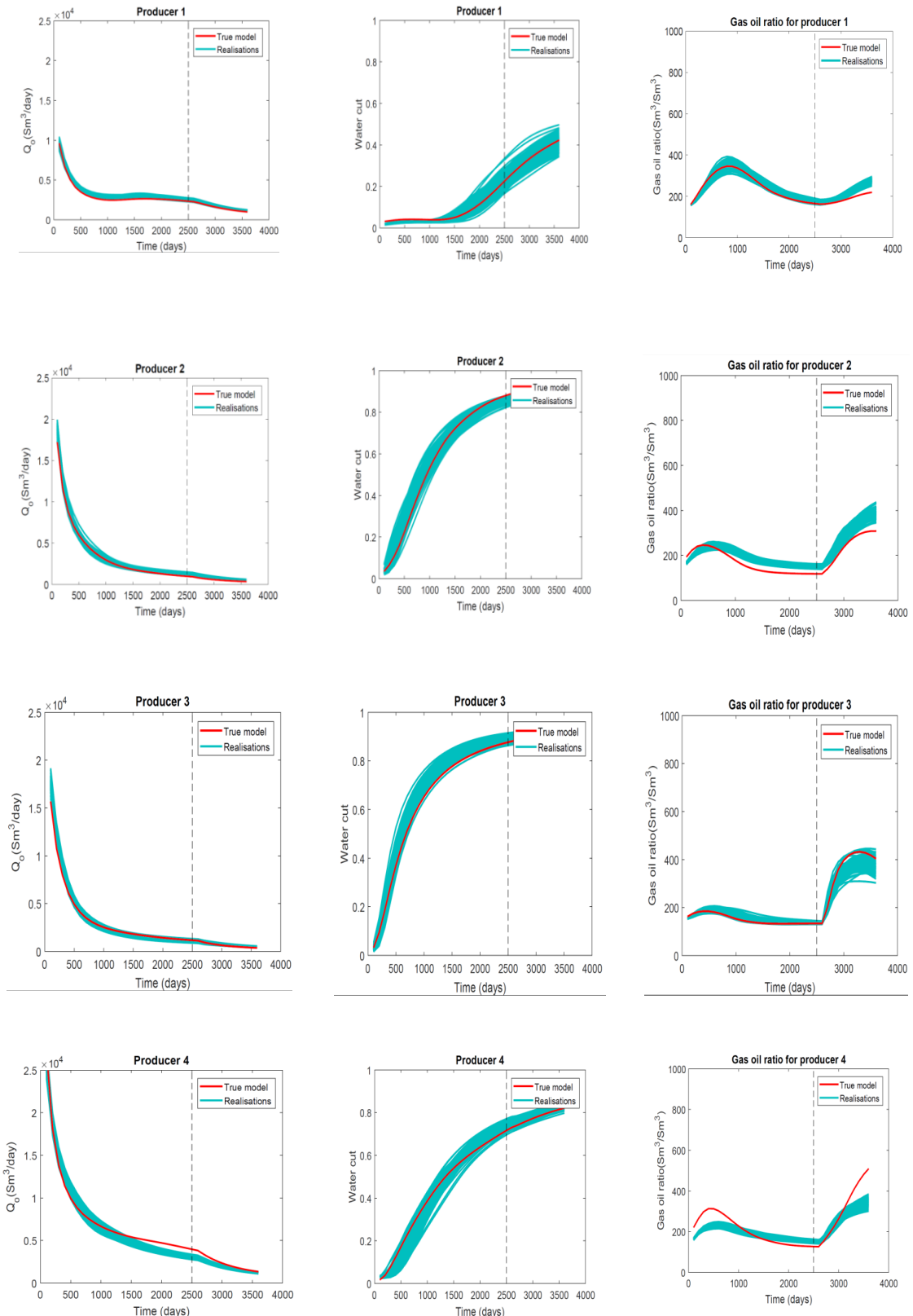


Figure 7.77(a): ES-MDA-Level set ensemble showing the match to oil production rate (column 1), match to water cut (column 2) and match to gas oil ratio (column 3). The red curve represent the true data and the cyan overlay lines represents the realisations. The vertical dashed line represents the historical (left of this line) and predcitin stages (right of this line)

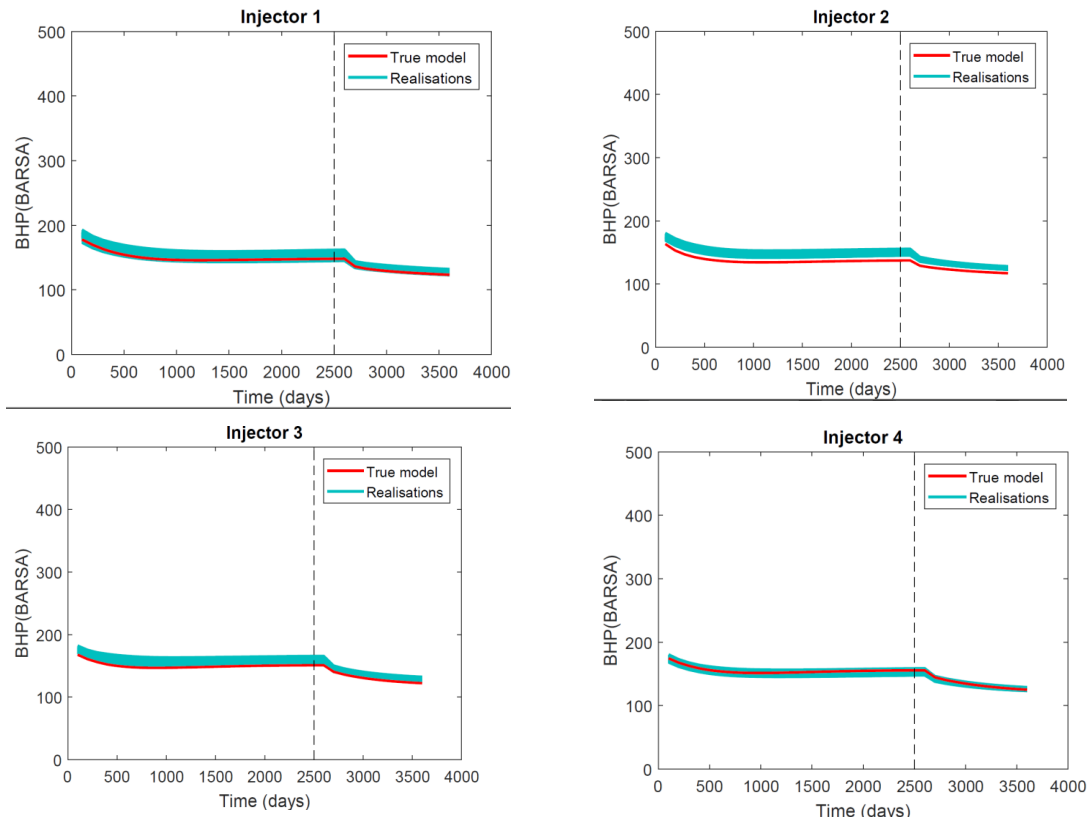


Figure 7.77(b): ES-MDA-Level set ensemble showing the match to bottom hole pressure of the injector wells. The red curve represent the true data and the cyan overlay lines represents the realisations. The vertical dashed line represents the historical (left of this line) and predcitin stages (right of this line)

Figure 7.78(a) shows the SELE ensemble showing the match to oil production rate (column 1), match to water cut (column 2) and match to gas oil ratio (column 3). Figure 7.78(b) shows the *SELE* ensemble matches to bottom hole pressure of the injector wells

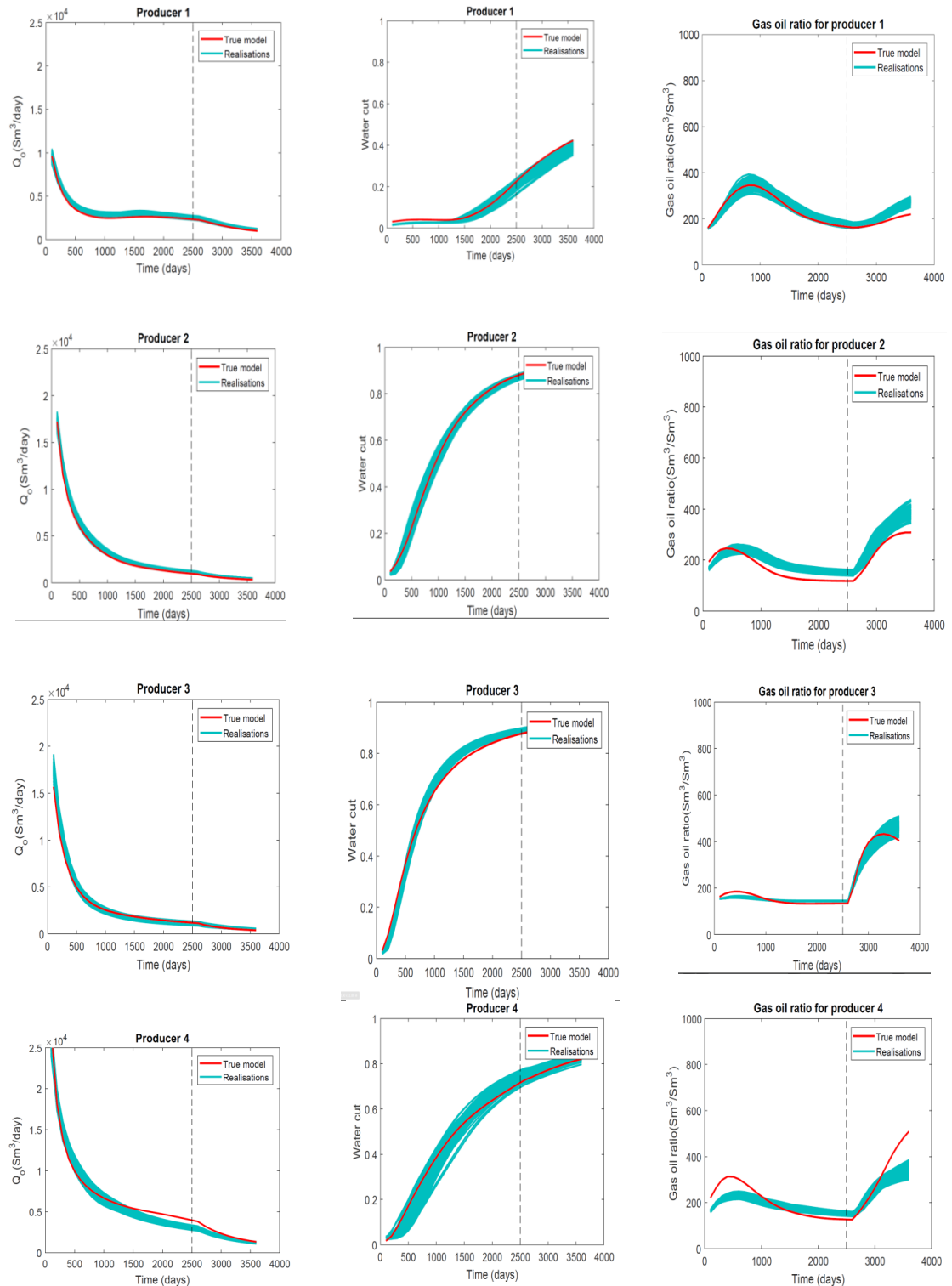


Figure 7.78(a): SELE ensemble showing the match to oil production rate (column 1), match to water cut (column 2) and match to gas oil ratio (column 3). The red curve represent the true data and the cyan overlay lines represents the realisations. The vertical dashed line represents the historical (left of this line) and predcitin stages (right of this line)

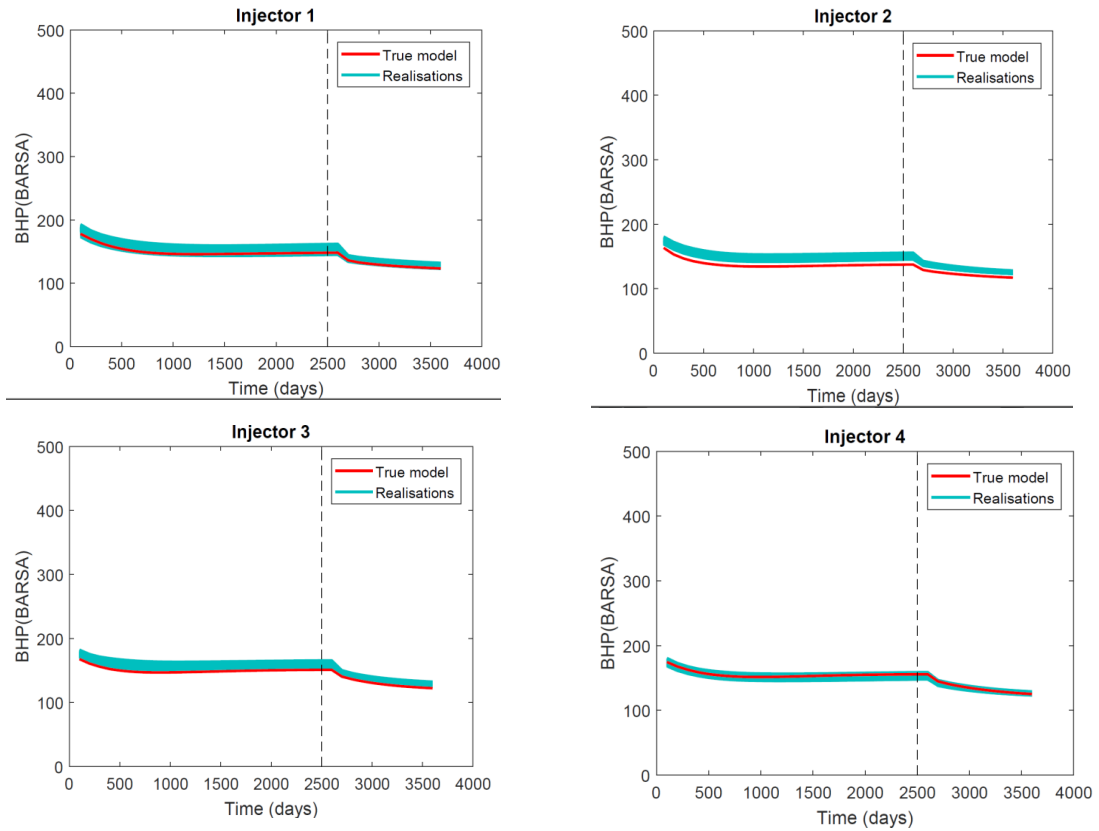


Figure 7.78(b): SEL ensemble showing the match to bottom hole pressure of the injector wells. The red curve represent the true data and the cyan overlay lines represents the realisations. The vertical dashed line represents the historical (left of this line) and predcitin stages (right of this line)

Structural Similarity Index metric (SSIM)

Figure 7.79 shows the permeability reconstruction of the three methods used to the true reservoir model.

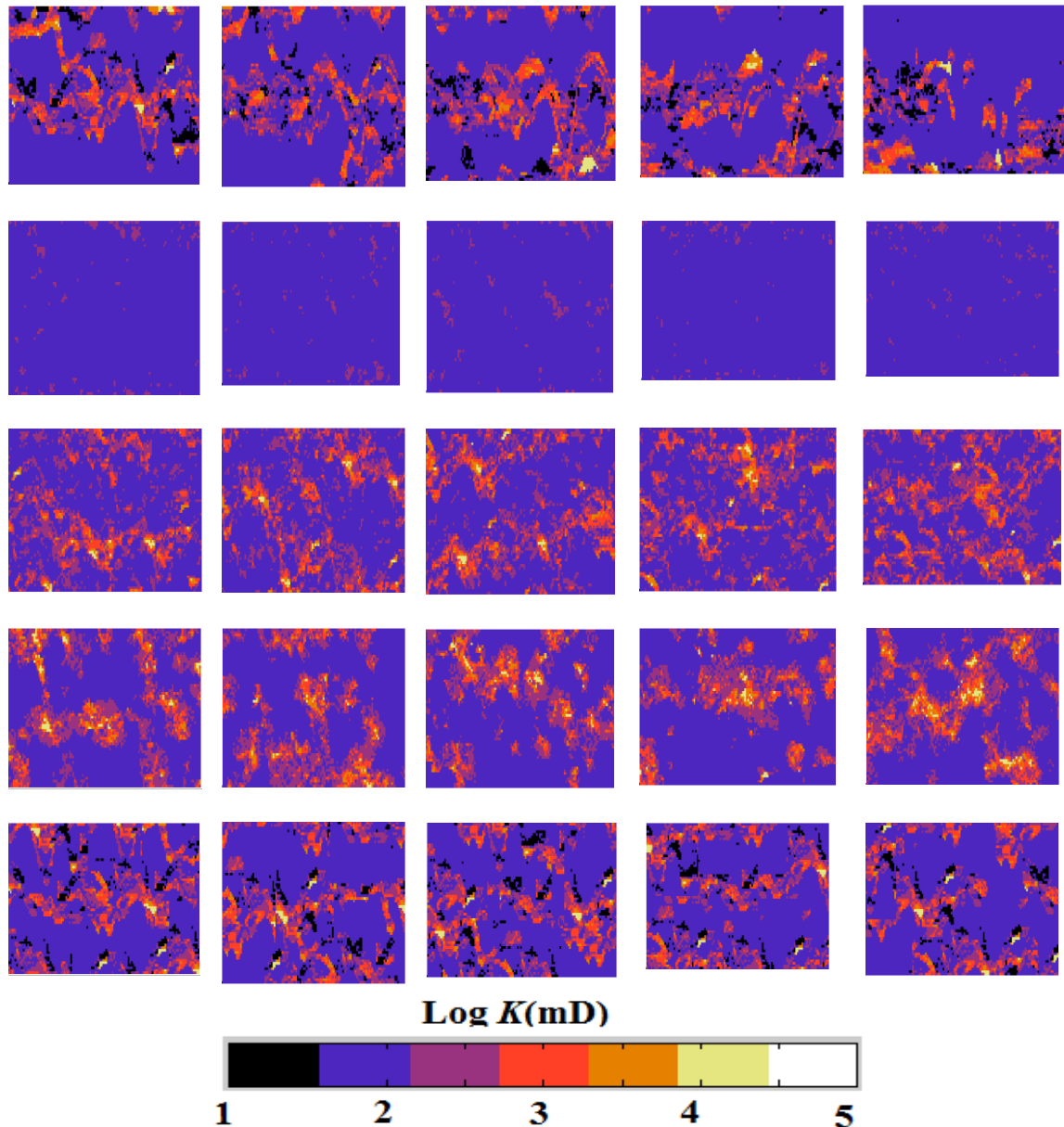


Figure 7.79: Permeability field of the five models shown row-wise (left-to-right). (First row) True permeability model, (second row) mean permeability of initial ensemble, (third row) mean permeability recovered with the ES-MDA algorithm, (fourth row) means Permeability recovered with the ES-MDA-Level set algorithm and (fifth row) mean permeability recovered with the SELE scheme

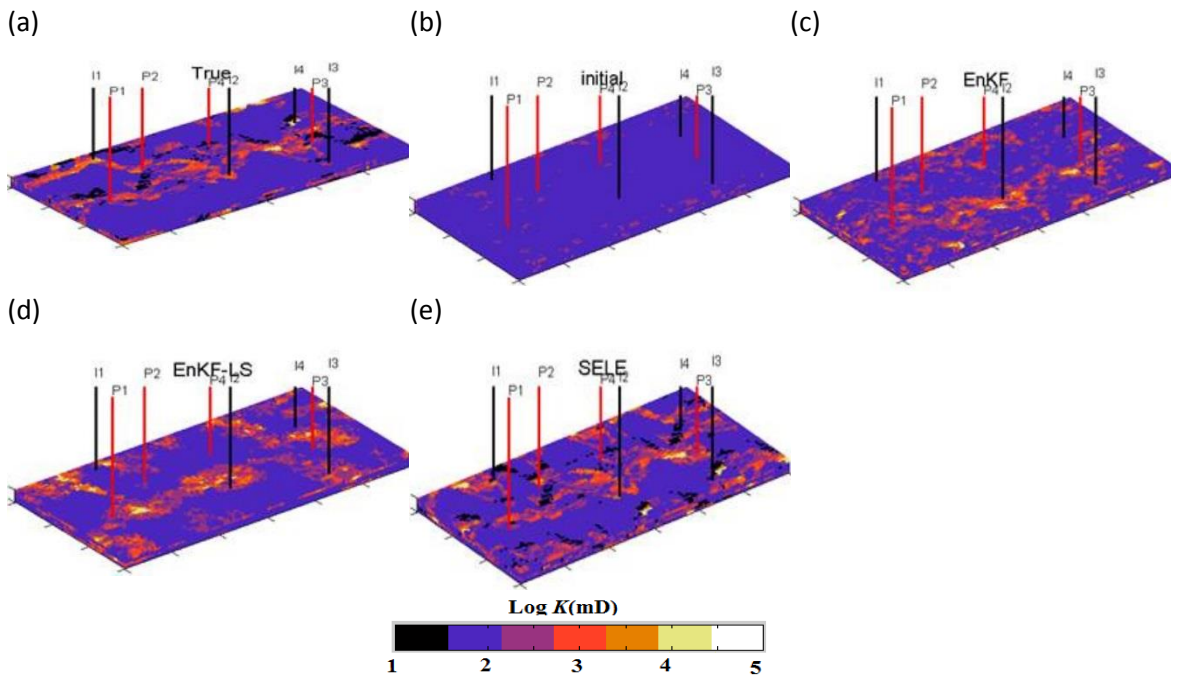


Figure 7.80: 3D Permeability field of the five models. (a) True permeability model, (b) mean permeability of initial ensemble, (c) Permeability recovered with the ES-MDA algorithm, (d) permeability recovered with the ES-MDA-level set scheme and (e) Permeability recovered with the SELE method

Table 7.20: *SSIM* values to true permeability field for the three history matched models of the ES-MDA-Level-set scheme standard ES-MDA and SELE method

Method	<i>SSIM</i> value of average permeability reconstruction
SELE	0.878
ES-MDA-Level set	0.792
ES-MDA	0.523

In the *SSIM* value highlighted in Table 7.20, we see that the *SELE* history matched realisation gave a higher similarity to the true model than the realisation obtained through the other four procedures.

7.6.9. Conclusion

- A new sparsity promoting framework for the enhanced recovery of subsurface permeability in the reservoir, using the ES-MDA and Level set parametrisation has been proposed.
- Numerically, the *SELE* algorithm and ES-MDA-Level set are superior to the classical ES-MDA proposed in previous works.

- This superiority is verified based on the average structural similarity index ($SSIM$) of the reconstructed permeability image to the true or reference permeability image, the lower final RMS function value and the number of data assimilation time step required for convergence.
- Further work will be to assimilate the electromagnetic data method for the non-linear Kaczmarz reconstruction of water saturation distribution into the innovation vector, in our SELE-promoting history matching algorithm.
- The SELE algorithm is limited to the choice of training image being used in the creation of the over complete dictionary. This could be gotten from priors through digital outcrop modelling.

Chapter 8-Overall Conclusion of Numerical experiments and results in the thesis with considerations for future work

In Numerical experiment 1, found in section 7.2, A novel method for the history matching of reservoirs with multiple lithofacies was introduced. The method estimates geological reservoir properties and facies boundaries by combining Ensemble Kalman Filter (EnKF) with the Level Set method. Each iteration of the automatic history matching involves the simultaneous update of the parameter field, porosity, and permeability, with the standard EnKF scheme and facies distribution. Computational time is reduced compared to Ensemble Kalman Filter (EnKF) as the Level Set evolves only around the boundary between different facies. A boundary known as the “narrow-band matrix” preserves shapes of the adjacent facies region and prevents the degradation in the classical EnKF inversion. The proposed algorithm is implemented on a synthetic 3D reservoir model with water flooding a Gaussian reservoir and a fractured reservoir. An initial ensemble of porosity and permeability are created using the sequential Gaussian simulation (SGS) for the Gaussian case and a multiple-point geostatistical algorithm (*FILTERSIM*) for the channelised and fracture case. The root mean square of the pressure and production data was used as the functional metric to measure the performance of the developed method. The proposed method outperforms the standard EnKF algorithm, regarding the accuracy of the reconstructed permeability, by preserving the boundaries. This is demonstrated based on the average structural similarity index (SSIM) of the reconstructed permeability image to the true or reference permeability image. In Numerical Experiment 2 found in section 7.3 Ensemble Kalman filter (EnKF) is widely used for history-matching applications. The repeating simulation runs during the EnKF scheme discourages the application of EnKF when the production history of the well is long, and the target is to incorporate the history matching to several aspects in the reservoir-geophysics workflow for calibrating the model. The ensemble smoother (ES) is a better alternative to be used in such cases. In this numerical experiment, a variant of the ensemble smoother (ES-MDA) is utilised. The history matching result of the recently proposed ES-MDA to EnKF on a

Gaussian synthetic reservoir is compared. The proposed ES-MDA method is tested on a Gaussian sandstone reservoir. The results show that the ES-MDA provides better data matches than those obtained with EnKF, EnKF by reducing the RMS from 14.25 for the EnKF to 3.5 for the ES-MDA and having a computational cost compared with the computational cost of EnKF. The resulting ES-MDA is coupled with our previously developed level set method and covariance localisation. The distance-based covariance localisation scheme is coupled with the previously developed Level set method. The methodology is introduced. Covariance localisation means localising the effect of an observation to the state variables that are ‘closer’ to the observations. The various localisation methods proposed in the literature have the common goal of removing the spurious terms in the cross-covariance matrix; this matrix is in turn used to update the state vectors during the ES-MDA update process. This is done by conditioning the Kalman Gain through a localising function. The motivation of covariance localisation is to achieve a similar level of ES-MDA performance if a larger ensemble size would have been used. However, it requires enormous computational resources to perform history matching if the ensemble size is large. Filter divergence and spurious long-range correlations were reduced leading to a better permeability reconstruction to the standard ES-MDA implementation. The method gave a lower RMS deviation to the true model as a result of the geometry of the channels being in close agreement to the true permeability model. In Numerical Experiment 3 found in section 7.4 We focus on the improvement of an integrated methodology for the automatic history matching of compartmentalised reservoirs using 4D seismic results and the Ensemble Kalman Filter method. We show the comparison of different history matching approaches using the Ensemble Kalman Filter (EnKF) to update the Fault Transmissibility Multipliers (FTM) initially computed with and without considering the 4D seismic results. The parameters modified during the history matching are two-phase fault transmissibility multipliers (FTM), absolute permeability and effective porosity of a synthetic 3D reservoir. The true impedance distribution and the changes in reservoir pressure and saturation computed from 4D seismic results. The estimation of two-phase fault transmissibility multipliers is hinged on the integration of the collected 4D seismic results and an apriori method validated in a previous work based

on a deterministic model, using the Levenberg Marquardt method (LM). The stochastic method utilised is the Sequential Gaussian Simulation (SGS) technique to generate 100 initial models. During history matching, the saturation distributions are computed from the forward modelling of a two-phase system (oil-water). The impedance maps are then calculated using the Gassmann equation and compared with the true impedance map as part of the History Matching. To validate the results, the cost function which is made up of two components is calculated, the first is the structural similarity index of the reconstructed impedance images to the real impedance image and the second is the RMS, L_2 -norm of the difference between the true (real) and the simulated pressure-production data. The EnKF history matching utilising the two-phase FTM values considering 4D seismic results produced lower cost function values in comparison with the model using the initial FTM multiplier without considering 4D seismic results. The EnKF history matching algorithm utilising 4D seismic presented in this work produced results closer to the true reservoir impedance map compared to a previous 4D gradient based history matching method. In Numerical Experiment 4 found in section 7.5 We couple a history matching level-set enhanced ensemble Kalman filter (EnKF) algorithm from our previous work with time-lapse EM data using a non-linear Kaczmarz-type approach for the estimation of water saturation distributions in an oil reservoir from EM data. The main focus is on the coupling of the inverse Maxwell problem in geophysical imaging with the fluid flow estimation from production data. The water saturation field is inferred from low frequency cross-borehole electromagnetic induction tomography (EMIT) data using the well-known Archie equations. These internal estimates of saturation are then plugged into one step of the Ensemble Kalman filter for matching data by modifying some reservoir parameters. Numerical results show that this integrated assimilation of EM inferred internal water saturation data during the EnKF inversion technique yields in an efficient way improved results compared to history matching without integrating time-lapse EM data. In Numerical Experiment 5, found in section 7.6, A novel shape reconstruction method called ‘SELE’ which denotes Sparsity-Ensemble optimization-Level-set-Ensemble optimisation, implementing a coupling of a Level-set-Ensemble Smoother Multiple Data Assimilation (ES-MDA) with compressed sensing/Machine

Learning (CS) is proposed. Due to the ill-determined characteristic of history matching, several realisations may match quantitatively to the true model but vary qualitatively in the permeability replicates. ‘SELE’ solves this ill-posed problem by using a sparsity promoting ES-MDA approach. An initial over complete learned dictionary is created using an unsupervised learning algorithm called K-SVD.

Further parametrisation to avoid a huge burden on complexity is achieved using the discrete cosine transform (DCT) on the initial realisations first, which is then after learned with the K-SVD. K-SVD is then combined with a greedy Orthogonal, Matching Pursuit algorithm (OMP) for the parametrisation of the petrophysical properties (permeability/ or porosity fields). During the history matching step, the ensemble state which consists of these sparse coefficients coupled with the level set representation of these properties is generated. The analysed sparse coefficients are then mapped back to spatial fields using this K-SVD dictionary. The efficiency of the algorithm is shown with numerical examples. The CS algorithm enhances the reconstruction of channelised geological structures by transforming the ES-MDA assimilation step to a sparse domain which captures the diverse geological scenarios in play. Numerical examples are shown and quantify the ‘SELE’ shape reconstruction by using a structural similarity index metric (SSIM). The proposed method shows rapid convergence to the true model and higher SSIM index to the true model permeability distribution.

For future work, supervised learning algorithms could be employed for classification of reservoir models. Running the forward problem for each realisation in the ensemble is time consuming. In this thesis even though a parallel implementation reduced the computational time required for forwarding, surrogate modelling coupling methods such as Proper Orthogonal Decomposition-Trajectory Piecewise Linearization (POD-TPWL) could be used in place of the full fidelity Eclipse reservoir simulator. This in turn could be used with the developed methods in this thesis for history matching. Another area could be in using deep learning variational autoencoder for parametrisation of the static petrophysical properties. The autoencoder is an encoder-decoder deep learning architecture where a reduced order modelling of the full permeability field ensemble could be realised. This reduced order could then be used in the ES-

MDA/EnKF inversion. The updated reduced order models could be put back into the decoder part of the learned network and the full permeability field recovered for the next iteration. In summary deep learning algorithms should be embedded more into the reservoir model calibration to improve geological realism during history matching.

Appendix

A1 - Reservoir Fluid Properties

A.1.1 Reservoir rock-fluid interaction

In reservoir engineering, they are fundamental rock-fluid properties that are necessary to describe reservoir dynamics in reservoir simulation literature (Dake, 2001). These properties are Wettability, Compressibility, Fluid saturations, Effective and relative permeability, Capillary pressure, Porosity, Absolute permeability-use of Darcy's Law, Core Analysis.

- Wettability

It is the likelihood of one fluid to cling to the surface body of rock in the presence of other fluids (Dake, 2001). Reservoirs may be of intermediate wettability, oil wet or water-wet. The initial conditions of most reservoirs are that they are water-wet because they are initially saturated with water before the migration of oil begins into the reservoir system.

If $0 < \theta < 90$ it is referred to as being water-wet

If $\theta > 90$ it is known as being oil wet.

Wettability is measured by directly analysing core samples taken from the reservoir using wire-line logging, and determining the contact angle between the fluids in contact with the reservoir rock and the reservoir rock.

- Compressibility

Overburden pressure is the pressure acting on the reservoir rock situated below as a result of the weight of the rocks overlaid on them (Dake, 2001). This overburden pressure increases at the rate of 1psi/ft (Dake, 2001). They are two ways reservoir rocks support this weight, either by using pressure support with the aid of the fluid properties of the pores or with structural support with the utilisation of the rock matrix. The production of hydrocarbons leads to a decline in pressure which concurrently leads to an increase in overburden pressure that is being supported by the

matrix of the rock. This then reduces the pore volume of the rock and the bulk volume of the rock isothermally. The pore volume compressibility c_f is the reduction in the pore volume V_p of the rock.

The pore volume compressibility is defined mathematically as,

$$c_f = \frac{1}{V_p} \frac{dV_p}{dp} \text{ psi}^{-1} \quad \text{a.1}$$

The pressure decrease as the pore volume decreases. c_f is measured by the use of correlations such as the Halls correlation (Craft & Hawkins, 1991) which shows compressibility being a function of the porosity of the rock. Hals correlation is agreeable with consolidated sandstones and carbonates

Compressibility is used heavily in the material balance equation for volume balance where,

The production of fluids

$$\begin{aligned} &= \text{Volume of fluid initially in place} \\ &\quad - \text{volume of fluid finally in place} \end{aligned}$$

The concept of material balance in reservoir engineering is governed by the equation below, where

$$\text{Production} = \text{Water influx} + \text{Expansion}$$

In a depletion drive mechanism of a reservoir, the oil production mechanism is simply the expansion of the reservoir fluids. The isothermal compressibility of the expansion fluid is;

$$C = \frac{1}{V} \frac{dV}{dp}$$

a.2

Where C = isothermal compressibility

p =pressure

V =volume and dV are the volumes of fluid produced from the reservoir and dp are the pressure drop occurring in the reservoir

$$dV = cVdp \quad a.3$$

For a continuous declining reservoir pressure, the total production from the reservoir will be equal to,

$$dV_{Tot} = dV_o + dV_w + dV_p \quad a.4$$

$dV_o=c_o V_o dp$ is the expansion of the oil

$dV_w=c_w V_w dp$ is the expansion of the connate water

$dV_p=c_f V_p dp$ is the reduction in pore volume

And $c_{o,w}$ is the isothermal compressibility of the oil and connate water respectively.

- Fluid saturations

The fluid saturation of a certain fluid is the fraction of the total pore space that is occupied by the fluid. (Dake, 2001)

$$s_w = \frac{V_w}{V_p} = \text{water saturation} \quad a.5$$

$$s_o = \frac{v_o}{v_p} = \text{oil saturation}$$

a.6

$$s_g = \frac{v_g}{v_p} = \text{gas saturation}$$

a.7

$$s_w + s_o + s_g = 1$$

a.8

$v_{o,w,g}$ = volume of the fluid (oil,water and gas)

v_p = pore volume

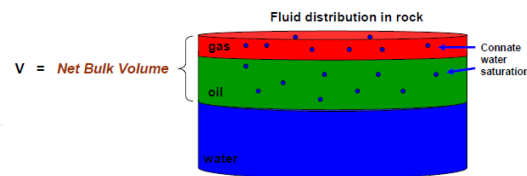


Figure A1: Schematic of an oil reservoir

$$V \times \varphi = \text{pore volume}$$

a.9

$$V \times \varphi \times (1 - s_{wc})$$

= hydrocarbon pore volume

a.10

φ =porosity of the rocks

s_{wc} =connate water saturation

Fluid saturation is measured with the aid of core samples gotten from the reservoir through the use of wireline or well logs.

- Effective and Relative permeability

Other fluids present in the rock impairs the ease of a fluid to flow in rock. Effective permeability is the permeability observed in a rock towards a certain fluid in the presence of other fluids also present in the rock (Dake, 2001)

k_o =effective permeability to oil

k_w =effective permeability to water

k_g =effective permeability to gas

The ratio of the effective permeability to the absolute permeability ratio is the relative permeability. Absolute permeability of fluid measures the ability of the rock (permeable) to transmit a certain fluid in the situation where only one fluid is present in the rock. Relative permeability data shows the effect of fluid saturation, pore geometry, wettability, saturation history and fluid distribution of the flow dynamics of the reservoir system (Dake, 2001)

$$k_{rg} = \frac{k_g}{k} = \text{relative permeability to gas}$$

a.11

$$k_{rw} = \frac{k_w}{k} = \text{relative permeability to water}$$

a.12

$$k_{ro} = \frac{k_o}{k} = \text{relative permeability to oil}$$

a.13

Where k is the absolute permeability. Relative permeability modifiers Darcy's equation for two-phase flow, where

$$Q = \frac{k_{ro} k A}{\mu} \frac{dP}{dL}$$

a.14

k_{ro} is effective permeability to oil in this case and Q is the oil production rate in bbls(barrels) or Stb(stock-tank barrels). Similar subscript for water and gas are gotten in the same way.

Absolute permeability is gotten from Darcy's Equation,

$$Q = -\frac{KA}{\mu} \frac{dP}{dL} \quad a.15$$

A is the cross-sectional area, μ is the viscosity of the fluid, dP is the pressure drop in the reservoir between the reservoir pressure and the workface pressure.

$$dp = P_r - p_{wf} \quad a.16$$

where p_{wf} is the work flowing pressure and is a function of the well head pressure at the surface, the pressure due to hydrostatic gravity and pressure due to friction losses.

Effective and relative permeability are measured from mathematical models, core analysis, well test analysis(for effective permeability) and history matching techniques (Dake, 2001). Their application in reservoir engineering is in the calculation of ultimate recovery from the reservoir, flow rates, and the displacement efficiency.

- Capillary pressure

Whenever two immiscible fluids are in contact, there exists a capillary pressure that is a function of the saturation of fluid within the rock. Capillary pressure is simply the pressure difference that arises between the curved interfaces between these two immiscible fluids (Dake, 1978). It is relevant at the pore throats of reservoir rocks when they are significant surface forces.

The pressure in the capillary tube can be defined as,

$$p_c = \frac{2\sigma_{wo} \cos\theta}{r} = (\rho_0 - \rho_w)gh$$

a.17

Where r = tube radius

θ = contact angle

σ_{wo} = contact angle

h = height of the water column, g = gravity

$\rho_{0,w}$ = fluid density

Capillary pressure is responsible for the transition to the free water level (100% water)

to the connate water saturation s_{wc} in the oil zone

This transition zone is known as the vertical thickness h calculated from

$$h(ft) = \left(\frac{144p_c}{\rho_w - \rho_0} \right)$$

a.18

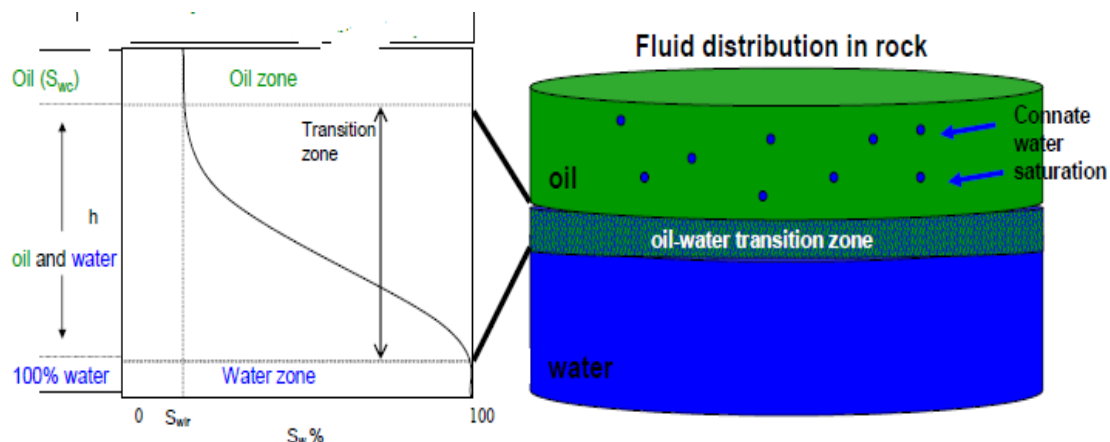


Figure A2: Capillary pressure schematic as it relates to the oil reservoir

If the capillary pressure is equal to 0 (a common occurrence in reservoirs that have high permeability and good vertical permeability), then there will be a minimal or no transition zone in the reservoir.

Capillary pressure is related to the pore size distribution, fluid saturation, and the saturation history (Dake, 2001). The saturation history of the reservoir can either be an imbibition process or a drainage process. In the imbibition process, the water is displacing the oil in the reservoir, and the wetting phase is increasing in the case of water flooding. In the drainage process, there is a constant decrease in the wetting phase (oil migration into the reservoir) which is assumed the initial condition of the reservoir. Capillary pressure is measured by the centrifuge method or the porous plate method (Dake, 1978). It is applied in reservoir engineering in calculating the hydrocarbons in place by determining the saturation values.

- Porosity

Porosity is the amount or the measure of the volume of the reservoir rock that is capable of containing the reservoir fluid (Dake, 2001)

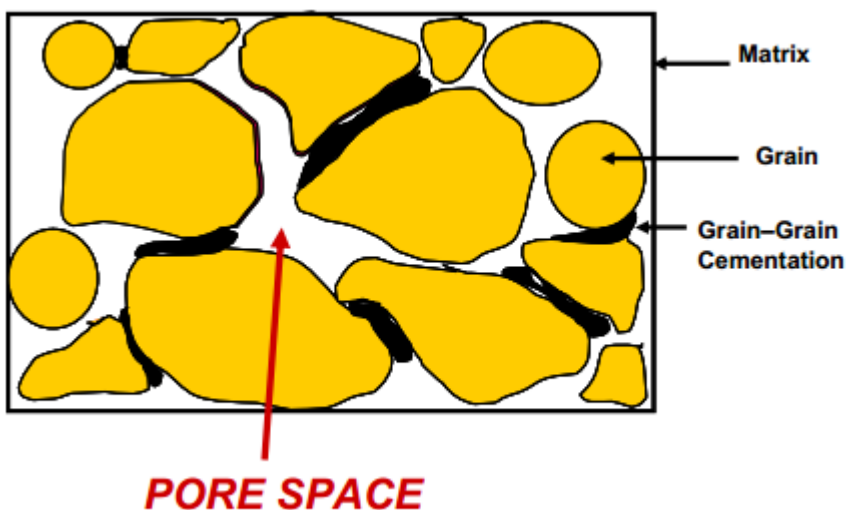


Figure A3: Schematic showing the porosity of the rock

Porosity is the ratio of the pore volume (or the void space within the rock) to the total bulk volume of the rock

$$\varphi = \frac{v_p}{v_b} \times 100$$

a.19

Where,

v_p =pore volume (space in the rock)

v_b =bulk volume

There are four main types of porosity. The first is primary porosity (which is formed during initial intergranular deposition). The second is secondary porosity (it is of a fracture mechanism and formed during the stage of diagenesis). The third is absolute porosity (it is a measure of the total pore spaces found in a reservoir rock as a unit of its overall bulk volume) and effective porosity (a measure of the interconnected pore spaces found in the reservoir rock) (Dake, 2001)

In reservoir engineering, effective porosity is the porosity of interest. Effective porosity is measured from well logs such as the sonic, density NMR and neutron logs. Effective porosity is measured by direct measurements from cores. The volume of petroleum fluids in a reservoir depends on the porosity.

A.1.2 Darcy's Law

It explains the concept of permeability. Flow characteristics of the fluid in the reservoir are vital for the prediction of certain qualities that will aid the decision made by the reservoir engineer. The rate of production of these reservoir fluids is important for various economic reasons.

Darcy's law states "the rate of flow of a homogeneous fluid through a porous medium is proportional to the pressure of hydraulic gradient and the cross-sectional area normal to flow direction and inversely proportional to the fluid viscosity."

$$V_s = \frac{-K}{\mu v} \left(\frac{\bar{v} \partial p}{\partial s} + \frac{\partial z}{\partial s} \right)$$

a.20

where

μ = absolute viscosity

k = homogenous fluid permeability

\bar{v} = specific volume = $\frac{1}{\rho g}$

V_s = macroscopic velocity in positive s

g = acceleration due to gravity

ρ = density

z = elevation

The quantities in brackets in equation a.20 is known as the total fluid potential

Equation a.20 can be rewritten as,

$$V_s = \frac{-K}{\mu v} \frac{\partial \Phi}{\partial s}$$

a.21

Where Φ is the total fluid potential.

Assumptions made in formulating Darcy's Equation are

- 1) There is no electrokinetic effect
- 2) The flow is assumed laminar and not turbulent
- 3) Permeability is independent of temperature, fluid, location and pressure
- 4) There is no Klinkenberg effect
- 5) Homogenous single-phase fluid
- 6) Zero chemical reaction between the fluid and the media.

A.1.3 Two-Phase relative permeability

Two approximations are used to calculate the relative permeability of two phases flowing in the reservoir. These approximations are the Correy approximation (Correy, 1956) and the Naar-Henderson approximation (Naar, 1962).

- 1) For the Correy approximation: This approximation is used for the drainage process such as gas drive where the saturation of the water is being reduced.

The displaced phase relative permeability,

$$k_o = (1 - S)^4 \quad \text{a.22}$$

The Displacing phase relative permeability

$$k_d = S^3(2 - S) \quad \text{a.23}$$

Where $S = \frac{S_D}{1 - S_{wc}}$ a normalizing saturation function

- 2) For the Naar-Henderson approximation: This approximation is used for the imbibitions process (where the saturation of water is being increased in the reservoir)

The Displaced phase relative permeability,

$$k_o = \frac{(1 - 2S)^{\frac{3}{2}}}{2 - (1 - 2S)^{\frac{1}{2}}} \quad \text{a.24}$$

The displacing phase relative permeability,

$$k_d = S^4 \quad \text{a.25}$$

Where

$$S = \frac{S_D - S_{wc}}{1 - S_{wc}}$$

a.26

A.1.4 Three-phase relative permeability

The concept provided by Stone et al. models the relative permeability of three phases flowing in the reservoir. This model combines the theory of channel flow in the porous media, with probability concept to arrive at a simple result for determining the relative permeability of oil in the presence of gas and water flow.

The following equation estimates the oil relative permeability

$$k_{ro} = (k_{row} + k_{rw})(k_{rog} + k_{rg}) - (k_{rw} + k_{rg})$$

a.27

$$k_{ro} \geq 0$$

A.1.5 Under saturated reservoirs

An undersaturated reservoir is a reservoir where there is no gas cap formed, and no gas comes out of solution with the oil in reservoir conditions (Dake, 1978). The undersaturated reservoir has a pressure higher than the bubble-point pressure of the reservoir. For an undersaturated reservoir, when the reservoir pressure drops to a point lower than the bubble point pressure gas will come out of the solution in the reservoir leading to a free gas saturation(S_g). In the initial condition when there is a small amount of gas present, the gas will be immobile (it will not flow because it remains trapped in the pores of the formation). The free gas solution will rise over time as more gas comes out of solution, at that point, it reaches a critical value and the gas becomes mobile. The free gas will flow under an applied pressure gradient.

A.1.6 Saturated Reservoir

For a saturated reservoir, gas comes out of solution in the oil because the reservoir pressure is below the bubble-point pressure.

A.1.7 Gas Expansion Factor

The gas formation volume factor B_g can also be expressed in terms of the gas expansion factor (Dake, 2001). E, where

$$E = \frac{\text{volume of 1 mole of gas at standard conditions}}{\text{volume of 1 mole of gas at reservoir conditions}}$$

a.28

Standard conditions in a reservoir are taken at 14.7 psia and 60°F,

$$E = \frac{35.37P}{ZT}$$

a.29

Z is the compressibility factor of gas at reservoir conditions T(temperature) and P(pressure).

Therefore,

$$B_g = \frac{1}{5.615E} \frac{rb}{scf}$$

a.30

For an under-saturated reservoir (where the pressure is above the bubble-point pressure of the reservoir) E and B_g are normally not given

A.1.8 Volumetric Estimation of Fluid Reserves

For an initially under saturated reservoir,

V= bulk volume of the reservoir in acre-feet

Φ = porosity of the rock in the reservoir (fractional)

s_{wc} = connate water saturation (fractional)

The volume of oil that is initially in place

$$v\varphi(1 - s_{wc}) 7758$$

a.31

The volume of oil measured will be in reservoir barrels (1 acre-feet=7758 barrels)

To calculate the stock tank of oil initially in place, we divide the equation by the initial oil formation volume factor B_{oi} .

Hence,

$$N = \frac{v\varphi(1 - s_{wc}) 7758}{B_{oi}} \quad \text{a.32}$$

The values of B_{oi} , s_{wc} and φ is averaged over the whole reservoir. In order to arrive at a good volumetric estimate, it is essential to have accurate information about the position of the precise oil-water contact and good quality geological data. Appraisal and exploration drilling can provide data on which reliable estimates of the average values of connate water saturation and porosity

The recovery efficiency is given by

$$\frac{N_p}{N} = 1 - \frac{(1 - S_{wc} - S_g)B_{oi}}{(1 - S_{wc})B_o} \quad \text{a.33}$$

$\frac{N_p}{N}$ is the recovery ratio.

A.2: The flow potential

It is assumed in the fluid mechanics of porous media, that the macroscopic fluid velocity vectors are normal to the equipotential surface, and the magnitude of these vectors is proportional to the potential gradient.

Let Φ be the fluid potential which is the mechanical energy per unit mass of the fluid at any location.

The total work done in the transportation of this fluid is given by

$$\Phi_1 = \int_{\dot{p}}^{p_1} \bar{v} dp + z_1 + \frac{\mu_1^2}{2g}$$

a.34

Neglecting the velocity term in porous media, equation a.7 becomes,

$$\Phi_1 = \int_{\dot{p}}^{p_1} \bar{v} dp + z_1$$

a.35

For an incompressible fluid,

$$\Phi_1 = \bar{v}(p_1 - p) + z_1$$

a.36

A.2.1 Real gas flow potential

Properties of most gasses are assumed independent of pressure under ideal conditions. In reservoir conditions, gasses are far from ideal, and variations arise due to viscosity change with pressure and gas deviation factor (Z) variation with pressure.

Al-Hussainy et al. (Al-Hussainy, 1966). Developed the real gas potential function that is described below,

$$m(\dot{p}) = 2 \int_{p_m}^p \frac{\dot{p}}{\mu(\dot{p})z(\dot{p})} d\dot{p}$$

a.37

Where P=Gas pressure, z=gas deviation factor, \dot{p} = a dummy variable of integration, μ =viscosity, p_m = an arbitrary datum pressure.

A.2.2 Steady and unsteady flow

Assuming a fluid flowing through a porous media with velocity V . The velocity is a function of distance(s) and time(t)

Hence, we will have,

$$dv = \left(\frac{\partial v}{\partial t}\right)_s dt + \left(\frac{\partial v}{\partial s}\right)_t ds \quad a.38$$

Differentiating equation a.38 concerning time we will have,

$$\frac{dv}{dt} = \left(\frac{\partial v}{\partial t}\right)_s + \left(\frac{\partial v}{\partial s}\right)_t \frac{ds}{dt} \quad a.39$$

$\frac{ds}{dt}$ = velocity. equation can be rewritten as,

$$\frac{dv}{dt} = \left(\frac{\partial v}{\partial t}\right)_s + \left(\frac{\partial v}{\partial s}\right)_t v \quad a.40$$

Total acceleration = local acceleration + convectional acceleration

$$\left(\frac{dv}{dt}\right)_s = 0 \text{ for steady state flow} \quad a.41$$

$$\left(\frac{dv}{dt}\right)_s \neq 0 \text{ for unsteady flow} \quad a.42$$

The pressure of the fluid in a reservoir is a function of the radius of the reservoir boundary, and the time it takes the fluid to cross this boundary

$$P(r_w t)$$

, then

$$\left(\frac{dp}{dt}\right)_s = 0$$

A.3 Fluid Types

There are three broad classifications of reservoir fluids namely

- 1) Incompressible fluid flow: Constant density fluid
- 2) Slightly compressible fluid flow: A measurable change of density with pressure
- 3) Compressible fluid flow: Significant change of density with pressure

The equation of state equation that relates these different forms of compression is

$$\rho = \rho_o e^{c(p-p_o)}$$

C=compressibility, p_o =datum pressure, p =any pressure

For incompressible fluid, $c=0$ and $\rho=\rho_o$

For slightly compressible fluid,

$$\rho = \rho_o + \rho_o c(\Delta p)$$

$$\Delta p = p - p_o$$

A.4 Reservoir Simulation Equations numerically solved by ECLIPSE

A combination of the governing equations together with the initial conditions and necessary boundary conditions form the mathematical model of the system. The necessary steps involved are;

- 1) Selecting the elemental volume of the system that may be radial, areal, spherical and 3-D

- 2) Writing all the fluxes into and out of the volume over a time interval
- 3) Equating the fluxes to changes within the observed system during this time.
- 4) Taking the limit as the elemental volume shrinks to an infinitesimal size.

$\text{Lim} \Delta t \rightarrow 0$

$$\Delta x \rightarrow 0$$

The resulting equation is the required differential equation governing the flow through the porous media.

Analysing a control volume, through which a single phase of the hydrocarbon is flowing through (the x-direction) at any instant

$$\text{Mass rate in} - \text{Mass rate out} = \text{Mass rate of accumulation}$$

a.47

$$(v_x \rho_x \Delta y \Delta z) - (v_{x+\Delta x} \rho_{x+\Delta x} \Delta y \Delta z) = (\Delta x \Delta y \Delta z) \phi \frac{(\rho_{t+\Delta t} - \rho_t)}{\Delta t}$$

a.48

Dividing by $\Delta x \Delta y \Delta z$ we will have,

$$-\frac{(v_{x+\Delta x} \rho_{x+\Delta x}) - (v_x \rho_x)}{\Delta x} = \phi \frac{(\rho_{t+\Delta t} - \rho_t)}{\Delta t}$$

Taking the limit $\left\{ \frac{\Delta x}{\Delta t} \right\}$ goes to zero simultaneously we will have

$$\frac{\partial(v\rho)}{\partial x} = -\phi \frac{\partial \rho}{\partial t}$$

a.49

Equation a.49 is the continuity equation for a linear system.

From Darcy's equation,

$$\nu = -\frac{k\partial p}{\mu\partial x}$$

a.50

$$\frac{\partial \left(-\frac{k\partial p}{\mu\partial x} \rho \right)}{\partial x} = -\Phi \frac{\partial \rho}{\partial t}$$

a.51

From the definition of compressibility, c

$$c = \frac{1}{V} \left(\frac{dV}{dP} \right)_T$$

a.52

Expanding the left-hand side

$$-\left(\frac{k}{\mu} \frac{\partial^2 P}{\partial x^2} \rho + \frac{k}{\mu} \frac{\partial p}{\partial x} \frac{\partial \rho}{\partial x} \right) = -\Phi \frac{\partial \rho}{\partial t}$$

a.53

$$\frac{\partial \rho}{\partial x} = \frac{\partial \rho}{\partial P} \frac{\partial p}{\partial x}$$

a.54

$$\frac{\partial \rho}{\partial t} = \frac{\partial \rho}{\partial P} \frac{\partial p}{\partial t}$$

a.55

Substituting we will then have

$$-\left(\frac{k}{\mu} \frac{\partial^2 P}{\partial x^2} \rho + \frac{\partial \rho}{\partial P} \frac{\partial p}{\partial x} \frac{\partial \rho}{\partial x}\right) = -\Phi \frac{\partial \rho}{\partial P} \frac{\partial p}{\partial t}$$

a.56

$$-\left(\frac{k}{\mu} \frac{\partial^2 P}{\partial x^2} \rho + \frac{\partial \rho}{\partial P} \left(\frac{\partial p}{\partial x}\right)^2\right) = -\Phi \frac{\partial \rho}{\partial P} \frac{\partial p}{\partial t}$$

a.57

Neglecting the $\left(\frac{\partial p}{\partial x}\right)^2$ term because of the assumption of small pressure gradient, multiplying by -1 yields,

$$\frac{k}{\mu} \frac{\partial^2 P}{\partial x^2} \rho = \Phi \frac{\partial \rho}{\partial P} \frac{\partial p}{\partial t}$$

a.58

Dividing by density ρ and using the definition of compressibility to be,

$$C = \frac{1}{\rho} \frac{\partial \rho}{\partial p}$$

The resulting equation will then be,

$$\frac{k}{\mu} \frac{\partial^2 P}{\partial x^2} = \Phi C \frac{\partial p}{\partial t}$$

a.59

$$\frac{\partial^2 P}{\partial x^2} = \frac{\mu \Phi C}{k} \frac{\partial p}{\partial t}$$

a.60

Equation a.33 is known as the diffusivity equation for single-phase flow in one dimension.

For other coordinate systems, we will have,

$$\frac{\partial^2 P}{\partial x^2} + \frac{\partial^2 P}{\partial y^2} = \frac{\mu \Phi c}{k} \frac{\partial p}{\partial t}$$

for two-dimensional systems

a.61

$$\frac{\partial^2 P}{\partial r^2} + \frac{1}{r} \frac{\partial P}{\partial r} = \frac{\mu \Phi c}{k} \frac{\partial p}{\partial t}$$

for radial flow systems

a.62

A.4.1 Multiphase flow equations

For oil

Starting with an elemental volume of the reservoir system the basic equation is derived by combining the equation of state, continuity equation, and Darcy's equation.

We will have,

$$\left[-A \frac{K_o}{\mu_o B_o} \frac{\partial P}{\partial x} \right]_x - \left[-A \frac{K_o}{\mu_o B_o} \frac{\partial P}{\partial x} \right]_{x+\Delta x} = \nu \left[\frac{\left(\frac{\phi S_o}{B_o} \right)^{n+1} - \left(\frac{\phi S_o}{B_o} \right)^n}{\Delta t} \right]$$

a.63

$$A = \Delta y \Delta z$$

$$V = \Delta x \Delta y \Delta z$$

Equation a.63 in the limit becomes,

$$\frac{\partial}{\partial x} \left(\frac{K_o}{\mu_o B_o} \frac{\partial P}{\partial x} \right) = \frac{\partial}{\partial t} \left(\frac{\phi S_o}{B_o} \right)$$

a.64

Considering a radial system, the equivalent will be

$$\frac{1}{r} \frac{\partial}{\partial r} \left(r \frac{K_o}{\mu_o B_o} \frac{\partial P}{\partial r} \right) = \frac{\partial}{\partial t} \left(\frac{\phi S_o}{B_o} \right)$$

a.65

For Gas

$$\begin{aligned}
 & \left[-A \left(\frac{K_g}{\mu_g B_g} + \frac{R_{so} K_o}{\mu_o B_o} + \frac{R_{sw} K_w}{\mu_w B_w} \right) \frac{\partial P}{\partial x} \right]_x - \left[-A \left(\frac{K_g}{\mu_g B_g} + \frac{R_{so} K_o}{\mu_o B_o} + \frac{R_{sw} K_w}{\mu_w B_w} \right) \frac{\partial P}{\partial x} \right]_{x+\Delta x} \\
 &= v \left[\frac{\phi \left(\frac{S_g}{B_g} + \frac{R_{so} S_o}{B_o} + \frac{R_{sw} S_w}{B_o} \right)^{n+1} - \phi \left(\frac{S_g}{B_g} + \frac{R_{so} S_o}{B_o} + \frac{R_{sw} S_w}{B_o} \right)^n}{\Delta t} \right]
 \end{aligned}$$

a.66

Equation a.66 becomes in the limit,

$$\frac{\partial}{\partial x} \left[\left(\frac{K_g}{\mu_g B_g} + \frac{R_{so} K_o}{\mu_o B_o} + \frac{R_{sw} K_w}{\mu_w B_w} \right) \frac{\partial P}{\partial x} \right] = \frac{\partial}{\partial t} \left[\phi \left(\frac{S_g}{B_g} + \frac{R_{so} S_o}{B_o} + \frac{R_{sw} S_w}{B_o} \right) \right]$$

a.67

For a radial system, we will have the following equation similar to that of the oil in a single phase,

$$\frac{1}{r} \frac{\partial}{\partial r} \left[r \left(\frac{K_g}{\mu_g B_g} + \frac{R_{so} K_o}{\mu_o B_o} + \frac{R_{sw} K_w}{\mu_w B_w} \right) \frac{\partial P}{\partial x} \right] = \frac{\partial}{\partial t} \left[\phi \left(\frac{S_g}{B_g} + \frac{R_{so} S_o}{B_o} + \frac{R_{sw} S_w}{B_o} \right) \right]$$

a.68

The water phase is the same as the oil phase.

$$\frac{\partial}{\partial x} \left(\frac{K_w}{\mu_w B_w} \frac{\partial P}{\partial x} \right) = \frac{\partial}{\partial t} \left(\phi \frac{S_w}{B_w} \right)$$

a.69

Expansion in the Radial form

Multiplying equation a.68 by B_o and expanding by differentiation we will have,

$$\begin{aligned}
& \frac{B_o}{r} \left[r \frac{K_o}{\mu_o B_o} \frac{\partial^2 P}{\partial r^2} + r \frac{K_o}{\mu_o} \frac{\partial P}{\partial r} \left(-1 \frac{1}{B_0^2} \right) \frac{\partial B_o}{\partial P} \frac{\partial P}{\partial r} + \frac{1}{r} \frac{K_o}{\mu_o B_o} \frac{\partial P}{\partial r} \right] \\
& = \phi B_o \left(\frac{1}{B_o} \frac{\partial S_o}{\partial t} + \frac{S_o}{-B_0^2} \frac{\partial B_o}{\partial P} \frac{\partial P}{\partial t} \right)
\end{aligned}$$

a.70

Thus,

$$\frac{K_o}{\mu_o} \frac{\partial^2 P}{\partial r^2} + \frac{1}{r} \frac{K_o}{\mu_o} \frac{\partial P}{\partial r} = \phi \left(\frac{\partial S_o}{\partial t} - \frac{S_o}{B_o} \frac{\partial B_o}{\partial P} \frac{\partial P}{\partial t} \right)$$

a.71

Which becomes,

$$\frac{\partial}{\partial r} \left(\frac{1}{r} \frac{\partial P}{\partial r} \right) \frac{K_o}{\mu_o} = \phi \left(\frac{\partial S_o}{\partial t} - \frac{S_o}{B_o} \frac{\partial B_o}{\partial P} \frac{\partial P}{\partial t} \right)$$

a.72

The three-phase unsteady –state flow of oil, gas and water in a radial system is

$$\frac{1}{r} \frac{\partial}{\partial r} \left(r \frac{\partial P}{\partial r} \right) = \frac{\phi c_t}{k/\mu_t} \frac{\partial P}{\partial t}$$

a.73

Where,

$$c_t = -\frac{S_o}{B_o} \frac{\partial B_o}{\partial P} + \frac{S_o B_g}{B_o} \frac{\partial R_{so}}{\partial P} - \frac{S_w}{B_w} \frac{\partial B_w}{\partial P} + \frac{S_w B_g}{B_w} \frac{\partial R_{sw}}{\partial P} - \frac{S_g}{B_g} \frac{\partial B_g}{\partial P}$$

a.74

$$\left(\frac{k}{\mu}\right)_t = \frac{K_o}{\mu_o} + \frac{K_w}{\mu_w} + \frac{K_g}{\mu_g}$$

a.75

A.4.2 Finite Difference Model

Considering the equation below,

$$\frac{\partial^2 P}{\partial x^2} = \frac{\mu \Phi c}{k} \frac{\partial p}{\partial t}$$

P=pressure, μ for fluid viscosity, k for permeability, Φ for porosity and c for total compressibility of the rock and fluid

A.4.3 Discretization

Numerical solutions are better employed in the solution of the partial differential equations because it finds solutions at certain discrete points in space and time. The spatial domain that represents the reservoir system is divided into cells or grids and a series of time steps is advocated discretise the time domain. The analytical methods, on the other hand, gives a continuous solution in space and time(that is if any such solution can be found). The continuous partial differential equations are transformed into the equivalent discrete form of the equation using the finite-difference method.

Replacing the partial differential equations by a finite difference approximation based on Taylor's series expansion, the differential equation is then discretised into the finite-difference form. A numerical solution can be obtained with the finite difference form of the problems described by the partial differential equations taking into account the specified boundary conditions.

A.4.4 Spatial discretisation

In the numerical model, the grids are often rectangular. In local hybrid gridding or single-well monitoring systems, radial grids are often used in such scenarios. The grid system is usually defined by a N_x for a one- dimensional system, $N_x N_y$ for a two-dimensional system and $N_x N_y N_z$ for the three-dimensional system. The index is

known as the center, and unknown parameters such as pressure is calculated right at the center of the gridblock. A block centered grid block is one where the unknown parameters are calculated at the center of the grid.

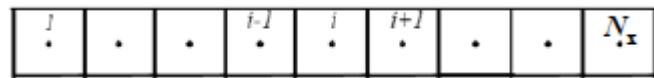


Figure A4: One-dimensional grid system (Crichlow, 1977).

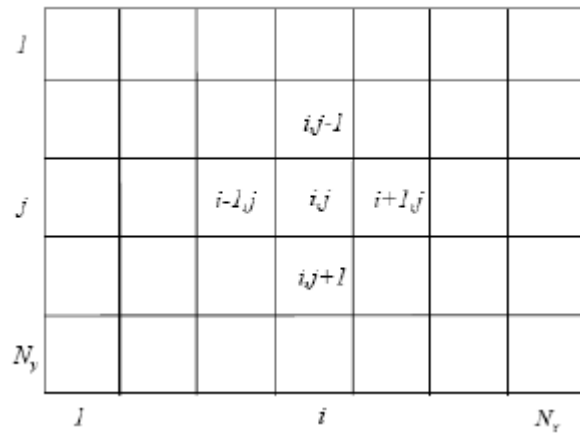


Figure A5: 2-dimensional grid system (Crichlow, 1977).

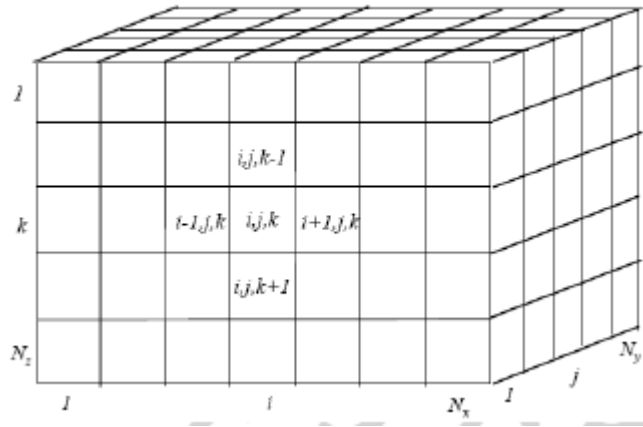


Figure A6: 3-dimensional grid system (Crichlow, 1977).

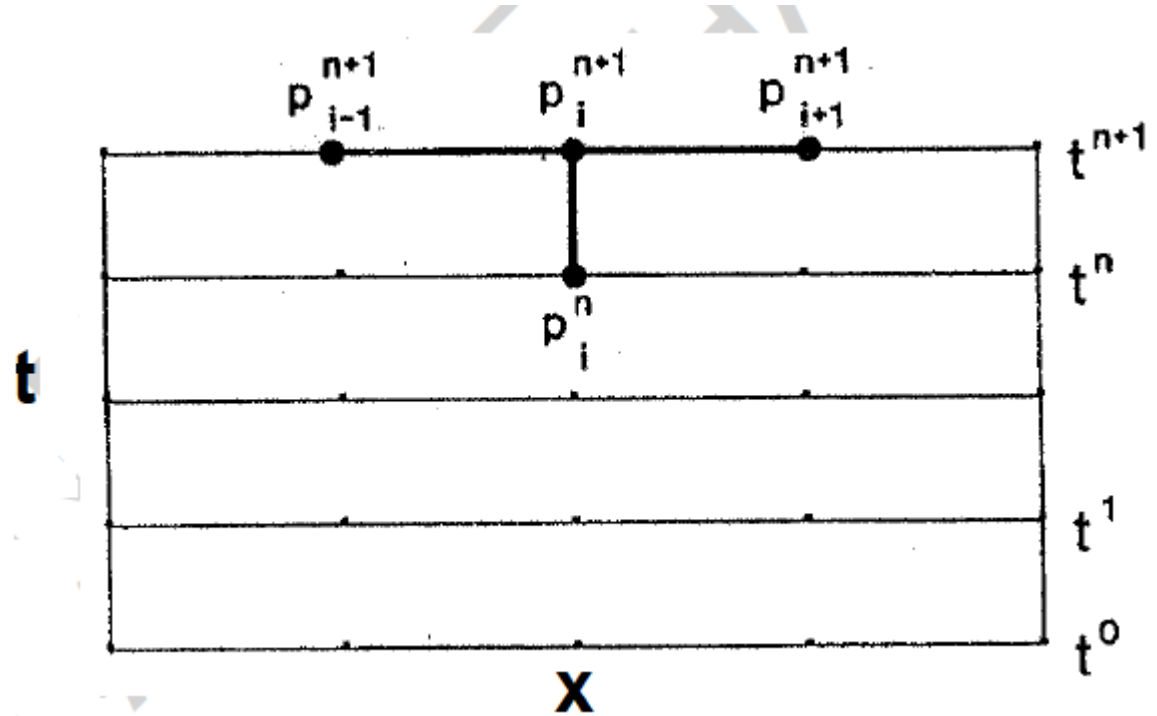


Figure A7: Discretization in the time domain (Crichlow, 1977)

For a one-dimensional problem, the pressure value p at $x + \Delta x$ is

$$p(x + \Delta x) = p(x) + \Delta x \frac{\partial p(x)}{\partial x} + \frac{\Delta x^2}{2!} \frac{\partial^2 p(x)}{\partial x^2} + \frac{\Delta x^3}{3!} \frac{\partial^3 p(x)}{\partial x^3} + \frac{\Delta x^4}{4!} \frac{\partial^4 p(x)}{\partial x^4} + \frac{\Delta x^n}{n!} \frac{\partial^n p(x)}{\partial n} + \dots$$
a.76

The value of $p(x - \Delta x)$ is similarly,

$$p(x - \Delta x) = p(x) - \Delta x \frac{\partial p(x)}{\partial x} + \frac{\Delta x^2}{2!} \frac{\partial^2 p(x)}{\partial x^2} - \frac{\Delta x^3}{3!} \frac{\partial^3 p(x)}{\partial x^3} + \frac{\Delta x^4}{4!} \frac{\partial^4 p(x)}{\partial x^4} - \frac{\Delta x^n}{n!} \frac{\partial^n p(x)}{\partial n}$$
a.77

Δx = distance of the center of two adjacent gridblocks

i =location of gridblock

x_i =location of the center of grid block i

$i + 1$ = Neighboring grid block to the right of i

x_{i+1} = location of the center of grid block $i + 1$

$i - 1$ =neighbouring grid block to the left of i

x_{i-1} =location of center of grid block $i - 1$

Combining equation a.77 and a.78 we will then have,

$$\frac{\partial^2 p(x)}{\partial x^2} = \frac{p(x - \Delta x) - 2p(x) + p(x + \Delta x)}{\Delta x^2} - \frac{2\Delta x^2}{4!} \frac{\partial^4 p(x)}{\partial x^4} \quad \text{a.78}$$

Using the notations described above, equation a.78 can be written as,

$$\frac{\partial^2 p(x)}{\partial x^2} \approx \frac{p_{i-1} - 2p_i + p_{i+1}}{\Delta x^2} + O(\Delta x^2) \quad \text{a.79}$$

Substituting, we arrive at the final difference form of the single-phase diffusivity equation

$$\frac{p_{i-1} - 2p_i + p_{i+1}}{\Delta x^2} = \frac{\mu \Phi c}{k} \frac{p_i^{n+1} - p_i^n}{\Delta t} \quad \text{a.80}$$

For the implicit case,

$$p_{i-1}^{n+1} - 2p_i^{n+1} + p_{i+1}^{n+1} = \frac{\Delta x^2 \mu \Phi c}{k} \frac{p_i^{n+1} - p_i^n}{\Delta t} \quad \text{a.81}$$

Collecting like terms together we will then have,

$$p_{i-1}^{n+1} - \left(2 + \frac{\Delta x^2}{\Delta t} \right) p_i^{n+1} + p_{i+1}^{n+1} = \frac{\Delta x^2 \mu \Phi c}{k} \frac{p_i^n}{\Delta t} \quad \text{a.82}$$

Equation a.82 is a single equation with three unknowns. This equation is expressed in the form

$$a_i p_{i-1} + b_i p_i + c_i p_{i+1} = d_i \quad \text{a.83}$$

Where,

$$a_i p_{i-1} = p_{i-1}^{n+1}$$

$$b_i = -\left(2 + \frac{\Delta x^2}{\Delta t}\right)$$

$$c_i p_{i+1} = p_{i+1}^{n+1}$$

$$d_i = \frac{\Delta x^2 \mu \Phi c}{k} \frac{p_i^n}{\Delta t}$$

The equation above can either be explicit if the expressions of the pressure on the left-hand side are the time step n (previous time step). It can be implicit if the expressions of the pressure on the left hand side is at the time step $n + 1$

For the implicit case, it is called an IMPES method meaning implicit pressure, explicit saturation. The matrix pressure equation of equation a.83 of the form,

$$AP = d \quad \text{a.84}$$

$$\begin{bmatrix} a_i b_i c_i & & \\ & a_i b_i c_i & \\ & & a_i b_i c_i \end{bmatrix} \times \begin{bmatrix} p_i \\ p_i \\ p_i \end{bmatrix} = \begin{bmatrix} d_i \\ d_i \\ d_i \end{bmatrix}$$

a.85

A is a tridiagonal matrix containing the coefficients a , b and c

Equation a.95 is solved implicitly with the Eclipse Reservoir simulator by iterative methods such as the Thomas algorithm (LU decomposition) (Rachford, 1955). It can

also be solved by the Alternating direction implicit procedure(ADIP) (Rachford, 1955), iterative Alternating-Direction Implicit method (Crichlow, 1977), Line successive over-relaxation(LSOR) (Crichlow, 1977), strongly implicit procedure(SIP).

Once we get the pressure equation at n+1 implicitly, we solve the saturation equation explicitly.

The saturation equation is

$$\frac{S_o}{B_o}^{n+1} = \frac{S_o}{B_o}^n + \frac{\Delta t}{\Phi} \left(\frac{\partial}{\partial x} \left(\frac{K_o}{\mu_o B_o} \frac{\partial \Phi}{\partial x} \right) \right)$$

Where

$$\Phi = p + \rho g h$$

For the initial condition, we specify the process to begin the time step sequence.

N=0 for initial condition and the initial pressure that exists before production is usually assigned to the grid blocks

The boundary conditions may either be Dirichlet (fixed pressure) or Neumann (fixed first partial derivatives). These conditions specify the equations at first and the last grid blocks. In the present work these equations are not solved directly but rather the Eclipse reservoir simulator is used.

MATLAB codes

Codes for Numerical Experiment 2- Comparison of Ensemble-based methods integrated with imaging and regularisation techniques

The code below shows the application of the ES-MDA technique to a Gaussian sandstone reservoir. Comparing to the standard EnKF has been done in the 1st year of the researcher.

This code is a group of MATLAB scripts used for numerical experiment 2.

The code couples several methods that carry out an integrated reservoir model calibration with seismic, electromagnetic, compressed sensing and discrete cosine transform on the Gaussian reservoir, MASATER0. The code is easy to implement and requires the availability of the Eclipse reservoir simulator and MATLAB research licence. The code starts with defining the size of the reservoir model, ensemble construction and size (designed a priori from the SGeMS), the true well, seismic or electromagnetic data, over complete learned dictionaries(unsupervised learning) and initialisation of the ensemble. The forward problem is run in parallel for the computational time reduction, utilising all cores of the local machine for running the Eclipse simulator. The inverse modelling, data processing and petrophysical maps are generated automatically after the end of the history matching loop.

```
%-----
-----%
% History matching using several methods with ESMDA (Ensemble smoother
% multiple data assimilation)
% Running Ensembles
% the code couples ECLIPSE reservoir simulator with MATLAB used to implement
my ideas on history matching of
% The MASTERO Gaussian Reservoir.
% Extra source of data is 4D seismic data and Electromagnetic data inverted
% to water saturation using our Kazsmarz equation
% Author: Clement Etienam , PhD Petroleum Engineering 2015-2018
% Supervisor: Dr Rosmary Villegas
% Co-Supervisor: Dr Masoud Babei
% Co-Supervisor: Dr Oliver Dorn
%-----
-----%
%%

clc
clear
disp('choose from the methods listed below for history matching with ESMDA')
disp('1-main_ESMDA')
disp('2-main_ESMDA_Localization-covariance localization')
disp('3- main_DCT(discrete cosine transform method coupled with ESMDA)')
disp('4-main_sparsity(compressed sensing) with ESMDA')
disp('5-main_4Dseismic_ESMDA +production data')
disp('6-main_4Dseismic+Electromagnetic_ESMDA(DCT parametrized) +production
data')
disp('7-main_Electromagnetic_ESMDA +production data')
disp('8-main_ESMDA+ DCT parametrisation on Seismic data uncertain')
```

```

disp('9-main_ESMDA+ DCT parametrisation on Electromagnetic data uncertain')
method=input(' Enter the required data assimilation scheme method ');
% N - size of ensemble
N=input( ' enter the number of realizations(ensemble size) '); %100
nx=input( ' enter the number of grid blocks in x direction '); %84
ny=input( ' enter the number of grid blocks in y direction '); %27
nz=input( ' enter the number of grid blocks in z direction '); % 4
alpha=input(' enter the alpha value '); %4-8
% alpha is the number of iteration and damping coefficient
history=input(' enter the number of timestep for the history period '); %16
disp( 'Load the true permeability and porosity')
load rossmary.GRDECL; %true permeability field
load rossmaryporo.GRDECL; %True porosity field
oldfolder=cd;
cd(oldfolder) % setting original directory
disp(' import the true observation data ');
True= importdata('Real.RSM',' ',7);
True=True.data;
TO1=True(:,6);
TW1=True(:,8);
TP1=True(:,9);
disp(' make the true observation')
for ihistory=1:history
obs=zeros(3,1);
obs(1,:)=TO1(ihistory,:);
obs(2,:)=TW1(ihistory,:);
obs(3,:)=TP1(ihistory,:);
observation(:,ihistory)=obs;
end
%% extract the true water for base survey
true31 = importdata('true.F0001',' ',2938); %true water sat for year 83
true31=true31.data;
truewater83=true31;
SO=ones(2268,4)-true31;
truepressure = importdata('true.F0001',' ',669);
truepressure=truepressure.data;
truepressure83=truepressure;
Pr=truepressure83;
PORO = importdata('porojoy.DAT',' ',1); % true porosity field
PORO=PORO.data;
ImpP=Gassmann(PORO,Pr,SO);
ImpP83=reshape(ImpP,2268,1); % True impedance at year 83;
trueimpedance83=repmat(ImpP83,1,N);
%% extract true water and impedance for monitor survey
true32 = importdata('true.F0016',' ',2938); %true water sat for the time 89
timestep
true32=true32.data;
truewater89=true32;
SO=ones(2268,4)-true32;
truepressure89 = importdata('true.F0016',' ',669);
truepressure89=truepressure89.data;
Pr=truepressure89;
PORO = importdata('porojoy.DAT',' ',1);
PORO=PORO.data;
ImpP=Gassmann(PORO,Pr,SO);
ImpP89=reshape(ImpP,2268,1);
trueimpedance89=repmat(ImpP89,1,N);
EMwater=truewater89; % for history matching electromagnetic data
oldfolder=cd;
%% Creating Folders
disp( 'create the folders')
for j=1:N
f = 'MASTER';
folder = strcat(f, sprintf('%.5d',j));
mkdir(folder);
end
%% Copying simulation files

```

```

disp( 'copy simulation files for the forward problem')
for j=1:N
f = 'MASTER';
folder = strcat(f, sprintf('%.5d',j));
copyfile('FAULT.DAT',folder)
copyfile('MASTER0.DATA',folder)
copyfile('Gassmann.m',folder)
copyfile('field2Metric.m',folder)
copyfile('Eclipse2Matlab.m',folder)
copyfile('Matlab2Eclipse.m',folder)
copyfile('resize.m',folder)
end
tic;
for iyobo=1:alpha
fprintf('Now running the code for iteration %d .\n', iyobo);
%% Loading Porosity and Permeability ensemble files
disp(' load the permeability and porosity fields')
if iyobo==1
    disp('permeability loaded from initial ensemble')
load sgsimporo.out; %initial porosity
load sgsim.out; %initial permeability
perm=reshape(sgsim,nx*ny*nz,N);
poro=reshape(sgsimporo,nx*ny*nz,N);
else
    disp('permeability loaded from UPDATED ensemble')
perm=reshape(mumyperm,nx*ny*nz,N);
poro=reshape(mumyporo,nx*ny*nz,N);
end
cd(olddfolder) % setting original directory
%% Saving POROVANCOUVER and KVANCOUVER
for i=1:N %list of folders
    f = 'MASTER';
    folder = strcat(f, sprintf('%.5d',i));
    cd(folder) % changing directory
    PORO2=poro(:,i);
    PERMX2=perm(:,i);
    save('KVANCOUVER.DAT','PERMX2','-ascii');
    save('POROVANCOUVER.DAT','PORO2','-ascii');
    cd(olddfolder) % returning to original cd
end
%% Inserting KEYWORDS PORO and PERMY

parfor i=1:N %list of folders
    f = 'MASTER';
    folder = strcat(f, sprintf('%.5d',i));
    cd(folder)
CStr = regexp(fileread('KVANCOUVER.DAT'), char(10), 'split');
CStr2 = strrep(CStr, 'toReplace', 'Replacement');
CStr2 = cat(2, {'PERMY'}, CStr2(1:end));
CStr2 = cat(2, CStr2(1:end), {'/'});
FID = fopen('KVANCOUVER.DAT', 'w');
if FID < 0, error('Cannot open file'); end
fprintf(FID, '%s\n', CStr2{:});
fclose(FID)
CStr = regexp(fileread('POROVANCOUVER.DAT'), char(10), 'split');
CStr2 = strrep(CStr, 'toReplace', 'Replacement');
CStr2 = cat(2, {'PORO'}, CStr2(1:end));
CStr2 = cat(2, CStr2(1:end), {'/'});
FID = fopen('POROVANCOUVER.DAT', 'w');
if FID < 0, error('Cannot open file'); end
fprintf(FID, '%s\n', CStr2{:});
fclose(FID);
cd(olddfolder) % setting original directory
end
%% Running Simulations
disp( 'Solve the Non-Linear fluid flow Forward Problem' )
cd(olddfolder) % setting original directory

```

```

parfor i=1:N %list of folders
    f = 'MASTER';
    folder = strcat(f, sprintf('%.5d',i));
    cd(folder)
    fid = fopen('MASTER0.bat', 'w');
    fprintf(fid,'@ECHO OFF\n');
    % fprintf(fid,'SET SLBSLS_LICENSE_FILE=27008@eclipse.cc.ic.ac.uk\n');
    fprintf(fid,'SET SLBSLS_LICENSE_FILE=27000@10.99.15.78\n');
    fprintf(fid,'@ECHO OFF\n');
    fprintf(fid,['c:\\ecl\\macros\\$eclipse ', 'MASTER0'], '\n');
    fclose(fid);
    %while ~exist('MASTER0.F0016','file')
        system('MASTER0.bat')
    %end
    cd(olddfoder) % setting original director
end
disp(' plot production profile for the run')
oldfolder=cd;
cd(olddfoder) % setting original directory
%% Plot the Production profile of ensemble
disp(' start the plotting ')
for i=1:N %list of folders
    f = 'MASTER';
    folder = strcat(f, sprintf('%.5d',i));
    cd(folder);
    A1 = importdata('MASTER0.RSM', ' ',7);
    A1=A1.data;
    WOPR1=A1(:,3);
    WWPR1=A1(:,5);
    WBHP1=A1(:,6);
    Time=A1(:,1);
    WOPRA(:,i)=WOPR1;
    WWPRB(:,i)=WWPR1;
    WBHPC(:,i)=WBHP1;

    cd(olddfoder);
end
cd(olddfoder) % returning to original directory
%Import true data
True= importdata('Real.RSM', ' ',7);
True=True.data;
TO1=True(:,6);
TO2=True(:,8);
TO3=True(:,9);
linecolor1 = colordg(4);
%% Plot for Well Bottom Hole Pressure
figure()
plot(Time,WOPRA(:,1:N),'Color',linecolor1,'LineWidth',2)
xlabel('Time (days)', 'FontName', 'Helvetica', 'FontSize', 13);
ylabel('Q_o(STB/DAY)', 'FontName', 'Helvetica', 'FontSize', 13);
ylim([5000 25000])
title('Producer Oil production Rate', 'FontName', 'Helvetica', 'FontSize', 13)
a = get(gca, 'Children');
hold on
plot(Time,TO1,'r','LineWidth',1)
b = get(gca, 'Children');
set(gca, 'FontName', 'Helvetica', 'FontSize', 13)
set(gcf, 'color', 'white')
line([1500 1500], [5000 25000],'Color','black','LineStyle','--')
h = [b;a];
legend(h, 'True model', 'Realisations', 'location', 'northeast');
hold off
saveas(gcf,sprintf('PRO-Oilrate_iter%d.fig',iyobo))
close.figure)
figure()
plot(Time,WWPRB(:,1:N),'Color',linecolor1,'LineWidth',2)
xlabel('Time (days)', 'FontName', 'Helvetica', 'FontSize', 13);

```

```

ylabel('Q_w(STB/DAY)', 'FontName', 'Helvetica', 'FontSize', 13);
ylim([1 200])
title('Producer Water production Rate', 'FontName', 'Helvetica', 'FontSize', 13)
a = get(gca, 'Children');
hold on
plot(Time, TO2, 'r', 'LineWidth', 1)
b = get(gca, 'Children');
set(gca, 'yscale', 'log', 'FontName', 'Helvetica', 'FontSize', 13)
set(gca, 'FontName', 'Helvetica', 'FontSize', 13)
set(gcf, 'color', 'white')
line([1500 1500], [1 200], 'Color', 'black', 'LineStyle', '--')
h = [b;a];
legend(h, 'True model', 'Realisations', 'location', 'northeast');
hold off
saveas(gcf, sprintf('PRO-WATER_iter%d.fig', iyobo))
close(figure)
figure()
plot(Time, WBHPC(:,1:N), 'Color', linecolor1, 'LineWidth', 2)
xlabel('Time (days)', 'FontName', 'Helvetica', 'FontSize', 13);
ylabel('BHP(Psia)', 'FontName', 'Helvetica', 'FontSize', 13);
ylim([1500 4000])
title('Injector BHP', 'FontName', 'Helvetica', 'FontSize', 13)
a = get(gca, 'Children');
hold on
plot(Time, TO3, 'r', 'LineWidth', 1)
b = get(gca, 'Children');
set(gca, 'FontName', 'Helvetica', 'FontSize', 13)
set(gcf, 'color', 'white')
line([1500 1500], [1500 4000], 'Color', 'black', 'LineStyle', '--')
h = [b;a];
legend(h, 'True model', 'Realisations', 'location', 'northeast');
hold off
saveas(gcf, sprintf('Injector-WBHP_iter%d.fig', iyobo))
close(figure)
for i=1:N
    EWOP1(i,:)=immse(WOPRA(:,i),TO1);
    EWOP2(i,:)=immse(WOPRB(:,i),TO2);
    EWOP3(i,:)=immse(WBHPC(:,i),TO3);
end
TOTALERROR=ones(N,1);
TOTALERROR=(EWOP1./std(TO1))+(EWOP2./std(TO2))+(EWOP3./std(TO3));
TOTALERROR=TOTALERROR./16;
jj=min(TOTALERROR);
index = TOTALERROR;
bestnorm = find(index == min(index));
fprintf('The best Norm Realization for production data match is number %i with
value %4.6f \n', bestnorm, jj);
reali=[1:N];
figure()
bar(reali, index, 'cyan');
xlabel('Realizations', 'FontName', 'Helvetica', 'FontSize', 13);
ylabel('RMSE value', 'FontName', 'Helvetica', 'FontSize', 13);
title('Production data Cost function for
Realizations', 'FontName', 'Helvetica', 'FontSize', 13)
set(gcf, 'color', 'white');
hold on
scatter(reali, index, 'black', 'filled');
xlim([1,N]);
xlabel('Realizations', 'FontName', 'Helvetica', 'FontSize', 13);
ylabel('RMSE value', 'FontName', 'Helvetica', 'FontSize', 13)
saveas(gcf, sprintf('RMS_iter%d.fig', iyobo))
close(figure)
disp(' program almost executed ');
decreasingnorm(:,iyobo)=index;
disp('Get the simulated files for all the time step')
oldfolder=cd;
cd(oldfolder) % setting original directory

```

```

overallsim=zeros(3,history,N);
for ii=1:N %list of folders
    f = 'MASTER';
    folder = strcat(f, sprintf('%.5d',ii));
    cd(folder)
    True= importdata('MASTER0.RSM',' ',7);
True=True.data;
TO1=True(:,3);
TW1=True(:,5);
TP1=True(:,6);
for i=1:history
obs=zeros(3,1);
obs(1,:)=TO1(i,:);
obs(2,:)=TW1(i,:);
obs(3,:)=TP1(i,:);
observationsim(:,i)=obs;
end
overallsim(:, :, ii)=observationsim;
cd(olddfilder) % returning to original directory

end
disp(' done saving simulated production data')
cd(olddfilder) % returning to original directory
[PclementEn83,SclementEn83,PclementEn89,SclementEn89]=getitnow(100);
PclementEn83=reshape(PclementEn83,nx*ny*nz*N,1); %pressure ensemble initial
SclementEn83=reshape(SclementEn83,nx*ny*nz*N,1); %water saturation ensemble
initial
PclementEn89=reshape(PclementEn89,nx*ny*nz*N,1); %pressure ensemble final
SclementEn89=reshape(SclementEn89,nx*ny*nz*N,1); %water saturation ensemble
final
cd(olddfilder) % returning to original directory
disp('save the ensemble to see how good')
pressureensemble83(:,iyobo)=PclementEn83;
pressureensemble89(:,iyobo)=PclementEn89;
saturationensemble83(:,iyobo)=SclementEn83;
saturationensemble89(:,iyobo)=SclementEn89;
%% Construction of Synthetic Seismic using Gassmann's equation
disp('Construction of Synthetic Seismic using Gassmanns equation')
[IEn83,IEn89]=getitimp(N,nx,ny,nz);
[Sall,Pall]=getstatesall(N);
%% Enter the assimilation loop
disp('now entering the assimilation loop')
switch method
    case 1
        disp('method 1 specified-standard ESMDA')
        [mumyperm,mumyporo]=main_ESMDA(nx,ny,nz,N,observation,overallsim,rossmary,ross
maryporo,perm,poro,history,alpha,Sall,Pall);
    case 2
        disp('method 2 specified-Localization with ESMDA')
        [mumyperm,mumyporo]=main_ESMDA_Localization(nx,ny,nz,N,observation,overallsim,
rossmary,rossmaryporo,perm,poro,history,alpha,Sall,Pall);
    case 3
        disp('method 3 specified-DCT')
        [mumyperm,mumyporo]=main_DCT(nx,ny,nz,N,observation,overallsim,rossmary,rossma
ryporo,perm,poro,history,alpha,Sall,Pall);
    case 4
        disp('method 4 specified-Sparsity')
        [mumyperm,mumyporo]=main_sparsity(nx,ny,nz,N,observation,overallsim,rossmary,r
ossmaryporo,perm,poro,history,alpha,Yes2PUNQ,YesPUNQporo,Sall,Pall);
    case 5
        disp('method 5 specified-main_4Dseismic_ESMDA +production data')
        [mumyperm,mumyporo]=main_4Dseismic_ESMDA(nx,ny,nz,N,observation,overallsim,ros
smary,rossmaryporo,perm,poro,history,alpha,trueimpedance83,trueimpedance89,IEn
83,IEn89,Sall,Pall);
    case 6
        disp('method 6 specified-4DEMparametrized')
        [mumyperm,mumyporo]=main_4DEMpara_ESMDA(nx,ny,nz,N,observation,overallsim,ross

```

```

mary, rossmaryporo, perm, poro, history, alpha, trueimpedance83, trueimpedance89, EMwater, IEn83, IEn89, SEn89, Sall, Pall);
    case 7
        disp( 'method 7 specified-EM-ESMDA')
        [mumyperm,mumyporo]=main_EM_ESMDA(nx,ny,nz,N,observation,overallsim,rossmary,rossmaryporo,perm,poro,history,alpha,EMwater,SEn89,Sall,Pall);
    case 8
        disp( 'method 8 specified-4D+ESMDA')
        [mumyperm,mumyporo]=main_4Dfull_ESMDA(nx,ny,nz,N,observation,overallsim,rossmary,rossmaryporo,perm,poro,history,alpha,trueimpedance83,trueimpedance89,IEn83,IEn89,Sall,Pall);
    case 9
        disp( 'method 9 specified-EMparametrized')
        [mumyperm,mumyporo]=main_EMpara_ESMDA(nx,ny,nz,N,observation,overallsim,rossmary,rossmaryporo,perm,poro,history,alpha,EMwater,SEn89,Sall,Pall);
    otherwise
        disp('method not specified correctly')
    end
perm=reshape(mumyperm,nx*ny*nz,N);
poro=reshape(mumyporo,nx*ny*nz,N);
fprintf('Finished Iteration %d .\n', iyobo);
end
%% Exit the loop
%% Now run the code to see the final history matching step
disp( 'now run the code after the last Iteration to see how good')
fprintf('Get the RMS after exiting the loop');
%% Loading Porosity and Permeability ensemble files
disp(' use the permeability and porosity fields after Last iteration')
cd(olddfolder) % setting original directory
for i=1:N %list of folders
    f = 'MASTER';
    folder = strcat(f, sprintf('%.5d',i));
    cd(folder) % changing directory
    PORO2=poro(:,i);
    PERMX2=perm(:,i);
    save('KVANCOUVER.DAT','PERMX2','-ascii');
    save('POROVANCOUVER.DAT','PORO2','-ascii');
    cd(olddfolder) % returning to original cd
end
%% Inserting KEYWORDS PORO and PERMY
parfor i=1:N %list of folders
    f = 'MASTER';
    folder = strcat(f, sprintf('%.5d',i));
    cd(folder)
CStr = regexp(fileread('KVANCOUVER.DAT'), char(10), 'split');
CStr2 = strrep(CStr, 'toReplace', 'Replacement');
CStr2 = cat(2, {'PERMY'}, CStr2(1:end));
CStr2 = cat(2, CStr2(1:end), {'/'});
FID = fopen('KVANCOUVER.DAT', 'w');
if FID < 0, error('Cannot open file'); end
fprintf(FID, '%s\n', CStr2{:});
fclose(FID);
CStr = regexp(fileread('POROVANCOUVER.DAT'), char(10), 'split');
CStr2 = strrep(CStr, 'toReplace', 'Replacement');
CStr2 = cat(2, {'PORO'}, CStr2(1:end));
CStr2 = cat(2, CStr2(1:end), {'/'});
FID = fopen('POROVANCOUVER.DAT', 'w');
if FID < 0, error('Cannot open file'); end
fprintf(FID, '%s\n', CStr2{:});
fclose(FID);
cd(olddfolder) % setting original directory
end
%% Running Simulations
disp( 'Solve the Non-Linear fluid flow Forward Problem' )
cd(olddfolder) % setting original directory
parfor i=1:N %list of folders
    f = 'MASTER';

```

```

folder = strcat(f, sprintf('%.5d',i));
cd(folder)
fid = fopen('MASTER0.bat', 'w');
fprintf(fid, '@ECHO OFF\n');
fprintf(fid, 'SET SLBSLS_LICENSE_FILE=27000@10.99.15.78\n');
fprintf(fid, '@ECHO OFF\n');
fprintf(fid, ['c:\\ecl\\macros\\$eclipse ', 'MASTER0'], '\n');
fclose(fid);
    system('MASTER0.bat')
cd(olddfoder) % setting original directory
end
disp(' plot production profile for the final run')
N=100;
oldfolder=cd;
cd(olddfoder) % setting original directory
%% Plot the Production profile of ensemble
disp(' start the plotting ');
for i=1:N %list of folders
f = 'MASTER';
folder = strcat(f, sprintf('%.5d',i));
cd(folder);
A1 = importdata('MASTER0.RSM', ' ', 7);
A1=A1.data;
WOPR1=A1(:,3);
WWPR1=A1(:,5);
WBHP1=A1(:,6);
Time=A1(:,1);
WOPRA(:,i)=WOPR1;
WWPRB(:,i)=WWPR1;
WBHPC(:,i)=WBHP1;
cd(olddfoder);
end
cd(olddfoder) % returning to original directory
%Import true data
True= importdata('Real.RSM', ' ', 7);
True=True.data;
TO1=True(:,6);
TO2=True(:,8);
TO3=True(:,9);
linecolor1 = colordg(4);
%% Plot for Well Bottom Hole Pressure
figure()
plot(Time,WOPRA(:,1:N),'Color',linecolor1,'LineWidth',2)
xlabel('Time (days)', 'FontName', 'Helvetica', 'FontSize', 13);
ylabel('Q_o(STB/DAY)', 'FontName', 'Helvetica', 'FontSize', 13);
ylim([5000 25000])
title('Producer Oil production Rate', 'FontName', 'Helvetica', 'FontSize', 13)
a = get(gca, 'Children');
hold on
plot(Time,TO1,'r','LineWidth',1)
b = get(gca, 'Children');
set(gca, 'FontName', 'Helvetica', 'FontSize', 13)
set(gcf, 'color', 'white')
line([1500 1500], [5000 25000], 'Color', 'black', 'LineStyle', '--')
h = [b;a];
legend(h, 'True model', 'Realisations', 'location', 'northeast');
hold off
saveas(gcf,sprintf('PRO-Oilrate_iter%d.fig',iyobo))
close(figure)
figure()
plot(Time,WWPRB(:,1:N),'Color',linecolor1,'LineWidth',2)
xlabel('Time (days)', 'FontName', 'Helvetica', 'FontSize', 13);
ylabel('Q_w(STB/DAY)', 'FontName', 'Helvetica', 'FontSize', 13);
ylim([1 200])
title('Producer Water production Rate', 'FontName', 'Helvetica', 'FontSize', 13)
a = get(gca, 'Children');
hold on

```

```

plot(Time,TO2, 'r', 'LineWidth',1)
b = get(gca, 'Children');
set(gca, 'yscale','log', 'FontName','Helvetica', 'FontSize', 13)
    set(gca, 'FontName','Helvetica', 'FontSize', 13)
set(gcf,'color','white')
line([1500 1500], [1 200], 'Color','black', 'LineStyle','--')
h = [b;a];
legend(h,'True model','Realisations','location','northeast');
hold off
saveas(gcf,sprintf('PRO-WATER_iter%d.fig',iyobo))
close(figure)
figure()
plot(Time,WBHP(:,1:N), 'Color',linecolor1, 'LineWidth',2)
xlabel('Time (days)', 'FontName','Helvetica', 'FontSize', 13);
ylabel('BHP(Psia)', 'FontName','Helvetica', 'FontSize', 13);
    ylim([1500 4000])
title('Injector BHP', 'FontName','Helvetica', 'FontSize', 13)
a = get(gca, 'Children');
hold on
plot(Time,TO3, 'r', 'LineWidth',1)
b = get(gca, 'Children');
    set(gca, 'FontName','Helvetica', 'FontSize', 13)
set(gcf,'color','white')
line([1500 1500], [1500 4000], 'Color','black', 'LineStyle','--')
h = [b;a];
legend(h,'True model','Realisations','location','northeast');
hold off
saveas(gcf,sprintf('Injector-WBHP_iter%d.fig',iyobo))
close(figure)
for i=1:N
    EWOP1(i,:)=immse(WOPRA(:,i),TO1);
    EWOP2(i,:)=immse(WWPRB(:,i),TO2);
    EWOP3(i,:)=immse(WBHP(:,i),TO3);
end
TOTALERROR=ones(N,1);
TOTALERROR=(EWOP1./std(TO1))+(EWOP2./std(TO2))+(EWOP3./std(TO3));
TOTALERROR=TOTALERROR./16;
jj=min(TOTALERROR);
index = TOTALERROR;
bestnorm = find(index == min(index));
fprintf('The best Norm Realization for production data match is number %i with
value %4.6f \n',bestnorm,jj);
decreasingseries=zeros(N,iyobo+1);
decreasingseries(:,1:iyobo)=decreasingnorm;
decreasingseries(:,iyobo+1)=index;
reali=[1:N];
figure()
bar(reali,index,'cyan');
xlabel('Realizations', 'FontName','Helvetica', 'FontSize', 13);
ylabel('RMSE value', 'FontName','Helvetica', 'FontSize', 13);
title('Production data Cost function for
Realizations', 'FontName','Helvetica', 'FontSize', 13)
set(gcf,'color', 'white');
hold on
scatter(reali,index,'black','filled');
    xlim([1,N]);
xlabel('Realizations', 'FontName','Helvetica', 'FontSize', 13);
ylabel('RMSE value', 'FontName','Helvetica', 'FontSize', 13)
    saveas(gcf,'RMS_final','fig')
close(figure)
disp(' Final RMS computation executed ');
disp('output the permeability and porosity history matched model for the last
iteration')
file = fopen('sgsimfinal.out','w+'); %output the dictionary
for k=1:numel(mumyperm)
fprintf(file, ' %4.6f \n',mumyperm(k) );
end

```

```

file2 = fopen('sgsimporofinal.out','w+'); %output the dictionary
for k=1:numel(mumyporo)
fprintf(file2,' %4.6f \n',mumyporo(k) );
end
file4 = fopen('evolvingNorm.out','w+');
for k=1:numel(decreasingseries)
fprintf(file4,' %4.4f \n',decreasingseries(k) );
end
disp('save the ensemble of pressure and saturation for all iterations')
save('PEn83.out','pressureensemble83','-ascii');
save('SEn83.out','saturationensemble83','-ascii');
save('PEn89.out','pressureensemble89','-ascii');
save('SEn89.out','saturationensemble89','-ascii');
bestnorm=double(bestnorm);
disp('1=yes')
disp('2=no' )
response=input('Do you want to plot the permeability map ');
disp('Well locations consisting of producer well')
iProd = [10, 70]; %1 injector well
jProd = [10, 10]; % 1 producer well
if response==1
    disp('Pixel map needed')
    [bestnorm3,PlogK]=clementPlot(nx,ny,nz,iProd,
jProd,mumyperm,rossmary,N,bestnorm);
    clementPlotporo(nx,ny,nz,iProd, jProd,mumyporo,rossmaryporo,N,bestnorm3);
    disp(' red is producer and black is injector')
    %run('clementPlot.m')
else
    disp (' pixel map not needed')
end
fprintf('Finished Iterations with the History matching method %d .\n',
method);
if method==1
disp('The method used was standard ESMDA implemented with main_ESMDA')
elseif method==2
disp('The method used was ESMDA with Localization')
elseif method==3
disp('The method used was ESMDA implemented with main_DCT( discrete cosine
transform method coupled with ESMDA)')
elseif method==4
disp('The method used was compressed sensing ESMDA implemented with
main_sparsity(compressed sensing)')
elseif method==5
disp('The method used was main_4Dseismic(DCT parametrised)_ESMDA +production
data')
elseif method==6
disp('The method used was main_4Dseismic+Electromagnetic_ESMDA(DCT
parametrized) +production data')
elseif method==7
disp('The method used was main_Electromagnetic_ESMDA +production
data')
elseif method==8
disp('The method used was main_ESMDA+ Seismic data uncertain')
else
    disp('The method used was main_ESMDA+ DCT parametrisation on Electromagnetic
data uncertain')
end
disp(' The overall program has been executed, and the history matched files
saved in the folder ');
toc

```

The ES-MDA function is explained below;

```

function
[mumyperm,mumyporo]=main_ESMDA(nx,ny,nz,N,observation,overallsim,rossmary,ross
maryporo,perm,poro,history,alpha,Sall,Pall);
% N - size of ensemble
sgsim=reshape(perm,nx*ny*nz,N);
sgsimporo=reshape(poro,nx*ny*nz,N);
Sall=reshape(Sall,nx*ny*nz,history,N);
Pall=reshape(Pall,nx*ny*nz,history,N);
Sim11=reshape(overallsim,3,history,N);
%History matching using ESMDA
for i=1:history
    fprintf('Now assimilating timestep %d .\n', i);
    Sim1=Sim11(:,i,:);
    Sim1=reshape(Sim1,3,N);
    Saturation=Sall(:,i,:);
    Saturation=reshape(Saturation,nx*ny*nz,N);
    Pressure=Pall(:,i,:);
    Pressure=reshape(Pressure,nx*ny*nz,N);
    f=observation(:,i);
    [DupdateK,Dupdateporo] = ESMDA (sgsim,sgsimporo,f, N,
    Sim1,alpha,Saturation,Pressure);
    sgsim=DupdateK;
    sgsimporo=Dupdateporo;
    fprintf('Finished assimilating timestep %d \n', i);
end
disp('recover the full permeability and porosity field')
[output,outputporo] = honour2(rossmary, rossmaryporo, N,Dupdateporo,DupdateK);
mumyperm=output;
mumyporo=outputporo;
disp(' program executed ');
end

```

Case 2

The MATLAB scripts below shows the implementation of the logic, adapting a compact support fifth order covariance matrix with the Level set technique developed in the researcher's previous work

The reservoir is channelized.

The main script

```

%-----
% History matching using several methods with ESMDA (Ensemble smoother
% multiple data assimilation)
% Running Ensembles
% the code couples ECLIPSE reservoir simulator with MATLAB used to implement
my ideas on history matching of
% The SPE 10 Reservoir.
% Author: Clement Etienam , PhD Petroleum Engineering 2015-2018
% Supervisor: Dr Rossmay Villegas
% Co-Supervisor: Dr Masoud Babai
% Co-Supervisor: Dr Oliver Dorn
%-----
%%
clc
clear
tic
%% Query the user

```

```

disp('choose from the methods listed below for history matching with ESMDA')
disp('1-main_ESMDA')
disp('2-main_Levelset')
disp('3- main_DCT( discrete cosine transform method coupled with ESMDA)')
disp('4-main_sparsity(compressed sensing) with ESMDA')
disp('5-SELE_PhD (My method coupling machine learning with Level set)')
disp('6-main_DCT_Levelset(My method coupling DCT with Level set)')
disp('7-main_DCT_LS2 (Level set and DCT update)')
disp('8-main_sparsity_LS(Level set update)')
disp('9-main_Levelset_Boundary ')
disp('10-main_Velocity_LS')
disp('11-main_ESMDA_Localization-covariance localization')
disp('12-main_Levelset_Cov-covariance localization with Levelset')
disp('13-main_Levelset_Cov-covariance localization with Levelset but
permeability constant')
disp('14-main_supervised-Supervised learning ')
disp('15-main_dynamicsparsity ')
method=input(' Enter the required data assimilation scheme method ');
disp(' Now the smoothing query from the user ')
disp('Enter- 1 if needed smoothing of the pixel maps')
disp('Enter 2 -if you dont need smoothing of the pixel maps')
needed=input(' Do you want to smooth the pixel maps after history matching?
');
disp('1=yes')
disp('2=no' )
response=input('Do you want to plot the permeability map ');
disp(' Now the number of times to smooth it ')
numberoftimes=input(' Number of times to clean? ');
% cleaning the maps up to 2 times for ESMDA is good enough
%%
% N - size of ensemble
N=input(' enter the number of realizations(ensemble size) '); %100
nx=input(' enter the number of grid blocks in x direction '); %120
ny=input(' enter the number of grid blocks in y direction '); %60
nz=input(' enter the number of grid blocks in z direction '); % 5
tol=input(' enter the tolerance for pseudo inversion ');
alpha=input(' enter the alpha value '); %4-10 is enough
% alpha is the number of iteration and damping coefficient
history=input(' enter the number of timestep for the history period '); %36
disp('Load the true permeability and porosity')
load rossmary.GRDECL; %true permeability field
load rossmaryporo.GRDECL; %True porosity field
%% Import the true data to be history matched
oldfolder=cd;
cd(oldfolder) % setting original directory
disp(' import the true observation data ');
True= importdata('Real.RSM',' ',7);
True2= importdata('Real.RSM',' ',50);
True3= importdata('Real.RSM',' ',93);
True4= importdata('Real.RSM',' ',136);
True=True.data;
True2=True2.data;
True3=True3.data;
True4=True4.data;
TO1=True(:,3);
TO2=True(:,4);
TO3=True(:,5);
TO4=True(:,6);
TW1=True2(:,2);
TW2=True2(:,3);
TW3=True2(:,4);
TW4=True2(:,5);
TP1=True3(:,5);
TP2=True3(:,6);
TP3=True3(:,7);
TP4=True3(:,8);
TG1=True3(:,9);

```

```

TG2=True3(:,10);
TG3=True4(:,2);
TG4=True4(:,3);
TFOE=True4(:,8);
disp(' make the true observation')
for ihistory=1:history
obs=zeros(17,1);
obs(1,:)=TO1(ihistory,:);
obs(2,:)=TO2(ihistory,:);
obs(3,:)=TO3(ihistory,:);
obs(4,:)=TO4(ihistory,:);
obs(5,:)=TW1(ihistory,:);
obs(6,:)=TW2(ihistory,:);
obs(7,:)=TW3(ihistory,:);
obs(8,:)=TW4(ihistory,:);
obs(9,:)=TP1(ihistory,:);
obs(10,:)=TP2(ihistory,:);
obs(11,:)=TP3(ihistory,:);
obs(12,:)=TP4(ihistory,:);
obs(13,:)=TG1(ihistory,:);
obs(14,:)=TG2(ihistory,:);
obs(15,:)=TG3(ihistory,:);
obs(16,:)=TG4(ihistory,:);
obs(17,:)=TFOE(ihistory,:);
observation(:,ihistory)=obs;
end

%% End of section
oldfolder=cd;
%% Creating Folders
disp( 'create the folders')
for j=1:N
f = 'MASTER';
folder = strcat(f, sprintf('%.5d',j));
mkdir(folder);
end
%% Copying simulation files
disp( 'copy simulation files for the forward problem')
for j=1:N
f = 'MASTER';
folder = strcat(f, sprintf('%.5d',j));
copyfile('ACTNUM.DAT',folder)
copyfile('SPE10_PVTI.PVO',folder)
copyfile('SPE10_PVTI_RSVD.PVO',folder)
copyfile('SPE10_PVTI_WATER.PVO',folder)
copyfile('Eclipse2Matlab.m',folder)
copyfile('resize.m',folder)
copyfile('MASTER0.DATA',folder)
end
%% Unsupervised learning learned dictionaries
disp( 'Loading the overcomplete dictionary of permeability and porosity')
load Yes2.out; %Permeability dictionary
load Yes2poro.out; %porosity dictionary
disp( 'Loading the overcomplete dictionary of signed distance of permeability
and porosity')
load Yes2signed.out; %permeability signed distance
load Yes2signedporo.out; %porosity signed distance
if method==15
load reali.out; %permeability realizations (3600*1500 (1500 realizations))
realis=reali;
end
%% The big history matching iterative loop will start here
for iyobo=1:alpha
fprintf('Now running the code for iteration %d .\n', iyobo);
%% Loading Porosity and Permeability ensemble files
disp(' load the permeability and porosity fields')
if iyobo==1

```

```

    disp( 'permeability loaded from initial ensemble')
load sgsimporo2.out; %initial porosity
load sgsim.out; %initial permeability
perm=reshape(sgsim,72000,N);
poro=reshape(sgsimporo2,72000,N);
else
    disp( 'permeability loaded from UPDATED ensemble')
    perm=reshape(mumyperm,72000,N);
    poro=reshape(mumyporo,72000,N);
end
cd(olddfoder) % setting original directory
%% Saving permeability and porosity files
for i=1:N %list of folders
    f = 'MASTER';
    folder = strcat(f, sprintf('%.5d',i));

    cd(folder) % changing directory
    PORO2=poro(:,i);
    PERMY2=perm(:,i);
    save('PERMY2.GRDECL','PERMY2','-ascii');
    save('PORO2.GRDECL','PORO2','-ascii');
    cd(olddfoder) % returning to original cd
end

%% Inserting KEYWORDS PORO and PERMY

parfor i=1:N %list of folders
    f = 'MASTER';
    folder = strcat(f, sprintf('%.5d',i));
    cd(folder)
    CStr = regexp(fileread('PERMY2.GRDECL'), char(10), 'split');
    CStr2 = strrep(CStr, 'toReplace', 'Replacement');
    CStr2 = cat(2, {'PERMY'}, CStr2(1:end));
    CStr2 = cat(2, CStr2(1:end), {'/'});
    FID = fopen('PERMY2.GRDECL', 'w');
    if FID < 0, error('Cannot open file'); end
    fprintf(FID, '%s\n', CStr2{:});
    fclose(FID);
    CStr = regexp(fileread('PORO2.GRDECL'), char(10), 'split');
    CStr2 = strrep(CStr, 'toReplace', 'Replacement');
    CStr2 = cat(2, {'PORO'}, CStr2(1:end));
    CStr2 = cat(2, CStr2(1:end), {'/'});
    FID = fopen('PORO2.GRDECL', 'w');
    if FID < 0, error('Cannot open file'); end
    fprintf(FID, '%s\n', CStr2{:});
    fclose(FID);
    cd(olddfoder) % setting original directory
end

%% Running the Eclipse Simulations
disp( 'Solve the Non-Linear fluid flow Forward Problem' )
cd(olddfoder) % setting original directory
parfor i=1:N %list of folders
    f = 'MASTER';
    folder = strcat(f, sprintf('%.5d',i));
    cd(folder)
    fid = fopen('MASTER0.bat', 'w');
    fprintf(fid, '@ECHO OFF\n');
    % fprintf(fid,'SET SLBSLS_LICENSE_FILE=27008@eclipse.cc.ic.ac.uk\n');
    fprintf(fid,'SET SLBSLS_LICENSE_FILE=27000@10.99.15.78\n');
    fprintf(fid, '@ECHO OFF\n');
    fprintf(fid,['c:\\\\ecl\\\\macros\\\\$eclipse ', 'MASTER0'], '\n');
    fclose(fid);
    system('MASTER0.bat')
    cd(olddfoder) % setting original directory
end
disp(' plot production profile')
N=100;

```

```

oldfolder=cd;
cd(oldfolder) % setting original directory
%% Plot the Production profile of ensemble
disp(' start the plotting ');
for i=1:N %list of folders
f = 'MASTER';
folder = strcat(f, sprintf('%.5d',i));
%folder=oldfolder;
cd(folder);
%Saturation data lines [2939-5206]
A1 = importdata('MASTER0.RSM',' ',7);
A2 = importdata('MASTER0.RSM',' ',50);
A3 = importdata('MASTER0.RSM',' ',93);
A4 = importdata('MASTER0.RSM',' ',136);
A1=A1.data;
A2=A2.data;
A3=A3.data;
A4=A4.data;
WOPR1=A1(:,3);
WOPR2=A1(:,4);
WOPR3=A1(:,5);
WOPR4=A1(:,6);
Time=A1(:,1);
WWCT1=A2(:,2);
WWCT2=A2(:,3);
WWCT3=A2(:,4);
WWCT4=A2(:,5);
BHP1=A3(:,5);
BHP2=A3(:,6);
BHP3=A3(:,7);
BHP4=A3(:,8);
GORP1=A3(:,9);
GORP2=A3(:,10);
GORP3=A4(:,2);
GORP4=A4(:,3);
FOE=A4(:,8);
%Saturation
WOPRA(:,i)=WOPR1;
WOPRB(:,i)=WOPR2;
WOPRC(:,i)=WOPR3;
WOPRD(:,i)=WOPR4;
WCTA(:,i)=WWCT1;
WCTB(:,i)=WWCT2;
WCTC(:,i)=WWCT3;
WCTD(:,i)=WWCT4;
BHPA(:,i)=BHP1;
BHPB(:,i)=BHP2;
BHPC(:,i)=BHP3;
BHPD(:,i)=BHP4;
GORA(:,i)=GORP1;
GORB(:,i)=GORP2;
GORC(:,i)=GORP3;
GORD(:,i)=GORP4;
FOEA(:,i)=FOE;
cd(oldfolder);
end
cd(oldfolder) % returning to original directory
%Import true production data
True= importdata('Real.RSM',' ',7);
True2= importdata('Real.RSM',' ',50);
True3= importdata('Real.RSM',' ',93);
True4= importdata('Real.RSM',' ',136);
True=True.data;
True2=True2.data;
True3=True3.data;
True4=True4.data;

```

```

TO1=True(:,3);
TO2=True(:,4);
TO3=True(:,5);
TO4=True(:,6);
TW1=True2(:,2);
TW2=True2(:,3);
TW3=True2(:,4);
TW4=True2(:,5);
TP1=True3(:,5);
TP2=True3(:,6);
TP3=True3(:,7);
TP4=True3(:,8);
TG1=True3(:,9);
TG2=True3(:,10);
TG3=True4(:,2);
TG4=True4(:,3);
TFOE=True4(:,8)
grey = [0.4,0.4,0.4];
linecolor1 = colordg(4);
%% Plot for oil production rates
figure()
%subplot(2,2,1)
plot(Time,WOPRA(:,1:N),'Color',linecolor1,'LineWidth',2)
xlabel('Time (days)', 'FontName','Helvetica', 'FontSize', 13);
ylabel('Q_o(Sm^3/day)', 'FontName','Helvetica', 'FontSize', 13);
ylim([0 25000])
title('Producer 1','FontName','Helvetica', 'FontSize', 13)
a = get(gca,'Children');
hold on
plot(Time,TO1,'r','LineWidth',2)
b = get(gca,'Children');
set(gca, 'FontName','Helvetica', 'FontSize', 13)
set(gcf,'color','white')
line([2500 2500], [0 25000],'Color','black','LineStyle','--')
h = [b;a];
legend(h,'True model','Realisations','location','northeast');
hold off
saveas(gcf,sprintf('PRO1_OIL_iter%d.fig',iyobo))
close.figure()
%subplot(2,2,2)
figure()
plot(Time,WOPRB(:,1:N),'Color',linecolor1,'LineWidth',2)
xlabel('Time (days)', 'FontName','Helvetica', 'FontSize', 13);
ylabel('Q_o(Sm^3/day)', 'FontName','Helvetica', 'FontSize', 13);
ylim([0 25000])
title('Producer 2','FontName','Helvetica', 'FontSize', 13)
a = get(gca,'Children');
hold on
plot(Time,TO2,'r','LineWidth',2)
b = get(gca,'Children');
set(gca, 'FontName','Helvetica', 'FontSize', 13)
set(gcf,'color','white')
line([2500 2500], [0 25000],'Color','black','LineStyle','--')
h = [b;a];
legend(h,'True model','Realisations','location','northeast');
hold off
saveas(gcf,sprintf('PRO2_OIL_iter%d.fig',iyobo))
close.figure()

figure()
%subplot(2,2,3)
plot(Time,WOPRC(:,1:N),'Color',linecolor1,'LineWidth',2)
xlabel('Time (days)', 'FontName','Helvetica', 'FontSize', 13);
ylabel('Q_o(Sm^3/day)', 'FontName','Helvetica', 'FontSize', 13);
ylim([0 25000])
title('Producer 3','FontName','Helvetica', 'FontSize', 13)

```

```

a = get(gca, 'Children');
hold on
plot(Time,T03,'r','LineWidth',2)
b = get(gca, 'Children');
set(gca, 'FontName','Helvetica', 'FontSize', 13)
set(gcf,'color','white')
line([2500 2500], [0 25000], 'Color','black','LineStyle','--')
h = [b;a];
legend(h,'True model','Realisations','location','northeast');
hold off
saveas(gcf,sprintf('PRO3_OIL_iter%d.fig',iyobo))
close(figure)
figure()
%subplot(2,2,4)
plot(Time,WOPRD(:,1:N),'Color',linecolor1,'LineWidth',2)
xlabel('Time (days)', 'FontName','Helvetica', 'FontSize', 13);
ylabel('Q_o(Sm^3/day)', 'FontName','Helvetica', 'FontSize', 13);
ylim([0 25000])
title('Producer 4','FontName','Helvetica', 'FontSize', 13)
a = get(gca, 'Children');
hold on
plot(Time,T04,'r','LineWidth',2)
b = get(gca, 'Children');
set(gca, 'FontName','Helvetica', 'FontSize', 13)
set(gcf,'color','white')
line([2500 2500], [0 25000], 'Color','black','LineStyle','--')
h = [b;a];
legend(h,'True model','Realisations','location','northeast');
hold off
saveas(gcf,sprintf('PRO4_OIL_iter%d.fig',iyobo))
close(figure)
%% Plot for water cut
figure()
%subplot(2,2,1)
plot(Time,WCTA(:,1:N),'Color',linecolor1,'LineWidth',2)
xlabel('Time (days)', 'FontName','Helvetica', 'FontSize', 13);
ylabel('Water cut', 'FontName','Helvetica', 'FontSize', 13);
title('Producer 1','FontName','Helvetica', 'FontSize', 13)
a = get(gca, 'Children');
hold on
plot(Time,TW1,'r','LineWidth',2)
b = get(gca, 'Children');
set(gca, 'FontName','Helvetica', 'FontSize', 13)
set(gcf,'color','white')
line([2500 2500], [0 1], 'Color','black','LineStyle','--')
h = [b;a];
legend(h,'True model','Realisations','location','northeast');
hold off
saveas(gcf,sprintf('PRO1_WATER_iter%d.fig',iyobo))
close(figure)
figure()
%subplot(2,2,2)
plot(Time,WCTB(:,1:N),'Color',linecolor1,'LineWidth',2)
xlabel('Time (days)', 'FontName','Helvetica', 'FontSize', 13);
ylabel('Water cut', 'FontName','Helvetica', 'FontSize', 13);
title('Producer 2','FontName','Helvetica', 'FontSize', 13)
a = get(gca, 'Children');
hold on
plot(Time,TW2,'r','LineWidth',2)
b = get(gca, 'Children');
set(gca, 'FontName','Helvetica', 'FontSize', 13)
set(gcf,'color','white')
line([2500 2500], [0 1], 'Color','black','LineStyle','--')
h = [b;a];
legend(h,'True model','Realisations','location','northeast');
hold off
saveas(gcf,sprintf('PRO2_WATER_iter%d.fig',iyobo))

```

```

close(figure)
figure()
%subplot(2,2,3)
plot(Time,WCTC(:,1:N),'Color',linecolor1,'LineWidth',2)
xlabel('Time (days)', 'FontName','Helvetica', 'FontSize', 13);
ylabel('Water cut', 'FontName','Helvetica', 'FontSize', 13);
title('Producer 3', 'FontName','Helvetica', 'FontSize', 13)
a = get(gca,'Children');
hold on
plot(Time,TW3,'r','LineWidth',2)
b = get(gca,'Children');
set(gca, 'FontName','Helvetica', 'FontSize', 13)
set(gcf,'color','white')
line([2500 2500], [0 1],'Color','black','LineStyle','--')
h = [b;a];
legend(h,'True model','Realisations','location','northeast');
hold off
saveas(gcf,sprintf('PRO3_WATER_iter%d.fig',iyobo))
close(figure)
figure()
plot(Time,WCTD(:,1:N),'Color',linecolor1,'LineWidth',2)
xlabel('Time (days)', 'FontName','Helvetica', 'FontSize', 13);
ylabel('Water cut', 'FontName','Helvetica', 'FontSize', 13);
title('Producer 4', 'FontName','Helvetica', 'FontSize', 13)
a = get(gca,'Children');
hold on
plot(Time,TW4,'r','LineWidth',2)
b = get(gca,'Children');
set(gca, 'FontName','Helvetica', 'FontSize', 13)
set(gcf,'color','white')
line([2500 2500], [0 1],'Color','black','LineStyle','--')
h = [b;a];
legend(h,'True model','Realisations','location','northeast');
hold off
saveas(gcf,sprintf('PRO4_WATER_iter%d.fig',iyobo))
close(figure)
%% Plot for BHP
figure()
plot(Time,BHPA(:,1:N),'Color',linecolor1,'LineWidth',2)
xlabel('Time (days)', 'FontName','Helvetica', 'FontSize', 13);
ylabel('BHP(BARSA)', 'FontName','Helvetica', 'FontSize', 13);
title('Injector 1', 'FontName','Helvetica', 'FontSize', 13)
a = get(gca,'Children');
hold on
plot(Time,TP1,'r','LineWidth',2)
b = get(gca,'Children');
set(gca, 'FontName','Helvetica', 'FontSize', 13)
set(gcf,'color','white')
line([2500 2500], [0 500],'Color','black','LineStyle','--')
h = [b;a];
legend(h,'True model','Realisations','location','northeast');
hold off
%saveas(gcf,'inj1_BHP','epsc')
saveas(gcf,sprintf('inj1_BHP_iter%d.fig',iyobo))
close(figure)
figure()
plot(Time,BHPB(:,1:N),'Color',linecolor1,'LineWidth',2)
xlabel('Time (days)', 'FontName','Helvetica', 'FontSize', 13);
ylabel('BHP(BARSA)', 'FontName','Helvetica', 'FontSize', 13);
title('Injector 2', 'FontName','Helvetica', 'FontSize', 13)
a = get(gca,'Children');
hold on
plot(Time,TP2,'r','LineWidth',2)
b = get(gca,'Children');
set(gca, 'FontName','Helvetica', 'FontSize', 13)
set(gcf,'color','white')
line([2500 2500], [0 500],'Color','black','LineStyle','--')

```

```

h = [b;a];
legend(h,'True model','Realisations','location','northeast');
hold off
saveas(gcf,sprintf('inj2_BHP_iter%d.fig',iyobo))
close(figure)
figure()
plot(Time,BHPC(:,1:N),'Color',linecolor1,'LineWidth',2)
xlabel('Time (days)', 'FontName', 'Helvetica', 'FontSize', 13);
ylabel('BHP(BARSA)', 'FontName', 'Helvetica', 'FontSize', 13);
title('Injector 3', 'FontName', 'Helvetica', 'FontSize', 13)
a = get(gca,'Children');
hold on
plot(Time,TP3,'r','LineWidth',2)
b = get(gca,'Children');
set(gca, 'FontName', 'Helvetica', 'FontSize', 13)
set(gcf,'color','white')
line([2500 2500], [0 500], 'Color','black','LineStyle','--')
h = [b;a];
legend(h,'True model','Realisations','location','northeast');
hold off
saveas(gcf,sprintf('inj3_BHP_iter%d.fig',iyobo))
close(figure)
figure()
plot(Time,BHPD(:,1:N),'Color',linecolor1,'LineWidth',2)
xlabel('Time (days)', 'FontName', 'Helvetica', 'FontSize', 13);
ylabel('BHP(BARSA)', 'FontName', 'Helvetica', 'FontSize', 13);
title('Injector 4', 'FontName', 'Helvetica', 'FontSize', 13)
a = get(gca,'Children');
hold on
plot(Time,TP4,'r','LineWidth',2)
b = get(gca,'Children');
set(gca, 'FontName', 'Helvetica', 'FontSize', 13)
set(gcf,'color','white')
line([2500 2500], [0 500], 'Color','black','LineStyle','--')
h = [b;a];
legend(h,'True model','Realisations','location','northeast');
hold off
saveas(gcf,sprintf('inj4_BHP_iter%d.fig',iyobo))
close(figure)

%% Plot for GOR
figure()
plot(Time,GORA(:,1:N),'Color',linecolor1,'LineWidth',2)
xlabel('Time (days)', 'FontName', 'Helvetica', 'FontSize', 13);
ylabel('Gas oil ratio(Sm^3/Sm^3)', 'FontName', 'Helvetica', 'FontSize', 13);
title('Gas oil ratio for producer 1', 'FontName', 'Helvetica', 'FontSize', 13)
a = get(gca,'Children');
hold on
plot(Time,TG1,'r','LineWidth',2)
b = get(gca,'Children');
set(gca, 'FontName', 'Helvetica', 'FontSize', 13)
set(gcf,'color','white')
line([2500 2500], [0 1000], 'Color','black','LineStyle','--')
h = [b;a];
legend(h,'True model','Realisations','location','northeast');
hold off
saveas(gcf,sprintf('PRO1_GOR_iter%d.fig',iyobo))
close(figure)
figure()
plot(Time,GORB(:,1:N),'Color',linecolor1,'LineWidth',2)
xlabel('Time (days)', 'FontName', 'Helvetica', 'FontSize', 13);
ylabel('Gas oil ratio(Sm^3/Sm^3)', 'FontName', 'Helvetica', 'FontSize', 13);
title('Gas oil ratio for producer 2', 'FontName', 'Helvetica', 'FontSize', 13)
a = get(gca,'Children');
hold on
plot(Time,TG2,'r','LineWidth',2)
b = get(gca,'Children');

```

```

set(gca, 'FontName','Helvetica', 'FontSize', 13)
set(gcf,'color','white')
line([2500 2500], [0 1000], 'Color','black','LineStyle','--')
h = [b;a];
legend(h,'True model','Realisations','location','northeast');
hold off
saveas(gcf,sprintf('PRO2_GOR_iter%d.fig',iyobo))
close(figure)

figure()
plot(Time,GORC(:,1:N),'Color',linecolor1,'LineWidth',2)
xlabel('Time (days)', 'FontName','Helvetica', 'FontSize', 13);
ylabel('Gas oil ratio( $S_m^{3}/S_m^{3}$ )', 'FontName','Helvetica', 'FontSize', 13);
title('Gas oil ratio for producer 3', 'FontName','Helvetica', 'FontSize', 13)
a = get(gca,'Children');
hold on
plot(Time,TG3,'r','LineWidth',2)
b = get(gca,'Children');
set(gca, 'FontName','Helvetica', 'FontSize', 13)
set(gcf,'color','white')
line([2500 2500], [0 1000], 'Color','black','LineStyle','--')
h = [b;a];
legend(h,'True model','Realisations','location','northeast');
hold off
saveas(gcf,sprintf('PRO3_GOR_iter%d.fig',iyobo))
close(figure)

figure()
plot(Time,GORD(:,1:N),'Color',linecolor1,'LineWidth',2)
xlabel('Time (days)', 'FontName','Helvetica', 'FontSize', 13);
ylabel('Gas oil ratio( $S_m^{3}/S_m^{3}$ )', 'FontName','Helvetica', 'FontSize', 13);
title('Gas oil ratio for producer 4', 'FontName','Helvetica', 'FontSize', 13)
a = get(gca,'Children');
hold on
plot(Time,TG4,'r','LineWidth',2)
b = get(gca,'Children');
set(gca, 'FontName','Helvetica', 'FontSize', 13)
set(gcf,'color','white')
line([2500 2500], [0 1000], 'Color','black','LineStyle','--')
h = [b;a];
legend(h,'True model','Realisations','location','northeast');
hold off
saveas(gcf,sprintf('PRO4_GOR_iter%d.fig',iyobo))
close(figure)
figure()
plot(Time,FOEA(:,1:N),'Color',linecolor1,'LineWidth',2)
xlabel('Time (days)', 'FontName','Helvetica', 'FontSize', 13);
ylabel('Oil recovery ratio', 'FontName','Helvetica', 'FontSize', 13);
title('Field oil recovery ratio', 'FontName','Helvetica', 'FontSize', 13)
a = get(gca,'Children');
hold on
plot(Time,TFOE,'r','LineWidth',2)
b = get(gca,'Children');
set(gca, 'FontName','Helvetica', 'FontSize', 13)
set(gcf,'color','white')
line([2500 2500], [0 1], 'Color','black','LineStyle','--')
h = [b;a];
legend(h,'True model','Realisations','location','northeast');
hold off
saveas(gcf,sprintf('Oilrecovery_iter%d.fig',iyobo))
%% Get the Norm to production data
disp( 'Get the Norm to production data mismatch')
close(figure)
for i=1:N
    EWOP1(i,:)=immse(WOPRA(:,i),TO1);
    EWOP2(i,:)=immse(WOPRB(:,i),TO2);
    EWOP3(i,:)=immse(WOPRC(:,i),TO3);

```

```

EWOP4(i,:)=immse(WOPRD(:,i),TO4);
EWCT1(i,:)=immse(WCTA(:,i),TW1);
EWCT2(i,:)=immse(WCTB(:,i),TW2);
EWCT3(i,:)=immse(WCTC(:,i),TW3);
EWCT4(i,:)=immse(WCTD(:,i),TW4);
EBHP1(i,:)=immse(BHPA(:,i),TP1);
EBHP2(i,:)=immse(BHPB(:,i),TP2);
EBHP3(i,:)=immse(BHPC(:,i),TP3);
EBHP4(i,:)=immse(BHPD(:,i),TP4);
EGORP1(i,:)=immse(GORA(:,i),TG1);
EGORP2(i,:)=immse(GORB(:,i),TG2);
EGORP3(i,:)=immse(GORC(:,i),TG3);
EGORP4(i,:)=immse(GORD(:,i),TG4);
end
TOTALERROR=ones(N,1);
TOTALERROR=(EWOP1./std(TO1))+(EWOP2./std(TO2))+(EWOP3./std(TO3))+...
(EWOP4./std(TO4))+(EWCT1./std(TW1))+(EWCT2./std(TW2))...
+(EWCT3./std(TW3))+(EWCT4./std(TW4))+(EBHP1./std(TP1))...
+(EBHP2./std(TP2))+(EBHP3./std(TP3))+(EBHP4./std(TP4))...
+(EGORP1./std(TG1))+(EGORP2./std(TG2))+(EGORP3./std(TG3))+(EGORP4./std(TG4));
TOTALERROR=TOTALERROR./36;
jj=min(TOTALERROR);
index = TOTALERROR;
bestnorm = find(index == min(index));
%Pssim = Pnew(:,bestssim); %best due to ssim
fprintf('The best Norm Realization is number %i with value %4.4f
\n',bestnorm,jj);
% JOYLINE=[1:100];
% figure()
%bar(JOYLINE,TOTALERROR);
reali=[1:N];
figure()
bar(reali,index,'cyan');
xlabel('Realizations', 'FontName','Helvetica', 'FontSize', 13);
ylabel('RMSE value', 'FontName','Helvetica', 'FontSize', 13);
title('Cost function for Realizations','FontName','Helvetica', 'FontSize', 13)
set(gcf,'color', 'white');
hold on
scatter(reali,index,'black','filled');
xlabel('Realizations', 'FontName','Helvetica', 'FontSize', 13)
ylabel('RMSE value', 'FontName','Helvetica', 'FontSize', 13)
hold off
xlim([1,N]);
saveas(gcf,sprintf('RMS_iter%d.fig',iyobo))
close();
disp(' program almost executed ');
decreasingnorm(:,iyobo)=index;
%% Get simulated files for all the time steps
disp( 'Get the simulated files for all the time step')
N=100;
oldfolder=cd;
cd(oldfolder) % setting original directory
overallsim=zeros(17,history,N);
for ii=1:N %list of folders
    f = 'MASTER';
    folder = strcat(f, sprintf('%5d',ii));
    cd(folder)
    True= importdata('MASTER0.RSM',' ',7);
    A2 = importdata('MASTER0.RSM',' ',50);
    A3 = importdata('MASTER0.RSM',' ',93);
    A4 = importdata('MASTER0.RSM',' ',136);
    True=True.data;
    A2=A2.data;
    A3=A3.data;
    A4=A4.data;

```

```

TO1=True(:,3);
TO2=True(:,4);
TO3=True(:,5);
TO4=True(:,6);
    WWCT1=A2(:,2);
    WWCT2=A2(:,3);
    WWCT3=A2(:,4);
    WWCT4=A2(:,5);
    BHP1=A3(:,5);
    BHP2=A3(:,6);
    BHP3=A3(:,7);
    BHP4=A3(:,8);
    GORP1=A3(:,9);
    GORP2=A3(:,10);
    GORP3=A4(:,2);
    GORP4=A4(:,3);
    FOE=A4(:,8);
for i=1:history
obs=zeros(17,1);
obs(1,:)=TO1(i,:);
obs(2,:)=TO2(i,:);
obs(3,:)=TO3(i,:);
obs(4,:)=TO4(i,:);
obs(5,:)=WWCT1(i,:);
obs(6,:)=WWCT2(i,:);
obs(7,:)=WWCT3(i,:);
obs(8,:)=WWCT4(i,:);
obs(9,:)=BHP1(i,:);
obs(10,:)=BHP2(i,:);
obs(11,:)=BHP3(i,:);
obs(12,:)=BHP4(i,:);
obs(13,:)=GORP1(i,:);
obs(14,:)=GORP2(i,:);
obs(15,:)=GORP3(i,:);
obs(16,:)=GORP4(i,:);
obs(17,:)=FOE(i,:);
observationsim(:,i)=obs;
end
overallsim(:,:,ii)=observationsim;
cd(olddfolder) % returning to original directory
end
cd(olddfolder) % returning to original directory
[SEn83,PEn83]=getstatesall(N,history);
%% Enter the assimilation loop
disp('now entering the assimilation loop')
switch method
    case 1
        disp( 'method 1 specified-standard ESMDA')
        [mumyperm,mumyporo]=main_ESMDA(N,tol,observation,overallsim,rossmary,rossmaryp
oro,perm,poro,history,alpha);
    case 2
        disp( 'method 2 specified-ESMDA and Levelset')
        [mumyperm,mumyporo]=main_Levelset(nx,ny,nz,N,tol,observation,overallsim,rossma
ry,rossmaryporo,perm,poro,history,alpha);
    case 3
        disp( 'method 3 specified-DCT')
        [mumyperm,mumyporo]=main_DCT(N,tol,observation,overallsim,rossmary,rossmarypor
o,perm,poro,history,alpha);
    case 4
        disp( 'method 4 specified-Sparsity')
        [mumyperm,mumyporo]=main_sparsity(N,tol,observation,overallsim,rossmary,rossma
ryporo,perm,poro,history,alpha);
    case 5
        disp( 'method 5 specified-Sparsity and Levelset')
        [mumyperm,mumyporo]=SELE_PhD(nx,ny,nz,Yes2,Yes2poro,N,tol,observation,overalls
im,rossmary,rossmaryporo,perm,poro,history,alpha);
    case 6

```

```

    disp( 'method 6 specified-DCT and Level set')
    [mumyperm,mumyporo]=main_DCT_Levelset(nx,ny,nz,N,tol,observation,overallsim,ro
ssmary,rossmaryporo,perm,poro,history,alpha);
    case 7
        disp( 'method 7 specified- DCT and Level set 2')
        [mumyperm,mumyporo]=main_DCT_LS2(nx,ny,nz,N,tol,observation,overallsim,rossmar
y,rossmaryporo,perm,poro,history,alpha);
    case 8
        disp( 'method 8 specified-Sparsity and LS')
        [mumyperm,mumyporo]=main_sparsity_LS(Yes2signed,Yes2signedporo,nx,ny,nz,Yes2,Y
es2poro,N,tol,observation,overallsim,rossmary,rossmaryporo,perm,poro,history,a
lpha);
    case 9
        disp( 'method 9 specified-Levelset upadate with Boundary')
        [mumyperm,mumyporo]=main_Levelset_Boundary(nx,ny,nz,N,tol,observation,overall
sim,rossmary,rossmaryporo,perm,poro,history,alpha);
    case 10
        disp( 'method 10 specified-Velocity and LS')
        [mumyperm,mumyporo]=main_Velocity_LS(nx,ny,nz,N,tol,observation,overallsim,ros
smary,rossmaryporo,perm,poro,history,alpha);
    case 11
        disp( 'method 11 specified-Localization with ESMDA')
        [mumyperm,mumyporo]=main_ESMDA_Localization(N,tol,observation,overallsim,ros
smary,rossmaryporo,perm,poro,history,alpha);
    case 12
        disp( 'method 12 specified-Localization with ESMDA and Levelset')
        [mumyperm,mumyporo]=main_Levelset_Cov(nx,ny,nz,N,tol,observation,overallsim,ro
ssmary,rossmaryporo,perm,poro,history,alpha);
    case 13
        disp( 'method 13 specified-Localization with ESMDA and
Levelset,permeability only vale in states')
        [mumyperm,mumyporo]=main_Levelset_Cov_Perm(nx,ny,nz,N,tol,observation,overall
sim,rossmary,rossmaryporo,perm,history,alpha);
    case 14
        disp( 'method 14 specified-Localization with ESMDA-Levelset-supervised
learning')
        [mumyperm,mumyporo]=main_supervised(nx,ny,nz,N,tol,observation,overallsim,ross
mary,rossmaryporo,perm,poro,history,alpha);
    case 15
        disp( 'method 15 specified-Dynamic Sparsity update unsupervised learning')
        [mumyperm,mumyporo]=main_dynamicsparsity(nx,ny,nz,N,tol,observation,overallsim
,rossmary,rossmaryporo,perm,history,alpha,realis);
    otherwise
        disp('method not specified correctly')
end

perm=reshape(mumyperm,72000,N);
poro=reshape(mumyporo,72000,N);
fprintf('Finished Iteration %d .\n', iyobo);
end
%% Exit the loop
disp( 'now run the code after the last Iteration to see how good')
%% Loading Porosity and Permeability ensemble files
disp(' use the permeability and porosity fields after Last iteration')
cd(oldfolder) % setting original directory

%% Saving POROVANCOUVER and KVANCOUVE
for i=1:N %list of folders
    f = 'MASTER';
    folder = strcat(f, sprintf('.%5d',i))
    cd(folder) % changing directory

    PORO2=poro(:,i);
    PERMY2=perm(:,i);
    save('PERMY2.GRDECL','PERMY2','-ascii');
    save('PORO2.GRDECL','PORO2','-ascii');
    cd(oldfolder) % returning to original c

```

```

end
%% Inserting KEYWORDS PORO and PERMY
parfor i=1:N %list of folders
    f = 'MASTER';
    folder = strcat(f, sprintf('%.5d',i));
    cd(folder)
CStr = regexp(fileread('PERMY2.GRDECL'), char(10), 'split');
CStr2 = strrep(CStr, 'toReplace', 'Replacement');
CStr2 = cat(2, {'PERMY'}, CStr2(1:end));
CStr2 = cat(2, CStr2(1:end), {'/'});
FID = fopen('PERMY2.GRDECL', 'w');
if FID < 0, error('Cannot open file'); end
fprintf(FID, '%s\n', CStr2{:});
fclose(FID);
CStr = regexp(fileread('PORO2.GRDECL'), char(10), 'split');
CStr2 = strrep(CStr, 'toReplace', 'Replacement');
CStr2 = cat(2, {'PORO'}, CStr2(1:end));
CStr2 = cat(2, CStr2(1:end), {'/'});
FID = fopen('PORO2.GRDECL', 'w');
if FID < 0, error('Cannot open file'); end
fprintf(FID, '%s\n', CStr2{:});
fclose(FID);
cd(olddfoder) % setting original directory
end
%% Running Simulations
disp( 'Solve the Non-Linear fluid flow Forward Problem' )
cd(olddfoder) % setting original directory
parfor i=1:N %list of folders
    f = 'MASTER';
    folder = strcat(f, sprintf('%.5d',i));
    cd(folder)
    fid = fopen('MASTER0.bat', 'w');
    fprintf(fid, '@ECHO OFF\n');
    % fprintf(fid,'SET SLBSLS_LICENSE_FILE=27008@eclipse.cc.ic.ac.uk\n');
    fprintf(fid, 'SET SLBSLS_LICENSE_FILE=27000@10.99.15.78\n');
    fprintf(fid, '@ECHO OFF\n');
    fprintf(fid, ['c:\\\\ecl\\\\macros\\\\$eclipse ', 'MASTER0'], '\n');
    fclose(fid);
    system('MASTER0.bat')
    cd(olddfoder) % setting original directory
end
disp(' plot production profile')
N=100;
olddfoder=cd;
cd(olddfoder) % setting original directory
%% Plot the Production profile of ensemble
disp(' start the plotting ');
for i=1:N %list of folders
    f = 'MASTER';
    folder = strcat(f, sprintf('%.5d',i));
    %folder=olddfoder;
    %cd 'C:\Work\GSLIB\sgsim\EnKFMATLABRun'
    cd(folder)

    %Saturation data lines [2939-5206]
    A1 = importdata('MASTER0.RSM', ' ', 7);
    A2 = importdata('MASTER0.RSM', ' ', 50);
    A3 = importdata('MASTER0.RSM', ' ', 93);
    A4 = importdata('MASTER0.RSM', ' ', 136);
    A1=A1.data;
    A2=A2.data;
    A3=A3.data;
    A4=A4.data;
    WOPR1=A1(:,3);
    WOPR2=A1(:,4);
    WOPR3=A1(:,5);

```

```

WOPR4=A1 (:, 6);
Time=A1 (:, 1);
WWCT1=A2 (:, 2);
WWCT2=A2 (:, 3);
WWCT3=A2 (:, 4);
WWCT4=A2 (:, 5);
BHP1=A3 (:, 5);
BHP2=A3 (:, 6);
BHP3=A3 (:, 7);
BHP4=A3 (:, 8);
GORP1=A3 (:, 9);
GORP2=A3 (:, 10);
GORP3=A4 (:, 2);
GORP4=A4 (:, 3);
FOE=A4 (:, 8);
WOPRA (:, i)=WOPR1;
WOPRB (:, i)=WOPR2;
WOPRC (:, i)=WOPR3;
WOPRD (:, i)=WOPR4;
WCTA (:, i)=WWCT1;
WCTB (:, i)=WWCT2;
WCTC (:, i)=WWCT3;
WCTD (:, i)=WWCT4;
BHPA (:, i)=BHP1;
BHPB (:, i)=BHP2;
BHPC (:, i)=BHP3;
BHPD (:, i)=BHP4;
GORA (:, i)=GORP1;
GORB (:, i)=GORP2;
GORC (:, i)=GORP3;
GORD (:, i)=GORP4;
FOEA (:, i)=FOE;
cd(olddfolder);
end
cd(olddfolder) % returning to original directory
%Import true production data
True= importdata('Real.RSM',' ',7);
True2= importdata('Real.RSM',' ',50);
True3= importdata('Real.RSM',' ',93);
True4= importdata('Real.RSM',' ',136);
True=True.data;
True2=True2.data;
True3=True3.data;
True4=True4.data;
TO1=True (:, 3);
TO2=True (:, 4);
TO3=True (:, 5);
TO4=True (:, 6);

TW1=True2 (:, 2);
TW2=True2 (:, 3);
TW3=True2 (:, 4);
TW4=True2 (:, 5);
TP1=True3 (:, 5);
TP2=True3 (:, 6);
TP3=True3 (:, 7);
TP4=True3 (:, 8);
TG1=True3 (:, 9);
TG2=True3 (:, 10);
TG3=True4 (:, 2);
TG4=True4 (:, 3);
TFOE=True4 (:, 8);
grey = [0.4,0.4,0.4];
linecolor1 = colordg(4);
%% Plot for oil production rates
figure()
plot(Time,WOPRA (:, 1:N), 'Color', linecolor1, 'LineWidth', 2)

```

```

xlabel('Time (days)', 'FontName', 'Helvetica', 'FontSize', 13);
ylabel('Q_o(Sm^3/day)', 'FontName', 'Helvetica', 'FontSize', 13);
ylim([0 25000])
title('Producer 1', 'FontName', 'Helvetica', 'FontSize', 13)
a = get(gca, 'Children');
hold on
plot(Time, TO1, 'r', 'LineWidth', 2)
b = get(gca, 'Children');
set(gca, 'FontName', 'Helvetica', 'FontSize', 13)
set(gcf, 'color', 'white')
line([2500 2500], [0 25000], 'Color', 'black', 'LineStyle', '--')
h = [b;a];
legend(h, 'True model', 'Realisations', 'location', 'northeast');
hold off
saveas(gcf, 'PRO1_OILfinal', 'epsc')
saveas(gcf, 'PRO1_OILfinal', 'fig')
close(figure)
figure()
plot(Time, WOPRB(:,1:N), 'Color', linecolor1, 'LineWidth', 2)
xlabel('Time (days)', 'FontName', 'Helvetica', 'FontSize', 13);
ylabel('Q_o(Sm^3/day)', 'FontName', 'Helvetica', 'FontSize', 13);
ylim([0 25000])
title('Producer 2', 'FontName', 'Helvetica', 'FontSize', 13)
a = get(gca, 'Children');
hold on
plot(Time, TO2, 'r', 'LineWidth', 2)
b = get(gca, 'Children');
set(gca, 'FontName', 'Helvetica', 'FontSize', 13)
set(gcf, 'color', 'white')
line([2500 2500], [0 25000], 'Color', 'black', 'LineStyle', '--')
h = [b;a];
legend(h, 'True model', 'Realisations', 'location', 'northeast');
hold off
saveas(gcf, 'PRO2_OILfinal', 'epsc')
saveas(gcf, 'PRO2_OILfinal', 'fig')
close(figure)
figure()
plot(Time, WOPRC(:,1:N), 'Color', linecolor1, 'LineWidth', 2)
xlabel('Time (days)', 'FontName', 'Helvetica', 'FontSize', 13);
ylabel('Q_o(Sm^3/day)', 'FontName', 'Helvetica', 'FontSize', 13);
ylim([0 25000])
title('Producer 3', 'FontName', 'Helvetica', 'FontSize', 13)
a = get(gca, 'Children');
hold on
plot(Time, TO3, 'r', 'LineWidth', 2)
b = get(gca, 'Children');
set(gca, 'FontName', 'Helvetica', 'FontSize', 13)
set(gcf, 'color', 'white')
line([2500 2500], [0 25000], 'Color', 'black', 'LineStyle', '--')
h = [b;a];
legend(h, 'True model', 'Realisations', 'location', 'northeast');
hold off
saveas(gcf, 'PRO3_OILfinal', 'epsc')
saveas(gcf, 'PRO3_OILfinal', 'fig')
close(figure)
figure()
plot(Time, WOPRD(:,1:N), 'Color', linecolor1, 'LineWidth', 2)
xlabel('Time (days)', 'FontName', 'Helvetica', 'FontSize', 13);
ylabel('Q_o(Sm^3/day)', 'FontName', 'Helvetica', 'FontSize', 13);
ylim([0 25000])
title('Producer 4', 'FontName', 'Helvetica', 'FontSize', 13)
a = get(gca, 'Children');
hold on
plot(Time, TO4, 'r', 'LineWidth', 2)
b = get(gca, 'Children');
set(gca, 'FontName', 'Helvetica', 'FontSize', 13)
set(gcf, 'color', 'white')

```

```

line([2500 2500], [0 25000], 'Color','black','LineStyle','--')
h = [b;a];
legend(h,'True model','Realisations','location','northeast');
hold off
saveas(gcf,'PRO4_OILfinal','epsc')
saveas(gcf,'PRO4_OILfinal','fig')
close(figure)
figure()
plot(Time,WCTA(:,1:N),'Color',linecolor1,'LineWidth',2)
xlabel('Time (days)', 'FontName', 'Helvetica', 'FontSize', 13);
ylabel('Water cut', 'FontName', 'Helvetica', 'FontSize', 13);
title('Producer 1', 'FontName', 'Helvetica', 'FontSize', 13)
a = get(gca,'Children');
hold on
plot(Time,TW1,'r','LineWidth',2)
b = get(gca,'Children');
set(gca, 'FontName', 'Helvetica', 'FontSize', 13)
set(gcf,'color','white')
line([2500 2500], [0 1], 'Color','black','LineStyle','--')
h = [b;a];
legend(h,'True model','Realisations','location','northeast');
hold off
saveas(gcf,'PRO1_WATERfinal','epsc')
saveas(gcf,'PRO1_WATERfinal','fig')
close(figure)
figure()
plot(Time,WCTB(:,1:N),'Color',linecolor1,'LineWidth',2)
xlabel('Time (days)', 'FontName', 'Helvetica', 'FontSize', 13);
ylabel('Water cut', 'FontName', 'Helvetica', 'FontSize', 13);
title('Producer 2', 'FontName', 'Helvetica', 'FontSize', 13)
a = get(gca,'Children');
hold on
plot(Time,TW2,'r','LineWidth',2)
b = get(gca,'Children');
set(gca, 'FontName', 'Helvetica', 'FontSize', 13)
set(gcf,'color','white')
line([2500 2500], [0 1], 'Color','black','LineStyle','--')
h = [b;a];
legend(h,'True model','Realisations','location','northeast');
hold off
saveas(gcf,'PRO2_WATERfinal','epsc')
saveas(gcf,'PRO2_WATERfinal','fig')
close(figure)
figure()
plot(Time,WCTC(:,1:N),'Color',linecolor1,'LineWidth',2)
xlabel('Time (days)', 'FontName', 'Helvetica', 'FontSize', 13);
ylabel('Water cut', 'FontName', 'Helvetica', 'FontSize', 13);
title('Producer 3', 'FontName', 'Helvetica', 'FontSize', 13)
a = get(gca,'Children');
hold on
plot(Time,TW3,'r','LineWidth',2)
b = get(gca,'Children');
set(gca, 'FontName', 'Helvetica', 'FontSize', 13)
set(gcf,'color','white')
line([2500 2500], [0 1], 'Color','black','LineStyle','--')
h = [b;a];
legend(h,'True model','Realisations','location','northeast');
hold off
saveas(gcf,'PRO3_WATERfinal','epsc')
saveas(gcf,'PRO3_WATERfinal','fig')
close(figure)
figure()
plot(Time,WCTD(:,1:N),'Color',linecolor1,'LineWidth',2)
xlabel('Time (days)', 'FontName', 'Helvetica', 'FontSize', 13);
ylabel('Water cut', 'FontName', 'Helvetica', 'FontSize', 13);
title('Producer 4', 'FontName', 'Helvetica', 'FontSize', 13)
a = get(gca,'Children');

```

```

hold on
plot(Time,TW4,'r','LineWidth',2)
b = get(gca,'Children');
set(gca, 'FontName','Helvetica', 'FontSize', 13)
set(gcf,'color','white')
line([2500 2500], [0 1],'Color','black','LineStyle','--')
h = [b;a];
legend(h,'True model','Realisations','location','northeast');
hold off
saveas(gcf,'PRO4_WATERfinal','epsc')
saveas(gcf,'PRO4_WATERfinal','fig')
close.figure()
%% Plot for BHP
figure()
plot(Time,BHPA(:,1:N),'Color',linecolor1,'LineWidth',2)
xlabel('Time (days)', 'FontName','Helvetica', 'FontSize', 13);
ylabel('BHP(BARSA)', 'FontName','Helvetica', 'FontSize', 13);
title('Injector 1','FontName','Helvetica', 'FontSize', 13)
a = get(gca,'Children');
hold on
plot(Time,TP1,'r','LineWidth',2)
b = get(gca,'Children');
set(gca, 'FontName','Helvetica', 'FontSize', 13)
set(gcf,'color','white')
line([2500 2500], [0 500],'Color','black','LineStyle','--')
h = [b;a];
legend(h,'True model','Realisations','location','northeast');
hold off
saveas(gcf,'inj1_BHPfinal','epsc')
saveas(gcf,'inj1_BHPfinal','fig')
close.figure()
figure()
plot(Time,BHPB(:,1:N),'Color',linecolor1,'LineWidth',2)
xlabel('Time (days)', 'FontName','Helvetica', 'FontSize', 13);
ylabel('BHP(BARSA)', 'FontName','Helvetica', 'FontSize', 13);
title('Injector 2','FontName','Helvetica', 'FontSize', 13)
a = get(gca,'Children');
hold on
plot(Time,TP2,'r','LineWidth',2)
b = get(gca,'Children');
set(gca, 'FontName','Helvetica', 'FontSize', 13)
set(gcf,'color','white')
line([2500 2500], [0 500],'Color','black','LineStyle','--')
h = [b;a];
legend(h,'True model','Realisations','location','northeast');
hold off
saveas(gcf,'inj2_BHPfinal','epsc')
saveas(gcf,'inj2_BHPfinal','fig')
close.figure()
figure()
plot(Time,BHPC(:,1:N),'Color',linecolor1,'LineWidth',2)
xlabel('Time (days)', 'FontName','Helvetica', 'FontSize', 13);
ylabel('BHP(BARSA)', 'FontName','Helvetica', 'FontSize', 13);
title('Injector 3','FontName','Helvetica', 'FontSize', 13)
a = get(gca,'Children');
hold on
plot(Time,TP3,'r','LineWidth',2)
b = get(gca,'Children');
set(gca, 'FontName','Helvetica', 'FontSize', 13)
set(gcf,'color','white')
line([2500 2500], [0 500],'Color','black','LineStyle','--')
h = [b;a];
legend(h,'True model','Realisations','location','northeast');
hold off
saveas(gcf,'inj3_BHPfinal','epsc')
saveas(gcf,'inj3_BHPfinal','fig')
close.figure()

```

```

figure()
plot(Time,BHPD(:,1:N),'Color',linecolor1,'LineWidth',2)
xlabel('Time (days)', 'FontName','Helvetica', 'FontSize', 13);
ylabel('BHP(BARSA)', 'FontName','Helvetica', 'FontSize', 13);
title('Injector 4', 'FontName','Helvetica', 'FontSize', 13)
a = get(gca,'Children');
hold on
plot(Time,TP4,'r','LineWidth',2)
b = get(gca,'Children');
set(gca, 'FontName','Helvetica', 'FontSize', 13)
set(gcf,'color','white')
line([2500 2500], [0 500], 'Color','black','LineStyle','--')
h = [b;a];
legend(h,'True model','Realisations','location','northeast');
hold off
saveas(gcf,'inj4_BHPfinal','epsc')
saveas(gcf,'inj4_BHPfinal','fig')
close(figure)
%% Plot for GOR
figure()
plot(Time,GORA(:,1:N),'Color',linecolor1,'LineWidth',2)
xlabel('Time (days)', 'FontName','Helvetica', 'FontSize', 13);
ylabel('Gas oil ratio( $\text{Sm}^3/\text{Sm}^3$ )', 'FontName','Helvetica', 'FontSize', 13);
title('Gas oil ratio for producer 1', 'FontName','Helvetica', 'FontSize', 13)
a = get(gca,'Children');
hold on
plot(Time,TG1,'r','LineWidth',2)
b = get(gca,'Children');
set(gca, 'FontName','Helvetica', 'FontSize', 13)
set(gcf,'color','white')
line([2500 2500], [0 1000], 'Color','black','LineStyle','--')
h = [b;a];
legend(h,'True model','Realisations','location','northeast');
hold off
saveas(gcf,'PRO1_GORfinal','epsc')
saveas(gcf,'PRO1_GORfinal','fig')
close(figure)
figure()
plot(Time,GORB(:,1:N),'Color',linecolor1,'LineWidth',2)
xlabel('Time (days)', 'FontName','Helvetica', 'FontSize', 13);
ylabel('Gas oil ratio( $\text{Sm}^3/\text{Sm}^3$ )', 'FontName','Helvetica', 'FontSize', 13);
title('Gas oil ratio for producer 2', 'FontName','Helvetica', 'FontSize', 13)
a = get(gca,'Children');
hold on
plot(Time,TG2,'r','LineWidth',2)
b = get(gca,'Children');
set(gca, 'FontName','Helvetica', 'FontSize', 13)
set(gcf,'color','white')
line([2500 2500], [0 1000], 'Color','black','LineStyle','--')
h = [b;a];
legend(h,'True model','Realisations','location','northeast');
hold off
saveas(gcf,'PRO2_GORfinal','epsc')
saveas(gcf,'PRO2_GORfinal','fig')
close(figure)
figure()
plot(Time,GORC(:,1:N),'Color',linecolor1,'LineWidth',2)
xlabel('Time (days)', 'FontName','Helvetica', 'FontSize', 13);
ylabel('Gas oil ratio( $\text{Sm}^3/\text{Sm}^3$ )', 'FontName','Helvetica', 'FontSize', 13);
title('Gas oil ratio for producer 3', 'FontName','Helvetica', 'FontSize', 13)
a = get(gca,'Children');
hold on
plot(Time,TG3,'r','LineWidth',2)
b = get(gca,'Children');
set(gca, 'FontName','Helvetica', 'FontSize', 13)
set(gcf,'color','white')
line([2500 2500], [0 1000], 'Color','black','LineStyle','--')

```

```

h = [b;a];
legend(h,'True model','Realisations','location','northeast');
hold off
saveas(gcf,'PRO3_GORfinal','epsc')
saveas(gcf,'PRO3_GORfinal','fig')
close(figure)

figure()
plot(Time,GORD(:,1:N),'Color',linecolor1,'LineWidth',2)
xlabel('Time (days)', 'FontName', 'Helvetica', 'FontSize', 13);
ylabel('Gas oil ratio( $\text{Sm}^3/\text{Sm}^3$ )', 'FontName', 'Helvetica', 'FontSize', 13);
title('Gas oil ratio for producer 4', 'FontName', 'Helvetica', 'FontSize', 13)
a = get(gca,'Children');
hold on
plot(Time,TG4,'r','LineWidth',2)
b = get(gca,'Children');
set(gca, 'FontName','Helvetica', 'FontSize', 13)
set(gcf,'color','white')
line([2500 2500], [0 1000], 'Color','black','LineStyle', '--')
h = [b;a];
legend(h,'True model','Realisations','location','northeast');
hold off
saveas(gcf,'PRO4_GORfinal','epsc')
saveas(gcf,'PRO4_GORfinal','fig')
close(figure)
figure()
plot(Time,FOEA(:,1:N),'Color',linecolor1,'LineWidth',2)
xlabel('Time (days)', 'FontName', 'Helvetica', 'FontSize', 13);
ylabel('Oil recovery ratio', 'FontName', 'Helvetica', 'FontSize', 13);
title('Field oil recovery ratio', 'FontName', 'Helvetica', 'FontSize', 13)
a = get(gca,'Children');
hold on
plot(Time,TFOE,'r','LineWidth',2)
b = get(gca,'Children');
set(gca, 'FontName','Helvetica', 'FontSize', 13)
set(gcf,'color','white')
line([2500 2500], [0 1], 'Color','black','LineStyle', '--')
h = [b;a];
legend(h,'True model','Realisations','location','northeast');
hold off
saveas(gcf,'Oilrecoveryfinal','epsc')
saveas(gcf,'Oilrecoveryfinal','fig')
%% Get the Norm to production data
disp('Get the Norm to production data mismatch')
close(figure)
for i=1:N
    EWOP1(i,:)=immse(WOPRA(:,i),TO1);
    EWOP2(i,:)=immse(WOPRB(:,i),TO2);
    EWOP3(i,:)=immse(WOPRC(:,i),TO3);
    EWOP4(i,:)=immse(WOPRD(:,i),TO4);
    EWCT1(i,:)=immse(WCTA(:,i),TW1);
    EWCT2(i,:)=immse(WCTB(:,i),TW2);
    EWCT3(i,:)=immse(WCTC(:,i),TW3);
    EWCT4(i,:)=immse(WCTD(:,i),TW4);
    EBHP1(i,:)=immse(BHPA(:,i),TP1);
    EBHP2(i,:)=immse(BHPB(:,i),TP2);
    EBHP3(i,:)=immse(BHPC(:,i),TP3);
    EBHP4(i,:)=immse(BHPD(:,i),TP4);
    EGORP1(i,:)=immse(GORA(:,i),TG1);
    EGORP2(i,:)=immse(GORB(:,i),TG2);
    EGORP3(i,:)=immse(GORC(:,i),TG3);
    EGORP4(i,:)=immse(GORD(:,i),TG4);
end
TOTALERROR=ones(N,1);
TOTALERROR=(EWOP1./std(TO1))+(EWOP2./std(TO2))+(EWOP3./std(TO3))+...
(EWOP4./std(TO4))+(EWCT1./std(TW1))+(EWCT2./std(TW2))...
+(EWCT3./std(TW3))+(EWCT4./std(TW4))+(EBHP1./std(TP1))...

```

```

+ (EBHP2./std(TP2)) + (EBHP3./std(TP3)) + (EBHP4./std(TP4)) ...

+ (EGОРР1./std(TG1)) + (EGОРР2./std(TG2)) + (EGОРР3./std(TG3)) + (EGОРР4./std(TG4));
TOTALERROR=TOTALERROR./36;
jj=min(TOTALERROR);
indexfinal = TOTALERROR;
bestnorm = find(indexfinal == min(indexfinal));
%Pssim = Pnew(:,bestssim); %best due to ssim
fprintf('The best Norm Realization is number %i with value %4.4f
\n',bestnorm,jj);
decreasingseries=zeros(N,iyobo+1);
decreasingseries(:,1:iyobo)=decreasingnorm;
decreasingseries(:,iyobo+1)=indexfinal;
reali=[1:N];
%%
figure()
bar(reali,indexfinal,'cyan');
xlabel('Realizations', 'FontName','Helvetica', 'FontSize', 13);
ylabel('RMSE value', 'FontName','Helvetica', 'FontSize', 13);
title('Cost function for Realizations','FontName','Helvetica', 'FontSize',
13)
set(gcf,'color', 'white');
hold on
scatter(reali,indexfinal,'black','filled');
xlabel('Realizations', 'FontName','Helvetica', 'FontSize', 13)
ylabel('RMSE value', 'FontName','Helvetica', 'FontSize', 13)
hold off
xlim([1,N]);
saveas(gcf,'RMSfinal','epsc')
saveas(gcf,'RMSfinal','fig')
close(figure)
disp(' Final RMS computation executed ');
disp(' Smooth the final permeability and porosity Maps ');
if needed==1
for ki=1:numberoftimes
[mumyperm,mumyporo]=clean(nx,ny,nz,N,mumyperm,mumyporo,rossmary,rossmaryporo);
end
end
disp('output the permeability and porosity history matched model for the last
iteration')
file = fopen('sgsimfinal.out','w+'); %
for k=1:numel(mumyperm)
fprintf(file, '%4.6f \n',mumyperm(k) );
end
file2 = fopen('sgsimporofinal.out','w+'); %
for k=1:numel(mumyporo)
fprintf(file2, '%4.6f \n',mumyporo(k) );
end
file3 = fopen('genesisNorm.out','w+');
for k=1:numel(decreasingnorm)
fprintf(file3, '%4.4f \n',decreasingnorm(k) );
end
file4 = fopen('evolvingNorm.out','w+');
for k=1:numel(decreasingseries)
fprintf(file4, '%4.4f \n',decreasingseries(k) );
end
disp('Well locaions consisting of injector and producer well')
iInj = [30, 58, 90, 101]; % 16 wells configuration, injection wells
jInj = [55, 18, 6, 39]; % 16 wells configuration, injection wells
iProd = [14, 38, 96, 67]; % 16 wells configuration, production wells
jProd = [25, 39, 23, 41]; % 16 wells configuration, production wells
CMRmap=[0 0 0;.3 .15 .75;.6 .2 .50;1 .25 .15;.9 .5 0;.9 .9 .5;1 1 1];
if response==1
disp('Pixel map needed')
[bestnorm3,PlogK]=clementPlot(mumyperm,rossmary,N,bestnorm,CMRmap);
xr=reshape(PlogK,nx*ny,nz);

```

```

plottinglocations(xr, nx, ny,nz, 'Layer', iInj, jInj, iProd, jProd, min(xr),
max(xr),CMRmap);
disp(' green are injector wells and blue are producers')
    %run('clementPlot.m')
else
    disp (' pixel map not needed')
end
%%
fprintf('Finished Iterations with the History matching method %d .\n',
method);
if method==1
disp('The method used was standard ESMDA impelemented with main_ESMDA')
elseif method==2
disp('The method used was ESMDA with Levelset impelemented with
main_Levelset')
elseif method==3
disp('The method used was ESMDA impelemented with main_DCT( discrete cosine
transform method coupled with ESMDA)')
elseif method==4
disp('The method used was compressed sensing ESMDA impelemented with
main_sparsity(compressed sensing)')
elseif method==5
disp('The method used was SELE_PhD (My method coupling machine learning with
Level set)')
elseif method==6
disp('The method used was main_DCT_Levelset(My method coupling DCT with Level
set)')
elseif method==7
disp('The method used was main_DCT_LS2 (Level set and DCT update)')
elseif method==8
disp('The method used was main_sparsity_LS(Level set update)')
elseif method==9
disp('The method used was main_Levelset_Boundary ')
elseif method==10
disp('The method used was main_Velocity_LS')
elseif method==11
disp('The method used was main_ESMDA_Localization-covariance localization')
elseif method==12
disp('The method used was main_Levelset_Cov-covariance localization with
Levelset')
elseif method==13
    disp('The method used was main_Levelset_Cov-covariance localization with
Levelset perm only')
elseif method==14
    disp('The method used was method 14 specified-Localization with ESMDA-
Levelset-supervised learning')
else
    disp(' The method used was dynamic update with sparsity')
end
disp(' The overall program has been executed and the history matched files
saved in the folder ');
toc

```

The function that couples Level set with Covariance localization

```

function
[mumyperm,mumyporo]=main_Levelset_Cov(nx,ny,nz,N,tol,observation,overallsim,ro
ssmary,rossmaryporo,perm,poro,history,alpha);
disp( 'History matching data assimilation technique using ESMDA+Level set and
covaraice localization for SPE10 Reservoir' )
disp( 'We apply the narrow band function here' )
disp( 'permeability and porosity are the petro-physical properties of interest'
)
disp( 'PhD Student: Clement Etienam' )
disp( 'Supervisor: Dr Rossmary Villegas' )
disp( 'Co-supervisor: Dr Masoud Babei' )
disp( 'Co-supervisor: Dr Oliver Dorn' )

```

```

disp(' extract the active grid cells' )
sgsim=reshape(perm,72000,N);
sgsimporo=reshape(poro,72000,N);
for i=1:N
sgsimuse=reshape(sgsim(:,i),120,60,10);
sgs=sgsimuse(:,:,3:7);
ex=reshape(sgs,36000,1);
sg(:,i)=ex;
end
for i=1:N
sgsimporouse=reshape(sgsimporo(:,i),120,60,10);
sgsporo=sgsimporouse(:,:,3:7);
exporo=reshape(sgsporo,36000,1);
sgporo(:,i)=exporo;
end
Sim11=reshape(overallsim,17,history,N);
sgout=zeros(36000*N,1);
sgoutporo=zeros(36000*N,1);
for ii=1:36000*N
if(sg(ii)>=100)
sgout(ii)=1;
end
for ii=1:36000*N
if(sgporo(ii)>=0.1805)
sgoutporo(ii)=1;
end
end
disp (' get the signed distance of permeability and porosity fields')
clement=getsigned(sgout,nx,ny);
clementporo=getsigned(sgoutporo,nx,ny);
disp( 'get the narrowband function of permeability and porosity fields')
nbandall=regionband(sgout,N,nx,ny,nz);
nbandallporo=regionband(sgoutporo,N,nx,ny,nz);
%History matching using ESMDA and Level set starts here
for i=1:history
fprintf('Now assimilating timestep %d .\n', i);
f=observation(:,i); %true observation
Sim1=Sim11(:,i,:);
Sim1=reshape(Sim1,17,N); %simulated data

disp('assimilate the historical production data with covariance localization
included')
[sgsim2,DupdateK,updatedlevelset,updatedlevelsetporo,clement,clementporo] =
Assimilate_Levelset_Cov(sg,sgporo,f,
N,Sim1,clement,clementporo,nbandall,nbandallporo,alpha,10);
nbandall=regionband(updatedlevelset,N,nx,ny,nz);
nbandallporo=regionband(updatedlevelsetporo,N,nx,ny,nz);
sg=DupdateK;
sgporo=sgsim2;
fprintf('Finished assimilating timestep %d \n', i);
end
sgsim11=(DupdateK);
disp( 'rectify the conflict of permeabilit and porosity fields with updated
Level set')
sgsim11=reshape(sgsim11,36000*N,1);
sgsim2=reshape(sgsim2,36000*N,1);
updatedlevelset=reshape(updatedlevelset,36000*N,1);
updatedlevelsetporo=reshape(updatedlevelsetporo,36000*N,1);
updatedperm=zeros(36000*N,1);
updatedporo=zeros(36000*N,1);
for ii=1:36000*N
if(sgsim11(ii)>=100)
updatedperm(ii)=1;
end
if(sgsim2(ii)>=0.1805)
updatedporo(ii)=1;

```

```

        end
    end
requiredK=zeros(36000*N,1);
requiredporo=zeros(36000*N,1);
for iii=1:36000*N
    if (updatedperm(iii)==updatedlevelset(iii))
        requiredK(iii)=sgsim1(iii);
    end
    if (updatedporo(iii)==updatedlevelsetporo(iii))
        requiredporo(iii)=sgsim2(iii);
    end
    if ((updatedperm(iii) ~= updatedlevelset(iii)) && (updatedlevelset(iii)==0))
        requiredK(iii)=95;
    end
    if ((updatedperm(iii) ~= updatedlevelset(iii)) && (updatedlevelset(iii)==1))
        requiredK(iii)=105;
    end
    if ((updatedporo(iii) ~= updatedlevelsetporo(iii)) &&
(updatedlevelsetporo(iii)==0))
        requiredporo(iii)=0.1795 ;
    end
    if ((updatedporo(iii) ~= updatedlevelsetporo(iii)) &&
(updatedlevelsetporo(iii)==1))
        requiredporo(iii)=0.1895;
    end
end
requiredK=abs(requiredK);
requiredporo=abs(requiredporo);
disp('condition the field and honour')
[output,outputporo] = honour2(rosmmary, rossmaryporo,
N,requiredporo,requiredK);
permsteps=reshape(output,36000*N,1);
porosteps=reshape(outputporo,36000*N,1);
disp(' output to ASCII files the states at each time step ');
sgassimi=permsteps;
sgporoassimi=porosteps;
save('Permall.out','sgassimi','-ascii');
save('Poroall.out','sgporoassimi','-ascii');
permanswers=reshape(sgassimi,36000,N);
poroanswers=reshape(sgporoassimi,36000,N);
for i=1:N
sgsim=zeros(120,60,10);
sgsimporo=zeros(120,60,10);
sgsim(:,:,3:7)=reshape(permanswers(:,i),120,60,5);
sgsimporo(:,:,3:7)=reshape(poroanswers(:,i),120,60,5);
sgsimmijana(:,i)=reshape(sgsim,72000,1);
sgsimporomijana(:,i)=reshape(sgsimporo,72000,1);
end
mumyperm=sgsimmijana;
mumyporo=sgsimporomijana;
end

function
[sgsim2,DupdateK,updatedlevelset,updatedlevelsetporo,clement,clementporo] =
Assimilate_Levelset_Cov(sg,sgporo,f,
N,Sim1,clement,clementporo,nbandall,poro,alpha,c);

%
% PARAMETERS:
% f          - True data
% sg         - an ensemble of permeability realisations
% sgporo     - an ensemble of permeability realisations
% N          - ensemble size
% Sim1       - Simulated measurements
% Clement    - an ensemble of permeability realisations signed distance
% N          - ensemble size
% c          - correlation length (scaled by a factor of 10)

```

```

% nbandall,nbandporo - an ensemble of narrow band matrix of
permeability and porosity signed distance realisations
% alpha - damping coefficient

%-----
disp( 'History matching data assimilation technique using ESMDA with Levelset
and covariance localization for SPE 10 Reservoir' )
disp( 'PhD Student: Clement Etienam' )
disp( 'Supervisor: Dr Rossmay Villegas' )
disp( 'Co-supervisor: Dr Masoud Babei' )
disp( 'Advisor: Dr Oliver Dorn' )
disp(' load the files ');
A=zeros(120,60,5);
for j=1:5
    A(14,25,j)=1;
    A(38,39,j)=1;
    A(96,23,j)=1;
    A(67,41,j)=1;
    A(30,55,j)=1;
    A(58,18,j)=1;
    A(90,6,j)=1;
    A(14,25,j)=1;
    A(101,39,j)=1;

end
disp( 'calculate the Euclidean distance function to the six producer wells')
lf=reshape(A,120,60,5);
for j=1:5;
    sdf=lf(:,:,j);
    [usdf,IDX] = bwdist(sdf);
    usdf=reshape(usdf,7200,1);
    young(:,:,j)=usdf;
end
sdfbig=reshape(young,36000,1);
sdfbig1=abs(sdfbig);
z=sdfbig1;
% the value of the range should be computed accurately.
%c=range(z);

c0OIL1=zeros(36000,1);
disp( 'compute the gaspari-cohn coefficent')
[c0OIL1] = calc_loccoeffs(c, 'Gaspari_Cohn', z);
disp(' get the gaspari cohn for the stochastic gradient')
schur=c0OIL1;
Bsch = repmat(schur,1,N);
yoboschur=ones(72000,N);
yoboschur(1:36000,:)=Bsch;
yoboschur(36001:72000,:)=Bsch;
sgsim1=log(sg);
clement=reshape(clement,36000,N);
clementporo=reshape(clementporo,36000,N);
sgsim1l = reshape(sgsim1,36000,N);
sgsim1lporo = reshape(sgporo,36000,N);
disp(' generate Gaussian noise for the observed measurments ');
stddWOPR1 = 0.15*f(1,:);
stddWOPR2 = 0.15*f(2,:);
stddWOPR3 = 0.15*f(3,:);
stddWOPR4 = 0.15*f(4,:);
stddWWCT1 = 0.2*f(5,:);
stddWWCT2 = 0.2*f(6,:);
stddWWCT3 = 0.2*f(7,:);
stddWWCT4 = 0.2*f(8,:);
stddBHP1 = 0.2*f(9,:);
stddBHP2 = 0.2*f(10,:);

```

```

stddBHP3 = 0.2*f(11,:);
stddBHP4 = 0.2*f(12,:);
stddGORP1 = 0.2*f(13,:);
stddGORP2 = 0.2*f(14,:);
stddGORP3 = 0.2*f(15,:);
stddGORP4 = 0.2*f(16,:);
unierec=0.1*f(17,:);

Error1=ones(17,N);
Error1(1,:)=normrnd(0,stddWOPR1,1,N);
Error1(2,:)=normrnd(0,stddWOPR2,1,N);
Error1(3,:)=normrnd(0,stddWOPR3,1,N);
Error1(4,:)=normrnd(0,stddWOPR4,1,N);
Error1(5,:)=normrnd(0,stddWWCT1,1,N);
Error1(6,:)=normrnd(0,stddWWCT2,1,N);
Error1(7,:)=normrnd(0,stddWWCT3,1,N);
Error1(8,:)=normrnd(0,stddWWCT4,1,N);
Error1(9,:)= normrnd(0,stddBHP1,1,N);
Error1(10,:)= normrnd(0,stddBHP2,1,N);
Error1(11,:)= normrnd(0,stddBHP3,1,N);
Error1(12,:)= normrnd(0,stddBHP4,1,N);
Error1(13,:)= normrnd(0,stddGORP1,1,N);
Error1(14,:)= normrnd(0,stddGORP2,1,N);
Error1(15,:)= normrnd(0,stddGORP3,1,N);
Error1(16,:)= normrnd(0,stddGORP4,1,N);
Error1(17,:)= normrnd(0,unierec,1,N);

Cd2 = (Error1*Error1')./(N-1);
for i=1:N
    Dj(:,i)=f+Error1(:,i);

end
disp(' generate the ensemble state matrix containing parameters and states ');
overall=zeros(144017,N); %ensemble state for EnKF
overall(1:36000,1:N)=sgsim1l;
overall(36001:72000,1:N)=sgsim1lporo;
overall(72001:108000,1:N)=clement;
overall(108001:144000,1:N)=clementporo;
overall(144001:144017,1:N)=Sim1;
Y=overall; %State variable,it is important we include simulated measurements
in the ensemble state variable
nbandall=reshape(nbandall,36000,N);
nbandallporo=reshape(nbandallporo,36000,N);
nbandI=ones(144017,N); %narrow band and covariance correlation matrix
nbandI(72001:108000,1:N)=nbandall;
nbandI(108001:144000,1:N)=nbandallporo;
nbandI(1:72000,1:N)=yoboschur;
M = mean(Sim1,2);
% Mean of the ensemble state
M2=mean(overall,2);
% Get the ensemble states pertubations
for j=1:N
    S(:,j)=Sim1(:,j)-M;
end
for j=1:N
    yprime(:,j)=overall(:,j)-M2;
end
disp(' update the stochastic gradient ');
Cyd=(yprime*S')./((N-1));
Cdd=(S*S')./((N-1));
[Usig,Sig,Vsig] = svd(Cdd+(alpha.*Cd2));
xsmall = diag(Sig);
Bsig = cumsum(xsmall);
valuesig=Bsig(end);
valuesig=valuesig*0.9999;
indices = find(cumsum(xsmall) >= valuesig );
toluse=xsmall(indices,:);

```

```

tol=toluse(1,:);
disp(' update the new ensemble ');
Ynew=Y+((Cyd*pinv((Cdd+(alpha.*Cd2))))*(Dj-Sim1)).*nbandI;
disp(' extract the updated states ')
value1=Ynew(1:36000,1:N);

DupdateK=exp(value1);
sgsim2=Ynew(36001:72000,1:N);
updatedlevelset=Ynew(72001:108000,1:N);
clement=Ynew(72001:108000,1:N);
updatedlevelset(updatedlevelset>0)=1;
updatedlevelset(updatedlevelset<=0)=0;
updatedlevelsetporo=Ynew(108001:144000,1:N);
clementporo=Ynew(108001:144000,1:N);
updatedlevelsetporo(updatedlevelsetporo>0)=1;
updatedlevelsetporo(updatedlevelsetporo<=0)=0;
end

```

Covariance localisation function

```

% Calculates localisation coefficients
%
% @param radius - localisation radius
% @param tag - tag to choose a particular function
% @param dist - vector of distances
% @return coeffs - vector of localisation coefficients

% Author: Clement Etienam PhD Petroleum Engineering 2015-2018
% Purpose: Calculates localisation coefficients
%
% Description: Note: Implications of using particular localisation matrix
% have not been fully investigated yet. At this moment,
'Gauss'
% and 'Gaspari_Cohn' seem to be the two safest options.

%%

function [coeffs] = calc_loccoeffs(radius, tag, dist)
coeffs = zeros(size(dist));
switch tag
    case 'Gauss'
        R = radius;
        coeffs = exp(-0.5 * (dist / R) .^ 2);
    case 'Gaspari_Cohn'
        R = radius * 1.7386;
        ind1 = find(dist <= R);
        r2 = (dist(ind1) / R) .^ 2;
        r3 = (dist(ind1) / R) .^ 3;
        coeffs(ind1) = 1 + r2 .* (- r3 / 4 + r2 / 2) + r3 * (5 / 8) - r2 * (5 / 3);
        ind2 = find(dist > R & dist <= R * 2);
        r1 = (dist(ind2) / R);
        r2 = (dist(ind2) / R) .^ 2;
        r3 = (dist(ind2) / R) .^ 3;
        coeffs(ind2) = r2 .* (r3 / 12 - r2 / 2) + r3 * (5 / 8) + r2 * (5 / 3) - r1 * 5 + 4 - (2 / 3) ./ r1;
    case 'Cosine'
        R = radius * 2.3167;
        ind = find((dist <= R));
        r = dist(ind) / R;
        coeffs(ind) = (1 + cos(r * pi)) / 2;

```

```

case 'Cosine_Squared'

R = radius * 3.2080;
ind = find((dist <= R));
r = dist(ind) / R;
coeffs(ind) = ((1 + cos(r * pi)) / 2) .^ 2;

case 'Lewitt'

R = radius * 4.5330;
m = 10;
alpha = 1;
ind = find(dist <= R);
for i = ind
    r = dist(i) / R;
    rr = 1 - r^2;
    coeffs(i) = rr^(m/2) * besseli(m, alpha * rr^0.5) / besseli(m,
alpha);
end

case 'Exp3'

R = radius;
coeffs = exp(-0.5 * (dist / R) .^ 3);

case 'Cubic'

R = radius * 1.8676;
ind = find(dist < R);
coeffs(ind) = (1 - (dist(ind) / R) .^ 3) .^ 3;

case 'Quadro'

R = radius * 1.7080;
ind = find(dist < R);
coeffs(ind) = (1 - (dist(ind) / R) .^ 4) .^ 4;

case 'Step'

R = radius;
ind = find(dist < R);
coeffs(ind) = 1;

case 'None'

coeffs(:) = 1;

otherwise
    error(sprintf('\n EnKF: error: calc_loccoeffs(): unknown localisation
tag "%s".\n Possible tags:\n    "Gauss"\n    "Gaspari_Cohn"\n    "Cosine"\n
"Cosine_Squared"\n    "Lewitt"\n    "Exp3"\n    "Cubic"\n    "Quadro""\n
"Step""\n    "None"', char(tag)));
end

return

```

This function is to extract the pressure and saturation fields from restart files after the run from ECLIPSE

```

function [SEn83,PEn83]=getstatesall(N,history);

disp(' This code is to get the pressure and saturation fields for all the
states in SPE10')
for j=1:N

```

```

f = 'MASTER';
%folder = strcat(f, num2str('%.5d',j));
folder = strcat(f, sprintf('%.5d',j));
%sprintf('%.5d',23)
copyfile('Eclipse2Matlab.m',folder)
copyfile('resize.m',folder)
end
oldfolder=cd;
cd(oldfolder) % setting original directory
for i=1:N %list of folders
    f = 'MASTER';
    folder = strcat(f, sprintf('%.5d',i));
    cd(folder);
    parfor j=1:history %desired time steps
        ff = 'MASTER0.F';
        SW1983 = importdata(strcat(ff, sprintf('%.4d',j))), ' ',12020); %change here
    for 1st and 10th timestep
        SW1983=SW1983.data;
        A=SW1983;
        B22=Eclipse2Matlab(A);
        B2=resize(B22,[36000,1]);
        B(:,j)=B2;
    end
    Bpad = B;
    parfor jj=1:history % desired time steps
        fff = 'MASTER0.F';
        P1983 = importdata(strcat(fff, sprintf('%.4d',jj))), ' ',3019);
        P1983=P1983.data;
        C=P1983;
        D22=Eclipse2Matlab(C);
        D2=resize(D22,[36000,1]);
        D(:,jj)=D2;
    end
    Dpad = D;
    SEn83(:,:,i)=Bpad;
    PEn83(:,:,i)=Dpad;
    cd(oldfolder);
end
cd(oldfolder) % returning to original directory
end
function B=Eclipse2Matlab(A)
%Reshape from eclipse to matlab
[m,n]=size(A);
for k=1:m*n; % matrix of eclipse data
    y=mod(int32(k)-1,4)+1; % value of i
    x=idivide(int32(k)-1,4) + 1; % value of j
    B(k)=A(x,y); % new matrix in matlab shape
    B=B';
end
end

```

Codes for Numerical Experiment 5- Combining Machine learning techniques with a History Matching - Level set approach

The main script is similar to numerical experiment 2 above, the only difference is the function that computes the sparse coeffeicnets of the spatial permeability and porosity fields, the signed distance level set functions,narrow band matrix and integrates all this for the history matching loop.The rectification of the conflict between the level set update and permeability/porosity pixel update is taken into account at the tail end of the function

```

function
[mumyperm,mumyporo]=SELE_PhD(nx,ny,nz,Yes2,Yes2poro,N,tol,observation,overalls
im,rossmary,rossmaryporo,perm,poro,history,alpha);
disp( 'History matching data assimilation technique using SELE-ES-MDA for
SPE10 Reservoir' )
disp( 'SELE denotes Sparsity Ensemble filter Level set Ensemble filter' )
disp( 'PhD Student: Clement Etienam' )
disp( 'Supervisor: Dr Rosmary Villegas' )
disp( 'Co-supervisor: Dr Masoud Babei' )
disp( 'Co-supervisor: Dr Oliver Dorn' )
oldfolder=cd;
cd(oldfolder) % setting original directory
sgsim=reshape(perm,72000,N);
sgsimporo=reshape(poro,72000,N);
for i=1:N
sgsimuse=reshape(sgsim(:,i),120,60,10);
sgs=sgsimuse(:,:,3:7);
ex=reshape(sgs,36000,1);
sg(:,i)=ex;
end
for i=1:N
sgsimporouse=reshape(sgsimporo(:,i),120,60,10);
sgsporo=sgsimporouse(:,:,3:7);
exporo=reshape(sgsporo,36000,1);
sgporo(:,i)=exporo;
end
sgout=zeros(3600000,1);
sgoutporo=zeros(3600000,1);
for ii=1:3600000
if(sg(ii)>=100)
sgout(ii)=1;
end
end
for ii=1:3600000
if(sgporo(ii)>=0.1805)
sgoutporo(ii)=1;
end
end
end
disp (' get the signed distance of permeability and porosity field')
clement=getsigned(sgout,nx,ny);
clementporo=getsigned(sgoutporo,nx,ny);

disp( 'get the narrowband function of the facies of permeability and porosity
fields')
nbandall=regionband(sgout,N,nx,ny,nz);
nbandallporo=regionband(sgoutporo,N,nx,ny,nz);
disp( ' covert spatial permeability to sparse')
sgsparse=Sparse(log(sg),Yes2);
sgsparseporo=Sparse(sgporo,Yes2poro);
cd(oldfolder)
Sim11=reshape(overallsim,17,history,N);
for i=1:history
fprintf('Now assimilating timestep %d .\n', i);

Sim1=Sim11(:,i,:);
Sim1=reshape(Sim1,17,N);

f=observation(:,i);
[Dj,Cd2,sgsim2,DupdateK,updatedlevelset,updatedlevelsetporo,clement2,clementpo
ro2] = ESMDA_SELE_PhD (sgsparse,sgsparseporo,f, N,
Sim1,tol,alpha,clement,clementporo,nbandall,nbandallporo);
nbandall=regionband(updatedlevelset,N,nx,ny,nz);
nbandallporo=regionband(updatedlevelsetporo,N,nx,ny,nz);
Djpertubed(:,:,i)=Dj;
sgsparse=reshape(DupdateK,1500,N);

```

```

sgsparseporo=reshape(sgsim2,1500,N);
clement=clement2;
clementporo=clementporo2;
fprintf('Finished assimilating timestep %d \n', i);
end
disp( 'recover the full permeability field')
joyy=reshape(Yes2,36000,1500)*sgsparse;
joyyporo=reshape(Yes2poro,36000,1500)*sgsparseporo;

sgsim11=exp(joyy);
sgsim2=joyyporo;
disp( 'rectify the conflict between the permeability and porosity fields')
sgsim11=reshape(sgsim11,36000*N,1);
sgsim2=reshape(sgsim2,36000*N,1);
updatedlevelset=reshape(updatedlevelset,36000*N,1);
updatedlevelsetporo=reshape(updatedlevelsetporo,36000*N,1);
updatedperm=zeros(36000*N,1);
updatedporo=zeros(36000*N,1)
for ii=1:3600000
    if(sgsim11(ii)>=100)
        updatedperm(ii)=1;
    end
    if(sgsim2(ii)>=0.1805)
        updatedporo(ii)=1;
    end
end
requiredK=zeros(3600000,1);
requiredporo=zeros(3600000,1);
for iii=1:3600000
    if (updatedperm(iii)==updatedlevelset(iii))
        requiredK(iii)=sgsim11(iii);
    end

    if (updatedporo(iii)==updatedlevelsetporo(iii))
        requiredporo(iii)=sgsim2(iii);
    end
    if ((updatedperm(iii) ~= updatedlevelset(iii)) && (updatedlevelset(iii)==0))
        requiredK(iii)=95;
    end
    if ((updatedperm(iii) ~= updatedlevelset(iii)) && (updatedlevelset(iii)==1))
        requiredK(iii)=105;
    end

    if ((updatedporo(iii) ~= updatedlevelsetporo(iii)) &&
(updatedlevelsetporo(iii)==0))
        requiredporo(iii)=0.1795;
    end
    if ((updatedporo(iii) ~= updatedlevelsetporo(iii)) &&
(updatedlevelsetporo(iii)==1))
        requiredporo(iii)=0.1815;
    end
end
requiredK=abs(requiredK);
requiredporo=abs(requiredporo);
disp( 'condition the field and honour')
[output,outputporo] = honour2(rossmary, rossmaryporo,
N,requiredporo,requiredK);
permsteps=reshape(output,36000*N,1);
porosteps=reshape(outputporo,36000*N,1);
permanswers=reshape(permsteps,36000,N);
poroanswers=reshape(porosteps,36000,N);
for i=1:N
sgsim=zeros(120,60,10);
sgsimporo=zeros(120,60,10);
sgsim(:,:,3:7)=reshape(permanswers(:,:,i),120,60,5);

```

```

sgsimporo(:,:,3:7)=reshape(poroanswers(:,i),120,60,5);
sgsimmijana(:,i)=reshape(sgsim,72000,1);
sgsimporomijana(:,i)=reshape(sgsimporo,72000,1);
end
mumyperm=sgsimmijana;
mumyporo=sgsimporomijana;
disp(' program executed ');
end
function
[Dj,Cd2,sgsim2,DupdateK,updatedlevelset,updatedlevelsetporo,clement,clementpor
o] = ESMDA_SELE_PhD (sgsparse,sgsparseporo,f, N,
Sim1,tol,alpha,clement,clementporo,nbandall,nbandallporo);
%%History matching data assimilation technique
%%PhD Student: Clement Etienam
%%Supervisor: Dr Rossmary Villegas
%%Co-supervisor: Dr Masoud Babei
%DESCRIPTION:
%
% PARAMETERS:
%   f           - True data
%   sgsim       - ensemble of simulate states
%   N           - ensemble size
%   Sim         - Simulated measurments
%
%-----
disp( 'History matching data assimilation technique using standard ESMDA_SELE
for SPE10 Reservoir' )
disp( 'PhD Student: Clement Etienam' )
disp( 'Supervisor: Dr Rossmary Villegas' )
disp( 'Co-supervisor: Dr Masoud Babei' )
disp( 'Advisor: Dr Oliver Dorn' )
disp(' load the files ');

sgsim1=sgsparse;
sgsim11 = reshape(sgsim1,1500,N);
clement=reshape(clement,36000,N);

sgsim11poro = reshape(sgsparseporo,1500,N);

disp(' generate Gaussian noise for the observed measurments ');
stddWOPR1 = 0.15*f(1,:);
stddWOPR2 = 0.15*f(2,:);
stddWOPR3 = 0.15*f(3,:);
stddWOPR4 = 0.15*f(4,:);
stddWWCT1 = 0.2*f(5,:);
stddWWCT2 = 0.2*f(6,:);
stddWWCT3 = 0.2*f(7,:);
stddWWCT4 = 0.2*f(8,:);
stddBHP1 = 0.2*f(9,:);
stddBHP2 = 0.2*f(10,:);
stddBHP3 = 0.2*f(11,:);
stddBHP4 = 0.2*f(12,:);
stddGORP1 = 0.2*f(13,:);
stddGORP2 = 0.2*f(14,:);
stddGORP3 = 0.2*f(15,:);
stddGORP4 = 0.2*f(16,:);
unierec=0.1*f(17,:);

Error1=ones(17,N);
Error1(1,:)=normrnd(0,stddWOPR1,1,N);
Error1(2,:)=normrnd(0,stddWOPR2,1,N);
Error1(3,:)=normrnd(0,stddWOPR3,1,N);
Error1(4,:)=normrnd(0,stddWOPR4,1,N);
Error1(5,:)=normrnd(0,stddWWCT1,1,N);
Error1(6,:)=normrnd(0,stddWWCT2,1,N);
Error1(7,:)=normrnd(0,stddWWCT3,1,N);
Error1(8,:)=normrnd(0,stddWWCT4,1,N);
Error1(9,:)= normrnd(0,stddBHP1,1,N);

```

```

Error1(10,:)= normrnd(0,stddBHP2,1,N);
Error1(11,:)= normrnd(0,stddBHP3,1,N);
Error1(12,:)= normrnd(0,stddBHP4,1,N);
Error1(13,:)= normrnd(0,stddGORP1,1,N);
Error1(14,:)= normrnd(0,stddGORP2,1,N);
Error1(15,:)= normrnd(0,stddGORP3,1,N);
Error1(16,:)= normrnd(0,stddGORP4,1,N);
Error1(17,:)= normrnd(0,unierec,1,N);
Cd2 = (Error1*Error1')./(N-1); % measurement error auto covariance
for i=1:N
    Dj(:,i)=f+Error1(:,i);
end
disp(' generate the ensemble state matrix containing parameters and states ')
overall=zeros(75017,N); %ensemble state
overall(1:1500,1:N)=sgsim1; %sparse permeability
overall(1501:3000,1:N)=sgsim1poro; %sparse porosity
overall(3001:39000,1:N)=clement; %signed distance permeability
overall(39001:75000,1:N)=clementporo; %signed distance porosity
overall(75001:75017,1:N)=Sim1; %simulated data
Y=overall; %State variable,it is important we include simulated measurements
in the ensemble state variable
nbandall=reshape(nbandall,36000,N);
nbandI=ones(75017,N); %narrow band overall matrix
nbandI(3001:39000,1:N)=nbandall; %permeability narrow band
nbandI(39001:75000,1:N)=nbandallporo; %porosity narrow band
M = mean(Sim1,2);
% Mean of the ensemble state
M2=mean(overall,2);
%M=M'
% Get the ensemble states pertubations
for j=1:N
    S(:,j)=Sim1(:,j)-M;
end
for j=1:N
    yprime(:,j)=overall(:,j)-M2;
end

disp(' update the new ensemble ');
Cyd=(yprime*S')./((N-1));
Cdd=(S*S')./((N-1));
disp(' update the new ensemble ');
Ynew=Y+((Cyd*pinv((Cdd+alpha.*Cd2)))*(Dj-Sim1)).*nbandI;
disp(' extract the updated states ')
value1=Ynew(1:1500,1:N);
UpdateK=value1;
updatedlevelset=Ynew(3001:39000,1:N);
clement=Ynew(39001:75000,1:N);
updatedlevelset(updatedlevelset>0)=1;
updatedlevelset(updatedlevelset<=0)=0;
sgsim2=Ynew(1501:3000,1:N);
updatedlevelsetporo=Ynew(3001:39000,1:N);
clementporo=Ynew(39001:75000,1:N);
updatedlevelsetporo(updatedlevelsetporo>0)=1;
updatedlevelsetporo(updatedlevelsetporo<=0)=0;
end

```

Function to get the signed distance level set function

```

function [clement]=getsigned(sgout,nx,ny)
nfacies_en1=sgout;
sdf=zeros(nx,ny);
sgn(nx,ny)=1;
sdf_dt=zeros(nx,ny,5);
LF=reshape(nfacies_en1,36000,100);
for ii=1:100

```

```

lf=reshape(LF(:,ii),nx,ny,5);
for j=1:5
    sdf=lf(:,:,j);
    unie=lf(:,:,j);
    unie(unie==1)=1;
    unie(unie==0)=-1;
    usdf = ac_reinit(sdf,unie);
    usdf=reshape(usdf,7200,1);
    young(:,j)=usdf;
end
sdfbig=reshape(young,36000,1);
clement(:,ii)=sdfbig;
end
clement(clement==0)=-1;
disp(' output permeability signed distance ');
end

function u = ac_reinit(u,unie)
c = contours(u,[0,0]);
xy = zy_extract_pt_from_contours(c);
if isempty(xy), u = []; return; end
u0 = zeros(size(u));
u0(sub2ind(size(u), round(xy(2,:)),round(xy(1,:)))) = 1;
u = double(bwdist(u0)).*sign(unie);
end

```

Function to get the narrow-band

```

function nbandall=regionband(sgout,N,nx,ny,nz)
sgout=reshape(sgout,36000,N);
for ii=1:N
    lf=reshape(sgout(:,ii),nx,ny,nz);
    for j=1:5
        sdf=lf(:,:,j);

        usdf = boundarymask(sdf);
        usdf=reshape(usdf,7200,1);
        young(:,j)=usdf;

    end
    sdfbig=reshape(young,36000,1);
    sdfbig=double(sdfbig);
    nbandall(:,ii)=sdfbig;
end
end

```

Function to get the sparse coefficients of the permeability and porosity fields using orthogonal matching pursuit (OMP)

```

function sgsparse=Sparse(sg,Yes2);
disp(' add necessary file path ');
addpath(genpath('C:\Work\GSLIB\sgsim\ETIENAM answers SPE 10\ompbox10'));
addpath(genpath('C:\Work\GSLIB\sgsim\ETIENAM SPE 10 SPARSITY'));
disp(' Load the relevant files ');
load sgsim.out;
sgsim=reshape(sg,36000,100);
X=sgsim;
disp(' ');

```

```

disp(' ***** Orthogonal matching pursuit of permeability *****');
%[m,n] = size(X);
D=reshape(Yes2,36000,1500);
G=D'*D;
T=1500; %70 is the best
gammaperm = omp(D,X,G,T,'messages',1);
sparseperm=full(gammaperm);
yusuf=sparseperm;
sgsparse=yusuf;
%% show results %%
figure;
% subplot(1,2,1)
stem(gammaperm);
title('sparse coefficients of permeability','FontName','Helvetica',
'FontSize', 13);
xlabel('Weights','FontName','Helvetica', 'FontSize', 13);
ylabel('Basis index','FontName','Helvetica', 'FontSize', 13);
set(gca, 'FontName','Helvetica', 'FontSize', 13)
set(gcf,'color','white')

end

X = varargin{2};
G = varargin{3};
T = varargin{4};
DtX = [];
else
    error('Invalid number of parameters');
end

```

EnKF.m

```

function U = EnKF (D, Y, A, scheme, R, tol, beta)
%-----
%EnKF Assimilation code
%PhD Student: Clement Oku Etienam
%Supervisor: Dr Rosmary Villegas
%Co-supervisor: Dr Masoud Babaei
%    function U = EnKF (D, Y, A, scheme, R, tol, beta)
%
% DESCRIPTION:
%    Various EnKF update schemes following Evensen (2009).
%
% PARAMETERS:
%    D          - ensemble of simulated measurements
%    Y          - ensemble of perturbed measurements
%    A          - ensemble of simulated states
%    scheme     - EnKF scheme: 1 inverse computed using Matlab functions \
and /
%                                and full rank R
%                                2 pseudo inverse of C with full rank R
%                                3 subspace pseudo inverse of C with low
%                                rank Re (default)
%    R          - vector with measurement error variances
%    tol        - tolerance used in pseudo inversion (default: 0.01)
%    beta       - step size (default: 1)
%
% We aim to get the analysed ensemble as U:
% Updated ensemble of model states= U
%-----
if nargin < 7, beta = 1.0; end
if nargin < 6, tol = 0.01; end
if nargin < 4, scheme = 3; end
if (scheme ~=3 && (nargin < 5 || isempty(R)))

```

```

    error('*** EnKF: inconsistent input specification ***')
end
% *** this line only needed as long as diagonal R is assumed ***
%R = diag(R);
% number of state variables and ensemble size
ns = size(A,1);
ne = size(A,2);
% measurements
y = mean(Y,2);
m = numel(y);
% ensemble of measurement perurbations
E = Y - repmat(y,1,ne);

% simulated measurement anomaly matrix
S = D-repmat(mean(D,2),1,ne);
if m == 1 % use scalar inverse in case of single measurement
    if scheme == 3
        % LOW RANK R
        C = (S*S' + E*E')/(ne-1);
    else
        % FULL RANK R
        C = S*S'/(ne-1) + R;
    end
    U = A + beta * sqrt(ne-1).\\((A - repmat(mean(A,2),1,ne)) * S')*(Y -
D)/C);
else % more than one measurement
    % INVERSE WITH \ AND / AND FULL RANK R
    if scheme == 1
        S = S / sqrt(ne-1);
        if m <= ne
            C = S*S' + R;
            W = S' / C;
        else
            W = (eye(ne) + (S'/R)*S) \ S'/R;
        end
        U = A + beta * sqrt(ne-1).\\(A - repmat(mean(A,2),1,ne)) * (W*(Y - D));
    else
        % EXPLICIT PSEUDO INVERSE WITH FULL RANK R
        if scheme == 2
            C = S*S' + (ne-1)*R; % assumes diagonal R
            [U, Z] = eig(C);
            s0 = 0;
            for i = 1 : m
                s0 = s0 + Z(i,i);
            end
            s1 = 0.0; n = 0;
            for i = m: -1 : 1 % Z(m,m) contains largest eigenvalue
                if (s1/s0 < 1-tol) && Z(i,i) > 0.0
                    n = n + 1;
                    s1 = s1 + Z(i,i);
                    Z(i,i) = 1.0/Z(i,i);
                else
                    Z(i,i) = 0.0;
                end
            end
            % inverse of C
            C = U * Z * U';
        end
        % SUBSPACE PSEUDO INVERSE SCHEME FOR LOW RANK R
        if scheme == 3
            % SVD: S = U0 * Z0 * V0'
            p0 = min(m,ne);
            [U0,Z0,~] = svd(S,'econ'); % Z0: p0 x p0, U0: m x p0
            s0 = 0;
        end
    end
end

```

```

for i = 1 : p0
    s0 = s0 + Z0(i,i);
end
s1 = 0.0; n = 0;
for i = 1 : p0
    if (s1/s0 < 1-tol) && Z0(i,i) > 0.0
        n = n + 1;
        s1 = s1 + Z0(i,i);
        Z0(i,i) = 1.0/Z0(i,i);
    else
        Z0(i,i) = 0.0;
    end
end
% construct X0
X0 = Z0 * U0' * E; % X0: p0 x ne
% SVD: X0 = U1 * Z1 * V1'
p1 = min(p0,ne);
[U1,Z1,~] = svd(X0,'econ'); % Z1: p1 x p1, U1: p0 x p1
s0 = 0;
for i = 1 : p1
    s0 = s0 + Z1(i,i);
end
s1 = 0.0; n = 0;
for i = 1 : p1
    if (s1/s0 < 1-tol) && Z1(i,i) > 0.0
        n = n + 1;
        s1 = s1 + Z1(i,i);
        Z1(i,i) = 1.0/(Z1(i,i)^2+1.0);
    else
        Z1(i,i) = 1.0;
    end
end
% construct X1
X1 = U0 * Z0' * U1; % X1: m x p1
% inverse of C
C = X1 * Z1 * X1'; % C: m x m
end
% ensemble update for pseudo inverse schemes
if (2*ns*m*ne < (ns+m)*ne^2)
    % few measurements
    U = A + beta * ((A - repmat(mean(A,2),1,ne)) * S') * (C * (Y - D));
else
    % many measurements
    U = A * (eye(ne) + beta * S' * C * (Y - D));
end
end
end

```

Gassman.m

```

function [ImpP, ImpS]=Gassmann(PORO,Pr,SO)

% Author: Clement Etienam, PhD Petroleum Engineering 2015-2018
% Supervisor: Dr Rossmary Villegas
% Co-Supervisor: Dr Masoud Babei
% Co-Supervisor: Dr Oliver Dorn
%Poro - porosity (array shape)
%P - pressure (psi, eclipse formatted)
%SO - oil saturation (eclipse formatted)

% Temperature (degrees Celsius)
% 217 F
T = 103; % C

%Importing porosity and permeability values
POROVANCOUVER = PORO;

```

```

%D Data analysis
avePorosity = mean(POROVANCOUVER);
minPorosity = min(POROVANCOUVER);
maxPorosity = max(POROVANCOUVER);
stDevPorosity = std(POROVANCOUVER);
%%
% sorting out indices
for i = 1:size(POROVANCOUVER)
zIndex(i) = idivide(int16(i)-1,2268) + 1;
xyIndex(i) = mod(int16(i)-1,2268)+1;
yIndex(i) = idivide(int16(xyIndex(i))-1,84) + 1;
xIndex(i) = mod(xyIndex(i)-1,84) +1;
% {z} (x,y)
porosity{zIndex(i)}(xIndex(i),yIndex(i)) = POROVANCOUVER(i);
end
% Read in pressure and oil saturation files
PressureAfter1Year=Pr;
OilSatAfter1Year=SO;
% labeling the imported data
for i = 1:2268 %84*27
    for j = 1:4
        aux(i,j) = (i - 1)*4 + j;
        xyIndex2(i,j) = mod(aux(i,j) - 1, 2268) + 1;
        yIndex2(i,j) = idivide(int16(xyIndex2(i,j))-1,84) + 1;
        xIndex2(i,j) = mod(xyIndex2(i,j) - 1,84) +1;
        zIndex2(i,j) = idivide(int16(aux(i,j) - 1),2268) + 1;
        % psia to MPa
        pressure{zIndex2(i,j)}(xIndex2(i,j),yIndex2(i,j)) = ...
            field2Metric(PressureAfter1Year(i,j), 'psi')*1E-6;
        saturation{zIndex2(i,j)}(xIndex2(i,j),yIndex2(i,j)) = ...
            OilSatAfter1Year(i,j);
    end
end
%%
%%%%Water data%%%%%
% The water formation volume factor at the reference pressure
BWater = 1.029; % rb/stb
% Compressibility
CWater = 3.13E-6; % 1/psi
% Density
rhoWater = field2Metric(64.00, 'lbft3'); % kg/m3
%%%%%%%
%%%%%Oil data%%%%%
% Gas Specific gravity
G = 0.8515;
% 600 SCF/BBL -> m3/m3
RG = 0; %600*0.0283168466/0.158987295;
% Oil API
API = 141.5/G - 131.5; % need rhoOil in g/cm^3
%%%%%%%
%%%%%Matrix data%%%%%
%
% From permeability - porosity graphs, assumed made of quartz and feldspar
% quartz dominant
%
% Compressibility
CMatrix = 0.30E-05; % 1/psi ;
%
% Density
% From Carmichael (1986)
% Try different percentage of quartz
SQuartz = 0.6;
SFeldspar = 1 - SQuartz;
rhoQuartz = 2.65*1000; % kg/m3
KQuartz = 37E9; % Pa

```

```

GQuartz = 44E9; % Pa
rhoFeldspar = 2.62*1000; % kg/m3
KFeldspar = 37.5E9; % Pa
GFeldspar = 15E9; % Pa
KMatrix = ones(84,27)*(SQuartz.*KQuartz + SFeldspar.*KFeldspar)/2 + ...
           (SQuartz./KQuartz + SFeldspar./KFeldspar).^( -1)/2;
%%%%%%%%%%%%%%%
%%%%%%%Frame data%%%%%
% Lab data
rhoDry = ones(84,27)*2169;
KDry = ones(84,27)*field2Metric(2E6, 'psi') ;
GDry = ones(84,27)*field2Metric(1.368E6, 'psi');

% Calculate parameters from input data for each z value
for i = 1:4
    P = pressure{i};
    Soil = saturation{i};
    phi = porosity{i};
    % Oil data (Batzle and Wang)
    rho0 = 141.5/(API + 131.5); % g/cm3
    % volume formation factor
    B0 = 0.9718 + 0.00038*(2.4*RG*sqrt(G/rho0)+ T + 17.8).^(1.175);
    % pseudo density
    rhopseudo = rho0/B0*(1+0.001*RG)^-1; % g/cm3
    % density of oil with gas
    rhoG = (rho0 + 0.0012*G*RG)/B0; % g/cm3
    % density corrected for pressure and temperature
    rhoOil = 1000*(rho0 + (0.00277.*P - 1.71E-7.*P.^3)*(rhoG - 1.148).^2 +
...
    P.*3.49E-4)/(0.972 + 3.81E-4*(T + 17.78)^1.175); % kg/m3

    % Oil velocity from API (Batzle and Wang)
    % Simplified version of the equation in the report
    VOil = 2096*(rhopseudo/(2.6 - rhopseudo))^0.5 - 3.7*T + 4.64*P +...
        0.0115*T.*P*(4.12*(1.08/rhopseudo - 1).^0.5 - 1); %m/s
    % Bulk modulus of oil
    KOil = rhoOil.*VOil.^2; % Pa
    % Bulk modulus of water
    KWater = field2Metric(1./CWater, 'psi'); % Pa
    % Woodcock's equation
    KFluid = ((1 - Soil)./KWater + Soil./KOil).^( -1); %Pa
    rhoFluid = (1 - Soil).*rhoWater + Soil.*rhoOil; % kg/m3
    % Gassmann equations (in SI units)
    KSat{i} = KDry + ...
        (1 - KDry./KMatrix).^2./((phi./KFluid + (1 - phi)./KMatrix - ...
    KDry./KMatrix.^2));
    GSat = GDry;
    % Density equation
    rhoSat{i} = rhoDry + phi.*rhoFluid;
end

%%
% Backus Average
for i = 1:max(xIndex)
    for j = 1:max(yIndex)
        for k = 1:max(zIndex)
            element(k) = 1/(KSat{k}(i,j) + 4/3*GSat(i,j));
            density(k) = rhoSat{k}(i,j);
        end
        D(i,j) = GSat(i,j);
        C(i,j) = mean(element)^(-1);
        rho(i,j) = mean(density);
    end
end

% P and S wave velocities

```

```

VP = (C./rho).^0.5; % m/s
VS = (D./rho).^0.5;

% Seismic data (output)
VP = field2Metric(VP, 'ms'); % ft/s
VS = field2Metric(VS, 'ms');
rho = rho/1000; % g/cm3
% Impedance
ImpP = rho.*VP;
ImpS = rho.*VS;
% mean values
VPMean = mean(mean(VP));
VSMean = mean(mean(VS));
ImpPMean = mean(mean(ImpP));
ImpSMean = mean(mean(ImpS));
rhoSatMean = mean(mean(rho));

% Difference from mean value
VPD = (VP - VPMean)./VPMean*100;
VSD = (VS - VSMean)./VSMean*100;
ImpPD = (ImpP - ImpPMean)./ImpPMean*100;
ImpSD = (ImpS - ImpSMean)./ImpSMean*100;
rhoSatD = (rho - rhoSatMean)./rhoSatMean*100;

```

end

Colordg.m

```

function linecolor = colordg(n);
%COLORDG - Choose 1 out of 10 different colors for a line plot
%The first seven colors are exactly the same as Matlab's default
%AXES Colororder property.
%
%Syntax: linecolor = colordg(n);
%
%Input: N , value between 1 and 10, giving the following colors
%
% 1 BLUE
% 2 GREEN (medium dark)
% 3 RED
% 4 TURQUOISE
% 5 MAGENTA
% 6 YELLOW (dark)
% 7 GREY (very dark)
% 8 ORANGE
% 9 BROWN
% 10 YELLOW (pale)
%Output: LINECOLOR (1 x 3 row vector)
%Example: linecolor = colordg(8);
%Author: clement Etienam
%PhD Supervisor: Dr Rosmary Villegas
color_order = ...
[ 0 0 1 % 1 BLUE
0 0.5 0 % 2 GREEN (medium dark)
1 0 0 % 3 RED
0 0.75 0.75 % 4 TURQUOISE
0.75 0 0.75 % 5 MAGENTA
0.75 0.75 0 % 6 YELLOW (dark)
0.25 0.25 0.25 % 7 GREY (very dark)
1 0.50 0.25 % 8 ORANGE
0.6 0.5 0.4 % 9 BROWN
1 1 0 ]; % 10 YELLOW (pale)

linecolor = color_order(n,:);
%END of code

```

Bibliography

- Aanonsen, S., Oliver, D., Reynolds, A. & Valles, B., 2009. The Ensemble Kalman Filter in Reservoir Engineering--a Review. *SPE Journal*, 14(3), pp. 393-412.
- Abubakar, A., Habashy,T.M., Druskin,V.,Kniznherman, L., Alumbaugh, D.,2008. 2.5D forward and inverse modelling for interpreting low-frequency electromagnetic measurements. *Geophysics*, 73(4), pp. F165-F177.
- Agbalaka, C. C. & Oliver, S. D., 2008. Application of the EnKF and localization to automatic history matching of facies distribution and production data. *Mathematical Geosciences*, Volume 40, pp. 353-374.
- Agarwal, B., H. Hermansen, J. Sylte, and L. Thomas., 2000 Reservoir characterization of Ekofisk field: A giant, fractured chalk reservoir in the Norwegian North Sea{history match, *SPE Reservoir Evaluation & Engineering*, 3(6), 534-543.
- Aharon, M., Elad, M. & Bruckstein, A., 2006. K-SVD: An Algorithm for Designing Overcomplete Dictionaries for Sparse Representation. *IEEE Transactions on Signal Processing*, 54(11), pp. 4311-4322.
- Al-Busafi, B., 2005. *Incorporation of Fault Rock Properties into Production Simulation Models - PhD Thesis*, s.l.: s.n.
- Al-Busafi, B., Fisher, Q. & Harris, S., 2005. The importance of incorporating the multi-phase flow properties of fault rocks into production simulation models. *Marine and Petroleum Geology*, Volume 22, pp. 365-374.
- Al-Hinai, S.,Fisher, Q., Al-Busafi, B.,Guise, P.,Grattoni, C., 2006. *Recent application of special core analysis to fault rocks*. International Symposium of the Society of Core Analysts held in Trondheim, Norway, s.n.
- Al-Hussainy, R., 1966. The flow of real gases through porous media. *Society of petroleum engineers*, p. 624.
- Al-Otaibi, S. S. & Al-Majed, A. A., 1998. Factors affecting pseudo relative permeability curves. *Journal of Petroleum Science and Engineering*, 21(3-4), pp. 249-261.

Alumbaugh, D. L. & Morrison, H. F., 1995. Monitoring subsurface changes over time with cross-well electromagnetic tomography. *Geophysical prospecting*, Volume 43, pp. 873-902.

Anderson, J. L., 2001. An ensemble adjustment Kalman filter for data assimilation, *Monthly Weather Review*, 129(12), pp.2884-2903.

Anderson, J. L., 2007. An adaptive covariance inflation error correction algorithm for ensemble filters, *Tellus A*, 59(2), pp. 210-224.

Anderson, J. L., 2008. Exploring the need for localization in ensemble data assimilation using a hierarchical ensemble filter, *Physica D: Nonlinear Phenomena*, 230(1-2), pp. 99-111.

Anderson, J. L. and S. L. Anderson, 1999. A Monte Carlo implementation of the nonlinear filtering problem to produce ensemble assimilations and forecasts, *Monthly Weather Review*, 127(12), pp.2741-2758.

Andrews, A., 1968. A square root formulation of the Kalman covariance equations, *AIAA*, 6(6), 1165-1168.

Anterion, F., B. Karcher, and R. Eymard, 1989. Use of parameter gradients for reservoir history matching, in Proceedings of the *10th SPE Reservoir Simulation Symposium, Houston, Texas*, 6-8 February, SPE 18433.

Archie, G. E., 1942. The Electrical Resistivity Logs as an Aid in Determining Some Reservoir Characteristics. *SPE*, 146(1), pp. 54-62.

Arroyo-Negrete, E., D. Devegowda, A. Datta-Gupta, and J. Choe, 2008. Streamline assisted ensemble Kalman filter for rapid and continuous reservoir model updating, *SPE Reservoir Evaluation & Engineering*, 11(6), 1046-1060.

Aster R, Borchers. B., Thurber. C., 2005. *Parameter estimation and inverse problems*. 1 ed. .:Elsevier Academic Press.

Aziz, K. & Settari, A., 1979. *Petroleum Reservoir Simulation*. .:Applied Science Publishers.

Aublinger, C., 2015. Shape Factor Estimation and WAG Simulation in Naturally Fractured Reservoirs

Barenblatt, G. ., Zheltov, I. ., & Kochina, I.. 1960. Basic concepts in the theory of seepage of homogeneous liquids in fissured rocks [strata]. *Journal of Applied Mathematics and Mechanics*, 24(5), 1286–1303.[http://doi.org/10.1016/0021-8928\(60\)90107-6](http://doi.org/10.1016/0021-8928(60)90107-6)

Barker, J. & Fayers, F., 1994. Transport Coefficients for Compositional Simulation With Coarse Grids in Heterogeneous Media. *SPE Advanced Technology Series*, 2(02).

Benguigui, A., Yin, Z. & MacBeth, C., 2014. A method to updated fault transmissibility multipliers in the flow simulation model directly from 4D Seismic. *Journal of Geophysics and Engineering*, 11(2).

Bertino, L., G. Evensen, and H. Wackernagel, 2003. Sequential data assimilation techniques in oceanography, *International Statistical Review*, 71(2), 223-241.

Bianco A, Cominelli. A. Dovera. L. Naevdal. G. Valles. B., 2007. *History matching and production forecast uncertainty by means of the ensemble Kalman filter*. London, SPE Europec/EAGE Annual Conference.

Biondi B, Mavko. G., Mukerji., T. Ricket.,J., Lumely D.,Deutsch,C.,Gundeso,R.,Thiele, M., 1998. *Reservoir monitoring: a multidisciplinary feasibility study*. s.l.: The Leading edge.

Bi, Z., Oliver, D. & Reynolds, A. S., 2000. *Conditioning 3D Stochastic Channels to Pressure Data*. 5(4), 474-484 ed. s.l.: SPE Journal.

Bohling, G., October 2005. Introduction to Geostatistics and Variogram Analysis. In: U. o. Kansas, ed. Kansas: University of Kansas, p. 20.

Bourdarot, G, 1998.Well, Testing; Interpretation Methods (Editions T).Center for Petroleum engineering and project development

Burgers, G., P. van Leeuwen, and G. Evensen,1998. Analysis scheme in the ensemble Kalman filter, *Monthly Weather Review*, 126(6), 1719-1724.

Caers, J., 2002. *History matching under training-image based geological model constraints*. s.l.: Stanford University.

Candes, E. J., Romberg, J. & Tao, T., 2006. Robust uncertainty principles: Exact signal reconstruction from high incomplete frequency information. *Information Theory, IEEE Transactions on*, 52(2), pp. 489-509.

Carbonate Reservoirs. 2016. Retrieved June 12, 2017, from http://www.slb.com/services/technical_challenges/carbonates.aspx

Chang, H., Zhang, D. & Lu, Z., 2010. History matching of facies distribution with the EnKF and level set parameterization. *Journal of Computational Physics*, 229(1), pp. 8011-8030.

Chavent, G. M., Dupuy,M, and Lemonnier,P, 1975. History matching by use of optimal control theory, *SPE Journal*, 15(1), 74-86.

Chen, C., Li,G., and A. C. Reynolds,2010. Closed-loop reservoir management on the Brugge test case, *Computational Geosciences*, 14(4), 691-703.

Chen, W. H., Gavalas.G.R, Seinfeld, J.H, and Wasserman,M.L,1974. A new algorithm for automatic history matching, *SPE Journal*, 14(6), 593-608.

Chen, Y. and Oliver,D.,2009. Cross-covariance and localization for EnKF in multiphase flow data assimilation, *Computational Geosciences*, 14(4), 579-601.

Chen, Y. and Oliver,D.,2010. Ensemble-based closed-loop optimization applied to Brugge field, *SPE Reservoir Evaluation & Engineering*, 13(1), 56-71.

Chen, Y. and Oliver,D., .2011 Ensemble randomized maximum likelihood method as an iterative ensemble smoother, *Mathematical Geosciences*, Online First.

Cole, S., Lumley, D., Meadows, M. & Tura, A., 2002. *Pressure and Saturation Inversion of 4D Seismic Data by Rock Physics Forward Modeling*. Salt Lake City, Utah, Society of Exploration Geophysicists.

Cominelli A, Dovera. L. Vimercati. S., Naevdal. G., 2009. *Benchmark study of ensemble Kalman filter methodology: History Matching and uncertainty quantification for deep water oil reservoir*. Doha, Qatar, International Petroleum Technology conference.

Correy, A., 1956. Three Phase relative permeability. *Society of petroleum engineers*, Volume two, p. 349.

Craft, B. C. & Hawkins, M., 1991. *Applied Petroleum Reservoir Engineering*. S .l.: Prentice Hall.

Crichlow, H. B., 1977. *MODERN RESERVOIR ENGINEERING-A Simulation Approach*. 1st ed. Oklahoma: Prentice-Hall, Inc.Englewood Cliffs, New Jersey 07632.

Christie M.A. and Blunt M.J.,2001. Tenth SPE comparative solution project: A comparison of upscaling techniques. Proceedings of the 2001 SPE Reservoir Simulation Symposium, Houston, SPE.

Dake, L., 1978. *Fundamentals of Reservoir Engineering*. S .l.: Elsevier.

Dake, L., 2001. *The Practise of Reservoir Engineering*. Revised ed. s.l.: Elesevier.

Deutsch C and Journal, A., 1995. Stochastic reservoir modelling using simulated annealing and genetic algorithm. *SPE Formation Evaluation*, 10(1).

Deutsch, C. V. & Journel, A. G., 1998. *GSLIB Geostatistical Software Library and User's Guide*. NY(EUA) ed. New York: Oxford University Press.

Dong, Y., 2005. *Integration of time-lapse seismic data into automatic history matching*, Oklahoma: The University of Oklahoma, USA.

Dorn, O., Bertete-Aguirre, H. & Papanicolaou, G. C., 2007. Adjoint fields and sensitivities for 3D electromagnetic imaging in isotropic and anisotropic media.

Dorn, O. & Villegas, R., 2008. History matching of petroleum reservoirs using a level set technique. *Inverse problems*, p. 24.

Dovera, L. & Della Rossa, E., 2007. Ensemble Kalman filter for gaussian mixture models. *Petroleum Geostatistics*, 1(A16), pp. 10-14.

Ehrendorfer, M., 2007. A review of issues in ensemble-based Kalman filtering. *Metereologische Zeitschrift*, 16(6).

Elfeel, M. A. 2014. *Improved upscaling and reservoir simulation of enhanced oil recovery processes in naturally fractured reservoirs*. Heriot-Watt University.

Elsheikh, A., Jackson, M. & Laforce, T., 2012. Bayesian Reservoir History Matching Considering Parameter Uncertainties. *Mathematical Geosciences*, Issue 44, pp. 515-543.

Elsheikh, A., Wheeler, M. & Hoteit, I., 2013. Sparse calibration of subsurface flow models using nonlinear orthogonal matching pursuit and an iterative stochastic ensemble method. *Advances in Water Resources*, 56(1), pp. 14-26.

Emerick, A. A., 2018. Deterministic Ensemble Smoother with Multiple Data Assimilation as an Alternative for History Matching Seismic Data. *Computational Geosciences*.

Emerick, A. A. and Reynolds A. C., 2010. EnKF-MCMC, in Proceedings of the SPE EUROPEC/EAGE Annual Conference and Exhibition, Barcelona, Spain, 4-17 June, SPE 131375.

Emerick, A. A. and Reynolds A. C., 2011 Combining sensitivities and prior information for covariance localisation in the ensemble Kalman filter for petroleum reservoir applications, *Computational Geosciences*, 15(2), 251-269.

Emerick, A. A. and Reynolds A. C., 2011 History matching a field case using the ensemble Kalman filter with covariance localisation, *SPE Reservoir Evaluation& Engineering*, 14(4), 423-432.

Emerick, A. A. and Reynolds A. C., 2012. Combining the ensemble Kalman filter with Markov chain Monte Carlo for improved history matching and uncertainty characterisation, *SPE Journal*, in the press.

Emerick, A. A. and Reynolds A. C., 2013 Ensemble smoother with multiple data assimilation, *Computers & Geosciences*.

Emerick, A. A. and Reynolds A. C., 2012. History matching production and seismic data in a real field case using the ensemble smoother with multiple data assimilation.

Emerick, A. A. and Reynolds A. C., 2012. History matching time-lapse seismic data using the ensemble Kalman filter with multiple data assimilations, *Computational Geosciences*, Online First, 2012.

Ertekin, T., Abou-Kassem, J. H. & King, G. R., 2001. *Basic Applied Reservoir Simulation - SPE Textbook Series Vol.7*. s.l.: Society of Petroleum Engineers Inc.

Etienam, C., Mahmood, I. & Villegas, R., 2017. *History matching of Reservoirs by Updating Fault Properties Using 4D Seismic Results and Ensemble Kalman Filter*. Paris, SPE.

Etienam, C., Villegas, R & Babaei, M., 2016. *Integrated Structural Reconstruction and History Matching Using Ensemble Filter and Low-frequency Electromagnetic Data*. EAGE conference proceeding. *EAGE-SPE Annual Conference & Exhibition, Vienna, Austria*.

Etienam, C., Villegas, R., Babaei, M & Dorn,O 2018. *An Improved Reservoir Model Calibration through Sparsity Promoting ES-MDA*. ECMI conference proceeding. 20th European Conference on Mathematics for Industry (ECMI) 18-22 June 2018, Budapest, Hungary

Evensen G, H. J. R. E. S. K. a. E. O., 2007. Using the enkf for assisted history matching of a north sea reservoir model. *SPE Reservoir simulation symposium*, Volume 1, pp. SPE 89942-PA.

Evensen, G., 1994. Sequential data assimilation with a nonlinear quasi-geostrophic model using Monte Carlo methods to forecast error statistics. *Journal of Geophysical Research*, 99(C5), pp. 10143-10162.

Evensen, G., 2003. The Ensemble Kalman Filter: Theoretical formulation and practical implementation. *Ocean Dynamics*, 53(4), pp. 343-367.

Evensen, G., 2004. Sampling strategies and square root analysis schemes for the EnKF, *Ocean Dynamics*, 54(6), pp. 539-560.

Evensen, G., 2009. *Data Assimilation, The Ensemble Kalman filter*. 2nd ed. Berlin: Springer.

Evensen, G., 2009. The ensemble Kalman filter for combined state and parameter estimation, *IEEE Control Systems Magazine*, pp. 83-104.

Evensen, G., Eikrem, K. S 2018. *Conditioning reservoir models on rate data using ensemble smoothers*. Computational Geosciences, 22(5), pp. 1251-1270.

Evensen, G. and P. J. van Leeuwen, 2000 An ensemble Kalman smoother for nonlinear dynamics, *Monthly Weather Review*, 128(6), pp. 1852-1867.

Fahimuddin, A., March 2010. *4D Seismic History Matching Using the Ensemble Kalman Filter: Possibilities and challenges*, Bergen: University of Bergen.

Fenton.G.A, 2010. *Best Linear Unbiased Estimate and Kriging in stochastic analysis and inverse modelling*, s.l.: s.n.

Fisher, Q. J. & Jolley, S. J., 2007. Treatment of faults in production simulation models. In: *Structurally Complex Reservoirs*. S.l.: Geological Society of London, pp. 219-233.

Gao, G., Abubakar, A. & Habashy, T. M., 2004. Joint Petrophysical inversion of electromagnetic and full-waveform seismic data. *Geophysics*, 77(3), pp. WA3-WA18.

Gassmann, F., 1951.) Über die Elastizität poröser Medien: Vierteljahrsschrift der Naturforschenden Gesellschaft in Zürich.

Golmohammadi, Azarang, and Behnam Jafarpour. 2016. "Simultaneous geologic scenario identification and flow model calibration with group-sparsity formulations." *Advances in Water Resources* 92: 208-227

Goovaerts, P., 1997. *Geostatistics for Natural Resources Evaluation*. s.l.: Oxford University Press.

Gosselin O, Aanonsen. S. Aavarts. M. Cominelli. A.,Gonard.R.,Kolasinski.,M, Ferdinandadi,F., Kovacic.,L.,Neylon,K., 2003. *History matching using time-lapse seismic(HUTS)*. Colorado, USA, Society of Petroleum Engineers.

Habashy, M. & Abubakar, A., 2004. A general framework for constraint minimization for the inversion of electromagnetic measurements. *Progress in Electromagnetic Research*, 46(1), pp. 265-312.

Haibin, C. & Zhang, D., 2015. Jointly updating the mean size and spatial distribution of facies in reservoir history matching. *Computational Geosciences*.

Hanke, M.,1997. A regularizing Levenberg-Marquardt scheme, with applications to inverse groundwater filtration problems. *Inverse problems* 13(1), pp. 79–95

Hastings, W. K.,1970. Monte Carlo sampling methods using Markov chains and their applications, *Biometrika*, 57(1), 97-109.

Haugen, V., G. Naevdal, L.-J. Natvik, G. Evensen, A. M. Berg, and K. M. Flores,.2008. History matching using the ensemble Kalman filter on a North Sea field case, *SPE Journal*, 13(4), 382-391.

Heel, A. P. G. Van, Boerrigter, P. M., & E, S. I. 2006. Shape-Factor in Fractured Reservoir Simulation, 1–12.

Hill, H. J. & Milburn, J. D., 1956. Effect of Clay and Water salinity on Electromechanical Behaviour of Reservoir Rocks. *Petroleum Transactions*, 207(1), pp. 65-72.

Hodgetts, D. D., 2011. *Geostatistics and Stochastic Reservoir modelling - Basic geostatistics for reservoir characterization and introduction to stochastic reservoir modelling in PETREL*. s.l.: The University of Manchester - School of Earth, Atmospheric & Environmental Sciences.

Houtekamer, P. L. and H. L. Mitchell,.1998. Data assimilation using an ensemble Kalman filter technique, *Monthly Weather Review*, 126(3), 796-811.

Houtekamer , P. & Mitchell , H., 2001. A sequential ensemble Kalman filter for atmospheric data assimilation. *American Meterological Society*, Volume 1.

Houtekamer, P. L. and H. L. Mitchell, 2005. Ensemble Kalman filtering, *Quarterly Journal of the Royal Meteorological Society*, 131, pp. 3269-3289.

Hu, W., Abubakar, A. & Habashy, T. M., 2009. Joint Electromagnetic and seismic inversion using structural constraints. *Geophysics*, 74(6), pp. R99-R109.

Islam, M. R., Moussavizadegan, S., Mustafiz, S. & Abou-Kassem, J., 2010. *Advanced Petroleum Reservoir Simulation*. S.l.: Scrivener Publishing LLC.

IF, F., & Frykman, P. 2005. Estimation of shape factors in fractured reservoirs. *Petroleum Geology: North-West Europe and Global Perspectives—Proceedings of the 6th Petroleum Geology Conference*, 545–547.

Iglesias, M.A., Dawson, C. 2013. The regularizing Levenberg-Marquardt scheme for history matching of petroleum reservoirs. *Computational Geosciences* 17, pp.1033–1053

Jacquard., P. & Jain., C., 1965. *Permeability Distribution from Field Pressure Data*. s.l.: SPE.

Jafarpour, B., 2011. Wavelet reconstruction of geologic facies from nonlinear dynamic flow measurements. *Geosciences and Remote sensing, IEEE Transactions*, 49(5), pp. 1520-1535.

Jafarpour, B. & McLaughlin, D. B., 2007. *History matching with an ensemble Kalman filter and discrete cosine parametrization*. Anaheim, California, SPE.

Jansen, J., D. Brouwer, G. Naevdal, and C. van Kruijsdijk, 2005. Closed-loop reservoir management, *First Break*, 23, 43-48.

Jansen, J. D., S. D. Douma, D. R. Brouwer, P. M. J. V. den Hof, and A. W. Heemink, 2009. Closed-loop reservoir management, in Proceedings of the *SPE Reservoir Simulation Symposium*, The Woodlands, Texas, 2-4 February, SPE 119098.

Jing, P. & Zhang, D., 2013. History matching of fracture distributions by ensemble Kalman filter combined with vector based level set parametrization. *Journal of Petroleum Science and Engineering*, Issue 1.

Jolley, S. et al., 2007. Faulting and fault sealing in production simulation models: Brent Province, northern North Sea. *Petroleum Geoscience*, Volume 13, pp. 321-340.

Kalman, R., 1960. A new approach to linear filtering and prediction problems. *Transactions of the ASME-Journal of Basic Engineering*, p. 82.

Katterbauer, K., Hoteit, I. & Sun, S., March 2014. *A Time Domain Update Method for Reservoir History Matching of Electromagnetic Data*. Kuala Lumpur, Malaysia, Offshore Technology Conference.

Katterbauer, K. & Sun, S., 2015. History matching of Electromagnetically Heated Reservoirs Incorporating Full-Wavefield Seismic and Electromagnetic Imaging. *Society of Petroleum Engineers*.

Kawar R, C. R. K. M., 2003. *The workflow of 4D Seismic*. SPE 13th Middle East Oil show and conference, SPE 81527.

Kazemi, H., Merrill Jr, L. S., Porterfield, K. L., & Zeman, P. R. 1976. Numerical Simulation of Water-Oil Flow in Naturally Fractured Reservoirs. *Society of Petroleum Engineers Journal*, 16(6), 317–326. <http://doi.org/10.2118/5719-PA>

Kepert, J. D., 2004. On ensemble representation of the observation-error covariance in the ensemble Kalman filter, *Ocean Dynamics*, 54(6), 561-569.

Khaninezhad, M. M., Jafarpour, B. & Li, L., 2012. Sparse geologic dictionaries for subsurface flow model calibration: Part 1, Inversion formulation. *Advances in Water Resources*, 39(1), pp. 106-121.

Khaninezhad, Mohammad-Reza, and Behnam Jafarpour. 2017. Discrete Regularization for Calibration of Geologic Facies Against Dynamic Flow Data, *Water Resources Research*, In SPE Reservoir Simulation Conference. Society of Petroleum Engineers

Kirsch, 1996. *Introduction to the mathematical theory of inverse problems*. New York: Springer-Verlag.

Kleppe, J. 2003. *Introduction to fractured reservoir simulation*.

Knipe, R. J., Fisher, Q. & Jones, G., 1997. Fault seal analysis: successful methodologies, application and future directions. *Hydrocarbon Seals: Importance for exploration and production*, Volume 7, pp. 15-38.

Knipe, R., Jones, G. & Fisher, Q., 1998. Faulting, fault sealing and fluid flow in hydrocarbon reservoirs: *Geological Society of London, Special Publications*, Volume vii-xxi.

K.S, L., & W.K.S., P. 2013. Assessment of different matrix-fracture shape factor in double porosity medium. *Journal of Applied Sciences*, 308–314.
<http://doi.org/10.1017/CBO9781107415324.004>

Kyte, J. & Berry, D., 1975. New Pseudo Functions To Control Numerical Dispersion. *Society of Petroleum Engineers*, 15(04).

Landrø M, S. O. H. E. E. B. S. L., 1999. The Gullfaks 4D seismic study. *Petroleum Geoscience*, Volume 5 Nos 3.

Law K J H & Stuart A M , 2012 Evaluating Data Assimilation Algorithms Mon. Weather Rev 140 37-57

Leeuwenburgh, O., G. Evensen, and L. Bertino, 2005. The impact of ensemble filter definition on the assimilation of temperature profiles in the tropical Pacific, *Quarterly Journal of the Royal Meteorological Society*, 131, 3291-3300.

Lemonnier, P., & Bourbiaux, B. 2010. Simulation of Naturally Fractured Reservoirs. State of the Art. *Oil & Gas Science and Technology – Revue de l’Institut Français Du Pétrole*, 65(2), 263–286. <http://doi.org/10.2516/ogst/2009067>

Le, D.H., Emerick, A.A., Reynolds, A.C. 2016. An adaptive ensemble smoother with multiple data assimilation for assisted history matching. *SPE J.* 21(6), 2195–2207.
<https://doi.org/10.2118/173214-PA>

Lee, J., and P. K. Kitanidis. 2013. Bayesian inversion with total variation prior to discrete geologic structure identification. *Water Resources Research* 49, no. 11: 7658-7669.

Liang, B., 2007. *An Ensemble Kalman Filter Module for Automatic History matching*, Austin: University of Texas, Austin.

Li, G., M. Han, R. Banerjee, and A. C. Reynolds, 2010. Integration of well test pressure data into heterogeneous geological reservoir models, *SPE Reservoir Evaluation & Engineering*, 13(3).

Li, G. and A. C. Reynolds, 2009. Iterative ensemble Kalman filters for data assimilation, *SPE Journal*, 14(3), 496-505.

Li, R., A. C. Reynolds, and D. S. Oliver, 2003. History matching of three-phase flow production data, *SPE Journal*, 8(4), 328-340, 2003.

Lia, O. et al., 1997. Uncertainties in reservoir production forecasts. *AAPG Bulletin*, Issue 81, pp. 775-801.

Lim, K. T., & Aziz, K. 1995. Matrix-fracture transfer shape factors for dual porosity simulators. *Journal of Petroleum Science and Engineering*, 13(3-4), 169–178.
[http://doi.org/10.1016/0920-4105\(95\)00010-F](http://doi.org/10.1016/0920-4105(95)00010-F)

Liu, E. & Jafarpour, B., 2013. Learning sparse geologic dictionaries from low-rank representations of facies connectivity for flow model calibration. *Water resources*, Volume 49, pp. 7088-7101.

Liu, N. & Oliver, S. D., 2005. Critical evaluation of the ensemble Kalman filter on history matching of geological facies. *SPE Reservoir Evaluation & Engineering*, 8(6), pp. 470-477.

Lorentzen, R. J., Flornes, M. K. & Naevdal, G., 2012. History matching Channelized Reservoirs Using the Ensemble Kalman Filter. *Society of Petroleum Engineers*, 17(1).

Lorentzen, R. J., Naevdal, G. & Shafeirad, A., 2013. Estimating Facies fields by use of the Ensemble Kalman Filter and Distance Functions-Applied to Shallow-Marine Environment. *Society of Petroleum Engineers*, 18(1), pp. 146-158.

Lorentzen, R. J., A. Shaifeirad, and G. Naevdal, 2009. Closed loop reservoir management using the ensemble Kalman filter and sequential quadratic programming, in

Proceedings of the *SPE Reservoir Simulation Symposium*, The Woodlands, Texas, 2{4 February, SPE 119101.

Lorentzen, R. J. and G. Naevdal, 2011. An iterative ensemble Kalman filter, *IEEE Transactions on Automatic Control*, 56(8), 1990-1995.

Lorentzen, R. J., K. K. Fjelde, J. Froyen, A. C. Lage, G. Naevdal, and E. H. Vefring, 2001. Underbalanced and low-head drilling operations: Real-time interpretation of measured data and operational support, in *Proceedings of the SPE Annual Technical Conference and Exhibition*, New Orleans, Louisiana, 30 September-3 October, SPE 71384.

Luenberger, D., 1967. *Optimization by vector space methods*. New York: John Wiley & Sons Inc.

Lumley, D., 1999. Meren Field Nigeria: A 4D case study. *SEG Extended Abstracts*, p. 1628.

Macbeth, C., 2004. A classification for the pressure sensitivity properties of a sandstone rock frame. *Geophysics*, Volume 69, pp. 497-510.

Macbeth, C., Floricich, M. & Soldo, J., 2006. Going quantitative with 4D seismic analysis. *Geophysical Prospecting*, Volume 54, pp. 303-317.

Maharaja, A., 2008. TiGenerator: Object-based training image generator. *Computers & Geosciences*, Volume 34, pp. 1753-1761.

Manzocchi, T., Heath, A., Walsh, J. J. & Childs, C., 2002. The representation of two-phase fault-rock properties in flow simulation models. *Petroleum Geoscience*, Volume 8, pp. 119-132.

Manzocchi, T., Walsh, J., P.Neil & Yielding, G., 1999. Fault transmissibility multipliers for flow simulation models. *Petroleum Geoscience*, Volume 5, pp. 53-63.

Marsala, A. et al., 2008. *Crosswell electromagnetic tomography: from resistivity mapping to interwell fluid distribution*. s.l., International Petroleum Technology Conference, 2008.

Mathworks, MATLAB 2016. www.mathworks.com. [Online]
[Accessed 20 June 2016].

Maybeck, P., 1979. *Stochastic models, estimation and control*. 1 ed. New York: Academic Press.

Ma, Y. Z. & Pointe, P. R. L., 2011. *Uncertainty Analysis and Reservoir Modeling: Developing and Managing Assets in an Uncertain World*. Memoir 96 ed. s.l.: AAPG.

Mora, C. A., & Wattenbarger, R. A. 2009. Analysis and verification of dual porosity and CBM shape factors. *Journal of Canadian Petroleum Technology*, 48(2), 17–21.
<http://doi.org/10.2118/09-02-17>

More, J. & Sorensen, D., 1983. Computing a trust region step. *SIAM J. Statistical Computation*, 4(3), pp. 553-572.

Moreno, D. L., 2011. *Continuous Facies Updating Using the Ensemble Kalman Filter and the Level set method*. s.l., Mathematical Geosciences.

Moreno, L. D. & Aanonsen, I. S., 2008. Conditioning geological facies to production and well data using the ensemble Kalman filter and the level set method: a study on ensemble size and localization. *SPE Journal*.

Moreno, L. D. & Aanonsen, S. I., 2007. *Stochastic facies modelling using the level set method*. Cascais, Portugal, In proceedings of EAGE-Petroleum Geostatistics Conference.

Naar, J. W. a. H. J., 1962. Imbibition relative permeability in unconsolidated porous media. *Society of petroleum engineers*, Volume two, p. 13.

Nævdal G, J. L. S. E., 2005. Reservoir monitoring and continuous model updating using the ensemble Kalman filter. *SPE Journal* 10.

Nævdal, G., Johnsen, L. M., Aanonsen, I. S. & Vefring, E. H., 2003. Reservoir monitoring and continuous model updating using ensemble Kalman filter. *SPE Journal*, 1(10), pp. 66-74.

Nocedal, J. and Wright, S.J, 1999. *Numerical Optimization*, Springer, New York.

Nikravesh, M., Zadeh, L. & Aminzadeh, F., 2003. *Soft Computing and Intelligent Data Analysis in Oil Exploration*. s.l.: Elsevier.

Odling, N.E, 1997, Scaling and connectivity of joint systems in sandstones from western Norway: *Journal of structural geology*, v.19, no 10,p.1257-1271

Oldenziel, T., 2003. *Time-lapse seismic within reservoir engineering*, The Netherlands: PhD Thesis, Delft University of Technology.

Oliver, D., 1996. Multiple realizations of the permeability field from well-test data. *SPE Journal*, 1(2).

Oliver, D. S. and Y. Chen,2009. Improved initial sampling for the ensemble Kalman filter, *Computational Geosciences*, 13(1), pp.13-27, 2009.

Oliver, D. S. & Chen, Y., 2010. Recent progress on reservoir history matching: a review. s.l.: *Computational Geoscience - Springer Science*.

Oliver, D. S., N. He, and A. C. Reynolds, 1996. Conditioning permeability fields to pressure data, in Proceedings of the *European Conference for the Mathematics of Oil Recovery*.

Oliver, D. S., Reynolds, A. C. & Liu, N., 2008. *Inverse Theory for Petroleum Reservoir Characterization and History Matching*. s.l.: Cambridge University Press.

Omre, 2000. *Stochastic reservoir models conditioned to non-linear production history observations*. Cape town: Geostatistics 2000.

Osher, s. & Fedkiw, R., 2003. *Level set methods and dynamic implicit surfaces*. s.l.: Springer-Verlag New York Inc.

Osher, S. & Sethian, J. A., November 1998. Fronts propagating with curvature-dependent speed: Algorithms based on Hamilton-Jacobi formulations. *Journal of computational physics*, 79(1), pp. 12-49.

Pittman, E., 1981. Effect of fault-related granulation on porosity and permeability of quartz sandstones. *AAPG Bulletin*, Volume 65, pp. 2381-2387.

Quintard, M., & Whitaker, S. 1996. Transport in chemically and mechanically heterogeneous porous media. I: Theoretical development of region-averaged equations for slightly compressible single-phase flow. *Advances in Water Resources*, 19(1), 29–47. [http://doi.org/10.1016/0309-1708\(95\)00023-C](http://doi.org/10.1016/0309-1708(95)00023-C)

R.S, V., 1962. *Matrix Iterative analysis*. 1 ed. Englewood Cliffs, N.J Prentice Hall.

Rachford, D. P. a. H., 1955. *The Numerical solution of parabolic and elliptical Differential Equations*. 1 ed. New York: J.Soc.Industry.Appl.Math.

Rachford, P. D. a., 1955. The numerical solution of parabolic and elliptic Differential Equations. *Journal of the society of industrial and applied mathematics*, Issue 3, pp. 28-41.

Ravanelli, F. & Hoteit, I., 2013. *History matching time-lapse Crosswell data using the ensemble Kalman filter*. s.l., SPE journal.

Reynolds, A. C., N. He, L. Chu, and Oliver D. S., 1996. Reparameterization techniques for generating reservoir descriptions conditioned to variograms and welltest pressure data, *SPE Journal*, 1(4), 413-426,

Reynolds, A. C., N. He, and Oliver D. S., 1999. Reducing uncertainty in the geostatistical description with well-testing pressure data, in Reservoir Characterization-Recent Advances, (edited by R. A. Schatzinger and J. F. Jordan), pp. 149-162, *American Association of Petroleum Geologists*.

Reynolds, A. C., Zafari M., and Li G., 2006. Iterative forms of the ensemble Kalman filter, in Proceedings of 10th European Conference on the Mathematics of Oil Recovery, Amsterdam, 4-7 September 2006.

Report and Dresser, 1982. *Well, logging and Interpretation Techniques*. second ed. s.l.:s.n.

Richard.c.Selley, 2007. *Elements of petroleum geology*. second ed. s.l.:s.n.

Rider, M. H., 2002. *The geological interpretation of well logs*. 2nd Edition ed. s.l.: Rider-French Consulting Ltd.

Ringrose, P., Sorbie, K., Corbett, P. & Jensen, J., 1992. Immiscible flow behaviour in laminated and cross-bedded sandstones. *Journal of Petroleum Science and Engineering*, 9(2), pp. 103-124.

Roggero F, D. D. B. P. L. O., 2007. *Matching of production history and 4D seismic data-application to the Girassol Field offshore Angola*. Anaheim, California, SPE.

Saito, H., 2006. Time-lapse Crosswell seismic tomography for monitoring injected CO₂ in an onshore aquifer, Nagoaka, Japan. *Exploration Geophysics*, 37(1), pp. 30-36.

Sandø I, M. O. a. E. R., 2009. 4D geophysical data. *GEO Ex-Pro*, Issue 5.

Sarma, P., L. Durlofsky, K. Aziz, and W. Chen, 2006. Efficient real-time reservoir management using adjoint-based optimal control and model updating, *Computational Geosciences*, 10, 3-36.

Sarma, P., L. J. Durlofsky, and K. Aziz,,2008. Kernel principal component analysis for efficient differentiable parameterization of multipoint geostatistics, *Mathematical Geosciences*, 40, 3-32, 2008.

Satter, A., Iqbal, G. & Buchwalter, J. L., 2008. *Practical Enhanced Reservoir Engineering: Assisted with Simulation Software*. s.l.: PennWell Books.

Schlumberger GeoQuest, 2014. *ECLIPSE 100(Black Oil): Reference Manual and Technical Description*. Houston: s.n.

Schulze-Riegert, R. & Ghedan, S., 2007. *Modern techniques for history matching..* s.l.: 9th International Forum on Reservoir Simulation.

Seiler A,. 2009. Advanced reservoir management workflow using an EnKF based assisted history matching method. *SPE Reservoir Simulation Symposium*, p. SPE 118906.

Sherman, J., Morrison, W.J.1950. Adjustment of an inverse matrix corresponding to a change in one element of a given matrix. *The Annals of Mathematical Statistics* 21, 124–127.

Siavash, N., Leung, J. & Trivedi, J., 2015. Characterization of Non-Gaussian Geologic Facies Distribution Using Ensemble Kalman Filter with Probability Weighted Re-Sampling. *Mathematical Geosciences*.

Skjervheim J-A, 2007. *Continuous Updating of a coupled reservoir-seismic model using ensemble Kalman filter technique*, Bergen, Norway: PhD Thesis, University of Bergen.

Skjervheim, J.-A. E. G. A. S. R. B. J. T., 2007. Incorporating 4D seismic data in reservoir simulation models usig ensemble Kalman filter. *SPE Journal*, pp. SPE 958789-PA.

Skjervheim, J.-A., G. Evensen, J. Hove, and J. G. Vabo,2011. An ensemble smoother for assisted history matching, in Proceedings of the *SPE Reservoir Simulation Symposium*, The Woodlands, Texas, USA, 21-23 February, SPE 141929.

Stordal, A.2014. Iterative Bayesian inversion with Gaussian mixtures: finite sample implementation and large sample asymptotics. *Computational Geosciences*. DOI 10.1007/s10596-014-9444-9

Strebelle, S., 2000. *Sequential simulation drawing structures from training images*, Stanford, CA: Stanford University.

Strebelle, S., 2002. Conditional simulation of complex geological structures using multiple-point statistics. *Mathematical Geology*, 1(34).

Strebelle, S. B. & Journel, G. A., 2001. Reservoir modelling using Multiple-point Statistics. *SPE 71324*.

Strebelle, S., Caers, J. & Payrazyan, S., 2003. Modelling of a deepwater turbidite reservoir conditional to seismic data using principal component analysis and multiple-point geostatistics. *SPE*, 8(3).

Strebelle, S. & Levy, M., 2008. Using multiple-point statistics to build geologically realistic reservoir models: the MPS/FDM workflow. In: *The Future of Geological Modelling in Hydrocarbon Development*. s.l.: Geological Society of London.

Stroud, K. & Booth, D. J., 2007. *Engineering Mathematics*. 6th ed. s.l.: Palgrave Macmillan.

Stuart A M ,2010 *Inverse problems: A Bayesian perspective* Acta Numerica 19 451-559.

Szunyogh, I., Kostelich E. J., Gyarmati G., Patil D. J., Hunt B. R., Kalnay E., Ott E., and Yorke J. A.,2005. Assessing a local ensemble Kalman filter: perfect model experiments with the national centres for environmental prediction global model, *Tellus A*, 57, 528-545.

Tarantola, 2005. *Inverse problem theory and methods for model parameter estimation*. 1 ed. Philadelphia: SIAM.

Tarrahi, M. & Afra, S., 2016. Improved Geological model calibration through Sparsity-promoting Ensemble Kalman Filter. *Offshore Technology Conference*.

Tavakoli, R. and A. C. Reynolds,2010. History matching with parameterization based on the SVD of a dimensionless sensitivity matrix, *SPE Journal*, 15(12), pp. 495-508.

Tavakoli, R. and A. A. Reynolds,2011. Monte Carlo simulation of permeability fields and reservoir performance predictions with SVD parameterization in RML compared with EnKF, *Computational Geosciences*, 15(1), 99-116.

Thulin, K., G. Naevdal, H. J. Skaug, and S. I. Aanonsen,2011. Quantifying Monte Carlo uncertainty in the ensemble Kalman filter, *SPE Journal*, 16(1), pp. 172-182.

Tierney, L.,1994, Markov chains for exploring posterior distributions, *Annals of Statistics*, 22(4), 1701-1728.

Tropp, J. A. & Gilbert, C. A., 2007. Signal recovery from random measurements via orthogonal matching pursuit. *Information Theory, IEEE Transactions on*, 53(12), pp. 4655-4666.

Van Leeuwen, P. J., 1999. Comment on "Data assimilation using an ensemble Kalman filter technique", *Monthly Weather Review*, 127(6), 1374-1377.

Van Leeuwen, P. J., 2001. An ensemble smoother with error estimates, *Monthly Weather Review*, 129, 709-728.

Van Leeuwen, P. J. and Evensen G., 1996. Data assimilation and inverse methods in terms of a probabilistic formulation, *Monthly Weather Review*, 124, 2898-2913.

Vega, S. & Berteussen, K., 2007. *Is Gassmann the Best Model For Fluid Substitution In Heterogeneous Carbonates?*. San Antonio, Texas, Society of Exploration Geophysicists.

Villegas, R., Dorn, O. & Kindelan, M., 2005. Simultaneous characterisation of geological shapes and permeability distributions using the level set method. *SPE*.

Villegas, R., Etienam, C., Dorn, O., & Babaei, M., 2018. The shape and Distributed Parameter Estimation for History Matching using a Modified Ensemble Kalman Filter and Level Sets. ; Submitted to *Inverse problems Science and Engineering*.

Villegas, R., Etienam, C & F. Rahma. 2018. CO₂ Sequestration Using Ensemble Kalman Filter and Considering a Sustainability Approach. SPE paper SPE-185780-MS. *80th EAGE-SPE Annual Conference & Exhibition, Copenhagen, 11-14 June 2018*.

Villegas, R., Fisher, Q. & Anon, A., 2009. *Optimizing fluid-rock properties in compartmentalized reservoirs by using 4D Seismic Data*. 2nd International Conference on Faults and Top Seals, Montpellier, s.n.

Waggoner J, C. A. a. S. R., 2002. *Improved reservoir modelling with time-lapse seismic in a Gulf of Mexico gas condensate reservoir*. San Antonio, USA, SPE 77514.

Wang, C., G. Li, and A. C. Reynolds, 2009. Production optimization in closed-loop reservoir management, *SPE Journal*, 14(3), 506-523.

Wang, Z., Bovik, A. C., Sheikh, H. R. & Simoncelli, E. P., 2004. Image quality assessment: from error visibility to structural similarity. *Image processing IEEE transactions*, 13(4), pp. 600-612.

Warren, J. E. & Root, P. J., 1963. The behaviour of naturally fractured reservoirs. *SPE Reservoir Engineering*, 1(May), pp. 243-252.

Whitaker, J. S., T. M. Hamill, X. Wei, Y. Song, and Z. Toth, Ensemble data assimilation with the NCEP global forecast system, *Monthly Weather Review*, 136, 463{482, 2008.

Wilt, M. & Alumbaugh, D., 2003. Oilfield reservoir characterization and monitoring using electromagnetic geophysical techniques. *Journal of Petroleum Science and Engineering*, 39(1), pp. 85-97.

Wilt, M. J., 1995. Crosswell electromagnetic tomography: System design considerations and field results. *Geophysics*, 60(3), pp. 871-885.

Wu, J., Boucher, A. & Journel, G. A., 2006. A 3D code for mp simulation of continuous and categorical variables: FILTERSIM. *SPE*.

Wu, Z., Reynolds, A. & Oliver, D., 1999. *Conditioning Geostatistical Models to Two-Phase Production Data*. 3(2), 142-155 ed. s.l.: SPE Journal.

Yamasaki, S., 2009. A level set based topology optimization method using the discretized signed distance function as the design variables. *Structural and Multidisciplinary Optimization*.

Zhao, Y., Reynolds, A. C. & Li, G., 2008. *Generating facies maps by assimilating production data and seismic data with the ensemble Kalman filter*. Tulsa, SPE/DOE Symposium on Improved Oil Recovery.

Zhdanov, M., 2010. Electromagnetics geophysics: Notes from the past and road ahead. *Geophysics*, 75(5), pp. 75A49-75A66.

Zijlstra, E. B., Reemst, P. H. & Fisher, Q. J., 2007. Incorporation of fault properties into production simulation models of Permian reservoirs from the southern North Sea. In: *Structurally Complex Reservoirs*. s.l.: Geological Society, London, Special Publications, p. 295–308.

